

UNIVERZA V LJUBLJANI  
BIOTEHNIŠKA FAKULTETA

Žiga PANDUR

**MEHANIZEM DELOVANJA KAVITACIJSKIH  
MEHURČKOV NA BAKTERIJSKO CELICO**

DOKTORSKA DISERTACIJA

Ljubljana, 2022

UNIVERZA V LJUBLJANI  
BIOTEHNIŠKA FAKULTETA

Žiga PANDUR

**MEHANIZEM DELOVANJA KAVITACIJSKIH MEHURČKOV NA  
BAKTERIJSKO CELICO**

DOKTORSKA DISERTACIJA

**MECHANISM OF ACTION OF THE CAVITATION BUBBLES ON  
BACTERIAL CELL**

DOCTORAL DISSERTATION

Ljubljana, 2022

Na podlagi Statuta Univerze v Ljubljani ter po sklepu Senata Biotehniške fakultete in Senata Univerze v Ljubljani z dne 15. 9. 2020 je bilo potrjeno, da Žiga Pandur izpolnjuje pogoje za opravljanje doktorata znanosti na doktorskem študiju Agroživilska mikrobiologija, znanstveno področje: agroživilska mikrobiologija. Doktorsko delo je bilo opravljeno v laboratorijih Oddelka za mikrobiologijo na Biotehniški fakulteti Univerze v Ljubljani. Delo je bilo financirano s strani Evropskega raziskovalnega sveta in Ministrstva za izobraževanje, znanost in šport Republike Slovenije v skladu z Uredbo o sofinanciranju doktorskega študija. Za mentorja je bil imenovan prof. dr. David Stopar in za somentorja prof. dr. Matevž Dular.

Mentor:           prof. dr. David STOPAR  
                       Univerza v Ljubljani, Biotehniška fakulteta, Oddelek za mikrobiologijo

Somentor:       prof. dr. Matevž DULAR  
                       Univerza v Ljubljani, Fakulteta za strojništvo, Katedra za energetsko strojništvo

Komisija za oceno in zagovor:

Predsednik:      izr. prof. dr. Blaž STRES  
                       Univerza v Ljubljani, Biotehniška fakulteta, Oddelek za mikrobiologijo

Član:              doc. dr. Martin PETKOVŠEK  
                       Univerza v Ljubljani, Fakulteta za strojništvo, Katedra za energetsko strojništvo

Član:              doc. dr. Ignacijo BILUŠ  
                       Univerza v Mariboru, Fakulteta za strojništvo, Katedra za energetsko, procesno in okoljsko inženirstvo

Datum zagovora: 15.12.2022

Doktorand: Žiga Pandur

## KLJUČNA DOKUMENTACIJSKA INFORMACIJA (KDI)

- ŠD Dd
- DK UDK 532.528:579.2:577.352(043)=163.6
- KG kavitacija, kavitacijski mehurčki, bakterijska celična stena, liposomi, sferoplasti, mikroorganizmi, *Escherichia coli*, mehanizem inaktivacije, čiščenje voda
- AV PANDUR, Žiga, mag. mikrobiol.
- SA STOPAR, David (mentor), DULAR, Matevž (somentor)
- KZ SI-1000 Ljubljana, Jamnikarjeva 101
- ZA Univerza v Ljubljani, Biotehniška fakulteta, Interdisciplinarni doktorski študij Bioznanosti, znanstveno področje agroživilska mikrobiologija
- LI 2022
- IN MEHANIZEM DELOVANJA KAVITACIJSKIH MEHURČKOV NA BAKTERIJSKO CELICO
- TD Doktorska Disertacija
- OP XI, 137, [75] str., 1 pregl., 9 sl., 4 pril., 200 vir.
- IJ sl
- JI sl/en
- AI Razpoložljivost neoporečne pitne vode postaja vse večja skrb v globaliziranem svetu. Kavitacija, kot nova obetajoča alternativna metoda pri procesu čiščenja vod, je pojav parnih mehurčkov v tekočinah ob hitrem lokalnem padcu tlaka, ki agresivno in hitro implodirajo, kar povzroča ekstremne fizikalno-kemijske razmere, ki imajo lahko uničujoč učinek na bakterije. Točen mehanizem inaktivacije bakterijskih celic s kavitacijo ni poznan. V doktorski disertaciji smo vpliv hidrodinamske in akustične kavitacije na lipidne vezikle, sferoplaste in bakterijske celice primerjali z vplivi fizikalno-kemijskih in mehanskih stresorjev. S selektivnim spremenjanjem izbranih komponent celične stene smo določili vpliv posameznih plasti na stabilnost celic pri kavitaciji in pokazali da je za stabilnost bakterij pri kavitaciji odločilen peptidoglikanski sloj. Za podrobnejše razumevanje interakcije med kavitacijskim mehurčkom in bakterijsko celico smo razvili novo metodo generiranja posameznega kavitacijskega mehurčka na mikrometrski časovni in prostorski skali, kar nam je omogočilo generiranje posameznega mikromehurčka v neposredni bližini bakterijske celice. Rezultati kažejo, da ima mikromehurček vpliv na bakterijske celice znotraj maksimalnega radija mikromehurčka. S pomočjo numeričnih analiz smo natančneje opisali razvoj kavitacijskega mehurčka in določili mejne sile, ki so potrebne za poškodovanje ali odtrganje celic iz površine. Rezultati teh naloge prispevajo k bistveno bolj podrobnemu razumevanju kavitacije na nivoju posameznega mehurčka in njegovemu vplivu na bakterije, kar bo omogočalo nadaljnji razvoj metod kavitacije za namene čiščenja vode.

### KEY WORDS DOCUMENTATION (KWD)

DN Dd  
DC UDK 532.528:579.2:577.352(043)=163.6  
CX cavitation, cavitation bubbles, bacterial cell wall, liposomes, spheroplasts, microrganisms, *Escherichia coli*, inactivation mechanism, water treatment  
AU PANDUR, Žiga  
AA STOPAR, David (supervisor), DULAR, Matevž (co-advisor)  
PP SI-1000 Ljubljana, Jamnikarjeva 101  
PB University of Ljubljana, Biotechnical Faculty, Interdisciplinary Doctoral Programme in Biosciences, field agrifood microbiology  
PY 2022  
TI MECHANISM OF ACTION OF THE CAVITATION BUBBLES ON BACTERIAL CELL  
DT Doctoral Dissertation  
NO XI, 137, [75] p., 1 tab., 9 fig., 4 ann., 200 ref.  
LA sl  
AL sl/en  
AB Due to escalating pollution, the world's clean water supplies are becoming seriously endangered. One of the novel promising methods in water cleaning is cavitation, where a sudden decrease in pressure triggers the formation of vapor and gas bubbles in a liquid medium. Fast and aggressive bubble implosions cause extreme physical-chemical conditions which inactivate bacteria and other contaminants. Despite an extensive research of cavitation, the exact mode of action on bacteria is not known. In doctoral dissertation we compare the effect of hydrodynamic and acoustic cavitation on lipid vesicles, spheroplasts and bacterial cells to the effect of various physio-chemical and mechanical stressors. Further, we evaluate the contribution of the individual cell wall layers on the resistance to cavitation. We show that peptidoglycan layer has the most important effect on cavitation resistance. For fundamental understanding of cavitation, we downscaled the cavitation phenomena to a single micrometer sized cavitation bubble and individual bacterial cell by developing a new method that delivers nanoscale spatial and temporal energy quantum to mechanically remove and destroy individual bacterial cells. The cavitation microbubble had an effect on bacterial cell when it was in proximity of the bubble. Numerical simulations enabled calculation of microbubble evolution and mechanical loads on bacterial cells and allow estimation of threshold values for wall shear stress and hydrodynamic force required for bacterial detachment and destruction. The new results will enable progress and development of cavitation technology towards more efficient and chemical free processes of water treatment.

## KAZALO VSEBINE

<b>KLJUČNA DOKUMENTACIJSKA INFORMACIJA (KDI)</b>	<b>III</b>
<b>KEY WORDS DOCUMENTATION (KWD)</b>	<b>IV</b>
<b>KAZALO VSEBINE</b>	<b>V</b>
<b>KAZALO ZNANSTVENIH DEL</b>	<b>VII</b>
<b>KAZALO PREGLEDNIC</b>	<b>VIII</b>
<b>KAZALO SLIK</b>	<b>IX</b>
<b>KAZALO PRILOG</b>	<b>X</b>
<b>OKRAJŠAVE IN SIMBOLI</b>	<b>XI</b>
<b>1 UVOD</b>	<b>1</b>
1.1 KAVITACIJA	1
1.2 KOLAPS POSAMEZNEGA MEHURČKA	5
1.3 BAKTERIJSKA CELICA	6
1.3.1 Citoplazemska membrana	7
1.3.2 Peptidoglikan	8
1.3.3 Zunanja membrana	8
1.3.4 Kapsula	9
1.4 VPLIV KAVITACIJE NA MIKROORGANIZME	9
1.5 NAMEN IN CILJI DOKTORSKE DISERTACIJE	10
1.6 RAZISKOVALNE HIPOTEZE	12
<b>2 ZNANSTVENA DELA</b>	<b>13</b>
2.1 OBJAVLJENA ZNANSTVENA DELA	13
2.1.1 Učinkovitost uničenja liposomov s hidrodinamsko kavitacijo v primerjavi z ostalimi kemijskimi, fizikalnimi in mehanskimi postopki	13
2.1.2 Študija morfologije gigantskih veziklov v neravnovesnih okoljih z Monte Carlo metodo	47

<b>2.1.3</b>	<b>Materialne lastnosti celične stene bakterije <i>E. coli</i> določajo odpornost celic na sonolizo</b>	<b>62</b>
2.2	OSTALO POVEZOVALNO ZNANSTVENO DELO	77
<b>2.2.1</b>	<b>Vpliv posameznega kavitacijskega mehurčka na bakterijsko celico</b>	<b>77</b>
2.2.1.1	Uvod	77
2.2.1.2	Materiali in metode	79
2.2.1.3	Rezultati	92
<b>3</b>	<b>RAZPRAVA IN SKLEPI</b>	<b>102</b>
3.1	RAZPRAVA	102
<b>3.1.1</b>	<b>Lipidni dvosloj</b>	<b>102</b>
<b>3.1.2</b>	<b>Bakterija <i>E. coli</i> in celice z oslabljenimi komponentami celične stene</b>	<b>106</b>
<b>3.1.3</b>	<b>Vpliv individualnega kavitacijskega mehurčka na individualno bakterijsko celico</b>	<b>109</b>
<b>3.1.4</b>	<b>Pregled doprinosha kandidata in ostalih sodelavcev v okviru doktorske disertacije</b>	<b>113</b>
3.2	SKLEPI	113
<b>3.2.1</b>	<b>Potrditev hipotez</b>	<b>114</b>
<b>4</b>	<b>POVZETEK (SUMMARY)</b>	<b>115</b>
4.1	POVZETEK	115
4.2	SUMMARY	117
<b>5</b>	<b>VIRI</b>	<b>120</b>
<b>ZAHVALA</b>		
<b>PRILOGE</b>		

## KAZALO ZNANSTVENIH DEL

- Pandur Ž., Dogsa I., Dular M., Stopar D. 2020. Liposome destruction by hydrodynamic cavitation in comparison to chemical, physical and mechanical treatments. Ultrasonics Sonochemistry, 61: 104826, doi: 10.1016/j.ulsonch.2019.104826: 11 str. .... 13
- Drab M., Pandur Ž., Penič S., Iglič A., Kralj-Iglič V., Stopar D. 2021. A Monte Carlo study of giant vesicle morphologies in nonequilibrium environments. Biophysical Journal, 120, 20: 4418-4428..... 47
- Pandur Ž., Dular M., Kostanjšek R., Stopar D. 2022. Bacterial cell wall material properties determine *E. coli* resistance to sonolysis. Ultrasonics Sonochemistry, 83: 105919, doi: 10.1016/j.ulsonch.2022.105919: 10 str. .... 62

## KAZALO PREGLEDNIC

Preglednica 1: Upoštevani materialni parametri obeh tekočin ..... 89

## KAZALO SLIK

Slika 1: Različni tipi nastanka akustične in hidrodinamske kavitacije (povzeto po Filipić in sod., 2022; Mo in sod., 2012; Šarc in sod., 2018; Kolbl Repinc in sod., 2022; Podbevšek in sod., 2021).....	4
Slika 2: Shematski prikaz Gram negativne bakterijske celične stene ( <i>E. coli</i> ). .....	11
Slika 3: Shematski prikaz eksperimentalne postavitve.. .....	80
Slika 4: Shematski prikaz interakcije mikromehurčka in bakterijske celice iz različnih perspektiv.....	84
Slika 5: Učinek hidrodinamske in akustične kavitacije na <i>E. coli</i> .....	77
Slika 6: Potek visokonapetostne razelektritve v tekočini in vpliv zarodnega mikromehurčka ali tlačnih valov na opazovane bakterijske celice. .....	94
Slika 7: Kavitacijski mehurček in njegov vpliv na bakterijske celice. ....	95
Slika 8: Računski model kavitacije mikromehurčka in določanje strižne napetosti ter hidrodinamske sile ob kavitaciji mikromehurčka.....	99
Slika 9: Mehanske obremenitve bakterijske celice pri kolapsu mikromehurčka .....	101

## KAZALO PRILOG

**Priloga A:** Objavljen pregledni članek vpliva hidrodinamske kavitacije na mikroorganizme.

**Priloga B:** Objavljen pregledni članek vpliva mehanskih lastnosti posameznih slojev bakterijske celične stene.

**Priloga C:** Dovoljenje založnika Elsevier za vključitev objavljenega raziskovalnega dela v doktorsko disertacijo z naslovom: A Monte Carlo study of giant vesicle morphologies in nonequilibrium environments (Biophysical Journal).

**Priloga D:** Dovoljenje založnika Elsevier za vključitev objavljenega raziskovalnega dela v doktorsko disertacijo z naslovom: Evolution of mechanical stability from lipid layers to complex bacterial envelope structures (Academic Press).

## OKRAJŠAVE IN SIMBOLI

CFU	kolonijsko število (ang. <i>colony forming units</i> )
DMPC	1,2-dimiristoil-sn-glicero-3-fosfoholin
DOPC	1,2-dioleoil-sn-glicerol-3-fosfoholin
DOPG	1,2-dioleoil-sn-glicerol-3-fosfat
DNK	deoksiribonukleinska kislina
EDTA	etilendiamintetraocetna kislina (ang. <i>ethylenediaminetetraacetic acid</i> )
EPS	ekstracelularni polisaharidi (ang. <i>extracellular polymeric substance</i> )
Fps	slike na sekundo (ang. <i>frames per second</i> )
Gfp	zeleni fluorescentni protein (ang. <i>green fluorescent protein</i> )
IPTG	izopropil- $\beta$ -D-1-tiogalaktopyranozid (ang. <i>Isopropyl-<math>\beta</math>-D-1-thiogalactopyranoside</i> )
Kn	kanamicin
LB	lizogeno gojišče (ang. <i>lysogeny broth</i> )
LPS	lipopolisaharid
OD650	optična gostota pri 650 nm (ang. <i>optical density at 650 nm</i> )
PGA	poli- $\beta$ -1,6-N-acetyl-D-glukozamin (ang. <i>poly-<math>\beta</math>-1,6-N-acetyl-D-glucosamine</i> )
PI	propidijev jodid (ang. <i>propidium iodide</i> )
PLL	poli-L-lizin
ROS	reakтивne kisikove zvrsti (ang. <i>reactive oxygen species</i> )
rpm	obrati na minuto (ang. <i>revolutions per minute</i> )

## 1 UVOD

Voda je ena izmed najpomembnejših molekul za obstoj življenja na Zemlji (Maher in Stevenson, 1988). Poleg tega igra voda zelo pomembno vlogo pri svetovni ekonomiji kot dobrina, ki omogoča obstoj in razvoj družbe. Okoljski vodni viri predstavljajo primerno okolje za obstoj in medij za prenos potencialno patogenih mikroorganizmov za človeka, živali in rastline (Gibson, 2014). Odpadne vode lahko vsebujejo patogene mikroorganizme, kot so bakterije (na primer iz rodov *Vibrio*, *Enterobacter*, *Escherichia*, *Klebsiella*, *Pseudomonas*) (Spiteri in sod., 2017) in enterične viruse (npr. norovirusi in kalicivirusi) (Chrysikopoulos in sod., 2013), ki lahko povzročijo resne okužbe ob stiku ali z zaužitjem onesnažene vode. Porajajoči se patogeni mikroorganizmi, virusi in druge nevarne snovi, kot so toksini v vodnih sistemih, postajajo vse večji problem (Chrysikopoulos in sod., 2013; Joyce in sod., 2010; Spiteri in sod., 2017). Razpoložljivost neoporečne pitne vode je vse večja skrb v globaliziranem svetu, tako v razvitih državah kot v državah v razvoju. Zaradi vse večjega onesnaževanja postajajo svetovne zaloge čiste vode resno ogrožene in za številne države je čista ter neoporečna voda postala luksuzna dobrina, ki ni več samoumevna. Zato postaja recikliranje odpadne vode in zagotavljanje neoporečnih virov pitne vode vse bolj pomembna panoga. Da bi zagotovili varno uporabo pitne vode, je dezinfekcija nujen korak v shemi čiščenja vode. Trenutne uporabljene metode za čiščenje odpadnih voda temeljijo na kemijskih ali fizikalnih postopkih. Dezinfekcija vode vključuje postopke, kot so kloriranje, ozoniranje in UV obsevanje. Te metode so do določene mere učinkovite, vendar imajo tudi pomanjkljivosti. UV-obsevanje povzroči reverzibilno poškodbo bakterijske DNK (Drakopoulou in sod., 2009) in ni zelo učinkovito, če so mikroorganizmi združeni v skupke - flokule (Ohrdes in sod., 2018). Ozonacija je učinkovit, a finančno drag proces, kjer lahko nastanejo strupeni in škodljivi stranski produkti (Gao in sod., 2016; Gogoi in sod., 2018; Schlütter-Vorberg in sod., 2015). Kemične metode dezinfekcije, kot je kloriranje, lahko povzročijo nastanek škodljivih stranskih produktov (Zou in Wang, 2017) in lahko povzročijo sekundarno onesnaženje (Rajasekhar in sod., 2012). Termični šok je najpogosteje uporabljeni metoda, ki pa je energetsko zelo potratna. Zato se je v zadnjem desetletju povečalo raziskovanje alternativnih metod in postopkov čiščenja odpadne vode, ki bi lahko izboljšale in zamenjale obstoječe postopke obdelave vode. Ena izmed obetavnih novih metod je hidrodinamska kavitacija, ki je v primerjavi s termičnimi šoki do 30-krat bolj energijsko učinkovita pri čiščenju vode (Šarc in sod., 2014).

### 1.1 KAVITACIJA

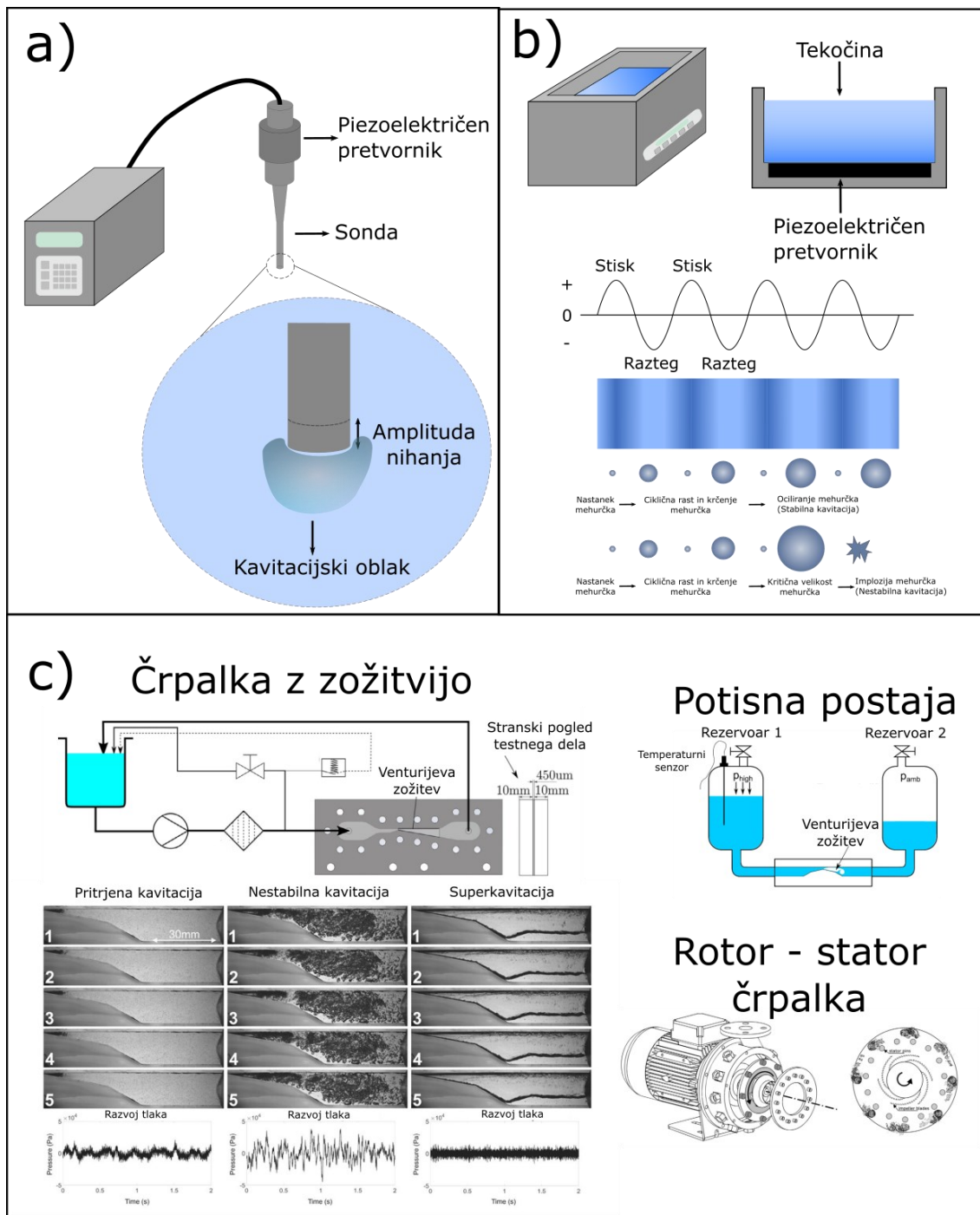
Kavitacija je pojav parnih mehurčkov v tekočini. Je hiter pojav, ki nastane zaradi lokalnega znižanja tlaka v tekočini, kar privede do nastanka majhnih mehurčkov (Franc in Michel, 2004). Po dvigu tlaka v tekočini na začetno stanje, se parni mehurček

agresivno sesede (implodira) (Young, 1989). Pri kavitaciji lahko pride do pojava lokalnih ekstremnih razmer, kot je visoka temperatura (več kot 1000 K), nastanka mikrocurkov s hitrostmi preko 100 m/s, nastanka tlačnih valov (več kot 100 MPa) in nastanka reaktivnih radikalnih zvrsti (Brennen, 1995; Chahine in Hsiao, 2015; Koda in sod., 2003; Suslick in sod., 2011). Glede na način nastanka kavitacijskih mehurčkov lahko kavitacijo razdelimo na: akustično kavitacijo, hidrodinamsko kavitacijo, optično kavitacijo ter kavitacijo delcev. Najpogostejsa tipa kavitacije sta akustična in hidrodinamska kavitacija. Razlika med omenjenima tipoma je kako pridemo do znižanja tlaka v tekočini: pri akustični kavitaciji (sonikacija) nastajajo zgoščenine in razredčine kapljevine zaradi prenašanja zvočnih valov skozi kapljevinu, medtem ko pri hidrodinamski kavitaciji pride do lokalnega znižanja tlaka zaradi pospešitve toka tekočine (Širok in sod., 2006). Pri optični kavitaciji pride do optičnega preboja v vodi s kratkim, fokusiranim in visoko energijskim laserskim žarkom, kjer nastane plazma, uparjanje tekočine in posledično kavitacijski mehurček. Pri kavitaciji delcev pride do absorpcije energije elementarnih delcev, npr. absorpcija protonskega žarka v živem srebru kar povzroči nastanek kavitacijskega mehurčka (Young, 1989).

Akustično valovanje vzbujamo s piezoelektričnim pretvornikom, ki pretvori visoko frekvenčno električno energijo v mehansko vibracijo, kar povzroči nastanek zgoščenin in redčin v kapljevini. Tako generirani akustični valovi imajo lahko frekvenco nihanja v razponu od kHz do MHz. Najbolj pogosta tipa ultrazvočnih naprav za generiranje akustične kavitacije sta ultrazvočna sonda in ultrazvočna kad (Slika 1). Pri ultrazvočni sondi je vir akustičnih valov radialna sonda, ki ima v večini primerov premer konice do nekaj centimetrov. Pri sondi se kavitacijski oblak ustvari pod konico sonde, kjer konica niha z določeno frekvenco in amplitudo. Akustična energija se prenaša preko majhne površine konice sonde, zato sonde proizvajajo visoko intenziteto kavitacije. Zaradi fokusirane kavitacije v bližini sonde je potrebno pri večjih volumnih pri tem tipu naprave zagotoviti učinkovito mešanje po celotnem volumnu tekočine. Drugi najpogostejsi tip je ultrazvočna kad kjer so piezoelektrični pretvorniki postavljeni na dno kadi. Akustični valovi se prenašajo po celotnem volumnu tekočine, ki je v kadi. Zaradi večje površine piezoelektričnega pretvornika je takšen tip kavitacije nizko intenziven. V večini primerov prihaja do oscilacije mehurčkov zaradi akustičnega valovanja in ne do agresivnih kolapsov mehurčkov. Oscilirajoči mehurčki lahko ob površinah ustvarijo visok strig. Takšen tip kavitacije imenujemo stabilna kavitacija, medtem ko agresivno implozijo mehurčka imenujemo nestabilna kavitacija. Pri soniciranju se lahko uporablja kontinuirni način delovanja ali pa uporaba delovnih ciklov, kjer je soniciranje v krajsih časovnih intervalih prekinjeno. S tem zmanjšamo vpliv segrevanja vzorca med samim soniciranjem. Pri uporabi akustične kavitacije se največkrat uporablja šaržni način tretiranja, kjer istočasno obdelujemo celoten volumen. Zato je akustična kavitacija primerna za obdelavo relativno majhnega volumna tekočine – na primer v mililitrskem volumskem območju. Zaradi tega je nadgradnja sistema, ki

bi lahko bila primerna za velike volumne v industrijskih merilih otežena. Naprave za akustično kavitacijo se pojavljajo skoraj v vsakem raziskovalnem laboratoriju za namene čiščenja površin, mešanja tekočin, priprave emulzij, razplinjenja tekočin, procesiranja živil, uporabe v medicinske namene, obdelave mineralov, uničenja celic in ekstrakcije celičnih komponent ter produkcije majhnih unilamelarnih veziklov (Annegowda in sod., 2012; Canselier in sod., 2002; Eskin in sod., 2015; Peshkovsky in sod., 2013; Saranya in sod., 2014; Zupanc in sod., 2019).

Hidrodinamska kavitacija nastane zaradi sprememb v geometriji toka, običajno ob prehodu tekočine skozi zožitev ali zaradi ovire v toku. S tem se toku poveča hitrost in posledično zmanjša tlak. Ob zadostnem padcu tlaka se pojavi kavitacija. Dinamika hidrodinamske kavitacije je odvisna od karakteristike toka tekočine in geometrije obtekanega objekta oziroma zožitve (Širok in sod., 2006). Ob nastanku mehurčka je večina energije shranjena v okoliški tekočini katera se sprosti ob povratku tlaka v začetno stanje. Na intenzivnost kolapsa vpliva tlačni gradient, ki vpliva na dinamiko poteka dogodka. Hidrodinamsko kavitacijo lahko razdelimo na tri tipe: 1. pritrjena kavitacija, 2. nestabilna (ang. »cloud shedding«) kavitacija in 3. superkavitacija. Pri pritrjeni kavitaciji so mehurčki skupaj in so pritrjeni na vodilno stran zožitve, kar lahko vidimo kot stabilen pritrjen kavitacijski oblak. V primeru, da se tok tekočine poveča oziroma se tlak pred zožitvijo poviša, postane kavitacijski oblak nestabilen in se prične deloma ali v celoti trgati (nestabilna kavitacija). Če se pretok ali tlak še dodatno povečata, se pričnejo posamezni mehurčki združevati v stabilen velik parni oblak. Tak pojav imenujemo superkavitacija. Najbolj pogosti tipi hidrodinamsko kavitacijskih naprav so: potisne postaje z zožitvami (ang. »blow through«), črpalke z zožitvami ter naprave z rotor-statorjem (prilagojene lopatice na črpalki) (Zupanc in sod., 2019). Največkrat uporabljen sistem je kombinacija črpalke in zožitve, kjer pa lahko pride do pojava kavitacije tudi v sami črpalki. Zato sistemi s črpalko niso najbolj primerni za karakterizacijo vpliva kavitacije na biološke delce. Pri napravah kjer uporabljamo stisnjeni zrak za potisk tekočine skozi zožitev (potisne naprave) se izognemo omenjenemu problemu vendar zahteva večje obdelovane volumne. Pri sistemih z zožitvami je največkrat uporabljen Venturijeva zožitev ali majhna okrogla zaslonka (ang. »orifice«). Pri rotor-stator tipu je geometrija izboklin razporejena po obodni površini rotorja ali v kombinaciji na rotorju in statorju, kjer je postavitev lahko simetrična ali asimetrična (Kolbl Repinc in sod., 2022). Shematski prikaz obeh tipov kavitacij skupaj z napravami je prikazano v sliki 1. Prednost hidrodinamske kavitacije je enostavno večanje velikostne skale naprave na industrijski nivo, medtem ko zmanjšanje delovnega volumna naprav na laboratorijski nivo (delovni volumen naprave v mililitrskem rangu) predstavlja precejšen izzik (Zupanc in sod., 2019).



Slika 1: Različni tipi nastanka akustične in hidrodinamske kavitacije.

Akustična kavitacija (a in b) ter hidrodinamska kavitacija (c). Ultrazvočna sonda (a) pretvarja električno energijo v mehanske vibracije na konci sonde, kjer se pojavi kavitacijski oblak. Pri ultrazvočni banjici (b) so piezoelektrični pretvorniki postavljeni na dno banjice in ultrazvočni valovi potujejo po celotnem volumnu kapljivine. Pri tem primeru velikokrat pride do stabilne kavitacije kjer mehurčki samo oscilirajo zaradi ultrazvočnega valovanja. Pri hidrodinamski kavitaciji (c) so največkrat uporabljene črpalke in zožitve (levo zgoraj), za potisk tekocene se lahko uporablja tudi stisneni zrak (blow through), lahko pa se prilagodi obliko lopatice črpalke (rotor-stator črpalka). Pri hidrodinamski kavitaciji lahko opazimo tri type kavitacije (levo spodaj): pritrjena, nestabilna kavitacija in superkavitacija. (slike povzete po Filipić in sod., 2022; Mo in sod., 2012; Šarc in sod., 2018; Kolbl Repinc in sod., 2022; Podbevsek in sod., 2021).

## 1.2 KOLAPS POSAMEZNEGA MEHURČKA

Kolaps posameznega mehurčka na milimetrski velikostni skali je dobro opisan pojav. Za nastanek posameznega milimetrskega kavitacijskega mehurčka se velikokrat uporablja optično kavitacijo, kjer z laserjem vnesemo v kapljevino v zelo kratkem času veliko količino energije (nanosekundni laserski pulz), pri čemer pride do nastanka nestabilnega parnega mehurčka, kar posledično privede do kavitacijskega kolapsa mehurčka. Z lasersko generiranim mehurčkom je možno generirati kavitacijske mehurčke z maksimalnim radijem od nekaj deset  $\mu\text{m}$  in vse do milimetrskega velikostnega ranga. Sama dinamika mehurčka je odvisna od okolice kjer se mehurček nahaja - v primeru kjer je v okolini mehurčka kapljevina pride do sferičnega kolapsa mehurčka. Kolaps kavitacijskega mehurčka v bližini trdne površine privede do nastanka curka ob imploziji mehurčka. V primeru trdne površine nastane osno simetričen curek, ki je usmerjen proti trdni površini. Oblika kolapsa mehurčka je pogojena z razmerjem oddaljenosti centra mehurčka od stene ( $d_b$ ) in maksimalnega radija mehurčka  $R_{r,\max}$ ) ( $\gamma = \frac{d_b}{R_{r,\max}}$ ), kjer je kritično razmerje za nastanek curka ob trdi steni  $\gamma = 2$  (Dular in sod., 2019). Na splošno je dinamika kolapsa mehurčka odvisna od različnih faktorjev kot so geometrija mejne plasti, materialne in strukturne lastnosti mejne plasti, prisotnosti striga, tlačnih valov, gravitacijskega polja ali prisotnosti in vpliva drugih mehurčkov (Reuter in Ohl, 2021).

Mikrometrski kavitacijski mehurčki so posebej pomembni za delovanje na bakterijske celice, saj so istega velikostnega reda kot bakterijske celice. Delovanje mikrometrskih kavitacijskih mehurčkov na bakterijske celice je slabo proučeno in je predmet raziskovanja v tej doktorski disertaciji. Interakcija posameznega mehurčka z mikrometrsko velikim delcem se lahko dogaja na treh velikostnih skalah: ko je mehurček znatno večji od delca (mm velikost), mehurček primerljiv velikosti delca ( $\mu\text{m}$  velikost) in mehurček manjši od delca (nm velikost). Pri znatno večjem mehurčku od delca sam delec naj ne bi direktno vplival na potek kolapsa mehurčka, kar nakazujejo raziskave kolapsa milimetrskega mehurčka s sedimentom (Teran in sod., 2018). Po drugi strani se pri manjših (nanometrskih) mehurčkih pričakuje, da niso relevantni za tak primer saj so izredno stabilni pri tlačnih oscilacijah (Franc in Michel, 2004). Interakcije posameznega mehurčka na milimetrski velikostni skali je opisal Borkent in sod. (2008), kjer so pokazali, da kolaps mehurčka v bližini nepritrjenega delca le tega potisne stran od mehurčka. Pri milimetrskem kolapsu mehurčka površinska napetost in viskoznost ne vplivata znatno na dinamiko kolapsa. Raziskav mikrometrskih mehurčkov do nedavnega ni bilo. Preliminarne raziskave na manjših mehurčkih (v mikrometrskem velikostnem rangu) pa kažejo, da površinska napetost in viskoznost lahko vplivajo na dinamiko kolapsa mehurčka, kar bi lahko vplivalo na izid poteka kavitacije mikrometrskega mehurčka (mikromehurčka) (Zevnik in Dular, 2022).

### 1.3 BAKTERIJSKA CELICA

Notranjost bakterijske celice predstavlja visoko regulirano okolje za razliko od okolice kjer so prisotna znatna nihanja. Za preživetje celic v takšnem nepredvidljivem okolju so bakterijske celice razvile vrsto različnih plasti v celični steni, katere jim skupaj omogočijo preživetje stresnih razmer (npr. mehanski stres, povišana temperatura, kislo okolje, odpornost na izsuševanje). Posamezna struktura v celični steni ima specifično funkcionalnost, ki pripomore k končni odpornosti celice na različne okoljske dejavnike (Madigan in sod., 2008). Ena izmed pogostih definicij celične smrti je porušitev integritete celične stene, kar povzroči izpust celične vsebine v okolico – pride do t.i. lize celic (Gregori in sod., 2001). Zato veliko metod bakterijske inaktivacije (npr. mehanske metode, določeni antibiotiki) temeljijo na porušitvi integritete celične stene kar privede do ireverzibilne lize celic. Po sestavi celične stene lahko ločimo bakterije v dve skupini: Gram negativne in Gram pozitivne. Barvanje po Gramu je klasificiranje bakterij na podlagi diferencialnega barvanja glede na različno sestavo celične skupine. Gram negativne celice imajo citoplazemske membrano, ki je povezana preko tankega peptidoglikanskoga sloja z asimetrično zunanjim lipopolisaharidno membrano. Lipopolisaharidna membrana ima na notranji strani fosfolipidni sloj, medtem ko so na zunanjem sloju lipopolisaharidne molekule. Gram pozitivne bakterije imajo citoplazemske membrano in debel peptidoglikanski sloj, ki služi kot mehanska in kemijska opora citoplazemski membrani (Madigan in sod., 2008). Poleg osnovnih plasti celične stene imajo lahko bakterijske celice še dodatne plasti kot so S-sloji, kapsularni sloj, eksopolisaharidni sloj (EPS), in plašč (Beveridge, 1981; Beveridge in Graham, 1991; Madigan in sod., 2008; Sleytr in Messner, 2009).

*Escherichia coli*, ki smo jo uporabljali v tej doktorski disertaciji je Gram negativna paličasta bakterija, ki je del mikrobiote prebavnega trakta živali in človeka. Nekateri sevi so patogeni za človeka (Madigan in sod., 2008). *E. coli* je modelni predstavnik Gram negativnih bakterij in je dobro preučen organizem. Zaradi hitre rasti, enostavnosti rokovanja se bakterija uporablja pri genskem inženiringu, produkciji farmacevtskih učinkovin ter drugih biotehnoloških panogah (Blount, 2015). Bakterija lahko raste v pH območju med 4,5 in 9, med 8 in 45 °C ter tlakom 1 - 400 atm (Ivančič in sod., 2013; Kumar in Libchaber, 2013; Wilks in Slonczewski, 2007).

V nadaljevanju so predstavljene štiri ključne plasti Gram negativne bakterijske celične stene in njihove fizikalno-kemijske lastnosti, ki so lahko potencialna tarčna mesta za delovanje kavitacijskih mehurčkov.

### 1.3.1 Citoplazemska membrana

Citoplazemska membrana je sestavljena iz lipidnega dvosloja. Lipidni dvosloji so izgrajeni iz amfifilnih molekul v vodnem okolju, kjer so polarne glave orientirane v vodno okolje, medtem ko so nepolarni repi maščobnih kislin orientirani v notranjosti strukture (Bangham in Horne, 1964). Glavna naloga lipidnega dvosloja v bioloških sistemih je selektivno ločevanje notranjosti celice od okolice. S tem lahko celica ohrani svojo entiteto, omogočen je selektivni transport hranil v celico ter odvečnih presnovkov iz celice (Tien in Ottova, 2003). Molekule so v lipidnem dvosloju šibko nekovalentno povezane med seboj. Struktura lipidnega dvosloja je poznana kot tekoči kristal, kjer ves čas prihaja do reorganizacije molekul kot so rotacijske in konformacijske spremembe, lateralna difuzija in spremembe oblike dvosloja (Nickels in sod., 2015; Pucadyil in sod., 2007; Singer in Nicholson, 1972). Bakterija *E. coli* ima več kot sto različnih posfolipidnih molekul v svoji membrani (Jeucken in sod., 2019). Različne posfolipidne molekule pripomorejo k asimetriji slojev kar pripomore k stabilnosti citoplazemske membrane v primerjavi s simetričnim dvoslojem (Lu in sod., 2016).

Najenostavnejši model citoplazemske membrane so posolipidni vezikli, sferične strukture, obdane s posolipidnim dvoslojem, ki razmejuje notranjost vezikla od tekočine v okolici (Locascio in sod., 2004). V povprečju je debelina lipidnega dvosloja 4 nm (Pandit in Klauda, 2012). Lipidni vezikli so široko uporabni v raziskovalne in industrijske namene. Na primer v medicini se uporablajo za tarčno dostavljanje zdravilnih učinkov in kot kontrastni agens pri ultrazvoku (Shashi in sod., 2012). Priprava lipidnih veziklov lahko poteka na različne načine kar omogoča pripravo veziklov v nanometrskem ali mikrometrskem velikostnem rangu. Vezikli v mikrometrskem velikostnem rangu predstavljajo dober modelni nadomestek bakterijski celici. Zaradi samo-orientiranja lipidnih molekul v polarnem topilu je dvosloj fluidna dinamična struktura kjer prihaja do neprestane reorganizacije lipidov v dvosloju kjer se lahko lipidi premeščajo znotraj posameznega sloja ali pa pride do premeščanja med zunanjim in notranjim slojem v dvosloju (Almeida in Vaz, 1995; Heerklotz in Epand, 2001). Privlak med molekulami v dvosloju je posledica elektrostatskih interakcij med polarnimi glavami in van der Waals povezavami med sosednjimi nepolarnimi repi, zato je lipidni dvosloj krhka in izredno podajna struktura (Auer in Weibel, 2017) in posledično občutljiv na različne spremembe v osmolarnosti, dodatku amfifilnih molekul, pH, temperature, ionske jakosti, itd. (Böckmann in sod., 2003; Böckmann in Grubmüller, 2004; Claessens in sod., 2004; Goertz in sod., 2011; Kato in sod., 2015; Kodama in sod., 2018; Koerner in sod., 2011; Sułkowski in sod., 2005). Vstavljanje amfifilnih molekul v dvosloj povzroči znatne oscilacije in motnje v dvosloju, ki lahko privede do razpada dvosloja. Mehanističen vpogled v dinamiko oscilacij dvosloja omogoča lažje razumevanje vloge in stabilnosti lipidnega dvosloja pri izpostavitvi letega zunanjim stresorjem. Zaradi fluidne narave lipidnega dvosloja pričakujemo, ob

zadostnem vložku energije, nastanek por v membrani ali uvihanja membrane, kar lahko povzroči ireverzibilne poškodbe v dvosloju in vezikel lahko posledično razpade (Bavi in sod., 2014).

### 1.3.2 Peptidoglikan

Pri bakterijah večinsko ne najdemo samo lipidnega dvosloja, ampak je zaradi turgorskega tlaka potrebna dodatna struktura, ki izboljša mehansko trdnost in pripomore k obliki bakterije – peptidoglikan (Jauffred in sod. 2007). Peptidoglikan je polimerna struktura, sestavljena iz N-acetilglukozamina in N-acetilmuraminske kisline, ki sta med seboj povezana z  $\beta$ -1,4 glikozidno vezjo v glikanske verige, ki se medsebojno povezujejo preko peptidnih enot (Vollmer, 2007). Delež navzkrižnih povezav v peptidoglikanu lahko variira od 20 % pri *E. coli* pa preko 90 % na primer pri *Staphylococcus aureus* (Rogers in sod., 1980). Skozi evolucijo so se bakterije ločile na dve skupini glede debeline celične stene, ki jih lahko ločimo z barvanjem po Gramu (Hiremath in Banigidad, 2011). Pri po Gramu negativnih bakterijah je peptidoglikanski sloj tanek, vsebuje 1-3 plasti in je debeline 1,5-15 nm (Vollmer in sod., 2008; Yao in sod., 1999), npr. pri *E. coli* v debelini med 2,5 in 6,4 nm (Gumbart in sod. 2014). Pri po Gramu pozitivnih bakterijah pa je prisoten večplastni peptidoglikanski sloj, ki lahko meri v debelino 30-100 nm (Silhavy in sod., 2010). Zaradi večje debeline peptidoglikanskoga ovoja lahko Gram pozitivne bakterije prenesejo višji turgorski tlak (Gumbart in sod. 2014; Vollmer, 2008). Za voljo mehanske vloge je peptidoglikan velikokrat tarčno mesto encimov in antibiotikov za lizo bakterijskih celic (Uehara in Bernhardt, 2011; Sarhar in sod., 2017). Peptidoglikan je viskoelastičen material, ki omogoča reverzibilno raztezanje pod vplivom turgorskega tlaka, kar daje celici obliko. V normalnem stanju celice je peptidoglikan natezno obremenjen zaradi turgorskega tlaka. Npr. pri *E. coli* se v primeru razgradnje citoplazemske membrane površina bakterije zmanjša za 45 % zaradi relaksacije peptidoglikana. V primeru sferičnih celic je turgorski tlak izotropen, medtem ko je pri paličastih celicah različen v vzdolžni in prečni osi bakterijske celice (Koch in sod., 1987). Peptidoglikan je bolj podajan v vzdolžni (daljši) osi (elastičen modul  $2,5 \times 10^7 \text{ Nm}^{-2}$ ) kakor v prečni smeri celice (elastičen modul  $4,5 \times 10^7 \text{ Nm}^{-2}$ ) (Yao in sod., 1999). Skladno s tem se pri osmotskem šoku dolžina celice *E. coli* znatno spremeni, medtem ko se premer celice ne spremeni bistveno (van den Bogaart in sod., 2007).

### 1.3.3 Zunanja membrana

Zunanja membrana je prisotna pri po Gramu negativnih bakterijah. Funkcija zunanje membrane je dodatna transportna bariera za molekule. Gre za izrazito nesimetrično membrano, kjer je notranja plast membrane sestavljena iz fosfolipidov, medtem ko je zunanja plast sestavljena iz lipopolisaharidov (LPS). LPS molekule so sestavljene iz

treh delov: Lipid A, negativno nabitega polisaharidnega jedra in O-antigena. Za viabilnost celice sta potrebna intakten lipid A in polisaharidno jedro (Erridge in sod., 2002). Zunanja membrana je povezana s peptidoglikanskim slojem preko Braunovega lipoporoteina (LPP) in Pal lipoporoteina (Braun in Rehn, 1969; Braun in Sieglin, 1970; Godlewska in sod. 2009). Negativni naboje LPS je nevtraliziran s  $\text{Ca}^{2+}$  ali  $\text{Mg}^{2+}$ , ki preko divalentnih mostičkov stabilizirajo zunanjo membrano (Auer in Weibel, 2017). Uporaba kelatorja (npr. EDTA) lahko privede do delne odstranitve (približno 40-50 %) LPS molekul iz membrane, kar destabilizira zunanjo membrano in s tem zelo oslabi kemijsko in mehansko strukturo bakterije (Amro in sod., 2000).

### 1.3.4 Kapsula

Dodatna struktura, ki lahko okrepi bakterijsko steno je kapsula (Araújo in sod., 2019). Debelina kapsule lahko meri v debelino do nekaj  $\mu\text{m}$  in služi za lažjo vezavo na površino ali medsebojno povezavo med celicami. Obenem služi kot dodatna fizična pregrada za prehod snovi do celice – na primer otežen dostop antibiotikov do celic (Bayer in Thurow, 1977; Costerton in sod., 1981; Roberts, 1996). Kapsula je sestavljena iz verige polisaharidov z visoko molekulsko maso, ki so kovalentno in nekovalentno povezani z zunanjim membranom (Beveridge in Graham, 1991). Pri celicah *E. coli* so štiri glavne kapsularne komponente: poli- $\beta$ -1,6-N-acetyl-D-glukozamin (PGA), kodrasti proteini, kolanska kislina in bakterijska celuloza ali celulozni derivati (Wang in sod. 2004; Itoh in sod., 2005; Itoh in sod., 2008; Smith in sod., 2017; Danese in sod., 2000; Thongsomboon in sod. 2018). Horvat in sod. (2019) so okarakterizirali vpliv kapsularnih komponent na mehanske lastnosti biofilma *E. coli* in pokazali na spremenjene mehanske lastnosti mutant, ki imajo okvarjene gene za produkcijo zunajceličnih komponent.

## 1.4 VPLIV KAVITACIJE NA MIKROORGANIZME

Do nedavnega je bila kavitacija poznana zgolj kot negativen pojav, ki zmanjšuje življenjsko dobo vodnih turbin zaradi erozije materiala, povzroča hrup ter zmanjšanje učinkovitosti naprav (Franc in Michel, 2004). Zaradi ekstremnih lokalnih razmer v okolini kolapsa kavitacijskega mehurčka in destruktivnega učinka na npr. trden material, bi lahko imeli kavitacijski mehurčki vpliv tudi na biološke delce, na primer mikroorganizme. Pretekle raziskave kažejo na obetavne rezultate inaktivacije različnih mikroorganizmov, na primer Azuma in sod. (2007) so dosegli popolno uničenje bakterije *Escherichia coli* s kavitacijskim curkom, primerljiv rezultat so dobili tudi Cerecedo in sod. (2018) pri uporabi kavitacijske črpalke. Hunter in sod. (2008) so z akustično kavitacijo dosegli 99 % inaktivacijo bakterije *E. coli*. Vseeno se rezultati raziskav lahko znatno razlikujejo glede na izbrani mikroorganizem, testirane pogoje, tip kavitacije in uporabljene naprave. Kljub splošni uporabi kavitacije v mikrobiologiji se

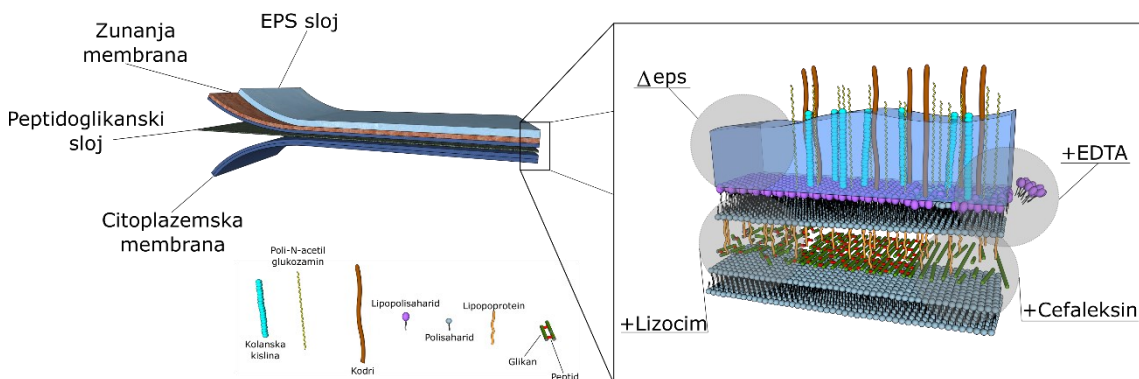
še vedno smatra kavitacija kot »fenomen črne škatle« kjer ni popolnoma jasno kaj se dogaja v procesu kavitacije z mikroorganizmi. Večina raziskovalcev pripisuje inaktivacijo bakterij mehanskemu vzroku – propad celic zaradi mehanskih poškodb celične stene. Nekateri pripisujejo inaktivacijo kemijskim vzrokom, kot so reaktivne kisikove zvrsti (ROS), vendar pa podrobni mehanizem delovanja ni poznan (Zupanc in sod., 2019), kar predstavlja glavno težavo pri širši uporabi kavitacije za uničenje bakterijskih celic. Bakterijske celice so izjemno odporne na različne okoljske dejavnike (Griffiths in Philippot, 2013). Razlog je v tem, da je bakterijska celica multikompozitni material, sestavljen iz večjega števila slojev z različnimi kemijskimi, biokemijskimi in biofizikalnimi lastnostmi. Trenutno ne poznamo kako kavitacija deluje na posamezne plasti bakterijske površine (npr. na lipidni dvosloj, peptidoglikan, zunanjemembrano) in kako ruši njihovo integriteto. Podobno slabo poznamo zaradi katerega fizikalno - kemijskega vpliva (npr. strižna sila, tlačne spremembe, temperatura, prosti radikali) je kavitacija pri bakterijah učinkovita in kako učinkovita je v primerjavi z ostalimi stresnimi dejavniki, ki vplivajo na stabilnost bakterijske celice.

### 1.5 NAMEN IN CILJI DOKTORSKE DISERTACIJE

V doktorski disertaciji smo s selektivnim pristopom preverili kako posamezne strukture oziroma kombinacije plasti bakterijske celične stene vplivajo na stabilnost celic pri kavitaciji. Kot najosnovnejši model celične membrane smo uporabili fosfolipidni vezikel, ki je imel fluorescentno označen lumen kar nam je omogočilo zajem konfokalnih fluorescentnih mikroskopskih slik in njihovo karakterizacijo pred in po tretiranju s kavitacijo in ostalimi fizikalno-kemijskimi stresorji. Natančen mehanizem razpada lipidnega dvosloja pri kavitaciji še ni bil dokazan. Predvidevamo, da pri kolapsu mehurčkov prihaja do tlačnih valov in ostalih mehanskih obremenitev, ki povzročijo nastanek por v dvosloju, kar povzroči puščanje iz notranjega lumna v okolico. Pore so prisotne v času tlačnih valov, vendar takoj, ko se zaključi valovanje se pore zaradi samocelilnih lastnosti fosfolipidnih dvoslojev zacelijo (Lin in Thomas, 2004; Marmottant in sod., 2008; Pong in sod., 2006; Schroeder in sod., 2007). Če pore zrastejo preko kritične velikosti pride do razpada dvosloja (Marmottant in sod., 2008, Small in sod., 2012). Soniciranje se že dolgo uporablja kot metoda pri pripravi majhnih unilamelarnih veziklov (Saunders in sod., 1962; Schroeder in sod., 2009). Vpliv hidrodinamske kavitacije na lipidni dvosloj še ni bil raziskan.

Modelni bakterijski sistem je bila bakterija *Escherichia coli* MG1655 DE3. Bakterija je mutanta divjega tipa *E. coli* K12, ki ima vstavljen gen za zeleni fluorescenčni protein (gfp), ki je pod regulacijo inducibilnega promotorja izopropil β-D-1-tiogalaktopyranozid (IPTG) in kanamicinskim selekcijskim markerjem. Bakteriji *E. coli* smo ošibili površinske strukture celične stene z uporabo reagentov (npr. cefaleksin, EDTA, lizocim). Balasundaram in Harrison (2006) sta predlagala, da kavitacija najprej

poškoduje zunanjo plast celice in nato postoma skozi več ciklov pride do poškodb notranje membrane in celične lize. S spremenjanjem lastnosti zunanje membrane preko EDTA kelatorja smo preverili vpliv zunanje membrane, saj je zunanja membrana v kombinaciji s peptidoglikanom znana kot glavni element za prenašanje turgorskega tlaka (Rojas in sod., 2018). Najbolj znan element, ki daje mehansko odpornost bakteriji je peptidoglikanski sloj. Peptidoglikanski sloj smo spremenili na dva načina – z encimom lizocim, ki hidrolizira glikozidne vezi (Ellison in Giehl, 1991) ali z antibiotikom cefaleksin, ki onemogoči navzkrižno povezovanje peptidnih verig kar povzroči nastanek filamentoznih celic (Sun in sod., 2014). V primeru sočasne uporabe EDTA, lizocima in cefaleksina dobimo gigantske sferoplaste, ki imajo intaktno samo citoplazemske membrano, medtem ko sta peptidoglikan in zunanja membrana večinsko odstranjena. Zaradi izgube peptidoglikanskega sloja takšne celice postanejo sferične oblike (Kikuchi in sod., 2015). Shematski prikaz spremenjanja komponent celične stene je prikazan na Slika 2. Primerjali smo tudi vpliv zunajceličnih komponent z uporabo mutante, ki ima okvarjene gene za sintezo kodrov (ang. curli), kolanske kisline in polisaharida zunanje ovojnici (poli- $\beta$ -1,6-GlcNAc – PGA).



Slika 2: Shematski prikaz Gram negativne bakterijske celične stene (*E. coli*).

Leva slika predstavlja poenostavljeno shemo plasti celične stene, kjer je na notranji strani celice citoplazemska membrana, kateri sledi tanek peptidoglikanski sloj. Na zunanji strani sta zunanja membrana in EPS sloj. Desna slika prikazuje poenostavljeno molekularno shemo omenjenih slojev v celični steni. Prikazana so tudi mesta, kjer je prišlo do sprememb celične stene v doktorski disertaciji – genetska mutanta  $\Delta\text{eps}$  ne izraža treh glavnih komponent EPS sloja (kolanske kisline, kodrov in PGA); dodatek kelatorja EDTA povzroči odstranjevanje LPS molekul in posledično reorganizacijo zunanje membrane; modifikacija peptidoglikanskega sloja je bila opravljena z encimom lizocim ter  $\beta$ -laktamskim antibiotikom cefaleksin.

Za natančnejše razumevanje vpliva kavitacije na biološke celice je potrebno raziskati interakcijo pojava na mikroskopskem nivoju – torej na nivoju posameznega mehurčka in posamezne mikrobne celice. Nekaj raziskav je bilo narejenih z evkariontskimi celicami, kjer so pokazali, da pride do prepuščanja in lize celic, kjer predlagajo kot možen vzrok poškodb nastanek mikrocurkov (Gac in sod., 2007; Li in sod., 2013; Rau in sod., 2006; Zhou in sod., 2012). Interakcija posameznega mehurčka z bakterijskimi

celicami tudi še ni bila opisana. Najbližje so bili Tandiono in sod. (2012) kjer so v mikrofluidnem sistemu akustično vzbudili naključne kavitacijske mehurčke v bližini bakterijske kulture kjer so opazili učinkovito lizo bakterijskih celic *E. coli* pri izpostavljenosti akustični kavitaciji v času 0,4 s. Za raziskovanje vpliva posameznega kavitacijskega mehurčka je ključen razvoj metode za ustvarjanje posameznega mikrometrskoga kavitacijskega mehurčka v bližini bakterijske celice, kar smo razvili v tej doktorski nalogi.

## 1.6 RAZISKOVALNE HIPOTEZE

Raziskovalni hipotezi v doktorski disertaciji sta:

- 1: Gruča hidrodinamsko generiranih kavitacijskih mehurčkov v primerjavi z običajnimi fizikalno-kemijskimi stresorji učinkovito lizira fosfolipidne vezikle, sferoplaste in bakterijske celice.
- 2: Z implozijo posameznega kavitacijskega mehurčka v bližini bakterijske celice pride do porušenja membranske integritete, kar omogoča lizo bakterijske celice.

## 2 ZNANSTVENA DELA

### 2.1 OBJAVLJENA ZNANSTVENA DELA

#### 2.1.1 Učinkovitost uničenja liposomov s hidrodinamsko kavitacijo v primerjavi z ostalimi kemijskimi, fizikalnimi in mehanskimi postopki

Pandur Ž., Dogsa I., Dular M., Stopar D. 2020. Liposome destruction by hydrodynamic cavitation in comparison to chemical, physical and mechanical treatments. Ultrasonics Sonochemistry, 61: 104826, doi: 10.1016/j.ulsonch.2019.104826: 11 str.

Izvleček:

Liposomi so uporabni v številnih raziskovalnih in industrijskih panogah, v medicini in diagnostiki. V članku je prvič prikazan vpliv hidrodinamske kavitacije na stabilnost liposomov v primerjavi z učinkovitostjo drugih kemijskih, fizikalnih in mehanskih postopkov. Hidrodinamsko kavitacijo smo primerjali z vplivom ionske jakosti, osmolarnosti (glukoza,  $\text{Na}^+$ ,  $\text{Ca}^{2+}$  in  $\text{Fe}^{3+}$ ), prostih radikalov, striga (pipetiranje, mešanje na mešalu, rotacijski strig), visokega tlaka, elektroporacija, centrifugiranja, površinsko aktivnih snovi (Triton X-100, etanol), mikrovalov, segrevanja, zamrzovanja – odtajevanja, ter ultrazvoka (ultrazvočna banjica in ultrazvočna sonda). Notranjost veziklov je bila fluorescentno označena s fluorescentnim barvilom (natrijev-fluoresceinat). S konfokalnim fluorescentnim vrstičnim mikroskopom smo izmerili intenziteto fluorescence posameznega liposoma in določili distribucije velikosti, intenzitete in števila liposomov pred in po izbranem tretmaju. Izmed vseh testiranih postopkov so imeli največji vpliv na liposome hidrodinamska kavitacija, mešanje na mešalu s steklenimi kroglicami in ultrazvok. Pokazali smo, da je lahko hidrodinamska kavitacija zelo učinkovita metoda za uničenje liposomov. V tem delu je prikazan obširen eksperimentalen pregled vpliva različnih kemijskih, fizikalnih in mehanskih postopkov, ki predstavlja osnovo za pripravo in nadaljnje rokovanie z liposomi.



To delo je ponujeno pod Creative Commons Priznanje avtorstva-Deljenje pod enakimi pogoji 4.0 Mednarodno licenco.



## Liposome destruction by hydrodynamic cavitation in comparison to chemical, physical and mechanical treatments



Žiga Pandur<sup>a,b</sup>, Iztok Dogsa<sup>a</sup>, Matevž Dular<sup>b</sup>, David Stopar<sup>a,\*</sup>

<sup>a</sup> University of Ljubljana, Biotechnical Faculty, Večna pot 111, Ljubljana 1000, Slovenia

<sup>b</sup> University of Ljubljana, Faculty of Mechanical Engineering, Aškerčeva 6, Ljubljana 1000, Slovenia

### ARTICLE INFO

**Keywords:**  
Hydrodynamic cavitation  
Giant lipid vesicles  
DOPC  
Stability  
Fluorescein release  
Confocal laser microscopy

### ABSTRACT

Liposomes are widely applied in research, diagnostics, medicine and in industry. In this study we show for the first time the effect of hydrodynamic cavitation on liposome stability and compare it to the effect of well described chemical, physical and mechanical treatments. Fluorescein loaded giant 1,2-dioleoyl-sn-glycero-3-phosphocholine (DOPC) lipid vesicles were treated with hydrodynamic cavitation as promising method in inactivation of biological samples. Hydrodynamic treatment was compared to various chemical, physical and mechanical stressors such as ionic strength and osmolarity agents (glucose, Na<sup>+</sup>, Ca<sup>2+</sup>, and Fe<sup>3+</sup>), free radicals, shear stresses (pipetting, vortex mixing, rotational shear stress), high pressure, electroporation, centrifugation, surface active agents (Triton X-100, ethanol), microwave irradiation, heating, freezing-thawing, ultrasound (ultrasonic bath, sonotrode). The fluorescence intensity of individual fluorescein loaded lipid vesicles was measured with confocal laser microscopy. The distribution of lipid vesicle size, vesicle fluorescence intensity, and the number of fluorescein loaded vesicles was determined before and after treatment with different stressors. The different environmental stressors were ranked in order of their relative effect on liposome fluorescein release. Of all tested chemical, physical and mechanical treatments for stability of lipid vesicles, the most detrimental effect on vesicles stability had hydrodynamic cavitation, vortex mixing with glass beads and ultrasound. Here we showed, for the first time that hydrodynamic cavitation was among the most effective physico-chemical treatments in destroying lipid vesicles. This work provides a benchmark for lipid vesicle robustness to a variety of different physico-chemical and mechanical parameters important in lipid vesicle preparation and application.

### 1. Introduction

A liposome or lipid vesicle is a lipid bilayer rolled up into a spherical shell with enclosed liquid within shell, which is separated from the outer (surrounding) liquid solution. Because of this fundamental similarity to the biological cell membrane, lipid vesicles have been used extensively as model systems to study properties and stability of lipid bilayers to different physico-chemical or biochemical parameters [1–5]. Lipid bilayer integrity is one of the main criteria to distinguish between viable and dead cells. If cell membrane is compromised, the essential cellular components leak out which results in cell death [6]. To assess bacteria viability, the membrane impermeable fluorescent dyes are regularly used (i.e. propidium iodide) [7–10]. Normally cell membranes are impermeable to a charged dye propidium iodide. However, if cell membrane is compromised, propidium iodide can enter into the cell

and intercalate with DNA which increases its fluorescence quantum yield [10]. Consequently, dead cells become fluorescent and can be distinguished from live cells with intact membranes, which are impermeable to propidium iodide [9]. In this work we have reversed the logic and packed fluorescence dye fluorescein inside the lipid vesicle and measured its leakage to the surrounding media upon hydrodynamic cavitation and other different physico-chemical treatments.

There are numerous protocols to make lipid vesicles of different size, lamellarity and composition reviewed by Laquini et al. [11]. Liposomes are classified according to vesicular size and lamellar structure as small unilamellar vesicles (20–40 nm), medium (40–80 nm), large (100–1000 nm) or giant (> 1000 nm) vesicles [12]. Oligolamellar vesicles are made from 2 to 10 bilayers, whereas multilamellar vesicles have several bilayers. Intrinsically the stability of lipid vesicles is dependent on curvature elastic free energy. Using model membranes, two

**Abbreviations:** DOPC, 1,2-dioleoyl-sn-glycero-3-phosphocholine; GUV, giant unilamellar vesicles; HC, hydrodynamic cavitation; DIC, differential interference contrast microscopy

\* Corresponding author.

E-mail address: [david.stopar@bf.uni-lj.si](mailto:david.stopar@bf.uni-lj.si) (D. Stopar).

<https://doi.org/10.1016/j.ulsonch.2019.104826>

Received 12 June 2019; Received in revised form 9 August 2019; Accepted 8 October 2019

Available online 19 October 2019

1350-4177/ © 2019 The Authors. Published by Elsevier B.V. This is an open access article under the CC BY license (<http://creativecommons.org/licenses/by/4.0/>).

instabilities could be observed: rupture and buckling. The former can be seen during pore formation and fragmentation, as a result of local perturbations of lipid organization [13], the latter gives rise to membrane bending or folding due to leaflet asymmetry or membrane tension modifications [14,15]. Generally, more curved the lipid vesicle, easier it is to fuse or break. This suggests that large or giant lipid vesicles should be more stable than smaller vesicles. Although the total curvature elastic free energy for a spherical liposome is the same for every size of sphere, its free energy for unit lipid is much higher for smaller vesicles. As the number of lipids in the vesicle decreases with smaller vesicles, the curvature free energy per lipid scales as  $R^2$ . This explains why supported lipid bilayers are made from unstable small vesicles rather than the other way around [16].

In spite of their great inherent stability, lipid vesicles constantly undergo remodelling, fusion, pore formation, and various means of lipid exchange [17–19]. The long-term stability of lipid vesicles can be dramatically affected by lipid acyl chain saturation. For example, saturated lipids are more resistant to oxidation than monounsaturated, which in turn are more stable compared to polyunsaturated lipids [20]. Lipid vesicles may be further destabilized by hydrolytic degradation. The lipid hydrolysis is dependent on several key factors including pH [21,22], temperature [22], buffer species [23,24], ionic strength [25,26], acyl chain length [27,28], headgroup composition [29] or state of the aggregation [30]. A major challenge to lipid vesicle stability is also mechanical stress, i.e. ultrasound [31], oscillating electric field [32,33], static pressure [34] and shock waves [35]. Due to their amphiphatic nature lipid vesicles integrity can be easily compromised by the addition of surface-active molecules. Amphiphilic compounds increase permeability of lipid vesicles by intercalating into lipid bilayer, which at concentrations higher than critical micellar concentrations, leads to disruption and solubilisation of lipid bilayer [36,37].

Although lipid vesicles can be destroyed in many ways, destruction of lipid vesicles with hydrodynamic cavitation (HC) has not been exploited yet. Cavitation occurs when small vapour bubbles are formed in liquid. Bubbles are triggered by sudden local decrease in pressure [38]. During pressure change, the bubble violently collapses and possibly rebounds, therefore extreme conditions near proximity of the bubble are likely to occur. It has been reported that extreme high temperatures (several 1000 K [39]) microjet formation (with fluid velocity up to 100 m/s [40]), pressure waves shocks (up to 100 MPa [41]), and formation of highly reactive radicals [42] may occur during bubble collapse. Due to its properties hydrodynamic cavitation has been used as the promising new treatment for bacterial inactivation [43–47]. The exact mechanism of bacteria inactivation, however, is still unknown [48]. The extreme conditions during collapse of the bubbles could have effect on bacterial cells, including the cell membrane. It is generally assumed that bacteria die because of membrane disruption [44,49,50]. Here, we report about the significant effect of hydrodynamic cavitation on model membrane leakage and stability.

To check the effect of hydrodynamic cavitation we have used giant lipid vesicles which are intrinsically more stable to breakage and better resist pore formation or fusion compared to smaller vesicles. We have focused the study on DOPC giant unilamellar lipid vesicles. The DOPC contains monounsaturated oleic acid (18:1, *cis*-9) and has often been used as a model lipid bilayer system [51–56]. The lumen of the vesicles was labelled with membrane impermeable fluorescent marker fluorescein. In the event of bilayer damage, the leakage of fluorescent marker is expected. We have employed a new fluorescence microscopy method to measure the fluorescence intensity of individual lipid vesicle loaded with fluorescein. The fluorescence intensity of the individual lipid vesicles was measured to determine the distribution of lipid vesicle size, shape, and dynamic response to hydrodynamic cavitation treatment and other physico-chemical stressors. Hydrodynamic cavitation was selected as a promising novel unexploited method in biological samples disruption, while other physico-chemical stressors have been selected to represent common challenges, to which lipid vesicles

(phospholipid bilayers) are exposed. Results indicate high potency of hydrodynamic cavitation for lipid vesicle destruction. This work provides a benchmark for lipid vesicle sensitivity to hydrodynamic cavitation treatment and to a variety of different physico-chemical parameters.

## 2. Materials and methods

### 2.1. Preparation of giant unilamellar lipid vesicles (GUV)

Giant DOPC unilamellar lipid vesicles were prepared as described by Moscho et al. [57]. By applying rapid evaporation method, the procedure allows the formation of preferentially unilamellar giant lipid vesicle. Shortly, DOPC was dissolved in chloroform to a concentration of 0.1 M. Then 115 µL of lipid solution was transferred into 250 mL round bottom flask containing 5.6 mL chloroform and 572 µL of methanol. Next, 40 mL of buffer solution (10 mM HEPES buffer, pH = 7.4) with added fluorescein sodium salt - ThermoFisher Scientific, USA (375 mg/mL) was carefully added along the flask walls to lipid solution. Organic solvent was removed with rotary evaporator (Büchi Rotavapor R-134, Büchi Waterbath B-480, Büchi Vacuum Controller V-850, Büchi Vacuum pump V-700) at 40 rpm under reduced pressure (final pressure 55 mbar, volume flow rate 1.8 m<sup>3</sup>/h) in a water bath with temperature set at 40 °C. Around evaporation point of chloroform and methanol we slowly reduced pressure in 5 mbar increments to obtain gentle boiling point of solution. After reaching final pressure of 55 mbar, we let solution to stay at that pressure for 2 min. In the next step, we separated vesicle fraction from the aqueous solution and excess fluorescein with centrifuging at 15700 × g for 10 min. Lipid vesicles in the pellet were resuspended in 40 mL 10 mM HEPES buffer. We repeated lipid vesicle washing three times, and after the third time vesicles were concentrated into 5 mL HEPES buffer. For all lipid vesicle stability experiments vesicles were prepared freshly. Lipid vesicle size was determined with DIC and fluorescence microscopy. As demonstrated by Moscho et al. [57] the method enables a simple, fast and effective method for the production of preferentially giant unilamellar DOPC lipid vesicles.

### 2.2. Stability of lipid vesicles

Giant DOPC lipid vesicles were exposed to different chemical, physical and mechanical stresses. For the stability experiments the concentration of GUV were between  $10^6$  and  $10^7$  vesicles/mL. Lipid vesicles were exposed to different stress exposure times up to 60 min. All reagents were prepared and diluted in 10 mM HEPES buffer solution. All experiments (except heating, freezing, and hydrostatic pressure) were made under ambient conditions (room temperature, ambient air pressure). The following conditions with intention to compromise GUV stability were tested:

- Hydrodynamic cavitation: HC was obtained with circular Venturi restriction tube, which was made from acrylic plastic with restriction hole diameter of 0.6 mm (technical drawing of venturi restriction is represented in Supplementary Fig. S21). 5 mL of sample was pushed through Venturi restriction from one syringe to another in 0.3 s, leading to the average velocity in the order of 50 m/s inside the Venturi. Despite the limitations, which were raised by Šarc et al. [58], we still estimated the value of cavitation number, which may be useful for reference and guidance, especially in the case of upscaling. Considering the downstream pressure, the vapor pressure at 22 °C and the flow velocity inside the restriction tube, the cavitation number of  $\sigma = 0.93$  can be determined. This is close, but still above the limit of chocked flow, which occurs at  $\sigma = 0.045$ . We pushed sample though restriction 100 times.
- Ultrasonic treatment: 800 µL of GUV solution was put into 1.5 mL microtubes and sonicated with ultrasonic horn probe type (MSE 150 W Ultrasonic disintegrator Mk2, exponential probe 1/8" –

- 3 mm) at nominal frequency of 20 kHz and at different amplitudes (3 µm, 6 µm, 9 µm, 12 µm, 15 µm, 18 µm, 21 µm) for 5 s. Horn was immersed into solution approximately 1/3 of whole sample volume. Samples were kept in cold ice water.
- c) Solubilization of lipid vesicles with Triton X-100: 9 µL of fluorescein loaded GUV solution was put on microscope slide and mixed with 1 µL of appropriate Triton X-100 solution (final concentrations of Triton X-100: 0.03, 0.05, 0.11, 0.21, 0.43, 0.85, and 1.7 mM). Samples were incubated at room temperature for up to 10 min.
  - d) Changing osmolarity of the lipid vesicle solution: 9 µL of fluorescein loaded GUV solution was put on microscope slide and mixed with 1 µL of appropriate glucose solution (final concentrations of glucose: 0.3, 0.6, 1.2, 2.5, and 5% (w/v)). Samples were incubated at room temperature for up to 10 min and observed with fluorescence microscopy.
  - e) Addition of ethanol: 9 µL of fluorescein loaded GUV solution was put on microscope slide and mixed with 1 µL ethanol solution (final concentrations of ethanol: 1.2%, 2.5%, 5% and 10%), incubated for up to 10 min and observed with fluorescence microscopy.
  - f) Changing ionic strength: 9 µL of fluorescein loaded GUV solution was put on microscope slide and mixed with 1 µL of NaCl, CaCl<sub>2</sub> or FeCl<sub>3</sub> solution (final concentrations of NaCl: 1, 10 and 100 mM; CaCl<sub>2</sub>: 0.1, 1, 10, and 100 mM; FeCl<sub>3</sub>: 0.01, 0.1, 1, 10, and 100 mM). Lipid vesicles were incubated for up to 10 min and observed with fluorescence microscopy.
  - g) Changing pH: 1.2 mL fluorescein loaded GUV solution was put into 15 mL centrifuge tube and pH was adjusted with 0.4 M HCl or NaOH in the range from pH 2 to 12. As the volumes of added HCl or NaOH were small we did not correct for the solution of the lipid vesicles. Lipid vesicles were incubated for up to 10 min and observed with fluorescence microscopy.
  - h) Fenton reaction: 16 µL of fluorescein loaded GUV solution was put into 1.5 mL microtubes and mixed with 2 µL of H<sub>2</sub>O<sub>2</sub> and 2 µL FeSO<sub>4</sub> solutions with a molar ratio 1:1, final concentrations of H<sub>2</sub>O<sub>2</sub> and FeSO<sub>4</sub> were 0.25, 0.5, 1, 2.5, and 5 mM. Samples were incubated in microtubes at room temperature for approximately 10 min. Next, lipid vesicles were observed with fluorescence microscopy.
  - i) Vortex mixing: 100 µL of fluorescein loaded GUV solution was put into 1.5 mL microtubes and mixed with vortex mixer (IKA MS 3 digital) for 4 min at different rotary speeds: 1000, 2000, and 3000 rpm. Microtube was held in upright position during vortex mixing. Lipid vesicles were immediately observed with fluorescence microscopy. In addition, we have vortex mixed samples with 1.5 mm silica beads. To 100 µL of fluorescein loaded GUV solution in 1.5 mL microtubes 0.1 g of silica beads were added and vortexed at different rotary speeds: 1000, 2000, and 3000 rpm for 4 min.
  - j) Pipetting: 100 µL of fluorescein loaded GUV suspension was put into 1.5 mL microtubes and 70 µL of sample was repeatedly pipetted with automatic pipette for 100, 500, and 1000 times. Next, lipid vesicles were observed with fluorescence microscopy.
  - k) Heating: 100 µL of fluorescein loaded GUV suspension was transferred into 1.5 mL microtubes and put into preheated thermoblock heater (Stuart SBH130DC). We incubated samples in a thermoblock for 10 min and cool them down prior to fluorescence microscopy. Lipid vesicle stability was tested at 40, 60, 80, and 100 °C. For long term stability vesicles were stored at room temperature in the dark.
  - l) Cooling: 100 µL of fluorescein loaded GUV suspension was transferred into 1.5 mL microtubes and put into cold room (4 °C) or frozen at -18 °C and -80 °C. Samples were frozen for approximately 1 h, thawed in hot water (~50 °C), and cooled to room temperature prior to microscopy observation.
  - m) Electroporation: 100 µL of fluorescein loaded GUV suspension was put into electroporation cuvette with 1 mm gap and transferred into electroporator (Eppendorf 2510). Samples were tested at different electric potential: 800, 1100, 1400, 1700, 2000, 2300, and 2500 V. Discharge time constant was 5 ms with 3.3 kOhm sample impedance. Lipid vesicles were immediately observed with fluorescence microscopy.
  - n) Microwave: 100 µL of fluorescein loaded GUV suspension was transferred into 1.5 mL microtubes, put into microwave (Daewoo KOR-6185, frequency: 2450 MHz) and heated for 1 min at different output powers (472 W, 623 W and 800 W). After heating, samples were cooled down to room temperature.
  - o) Shear rate treatment on rheometer: Shear rate experiments were performed on a rotational rheometer Physica MCR 302 (Anton Paar, Graz, Austria) at (25.00 ± 0.01) °C. 70 µL of lipid vesicle suspension was applied to a cone-plate measuring system (CP25) to ensure a constant shear rate within the entire shear gap. The samples were sheared at 2000, 6000, 10000, 14000 and 18500 s<sup>-1</sup> for 2 min. After shear treatment, lipid vesicles were immediately observed with fluorescence microscopy.
  - p) Hydrostatic pressure: Specially designed mechanical test rig was made to test static hydrostatic pressure in small liquid volumes. The test chamber was made from stainless-steel rod with hole of 5 mm H5 diameter and 60 mm length. On top of the chamber was piston with diameter of 5 mm H5 which provided displacement to create hydrostatic pressure. Piston had rubber O-ring φ5/φ1 mm to prevent leakage. Test rig is constructed out of leverage bar and test chamber mounting. Leverage bar was properly weighted to get desired pressure. Drawings of the test rig are presented in Supplementary Fig. S20. We put approximately 900 µL of sample into the testing chamber. Piston was pushed into the chamber to let air and excessive fluid out to obtain same tested volume (working volume was approximately 800 µL). After mounting test chamber into the testing rig, high pressure was applied for 5 min. Applied pressures were: 300, 600, 900, 1200, 1500 and 1800 bar.
  - q) Ultrasonic cleaning bath: 100 µL of fluorescein loaded GUV suspension was transferred into 1.5 mL microtubes and secured into microcentrifuge floating rack. Ultrasonic cleaning bath (ASonic PRO MED 50, Ultrasonic power: 120 W) was filled with water (water temperature was approx. 21 °C) and samples in floating rack were put into ultrasonic bath. Device has different operating modes – soft and normal modes. Operating frequency was 40 kHz. Samples were sonicated 5 s and 60 s at both operating modes (soft and normal mode). During the sonication, water temperature didn't surpass 25 °C during experiments.
  - r) Centrifugation: 100 µL of fluorescein loaded GUV suspension was transferred into 1.5 mL microtubes and centrifuged in centrifuge (Eppendorf Centrifuge 5424) for 10 min at different G-forces (10000 × g, 15700 × g, 20000 × g). Before we put sample on microscope slide, we mixed sample with vortex mixer for 10 s at 3000 rpm.

### 2.3. Stability of fluorescein sodium salt

For all tested conditions, we have checked the stability of fluorescein molecule fluorescence intensity. Fluorescein solution (375 mg/mL) in HEPES buffer was treated the same way as described in section above except that lipids were not added. After treatment, 300 µL of sample was put into 96-well black microtiter plate with clear bottom. Fluorescence intensity was measured with microplate reader (BioTek Instruments, Inc., Cytation 3, excitation: 500 nm, emission: 530 nm, gain: 50) and compared to the untreated control. Except for the low pH treatment, no decay of fluorescence intensity was observed.

We also tested stability of sodium fluorescein during storage at room temperature in dark. 5 mL of fluorescein solution (375 mg/mL) in HEPES buffer was stored in 15 mL centrifuge tubes. Every 3–4 days, 300 µL of sample was put into 96-well black microtiter plate with clear bottom and measured fluorescence. Fluorescence intensity was measured with microplate reader (BioTek Instruments, Inc., Cytation 3, excitation: 500 nm, emission: 530 nm, gain: 50).

#### 2.4. Fluorescence microscopy

The samples with fluorescein loaded giant unilamellar vesicles were visualized on fluorescence microscope Zeiss Axio Observer Z1 equipped with confocal unit LSM 800. Samples were prepared for microscopy with the following procedure: all samples were first vortex mixed for 5 s (at 3000 rpm), then 10 µL of untreated or treated sample was put on microscope slides, covered with 20 × 20 mm cover glass and sealed with VALAP wax (vaseline, lanolin, paraffin). Microscopic images were taken on 20x/0.4NA objective with 488 nm laser at 0.48% laser intensity. Pinhole was set to 100 µm (1.9 Airy Units ~11.3 µm thick section). Emission range was set 400–647 nm. Image acquisition mode was tiles imaging (2 × 2 tiles) on 5 random places on microscopic glass (on each corner of cover glass and one in the centre of sample). Single (2 × 2 tiled) image covered 1213.9 × 1213.9 µm of sample area. Acquired image frame size was 1024 × 1024 pixel. Pixel dwell time was 0.76 µsec, scan time 1.86 sec (scan speed was 8, averaging was set on number 2, digital magnification 0.5×).

#### 2.5. Analysis of microscopic images

Microscopic images were analysed with ImageJ 1.52i software. We set threshold to discriminate lipid vesicles from the background of the images and analysed with Particle analyser (set parameters: size = 4–100, circularity = 0.50–1.00). We obtained vesicle area and mean vesicle fluorescence intensity.

#### 2.6. Calculation of lipid vesicle parameters

To obtain fluorescence intensity of the individual vesicle the following corrections were performed: (i) fluorescence intensity of HEPES buffer was subtracted from mean fluorescence intensity of each vesicle, (ii) the background was further reduced by subtracting the image background value as obtained by "subtract background" function of ImageJ. As this value represents the background of the whole optical section void of vesicles, we have weighted its contribution relative to the thickness of space in z-direction not occupied by the vesicle. For example, the obtained fluorescence intensity of vesicle with 6 µm diameter in an image of 10 µm optical thickness has two contributions: fluorescence from background that originates from 4 µm thick void space and fluorescence from 6 µm thick vesicle, therefore 40% of background fluorescence value obtained from the background void of vesicles was included in vesicle fluorescence intensity correction. The vesicle diameter was calculated from vesicle area, by assuming the spherical shape of the vesicle. To obtain fluorescence intensity per unit volume, the fluorescence intensity of the vesicle was normalized by vesicle diameter. In the results the diameter normalized fluorescence intensity was calculated as an average over all vesicles and is presented as an average vesicle fluorescence. To calculate fluorescein amount per vesicle the diameter normalized fluorescence intensity was multiplied by vesicle volume. The total fluorescence for vesicles, as shown in the results, was obtained by summing fluorescence intensity of the individual vesicles.

The acquired confocal microscopic images had an optical slice thickness of 11.3 µm, thus only vesicles with diameters 11.3 µm or less (~98% of all vesicles) were included in the analysis. The vesicles with diameters < 2.4 µm were indistinguishable from the noise and were thus not included in the analysis. All results are represented relative to the untreated samples (controls).

#### 2.7. Data fitting

Results for long-term stability of fluorescein loaded GUV at room temperature in the dark over time were statistically analysed with Origin software. Each independent sample fluorescence intensity was first normalized to the initial state (day 0), next we fitted the

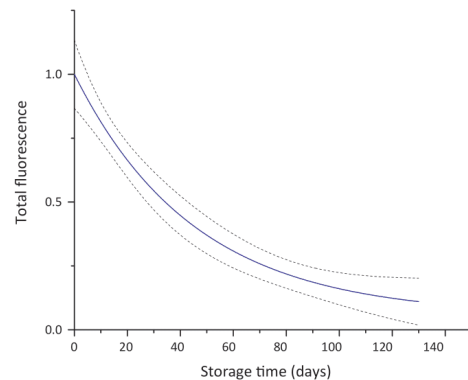


Fig. 1. GUV stability of DOPC at room temperature, stored in dark. Blue line represents an exponential decay function fitted to the normalized total fluorescence of fluorescein loaded vesicles during storage. Grey dashed lines represent 95% confidential interval ( $n = 3$ ). (For interpretation of the references to colour in this figure legend, the reader is referred to the web version of this article.)

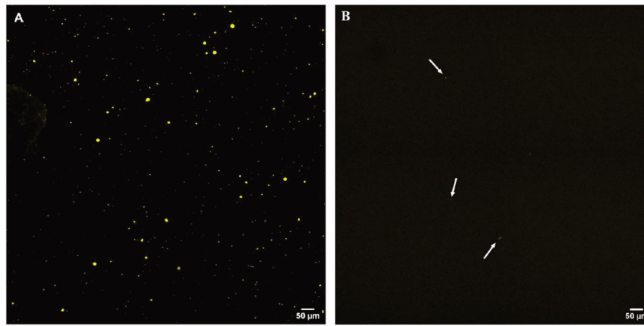
normalized results with the exponential decay function (ExpDec1 function).

### 3. Results

The long-term stability of DOPC giant unilamellar vesicles (GUV) loaded with fluorescein stored in the dark at room temperature is given in Fig. 1. The total fluorescence decreased exponentially. The average decay time, the time when the initial fluorescence decreased to 1/e was  $(31.5 \pm 8.5)$  days. Fluorescence intensity of the control fluorescein solution after 110 days of storage did not decrease significantly suggesting that the decrease of fluorescence intensity in GUV was not due to fluorescein decay. All the experiments on lipid vesicle stability were done on freshly prepared GUV and the duration of experiment with various physico-chemical stressors did not exceed 60 min. We therefore assumed that leakage and decay of fluorescein from untreated GUV was negligible. To compare the effect of different physico-chemical stressors on lipid vesicle stability all the results were normalized to the fluorescence intensity of the non-treated control GUV samples.

Hydrodynamic cavitation (HC) was recently introduced as method of choice to destroy bacteria [33–36]. Here we have tested for the first time the effect of HC on giant lipid vesicles as a model system for bacterial lipid bilayers. We have designed a new small volume hydrodynamic device (Supplementary Fig. S21) with Venturi restriction. The stability of GUV lipid vesicles treated with HC is shown in Fig. 2. A polydisperse distribution of vesicle size was observed before HC treatment. After 100 passes through Venturi restriction, only few small sized GUVs remained. The increase of background fluorescence, due to the leakage of fluorescein to the surrounding, was not measurable on fluorescent micrographs as it was below the detection limit of the microscope.

To further characterize the effect of HC on lipid vesicles, we analysed the individual lipid vesicles on microscopic images. The total fluorescence intensity, vesicle number, vesicle volume and vesicle fluorescence intensity of GUV relative to the untreated control sample are given in Fig. 3A. The results show that after 100 passes, the average lipid vesicles number, volume and total fluorescence intensity significantly decreased. Reduction in vesicle diameter is presented in Fig. 3B, where can be seen shift of vesicle size distribution toward



smaller vesicles size. There was small, but significant fraction of lipid vesicles that resist the hydrodynamic treatment. The average vesicle fluorescence intensity of the remaining vesicles did not change significantly relative to the untreated vesicles.

Cavitation bubbles can also be generated with propagation of acoustic waves through the liquid medium [59]. Application of low amplitude ( $3 \mu\text{m}$ ) ultrasound did not cause a major leak of fluorescein from the GUV (Fig. 4). With increasing amplitude, however, the total fluorescence decreases exponentially. At  $12 \mu\text{m}$  amplitude the majority of GUV were empty of fluorescein or destroyed. As given in Fig. 4 the number of GUV, the average volume of the remaining fluorescein labelled GUV, as well as the average liposome fluorescence decreased with increasing ultrasound amplitude. This indicates a disruption of the giant lipid vesicles at high amplitude treatments. The size distribution analysis of lipid vesicles (Fig. 4E) suggests that with increasing ultrasound amplitude the size distribution of GUV moved towards smaller sized vesicles. Consistently, the number of GUV independently determined by DIC microscopy also decreased. The decrease of the number of vesicles determined with DIC correlated with the number of lipid vesicles determined by fluorescence. This implies that the decrease of the total fluorescence intensity in GUV was mainly due to vesicle disintegration. Compared to ultrasound applied by a sonotrode, lipid vesicles treated with ultrasonic bath showed less effect on vesicles integrity (Supplementary Fig. S1). Increasing power output of the ultrasonic bath had similar effect to increasing amplitude of sonotrode.

The effects of different chemistry on GUV stability are given in Fig. 5. Only the highest concentrations used are shown in Fig. 5. The effect of other concentrations are given in Supplementary material (Fig. S2 – S6). Lipid vesicles were not resistant to osmolarity change.

Compared to the untreated control ~40% of fluorescein leaked out of lipid vesicles treated with 5% (w/v) glucose. Vesicles treated with 10% ethanol or 100 mM NaCl and CaCl<sub>2</sub> leaked even more fluorescein. Most of the GUV were disrupted upon addition of 100 mM FeCl<sub>3</sub>. When we induced free radical formation with Fenton reaction by mixing 2.5 mM FeSO<sub>4</sub> with 2.5 mM H<sub>2</sub>O<sub>2</sub> lipid vesicles disintegrated instantly. The addition of either 2.5 mM FeSO<sub>4</sub> or 2.5 mM H<sub>2</sub>O<sub>2</sub> to the GUV did not cause lipid vesicle disintegration (Supplementary Fig. S6).

It is surprising that the addition of 100 mM Fe<sup>3+</sup> ions had such a dramatic effect on GUV stability, in particular when compared to the addition of monovalent and divalent cations. It is known that the addition of ferric ion induces water hydrolysis and may significantly decrease pH [60]. The pH of 100 mM FeCl<sub>3</sub> solution was 1.9. This is very low and may have an effect on zwitterionic DOPC vesicles and fluorescence intensity of fluorescein marker [61,62]. To check this, we have measured fluorescein stability at different pH values. In Supplementary Fig. S7 we show that fluorescein is stable above pH 7.4, however at low pH fluorescein molecule decays. We have also changed the pH of lipid vesicle suspension. The results for total fluorescence are given only for pH 7.4 or higher (Supplementary Fig. S8). DOPC vesicles were most stable at pH 7.4. Increasing pH decreased the amount of total fluorescence in the vesicles as well as the number of fluorescein vesicles. The effect of low pH has been tested with DIC microscopy. We have observed significant decrease of the number of lipid vesicles which suggest that also low pH has a significant effect on DOPC lipid GUV stability.

Solubilization of GUV with Triton X-100 is given in Supplementary Fig. S9. At low concentrations of Triton X-100, below the critical micellar concentration, the addition of detergent did not significantly

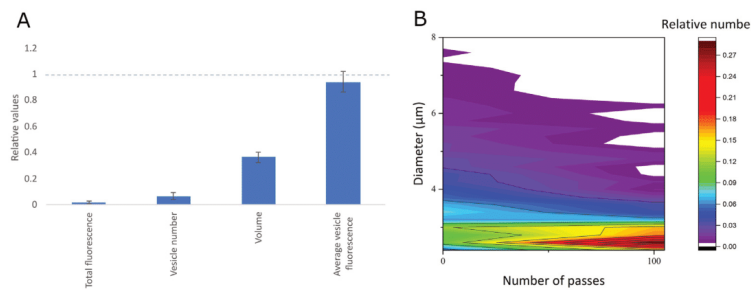
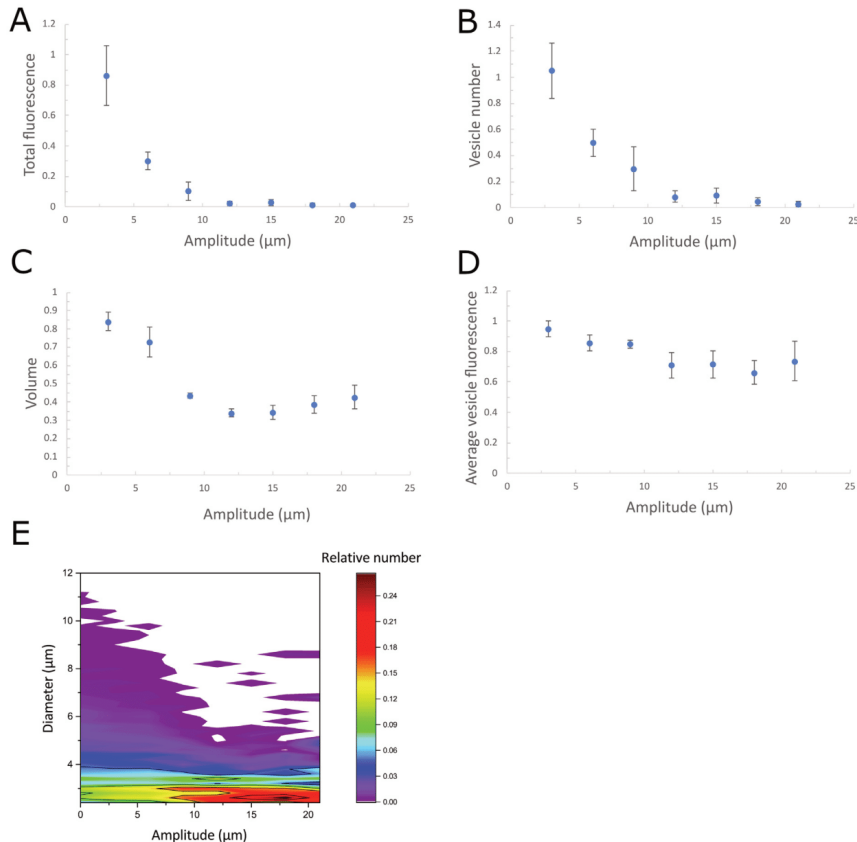


Fig. 3. Treatment of DOPC GUV with hydrodynamic cavitation. Panel A shows relative values of total fluorescence, the average vesicle number, vesicle volume and vesicle fluorescence relative to the untreated control, which is represented by dashed line (—). Panel B shows size distribution of individual fluorescein loaded vesicles during the hydrodynamic cavitation treatment. Average values and standard error are given in panel A (n = 5).



**Fig. 4.** The effect of different ultrasound amplitude on the total fluorescence of vesicles (A), relative number of fluorescein loaded vesicles (B), the average volume of the remaining vesicles (C), the average vesicle fluorescence of the remaining vesicles (D), and the vesicle size distribution at different amplitudes of ultrasound (E). The results in A-D represent the total fluorescence of vesicles, average number, volume and vesicle fluorescence relative to the untreated control, represented by value of 1. The average values and standard errors ( $n = 4$ ) are given for A-D.

compromised lipid vesicle stability. However, with increasing detergent concentration vesicles were progressively disrupted. At first the volume of lipid vesicles increased compared to untreated vesicles, most notably at 0.85 mM Triton X-100. The number of remaining lipid vesicles above the critical micellar concentration decreased drastically. We have observed that Triton X-100 first solubilized small sized GUV followed by disruption of larger vesicles at higher detergent concentrations (Supplementary Fig. S9E).

In addition to chemical stressors the GUV were exposed to different mechanical treatments as well (Fig. 6). Only the effect of the largest magnitude for a given stressor is given in Fig. 6. The effects for lower magnitudes are given in the Supplementary information. Pipetting lipid vesicle suspension several times had little effect on lipid integrity. If the number of pipetting was increased to unrealistically high number, i.e. 500 times or higher (Supplementary Fig. S10), small effect on lipid stability was observed. On the other hand, when shear stress was increased by vortexing, surprisingly, the total fluorescence increased relative to the untreated control. Since the relative average vesicle

volume and average vesicle fluorescence did not change, but the number of vesicles increased (Supplementary Fig. S11), it is likely that during vortexing more lipid vesicles were resuspended compared to the untreated control lipid vesicle suspension. If shear stress during vortexing was further increased by adding glass beads, vesicles were destroyed (Supplementary Fig. S12). We also applied rotational shear stress on lipid vesicle solution with rotational rheometer up to shear rate of  $18500\text{ s}^{-1}$ . Although this is considered to be a high shear rate, no significant effect on vesicle integrity was observed (Supplementary Fig. S13).

The electroporation had a strong effect on vesicle integrity and significantly decreased the total fluorescence and the number of vesicles. As given in Supplementary Fig. S14 the effect on vesicle volume, and average vesicle fluorescence was less pronounced. Increased temperature decreased lipid vesicle integrity only at temperatures above  $80^\circ\text{C}$ . Similarly freeze-thawing decreased the total fluorescence and volume but has less effect on the number and average vesicle fluorescence (Supplementary Fig. S15). The effect of static pressure on lipid

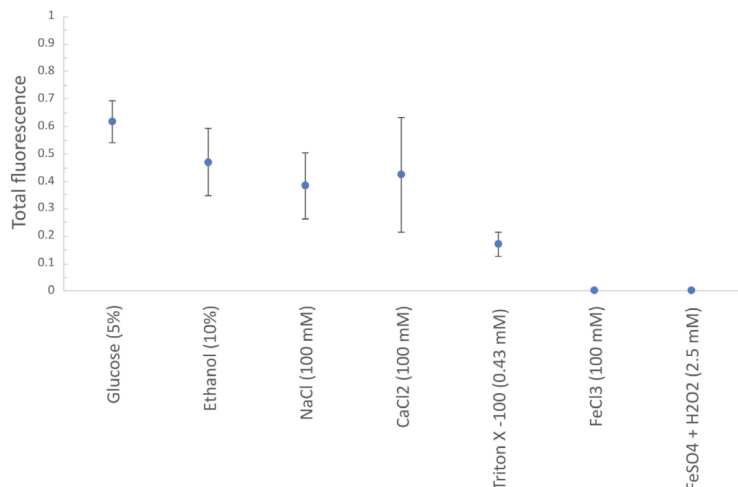


**Fig. 5.** The effect of different chemical treatments on DOPC integrity. The relative total fluorescence intensity is normalized relative to control untreated samples. Average values and standard errors are given ( $n = 4$  or 5).

stability is given in *Supplementary Fig. S16*, where it can be seen that vesicles are fairly stable to high pressures. Vesicle destruction can only be seen at pressures higher than 1200 bar. The effect of microwave treatment is given in *Supplementary Fig. S17*. The results suggest that microwaves induce leakage of fluorescein from the vesicles. The effect was dependent on the microwave output power. Microwaves did not have an effect on the number and volume of vesicles, but significantly

decreased average vesicle fluorescence. One of the most frequently used technique in the laboratory is centrifugation. The results of centrifugation on vesicle stability are given in *Supplementary Fig. S18*. With increasing g force lipid vesicles progressively leaked more. However, the effect of centrifugation was moderate.

The 3D comparison of lipid vesicle stability to different physicochemical and mechanical forces relative to the untreated lipid vesicles

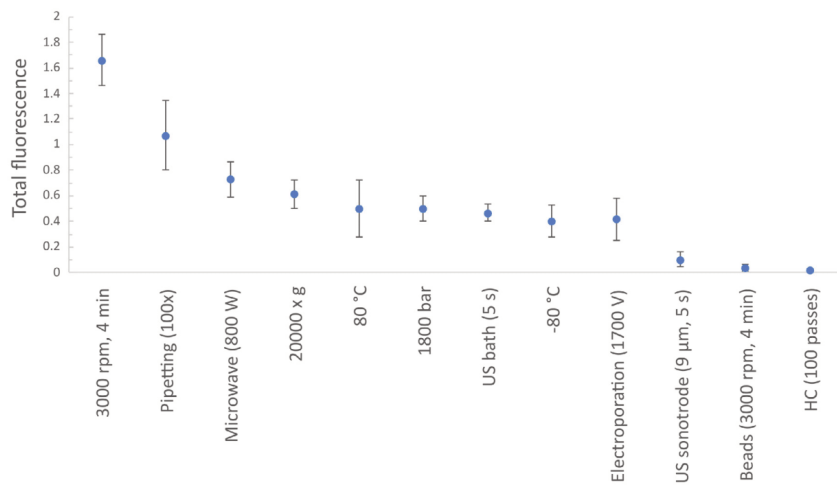


**Fig. 6.** DOPC vesicle integrity upon different mechanical and physical treatments of vesicles. The relative total fluorescence intensity after treatment compared to fluorescence intensity before treatment. Standard errors are given ( $n = 4$ ). Shown parameters from left to right: vortex mixing (3000 rpm, 4 min), pipetting (100x), microwave irradiation (output power 800 W), centrifugation (20000  $\times$  g, 10 min), heating (80 °C), high pressure (1800 bar), ultrasonic bath (40 kHz, 5 s) freezing-thawing (-80 °C), electroporation (1700 V), ultrasonication with sonotrode (9  $\mu$ m amplitude, 5 s), vortex mixing with beads (3000 rpm, 4 min), hydrodynamic cavitation (100 passes).

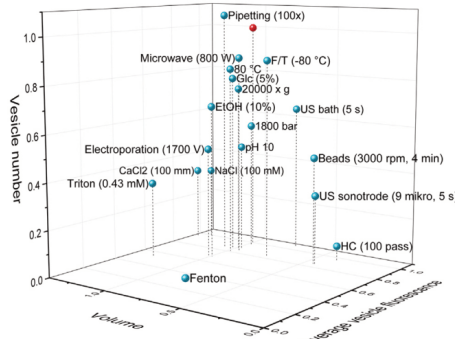


**Fig. 7.** Summary of relative importance of different environmental stressors on lipid vesicle stability. The data represent values of average vesicle volume, average vesicle fluorescence and number of vesicles relative to the untreated control. Red dot on graph represents the untreated control (all values are equal to 1.0). Abbreviations: F/T ( $-80^{\circ}\text{C}$ ) – freezing-thawing at  $-80^{\circ}\text{C}$ ;  $80^{\circ}\text{C}$  – heating on  $80^{\circ}\text{C}$ ; glc (5%) – glucose (5%);  $20000 \times g$  – centrifugation at  $20000 \times g$ ; EtOH (10%) – ethanol (10%); 1800 bar – high pressure (1800 bar); beads (3000 rpm, 4 min) – vortex mixing with beads at 3000 rpm for 4 min; HC (100 passes) – hydrodynamic cavitation (100 passes); Fenton –  $\text{FeSO}_4 + \text{H}_2\text{O}_2$  (2.5 mM). (For interpretation of the references to colour in this figure legend, the reader is referred to the web version of this article.)

for the worst-case scenario (i.e. the highest magnitude of the parameter used in this study) is given in Fig. 7. Several 2D slices such as vesicle volume : fluorescence, volume : number, and vesicle fluorescence : number are given in Supplementary Fig. S19. Vesicles responded to different environmental stressors either by changing volume, intravesicular fluorescein concentration, the number of vesicles, or a combination of this parameters.

This suggests that there are several mechanisms at work in decreasing lipid vesicle stability. Compared to other stressors, HC is a very effective method for lipid vesicle disintegration. It effectively decreases the number and size of lipid vesicles. The effect of hydrodynamic treatment on lipid vesicles is comparable to the effect of ultrasound with more pronounced decrease of vesicle number and higher fluorescence intensity of the remaining vesicles. HC reduces the number of lipid vesicles as effectively as free radicals; however, the volume of the remaining vesicles is smaller with higher fluorescence intensity.

#### 4. Discussion

The field of liposome research is immense. Due to their biological significance (i.e. bacterial membrane model system) and applications in different industries and medicine lipid vesicles and their stability remain an active area of research. In this study we have used hydrodynamic cavitation to destroy lipid vesicles and compared its effect to other chemical, physical and mechanical treatments. By normalizing different treatments to untreated control, we were able to compare the effect of different physico-chemical treatments on vesicle stability. The results clearly demonstrate that hydrodynamic cavitation is a very effective treatment method to destroy lipid vesicles. In the following we discuss different mechanisms of liposome destruction in order to infer possible mechanisms of lipid vesicle destruction by hydrodynamic cavitation.

One can imagine several mechanisms of lipid vesicle disruption that induce leakage of fluorescein from vesicles. Vesicles can become transiently porous and leak fluorescein with no substantial volume change during the process (e.g. electroporation). Lipid pores may form on a

longer timescale and grow to a critical size that leads to disintegration of lipid vesicle into several fragments that reassemble into smaller vesicles (e.g. shear stress). Lipid vesicle may buckle by shear stress and fragment to smaller vesicles. The ultimate disruption of lipid vesicles is solubilisation with surface active molecules (e.g. Triton X-100). Depending on the physico-chemical treatment, different combinations of the above-mentioned processes may occur in lipid vesicles disruption.

The results of this study indicate that all treatments tested had an effect on lipid stability either by decreasing lipid vesicle number, volume, fluorescence intensity or a combination of these parameters. The effect of salts, solvents, surface active agents, free radicals, temperature, and pressure on lipid vesicle stability have been well documented in the literature. Because our results do not deviate strongly from the published data they will not be further discussed. Much less, however, is known about the effect of high shear stress, centrifugation, vortex mixing, microwaves or hydrodynamic cavitation. The effect of shear stress was strongly dependent on the treatment applied. For example, pipetting had a negligible effect on lipid vesicle stability unless repeated at unrealistically high numbers. Lipid vesicles were stable in the shear rate range from 0 to  $18500 \text{ s}^{-1}$  on rotational rheometer. It has been demonstrated for the dilute and semi dilute regime that the rheological behaviour of small unilamellar DMPC bilayer vesicles is similar to that of a hard-sphere dispersion [63]. Although the tested shear rate range was rather large the results suggest that lipid vesicles do not deform sufficiently to allow for fluorescein leakage. Pal and Khakhar [64] showed size reduction of liposomes during constant shear stress ( $4000 \text{ s}^{-1}$ ) only after 6 h of applied shear stress. The proposed mechanism behind vesicle size reduction was deformation and rupture of vesicles above the critical diameter into smaller sized vesicles. They suggested that the breakage process was stochastic, since not all vesicles larger than critical diameter did not rupture.

The effect of microwave irradiation on lipid vesicle stability was significant. Already after one minute of treatment we have observed fluorescein leakage from lipid vesicles. The effect increased with increasing microwave power output. Saalman et al. [65] have showed that 2.45 GHz microwave irradiation significantly increased membrane permeability. Also, Orlando et al. [66] reported similar observations. In these experiments, however, lipid vesicles were subjected to long exposure times (several hours), whereas we exposed treated samples to microwave irradiation only for a short time.

The most detrimental mechanical treatments for lipid vesicles were vortex mixing with glass beads, ultrasound and hydrodynamic cavitation. The effect of vortex mixing was strongly increased when glass beads were added to the lipid solution. The number of vesicles and the volume of vesicles decreased significantly already after 4 min of vortex mixing with beads. Interestingly the fluorescence intensity of the remaining lipid vesicles decreased only slightly. This indicates that upon vigorous vortex mixing with glass beads lipid vesicles disintegrate and reseal to smaller vesicles almost instantaneously with no significant loss of fluorescein in the remaining vesicles.

Both, ultrasound and hydrodynamic treatment produced bubbles. During cavitation, when the bubble violently collapses extreme environmental conditions may be present. In collapsing bubble so called "hot spots" ( $\sim 4500 \text{ K}$  [39]) are created, it is expected that high shear stress exist during microjet bursts (shear rate in excess of  $100000 \text{ s}^{-1}$  [67]), high fluid velocities  $\sim 100 \text{ m/s}$  [40]), with resultant pressure waves and formation of free radicals. The collapse of bubbles during sonication is frequently correlated with the formation of free radicals [42]. Formation of highly reactive free radicals is very effective for vesicle disintegration as free radicals oxidize phospholipids. Our results for free radicals are consistent with the notion that oxidation of lipid bilayers leads to pore formation, destabilization and disintegration of bilayers [68]. Nevertheless, the exact mechanism of lipid vesicle disruption by ultrasound is still unknown. It is expected that low frequency ultrasound induces vesicle leakage by sonoporation due to pressure

oscillations and cavitation effects [69–71]. Ultrasound induced pores reseal as soon as the ultrasound is ceased and leakage from the vesicles stops [31,70,72,73]. Whereas most pores would be transient, allowing molecular transport before healing, some pores may grow to a critical size and cause liposome destruction [31,74]. In general terms our results are consistent with pore formation and fragmentation to smaller size vesicles upon ultrasound treatment. It has been reported that higher sonication frequencies cause vesicle reduction to smaller diameters [75]. Size distribution of vesicles in our experiments shifted towards smaller size with increasing amplitude of ultrasound. This is in agreement with the fact that ultrasound is used to prepare small unilamellar vesicles from large multilamellar vesicles [69,76]. Although our results agree with this findings there were some inconsistencies. Most notably a subpopulation of vesicles was resistant to sonication and even at increased ultrasound amplitude there was only a limited change of volume or leakage from the resistant vesicles. The volume of resistant vesicles unexpectedly slightly increased at higher amplitudes.

Similar cavitation phenomena may be induced by hydrodynamic cavitation. In this case, it is the acceleration of the fluid flow which causes local pressure to drop and induces bubble formation [38]. Although in principle both sono and hydrodynamic cavitation induce bubble formation the effects may differ (i.e. number of pressure pulses and cavitation intensity) [77,78]. We have induced cavitation bubble formation in a hydrodynamic flow with Venturi restriction. Results imply that hydrodynamic cavitation has a dramatic effect on vesicle stability comparable in magnitude to the effect of sonication, vortex mixing with glass beads, and free radicals. It proceeds from large vesicles to progressively smaller vesicles. The transformation from large to small vesicles must be fast as the remaining vesicles have approximately the same amount of fluorescein as untreated vesicles, which suggest a quick resealing of disrupted vesicles.

Application of sonication is widely used as cleaning or dispersing mechanism [79–81], on the other hand hydrodynamic cavitation is less commonly applied but much easier to induce. However, this is changing rapidly as many different applications of hydrodynamic cavitation are emerging nowadays [82–84]. Here, we showed for the first time that hydrodynamic cavitation is a powerful new tool to destroy lipid bilayers. Because lipid bilayer integrity is crucial for cell viability it is possible that reported bacterial inactivation by hydrodynamic cavitation is at least in part due to membrane disruption [48]. It remains to be seen if the disruption of membrane in more complex systems (i.e. bacterial spheroplast which lack bacterial cell wall or bacterial cells) by hydrodynamic cavitation is also very effective.

## 5. Conclusions

The experimental survey of a large collection of environmental stressors, among them many that have not been described yet in the literature demonstrate both extraordinary robustness of lipid vesicles to environmental challenges (i.e. high resistance to static pressure) as well as extreme fragility to hydrodynamic cavitation, ultrasound, free radicals or vortex mixing with glass beads. The results also demonstrate that fluorescence approach, based on individual lipid vesicle fluorescence intensity, can successfully describe lipid vesicle stability. By focusing our research to a single lipid vesicle composition, to giant unilamellar lipid vesicles size class, to a single method of preparation and detection we have obtained a consistent set of data that allowed us to compare the relative magnitude of different stressors on lipid vesicle stability. Based on the results we conclude that hydrodynamic cavitation is a highly effective method to destroy liposomes.

## Acknowledgments

The authors acknowledge the financial support from the European Research Council (ERC) under the European Union's Framework Program for research and innovation, Horizon 2020 (grant agreement

n° 771567 — CABUM) and the Slovenian Research Agency (research core funding No. P2-0401 and P4-0116). We would like to thank Mr. Tone Godeša for producing hydrostatic pressure test rig.

## Appendix A. Supplementary data

Supplementary data to this article can be found online at <https://doi.org/10.1016/j.ultsonch.2019.104826>.

## References

- [1] L.E. Locascio, W.N. Vreeland, A. Jahn, M. Gaitan, Liposomes as model cellular systems: liposome formation and applications in microfluidics, *Lab-on-Chips for Cелиomics* (2007) 59–81, [https://doi.org/10.1007/978-1-4020-2975-2\\_3](https://doi.org/10.1007/978-1-4020-2975-2_3).
- [2] S. Talegaonkar, P. Mishra, R. Khar, S. Biju, Vesicular systems: an overview, *Indian J. Pharm. Sci.* 68 (2006) 141, <https://doi.org/10.4103/0250-474X.25707>.
- [3] Y.-H.M. Chan, S.G. Boxer, Model Membrane Systems and Their Applications State of the field, *Curr. Opin. Chem. Biol.* 11 (2007) 581–587 <https://www.ncbi.nlm.nih.gov/pmc/articles/PMC2196400/pdf/nihms35927.pdf>.
- [4] B.N. Rao, K.R. Reddy, B. Mounika, S.R. Fathima, A. Tejaswini, *Vesicular Drug Delivery System : A Review* 12 (2019) 39–53.
- [5] C.G. Siontorou, G.P. Nikoleli, D.P. Nikolelis, S.K. Karapetis, Artificial lipid membranes: past, present, and future, *Membranes (Basel)* 7 (2017) 1–24, <https://doi.org/10.3390/membranes7030038>.
- [6] G. Gregori, S. Citterio, A. Ghiani, M. Labra, S. Sgorbati, S. Brown, M. Denis, Resolution of Viable and Membrane-Compromised Bacteria in Freshwater and Marine Waters Based on Analytical Flow Cytometry and Nucleic Acid Double Staining, *Appl. Environ. Microbiol.* 67 (2001) 4662–4670, <https://doi.org/10.1128/AEM.67.10.4662-4670.2001>.
- [7] F. Ou, C. McGoverin, S. Swift, P. Vanholbeek, Rapid and cost-effective evaluation of bacterial viability using fluorescence spectroscopy, *Anal. Bioanal. Chem.* (2019), <https://doi.org/10.1007/s00216-019-01848-5>.
- [8] M. Berney, F. Hammes, F. Bossard, H.-U. Wellenmann, T. Egli, Assessment and interpretation of bacterial viability by using the LIVE/DEAD BacLight Kit in combination with flow cytometry, *Appl. Environ. Microbiol.* 73 (2007) 3283–3290, <https://doi.org/10.1128/AEM.02750-06>.
- [9] L. Boulos, M. Prevost, B. Barbeau, J. Coallier, R. Desjardins, LIVE/DEAD(\*) BacLight(TM): Application of a new rapid staining method for direct enumeration of viable and total bacteria in drinking water, *J. Microbiol. Methods.* 37 (1999) 77–86, [https://doi.org/10.1016/S0167-7012\(99\)00048-2](https://doi.org/10.1016/S0167-7012(99)00048-2).
- [10] S.M. Stocks, Mechanism and use of the commercially available viability stain, *BacLight, Cytom. Part A* 61 (2004) 189–195, <https://doi.org/10.1002/cyto.a.20069>.
- [11] A. Laouini, C. Jaafar-Maaej, I. Limayem-Blouza, S. Sfar, C. Charcosset, H. Fessi, Preparation, Characterization and Applications of Liposomes: State of the Art, *J. Colloid Sci. Biotechnol.* 1 (2012) 147–168, <https://doi.org/10.1166/jcsb.2012.1020>.
- [12] K. Shashi, K. Satinder, P. Bharat, A complete review on: liposomes, *Int. Res. J. Pharm.* 3 (2012).
- [13] N. Bavi, Y. Nakayama, O. Bavi, C.D. Cox, Q.-H. Qin, B. Martinac, Biophysical implications of lipid bilayer rheometry for mechanosensitive channels, *Proc. Natl. Acad. Sci.* 111 (2014) 13864–13869, <https://doi.org/10.1073/pnas.1409011111>.
- [14] H. Wang, J. de Joannis, Y. Jiang, J.C. Gaulding, B. Albrecht, F. Yin, K. Khanna, J.T. Kindt, Bilayer Edge and Curvature Effects on Partitioning of Lipids by Tail Length: Atomistic Simulations, *Biophys. J.* 95 (2008) 2647–2657, <https://doi.org/10.1529/biophysj.108.131409>.
- [15] T. Shigematsu, K. Koshyama, S. Wada, Line tension of the pore edge in phospholipid / cholesterol bilayer from stretch molecular dynamics simulation 11 (2016) 1–10, <https://doi.org/10.1299/jbse.15-00422>.
- [16] L. Tayebi, D. Vashee, A.N. Parikh, Stability of Uni- and Multilamellar Spherical Vesicles, *ChemPhysChem.* 13 (2012) 314–322, <https://doi.org/10.1002/cphc.201100573>.
- [17] T.J. Pucadil, S. Mukherjee, A. Chattopadhyay, Organization and dynamics of NBD-labeled lipids in membranes analyzed by fluorescence recovery after photo-bleaching, *J. Phys. Chem. B.* 111 (2007) 1975–1983, <https://doi.org/10.1021/jp066092h>.
- [18] Science 175 (4023) (1972) 720–731, <https://doi.org/10.1126/science.175.4023.720>.
- [19] J.D. Nickels, J.C. Smith, X. Cheng, Lateral organization, bilayer asymmetry, and inter-lea fl et coupling of biological, membranes 192 (2015) 87–99.
- [20] M. Repetto, J. Semprine, A. Boeris, Lipid Peroxidation: Chemical Mechanism, Biological Implications and Analytical Determination, *Lipid Peroxidation* (2012) 3–30, <https://doi.org/10.5772/45943>.
- [21] M.P. Goertz, N. Goyal, G.A. Montano, B.C. Bunker, Lipid Bilayer Reorganization under Extreme pH Conditions (2011) 5481–5491, <https://doi.org/10.1021/la2001305>.
- [22] W.W. Sulkowski, D. Pentak, K. Nowak, A. Sulkowska, The influence of temperature, cholesterol content and pH on liposome stability, *J. Mol. Struct.* 744–747 (2005) 737–747, <https://doi.org/10.1016/j.molstruc.2004.11.075>.
- [23] M.M. Koerner, L.A. Palacio, J.W. Wright, K.S. Schweitzer, B.D. Ray, H.I. Petrache, Electroynamics of lipid membrane interactions in the presence of zwitterionic buffers, *Biophys. J.* 101 (2011) 362–369, <https://doi.org/10.1016/j.bpj.2011.05>.

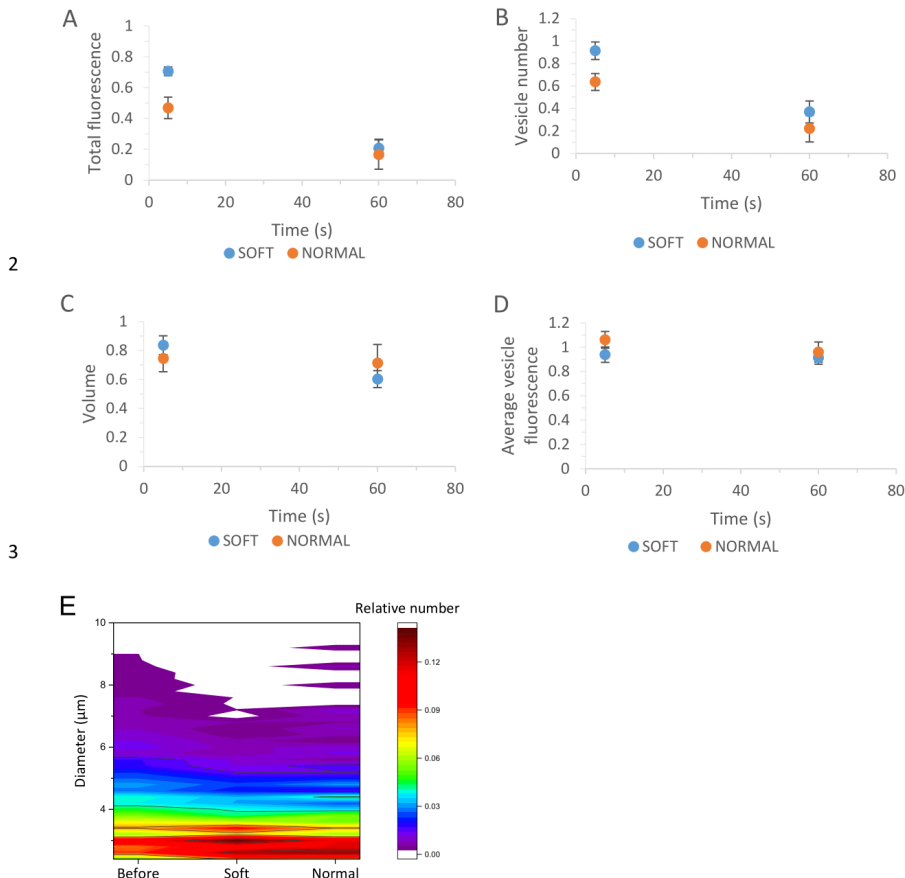
- [24] N. Kato, A. Ishijima, T. Inaba, F. Nomura, S. Takeda, K. Takiguchi, Effects of Lipid Composition and Solution Conditions on the Mechanical Properties of Membrane Vesicles (2015) 22–47, <https://doi.org/10.3390/membranes5010022>.
- [25] M.M.A.E. Claessens, B.F. Van Oort, F.A.M. Leermakers, F.A. Hoekstra, M.A.C. Stuart, Charged lipid vesicles: Effects of salts on bending rigidity, stability, and size, *Biophys. J.* 87 (2004) 3882–3893, <https://doi.org/10.1529/biophysj.103.036772>.
- [26] A. Kodama, M. Morandi, R. Ebihara, T. Jimbo, M. Toyoda, Y. Sakuma, M. Imai, N. Pu, M.I. Angelova, Migration of Deformable Vesicles Induced by Ionic Stimuli (2018), <https://doi.org/10.1021/acs.langmuir.8b02105>.
- [27] J. de Gier, J.G. Mandersloot, L.L.M. Van Deenen, Lipid composition and permeability of liposomes, *Biochim. Biophys. Acta - Biomembr.* 150 (1968) 666–675, [https://doi.org/10.1016/0005-2736\(68\)90056-4](https://doi.org/10.1016/0005-2736(68)90056-4).
- [28] H. Sakai, T. Gotoh, T. Imura, K. Sakai, K. Otake, M. Abe, Preparation and Properties of Liposomes Composed of Various Phospholipids with Different Hydrophobic Chains Using a Probabilistic Reverse Phase Evaporation Method 621 (2008) 613–621, <https://doi.org/10.5650/jos.57.613>.
- [29] C.R. Kensi, E.A. Dennis, Alkaline hydrolysis of phospholipids in model membranes and the dependence on their state of aggregation, *Biochemistry* 20 (1981) 6079–6085, <https://doi.org/10.1021/bi060524a025>.
- [30] M. Grit, D.J.A. Crommelin, Chemical stability of liposomes: implications for their physical stability, *Chem. Phys. Lipids* 64 (1993) 3–18, [https://doi.org/10.1016/0009-3084\(93\)90053-6](https://doi.org/10.1016/0009-3084(93)90053-6).
- [31] P. Marmottan, T. Biben, S. Hilgenfeldt, Deformation and rupture of lipid vesicles in the strong shear flow generated by ultrasound-driven microbubbles, *Proc. R. Soc. A Math. Phys. Eng. Sci.* 464 (2008) 1781–1800, <https://doi.org/10.1098/rspa.2007.0362>.
- [32] K.A. Riske, R. Dimova, Electro-deformation and poration of giant vesicles viewed with high temporal resolution, *Biophys. J.* 88 (2005) 1143–1155, <https://doi.org/10.1529/biophysj.104.050310>.
- [33] T. Portet, F. Camps I Febrer, J.M. Escoffre, C. Favard, M.P. Rols, D.S. Dean, Visualization of membrane loss during the shrinkage of giant vesicles under electropulsation, *Biophys. J.* 96 (2009) 4109–4121, doi:10.1016/j.bpj.2009.02.063.
- [34] W. Ding, M. Palaiokostas, G. Shahane, W. Wang, M. Orsi, Effects of High Pressure on Phospholipid Bilayers, *J. Phys. Chem. B* 121 (2017) 9597–9606, <https://doi.org/10.1021/acs.jpcb.7b07119>.
- [35] Y.R. Sliozberg, Structural Changes in Lipid Vesicles Generated by the Shock Blast Waves : Coarse-Grained Molecular Dynamics, Simulation (2013).
- [36] K. Inque, T. Kitagawa, Effect of lipid composition on sensitivity of lipid membranes to triton X-100, *Biochim. Biophys. Acta - Biomembr.* 426 (1976) 1–16, [https://doi.org/10.1016/0005-2736\(76\)90424-7](https://doi.org/10.1016/0005-2736(76)90424-7).
- [37] B.R. Casadei, C.C. Dominguez, E. De Paula, K.A. Riske, Direct visualization of the action of triton X-100 on giant vesicles of erythrocyte membrane lipids, *Biophys. J.* 106 (2014) 2417–2425, <https://doi.org/10.1016/j.bpj.2014.04.039>.
- [38] J.-P. Franc, J.-M. Michel, Fundamentals of Cavitation, Kluwer Academic Publishers, Dordrecht (2005), <https://doi.org/10.1007/1-4020-2233-6>.
- [39] K.S. Susic, N.C. Eddingsaas, D.J. Flammang, S.D. Hopkins, H. Xu, Extreme conditions during multibubble cavitation: sonoluminescence as a spectroscopic probe, *Ultrason. Sonochem.* 18 (2011) 842–846, <https://doi.org/10.1016/j.ultsonch.2010.12.012>.
- [40] G.L. Chahine, C.-T. Hsiao, Modelling cavitation erosion using fluid–material interaction simulations, *Interface Focus* 5 (2015) 20150016, <https://doi.org/10.1098/rsfs.2015.0016>.
- [41] C.E. Brennen, Cavitation and bubble dynamics, Oxford University Press, Oxford, 1995.
- [42] S. Koda, T. Kimura, T. Kondo, H. Mitome, A standard method to calibrate sonochemical efficiency of an individual reaction system, *Ultrason. Sonochem.* 10 (2003) 149–156, [https://doi.org/10.1016/S1350-4177\(03\)00084-1](https://doi.org/10.1016/S1350-4177(03)00084-1).
- [43] X. Sun, J.J. Park, H.S. Kim, S. Jin, S. Lee, A.S. Om, J.Y. Yoon, Experimental Investigation of the Thermal and Disinfection Performances of a Novel Hydrodynamic Cavitation Reactor, *Ultrason. Sonochem.* 49 (2018) 13–23, doi:10.1016/j.ultrasonch.2018.02.034.
- [44] L.M. Cerecedo, C. Dopazo, R. Gomez-Lus, Water disinfection by hydrodynamic cavitation in a rotor-stator device, *Ultrason. Sonochem.* 48 (2018) 71–78, <https://doi.org/10.1016/j.ultsonch.2018.05.015>.
- [45] J.G. Dalfré Filho, M.P. Assis, A.I.B. Genovez, Bacterial inactivation in artificially and naturally contaminated water using a cavitating jet apparatus, *J. Hydro-Environment Res.* (2015) 259–267, <https://doi.org/10.1016/j.jher.2015.03.001>.
- [46] L. Albanese, R. Ciriminna, F. Meneguzzo, M. Pagliaro, Energy efficient inactivation of saccharomyces cerevisiae via controlled hydrodynamic cavitation, *Energy Sci. Eng.* 3 (2015) 221–238, <https://doi.org/10.1002/esc.362>.
- [47] A. Šarc, J. Kosek, D. Stopar, M. Oder, M. Dular, Removal of bacteria *Legionella pneumophila*, *Escherichia coli*, and *Bacillus subtilis* by (super)cavitation, *Ultrason. Sonochem.* 42 (2018) 228–236, <https://doi.org/10.1016/j.ultsonch.2017.11.004>.
- [48] M. Zupanc, Ž. Pandur, T. Stepišnik Perdih, D. Stopar, M. Petkovsek, M. Dular, Effects of cavitation on different microorganisms: the current understanding of the mechanisms taking place behind the phenomenon. A review and proposals for further research, *Ultrason. Sonochem.* 57 (2019) 147–165, <https://doi.org/10.1016/j.ultsonch.2019.05.009>.
- [49] B. Balasundaram, S.T.L. Harrison, Study of physical and biological factors involved in the disruption of *E. coli* by Hydrodynamic Cavitation, *Biotechnol. Prog.* 22 (2006) 907–913, <https://doi.org/10.1021/bp0502173>.
- [50] B. Balasundaram, S.T.L. Harrison, Optimising orifice geometry for selective release of periplasmic products during cell disruption by hydrodynamic cavitation, *Biochem. Eng. J.* 54 (2011) 207–209, <https://doi.org/10.1016/j.bej.2011.03.002>.
- [51] S.J. Attwood, Y. Choi, Z. Leonenko, Preparation of DOPC and DPPC supported planar lipid bilayers for atomic force microscopy and atomic force spectroscopy, *Int. J. Mol. Sci.* 14 (2013) 3514–3539, <https://doi.org/10.3390/ijms14023514>.
- [52] P.R. Adhyapak, S.V. Panchal, A.V.N. Murthy, Cholesterol induced asymmetry in DOPC bilayers probed by AFM force spectroscopy, *Biochim. Biophys. Acta - Biomembr.* 1860 (1860) 953–959, <https://doi.org/10.1016/j.bbamem.2018.01.021>.
- [53] X. Chen, S. Liu, B. Deme, V. Cristiglio, D. Marquardt, R. Weller, P. Rao, Y. Wang, J. Bradshaw, Efficient internalization of TAT peptide in zwitterionic DOPC phospholipid membrane revealed by neutron diffraction, *Biochim. Biophys. Acta - Biomembr.* 1817 (1859) 910–916, <https://doi.org/10.1016/j.bbamem.2017.01.036>.
- [54] I.O.L. Bacellar, M.S. Baptista, H.C. Junqueira, M. Wainwright, F. Thalmann, C.M. Marques, A.P. Schröder, Permeability of DOPC bilayers under photoinduced oxidation: Sensitivity to photosensitizer, *Biochim. Biophys. Acta - Biomembr.* 1860 (1860) 2366–2373, <https://doi.org/10.1016/j.bbamem.2018.06.001>.
- [55] K.J. Fritsching, J. Kim, G.P. Holland, Probing lipid-cholesterol interactions in DOPC/eSM/Chol and DOPC/OPPC/Chol model lipid rafts with DSC and 13C solid-state NMR, *Biochim. Biophys. Acta - Biomembr.* 1828 (1828) 1889–1898, <https://doi.org/10.1016/j.bbamem.2013.03.028>.
- [56] P.J. Costa, I. Marques, V. Félix, Interaction of a calix[4]arene derivative with a DOPC bilayer: biomolecular simulations towards chloride transport, *Biochim. Biophys. Acta - Biomembr.* 1813 (1838) 890–901, <https://doi.org/10.1016/j.bbamem.2013.11.021>.
- [57] A. Moschi, O. Orwar, D.T. Chiu, B.P. Modi, R.N. Zare, Rapid preparation of giant unilamellar vesicles, *Proc. Natl. Acad. Sci.* 93 (1996) 11443–11447, <https://doi.org/10.1073/pnas.93.21.11443>.
- [58] A. Šarc, T. Stepišnik Perdih, M. Petkovsek, M. Dular, The issue of cavitation number value in studies of water treatment by hydrodynamic cavitation, *Ultrason. Sonochem.* 34 (2017) 51–59, <https://doi.org/10.1016/j.ultsonch.2016.05.020>.
- [59] T.J. Mason, Ultrasonic cleaning: An historical perspective, *Ultrason. Sonochem.* 29 (2016) 519–523, <https://doi.org/10.1016/j.ultsonch.2015.05.004>.
- [60] R.M. Cornell, U. Schwertmann, The Iron Oxides, Wiley-VCH Verlag GmbH & Co. KGaA, Weinheim, FRG, 2003, doi:10.1002/3527620297.
- [61] H. Sugita, I. Matsunaga, N. Yanagisawa, H. Tao, Y. Tsutsumi, K. Aoki, Effects of pH and Dissolved Ions on Fluorescence Intensity of Sodium Fluorescein, 2003, doi:10.1136/grs.93.21.11447.
- [62] Y. Zhou, R.M. Raphael, Solution pH alters mechanical and electrical properties of phosphatidylcholine membranes: Relation between interfacial electrostatics, intramembrane potential, and bending elasticity, *Biophys. J.* 92 (2007) 2451–2462, <https://doi.org/10.1529/biophysj.106.096362>.
- [63] K.H. de Haas, C. Blom, D. van den Ende, M.H.G. Duits, B. Haveman, J. Mellema, Rheological Behavior of a Dispersion of Small Lipid Bilayer Vesicles, *Langmuir* 13 (1997) 6658–6668, <https://doi.org/10.1021/la970564p>.
- [64] A. Pal, D.V. Khakhar, Breakage of vesicles in a simple shear flow, *Soft Matter* 15 (2019) 1979–1987, <https://doi.org/10.1039/c8sm01501e>.
- [65] E. Saalmann, B. Nordén, L. Arvidsson, Y. Hamnerius, P. Höjevik, K.E. Connell, T. Kurucsev, Effect of 2.45 GHz microwave radiation on permeability of unilamellar liposomes to 5(6)-carboxyfluorescein. Evidence of non-thermal leakage, *Biochim. Biophys. Acta - Biomembr.* 1064 (1991) 124–130, [https://doi.org/10.1016/0005-2736\(91\)90418-8](https://doi.org/10.1016/0005-2736(91)90418-8).
- [66] A.R. Orlando, G. Mossa, G. D’Inzeo, Effect of microwave radiation on the permeability of carbonic anhydrase loaded unilamellar liposomes, *Bioelectromagnetics*, 15 (1994) 303–313, doi:10.1002/bem.2250150405.
- [67] J. Katz, P. Reuter, H. Sagar, B. el Moctar, R. Mettin, Wall Shear Rates Induced by a Single Cavitation Bubble Collapse, in: Proc. 10th Int. Symp. Cavitation. (2019). doi:10.1115/1.861851\_ch208.
- [68] L. Cwiklik, P. Jungwirth, Massive oxidation of phospholipid membranes leads to pore creation and bilayer disintegration, *Chem. Phys. Lett.* 486 (2010) 99–103, <https://doi.org/10.1016/j.cplett.2010.01.010>.
- [69] A. Schroeder, J. Kost, Y. Barenholz, Ultrasound, liposomes, and drug delivery: principles for using ultrasound to control the release of drugs from liposomes, *Chem. Phys. Lipids.* 162 (2009) 1–16, <https://doi.org/10.1016/j.chemphyslip.2009.08.003>.
- [70] M. Pong, S. Umchid, A.J. Guarino, P.A. Lewin, J. Litniewski, A. Nowicki, S.P. Wren, In vitro ultrasound-mediated leakage from phospholipid vesicles, *Ultrasonics* 45 (2006) 133–145, <https://doi.org/10.1016/j.ultras.2006.07.021>.
- [71] D.L. Miller, S.V. Pislaru, J.F. Greenleaf, Sonoporation: Mechanical DNA delivery by ultrasonic cavitation, *Somat. Cell Mol. Genet.* 27 (2002) 115–134, <https://doi.org/10.1023/A:1022983907223>.
- [72] H.Y. Lin, J.L. Thomas, Factors affecting responsivity of unilamellar liposomes to 20 kHz ultrasound, *Langmuir* 20 (2004) 6100–6106, <https://doi.org/10.1021/la049866z>.
- [73] A. Schroeder, Y. Avnir, S. Weisman, Y. Najajreh, A. Gabizon, Y. Talmon, J. Kost, Y. Barenholz, Controlling liposomal drug release with low frequency ultrasound: Mechanism and feasibility, *Langmuir* 23 (2007) 4019–4025, <https://doi.org/10.1021/la0631668>.
- [74] E.F. Small, N.R. Dan, S.P. Wren, Low-frequency ultrasound-induced transport across non-raft-forming ternary lipid bilayers, *Langmuir* 28 (2012) 14364–14372, <https://doi.org/10.1021/la303183b>.
- [75] T. Yamaguchi, M. Nomura, T. Matsuzaka, S. Koda, Effects of frequency and power of ultrasound on the size reduction of liposome, *Chem. Phys. Lipids* 160 (2009) 58–62, <https://doi.org/10.1016/j.chemphyslip.2009.04.002>.
- [76] L. Saunders, J. Perrin, D. Gammie, Ultrasonic irradiation of some phospholipid sols, *J. Pharm. Pharmacol.* 14 (1962) 567–572, <https://doi.org/10.1111/j.2042-7158.1962.tb1141.x>.

Ž. Pandur, et al.

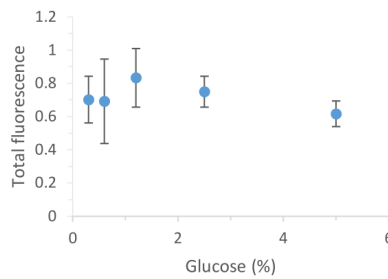
Ultrasonics - Sonochemistry 61 (2020) 104826

- [77] A. Ferrari, Fluid dynamics of acoustic and hydrodynamic cavitation in hydraulic power systems, Proc. R. Soc. A Math. Phys Eng. Sci. 473 (2017), <https://doi.org/10.1098/rspa.2016.0345>.
- [78] V.S. Moholkar, P. Senthil Kumar, A.B. Pandit, Hydrodynamic cavitation for sonochemical effects, Ultrason, Sonochem. 6 (1999) 53–65, [https://doi.org/10.1016/S1350-4177\(98\)00030-3](https://doi.org/10.1016/S1350-4177(98)00030-3).
- [79] J. Park, J. Church, Y. Son, K.T. Kim, W.H. Lee, Recent advances in ultrasonic treatment: Challenges and field applications for controlling harmful algal blooms (HABs), Ultrason. Sonochem. 38 (2017) 326–334, <https://doi.org/10.1016/j.ultsonch.2017.03.003>.
- [80] J. Wang, Z. Wang, C.L.Z. Vieira, J.M. Wolfson, G. Pingtian, S. Huang, Review on the treatment of organic pollutants in water by ultrasound technology, Ultrason.
- Sonochem. (2019), <https://doi.org/10.1016/j.ultsonch.2019.01.017>.
- [81] Y.L. Chen, H.H. Chang, Y.C. Chiang, C.P. Lin, Application and development of ultrasonics in dentistry, J. Formos. Med. Assoc. 112 (2013) 659–665, <https://doi.org/10.1016/j.jfma.2013.05.007>.
- [82] P.R. Gogate, A.M. Kabadi, A review of applications of cavitation in biochemical engineering/biotechnology, Biochem. Eng. J. 44 (2009) 60–72, <https://doi.org/10.1016/j.bej.2008.10.006>.
- [83] No Title, (n.d.). doi:10.1111/jfpe.13144.
- [84] C.R. Holkar, A.J. Jadhav, D.V. Pinjari, A.B. Pandit, Cavitationally Driven Transformations: A Technique of Process Intensification, Ind. Eng. Chem. Res. 58 (2019) 5797–5819, <https://doi.org/10.1021/acs.iecr.8b04524>.

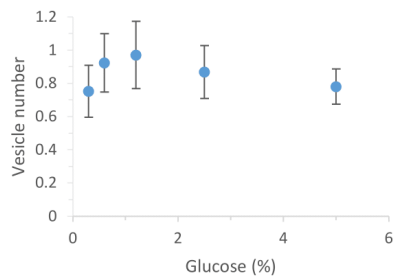
1    **Supplementary material**



A

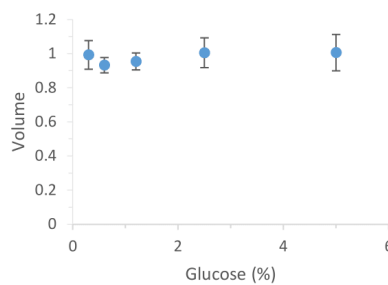


B

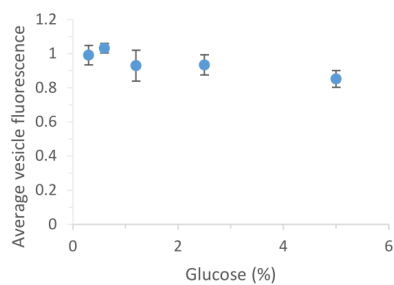


13

C



D

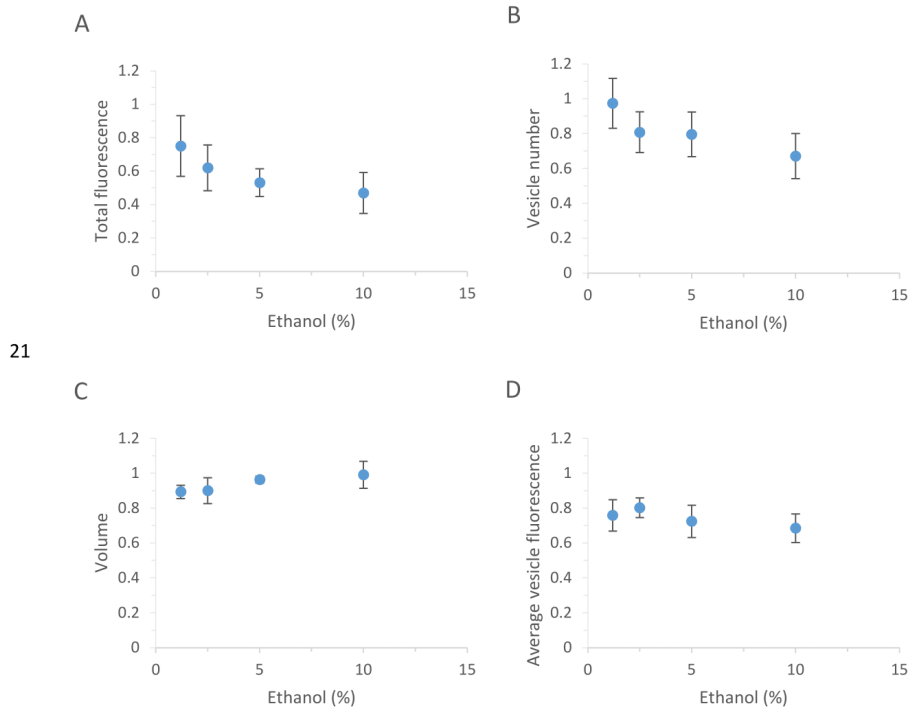


14

15 Supplementary Fig. S2: Addition of different glucose concentrations to DOPC vesicles: (A)  
16 shows relative amount of total fluorescence in vesicles, (B) shows relative number of  
17 fluorescein labelled vesicles, (C) shows relative average volume of vesicle and (D) shows

18

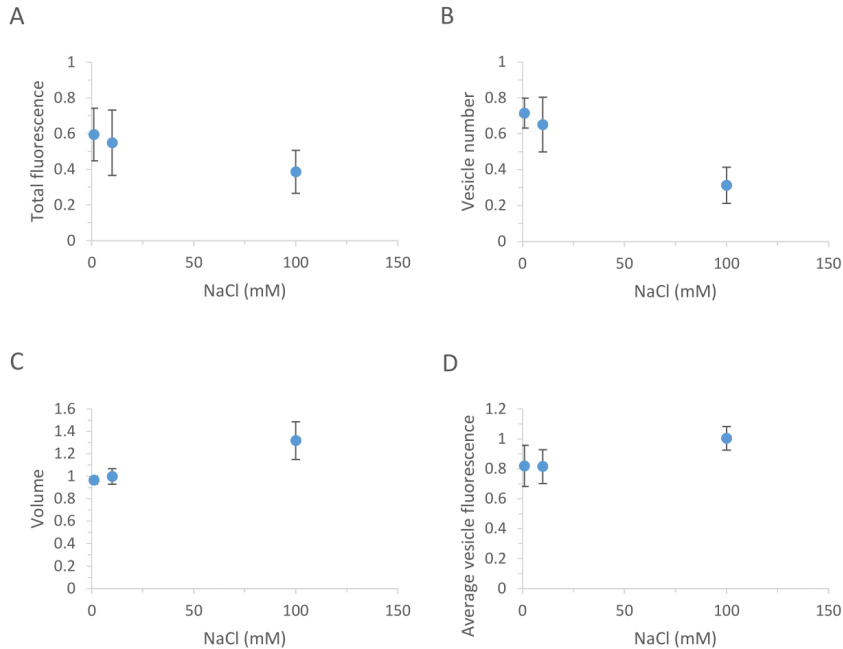
19 relative average fluorescence intensity of vesicle. Results represent relative values which were  
20 compared to sample before treatment. Error bars represent standard error ( $n = 5$ ).



21

22

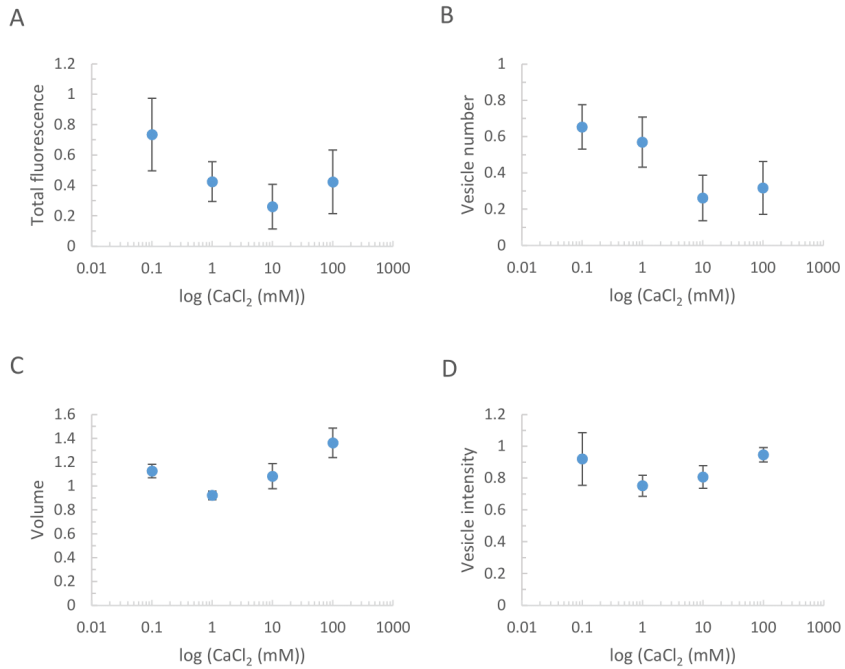
23     Supplementary Fig. S3: Addition of different ethanol concentrations to DOPC vesicles: (A)  
24     shows relative amount of total fluorescence in vesicles, (B) shows relative number of  
25     fluorescein labelled vesicles, (C) shows relative average volume of vesicle and (D) shows  
26     relative average fluorescence intensity of vesicle. Results represent relative values which were  
27     compared to sample before treatment. Error bars represent standard error (n = 5).



28

29

30     Supplementary Fig. S4: Addition of different NaCl concentrations to DOPC vesicles: (A) shows  
31     relative amount of total fluorescence in vesicles, (B) shows relative number of fluorescein  
32     labelled vesicles, (C) shows relative average volume of vesicle and (D) shows relative average  
33     fluorescence intensity of vesicle. Results represent relative values which were compared to  
34     sample before treatment. Error bars represent standard error ( $n = 4$ ).



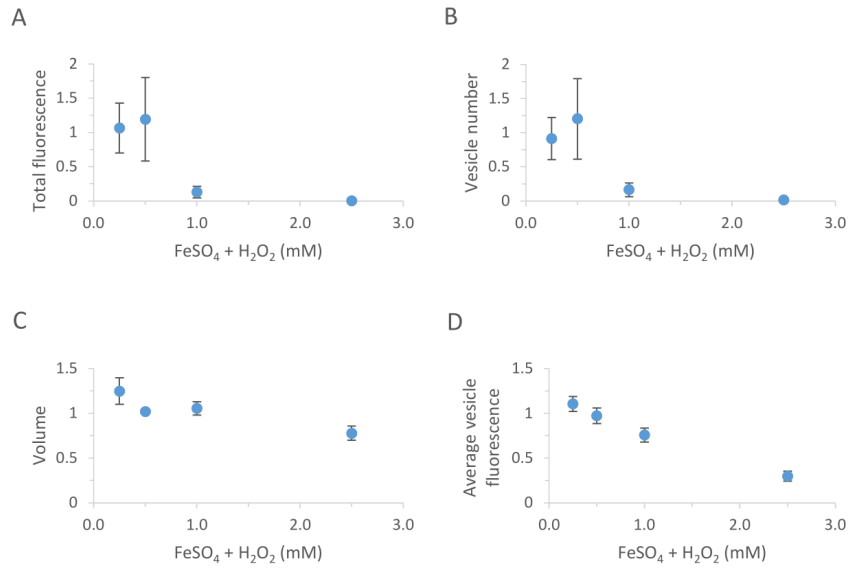
35

36

37

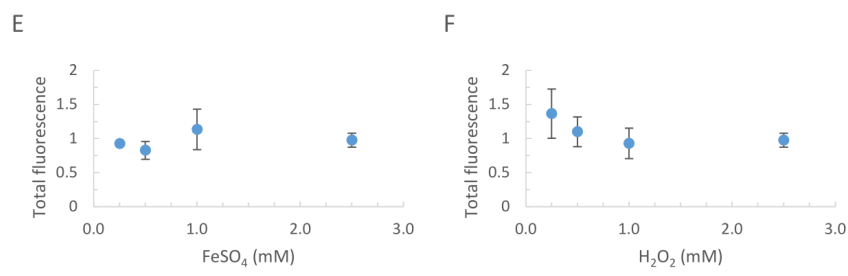
Supplementary Fig. S5: Addition of different CaCl<sub>2</sub> concentrations to DOPC vesicles: (A) shows relative amount of total fluorescence in vesicles, (B) shows relative number of fluorescein labelled vesicles, (C) shows relative average volume of vesicle and (D) shows relative average fluorescence intensity of vesicle. Results represent relative values which were compared to sample before treatment. Error bars represent standard error (n = 4).

42



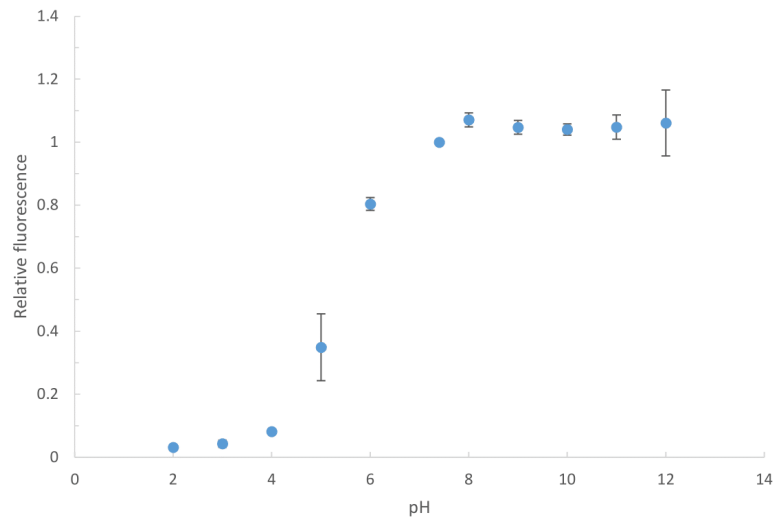
43

44



45

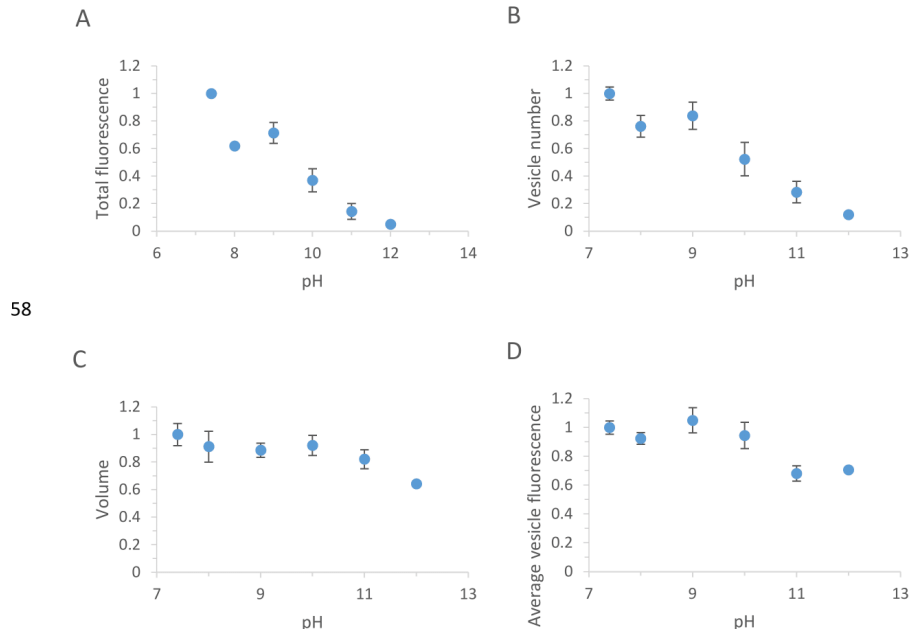
Supplementary Fig. S6: Addition of different  $\text{FeSO}_4$  and  $\text{H}_2\text{O}_2$  concentrations to DOPC vesicles: (A) shows relative amount of total fluorescence in vesicles, (B) shows relative number of fluorescein labelled vesicles, (C) shows relative average volume of vesicle and (D) shows relative average fluorescence intensity of vesicle. Error bars represent standard error for graphs A-D ( $n = 4$ ). Ratio between  $\text{FeSO}_4$  and  $\text{H}_2\text{O}_2$  was 1:1. (E) shows relative amount of total fluorescence in vesicles for addition of  $\text{FeSO}_4$  and (F) shows relative amount of total fluorescence in vesicles for addition of  $\text{H}_2\text{O}_2$ . E and F graph represents results of single experiment. Results represent relative values which were compared to sample before treatment.



53

54 Supplementary Fig. S7: Fluorescein stability at different pH in aqueous solution. The  
55 fluorescence intensity is normalized relative to control of pH 7.4. Error bars represent standard  
56 error ( $n = 3$ ).

57

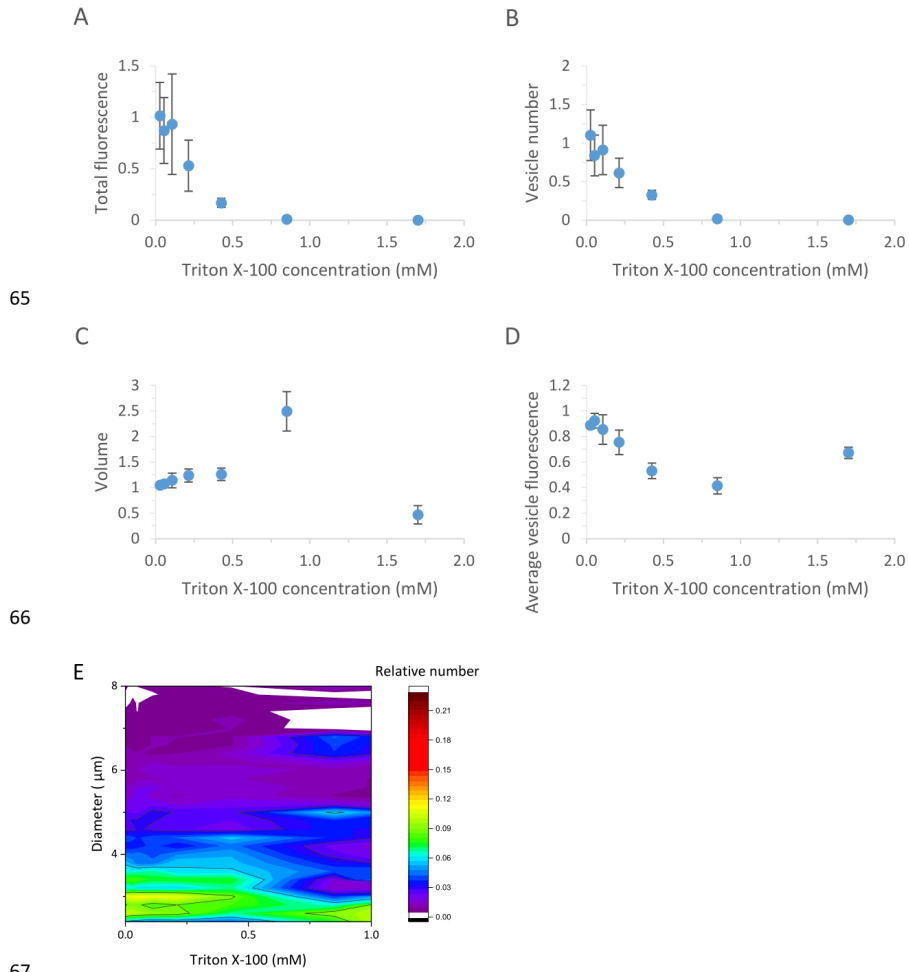


58

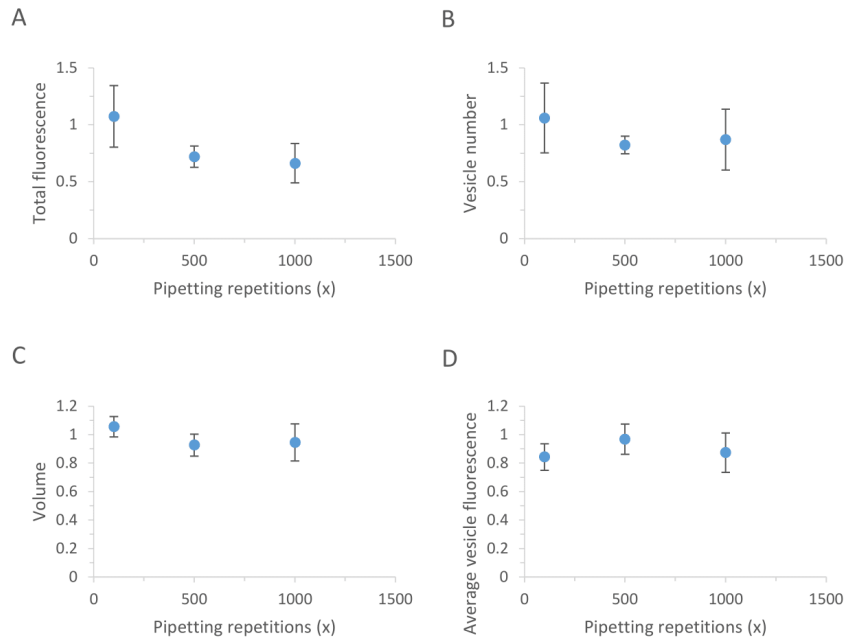
C

59

- 60   Supplementary Fig. S8: Effect of pH on DOPC vesicle integrity: (A) shows relative amount of  
61   total fluorescence in vesicles, (B) shows relative number of fluorescein labelled vesicles, (C)  
62   shows relative average volume of vesicle and (D) shows relative average fluorescence of  
63   vesicle. The relative total fluorescence intensity is normalized relative to control of pH 7.4.  
64   Error bars represent standard error ( $n = \text{at least } 5 \text{ or more}$ ).



65  
66  
67  
68      Supplementary Fig. S9: Effect of Triton X-100 addition on DOPC vesicles: (A) shows relative amount of total fluorescence in vesicles, (B) shows relative number of fluorescein labelled vesicles, (C) shows relative average volume of vesicle, (D) shows relative average fluorescence intensity of vesicle and (E) shows fractions of vesicle size distribution – there are represented results from 0 to 0.85 mM concentration as in highest (1.7 mM) concentration of Triton X-100 was too small population of vesicle for distribution analysis (less than 10 vesicles). Results represent relative values which were compared to sample before treatment. Error bars represent standard error (graph A-C, n = 4).



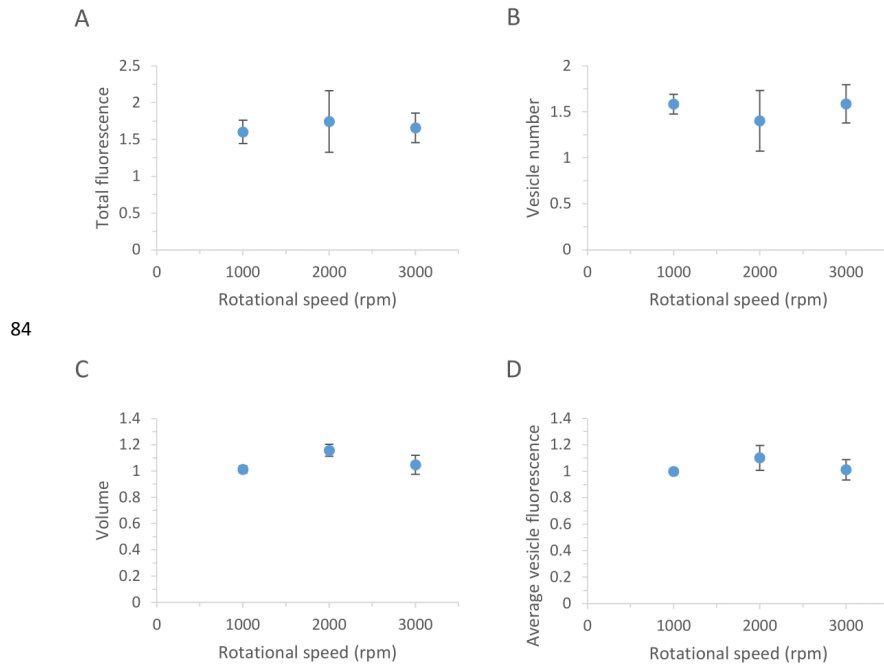
76

C

77

78     Supplementary Fig. S10: Effect of pipetting on DOPC vesicles: (A) shows relative amount of  
79     total fluorescence in vesicles, (B) shows relative number of fluorescein labelled vesicles, (C)  
80     shows relative average volume of vesicle and (D) shows relative average fluorescence of  
81     vesicle. Results represent relative values which were compared to sample before treatment.  
82     Error bars represent standard error ( $n = 4$ ).

83



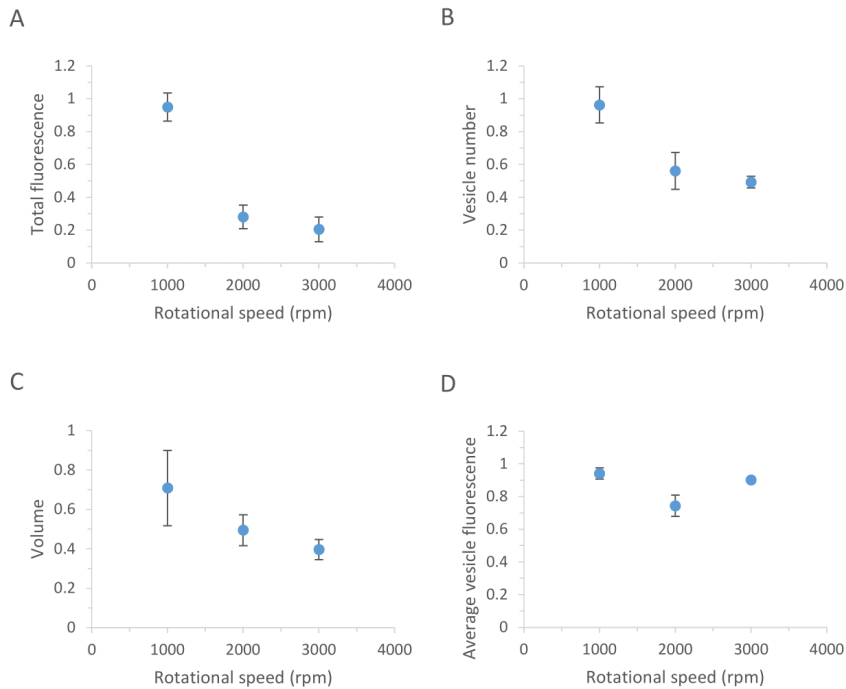
84

C

85

86 Supplementary Fig. S11: Effect of vortex mixing on DOPC vesicles: (A) shows relative amount  
87 of total fluorescence in vesicles, (B) shows relative number of fluorescein labelled vesicles, (C)  
88 shows relative average volume of vesicle and (D) shows relative average fluorescence of  
89 vesicle. All experiments were vortex mixed for 4 min. Results represent relative values which  
90 were compared to sample before treatment. Error bars represent standard error ( $n = 4$ ).

91



92

C

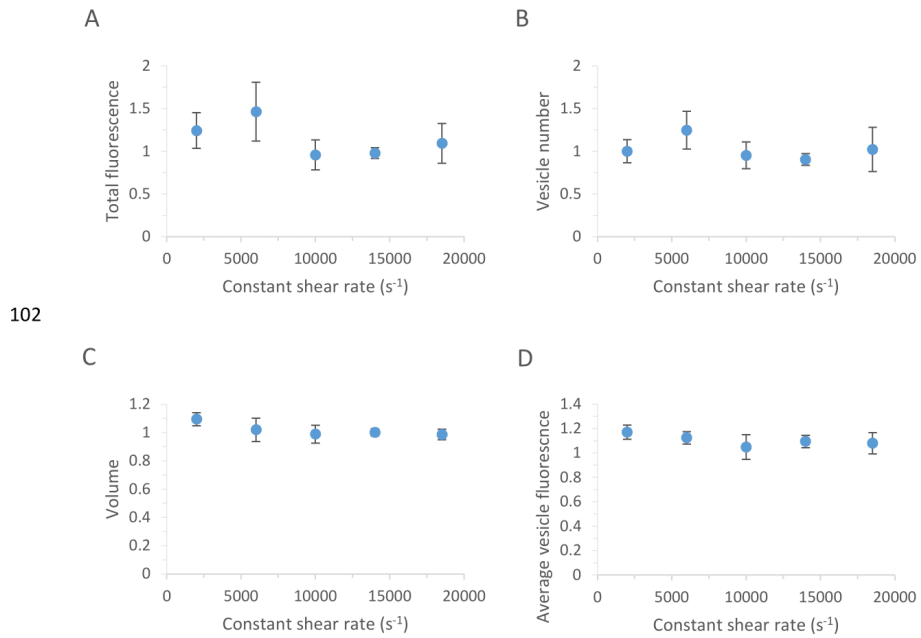
D

93

94

95     Supplementary Fig. S12: Effect of vortex mixing with glass beads on DOPC vesicles: (A)  
96     shows relative amount of total fluorescence in vesicles, (B) shows relative number of  
97     fluorescein labelled vesicles, (C) shows relative average volume of vesicle and (D) shows  
98     relative average fluorescence of vesicle. All experiments were vortex mixed for 4 min. Results  
99     represent relative values which were compared to sample before treatment. Error bars represent  
100    standard error (n = 4).

101



102

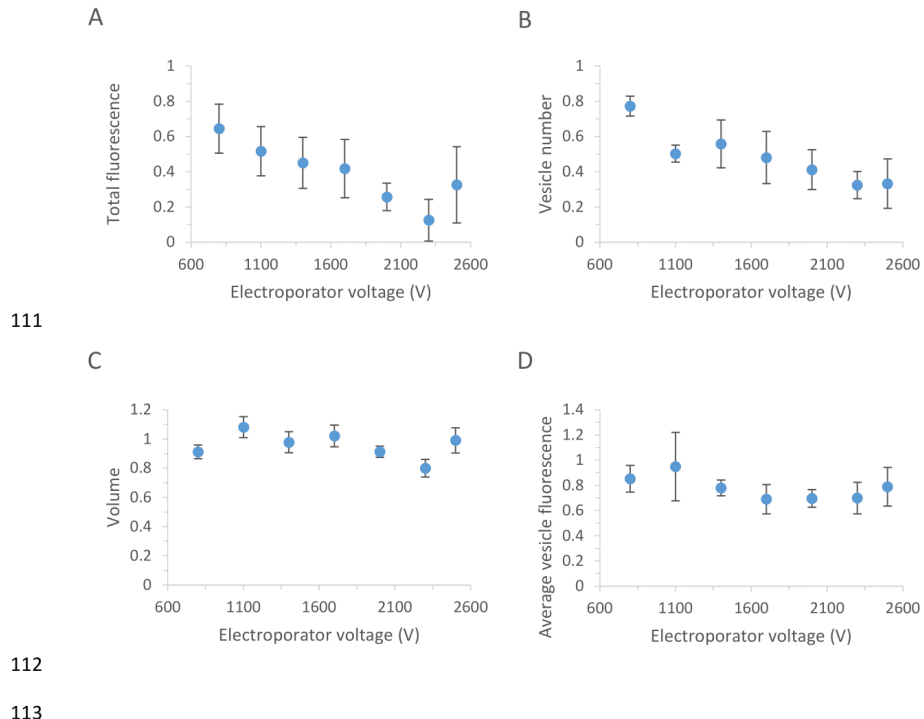
C

103

104     Supplementary Fig. S13: Effect of rotational shear stress on DOPC vesicles: (A) shows relative  
105     amount of total fluorescence in vesicles, (B) shows relative number of fluorescein labelled  
106     vesicles, (C) shows relative average volume of vesicle and (D) shows relative average  
107     fluorescence of vesicle. Results represent relative values which were compared to sample  
108     before treatment. Error bars represent standard error (n = 4).

109

110



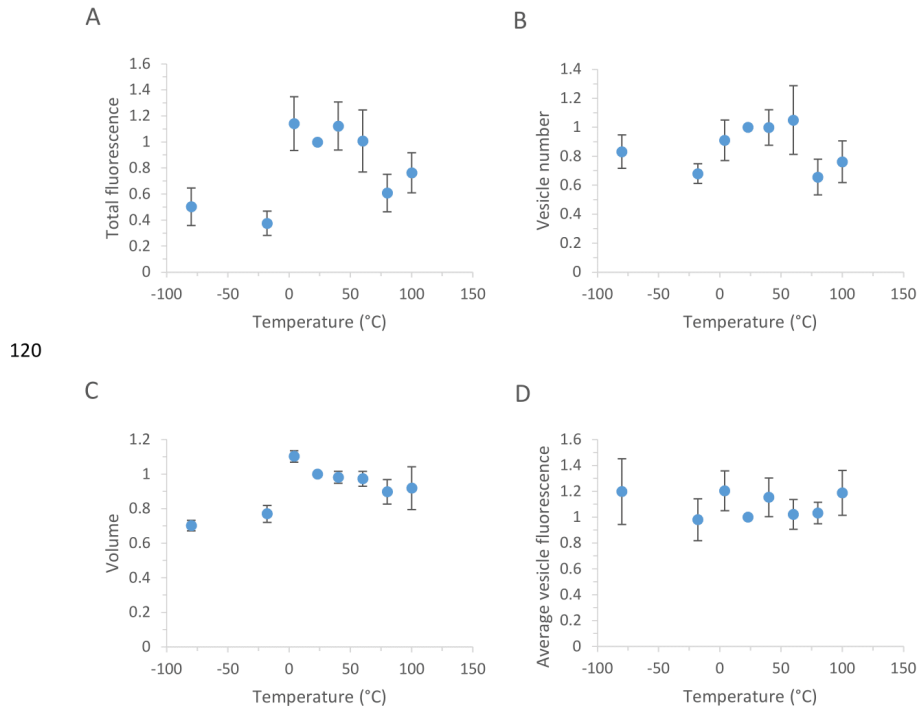
111

112

113

114     Supplementary Fig. S14: Effect of electroporation in DOPC vesicles: (A) shows relative  
115     amount of total fluorescence in vesicles, (B) shows relative number of fluorescein labelled  
116     vesicles, (C) shows relative average volume of vesicle and (D) shows relative average  
117     fluorescence of vesicle. Results represent relative values which were compared to sample  
118     before treatment. Error bars represent standard error ( $n = 4$ ).

119

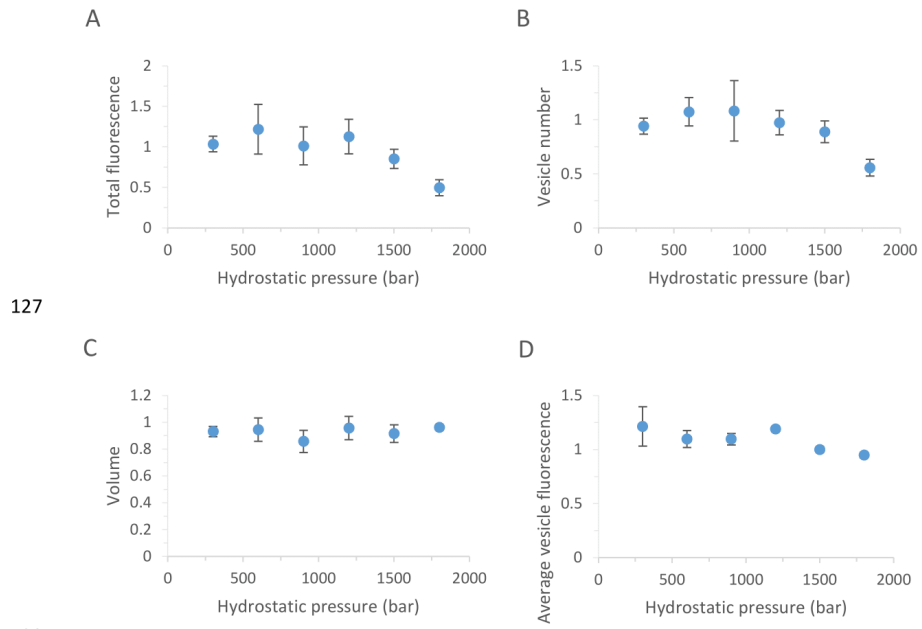


120

121

121

122     Supplementary Fig. S15: Effect of different temperature on DOPC stability: (A) shows relative  
123     amount of total fluorescence in vesicles, (B) shows relative number of fluorescein labelled  
124     vesicles, (C) shows relative average volume of vesicle and (D) shows relative average  
125     fluorescence of vesicle. Results represent relative values which were compared to sample  
126     before treatment. Error bars represent standard error ( $n = 4$ ).



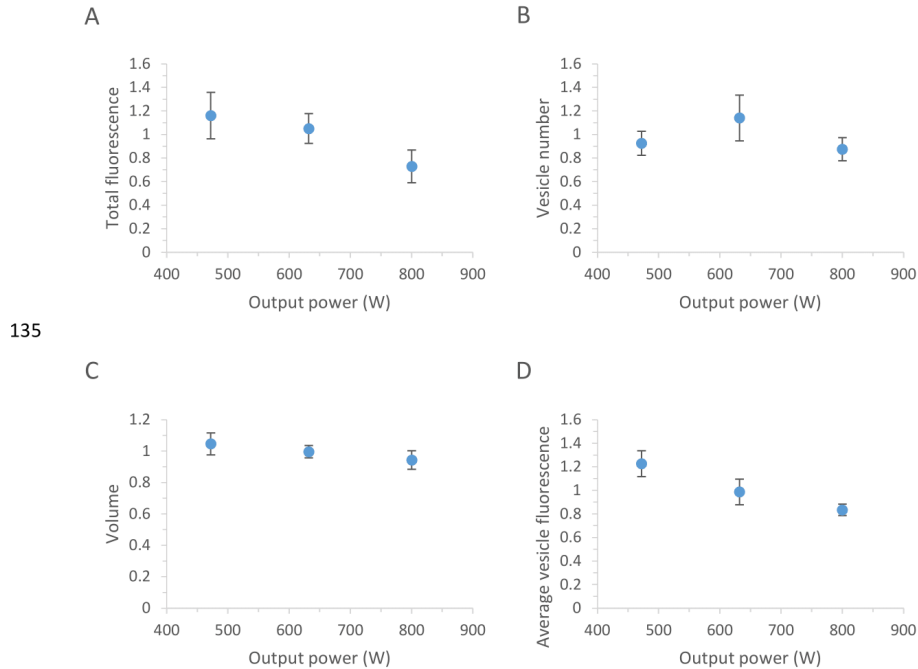
127

C

128

129     Supplementary Fig. S16: Effect of hydrostatic pressure on DOPC vesicles: (A) shows relative  
130 amount of total fluorescence in vesicles, (B) shows relative number of fluorescein labelled  
131 vesicles, (C) shows relative average volume of vesicle and (D) shows relative average  
132 fluorescence of vesicle. Results represent relative values which were compared to sample  
133 before treatment. Error bars represent standard error ( $n = 4$ ).

134



135

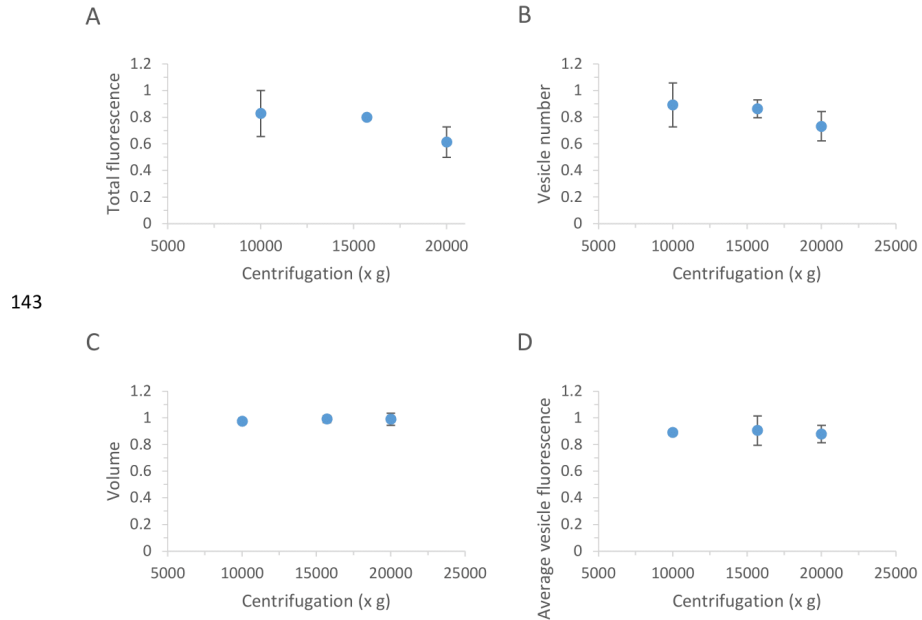
C

136

137     Supplementary Fig. S17: Effect of microwaves on DOPC vesicles: (A) shows relative amount  
138     of total fluorescence in vesicles, (B) shows relative number of fluorescein labelled vesicles, (C)  
139     shows relative average volume of vesicle and (D) shows relative average fluorescence of  
140     vesicle. Error bars represent standard error ( $n = 4$ ).

141

142



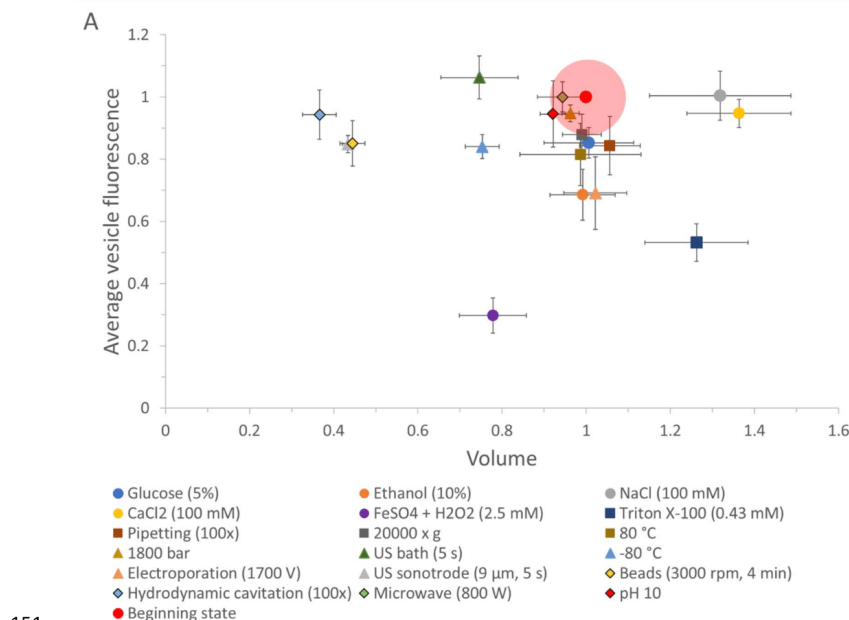
143

C

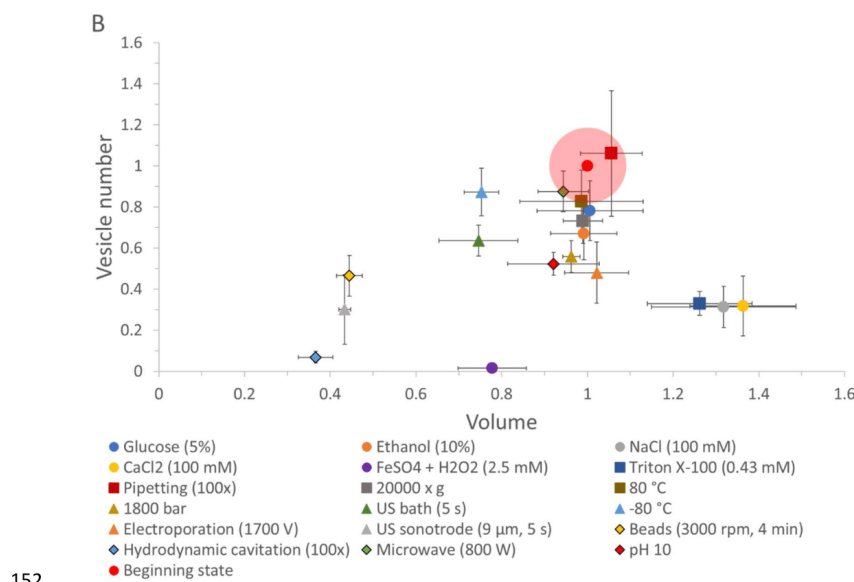
144

145 Supplementary Fig. S18: Effect of centrifugation on DOPC vesicles: (A) shows relative amount  
146 of total fluorescence in vesicles, (B) shows relative number of fluorescein labelled vesicles,  
147 (C) shows relative average volume of vesicle and (D) shows relative average fluorescence of  
148 vesicle. Results represent relative values which were compared to sample before treatment.  
149 Error bars represent standard error ( $n = 3$ ).

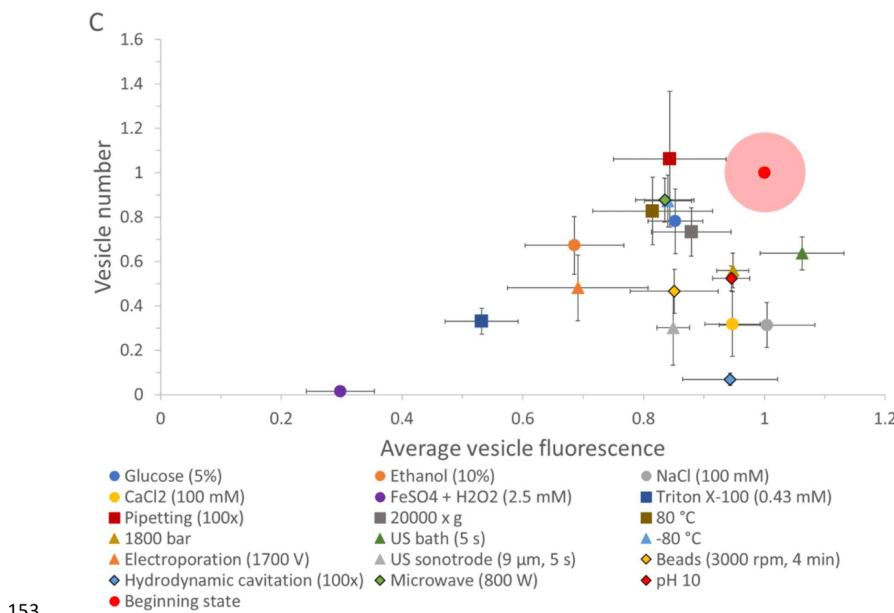
150



151



152



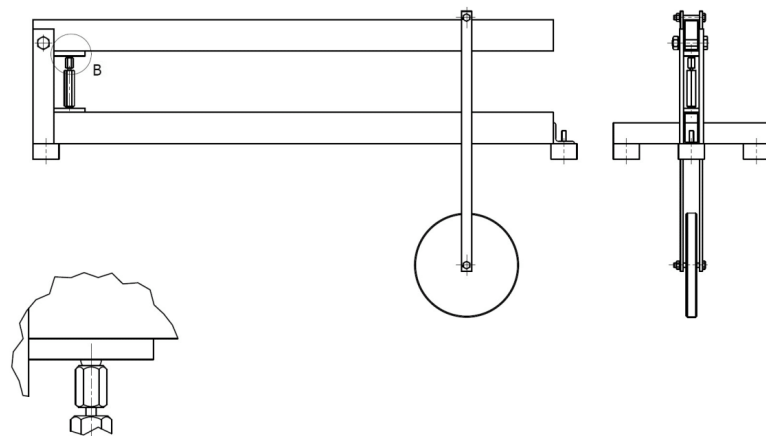
153

154      Supplementary Fig. S19: The effect of different environmental stressors on the stability of  
155      DOPC giant lipid vesicles. Only the largest value for the given chemical, physical or mechanical  
156      stressor are given. For the effect of other values of physico-chemical stressors one should look  
157      into the Supplementary Fig. S1 to S19. (A) relative vesicle volume : relative fluorescence  
158      intensity; (B) relative vesicle volume : relative vesicle number; (C) relative vesicle fluorescence  
159      intensity : relative vesicle number. Error bars represent standard error ( $n = 4$  or larger). Red dot  
160      represents the control lipid vesicle state before treatment with different physic-chemical  
161      stressors with the estimated experimental error (shaded red area).

162

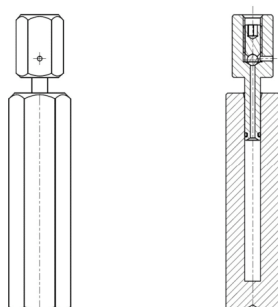
163

A



164

B

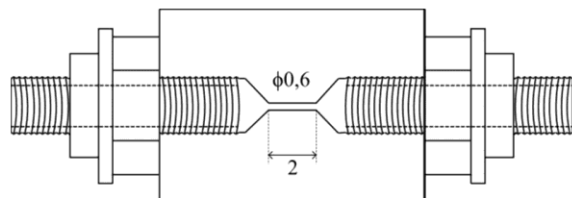


165

166    Supplementary Fig. S20: Hydrostatic pressure test rig. (A) shows whole compression unit with  
167    weights and in (B) is presented compression chamber for liquid sample of small volume.

168

169



170 Supplementary Fig. S21: Venturi restriction (0,6 mm diameter) scheme. All dimensions are in  
171 mm. It was coupled with 10 mL syringes to create hydrodynamic cavitation phenomena.

### **2.1.2 Študija morfologije gigantskih veziklov v neravnovesnih okoljih z Monte Carlo metodo**

Drab M., Pandur Ž., Penič S., Iglič A., Kralj-Iglič V., Stopar D. 2021. A Monte Carlo study of giant vesicle morphologies in nonequilibrium environments. Biophysical Journal, 120, 20: 4418-4428.

Izvleček:

Lipidni vezikli so mehke dinamične strukture. Predstavljajo najbolj enostavni model za študij stresnih vplivov okolja na biološke celice, vendar je njihovo morfološko proučevanje zaradi izrazito hitre dinamike med delovanjem stresnega dejavnika zelo oteženo. V tem delu smo razvili model za proučevanje morfoloških sprememb med delovanjem okoljskega stresorja. Lipidne vezikle smo *in situ* po izpostavljenosti kemijskemu stresorju morfološko okarakterizirali v realnem času z uporabo konfokalne laserske vrstične mikroskopije. Pokazali smo, da se je lipidni vezikel iz sferične oblike preobrazil v nesferične oblike, ki so spominjale na hruškaste oblik veziklov, uvhavanje veziklov, pojav večjega števila izrastkov (nanotub). Med posameznimi morfološkimi oblikami je prihajalo do hitre interkonverzije. Eksperimentalne rezultate dinamike oblik veziklov smo nato razložili z matematično analizo. S simulacijami po metodi Monte Carlo smo konstruirali 3D mrežo dvosloja, ki jeupoštevala postopno vgrajevanje molekul detergenta v lipidni dvosloj. Predpostavili smo, da je glavni vzrok za morfološke spremembe vezikla sprememba spontane ukrivljenosti membrane zaradi invertno konično oblikovanih molekul detergenta. Numerični rezultati se skladajo z eksperimentalnimi rezultati kar potrjuje primernost modela, ki nam omogoča vpogled v silovito dinamiko veziklov. Zaradi hitre dinamike in neravnovesnih sprememb je takšne spremembe težko proučevati, zato je v veliko pomoč matematičen model, ki omenjen pojav natančno popiše. Rezultati kažejo, da je z zunanjimi vplivi (kemijskimi ali mehanskimi) možno pognati membrano v visoko amplitudne oscilacije, ki imajo katastrofalne posledice za lipidni dvosloj.

## A Monte Carlo study of giant vesicle morphologies in nonequilibrium environments

Mitja Drab,<sup>1,2,\*</sup> Žiga Pandur,<sup>3</sup> Samo Penič,<sup>4</sup> Aleš Iglič,<sup>1,2</sup> Veronika Kralj-Iglič,<sup>2,5</sup> and David Stopar<sup>3</sup>

<sup>1</sup>Laboratory of Physics, Faculty of Electrical Engineering, <sup>2</sup>Laboratory of Clinical Biophysics, Faculty of Medicine, <sup>3</sup>Department of Food Science and Technology, Biotechnical Faculty, <sup>4</sup>Laboratory of Bioelectromagnetics, Faculty of Electrical Engineering, and <sup>5</sup>Laboratory of Clinical Biophysics, Faculty of Health Sciences, University of Ljubljana, Ljubljana, Slovenia

**ABSTRACT** It is known that giant vesicles undergo dynamic morphological changes when exposed to a detergent. The solubilization process may take multiple pathways. In this work, we identify lipid vesicle shape dynamics before the solubilization of 1,2-dioleoyl-sn-glycero-3-phosphocholine giant vesicles with Triton X-100 (TR) detergent. The violent lipid vesicle dynamics was observed with laser confocal scanning microscopy and was qualitatively explained via a numerical simulation. A three-dimensional Monte Carlo scheme was constructed that emulated the nonequilibrium conditions at the beginning stages of solubilization, accounting for a gradual addition of TR detergent molecules into the lipid bilayers. We suggest that the main driving factor for morphology change in lipid vesicles is the associative tendency of the TR molecules, which induces spontaneous curvature of the detergent inclusions, an intrinsic consequence of their molecular shape. The majority of the observed lipid vesicle shapes in the experiments were found to correspond very well to the numerically calculated shapes in the phase space of possible solutions. The results give an insight into the early stages of lipid vesicle solubilization by amphiphilic molecules, which is nonequilibrium in nature and very difficult to study.

**SIGNIFICANCE** This study reports on dynamic morphology changes of 1,2-dioleoyl-sn-glycero-3-phosphocholine lipid vesicles in the presence of detergent Triton X-100 and presents a novel, to our knowledge, three-dimensional Monte Carlo scheme that offers insight into the observed shape changes based on molecular geometry of amphiphiles in nonequilibrium environments.

### INTRODUCTION

Lipid vesicles are soft spherical structures. Under nonequilibrium conditions, driven by the influx of materials and energy, fascinating vesicle dynamic behavior has been observed, such as 1) tumbling, in which a vesicle undergoes a periodic flipping motion; 2) trembling, in which vesicle shape fluctuates and the orientation oscillates in time; and 3) tank treading, in which an ellipsoid vesicle's major axis maintains a fixed orientation with respect to the flow direction while the membrane rotates about the vorticity axis (1). The transitions between these dynamical modes depend on shear rate, viscosity ratio between the inner and outer fluid viscosities, and reduced volume, which is a measure of a vesicle's asphericity (2). Different morphological patterns may emerge in gradual and rapid environmental changes

even between the identical initial and final equilibrium states.

In this work, we will show that extensive lipid vesicle reshaping can be induced with the addition of detergent molecules. The detergent reshaping of lipid vesicle can lead to vesiculation and solubilization (3,4). Previously, shape transformations with a varying degree of similarity were observed when vesicles were exposed to baths of oleic or fatty acids (5,6), but the mechanisms of dynamic changes were not considered.

Phospholipids self-assemble in a way that prevents exposure of their hydrophobic moieties to water (7). A lipid vesicle is composed of two flexible layers of phospholipids in which, in an aqueous solution, polar headgroups are oriented outward facing the solution and the hydrophobic tails of the two layers are facing each other. Two factors primarily govern whether a lipid will form a stable bilayer: solubility and molecular shape. For self-assembled structures such as bilayers, the lipid should have low solubility in water, which can be described as a low critical micelle concentration (8,9).

Submitted March 22, 2021, and accepted for publication September 2, 2021.

\*Correspondence: mitja.drab@fe.uni-lj.si

Editor: Rumiana Dimova.

<https://doi.org/10.1016/j.bpj.2021.09.005>

© 2021 Biophysical Society.

4418 Biophysical Journal 120, 4418–4428, October 19, 2021



Above the critical micelle concentration, lipid molecules aggregate and form larger structures such as micelles, inverted micelles, or bilayers (10). The propensity for a lipid bilayer depends on shape of the lipid molecule (9,11–13). If a particular lipid monolayer structure has too large a deviation from zero spontaneous curvature, it will not form a lipid bilayer (14). Neglecting the anisotropy of the shape of lipid molecules (15,16), phospholipids such as phosphatidylethanolamine, phosphatic acid, diacylglycerol, and cardiolipin have a small polar headgroup/acyl chain ratio, which makes them roughly inverted conical in (dynamic) shape, which in turn imposes a negative monolayer curvature. Monolayers with these lipids bend in such a way that the headgroups come closer together and do not form lipid bilayers. Conversely, lipids with a large headgroup/acyl chain ratio, such as lysophosphatidylcholine or the large headgroups in phosphatidylinositol phosphates, that confers a conical shape to the lipids thereby favor the bending of the membrane into a positive curvature, bending the monolayer away from the headgroups (7,9,13). On the other hand, phosphatidylcholine and phosphatidylserine are cylindrical lipids that form a flat monolayer and consequently have a large propensity for lipid bilayers.

Introducing a conical or inverted-conical molecule into the lipid bilayer, such as a detergent, introduces stress. The partition coefficient that describes the detergent equilibrium between the bilayer and the aqueous solution is governed by the hydrophobicity of the detergent and its shape. The detergents are curvophilic, i.e., they have a tendency to form a positive spontaneous curvature (17). Curvophilic molecules are known to accumulate in the curved regions of bilayers, where the membrane inclusions may stabilize a hydrophilic pore (18), initiate a growth of tunnelling nanotubes (19–22), and affect endovesiculation (23,24) or membrane remodeling (25,26). It is hypothesized that incorporation of detergents and their association in the membrane will locally deform lipid bilayer structure by increasing positive local curvature of the binary mixture. More ordered membranes, such as those rich in long-saturated lipids and cholesterol, are less sensitive to solubilization (27).

In this work, we demonstrate a violent lipid vesicle dynamics and reshaping upon introduction of Triton X-100 (TR) detergent before giant 1,2-dioleoyl-*sn*-glycero-3-phosphocholine (DOPC) lipid vesicle solubilization. Shape changes were observed with confocal laser scanning fluorescence microscopy. The rates of flip-flop are known to be slow for artificial membranes, and thus, we assume that the induced spontaneous curvature is the prevailing mechanism driving shape change (28). Using Monte Carlo simulations, we show that vesicle reshaping can be reliably predicted by two parameters only: the concentration of the detergent incorporated into the lipid bilayer and the affinity between the curvophilic detergent molecules.

## MATERIALS AND METHODS

### Preparation of giant lipid vesicles

Giant DOPC lipid vesicles (GVs) were prepared by applying a rapid evaporation method as described by Moscho et al. (29). Briefly, DOPC was dissolved in chloroform to a concentration of 0.1 M. Then, 115  $\mu$ L of lipid solution was transferred into a 250 mL round-bottom flask containing 5.6 mL chloroform and 572  $\mu$ L methanol. Next, 40 mL buffer solution (10 mM HEPES buffer (pH 7.4)) with added fluorescein sodium salt (Thermo Fisher Scientific, Waltham, MA (0.3 mg/mL)) was carefully added along the flask walls to the lipid solution. Organic solvent was removed with a rotary evaporator (Büchi Rotavapor R-134, Büchi Waterbath B-480, Büchi Vacuum Controller V-850, Büchi Vacuum pump V-700; Büchi, Zagreb, Croatia) at 40 rotations per minute under reduced pressure (final pressure 55 mbar, volume flow rate 1.8  $\text{m}^3/\text{h}$ ) in a water bath with temperature set at 40°C. Around the evaporation point of chloroform and methanol, we slowly reduced the pressure in 5 mbar increments to reach a gentle boiling point of solution. After reaching the final pressure of 55 mbar, the solution is left there for 2 min. In the next step, we separated vesicle fraction from the aqueous solution and excess fluorescein with centrifuging at 15,700  $\times g$  for 10 min. Lipid vesicles in the pellet were resuspended in 40 mL 10 mM HEPES buffer. We repeated lipid vesicle washing three times, and after the third time, vesicles were concentrated into 5 mL HEPES buffer. For all experiments, the vesicles were freshly prepared. We used either fluorescein or rhodamine B as contrast agents packed in lipid vesicles. The final concentration of rhodamine B in 10 mM HEPES solution was 6 mg/mL. For vesicle membrane labeling, we used 3,3'-dioctyloxacarbocyanine perchlorate (DiO) lipophilic carbocyanine green fluorescent stain. Membrane-labeled vesicles were prepared as described above, with addition of 0.1 mol % DiO stain to DOPC mixture.

### Turbidity assay

A turbidity assay was performed as described by Ahyauch et al. (30). Shortly, in a 96-well microtiter plate, 90  $\mu$ L of vesicle solution was mixed with 10  $\mu$ L of TR. The final detergent concentration gradient ranged from 0.03 to 1.7 mM. The mixtures were left to equilibrate for 10 min at room temperature, and solubilization was assessed from the changes in turbidity (Optical Density at 650 nm, OD650) and medium fluorescence intensity (excitation: 500 nm; emission: 530 nm). Measurements were made with a Bitek Cytaion 3 microplate reader (BiTek, Winooski, VT).

### Microscopy

DOPC GVs were exposed to TR detergent under the microscope and monitored online to capture early lipid vesicle dynamics. In the experiments, the concentration of GVs was between  $10^6$  and  $10^7$  vesicles/mL. All experiments were made under ambient conditions (room temperature, ambient air pressure). 9  $\mu$ L of vesicle solution was pipetted onto a #1.5 microscope coverglass to form a hemispheric drop after positioning and focusing the solution on the microscope, which was  $\sim 1 \mu\text{L}$  of appropriate TR solution (final concentrations of TR were  $\sim 0.2$  mM). Image acquisition started right after the addition of detergent.

Dynamics of lipid solubilization with TR was visualized with laser microscope fluorescence microscope Zeiss Axio Observer Z1 equipped with confocal unit LSM 800 (Carl Zeiss, Oberkochen, Germany). Fluorescein, rhodamine B, and DiO were excited with 488 nm laser wavelength. Image acquisition was under an immersion oil 100 $\times$  objective with additionally cropped view range. Because the vesicles were freely moving in a drop of solution and occasionally went out of focus, manual vesicle tracking was needed to acquire the full sequence of vesicle dynamics. For visualization of vesicle response to subsolubilization detergent concentration, critical micellar concentrations, and supercritical detergent concentrations, a 20 $\times$  objective was used.

Drab et al.

### Theoretical model

When phospholipids can be idealized as a cylinder, as is the case for DOPC, the molecular volume is approximately equal to the product of the polar surface cross area and length of the hydrophobic chain. The packing parameter ( $p$ ) is then equal to 1 (9). Such amphiphiles are likely to form self-assembled flat bilayers because such packing entails a minimal exposure of hydrophobic chains to water. The molecular structure of TR, like most detergents, can be idealized as a cone. The volume of such a conical molecule is less than the product of the polar surface cross area and the length of the extended chain; therefore, its packing parameter is less than 1 (31). The exposure of hydrophobic chains is minimal when curved micelles are formed. A micelle has a spontaneous curvature that is by definition positive.

When phospholipid bilayers are mixed with a detergent, the two components are forced by entropy to reside in mixed aggregates. Before being solubilized, the bilayers retain their lamellar structure, but as the detergent/lipid ratio in the bilayers increases, detergent molecules agglomerate, leading to local membrane undulations.

In this model, the energy of a lipid vesicle is expressed as the sum of contributions of membrane bending and direct interactions between detergent inclusions (DI) embedded into the lipid membrane:

$$W = W_b + W_i, \quad (1)$$

where  $W_b$  is membrane bending energy and  $W_i$  is interaction between detergents. For the membrane bending energy, the standard Helfrich expression is used (32):

$$W_b = \frac{\kappa}{2} \int_A (C_1 + C_2 - C_0)^2 dA, \quad (2)$$

where the integral runs over the whole area of the membrane with bending stiffness  $\kappa$ ,  $C_1$  and  $C_2$  are the two principal curvatures, and  $C_0$  is the spontaneous curvature of the DI. On the patches occupied by the DIs, we therefore set  $C_0 = c_0$ , and elsewhere, we assume a symmetric membrane  $C_0 = 0$ . The DIs on the membrane are therefore modeled as isotropic patches of the membrane with given spontaneous curvature  $c_0$  (33–35). For patches occupied by the DIs, we set  $c_0 > 0$  because the positive sign of  $c_0$  means that the inclusions have a tendency to curve the membrane outwards. For direct interactions between neighboring DIs, we assume the step potential

$$W_i = -w \sum_{i < j} \mathcal{H}(r_0 - r_{ij}), \quad (3)$$

where  $w$  is a direct interaction constant, the sum runs over all DI pairs,  $r_{ij}$  are their mutual in-plane distances,  $\mathcal{H}(r)$  is the Heaviside step function, and  $r_0$  is the range of the direct interaction. We consider here attractive interactions  $w > 0$  that induce phase separation of the lipid bilayer (36).

### Monte Carlo simulations

The membrane is represented by a set of  $N$  vertices that are linked by tethers of variable length  $l$  to form a closed, dynamically triangulated, self-avoiding two-dimensional network of  $\sim 2N$  triangles and with the topology of a sphere (37,38). The lengths of the tethers can vary between a minimal and a maximal value,  $l_{min}$  and  $l_{max}$ , respectively. Self-avoidance of the network is ensured by choosing the appropriate values for  $l_{max}$  and the maximal displacement of the vertex  $s$  in a single updating step.

One Monte Carlo sweep (MCs) consists of individual attempts to displace each of the  $N$  vertices by a random increment in the sphere with radius  $s$ , centered at the vertex, followed by  $R_B/N$  attempts to flip a randomly chosen bond. We denote  $R_B$  as the bond-flip ratio, which defines how many attempts to flip a bond are made per one attempt to

move a vertex in one MCs. Note that the bond-flip ratio is connected to the lateral diffusion coefficient within the membrane, i.e., to the membrane viscosity (39). In this work, we have chosen  $R_B = 3$ ,  $s/l_{min} = 0.15$ , and  $l_{max}/l_{min} = 1.7$ . The dynamically triangulated network acquires its lateral fluidity from a bond-flip mechanism. A single bond flip involves the four vertices of two neighboring triangles. The tether connecting the two vertices in diagonal direction is cut and reestablished between the other two previously unconnected vertices. The self-avoidance of the network is implemented by ensuring that no vertex can penetrate through the triangular network and that no bond can cut through another bond.

The microstates of the membrane are sampled according to the Metropolis algorithm. The probability of accepting the change of the microstate due to vertex move or bond flip is  $\min[1, \exp(-\Delta E/kT)]$ , where  $\Delta E$  is the energy change,  $k$  is the Boltzmann constant, and  $T$  is absolute temperature. The energy for a given microstate is specified by Eq. 1. The bending energy is discretized as described by Gompper and Kroll (37,38). For each set of parameters, the system is initially thermalized. Ensemble averaging is done over 200 statistically independent microstates.

In this work, we set  $N_d$  of the total  $N = 1447$  vertices to represent DIs, which have spontaneous curvature  $c_0$  in the range between  $c_0 = 0$  (for flat proteins) and  $c_0 = 1/l_{min}$  for the most highly curved proteins that can be described well by the discrete mesh. For clarity, the explicit dimension of curvature is omitted throughout the text. All other vertices represent symmetric membrane and have zero spontaneous curvature. The fraction of curved inclusions on the membrane is given by

$$\rho = \frac{N_d}{N} \quad (4)$$

It should be noted that  $\rho$  does not represent a molar fraction of detergent added to the solution of GV directly, albeit being proportional to it. Rather,  $\rho$  serves as a qualitative measure of TR molecules found in the membrane and serves as the main parameter characterizing simulated vesicle morphologies.

We assume that the detergent binds to the membrane in a gradual process, which is accounted for in the simulations by an addition of a fraction of  $N_d$  DIs into the mesh every iteration at random positions on the mesh. The rate of inclusion addition is the same for all inclusion densities but varies from three to six to ensure the same simulation times. After each iteration, 2000 MCs are performed before new DIs are added again and the process is repeated. This gradual addition is crucial to account for the metastability of the process, as detergent-phospholipid mixtures may be stable for long periods of time without being at equilibrium (17). After the total number of DI  $N_d$  is reached, an additional 50 iterations with no new added DIs are performed with the aim of relaxing the energy of the final state even further. A typical simulation includes around 350 iterations and takes around 10 min to execute on a laptop with eight IntelCore i7-8550U cores.

It should be noted that the length of the simulation is determined experimentally; seeing that stable equilibrium shapes after adding all the inclusions at once are attained after around 300 iterations, this sets a benchmark for the cases of gradual adding of inclusions.

If the two vertices representing the DI are nearest neighbors, there is an additional energy term  $w$  assigned to their bond. The direct interaction constant  $w$  is assumed to be of the order of the thermal energy  $kT$ , where  $T_0 = 300$  K is room temperature, and the membrane bending stiffness  $\kappa$  is of the order of  $20 kT_0$ .

After a constant number of vertices in the discrete mesh is set ( $N = 1447$ ), the phase space of the Monte Carlo simulations consists of three independent parameters: proportion of curved inclusions ( $\rho$ ), spontaneous curvature of the curved inclusions ( $c_0$ ), and the nearest neighbor interaction constant ( $w$ ). To reflect the physical phenomena of the studied system of vesicles, these parameters have to be considered within approximate bounds. The proportion of curved inclusions ( $\rho$ ) varies from 0.28 to 0.8.

A Monte Carlo study of GV morphologies

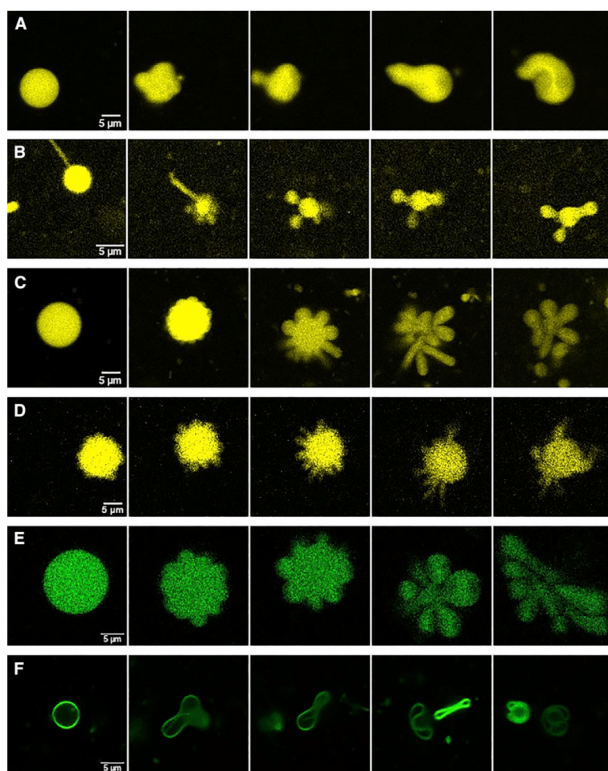


FIGURE 1 Microscopic image sequence of DOPC vesicle upon addition of TR under confocal fluorescence microscope. (A–D) represent different sequences of vesicle shape change in the experiments. Vesicles were packed with fluorescein (yellow pseudocolor). (E) is an image sequences of a vesicle packed with rhodamine B (green pseudocolor), which showed similar vesicle dynamics as fluorescein-packed vesicles. (F) shows a sequence of vesicle shape dynamics after addition of TR to a DiO membrane-labeled vesicle. To see these figures in color, go online.

## RESULTS

### DOPC and Triton X-100 experiments

The reshaping of DOPC lipid vesicles after the addition of TR is shown in Fig. 1. The initial shape of the vesicles before TR addition was spherical, as is apparent in the first column of Fig. 1. The vesicle lumen was contrasted with either fluorescein or rhodamine B and observed in confocal mode to enhance the resolution. After addition of the detergent, the spherical vesicle shape begins to deform. The dynamics of individual lipid vesicles is shown in time-lapse videos (Videos S1, S2, S3, S4, S5, and S6). Different patterns (shape families) were observed upon introduction of the detergent. A minority of lipid vesicles had a moderate shape change (Fig. 1 A). The lipid vesicles changed from spherical to cylindrical or became toroidal. A different sequence of shape changes was observed in Fig. 1 B, in which vesicles changed from spherical to pear-like structures with two unequal lobes, with one of the lobes—usually the smallest—potentially infolding. A large proportion of vesicles showed nanotube-like protrusions upon detergent addition, which could be classified into three patterns: 1) vesicles with a single very long nanotube extending several micrometers from the surface of the lipid vesicle (Fig. 1 C), 2) vesicles with several large protrusions (Fig. 1 D), and 3) lipid vesicles with many small nanotube protrusions of different length (Fig. 1 E). The fluorescence-labeled lipid vesicles were also subject to detergent solubilization, as were lipid vesicles labeled with fluorescein. There was a moderate shape change after detergent injection, with many similar morphological features as observed in fluorescein-labeled vesicles (Fig. 1 F).

The response of DOPC vesicles to different concentrations of added TR detergent is shown in Fig. S1. From the turbidity assay (Ahyayauch et al. (30)), it can be seen that at low detergent concentrations, OD<sub>650</sub> values did not

Drab et al.

change significantly, then increased at around the detergent critical micelle concentration, and thereafter decreased as a result of vesicle solubilization. With increasing detergent concentrations, there was a steady increase of fluorescence intensity, which suggests vesicle leakage. When all vesicles were solubilized, the fluorescence intensity reached a steady-state value. The red vertical band in Fig. S1 represents the detergent concentrations at which our experiments with vesicle dynamical shape changes were performed.

Additionally, we observed vesicle dynamics at different detergent concentrations (Videos S7, S8, and S9). In Video S7, there is a time-lapse sequence of vesicles immediately after the addition of the detergent at a subsolubilizing concentration of 0.03 mM. After the initial disturbance due to the detergent injection, no significant difference in vesicle shape could be observed in a given time frame (20 min). Vesicles did not solubilize during this time period. When a critical micellar concentration of 0.22 mM was added (Video S8), we observed a gradual change of vesicle shapes until the majority of vesicles solubilized. When we added a supercritical detergent concentration of 1.7 mM (Video S9), a rapid vesicle solubilization was observed in the direction of detergent front progression. Although vesicle shape dynamics could be observed, the dynamics was so rapid that it was visible only on a couple of frames. From these experiments, the outline of the dynamic phase diagram can be glimpsed. Obviously, the detergent concentration gradient has a significant impact on vesicle dynamic shape morphology and solubilization rate. With gradual DI inserted into the lipid bilayer, different vesicle shapes can be observed, whereas a large number of DI in a short time interval result in fast vesicle solubilization. To be able to see the observed vesicle shape dynamic, the detergent concentration is absolutely critical. Adding too little or too much detergent will either abolish morphological changes or speed up morphological changes and cause vesicle solubilization before recognizing shape dynamics. This is likely the reason why other researchers fail to notice the rapid vesicle shape dynamics upon detergent addition.

Although crossover between different shapes was observed, the vesicles mostly stayed within a given shape family. The vesicles of a given shape family, in particular those with small and large nanotube protrusions, were oscillating violently between different subshapes, making asymmetric stretches, twists, kicks, jumps, throws, and flips. In general, the motion of the lipid vesicle surface could be described as the “rocking and rolling” of a ship on the rough lipid ocean.

The observed morphological dynamics is very likely the result of the local detergent concentration. When the injected detergent concentration was high, the dynamics in the whole experimental system was so fast that we were not able to resolve the violent morphological fluctuations before the vesicle solubilization. On the other hand,

if the injected detergent concentration was low, the morphology did not change sufficiently during the experiment. The injected TR concentration in our experiments was ~0.2 mM, which is just below its critical micelle concentration (CMC). Only when the ratio of lipid/injected detergent was around 50:1 could we observe the morphological fluctuation dynamics. Because detergent was added locally and not mixed, the system did not reach equilibrium before the onset of morphological fluctuations. Most notably, the time of violent morphological changes varied between different vesicles (from 30 s up to 5 min). Once initiated, the morphological fluctuations in different vesicles followed similar paths. Because lipid vesicles were distributed at different distances from the detergent injection site, they could accumulate different concentrations of detergents and therefore follow different morphological sequences.

#### Monte Carlo simulation results

The results of Monte Carlo simulations are given in Fig. 2. Overall, the results of simulations reproduce very well the main patterns of vesicle behavior observed upon detergent addition (i.e., formation of spheroids, irregular structures, pear-like shapes, lobed structures, and nanotube-like protrusions). The final simulated microstates obtained after the gradual addition of detergent were dependent on the density of DIs ( $\rho$ ), the association between the detergent molecules ( $w$ ), and the curvature of the DI ( $c_0$ ). As given in Fig. 2, both the detergent density and the interaction between detergents have a major effect on the lipid vesicle shape. At low interactions between detergent molecules (i.e.,  $w = 0.5$ ), the increasing detergent concentration decreased the flat membrane patches and the vesicle shapes become irregular, sometimes with necklace-like protrusions that are commonly observed in vesicle systems (40). The vertices of the irregular vesicle shape were composed mainly of the detergent molecules. At detergent concentrations  $\rho > 0.6$ , the percolation threshold has been reached and the majority of the detergent molecules were interconnected. When the association between the detergent molecules was high (i.e.,  $w = 2$ ), the shape of the lipid vesicle became distorted already at much lower detergent concentrations. The vesicle structure evolved quickly into a lobed structure with increasing detergent concentration, and vesicles had a significantly increased surface/volume ratio. The detergent density was simulated from 0.28 to 0.8. Below  $\rho = 0.28$ , there were not enough curved DIs to have a significant effect on morphology, and vesicles generally retain their quasi-spherical shape. On the other hand, we found that at  $\rho > 0.8$ , vesicle shapes become pronouncedly spiculated and branched, with high local curvature. This should, in principle, initiate the pinching of detergent-loaded lipid micelles and start the solubilization of the lipid vesicle. Because the simulations did not include tearing of the membrane,

A Monte Carlo study of GV morphologies

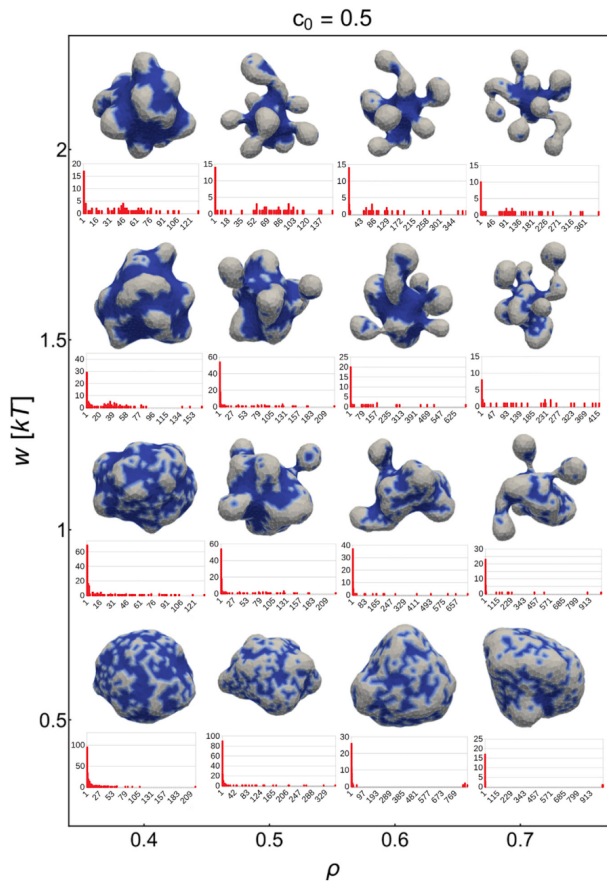


FIGURE 2 Final microstates of vesicles for gradual adding of curved inclusions ( $N_d$ ) every five iterations for  $c_0 = 0.5$ . The patches of flat membrane with no spontaneous curvature are shown in dark blue, and the gray areas correspond to positive spontaneous curvature  $c_0$  at which curved inclusions are present. In the corresponding cluster-size distributions, the y axis is the number of curved inclusions of each size, and the x axis is the curved inclusion cluster size as a sum of five simulations at given parameters. There were 300 iteration steps for each snapshot. To see these figures in color, go online.

we have limited the simulation up to and including a detergent density of  $\rho = 0.8$ .

To test the sensitivity of the simulation parameters, we have made several phase portraits for different model conditions. Fig. 3 shows a phase portrait of simulated vesicles at a constant curvature and association between the detergent molecules (i.e.,  $c_0 = 0.5$ ,  $w = 2$ ) at different detergent densities with increasing number of iteration steps. At low detergent concentration (i.e.,  $\rho = 0.4$ ), the increased number of iteration steps did not change the morphology of the lipid vesicle, although detergent molecules aggregated with increasing number of iteration steps and formed patches. The concave vesicles start to appear when detergent concentra-

tion gradually increased. The effect of increasing  $w$  correlates with the homogeneity of inclusion distribution, whereas increasing densities  $\rho$  result in more highly curved parts of the vesicle that bend outwards to accommodate for the spontaneous curvature of the inclusions. Protrusion growth was pronounced only at  $\rho > 0.5$  and  $w > 0.5$ , at which these two effects amplify budding of the membrane in a process that resembles vesiculation. Because the simulations did not account for membrane fission, the limit of such a vesiculation process result in highly tubular, branched morphologies at higher number of iteration steps. The vesiculation process can be followed with vesicle volume decrease (Fig. 3 D) and a concomitant increase of the

Drab et al.

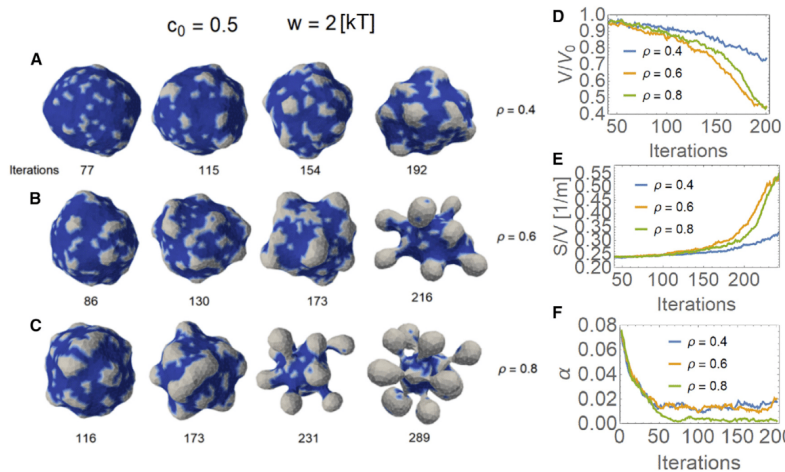


FIGURE 3 Sequential microstates of vesicles with an increasing number of curved inclusions ( $c_0 = 0.5$ ) on the membrane (marked as gray areas of the surface) for different end concentrations of inclusions  $\rho = 0.4$ ,  $\rho = 0.6$ , and  $\rho = 0.8$  for (A), (B), and (C), respectively. With increasing number of iteration steps, the reduced volume decreases (D), whereas the surface/volume ratio increases (E). (F) The asphericity  $\alpha$  as defined by Eq. 4. In all cases,  $w = 2$ . To see these figures in color, go online.

surface/volume ratio (Fig. 3 E). At low detergent concentrations, the vesiculation was indicated only at a very high number of iteration steps. Conversely, at high detergent concentrations ( $\rho > 0.5$ ), the surface/volume ratio increased at significantly lower number of iteration steps.

In general, with passing iteration steps, curved inclusions start to aggregate and form patches of the membrane with a preferred spontaneous curvature, leading to a formation of undulations and buds. Any deviation from quasispherical shapes leads to a decrease in volume and an increase of the surface/volume ratio. The change of vesicle shape could be assessed by calculating the asphericity parameter  $\alpha$ . Asphericity is the degree of deviation from a spherical shape, calculated as (41)

$$\alpha = \frac{(\lambda_1 - \lambda_2)^2 + (\lambda_2 - \lambda_3)^2 + (\lambda_3 - \lambda_1)^2}{2(\lambda_1 + \lambda_2 + \lambda_3)^2}, \quad (5)$$

where  $\lambda_i$  are the eigenvalues of the gyration tensor of the vesicle. For the thin rod limit,  $\alpha = 1$  ( $\lambda_1 = 1$ ,  $\lambda_2 = \lambda_3 = 0$ ), whereas  $\alpha = 0.25$  for disks. When the vesicle forms three or four spindles,  $\alpha$  starts to decrease (Fig. 3 F).

In the experiments, the concentration of detergent molecules in the membrane increased with time. In simulations, we have accounted for this by gradual addition of curved DI after every iteration. This was done to mimic the highly metastable and dynamic nature of the solubilization process and to allow shapes to attain the energy minima. To check

whether gradual incorporation of detergents is important for the outcome of the simulation, we have simulated the situation in which all curved DI were added at once to the lipid bilayer before the first iteration step. The phase portrait is given in Fig. 4. It is instructive to compare the gradual addition of detergent (Fig. 2) to the complete addition (Fig. 4). At low detergent interaction energy (i.e.,  $w = 0.5$ ), vesicle shapes stayed quasispherical for the gradual case but were highly branched and tubular for the complete detergent addition after the same number of iteration steps.

The shapes in gradual detergent additions start minimizing their bending energy when there are few curved inclusions present in the membrane, retaining their spherical morphology even after new inclusions were added to the surface. In complete detergent addition before the simulations (Fig. 4), curved inclusions start grouping together from the start of the simulation and formed patches of curved membrane that accumulated, resulting in highly curved morphologies that form spindles. In terms of cluster distributions of DIs, we see that gradual addition resulted in a diverged grouping: either most DIs were present in small patches, or they were a part of a superpatch containing almost all DIs on the membrane. In comparison, in the case of complete detergent addition, more medium-sized patches formed that evolved to membrane buds. These differences persisted even at larger  $w$  and  $\rho$ . Shapes obtained by gradual addition generally had thicker buds and protrusions, with a more pronounced central region of the membrane devoid of curved inclusions (Fig. 2), as opposed to

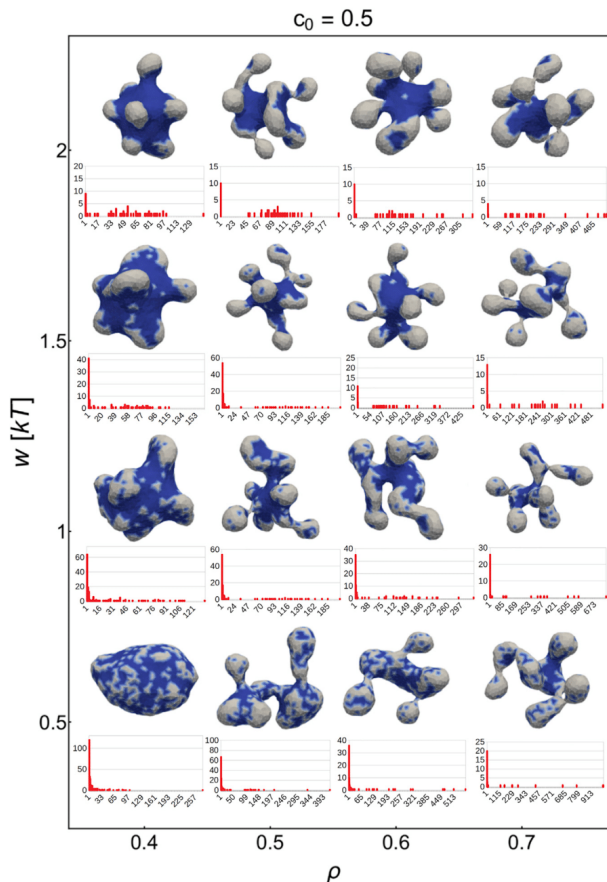


FIGURE 4 Final microstates of vesicles for which all curved inclusions ( $N_d$ ) were added before the first iteration for  $c_0 = 0.5$ . The patches of flat membrane with no spontaneous curvature are shown in dark blue, and the gray areas correspond to positive spontaneous curvature  $c_0$  at which curved inclusions are present. In the corresponding cluster-size distributions, the y axis is the number of curved inclusions of each size, and the x axis is the curved inclusion cluster size as a sum of five simulations at given parameters. Note the tubular worm-like structures lacking a centralized bulk vesicle usually present in gradual addition snapshots (Fig. 2). There were 300 iteration steps for each snapshot. To see these figures in color, go online.

shapes obtained by adding all detergent at once (Fig. 4). The latter were also more prone to resembling tubular structures with no apparent central part from which undulations emanated, a trait that was observed in nearly all shapes upon gradual detergent addition. This is due to the fact that curved inclusions are always added to the vacant positions on the surface and are therefore more likely to be locally flat. However, the complete addition of the detergent before the simulation can fall quickly into a kinetic trap, a relatively stable but not true equilibrium state, resulting in shapes that only elongate with more iterations, with much thinner necks connecting buds to the central shape (Fig. 4).

In conclusion, comparing the results of the simulation (Figs. 2 and 4) with the experimental results of detergent addition (Fig. 1), it is clear that the simulation with a gradual addition of detergents much better describes the dynamic evolution of lipid shapes than the simulation with complete detergent addition before the simulation.

The spontaneous curvature of DIs in the lipid bilayer is not known exactly. The results of simulating an increasing detergent spontaneous curvature are given in Fig. 5. It is important to note that spontaneous curvature  $c_0$  equal to zero leads to a trivial result yielding perfectly spherical vesicles. The increased detergent-inclusion curvature can have a pronounced effect on lipid vesicle shape already at low

Drab et al.

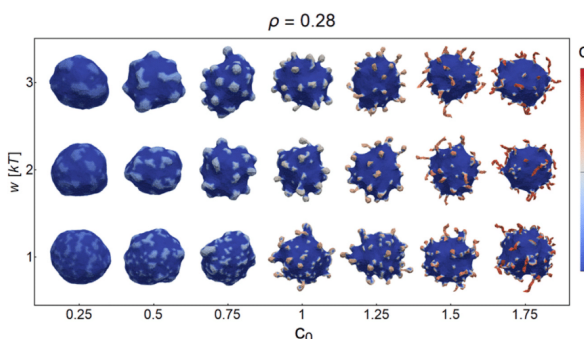


FIGURE 5 Snapshots of vesicle microstates for  $\rho = 0.28$ . The patches of flat membrane with no spontaneous curvature are shown in dark blue, and the heatmap colors correspond to areas of positive curvature where curved inclusions are present. The interaction parameter  $w$  regulates the homogeneity of the curved inclusion domains; at values  $w = 1$ , the interaction is relatively weak, resulting in a homogeneous distribution of inclusions across the vesicle, whereas increasing  $w$  results in more localized patches of curved membrane. Coupling this effect with high spontaneous curvature of inclusions results in the formation of protrusions shown in red. There were 300 iteration steps for each snapshot. To see these figures in color, go online.

detergent concentrations (i.e.,  $\rho = 0.28$ ). With increasing curvature, the number of protrusions increases. We have limited the simulations to values of  $c_0 < 1$  to avert from discontinuities. Theoretically, the highest possible  $c_0 = 1/l_{min}$ . The detergent neighbor interaction  $w$  was hardest to approximate because mechanisms of curved inclusion attraction are not well known. We found that an increasing  $w$  facilitates protrusion growth because it minimizes total energy but also regulates the homogeneity of the curved protrusion domains across the membrane.

## DISCUSSION

The structural changes of liposome-induced solubilization by detergents have been known experimentally for some time and take various solubilization pathways depending on the types of lipids and detergents. The morphology changes include shrinkage, bursting, budding, fission, peeling, and inside-out inversion. The equilibrium interactions between detergents and phospholipid bilayers (i.e., phase diagrams) have also been described (2,42). In the mixed system composed of lipids and detergents in aqueous solutions, the phase boundaries describe the range of partial lipid solubilization structures. A general consensus is that lipid bilayer solubilization proceeds in three stages (43). In stage 1, detergent partition between lipid bilayers and the aqueous media occurs, and in stage 2, a composition-induced disintegration of the bilayers forms long thread-like mixed micelles. In stage 3, at higher detergent concentrations, solubilization is followed by an entropy-derived rapid series of mixing large detergent-phospholipid mixed micelles with pure detergent micelles, yielding smaller mixed micelles with a higher detergent/phospholipid ratio. Theoretical approaches to the self-assembly of binary surfactant mixtures were mostly studied in stage 3 (43) with the onset of micellization and pore formation, but little is known about the mechanisms of membrane structural

changes in the intermediate stage, at which the binary mixtures coexist and the topology of the vesicles is not yet compromised. In particular, very little is known about structural behavior under nonequilibrium conditions, in which constant influx of detergent molecules introduces nonlinear dynamics in the lipid bilayer.

In this work, a possible mechanism of membrane structural changes seen in experiments with DOPC liposomes and TR mixtures before solubilization is presented within a simple Monte Carlo model. In the model, curved DI move laterally in the membrane and induce local curvature changes because of their molecular shape. This leads to a “rock-and-roll” dynamics of lipid vesicles seen in the experiments before micellization and solubilization of liposomes. Morphology changes observed in the experiments and simulations alike encompass symmetry breaking, resulting in protrusion growth and undulating geometries. The simulation qualitatively predicts the observed dynamic morphology changes up to a point of pore formation and micellization of the vesicles. It is found that the metastability of the process in the simulation is of crucial importance in predicting the three-dimensional shapes of lipid vesicles.

To our knowledge, such simulations are novel and predict morphology changes before pore formation and the total solubilization of liposomes. In future work, it would be interesting to couple the simulation parameters with differential scanning calorimetry (DSC), isothermal titration calorimetry, or infrared or NMR spectrometry results to study the effect of phase transitions of lipids in the membrane. To our knowledge, past studies tended to focus on the phase diagrams of late stages of solubilization with steady-state fluorescence spectroscopy (44) or isothermal titration calorimetry (45). Our findings are in line with recent molecular dynamics simulations of liposomes and detergents, which confirmed that the detergent adsorption induces spontaneous curvature of the vesicle bilayer, resulting in thin

neck formations connecting smaller spherical vesicles (46,47).

Lipid vesicles have been used extensively to understand the equilibrium and nonequilibrium dynamics of simplified biological cells that do not contain a cytoskeleton or have protein-loaded membrane. The results obtained in this study are therefore of interest for cell biology. The cells are regularly challenged by amphiphiles, which may induce lipid phase transition, cell shape alteration, and ultimately cell death (48,49). On the other hand, cells may autonomously control amphiphile concentration in the lipid bilayer (i.e., lysolipids) and thereby induce local or global shape change (14). Another venue in which one could benefit from the knowledge of nonequilibrium dynamics before solubilization is triggered liposome release of cargo in biomedical applications such as drug delivery and micro- or nanoscale reactors (50).

## CONCLUSION

In this work, the interaction between DOPC giant vesicles and nonionic detergent Triton X-100 was studied, with an emphasis on the processes before the solubilization. Intensive and dynamic changes of DOPC liposome morphology were observed. A possible mechanism for such a dynamic process is proposed that is based on the geometrical and associative properties of the detergent molecules that are adsorbed and laterally diffuse across the lipid vesicle. Three-dimensional Monte Carlo numerical simulations were used to study the phase space of metastable shapes, their dependence on detergent-inclusion spontaneous curvature, and the attraction between detergent molecules under nonequilibrium detergent concentrations. It is found that the gradual addition of curved detergent inclusions predicts very well the morphological shapes observed in experiment (spheroids, pears, undulations, lobes, spicules, and budding vesicles with thin necks connecting regions of quasispherical vesicles). The results are in line with the existing literature and shed a new, to our knowledge, light on the mechanical and dynamical aspects of the early stages of the solubilization process.

## SUPPORTING MATERIAL

Supporting material can be found online at <https://doi.org/10.1016/j.bpj.2021.09.005>.

## AUTHOR CONTRIBUTIONS

M.D.: investigation, methodology, visualization, writing—original draft, and writing—review and editing. Ž.P.: investigation, methodology, and writing—review and editing. S.P.: methodology and visualization. A.I.: conceptualization, supervision, and writing—review and editing. V.K.-I.: conceptualization, supervision, and writing—review and editing. D.S.: supervision, conceptualization, methodology, and writing—review and editing.

## ACKNOWLEDGMENTS

The authors are thankful to Professor Nir Gov for ideas that improved the manuscript.

We acknowledge the financial support from the research programs nos. P2-0232 and P3-0388 and research projects nos. J3-9262, J3-2533, L3-2621, and J1-9162, all from the Slovenian Research Agency. We also acknowledge the funding from the European Union's Horizon 2020 research and innovation programme VES4US No. 801338.

## REFERENCES

1. Kumar, D., C. M. Richter, and C. M. Schroeder. 2020. Conformational dynamics and phase behavior of lipid vesicles in a precisely controlled extensional flow. *Soft Matter*. 16:337–347.
2. Tomita, T., T. Sugawara, and Y. Wakamoto. 2011. Multitude of morphological dynamics of giant multilamellar vesicles in regulated nonequilibrium environments. *Langmuir*. 27:10106–10112.
3. Babnik, B., D. Miklavčič, ..., A. Iglič. 2003. Shape transformation and burst of giant POPC unilamellar liposomes modulated by non-ionic detergent C12E8. *Chem. Phys. Lipids*. 125:123–138.
4. Mavčič, B., B. Babnik, ..., V. Kralj-Iglič. 2004. Shape transformation of giant phospholipid vesicles at high concentrations of C12E8. *Bioelectrochemistry*. 63:183–187.
5. Peterlin, P., V. Arrigler, ..., P. Walde. 2009. Growth and shape transformations of giant phospholipid vesicles upon interaction with an aqueous oleic acid suspension. *Chem. Phys. Lipids*. 159:67–76.
6. Dervaux, J., V. Noireaux, and A. Libchaber. 2017. Growth and instability of a phospholipid vesicle in a bath of fatty acids. *Eur. Phys. J. Plus*. 132:1–10.
7. Tanford, C. 1980. The Hydrophobic Effect: Formation of Micelles and Biological Membranes, Second Edition. J. Wiley, New York.
8. Heerklotz, H., and R. M. Epanet. 2001. The enthalpy of acyl chain packing and the apparent water-accessible apolar surface area of phospholipids. *Biophys. J.* 80:271–279.
9. Israelachvili, J. N. 2015. Intermolecular and Surface Forces. Academic Press, London.
10. Lombardo, D., M. A. Kiselev, ..., P. Calandra. 2015. Amphiphiles self-assembly: basic concepts and future perspectives of supramolecular approaches. *Adv. Condens. Matter Phys.* 2015:151683.
11. Andersen, O. S., and R. E. Koeppe, II. 2007. Bilayer thickness and membrane protein function: an energetic perspective. *Annu. Rev. Biophys. Biomol. Struct.* 36:107–130.
12. McIntosh, T. J., and S. A. Simon. 2006. Roles of bilayer material properties in function and distribution of membrane proteins. *Annu. Rev. Biophys. Biomol. Struct.* 35:177–198.
13. Iglič, A., D. Drobne, and V. Kralj-Iglič. 2015. Nanostructures in Biological Systems: Theory and Applications. CRC Press, Boca Raton, FL.
14. Fuller, N., and R. P. Rand. 2001. The influence of lysolipids on the spontaneous curvature and bending elasticity of phospholipid membranes. *Biophys. J.* 81:243–254.
15. Mesarec, L., M. Drab, ..., A. Iglič. 2021. On the role of curved membrane nanodomains, and passive and active skeleton forces in the determination of cell shape and membrane budding. *Int. J. Mol. Sci.* 22:2348.
16. Kralj-Iglič, V., B. Babnik, ..., A. Iglič. 2006. Quadrupolar ordering of phospholipid molecules in narrow necks of phospholipid vesicles. *J. Stat. Phys.* 125:727–752.
17. Lichtenberg, D., H. Ahyaayach, and F. M. Goñi. 2013. The mechanism of detergent solubilization of lipid bilayers. *Biophys. J.* 105:289–299.
18. Fošnarič, M., V. Kralj-Iglič, ..., S. May. 2003. Stabilization of pores in lipid bilayers by anisotropic inclusions. *J. Phys. Chem. B.* 107:12519–12526.

Drab et al.

19. Kralj-Iglič, V., A. Iglič, ..., P. Peterlin. 2000. Stable tubular microexosomes of the erythrocyte membrane induced by dimeric amphiphiles. *Phys. Rev. E Stat. Phys. Plasmas Fluids Relat. Interdiscip. Topics.* 61:4230–4234.
20. Kralj-Iglič, V., H. Hägerstrand, ..., A. Iglič. 2005. Amphiphile-induced tubular budding of the bilayer membrane. *Eur. Biophys. J.* 34:1066–1070.
21. Drab, M., D. Stopar, ..., A. Iglič. 2019. Inception mechanisms of tunneling nanotubes. *Cells.* 8:626.
22. Mahapatra, A., C. Uysal, and P. Rangamani. 2021. The mechanics and thermodynamics of tubule formation in biological membranes. *J. Membr. Biol.* 254:273–291.
23. Bobrowska-Hägerstrand, M., V. Kralj-Iglič, ..., H. Hägerstrand. 1999. Torocyte membrane endovesicles induced by octaethylene glycol dodecylether in human erythrocytes. *Biophys. J.* 77:3356–3362.
24. Auth, T., and G. Gompper. 2009. Budding and vesiculation induced by conical membrane inclusions. *Phys. Rev. E Stat. Nonlin. Soft Matter Phys.* 80:031901.
25. Atilgan, E., and S. X. Sun. 2007. Shape transitions in lipid membranes and protein mediated vesicle fusion and fission. *J. Chem. Phys.* 126:03B604.
26. Reynwar, B. J., G. Illya, ..., M. Deserno. 2007. Aggregation and vesiculation of membrane proteins by curvature-mediated interactions. *Nature.* 447:461–464.
27. Sot, J., L. A. Bagatolli, ..., A. Alonso. 2006. Detergent-resistant, ceramide-enriched domains in sphingomyelin/ceramide bilayers. *Biophys. J.* 90:903–914.
28. Sudbrack, T. P., N. L. Archilha, ..., K. A. Riske. 2011. Observing the solubilization of lipid bilayers by detergents with optical microscopy of GUVs. *J. Phys. Chem. B.* 115:269–277.
29. Moscho, A., O. Orwar, ..., R. N. Zare. 1996. Rapid preparation of giant unilamellar vesicles. *Proc. Natl. Acad. Sci. USA.* 93:11443–11447.
30. Ahyayauch, H., M. I. Collado, ..., F. M. Goñi. 2012. Lipid bilayers in the gel phase become saturated by triton X-100 at lower surfactant concentrations than those in the fluid phase. *Biophys. J.* 102:2510–2516.
31. Israelachvili, J. N., S. Marčelja, and R. G. Horn. 1980. Physical principles of membrane organization. *Q. Rev. Biophys.* 13:121–200.
32. Helfrich, W. 1973. Elastic properties of lipid bilayers: theory and possible experiments. *Z. Naturforsch. C.* 28:693–703.
33. Iglič, A., T. Slivnik, and V. Kralj-Iglič. 2007. Elastic properties of biological membranes influenced by attached proteins. *J. Biomech.* 40:2492–2500.
34. Iglič, A., M. Lokar, ..., V. Kralj-Iglič. 2007. Possible role of flexible red blood cell membrane nanodomains in the growth and stability of membrane nanotubes. *Blood Cells Mol. Dis.* 39:14–23.
35. Fošnarič, M., S. Penič, ..., N. S. Gov. 2019. Theoretical study of vesicle shapes driven by coupling curved proteins and active cytoskeletal forces. *Soft Matter.* 15:5319–5330.
36. Veksler, A., and N. S. Gov. 2007. Phase transitions of the coupled membrane-cytoskeleton modify cellular shape. *Biophys. J.* 93:3798–3810.
37. Gompper, G., and D. Kroll. 1996. Random surface discretizations and the renormalization of the bending rigidity. *J. Phys. I.* 6:1305–1320.
38. Gompper, G., and D. Kroll. 2004. Triangulated-surface models of fluctuating membranes. In *Statistical Mechanics of Membranes and Surfaces*. D. Nelson, T. Piran, and S. Weinberg, eds. World Scientific, pp. 359–426.
39. Bivas, I., P. Hanusse, ..., O. Aguerre-Chariol. 1987. An application of the optical microscopy to the determination of the curvature elastic modulus of biological and model membranes. *J. Phys. (Paris).* 48:855–867.
40. Bhatia, T., S. Christ, ..., R. Lipowsky. 2020. Simple sugars shape giant vesicles into multispheres with many membrane necks. *Soft Matter.* 16:1246–1258.
41. Rudnick, J., and G. Gaspari. 1987. The shapes of random walks. *Science.* 237:384–389.
42. Arnulphi, C., J. Sot, ..., F. M. Goñi. 2007. Triton X-100 partitioning into sphingomyelin bilayers at subsolubilizing detergent concentrations: effect of lipid phase and a comparison with dipalmitoylphosphatidylcholine. *Biophys. J.* 93:3504–3514.
43. Helenius, A., and K. Simons. 1975. Solubilization of membranes by detergents. *Biochim. Biophys. Acta.* 415:29–79.
44. Juan-Colás, J., L. Dresser, ..., S. D. Quinn. 2020. The mechanism of vesicle solubilization by the detergent sodium dodecyl sulfate. *Langmuir.* 36:11499–11507.
45. Heerklotz, H., A. D. Tsamaloukas, and S. Keller. 2009. Monitoring detergent-mediated solubilization and reconstitution of lipid membranes by isothermal titration calorimetry. *Nat. Protoc.* 4:686–697.
46. Noguchi, H. 2013. Structure formation in binary mixtures of lipids and detergents: self-assembly and vesicle division. *J. Chem. Phys.* 138:024907.
47. Pizzirusso, A., A. De Nicola, ..., G. Milano. 2017. Biomembrane solubilization mechanism by Triton X-100: a computational study of the three stage model. *Phys. Chem. Chem. Phys.* 19:29780–29794.
48. Calvez, P., J. Jouhet, ..., A. Zapun. 2019. Lipid phases and cell geometry during the cell cycle of *Streptococcus pneumoniae*. *Front. Microbiol.* 10:351.
49. Marie, E., S. Sagan, ..., C. Tribet. 2014. Amphiphilic macromolecules on cell membranes: from protective layers to controlled permeabilization. *J. Membr. Biol.* 247:861–881.
50. Zylberberg, C., and S. Matosevic. 2016. Pharmaceutical liposomal drug delivery: a review of new delivery systems and a look at the regulatory landscape. *Drug Deliv.* 23:3319–3329.

**Biophysical Journal, Volume 120**

**Supplemental information**

**A Monte Carlo study of giant vesicle morphologies in nonequilibrium environments**

Mitja Drab, Žiga Pandur, Samo Penič, Aleš Iglič, Veronika Kralj-Iglič, and David Stopar

## Supporting Material

### A Monte-Carlo Study of Giant Vesicle Morphologies in Nonequilibrium Environments

#### Captions to Supporting Movies – Triton X-100 added to suspensions of DPPC vesicles.

Movie 1: A spherical vesicle develops undulations and multiple lobes after finally disintegrating into smaller vesicles.

Movie 2: A vesicle undergoes violent shape dynamics. In the first part of the video, a formation of thin protrusions can clearly be seen.

Movie 3: A spherical vesicle undergoes a strikingly symmetrical development with 4 roughly equal lobes after disintegrating into smaller vesicles.

Movie 4: A spherical vesicle retains its stable shape for almost two minutes after disintegrating. An interesting multi-vesicle structure can also be seen.

Movie 5: Another example of a changing shape of an initially spherical vesicle, this one goes from a sphere to an oblate to a multi-lobe structure after finally disintegrating.

Movie 6: An interesting shape transformation from a sphere to a cup-like shape that later segregates into daughter vesicles.

Movie 7: Addition of Triton-X100 detergent to vesicle suspension at a final concentration of 0.03 mM. During 20 min after addition of the detergent, only very few vesicle shape changes or vesicle solubilisation could be observed. Scale bar: 50 µm.

Movie 8: Addition of Triton-X100 detergent to vesicle suspension at a final concentration of 0.22 mM. After approx. 6 min vesicles with pear shape, vesicles with tethers, vesicles with blobs, etc. With time progression all vesicles gradually solubilized. Scale bar: 50 µm.

Movie 9: Addition of Triton-X100 detergent to vesicle suspension at a final concentration of 1.7 mM. Immediately after the addition of the detergent (approx. 30s) solubilisation of vesicle occurred. A fast moving solubilization line across the field of view can be seen, where vesicle shape changes very rapidly prior to vesicle solubilization. The detergent has been injected from the top left corner. Scale bar: 50 µm.

### Supporting Figures

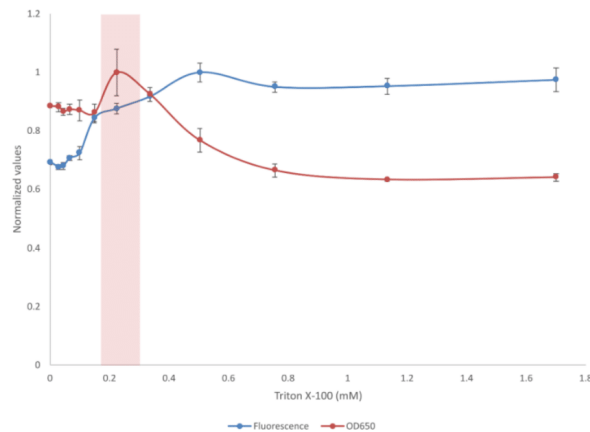


**Figure S1** Normalized values of fluorescence intensity in vesicle suspensions at different detergent concentrations. The red vertical band in represents detergent concentrations where our experiments with vesicle dynamical shape changes were performed.

### 2.1.3 Materialne lastnosti celične stene bakterije *E. coli* določajo odpornost celic na sonolizo

Pandur Ž., Dular M., Kostanjšek R., Stopar D. 2022. Bacterial cell wall material properties determine *E. coli* resistance to sonolysis. Ultrasonics Sonochemistry, 83: 105919, doi: 10.1016/j.ultsonch.2022.105919: 10 str.

Izvleček:

Iz rezultatov dinamike lipidnih dvosoljev v prejšnjem poglavju izhaja, da je mogoče z zunanjimi kemijskimi dejavniki povzročiti katastrofalne oscilacije v membrani. V tem delu smo z uporabo ultrazvoka preverili, kako se lahko različne strukture bakterijske celične stene upirajo mehansko povzročenim oscilacijam. V raziskavi smo sistematično spremenili lastnosti celične stene bakterije *E. coli*, katere smo sonicirali z ultrazvočno sondijo (20 kHz frekvenca, kalorimetrična moč 6,73 W). Določili smo stopnjo uničenja bakterijskih celic z okvarjenimi kapsularnimi komponentami, spremenjeno zunano membrano, spremenjenim peptidoglikanskim ovojem, sferičnih celic (sferoplasti) in gigantskih sferoplastov. Prav tako smo preverili odziv celic v različnem fiziološkem stanju – eksponentna in stacionarna faza rasti. Stacionarne celice so bile do 5-krat bolj odporne na soniciranje kakor celice v fazi rasti. Najbolj dovetne na inaktivacijo z vsiljenimi zunanjimi oscilacijami so bile celice z oslabljenim peptidoglikanskim slojem. Celice, ki so imele popolnoma odstranjen peptidoglikan (sferoplasti) so bile izjemno občutljive na soniciranje. Občutljivost sferoplastov je bila primerljiva z lipidnim dvoslojem (liposomi). Rezultati kažejo, da ima na učinkovitost soniciranja veliko vlogo struktura peptidoglikanskega sloja, obenem pa tudi fiziološko stanje bakterijskih celic.



To delo je ponujeno pod Priznanje avtorstva-Nekomercialno-Brez predelav 4.0 Mednarodno licenco.



## Bacterial cell wall material properties determine *E. coli* resistance to sonolysis



Žiga Pandur<sup>a,b</sup>, Matevž Dular<sup>b</sup>, Rok Kostanjšek<sup>a</sup>, David Stopar<sup>a,\*</sup>

<sup>a</sup> University of Ljubljana, Biotechnical Faculty, Večna pot 111, 1000 Ljubljana, SI-Slovenia

<sup>b</sup> University of Ljubljana, Faculty of Mechanical Engineering, Askerčeva 6, 1000 Ljubljana, SI-Slovenia

### ARTICLE INFO

Keywords:  
Viability  
Bacteria  
*Escherichia coli*  
Sonication  
Cell envelope

### ABSTRACT

The applications of bacterial sonolysis in industrial settings are plagued by the lack of the knowledge of the exact mechanism of action of sonication on bacterial cells, variable effectiveness of cavitation on bacteria, and inconsistent data of its efficiency. In this study we have systematically changed material properties of *E. coli* cells to probe the effect of different cell wall layers on bacterial resistance to ultrasonic irradiation (20 kHz, output power 6.73 W, horn type, 3 mm probe tip diameter, 1 ml sample volume). We have determined the rates of sonolysis decay for bacteria with compromised major capsular polymers, disrupted outer membrane, compromised peptidoglycan layer, spheroplasts, giant spheroplasts, and in bacteria with different cell physiology. The non-growing bacteria were 5-fold more resistant to sonolysis than growing bacteria. The most important bacterial cell wall structure that determined the outcome during sonication was peptidoglycan. If peptidoglycan was remodelled, weakened, or absent the cavitation was very efficient. Cells with removed peptidoglycan had sonolysis resistance equal to lipid vesicles and were extremely sensitive to sonolysis. The results suggest that bacterial physiological state as well as cell wall architecture are major determinants that influence the outcome of bacterial sonolysis.

### 1. Introduction

Sonication is widely used for dispersing, surface cleaning, degassing, food and beverage processing, medical scanning, nano synthesis, mineral processing, welding, cell disruption, and extraction of cellular components [1–6]. Another promising potential of sonication is disruption and inactivation of bacteria, for example in wastewater treatment plants [7]. The wider application of cavitation for bacterial inactivation is hampered by the lack of the knowledge of the mechanism of action of sonication on bacterial cells, variable effectiveness of cavitation on bacteria, and inconsistent data of its efficiency.

During sonication small vapour bubbles (cavities) form inside an initially homogeneous liquid medium by a sudden decrease in pressure with subsequent cavity collapse [8,9]. From a mechanical point of view the collapse of cavitation bubble produces extreme conditions such as pressure shocks up to several 100 MPa, microjets with velocities above 100 m/s, hot spots with extreme temperatures in order of several 1000 K [10–14]. From a chemical point of view, highly reactive radicals or antimicrobials can be formed due to local high temperatures [15]. In terms of biology, pressure oscillations during bubble collapse modify

permeability of cellular membrane (sonoporation), which is useful in cellular transfection or transformation [16] and can be used to inactivate bacteria [17,18].

Concentrated energy during collapse of cavitation bubbles can have major effects on bacterial cell integrity [19]. The exact mechanism of bacteria disruption, however, is not known [1,20–22]. It has been proposed that ultrasound weakens or disrupts bacterial cell envelope structure through a number of processes [1,23].

1. Damage of bacteria cell due to mechanical effects induced by pressure and pressure gradients during the collapse of cavitation bubbles within or near the bacteria.
2. Shear forces induced by microstreaming.
3. Chemical attack due to the formation of free radicals, which attack the cell wall layer structures leading to disintegration.
4. Formation of a bactericidal hydrogen peroxide.

The ability of *Escherichia coli* to survive physico-chemical stress is often related to material properties and multi-layered structure of cell wall [24–28]. *E. coli* cell envelope has cytoplasmic membrane,

\* Corresponding author.  
E-mail address: [david.stopar@bf.uni-lj.si](mailto:david.stopar@bf.uni-lj.si) (D. Stopar).

<https://doi.org/10.1016/j.ultronch.2022.105919>

Received 21 October 2021; Received in revised form 23 December 2021; Accepted 13 January 2022

Available online 18 January 2022

1350-4177/© 2022 The Author(s). Published by Elsevier B.V. This is an open access article under the CC BY-NC-ND license

(<http://creativecommons.org/licenses/by-nd/4.0/>).

peptidoglycan layer, outer membrane, capsular layer, slime-layer, loosely attached extracellular polymeric substances, pili, fimbriae, and flagella [29–32]. Each layer or structure has a unique chemical composition (Fig. 1), which in combination with the other layers form a multi-composite cell envelope structure that resist environmental stresses. The resistance of different cell wall structures to sonication is not known and has not been studied systematically.

Traditionally, peptidoglycan is considered to be the most important pressure bearing element of the bacterial cell envelope [33]. It is composed of glycan strands and peptide stems. The glycan strands are made of alternating N-acetylglucosamine (GlcNAc) and N-acetylmuramic acid (MurNAc) residues linked by  $\beta$ -1-4 glycosidic bonds. To provide mechanical stability glycan strands are cross-linked via peptide stems which generates mesh-like cell wall structure. Its viscoelastic properties allow cell reversible expansion under pressure and together with auxiliary proteins such as MreB give cell its shape [34,35]. Peptidoglycan is one of the most important targets for the action of antibiotics (i.e.,  $\beta$ -lactam antibiotics) and enzymes (i.e., lysozyme). The disruption of peptidoglycan layer causes cell lysis due to osmotic pressure fluctuations [36,37].

The outer membrane is another important structural element that in combination with peptidoglycan resist turgor pressure fluctuations [38,39]. The outer membrane has asymmetrical composition with an inner leaflet rich in phospholipids and an outer leaflet predominantly composed of polyanionic lipopolysaccharides (LPS) [40,41]. The polyanionic nature of LPS with numerous phosphate and acid sugar groups is stabilised by divalent cations ( $Mg^{2+}$  and  $Ca^{2+}$ ). If divalent cations are removed by chelators (i.e., EDTA) the structural integrity of the bacterial outer membrane is severely compromised [42,43].

Additional structural element that strengthens the bacterial cell

envelope is capsule [44]. Capsule can extend to great distances from the cell surface (often up to several micrometres) and is used as cementing substance to bind bacteria together or to a surface, and acts as a physical barrier to antibiotics [45–47]. Capsules are composed of high-molecular-weight capsular polysaccharide chains that are linked covalently and noncovalently to the outer membrane [30]. In *E. coli* four major extracellular polymer components have been identified: poly- $\beta$ -1,6-N-acetyl-D-glucosamine (PGA), curli proteins, colanic acid, and bacterial cellulose or cellulose derivates [48–53]. Recently, their effect on *E. coli* biofilm mechanical properties has been described [54].

In this work we have modified cell wall layers material properties of *E. coli* and probe the resistance of compromised cells to sonolysis. We have determined the rates of sonolysis decay for bacteria with compromised major capsular polymers, disrupted outer membrane, compromised peptidoglycan layer, as well as resistance of spheroplasts and giant spheroplasts (stripped bacterial cells with all cell wall layers removed except cytoplasmic membrane). The integrity of the intact and modified cell envelopes after sonolysis were tested in the exponential and stationary growth phase. The results suggest significantly different contribution of envelope layers to bacterial ability to resist sonolysis.

## 2. Methods

### 2.1. Growth and preparation of bacteria with weakened cell wall layers

Two bacterial strains were used in experiments: *E. coli* MG1655 strain with inducible green fluorescent protein (gfp) under IPTG (isopropyl  $\beta$ -D-thiogalactopyranoside) inducible promotor and an isogenic mutant of MG1655 strain (*eps*<sup>-</sup>) that does not produce  $\beta$ -1,6-N-acetyl-D-glucosamine (PGA), curli proteins, and colanic acid. Frozen

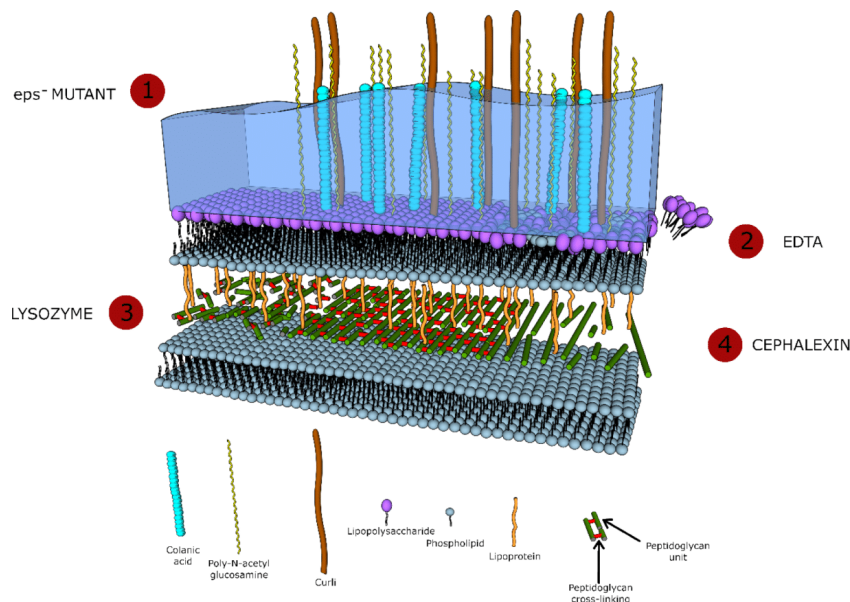


**Fig. 1.** Cell envelope layer structures that have been modified in different experiments. 1. capsule weakened isogenic *eps*<sup>-</sup> strain with deletions of genes for synthesis of PGA, colanic acid and curli proteins. 2. Outer membrane weakened by EDTA chelation of divalent ions. 3. Peptidoglycan weakened by lysozyme treatment, which cuts glycan 1-4  $\beta$  glycosidic bonds. 4. Peptidoglycan weakened with cephalixin that inhibits transpeptidases crosslinking. 5. Combination of treatments (2 + 3 + 4) to produce spheroplasts. Combination of treatments (2 + 3 + 4) to produce giant spheroplasts. Depicted are different layers with major chemical constituents.

stock culture from  $-80^{\circ}\text{C}$  were plated on lysogeny broth (LB) agar plates with kanamycin - Kn ( $50\ \mu\text{g}/\text{ml}$ ). Bacterial colonies from LB plates were used as inoculum for an overnight culture incubated at  $37^{\circ}\text{C}$  and shaken at 200 rpm under aerobic conditions. Next, 1 % of overnight medium was inoculated into a fresh LB Kn medium ( $50\ \mu\text{g}/\text{ml}$  kanamycin) and incubated at  $37^{\circ}\text{C}$ , 200 rpm until the exponential growth phase (optical density  $\text{OD}_{650}$  of  $\sim 0.5$  a.u) when cells were chemically treated. Experiments were performed also on cells in the stationary growth phase where cells were grown overnight (approx. 18 h incubation time) and then chemically treated.

Several modifications of cell wall layers were performed (Fig. 1). For peptidoglycan modification we used antibiotic cephalixin, which targets penicillin binding protein (PBP3, FtsI) involved in transpeptidases crosslinking [55]. To cells in the exponential or stationary growth phase cephalixin was added to a final concentration of  $50\ \mu\text{g}/\text{ml}$ . The suspension was incubated for 30 min at the growth conditions. Alternatively, peptidoglycan was modified with lysozyme, which cleaves glycosidic bonds. To the cell culture in the exponential or stationary growth phase we added lysozyme to a final concentration of  $100\ \mu\text{g}/\text{ml}$ . Cell suspension was incubated for 30 min at the growth conditions.

For the outer membrane modification, we used EDTA to sequester divalent  $\text{Ca}^{2+}$  and  $\text{Mg}^{2+}$  ions. The cell culture in the exponential or stationary growth phase was harvested with centrifugation at 4000 RCF for 3 min. Pellet was resuspended in 0,8 M sucrose. To the cell suspension we added EDTA to a final concentration of 3 mM and 25 mM Tris buffer ( $\text{pH} = 8,0$ ). After addition of reagents, cultures were further incubated for 30 min at the growth conditions.

For simultaneous modification of multiple cell wall layers, we produced giant spheroplasts as described by Sun et al. 2014 [56]. Filamentous cells were used to produce giant spheroplasts [57]. Briefly, 4 ml of LB suspension in the exponential growth phase ( $\text{OD} \sim 0,5$ ) was transferred into fresh 36 ml LB medium with cephalixin ( $50\ \mu\text{g}/\text{ml}$ ) and kanamycin ( $50\ \mu\text{g}/\text{ml}$ ). Bacterial culture was incubated at  $37^{\circ}\text{C}$  on a shaker at 200 rpm for 2 h. Filamentous cells were harvested with centrifugation at 4000 RCF for 3 min. Pellet was resuspended in 5 ml 0,8 M sucrose to which we have added EDTA to a final concentration of 3 mM, 25 mM Tris buffer ( $\text{pH} = 8,0$ ), and lysozyme to a final concentration of  $100\ \mu\text{g}/\text{ml}$ . After 10 min of incubation at room temperature, 2 ml of stop solution was added (1 M  $\text{MgCl}_2$ , 0,8 M sucrose, 10 mM Tris-HCl) to inactivate EDTA and to stabilize spheroplasts. For cultivation of filaments with different length, we used protocol described above for the preparation of giant spheroplasts and incubated cells in fresh LB medium with Cephalixin for various total times: 30, 60, 90 and 150 min to obtain filaments up to  $90\ \mu\text{m}$  length.

Additionally, we used a combination of EDTA and lysozyme only, which induces formation of smaller sized spherical cell (spheroplast). We followed the same preparation as described above, but without incubation with cephalixin. When removing growth medium, cells in the exponential growth phase were harvested from 40 ml of culture into 5 ml of 0,8 M sucrose, whereas for cells in the stationary growth phase 5 ml of growth medium were harvested into 5 ml 0,8 M sucrose.

## 2.2. Sonolysis

After preparation of bacterial cultures with modified cell wall envelope structures, 1 ml of samples were aliquoted into microcentrifuge tubes and stored on ice. For sonolysis experiments we used horn probe sonicator (MSE 150 W Ultrasonic disintegrator Mk2) equipped with the exponential probe  $168\ 1/8''$  – 3 mm, at nominal frequency of 20 kHz and at  $15\ \mu\text{m}$  amplitude. Probe was immersed approximately 15 mm into the liquid volume in a microcentrifuge tube. Samples were sonicated up to 90 s. At sonication times longer than 30 s we have used "duty-cycles", where 30 s of sonication was followed by 30 s of pause to avoid excessive sample heating, temperature did not exceed  $38,1 \pm (0,4)^{\circ}\text{C}$ .

## 2.3. Bacterial counts

After sonolysis samples were serially diluted in saline solution (0,9 % NaCl) and plated on LB Kn plates. For samples treated with EDTA or EDTA in combination with lysozyme or cephalixin serial dilutions in 0,8 M sucrose were made to avoid inactivation of EDTA due to the presence of ions in the solution. Culture plates were incubated overnight at  $37^{\circ}\text{C}$  and next day the number of colony forming units (CFU) were counted. For spheroplasts and giant spheroplasts bacterial counts after sonolysis were made on microscope to avoid counting of viable rod cells that were not transformed during the treatment.

## 2.4. Microscopy

For visualisation of cell morphology and viability assessment bacterial samples were visualized with fluorescence microscope Zeiss Axio Observer Z1 equipped with laser confocal unit LSM 800. For fluorescence microscopy, the wild-type strain was induced with IPTG (final concentration  $40\ \mu\text{M}$ ) to induce gfp synthesis, while for the *eps*-mutant we used SYTO-9 fluorescent stain (final concentration  $33,4\ \mu\text{M}$ ). In both cases we used excitation laser wavelength of 488 nm, and emission filter of 400–585 nm. To observe dead cells, samples were additionally stained with propidium iodide (PI) to a final concentration of  $40\ \mu\text{M}$  (excitation laser wavelength: 561 nm, emission filter: 585–700 nm). For accurate microscopic measurement, bacterial sample was fixed with 1 % agarose gel (Thermo Scientific Topvision Low melting point agarose) to prevent excess bacterial motion.

Resistance to sonolysis of spheroplasts and giant spheroplasts was quantified with microscopic image analysis.  $10\ \mu\text{L}$  of bacterial sample was put on microscopic glass slide and covered with 20x20 mm #1.5 cover glass. Samples on glass slides were sealed with VALAP sealant (mixture of Vaseline, lanolin and paraffin wax) [58]. Samples were observed under microscope after 5 min of incubation at a room temperature. Microscopic images (4x4 tiled images with 10 % overlay) were acquired through 6 random locations on microscopic glass slide for each treatment time. For spheroplasts we used 100x magnification lens, for giant spheroplasts we used 20x magnification lens. After image acquisition, images were analysed with ImageJ 1.53c software where the spheroplasts were counted.

## 2.5. Transmission electron microscopy

For transmission electron microscopy (TEM) of bacterial cultures the samples were fixed in 3,5 % glutaraldehyde in 0,1M PBS overnight at  $4^{\circ}\text{C}$ . After washing the fixative by 0,1 M PBS solution, the bacterial cells were pelleted by 3 min centrifugation at 4000 RCF and resuspended in 3 % low melting-point agarose. Sample was carefully mixed and incubated at room temperature until agarose fully solidified. Agar block was cut into smaller pieces approximately  $1 \times 1 \times 1\ \text{mm}$  in size, postfixed in 1 %  $\text{OsO}_4$  for an hour and rinsed with deionised water. Following dehydration in a series of gradient ethanol concentrations: 50 %, 70 %, 90 %, 96 %, and acetone, samples were embedded in Agar 100 resin (Agar Scientific). Ultrathin sections were transferred to copper grids, contrasted with uranyl acetate and lead citrate and visualized with CM100 (Philips) transmission electron microscope.

## 2.6. Statistical analysis

Experimental data (either CFU or number of spheroplasts obtained by microscopy) were statistically analysed. The decay rate was obtained by fitting the decrease of bacterial number density during sonolysis with equation Eq. (1).

$$y = y_0 + A_1 e^{-kt} \quad (1)$$

where  $y_0$  represents the initial value,  $A_1$  is amplitude,  $t$  is sonication

time, and  $k$  is decay rate. Fitted data parameter  $k$  of the individual experiments were collected and averaged. The average values were obtained from 5 independent biological experiments. A two-sample  $t$ -test assuming equal variances were used to test if cell wall layers treatments had significant effect on sonolysis resistance. Additionally, bacterial half-life ( $t_{1/2}$ ) was characterised as described in Eq. (2). Half-life depicts sonication time when half of the viable bacterial population was killed.

$$t_{1/2} = \frac{\ln(2)}{k} \quad (2)$$

#### 2.7. Measurements of sonicator output power

Calorimetric measurement was used to determine the output power of sonicator at 15  $\mu\text{m}$  amplitude. Shortly, 20 ml of water was put in a plastic tube that was thermally isolated with polystyrene. Water was cooled down to 5 °C before starting the experiment. During sonication water temperature was measured every 10 s. The total sonication time was 370 s. The sonicator output power was calculated with Eq. (3),

$$P = \frac{m^*c_p^*\Delta T}{t} \quad (3)$$

where  $m$  represents mass of the medium,  $c_p$  is heat capacity at constant pressure (for water 4185,5 J/K $^{\circ}$ Kg),  $\Delta T$  is increase in temperature, and  $t$  sonication time. The measured output of sonication power was 6,73±(0,13) W. Furthermore, we have calculated the energy required to reduce bacterial number to half of the initial concentration ( $E_{1/2}$ ) as described in Eq. (4)

$$E_{1/2} = t_{1/2} * P \quad (4)$$

where  $t_{1/2}$  represents half-life time (Eq. 2) of the viable bacteria during sonication and  $P$  is the sonication power.

#### 2.8. ROS detection

For ROS detection during sonication, we performed ROS assay with DTT as a marker. 10 mM solution of DTT was prepared in deionized water. 1 ml of DTT solution was sonicated up to 210 s (in 30 s increments). Generation of ROS was followed with absorbance measurements at 280 nm (oxidized DTT absorbs at 280 nm wavelength). Absorbance was measured on Spectrophotometer (Nanodrop 1000, Thermo Scientific).

### 3. Results

The effect of low frequency ultrasound sonolysis on a suspension of *E. coli* cells in the exponential and stationary growth phase is shown in Fig. 2. The cell number decayed exponentially. The decay rate was influenced by the physiological state of cells. The exponential cells were significantly more sensitive to sonication than stationary cells. The average decay rate constant ( $k$ ) was 0,16±(0,02) for the exponential and 0,03±(0,01) for the stationary bacteria. This implies that the stationary cells were on average 5.3-fold more resistant to sonolysis compared to the exponential cells. There was a significant decrease in the number of cells, but no visible cell debris (Supplementary Figure S1). The fraction of the cells with compromised cytoplasmic membrane was low before the ultrasound treatment and increased significantly after the treatment. Although the majority of bacteria lysed, there was a significant fraction of cells that survived sonolysis. The decay rate was not dependent on the initial bacterial densities (results not shown). To determine sonochemical effect we have performed Dithiothreitol (DTT) assay [59]. The results show no significant free radical production during sonication (Supplementary Figure S2).

To probe the effect of different cell wall layers on cell resistance to sonolysis we have modified bacterial cell wall structures and bacterial physiological states. Most of the chemical treatments did not decrease the number of viable cells prior to sonication so in this respect they were not antimicrobial. Only in production of spheroplasts the pre-treatment reduced viability (Supplementary Table S1). The morphologies of modified cells are given in Fig. 3. The exponential cells were rod shaped with dimensions 2,89±(0,67) × 0,74±(0,06)  $\mu\text{m}$ , in contrast cells in the stationary growth phase were smaller 1,44±(0,25) × 0,63±(0,06)  $\mu\text{m}$  (Fig. 3). When peptidoglycan layer in the exponential cells was modified with antibiotic cephalixin, which inhibits cross-linking of peptidoglycan molecules, cell size increased to 5,84±(0,96) × 0,86±(0,10)  $\mu\text{m}$  and cells formed filaments (Fig. 3A). Cephalixin treatment increased volume of the cells by 3.4-fold. On the other hand, cells treated with cephalixin in the stationary growth phase did not enlarge and form filaments. The peptidoglycan layer modified with lysozyme, that catalyses the hydrolysis of 1,4- $\beta$ -linkages between N-acetylmuramic acid and N-acetyl-D-glucosamine residues in peptidoglycan, had little effect on bacterial morphology and membrane integrity both in the exponential and stationary growth phase. Cells in the exponential growth phase treated with EDTA had the same size but severely compromised membranes as indicated by increased permeability to PI dye. Contrary, cells in the

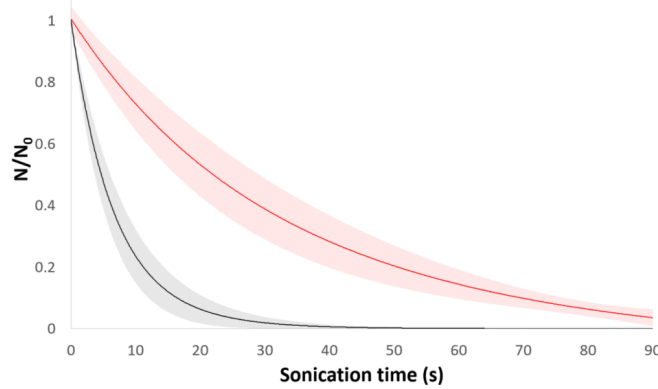


**Fig. 2.** Decay curves of exponential (black line) and stationary (red line) *E. coli* cells during sonication. Data were normalized to the initial bacterial numbers and fitted with Eq. 1. The mean decay curves with colour shaded bands representing standard deviations are shown ( $n = 5$ ).

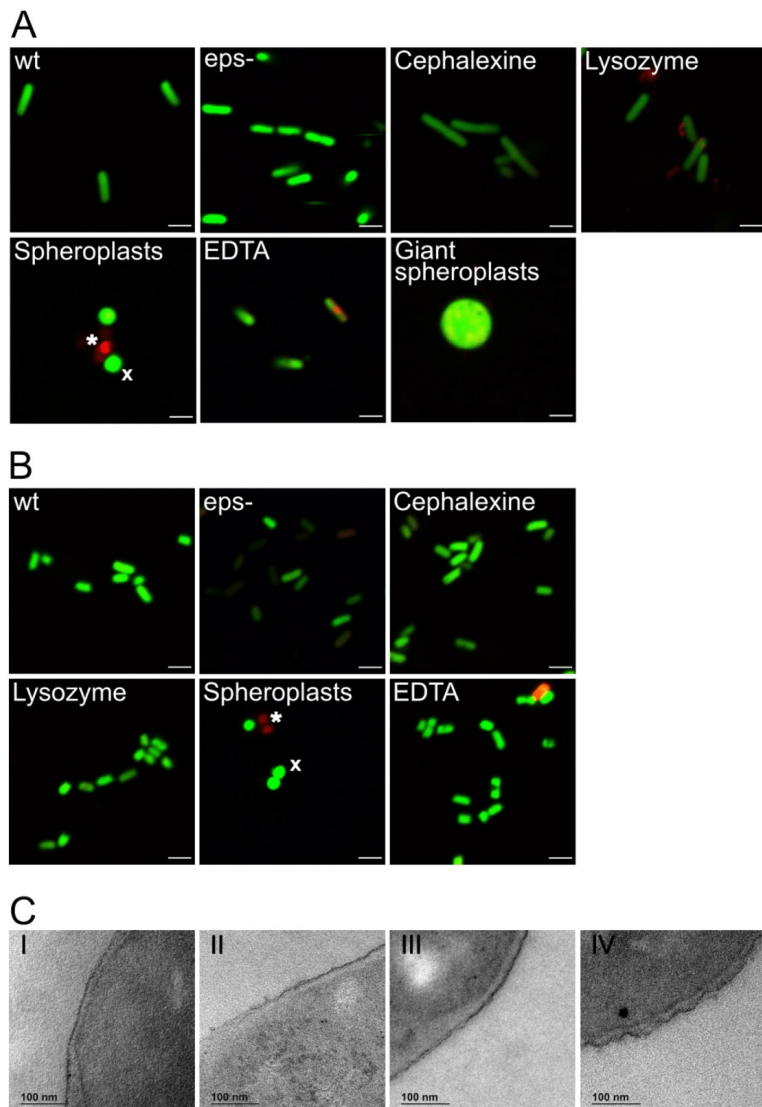


**Fig. 3.** Morphology of *E. coli* after different treatments that affect cell wall layer structure in the exponential (A) and stationary growth phase (B). Microscopic images are composite images from GFP (green fluorescence protein – indicating viable bacteria) and PI (red propidium iodide – indicating bacteria with compromised membrane). In spheroplast images, viable cells are indicated with “x” and cells with compromised membranes with “\*”. Scale bar represents 5 μm. (C) TEM micrographs of *E. coli* cells: (I) untreated cells in the exponential growth phase, (II) untreated cells in the stationary growth phase, (III) *eps-* mutant in stationary growth phase, and (IV) cephalaxin treated cells in exponential growth phase.

stationary growth phase were much less sensitive to EDTA treatment. The combined EDTA and lysozyme treatment resulted in spheroplast formation. Spheroplast formation reduced the number of viable cells (*Supplementary Table S1*). The cells that remained viable had spherical morphology with an average diameter of  $2,3 \pm (0,4)$   $\mu\text{m}$ . When cells were treated with a combination of EDTA, lysozyme, and cephalexin giant spheroplast formed, with a diameter of  $4,5 \pm (1,0)$   $\mu\text{m}$ . Giant spheroplasts could not be produced in the stationary growth phase because cephalexin does not work on non-growing cells. In general, in the stationary growth phase, most of the treatments did not have a significant impact on morphology. The exception was a combination of EDTA and lysozyme, which produced spheroplasts. TEM micrographs reveal similar cell wall ultrastructure for the exponential and stationary cells (*Supplementary Figure S4*). The cephalexin treated cells had higher degree of wrinkling of the cell wall observed with TEM (*Fig. 3* and *Supplementary Figure S5*). There was no visible difference in cell wall ultrastructure for the *eps-* mutant.

Cells with modified cell wall layers had different sensitivity for sonolysis (*Fig. 4*). For example, cells treated with cephalexin in the exponential growth phase showed significantly larger decay rate  $0,53 \pm (0,8)$  compared to cephalexin untreated cells  $0,16 \pm (0,02)$ . In cephalexin treated cells already after 10 s of sonication the fraction of viable cells was lower than 0.01. In contrast, cells in the stationary growth phase were insensitive to cephalexin treatment and there was no significant difference in sonolysis decay rate compared to untreated cells.

The effects of other cell wall layer modifications on sonolysis decay rates are given in *Fig. 5A*. Different treatments had no effect on stationary bacteria, except for spheroplasts, which were significantly more sensitive than untreated stationary cells. On the other hand, the exponential cells were much more sensitive to sonication (larger  $k$  values) and respond differently to cell wall modifications. Treatment with cephalexin, formation of spheroplasts, and formation of giant spheroplasts had a large effect on bacterial sensitivity to sonolysis. In particular, the giant spheroplast were very sensitive to sonolysis. Contrary, the removal of capsular polymers (*eps-* mutant), the outer membrane (EDTA), and lysozyme treatment did not change bacterial sensitivity to sonolysis.

The energy input to reduce viable bacteria to a half of their initial density was significantly lower for the growing compared to non-growing bacteria  $29,6 \pm (4,3)$  and  $170 \pm (70)$  J, respectively (*Fig. 5B*). For growing bacteria similar energy input was needed to reduce the

bacterial number for lysozyme or EDTA treated cells as well as *eps-* mutant strain. The least energy was required for cephalexin treated cells and giant spheroplast  $8,9 \pm (1,3)$  J and  $7,1 \pm (3,0)$  J, respectively.

The effect of bacterial size on decay rate is given in *Fig. 6*. The results suggest three qualitatively different decay rate regimes. The smallest stationary cells had the lowest decay rate. Slightly larger exponential cells had significantly higher decay rate (on average 8.5-fold). Exponential cells with modified peptidoglycan layer (giant spheroplast, filaments) had the largest decay rate (on average 3.8-fold larger compared to the unmodified cells in the exponential phase). Increasing the length of the filament by Cephalexin treatment (from 5 to 90  $\mu\text{m}$ ), had only a limited effect on decay rate (1.45-fold increase).

#### 4. Discussion

There are numerous proposed mechanisms of sonication that affect viability of bacteria [1,23] (i.e. physical, chemical, mechanical, biological) that occur simultaneously during sonication treatment. In this work we have focused on different cell wall layers material properties and their contributions to bacterial resistance to cavitation and sonolysis. This has not been described yet in the literature and provides a foundation for a successful application of sonolysis. As sonochemical effects do not contribute significantly (*Supplementary Figure S2*) to bacterial decay rate, in accordance with literature on low frequency sonication [60–62], we will mainly discuss bacterial mechanical properties and their effect on sonolysis resistance. The data suggest that cell size can have an effect on decay rate (*Fig. 6*). However, as cell wall architecture and cell physiological status have significantly larger effect on cell decay rates they will be primarily discussed.

The outermost cell layer modified was the capsular layer (*eps-* mutant in *Fig. 1*). The results suggest that removing the capsular polymers such as PGA, colanic acid, and curli proteins did not significantly increase sensitivity to sonication. Capsular components are synthesised more extensively under stress conditions (i.e., stationary growth phase) [63–65]. However, neither the exponential nor the stationary bacteria with removed capsular polymers (*eps-* mutant) were more sensitive to sonolysis than the wild type. This suggests that these components do not provide protection against sonolysis. In our previous work we have shown that capsular polymers determine rheological behaviour of *E. coli* biofilms [54]. In particular, they contribute to biofilm cohesive energy and are important in establishing intercellular bacterial stress resistant

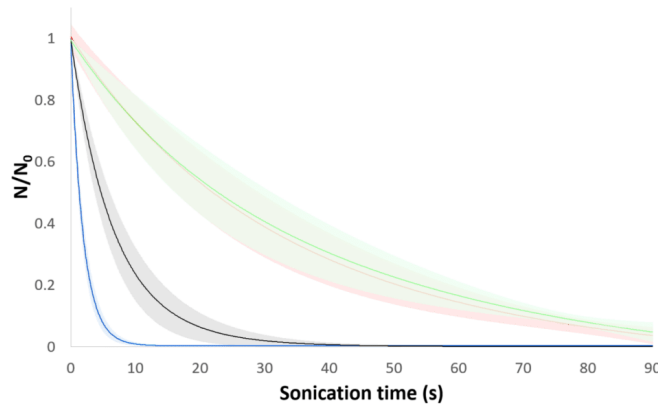


**Fig. 4.** Decay curves of cephalexin untreated (black line) and cephalexin treated (blue line) exponential cells, and cephalexin untreated (red line) and cephalexin treated (green line) stationary cells. The data were fitted with Eq. 1. The mean decay curves with colour shaded bands representing standard deviations are shown ( $n = 5$ ).

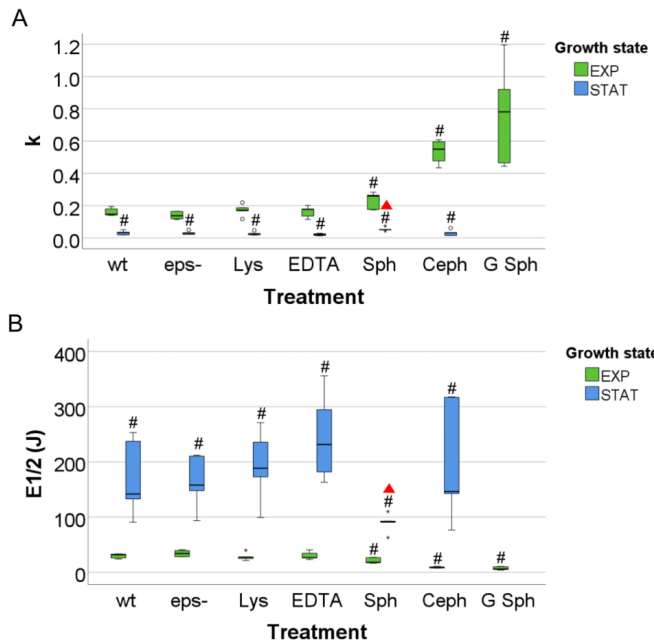


**Fig. 5.** (A) Sonication decay rate  $k$  and (B) cumulative energy required to halve the population of cells for the wild-type *E. coli* strain (wt) and cells with modified cell wall material properties for the exponential (green bars) and stationary cells (blue bars). The box plots are given ( $n = 5$ ). Black hashtag (#) indicate significant ( $\alpha = 0.05$ ) difference in decay rates compared to the wild-type strain in the exponential growth phase. Red triangle (▲) shows significant ( $\alpha = 0.05$ ) difference to the wild-type strain in the stationary growth phase. Abbreviations: wt (untreated cells), eps- (cells with removed capsular polymers), Lys (cells treated with lysozyme), EDTA (cells treated with EDTA), Sph (spheroplasts, cells treated with lysozyme and EDTA), Ceph (cells treated with Cephalexin), G Sph (giant spheroplasts, cells treated with Cephalexin, lysozyme and EDTA).

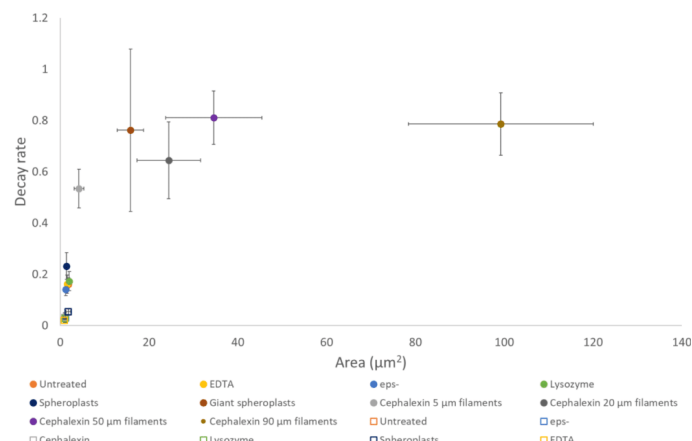


**Fig. 6.** The effect of cell size (presented as area of the cell) on sonication decay rate. Dots represent cells in the exponential growth phase, hollow squares represent cells in the stationary growth phase.

structures. We conclude that capsular layer does not contribute significantly to *E. coli* ultrasound resistance.

Cells treated with EDTA (Fig. 1), which weakens the outer membrane, had higher envelope permeability to PI dye in the exponential growth phase (Fig. 3A), but were not more sensitive to sonolysis.

Chelation of divalent cations with EDTA extracts divalent metal ions such as  $\text{Ca}^{2+}$  and  $\text{Mg}^{2+}$  from their binding sites within the outer membrane, weakening the LPS interactions [43]. In the presence of EDTA, the outer membrane loses its structural integrity and vast quantities (up to 50 % of total LPS) are released into solution [66–69]. The loss of LPS

molecules corresponds to appearance of irregularly shaped pits, bumps and dents along with rougher cell surface [42,70] that reduces envelope and cell stiffness [39]. Recently researchers observed increased permeability of the outer and inner membrane during sonication [71,72]. Additionally, sonication increased membrane rigidity and decreased membrane potential [71]. Although we have observed increased envelope permeability in EDTA treated cells we did not observe significant difference in sonolysis resistance, which suggest that the outer membrane structure does not contribute significantly to *E. coli* ultrasound resistance.

Peptidoglycan maintains bacterial shape and protects cytoplasmic membrane from turgor pressure stress [73]. We have used two external peptidoglycan modifications: treatment with antibiotic Cephalexin and with enzyme Lysozyme. Cephalexin is an antibiotic that irreversibly binds to and inactivates penicillin-binding proteins (PBPs) which interferes with cross-linking of peptide chains necessary for peptidoglycan strength and rigidity (Fig. 1) [36,74]. Cells treated with cephalexin were significantly more sensitive to sonolysis. Cephalexin is also used as a septation inhibitor for production of *E. coli* filaments [56,75,76]. Consistent with the literature we have observed filament morphology in the exponential cells treated with cephalexin (Fig. 3A and S3). It is interesting to note that filament cells were significantly more sensitive to sonolysis compared to the individual rod-shaped bacteria. Increasing the size of filaments for approximately 20 fold resulted in 1.4 increase in sonolysis sensitivity, which suggest that bacterial size has a small effect. In the stationary growth phase cephalexin did not induce morphological changes and did not sensitise cells for sonolysis. These results imply that actively grown cells with weakened peptidoglycan layer, but otherwise intact outer membrane and capsular layer, are sensitive to sonolysis.

Peptidoglycan can be weakened also by enzymatic hydrolysis of glycoside bonds with lysozyme (1,4- $\beta$ -N-acetyl muramidase), which leads to cell envelope instability (Fig. 1) [37]. The addition of lysozyme did not sensitise cells for sonolysis. In Gram-negative organisms such as *E. coli* the action of lysozyme may be hindered because the outer membrane shields peptidoglycan from the external environment [77]. Due to the absence of morphology changes, changes of permeability, or sonolysis decay rate we infer that lysozyme did not reach peptidoglycan (Fig. 3) [42]. To increase the access of lysozyme to its target we have combined lysozyme treatment with EDTA. After a combined treatment cells changed shape and become spherical, a clear indication of peptidoglycan modification (Fig. 3). It is generally accepted that spheroplasts have partially removed outer membrane and peptidoglycan layer but keep the intact cytoplasmic membrane [43,57,78,79]. The results indicate that spheroplasts are very sensitive to sonolysis (Table S1) both in the exponential and stationary growth phase.

The combination of lysozyme, EDTA, and cephalexin produced giant spheroplasts (Fig. 3.) that were extremely sensitive to sonolysis (Fig. 5A). In a combined action EDTA permeabilizes the outer membrane, which in turn permits lysozyme to cross into the periplasmic space where together with cephalexin completely degrades peptidoglycan thus allowing the formation of giant spheroplasts [42,80]. We observed that giant spheroplasts had increased permeability for PI dye and lower viability. When giant spheroplasts were sonicated, they rapidly lose viability. Essentially, a giant spheroplast represents a giant lipid bilayer vesicle. Previously we have shown that giant DOPC lipid vesicles are very sensitive to hydrodynamic and ultrasound cavitation [81]. When compared to other chemical, physical and mechanical stressors such as ionic strength and osmolarity agents, free radicals, shear stresses, high pressure, electroporation, centrifugation, surface active agents, microwave irradiation, heating, and freezing-thawing, ultrasound and hydrodynamic cavitation were among the most powerful. The giant DOPC vesicles were destroyed in less than 5 s at 20 kHz and amplitude of 10  $\mu\text{m}$  [81]. The results of decay of spheroplasts are consistent with lipid vesicle studies [82] and suggest that unprotected cytoplasmic membrane found in spheroplasts can be easily destroyed by cavitation. This also explains why animal cells, which do not have extra

protective layers to stabilise cytoplasmic membrane, are very sensitive to sonication [83].

The results of Cephalexin, EDTA, and lysozyme support the main conclusion that peptidoglycan contribute significantly to *E. coli* ultrasound resistance. Peptidoglycan is a complex molecule in which material properties, composition, architecture, and biophysical properties vary with bacterial strain, physiological conditions, and growth phase [84]. It is viscoelastic solid that allows reversible expansion under pressure and gives cell its shape. Normally peptidoglycan is under dynamic stress in the living cell due to the cell turgor pressure. In rod shaped bacteria it is more deformable in the direction of the long axis of the cell (elastic modulus  $2.5 \times 10^7 \text{ N m}^{-2}$ ) than in the direction perpendicular to the long axis (elastic modulus,  $4.5 \times 10^7 \text{ N m}^{-2}$ ) [85]. This is consistent with the observation that changes in the volume of osmotically shocked *E. coli* cells are mainly due to changes in the cell length, whereas cell diameter is virtually constant [86]. It was suggested that the anisotropy in elasticity of rod-shaped bacteria is the consequence of the predominant alignment of the flexible peptides in the direction of the long axis of the cell and of the more rigid glycan strands perpendicular to the direction of the long axis [87]. Cephalexin, which prevents peptide cross-linking in the direction of the long axis, had the largest effect on sonolysis decay rate. This suggest that the weakest point during sonication is the cell long axis, where cytoplasmic membrane during sonoporation likely becomes leaky. It was shown that spherical bacteria are more resistant to sonication treatments than rod shaped bacteria [23]. It should be noticed that in spherical bacteria cell peptidoglycan is fully developed and mechanical stress is isotropically distributed with no weak links as in rod shaped bacteria. Spheroplasts on the other hand have spherical geometry, but they do not possess functional peptidoglycan layer, which makes them extremely vulnerable to sonolysis.

In all experiments we have observed that stationary cells were significantly more resistant to sonolysis than exponential cells. This is likely the consequence of peptidoglycan remodelling. It has been shown that during the transition of *E. coli* from an exponential to a stationary phase the material properties, composition, and architecture of peptidoglycan are dramatically modified. For example, the relative abundance of Id-A2pm-A2pm cross-linked muropeptides increases from approximately 5 to 12 % of the total muropeptides [88], the degree of cross-linkage increases from 28 to 38 % cross-linked muropeptides, the mean glycan chain length decreases from roughly 33 down to 17 disaccharides per chain, and the lipoprotein-bound muropeptides increases from 9 to 14 % [88–90]. Such a remodelling of peptidoglycan increases the resistance to sonolysis. This has an important consequence for the application of sonolysis (i.e. water distribution systems). In these environments there are relatively few nutrients available for bacterial growth and bacteria are mostly starving [91]. Technically such bacteria are in the stationary growth phase and are significantly more resistant to sonolysis than actively growing cells.

## 5. Conclusions

In conclusion, variable effectiveness of cavitation on bacteria that have been reported in the literature provide an obstacle for implementation of cavitation in industrial settings. The results of this study imply that the most important bacterial structure that determines the outcome during sonication (20 kHz, output power 6,73 W, horn type, 3 mm probe tip diameter, 1 ml sample volume) is peptidoglycan. If peptidoglycan is remodelled, weakened, or absent the cavitation can be very efficient. Weakened peptidoglycan can be found in actively growing bacterial cells or cells that have been chemically treated with antibiotics or enzymes. In cells that lack peptidoglycan such as spheroplasts or eukaryotic cells sonoporation of cell membranes is much more effective and quickly kills cells.

**Declaration of Competing Interest**

The authors declare that they have no known competing financial interests or personal relationships that could have appeared to influence the work reported in this paper.

**Acknowledgments**

The authors acknowledge the financial support from the European Research Council (ERC) under the European Union's Framework Program for research and innovation, H2020-EU.1.1. (Grant agreement ID: 771567) and the Slovenian Research Agency (Core funding No. P2-0401 and P4-0116). We acknowledge the financial support from the Slovenian Research Agency to the Infrastructural Centre "Microscopy of Biological Samples", at Biotechnical faculty, University of Ljubljana, member of MRIC UL network.

**Appendix A. Supplementary data**

Supplementary data to this article can be found online at <https://doi.org/10.1016/j.ultsonch.2022.105919>.

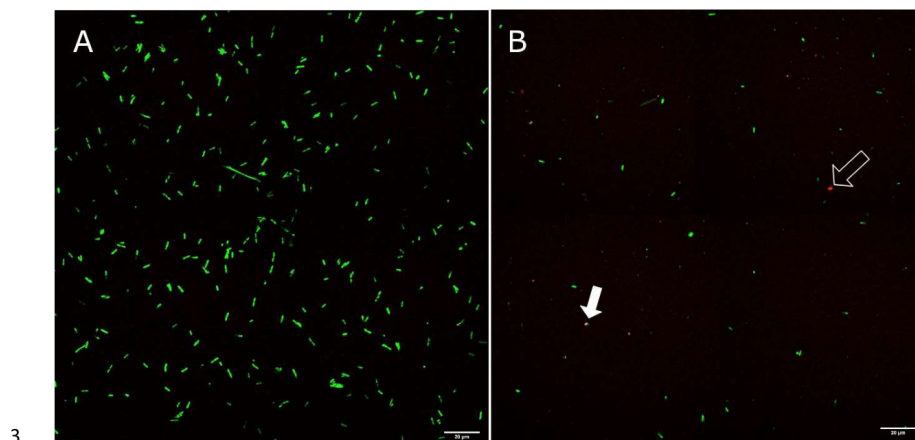
**References**

- [1] M. Zupanc, Ž. Pandur, T. Stepišnik Perdih, D. Stopar, M. Petkovsek, M. Dular, Effects of cavitation on different microorganisms: The current understanding of the mechanisms taking place behind the phenomenon. A review and proposals for further research, *Ultrason. Sonochem.* 57 (2019) 147–165, <https://doi.org/10.1016/j.ultsonch.2019.05.009>.
- [2] A.S. Peshkovsky, S.L. Peshkovsky, S. Bystryak, Scalable high-power ultrasonic technology for the production of translucent nanoemulsions, *Chem. Eng. Process. Process. Intensif.* 69 (2013) 77–82, <https://doi.org/10.1016/j.cep.2013.02.010>.
- [3] J.P. Canselier, H. Delmas, A.M. Wilhelm, B. Abismail, Ultrasound emulsification - An overview, *J. Dispers. Sci. Technol.* 23 (1–3) (2002) 333–349, <https://doi.org/10.1080/01932690208984209>.
- [4] D.G. Eskin, K. Al-Helal, I. Tzanakis, Application of a plate sonotrode to ultrasonic degassing of aluminum melt: Acoustic measurements and feasibility study, *J. Mater. Process. Technol.* 222 (2015) 148–154, <https://doi.org/10.1016/j.jmatprot.2015.03.006>.
- [5] H.V. Annegowda, R. Bhat, L. Min-Tze, A.A. Karim, S.M. Mansor, Influence of sonication treatments and extraction solvents on the phenolics and antioxidants in star fruits, *J. Food Sci. Technol.* 49 (4) (2012) 510–514, <https://doi.org/10.1007/s13197-011-0435-6>.
- [6] N. Saranya, P. Devi, S. Nithyanantham, R. Jeyalaxmi, Cells Disruption by Ultrasonication, *BionanoScience*, 4 (4) (2014) 335–337, <https://doi.org/10.1007/s12668-014-0149-2>.
- [7] F. Foladori, B. Laura, A. Gianni, Z. Giuliano, Effects of sonication on bacteria viability in wastewater treatment plants evaluated by flow cytometry-Fecal indicators: wastewater and activated sludge, *Water Res.* 41 (1) (2007) 235–243, <https://doi.org/10.1016/j.watres.2006.08.021>.
- [8] J.-P. Franc, J.-M. Michel, Fundamentals of Cavitation, Kluwer Academic Publishers, Dordrecht (2005), <https://doi.org/10.1007/1-4020-2233-6>.
- [9] T.J. Mason, Ultrasonic cleaning: An historical perspective, *Ultrason. Sonochem.* 29 (2016) 519–523, <https://doi.org/10.1016/j.ultsonch.2015.05.004>.
- [10] C.E. Bremen, Cavitation and bubble dynamics, Oxford University Press, Oxford, 1995.
- [11] G.L. Chahine, C.-T. Hsiao, Modelling cavitation erosion using fluid–material interaction simulations, *Interface Focus*, 5 (5) (2015) 20150016, <https://doi.org/10.1098/rsfs.2015.0016>.
- [12] K.S. Susic, N.C. Eddingsaas, D.J. Flannigan, S.D. Hopkins, H. Xu, Extreme conditions during multibubble cavitation: Sonoluminescence as a spectroscopic probe, *Ultrason. Sonochem.* 18 (4) (2011) 842–846, <https://doi.org/10.1016/j.ultsonch.2010.12.012>.
- [13] M. Petkovsek, M. Hocevar, M. Dular, Visualisation and measurements of shock waves in cavitating flow, *Exp. Therm. Fluid Sci.* 119 (2020) 110215, <https://doi.org/10.1016/j.expthermflusci.2020.110215>.
- [14] M. Dular, T. Pozar, J. Zevnik, R. Petkovsek, High speed observation of damage created by a collapse of a single cavitation bubble, *Wear.* 418–419 (2019) 13–23, <https://doi.org/10.1016/j.wear.2018.11.004>.
- [15] S. Koda, T. Kimura, T. Kondo, H. Mitome, A standard method to calibrate sonochemical efficiency of an individual reaction system, *Ultrason. Sonochem.* 10 (3) (2003) 149–156, [https://doi.org/10.1016/S1350-4177\(03\)00084-1](https://doi.org/10.1016/S1350-4177(03)00084-1).
- [16] Y. Song, T. Hahn, I.P. Thompson, T.J. Mason, G.M. Preston, G. Li, L. Paniwnyk, W. E. Huang, Ultrasound-mediated DNA transfer for bacteria, *Nucleic Acids Res.* 35 (2007) 1–9, <https://doi.org/10.1093/nar/gkm710>.
- [17] A. Šarc, J. Kosel, D. Stopar, M. Oder, M. Dular, Removal of bacteria *Legionella pneumophila*, *Escherichia coli*, and *Bacillus subtilis* by (super)cavitation, *Ultrason. Sonochem.* 42 (2018) 228–236, <https://doi.org/10.1016/j.ultsonch.2017.11.004>.
- [18] A. Šarc, M. Oder, M. Dular, Can rapid pressure decrease induced by supercavitation efficiently eradicate *Legionella pneumophila* bacteria? *Desalin. Water Treat.* 57 (5) (2016) 2184–2194, <https://doi.org/10.1080/19443994.2014.979240>.
- [19] P. Piyasena, E. Mohareb, R.C. McKellar, Inactivation of microbes using ultrasound: A review, *Int. J. Food Microbiol.* 87 (3) (2003) 207–216, [https://doi.org/10.1016/S0160-8395\(03\)00075-8](https://doi.org/10.1016/S0160-8395(03)00075-8).
- [20] C.W. Ho, T.K. Chew, T.C. Ling, S. Kamaruddin, W.S. Tan, B.T. Tey, Efficient mechanical cell disruption of *Escherichia coli* by an ultrasonicator and recovery of intracellular hepatitis B core antigen, *Process Biochem.* 41 (8) (2006) 1829–1834, <https://doi.org/10.1016/j.procbio.2006.03.043>.
- [21] M. Cameron, L.D. McMaster, T.J. Britz, Electron microscopic analysis of dairy microbes inactivated by ultrasound, *Ultrason. Sonochem.* 15 (6) (2008) 960–964, <https://doi.org/10.1016/j.ultsonch.2008.02.012>.
- [22] L.i. Zhang, Y. Jin, Y. Xie, X. Wu, T. Wu, Releasing polysaccharide and protein from yeast cells by ultrasound: Selectivity and effects of processing parameters, *Ultrason. Sonochem.* 21 (2) (2014) 576–581, <https://doi.org/10.1016/j.ultsonch.2013.10.016>.
- [23] E. Joyce, A. Al-Hashimi, T.J. Mason, Assessing the effect of different ultrasonic frequencies on bacterial viability using flow cytometry, *J. Appl. Microbiol.* 110 (2011) 862–870, <https://doi.org/10.1111/j.1365-2672.2011.04923.x>.
- [24] D. Scott Cayley, H.J. Gutman, M. Thomas Record, Biophysical characterization of changes in amounts and activity of *Escherichia coli* cell and compartment water and turgor pressure in response to osmotic stress, *Biophys. J.* 78 (4) (2000) 1748–1764.
- [25] M. Reuter, N.J. Hayward, S.S. Black, S. Miller, D.T.P. Dryden, I.R. Booth, Mechanosensitive channels and bacterial cell wall integrity: Does life end with a bang or a whimper? *J. R. Soc. Interface.* 11 (91) (2014) 20130850, <https://doi.org/10.1098/rsif.2013.0850>.
- [26] J. Lee, Gonul Kalentuc, Evaluation of the heat inactivation of *Escherichia coli* and *Lactobacillus plantarum* by differential scanning calorimetry, *Appl. Environ. Microbiol.* 68 (11) (2002) 5379–5386, <https://doi.org/10.1128/AEM.68.11.5379-5386.2002>.
- [27] P. Small, D. Blankenhorn, D. Welty, E. Zinser, J.L. Slonczewski, Acid and base resistance in *Escherichia coli* and *Shigella flexneri*: Role of rpoS and growth pH, *J. Bacteriol.* 176 (6) (1994) 1729–1737, <https://doi.org/10.1128/jb.176.6.1729-1737.1994>.
- [28] K.J.A. Hauben, K. Bernaerts, C.W. Michiels, Protective effect of calcium on inactivation of *Escherichia coli* by high hydrostatic pressure, *J. Appl. Microbiol.* 85 (4) (1998) 678–684, <https://doi.org/10.1111/j.1365-2672.1998.00577.x>.
- [29] U.B. Sleytr, B. Schuster, E.-M. Egelseer, D. Pum, S-layers: principles and applications, *FEMS Microbiol. Rev.* 38 (5) (2014) 823–864, <https://doi.org/10.1111/1574-6976.12063>.
- [30] T.J. Beveridge, L.L. Graham, Surface layers of bacteria, *Microbiol. Rev.* 55 (1991) 684–705, <http://www.ncbi.nlm.nih.gov/pubmed/1723487>.
- [31] C. Whitfield, Bacterial extracellular polysaccharides, *Can. J. Microbiol.* 34 (4) (1988) 415–420, <https://doi.org/10.1139/m88-073>.
- [32] A.B. Jonson, S. Normark, M. Rhen, Fimbriae, pili, flagella and bacterial virulence, *Contrib. Microbiol.* 12 (2005) 67–89, <https://doi.org/10.1159/000081690>.
- [33] A. Typagas, M. Banzhaf, C.G. Gross, W. Vollmer, From the regulation of peptidoglycan synthesis to bacterial growth and morphology, *Nat. Rev. Microbiol.* 10 (2) (2012) 123–136, <https://doi.org/10.1038/nrmicro2677>.
- [34] W. Margolin, Sculpting the Bacterial Cell, *Curr. Biol.* 19 (17) (2009) R812–R822, <https://doi.org/10.1016/j.cub.2009.06.033>.
- [35] H. Jiang, F. Si, W. Margolin, S. Sun, Mechanical Control of Bacterial Cell Shape, *Biophys. J.* 101 (2) (2011) 327–335, <https://doi.org/10.1016/j.bpj.2011.06.005>.
- [36] C.J. Harrison, D. Bratcher, *Cephalosporins, Cephalosporins : A Review* 29 (8) (2008) 264–273.
- [37] R.T. Ellison, T.J. Giehl, Killing of gram-negative bacteria by lactoferrin and lysozyme, *J. Clin. Invest.* 88 (4) (1991) 1080–1091, <https://doi.org/10.1172/JCI115407>.
- [38] J.W. Shaveitz, Microbiology: Peeling Back the Layers of Bacterial Envelope Mechanics, *Curr. Biol.* 28 (2018) R1210–R1211, <https://doi.org/10.1016/j.cub.2018.09.023>.
- [39] E.R. Rojas, G. Billings, P.D. Odermat, G.K. Auer, L. Zhu, A. Miguel, F. Chang, element in Gram-negative bacteria, (2018).
- [40] A.V. Hughes, D.S. Patel, G. Widmalm, J.B. Klouda, L.A. Clifton, W. Im, Physical Properties of Bacterial Outer Membrane Models: Neutron Reflectometry & Molecular Simulation, *Biophys. J.* 116 (6) (2019) 1095–1104, <https://doi.org/10.1016/j.bpj.2019.02.001>.
- [41] B. Bertani, N. Ruiz, J.M. Slauč, Function and Biogenesis of Lipopolysaccharides, *EcoSal Plus*, 8 (1) (2018), <https://doi.org/10.1128/ecosalplus.ESP-0001-2018>.
- [42] N.A. Amro, L.B. Kotra, K. Wadu-Mesthrige, A. Buldychev, S. Mobashery, G.Y. Liu, High-resolution atomic force microscopy studies of the *Escherichia coli* outer membrane: structural basis for permeability, *Langmuir*, 16 (2000) 2789–2796, <https://doi.org/10.1021/la991013x>.
- [43] L.A. Clifton, M.W.A. Skoda, A.P. Le Brun, F. Giesielski, I. Kuzmenko, S.A. Holt, J.H. Lakey, Effect of Divalent Cation Removal on the Structure of Gram-Negative Bacterial Outer Membrane Models, *Langmuir*, 31 (1) (2015) 404–412, <https://doi.org/10.1021/la504407v>.
- [44] G.R.d.S. Araújo, N.B. Viana, F. Gómez, B. Pontes, S. Frases, The mechanical properties of microbial surfaces and biofilms, *Cell Surf.* 5 (2019) 100028, <https://doi.org/10.1016/j.csur.2019.100028>.
- [45] J.W. Costerton, R.T. Irvin, K.J. Cheng, The bacterial glycocalyx in nature and disease, *Annu. Rev. Microbiol.* 35 (1) (1981) 299–324.

- [46] M.E. Bayer, H. Thurow, Polysaccharide capsule of *Escherichia coli*: microscope study of its size, structure, and sites of synthesis, *J. Bacteriol.* 130 (1977) 911–936, <http://www.ncbi.nlm.nih.gov/pmc/articles/PMC2400798/>.
- [47] I.S. Roberts, The Biochemistry and genetics of capsular polysaccharide production in bacteria, *Annu. Rev. Microbiol.* 50 (1) (1996) 285–315, <https://doi.org/10.1146/annurev.micro.50.1.285>.
- [48] X. Wang, X. Wang, J.F.P. Iii, J.F.P. Iii, T. Romeo, T. Romeo, The pgaABCD Locus of *Escherichia coli* Promotes the Synthesis of a Polysaccharide Adhesin Required for Biofilm Formation, *J. Bacteriol.* 186 (2004) 2724–2734, <https://doi.org/10.1128/JB.186.9.2724>.
- [49] Y. Itoh, X. Wang, B.J. Hinnebusch, J.F.P. Iii, Depolymerization of β-1,6-N-Acetyl-D-Glucosamine Disrupts the Integrity of the Cellulose Bacterial Biofilm, *J. Bac.* 187 (2005) 382–387, <https://doi.org/10.1128/JB.187.1.382>.
- [50] Y. Itoh, J.D. Rice, C. Goller, A. Pannuri, J. Taylor, J. Meissner, T.J. Beveridge, J. F. Preston, T. Romeo, Roles of pgaABCD genes in synthesis, modification, and export of the *Escherichia coli* biofilm adhesin poly-β-1,6-N-acetyl-D-glucosamine, *J. Bacteriol.* 190 (2008) 3670–3680, <https://doi.org/10.1128/JB.01920-07>.
- [51] D. Smith, J. Price, P. Burby, L. Blanco, J. Chamberlain, M. Chapman, The production of curli amyloid fibers is deeply integrated into the biology of *Escherichia coli*, *Bioolecules* 7 (4) (2017) 75, <https://doi.org/10.3390/biom07040075>.
- [52] P.N. Danese, L.A. Pratt, Exopolysaccharide Production Is Required for Development of Society, *182* (2000) 3593–3596, <https://doi.org/10.1093/aje/kw1220>.
- [53] W. Thongsomboon, D.O. Serra, A. Possling, C. Hadjineophytou, R. Hengge, L. Cegelski, Phosphoethanolamine cellulose: A naturally produced chemically modified cellulose, *Science* (80-) 359 (2018) 334–338.
- [54] M. Horvat, A. Pannuri, T. Romeo, I. Dogsa, D. Stopar, Viscoelastic response of *Escherichia coli* biofilms to genetically altered expression of extracellular matrix components, *Soft Matter*, 15 (25) (2019) 5042–5051.
- [55] H.S. Chung, Z. Yao, N.W. Goehring, R. Kishony, J.B. Kahne, Rapid β-lactam-induced lysis requires successful assembly of the cell division machinery, *Proc. Natl. Acad. Sci. U. S. A.* 106 (2009) 21872–21877, <https://doi.org/10.1073/pnas.0911674106>.
- [56] Y. Sun, T.-L. Sun, H. Huang, Physical Properties of *Escherichia coli* Spheroplast Membranes, *Biophys. J.* 107 (9) (2014) 2082–2090, <https://doi.org/10.1016/j.bpj.2014.09.034>.
- [57] M.O. Onitsuka, Y. Rikihisa, H.B. Maruyama, Biochemical and topographical studies on *Escherichia coli* cell surface. IV. Giant spheroplast formation from a filamentous cell, *J. Bacteriol.* 138 (2) (1979) 567–574, <https://doi.org/10.1128/JB.138.2.567-574.1979>.
- [58] Valap Sealant, Cold Spring Harb. Protoc. . 2015 (2015) pdb.rec082917. doi: 10.1101/pdb.rec082917.
- [59] B. Miljević, F. Hedayat, S. Stevanović, K.E. Fairfull-Smith, S.E. Bottle, Z. D. Ristovski, To Sonicate or Not to Sonicate PM Filters: Reactive Oxygen Species Generation Upon Ultrasonic Irradiation, *Aerosol Sci. Technol.* 48 (12) (2014) 1276–1284, <https://doi.org/10.1080/02786826.2014.981130>.
- [60] T.J. Mason, A.J. Cobley, J.E. Graves, D. Morgan, New evidence for the inverse dependence of mechanical and chemical effects on the frequency of ultrasound, *Ultrason. Sonochem.* 18 (1) (2011) 226–230, <https://doi.org/10.1016/j.ultsonch.2010.05.008>.
- [61] J. Jordens, B. Bamps, B. Gielen, L. Braeken, T. Van Gerven, The effects of ultrasound on micromixing, *Ultrason. Sonochem.* 32 (2016) 68–78, <https://doi.org/10.1016/j.ultsonch.2016.02.020>.
- [62] S. Nasseri, A.H. Mahvi, M. Seyedsalehi, K. Yaghmaeian, R. Nabizadeh, M. Alimohammadi, G.H. Safari, Degradation kinetics of tetracycline in aqueous solutions using peroxidisulfate activated by ultrasound irradiation: Effect of radical scavenger and water matrix, *J. Mol. Liq.* 241 (2017) 704–714, <https://doi.org/10.1016/j.molliq.2017.05.137>.
- [63] N. Cerca, K.K. Jefferson, Effect of growth conditions on poly-N-acetylgalcosamine expression and biofilm formation in *Escherichia coli*, *FEMS Microbiol. Lett.* 283 (2008) 36–41, <https://doi.org/10.1111/j.1574-6968.2008.01142.x>.
- [64] N. Majdalani, S. Gottesman, The Rcs phosphorelay: A complex signal transduction system, *Annu. Rev. Microbiol.* 59 (1) (2005) 379–405, <https://doi.org/10.1146/annurev.micro.59.050405.101230>.
- [65] K.E. Ebobiogboni, C.A. Biggs, Characterization of the extracellular polymeric substances produced by *Escherichia coli* using infrared spectroscopic, proteomic, and aggregation studies, *Biomacromolecules*, 9 (2) (2008) 686–695, <https://doi.org/10.1021/bm701043c>.
- [66] M. Vaara, Covalent structure of two novel neutrophile leucocyte-derived proteins of porcine and human origin, *Microbiol. Rev.* 56 (1992) 535–547, <https://doi.org/10.1111/prd.12107>.
- [67] R.E.W. Hancock, Alterations in structure of the cell envelope, *Ann. Rev. Microbiol.* 38 (1984) 237–264.
- [68] F.G. Ferris, T.J. Beveridge, Physicochemical roles of soluble metal cations in the outer membrane of *Escherichia coli* K-12, *Can. J. Microbiol.* 32 (1986) 594–601, <https://doi.org/10.1139/m86-110>.
- [69] L. Leive, Release of lipopolysaccharide by EDTA treatment of *E. coli*, *Biochem. Biophys. Res. Commun.* 21 (4) (1965) 290–296, [https://doi.org/10.1016/0006-291X\(65\)90191-9](https://doi.org/10.1016/0006-291X(65)90191-9).
- [70] H.-L. Alakomi, A. Paananen, M.-L. Suihki, I.M. Helander, M. Saarela, Weakening Effect of Cell Permeabilizers on Gram-Negative Bacteria Causing Biodegradation, *Appl. Environ. Microbiol.* 72 (7) (2006) 4695–4703, <https://doi.org/10.1128/AEM.00142-06>.
- [71] Q. He, D. Liu, M. Ashokumar, X. Ye, T.Z. Jin, M. Guo, Antibacterial mechanism of ultrasound against *Escherichia coli*: Alterations in membrane microstructures and properties, *Ultrasound. Sonochem.* 73 (2021) 105509, <https://doi.org/10.1016/j.ultsonch.2021.105509>.
- [72] L. Zhang, H. Qi, Z. Yan, Y. Gu, W. Sun, A.A. Zewde, Sonophotocatalytic inactivation of *E. coli* using ZnO nanofluids and its mechanism, *Ultrasound. Sonochem.* 34 (2017) 232–238, <https://doi.org/10.1016/j.ultsonch.2016.05.045>.
- [73] M.A. de Pedro, F. Cava, Structural constraints and dynamics of bacterial cell wall architecture, *Front. Microbiol.* 6 (2015), <https://doi.org/10.3389/fmicb.2015.00449>.
- [74] D.J. Waxman, J.L. Strominger, β-Lactam Antibiotics: Biochemical Modes of Action, ACADEMIC PRESS, INC. (1982), <https://doi.org/10.1016/b978-0-12-506303-6.50000-1>.
- [75] L.D. Renner, D.B. Weibel, Cardiolipin microdomains localize to negatively curved regions of *Escherichia coli* membranes, *Proc. Natl. Acad. Sci. U. S. A.* 108 (15) (2011) 6264–6269, <https://doi.org/10.1073/pnas.1015757108>.
- [76] K. Kikuchi, M. Sugiyama, C. Nishizawa-Harada, T. Kimura, The application of the *Escherichia coli* giant spheroplasts for drug screening with automated planar patch clamp system, *Biotechnol. Reports.* 7 (2015) 17–23, <https://doi.org/10.1016/j.biote.2015.04.007>.
- [77] P. Jollès, J. Jollès, What's new in lysozyme research? Always a model system, today as yesterday, *Mol. Cell. Biochem.* 63 (1984) 165–189, <https://doi.org/10.1007/BF00285225>.
- [78] D.C. Birdsell, E.H. Cota-Robles, Production and ultrastructure of lysozyme and ethylenediaminetetraacetate-lysozyme spheroplasts of *Escherichia coli*, *J. Bacteriol.* 93 (1) (1967) 427–437, <https://doi.org/10.1128/JB.93.1.427-437.1967>.
- [79] J.G. Voss, Lysozyme Lysis of Gram-Negative Bacteria without Production of Spheroplasts, *J. Gen. Microbiol.* 35 (2) (1964) 313–317, <https://doi.org/10.1099/00221287-35-2-313>.
- [80] R.E. Wooley, J.L. Blue, In-vitro effect of EDTA-TRIS-lysozyme solutions on selected pathogenic bacteria, *J. Med. Microbiol.* 8 (1) (1975) 189–194.
- [81] Ž. Pandur, I. Dogsa, M. Dular, D. Stopar, Liposome destruction by hydrodynamic cavitation in comparison to chemical, physical and mechanical treatments, *Ultrasound. Sonochem.* 61 (2020) 104826, <https://doi.org/10.1016/j.ultsonch.2019.104826>.
- [82] J. Zevnik, M. Dular, Liposome destruction by a collapsing cavitation microbubble: A numerical study, *Ultrasound. Sonochem.* 78 (2021) 105706, <https://doi.org/10.1016/j.ultsonch.2021.105706>.
- [83] T.C. Marentic, B. Kusler, G.G. Yaralioglu, S. Liu, E.O. Häggström, B.T. Khuri-Yakub, Microfluidic sonicator for real-time disruption of eukaryotic cells and bacterial spores for DNA analysis, *Ultrasound Med. Biol.* 31 (9) (2005) 1265–1277, <https://doi.org/10.1016/j.ultrasmedbio.2005.05.005>.
- [84] Ž. Pandur, D. Stopar, Evolution of mechanical stability from lipid layers to complex bacterial envelope structures (2020), <https://doi.org/10.1016/j.bab.2020.09.005>.
- [85] G. Van Den Bogaart, N. Hermans, V. Krasnikov, B. Poolman, Protein mobility and diffusive barriers in *Escherichia coli* : consequences of osmotic stress, *Mol. Microbiol.* 64 (2007) 858–871, <https://doi.org/10.1111/j.1365-2958.2007.05705.x>.
- [86] W. Vollmer, P. Born, Bacterial cell envelope peptidoglycan, in: *Microb. Glycobiol.*, Elsevier, 2010: pp. 15–28. doi:10.1016/B978-0-12-374546-0.00002-X.
- [87] R.C. Hughes, P.F. Thurman, E. Stokes, Estimates of the porosity of *Bacillus licheniformis* and *Bacillus subtilis* cell walls, *Z. Immunforsch. Exp. Klin. Immunol.* 149 (1975) 126–135. <http://www.ncbi.nlm.nih.gov/pmc/articles/PMC2400759/>.
- [88] B. Blasco, A.G. Pisabarro, M.A. de Pedro, Peptidoglycan biosynthesis in stationary-phase cells of *Escherichia coli*, *J. Bacteriol.* 170 (1) (1988) 5224–5228.
- [89] M.A. Snowden, H.R. Perkins, Peptidoglycan cross-linking in *Staphylococcus aureus*. An apparent random polymerisation process, *Eur. J. Biochem.* 191 (2) (1990) 373–377, <https://doi.org/10.1111/j.1432-1033.1990.tb19132.x>.
- [90] D. Gully, D. Gargani, K. Bonaldi, C. Grangeteau, C. Chaintréuil, J. Fardoux, P. Nguyen, R. Marchetti, N. Nouwen, A. Molinaro, P. Mergaert, E. Giraud, A Peptidoglycan-Remodeling Enzyme Is Critical for Bacteroid Differentiation in *Bradyrhizobium* spp. During Legume Symbiosis, *Mol. Plant-Microbe Interact.* 29 (6) (2016) 447–457, <https://doi.org/10.1094/MPMI-03-16-0052-R>.
- [91] J. Frías, F. Ribas, F. Lucena, Substrate affinity from bacterial strains and distribution water biofilms, *J. Appl. Bacteriol.* 76 (1994) 182–189, <https://doi.org/10.1111/j.1365-2672.1994.tb01614.x>.

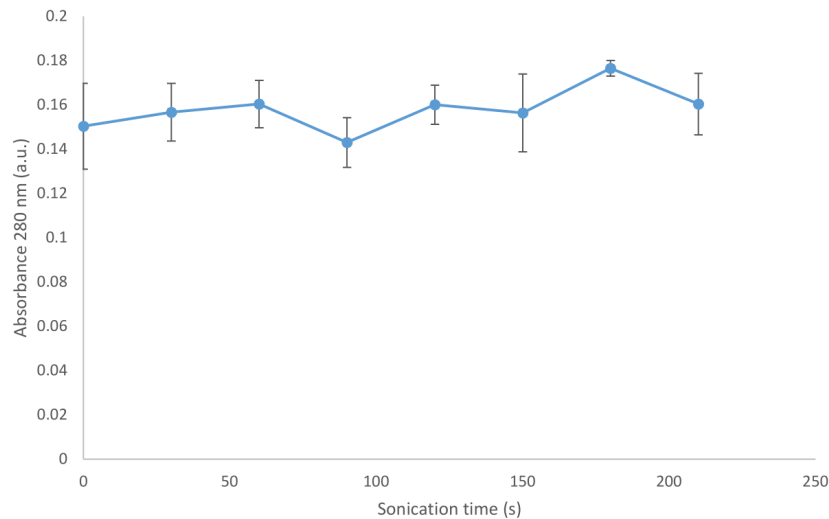
1    **Supplementary information**

2



4    **Fig. S1.** Microscopic images of exponential *E. coli*-gfp cells before and after the treatment with ultrasound for 20  
5    s. Cells with compromised membrane were stained with propidium iodide – PI (red). The total bacterial count after  
6    sonication significantly decreased. Most of the cells after sonication disintegrated and are not visible on the B  
7    panel. However, some of the cells remained and were either viable (green stained) or in the process of decaying  
8    (red or yellow stained indicated by arrows). The scale bar represents 20  $\mu\text{m}$ .

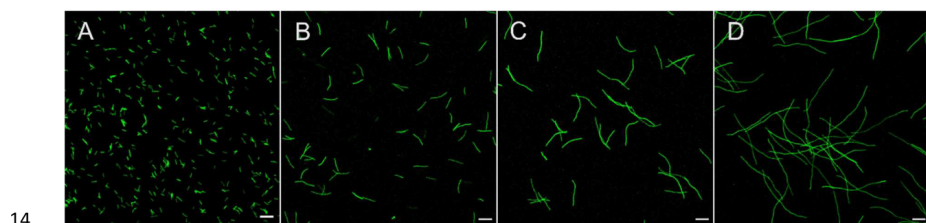
9



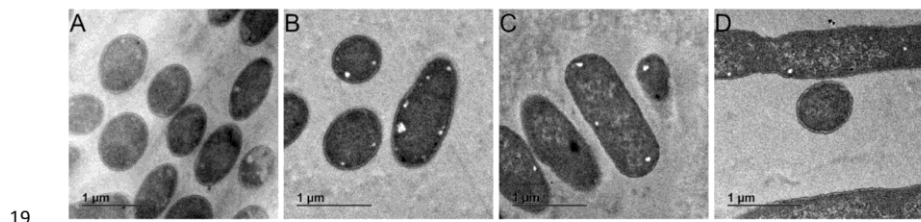
10

11 **Fig. S2:** DTT ROS assay. Samples were sonicated for 210 s and absorbance at 280 nm was determined in 10 mM  
12 DTT solution. Error bars represent standard deviation (n=3). No significant ROS was detected.

13

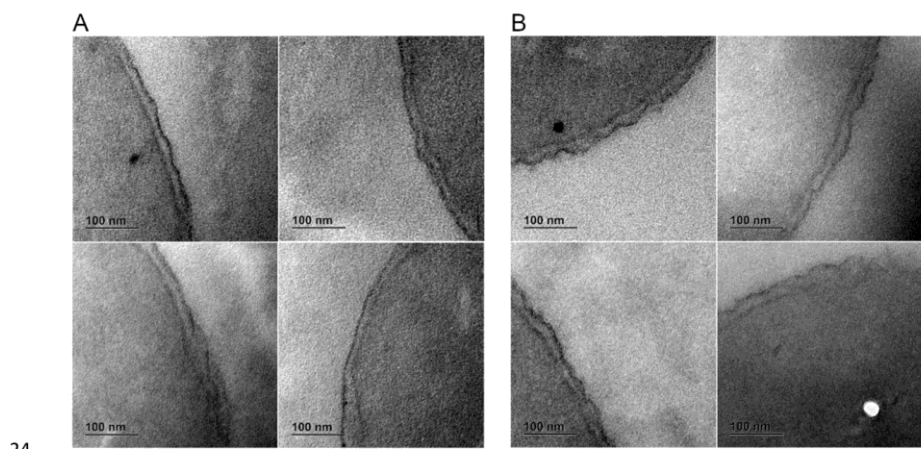


14  
15 **Fig. S3:** Confocal fluorescence images of filaments lengths (after different duration of Cephalexin treatment). A)  
16 image shows approx. 5  $\mu$ m long filaments (after 30 min of Cephalexin treatment); B) image shows approx. 20  $\mu$ m  
17 long filaments; C) image shows approx. 50  $\mu$ m long filaments; D) image shows approx. 90  $\mu$ m long filaments after  
18 150 min of Cephalexin treatment. Scale bar is 20  $\mu$ m.



20 **Fig. S4:** TEM micrographs of *E. coli* cells (A) gfp cells in stationary growth phase, (B) *eps-* mutant in stationary  
21 growth phase, (C) gfp cells in exponential growth phase and (D) gfp cells in exponential growth phase, treated  
22 with cephalexin.

23



25 **Fig. S5:** TEM micrographs of cell wall ultrastructure from *E. coli* cells in exponential growth phase (A) and cells  
26 treated with cephalexin (B). Note higher degree of wrinkling of outer membrane in cells treated with cephalexin.

27

28

29     **Table S1:** Bacterial counts (CFU/ml) prior to the cell wall modification, after cell wall modification, and after  
30     sonication (sonication time 90 s).

	Treatment	N <sub>0</sub> (CFU/ml)	N treated (CFU/ml)	N 90s sonication (CFU/ml)
EXponential Growth Phase	<i>Untreated</i>	1,5*10 <sup>9</sup> ± 3,0*10 <sup>8</sup>	1,5*10 <sup>9</sup> ± 3,0*10 <sup>8</sup>	6,5*10 <sup>5</sup> ± 2,7*10 <sup>5</sup>
	<i>eps-</i>	1,5*10 <sup>9</sup> ± 3,0*10 <sup>8</sup>	5,0*10 <sup>8</sup> ± 1,2*10 <sup>8</sup>	2,5*10 <sup>5</sup> ± 1,1*10 <sup>5</sup>
	<i>Lysozyme</i>	1,5*10 <sup>9</sup> ± 3,0*10 <sup>8</sup>	1,3*10 <sup>9</sup> ± 4,7*10 <sup>8</sup>	5,5*10 <sup>5</sup> ± 3,0*10 <sup>5</sup>
	<i>EDTA</i>	1,5*10 <sup>9</sup> ± 3,0*10 <sup>8</sup>	8,6*10 <sup>7</sup> ± 3,7*10 <sup>5</sup>	3,7*10 <sup>5</sup> ± 3,9*10 <sup>5</sup>
	<i>Cephalexin</i>	1,5*10 <sup>9</sup> ± 3,0*10 <sup>8</sup>	4,4*10 <sup>8</sup> ± 6,8*10 <sup>7</sup>	3,2*10 <sup>5</sup> ± 2,5*10 <sup>5</sup>
	<i>Spheroplasts</i>	1,5*10 <sup>9</sup> ± 3,0*10 <sup>8</sup>	2,0*10 <sup>6</sup> ± 1,3*10 <sup>6</sup>	8,0*10 <sup>3</sup> ± 9,7*10 <sup>3</sup>
Stationary Growth Phase	<i>Untreated</i>	1,1*10 <sup>10</sup> ± 1,4*10 <sup>9</sup>	1,1*10 <sup>10</sup> ± 1,4*10 <sup>9</sup>	4,7*10 <sup>8</sup> ± 2,2*10 <sup>8</sup>
	<i>eps-</i>	1,1*10 <sup>10</sup> ± 1,4*10 <sup>9</sup>	4,5*10 <sup>9</sup> ± 1,8*10 <sup>9</sup>	1,4*10 <sup>8</sup> ± 9,3*10 <sup>7</sup>
	<i>Lysozyme</i>	1,1*10 <sup>10</sup> ± 1,4*10 <sup>9</sup>	8,9*10 <sup>9</sup> ± 2,5*10 <sup>9</sup>	5,1*10 <sup>8</sup> ± 2,4*10 <sup>8</sup>
	<i>EDTA</i>	1,1*10 <sup>10</sup> ± 1,4*10 <sup>9</sup>	1,1*10 <sup>10</sup> ± 5,8*10 <sup>9</sup>	1,5*10 <sup>9</sup> ± 8,0*10 <sup>8</sup>
	<i>Cephalexin</i>	1,1*10 <sup>10</sup> ± 1,4*10 <sup>9</sup>	1,2*10 <sup>10</sup> ± 2,1*10 <sup>9</sup>	6,1*10 <sup>8</sup> ± 2,5*10 <sup>8</sup>
	<i>Spheroplasts</i>	1,1*10 <sup>10</sup> ± 1,4*10 <sup>9</sup>	2,3*10 <sup>7</sup> ± 3,8*10 <sup>7</sup>	6,5*10 <sup>5</sup> ± 3,6*10 <sup>5</sup>

31

32

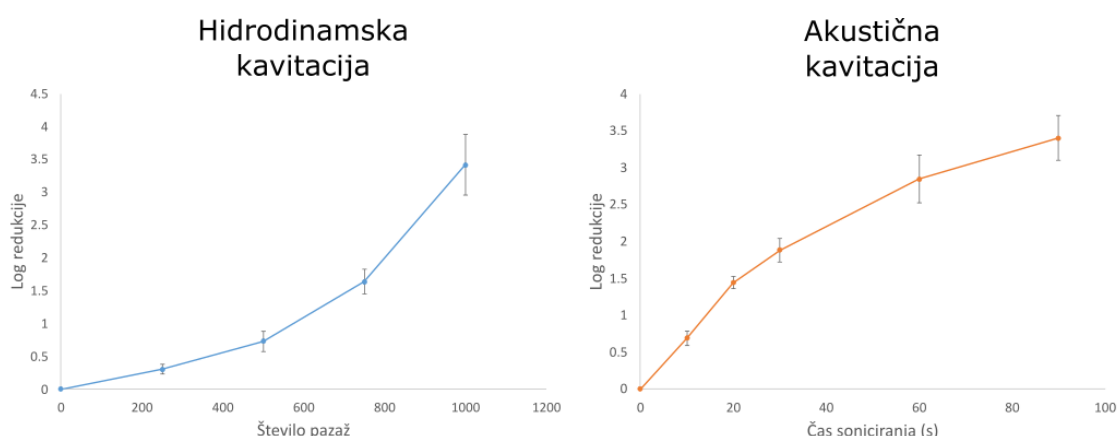
## 2.2 OSTALO POVEZOVALNO ZNANSTVENO DELO

Eksperimentalno delo in analiza eksperimentalnih rezultatov predstavljenega dela je plod lastnega dela z nasveti mentorja in somentorja, numerična analiza kavitacijskega mikromehurčka in odziva na bakterijske celice je plod dela sodelavca v raziskovalni skupini dr. Jure Zevnik, ki je omogočila natančnejši vpogled in opis pojava kavitacije mikromehurčka in odziva na bakterijske celice.

### 2.2.1 Vpliv posameznega kavitacijskega mehurčka na bakterijsko celico

#### 2.2.1.1 Uvod

V predhodnih poglavjih smo pokazali, da ima kavitacija velik vpliv na populacije lipidnih veziklov, bakterijskih sferoplastov, mehansko ošibljenih bakterijskih celic, kot tudi intaktnih bakterijskih celic. Na Slika 3 je prikazano, da je lahko populacija hidrodinamsko ali akustično generiranih mehurčkov učinkovito znižala število bakterijskih celic.



Slika 3: Učinek hidrodinamske in akustične kavitacije na *E. coli*.

Učinek hidrodinamske (levo, modra krivulja) in akustične (desno, oranžna krivulja) kavitacije na bakterijsko kulturo *E. coli* v eksponentni fazi rasti. Uporabljena mikrokavitacijska naprava za hidrodinamsko kavitacijo je imela Venturijevo zožitev z dimenzijsami 225x150 µm, pretok 1,6 ml/s, tlak na vstopni strani zožitve je bil 10 bar. Točke na krivulji predstavljajo povprečje dveh eksperimentalnih ponovitev, napaka je prikazana kot standardni odklon ponovitev. Akustična kavitacija je bila generirana z ultrazvočno sondijo (150 W), premer konice 3mm, 15 µm amplituda. Točke na krivulji predstavljajo povprečje petih eksperimentalnih ponovitev, napaka je prikazana kot standardni odklon ponovitev.

V teh eksperimentih smo generirali gručo kavitacijskih mehurčkov, ki je delovala na gručo lipidnih veziklov oziroma populacijo bakterijskih celic. Zaradi kompleksnosti kavitacijskega fenomena in za boljše razumevanje pojava je nujno potrebno kavitacijo skalirati na nivo posameznega mehurčka in posamezne celice. V tem poglavju predstavljamo še neobjavljene rezultate razvoja nove metode, ki omogoča proučevanje interakcije med posameznim kavitacijskim mikromehurčkom in bakterijsko celico.

Kavitacija je široko uporabljena metoda v raziskovalnem svetu in industriji, in se uporablja za namene čiščenja, dezinfekcije, za ustvarjanje disperzij, uničevanja celic in izolacijo celičnih komponent (Zupanc in sod., 2019). Makroskopski učinek kavitacije na bakterijske celice je rezultat številnih dogodkov implozije kavitacijskih mehurčkov na različnih časovnih skalah (Gogate in Pandit, 2005; Paliwal in Mitragotri, 2006; Zupanc in sod., 2019). Kljub številnim raziskavam, še vedno ni jasen natančen mehanizem (mehanski, fizikalni ali kemijski stresorji) kot vzrok za inaktivacijo bakterij. Kot omenja Prosperetti (2004), veliko raziskav je že bilo narejenih na temo mehurčkov, vendar še vedno ne poznamo točen mehanizem interakcije mehurčka z bakterijsko celico. Da bi lahko ocenili učinek izbranega kavitacijskega mehurčka na posamezno celico se je potrebno približati velikostni skali, ki je podobna velikosti bakterijskih celic, torej mikrometrski velikostni skali. Na tako majhni velikostni skali pa je izziv kako nadzorovati vzbujanje in pojav kavitacije. Kavitacija na mikrometrski skali namreč steče na mikrosekundni časovni skali.

Odziv bakterijske celice na mehanski stres pri različnih časovnih frekvencah je različen in nakazuje na gumijast odziv pri nizkih frekvencah, viskoelastični odziv pri srednjih frekvencah in drobljiv (steklast) odziv pri visokih frekvencah (Vadillo-Rodríguez in Dutcher, 2011). Srednje frekvence korelirajo karakterističnemu bakterijskem podvojevalnemu času, kjer so bakterije optimalno prilagojene na okolico in jih je v tem časovnem okvirju najtežje uničiti. Iz vidika materialnih lastnosti bakterijske celice bi morala biti bakterija najbolj dovzetna na propad pri visokofrekvenčnih mehanskih obremenitvah saj se lastnosti materiala spremenijo iz podajne strukture v krhko, kar bi v primeru bakterijske celice pomenilo nastanek ireverzibilnih celičnih poškodb in posledično lizo celic. Mehanski odziv bakterijskih celic pri nizkih in srednjih frekvencah je dokaj dobro opisan z metodami mikroskopije na atomsko silo, študij v laminarnih tokovih ter rast bakterij v gelih (Amir in sod., 2014; Tuson in sod., 2012; Vezenov in Barrett, 2013), medtem ko odziv bakterij na visokofrekvenčne mehanske obremenitve ni dobro raziskan.

Interakcija kavitacijskega mehurčka v velikosti nekaj deset mikrometrov ali več z evkrationtskimi celicami je že bila opisana (Jasikova in sod., 2019; O'Connor in sod., 2021; Ohl in sod., 2006; Rau in sod., 2006). V večini teh primerov so uporabili za generacijo kavitacije laserski preboj, ki omogoča natančen časoven in prostorski nadzor nastanka kavitacijskega mehurčka. Vendar pri laserskem preboju nastane plazma, ki povzroči nastanek visoko reaktivnih kisikovih radikalov, kateri lahko zamaskirajo mehanski efekt kavitacijskega mehurčka na biološko strukturo (Patinglag in sod., 2021; Sinibaldi in sod., 2019). Podobne raziskave pri bakterijah še ni bilo. Pri bakterijah se poleg otežene metodologije za generiranja majhnega mikromehurčka pojavi še dodaten izziv zaznavanja sprememb zaradi majhne velikosti bakterije, ki meji na difrakcijsko mejo svetlobnega mikroskopa.

V raziskavi smo opazovali interakcijo med kavitacijskim mikromehurčkom in posameznimi pritrjenimi bakterijskimi celicami *E. coli* v realnem času. Optična pinceta je omogočila natančno in hitro pozicioniranje mikromehurčka v bližini bakterijskih celic, kavitacijo mehurčka smo vzbudili s tlačnimi valovi, ki so nastali ob visokonapetostni razelektritvi. Kolaps mikromehurčka smo zajeli s hitro kamero, kjer smo z 0,7 µs časovnim intervalom zajemali potek kolapsa mikromehručka, ki je trajal nekaj mikrosekund. Vpliv kavitacijskega mikromehurčka na bakterijo je bil spremeljan s svetlobno in fluorescenčno mikroskopijo. Z dobljenimi eksperimentalnimi rezultati smo potrdili računsko analizo kolapsa mikromehurčka in njegovo interakcijo z bakterijo, ki nam je omogočil bolj natančen vpogled v dinamiko raziskovanega fenomena. S pomočjo računske analize smo ocenili mejne vrednosti za strižno napetost in hidrodinamsko silo, ki povzroči poškodovanje ali odtrganje bakterijske celice iz površine.

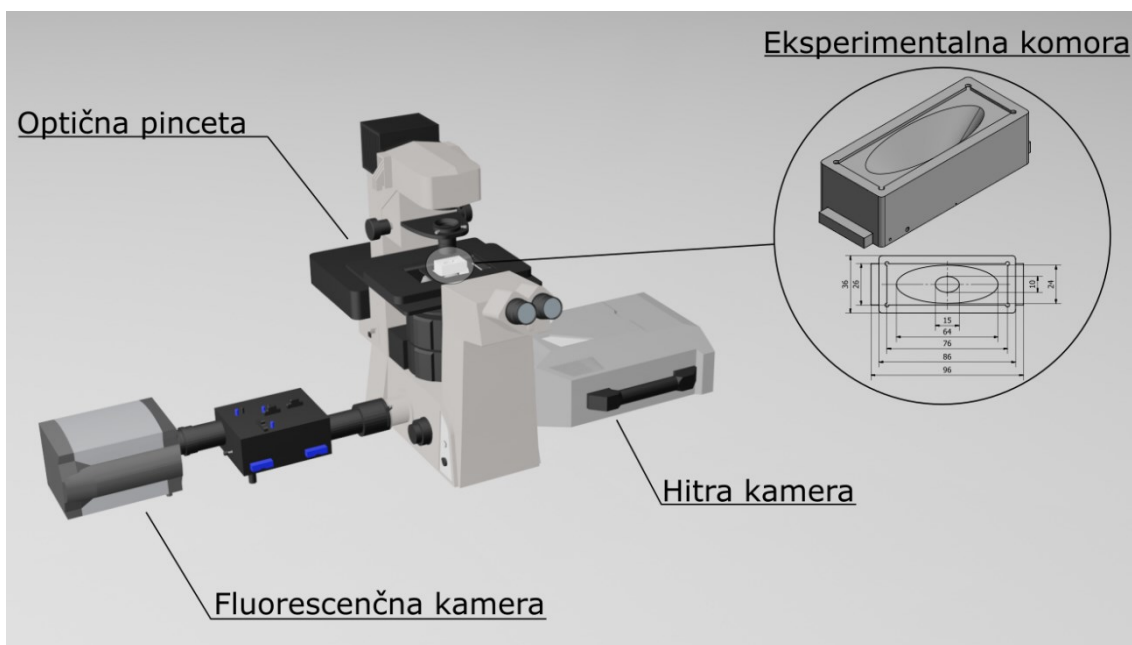
#### 2.2.1.2 Materiali in metode

##### **Generiranje kavitacijskega mikromehurčka**

Za nastanek mikrometrskoga kavitacijskega mehurčka smo uporabili kombinacijo optične pincete in visokonapetostne razelektritve. Z laserskim pulzom smo ustvarili stabilni mikrometrski mehurček, ki je služil kot zarodno jedro za kavitacijski mikromehurček. Nato smo ustvarili visokonapetostno razelektritev kjer so nastali tlačni valovi. Ti so povzročili razteg in kolaps zarodnega mehurčka. Obe metodi sta bili združeni v eksperimentalni komori, ki je bila nameščena na inverten mikroskop.

##### **Oblika eksperimentalne komore**

Komora je bila eliptične oblike in je bila narejena s 3D tiskalnikom. Tehnična skica komore je predstavljena na Slika 4. Večja ovalna odprtina je bila zaprta z objektnim stekelcem (76 x 26 mm, Menzel Gläser, Nemčija) in zatesnjena z epoksi lepilom. Manjša ovalna odprtina je bila zaprta z #1.5 krovnim stekelcem (60 x 24 mm, Menzel Gläser, Nemčija) in zatesnjena z VALAP tesnilno mešanicom (Valap Sealant, 2015). Za pozicioniranje visokonapetostne razelektritve v komori smo uporabili volframove igle, ki so bile postavljene na sredini komore, 0,5 mm nad krovnim stekelcem. Komora je bila napolnjena s svežo destilirano vodo (približno 15 ml), kateri smo dodali magnetne kroglice (končna koncentracija je bila približno  $3,7 \times 10^6$  kroglic/ml, Bangs Laboratories, ZDA). Pripravljena in zatesnjena komora je bila nameščena na inverten mikroskop Nikon Ti-U (Nikon Instruments Inc., ZDA).



Slika 4: Shematski prikaz eksperimentalne postavitev.

Optična pinceta je bila nameščena na inverten mikroskop skupaj s hitro in fluorescenčno kamero. S hitro kamero smo zajeli potek kolapsa mikromehurčka, s fluorescenčno kamero smo zajeli odziv bakterijskih celic na kolaps mikromehurčka. Eksperimentalna komora je bila nameščena na mikroskop z manjšo ovalno odprtino navzdol proti objektivom. V eksperimentalni komori smo z optično pinceto naredili mikromehurček, nato smo z visokonapetostno razelektritvijo ustvarili tlačne valove, ki so povzročili kavitiranje zarodnega mikromehurčka.

### Generiranje visokonapetostne razelektritve

Med visokonapetostno razelektritvijo je na mestu razelektritve nastal milimetrski kavitacijski mehurček, ki je generiral udarne tlačne valove (slika 6). Za generiranje razelektritve v deionizirani vodi smo uporabili piezoelektrični aktuator s 16 kV pulzom. Oblike naprave z vzmetnim mehanizmom omogoča ponovljive udarce na keramičen piezoelektrični aktuator. Kapacitivnost piezoaktuatorja je bila ocenjena na približno 30 pF. Za natančno pozicioniranje razelektritve smo uporabili mikrometrske volframove kirurške igle (Roboz surgical instrument, ZDA, RS-6065, 0,5 mm premer, zožane v mikrometrsko konico), katere smo postavili na željeno medsebojno razdaljo. Mehansko proženje aktuatorja je bilo računalniško krmiljeno preko LabView programske opreme. S spremenjanjem razdalje med iglama smo lahko regulirali maksimalen radij razelektritvenega mehurčka. V nadaljnjih eksperimentih smo imeli nastavljenou medsebojno razdaljo med iglama na 75 µm.

## Generiranje zarodnega mikromehurčka

Zarodni mehurček smo generirali s pomočjo laserskega sistema optične pincete (Aresis Tweez 300, Slovenija). Optična pinceta je opremljena s 1064 nm valovno dolžino laserja (nominalna moč 5 W). Akusto-optični zrcalni sistem omogoča natančno pozicioniranje mikrometrskih delcev. Delce z visoko absorpcijskim indeksom v infrardečem spektru valovanja (na primer zlati ali magnetni delci) lahko z obsevanjem laserja segrejemo, zaradi česar pride na površini delca do nastanka pare v okoliški kapljevini (Bhuyan in sod., 2018; Quinto-Su, 2014). S kratkim laserskim pulzom (17 µs) visoke intenzitete (moč obsevanja približno  $2 \times 10^8$  W/cm<sup>2</sup>), smo povzročili lokalni nastanek parnega mehurčka na površini magnetne kroglice (Bangs Laboratories, ZDA, ProMag 3 Series - 3 µm premer). Pozicioniranje magnetne kroglice je potekalo pri veliko nižjih intenzitetah laserja (moč obsevanja okrog  $2 \times 10^5$  W/cm<sup>2</sup>). Življenska doba zarodnega mikromehurčka je bila v rangu milisekunde do sekunde. Ko smo združili generiranje zarodnega mikromehurčka z visokonapetostno razelektritvijo in nastankom tlačnih valov je prišlo do hitre ekspanzije zarodnega mehurčka in nato implozije mikromehurčka na mikrosekundni časovni skali (Slika 7).

## Zajem slik s hitro kamero

Za zajem hitrih dogodkov kot je kolaps mikrometrskega zarodnega mehurčka smo uporabili hitro kamero Photron SA-Z type 2100K-M-64GB (Photron, Japonska). Pri zajemu slik razelektritvenega mehurčka smo uporabili objektiv z 10x povečavo, Nikon CFI E Plan Achromat 10X (Nikon Instruments Inc., ZDA) z nastavtvami kamere: 210000 sličic na sekundo (fps), hitrost zaslone 1 µs, resolucija 384x160 pikslov. Za zajem slik kolapsa mikromehurčka smo uporabili 60x objektiv z vodno imerzijo, Nikon CFI Apo NIR 60X W (Nikon Instruments Inc., ZDA) z nastavtvami kamere: 1440000 fps, 0,38 µs hitrost zaslone in resolucija slik 128x16 pikslov. Za zajem tlačnih valov pri razelektritvi smo uporabili kamero Kirana 7M s hitrostjo zajema 5000000 fps in femtosekundnim laserjem kot vir svetlobe. Zajem slik je bil sinhroniziran s proženjem kolapsa mikromehurčka.

## Karakterizacija tokovnega polja med kolapsom mikromehurčka

Eksperimentalna komora je bila napolnjena z deionizirano vodo in magnetnimi kroglicami kot je opisano zgoraj, dodali pa smo še steklene kroglice (4,2 µm diameter, Bang Laboratories, ZDA). Končna koncentracija kroglic v raztopini je bila približno  $10^4$  kroglic/ml. Steklene kroglice so bile postavljene z optično pinceto na določeno razdaljo od mesta kavitacijskega mehurčka. Zajem slik je potekal s hitro kamero kot je opisano zgoraj. Ob kolapsu mehurčka smo spremljali premik steklene kroglice. Položaj kroglice smo računalniško določili s programom ImageJ (1.53 f51) in vtičnikom TrackMate

(Tinevez in sod. 2017). Z vtičnikom smo najprej avtomatsko detektirali kroglico z Laplacian of Gaussian filtrom z nastavljenim premerom objekta 4,2  $\mu\text{m}$ . Dodatno smo zaznane objekte ročno preverili in jih po potrebi popravili. Za sledenje premika kroglice smo nadaljnje uporabili sledilnik »linear assignment problem« (LAP). S pridobitvijo položaja kroglice med kolapsom mikromehurčka smo lahko izračunali tok tekočine v bližini kavitirajočega mehurčka.

## Bakterijske celice

### Priprava bakterijske kulture

Uporabili smo bakterijsko kulturo *Escherichia coli* MG1655 z vstavljenim genom za sintezo zelenega fluorescentnega proteina (ang. green fluorescent potein - gfp) pod inducibilnim izopropil- $\beta$ -D-tiogalaktopiranozid (IPTG) promotorjem in selekcijskim markerjem z odpornostjo na antibiotik kanamicin (Kn). Zamrzljeno kulturo na  $-80^{\circ}\text{C}$  smo nacepili na trdno lizogeno agarsko (LB) gojišče z dodanim antibiotikom kanamicin ( $50 \mu\text{g}/\text{ml}$ ) z razmazom do posameznih kolonij. Nato smo posamezno bakterijsko kolonijo prenesli v tekoče LB gojišče s kanamicinom in IPTG ( $400 \mu\text{g}/\text{ml}$ ). Tako pripravljeno kulturo smo stresali preko noči na stresalniku s frekvenco stresanja 200 obratov /min v topli sobi na  $37^{\circ}\text{C}$ . Inkubacijski čas prekonočne kulture je bil približno 16 ur.

### Vezava bakterijskih celic

Za vezavo celic na steklo smo uporabili #1.5 mikroskopsko krovno steklo v dimenzijah  $60 \times 24 \text{ mm}$  (Menzel-Gläser, Nemčija). Najprej smo krovna stekelca očistili s soniciranjem v ultrazvočni banjici (PRO MED 50, at 120 W, 40 kHz, ASonic; Slovenija) in 96 % etanolu s časom soniciranja 20 min in pri normalni amplitudi. Nato smo očiščena stekelca sprali v deionizirani vodi ter jih osušili s komprimiranim zrakom. Suha krovna stekelca smo nato prenesli v napravo za čiščenje s plazmo (Harrick Plasma Inc, ZDA) kjer smo še dodatno očistili stekelca s plazmo pri visokem radiofrekvenčnem načinu in zrakom. Čas obdelovanja s plazmo je bil 60 s. Po tretiranju s plazmo smo na sredino stekelca dodali  $50 \mu\text{l} 0,1\% (\text{w/v})$  vodne raztopine poli-L-lizin (PLL) (Sigma-Aldrich, ZDA) in inkubirali kapljico 10 min pri sobni temperaturi. Po inkubaciji smo odvečno PLL raztopino sprali s čisto deionizirano vodo in osušili stekelca na zraku. Tako pripravljena stekelca smo shranili na suhem in v temi do uporabe pri eksperimentih. Nato smo vzeli 10 ml prekonočne kulture bakterije *E. coli*, katero smo centrifugirali 4 minute pri 5000 relativnih centrifugalnih enotah (rcf) pri sobni temperaturi. Supernatant smo odlili in resuspendirali pelet celic v sveži deionizirani vodi. Postopek smo ponovili 3-krat. Po tretjem centrifugiranju smo celice skoncentrirali v  $100 \mu\text{l}$  deionizirane vode.  $50 \mu\text{l}$  skoncentrirane kulture smo nanesli na sredino krovnega

stekelca s PLL in pustili stati kulturo na stekelcu 5 min pri sobni temperaturi. Po koncu inkubacije smo nevezane celice nežno sprali z deionizirano vodo, stekelce z vezanimi bakterijami na steklo pa smo položili čez manjšo ovalno odprtino komore in zatesnili z VALAP tesnilom. Pred tem smo eksperimentalno komoro pripravili kot je opisano zgoraj, le da smo v tekočino dodatno dodali 15 µl membransko nepropustnega fluorescentnega barvila propidijev jodid (PI).

### Fluorescenčna mikroskopija

Za vizualizacijo bakterijskih celic smo uporabili visoko občutljivo EMCCD kamero (Andor Ixon 888 Ultra, Oxford Instruments, Združeno kraljestvo). Za simultan zajem več flurescenčnih kanalov smo dodatno uporabili še optični sistem Cairn Optosplit III (Cairn Research, Združeno kraljestvo). Za vzbujanje vseh celic smo uporabili gfp proteina (eksitacija s 460 nm pri 30 % intenziteti, emisijski filter 525/40 nm). Celice, ki so bile poškodovane so se obarvale z barvilm PI, za katerega smo obsvetili vzorec s 550 nm valovno dolžino in 30 % intenziteto, emisijski filter je bil 640/40 nm. Čas izpostavljenosti senzorja signalu je bil pri obeh kanalih 100 ms. Interval zajema slik na obeh kanalih je bil nastavljen na 5 s časovni interval. Skupen čas zajemanja slik je bil 5 min. Zaradi hitrega bledenja gfp fluorokroma smo dodatno zajeli mikroskopske slike še s svetlobno presevno tehniko pred začetkom in po koncu zajemanja fluorescenčnih slik. Resolucija zajetih slik je bila 1024x512 piksov (vidno polje: 223,5 x 111,7 µm).

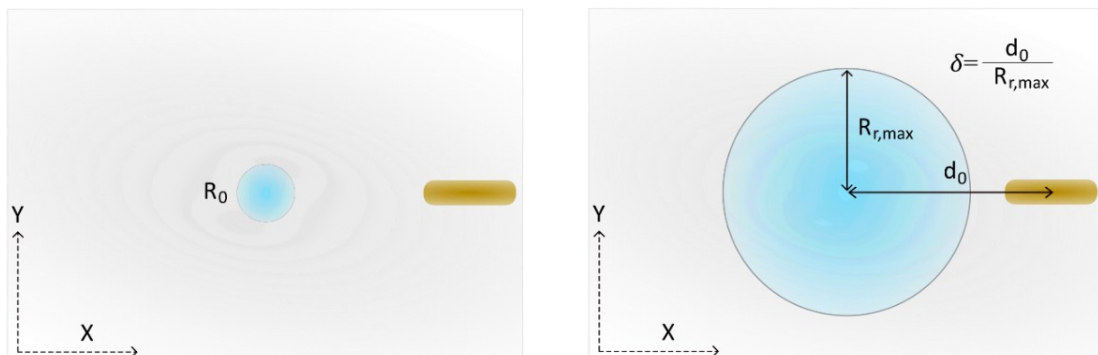
### Analiza slik

Mikroskopske slike smo analizirali z računalniškim programom ImageJ (1.53 f51). najprej smo mikroskopske slike iz različnih kanalov (svetlobna, gfp in PI) poravnali med kanali. Nato smo preko macro ukaza izvedli serijo analiz, da smo dobili lokacijo posameznih bakterij na vsakem kanalu. Najprej smo iz posnetkov hitre kamere določili center in maksimalni radij kavitacijskega mehurčka. Na podlagi pozicije in maksimalnega radija kavitacijskega mehurčka smo centrirali mikroskopske slike na center kavitacijskega mehurčka in obrezali sliko na 2x maksimalni radij mikromehurčka. Z obrezanimi slikami in pravovnim segmentiranjem slik smo dobili bakterijske celice pred in po kolapsu mikromehučka (svetlobna mikroskopija). Slike so bile še dodatno ročno pregledane, kjer smo celice, ki so se prekrivale ročno ločili na dva objekta. Na binarnih slikah posameznih celic smo uporabili vtičnik »Analyze Particles« kjer smo dobili koordinate o centru posameznega objekta, torej bakterije. Odtrgane celice smo določili z matematičnim odštevanjem binarnih slik pred in po kolapsu. Dodatno smo analizirali fluorescenčne slike kjer so se celice obarvale s propidijevim jodidom, katere celice smo označili kot poškodovane. Poškodovane celice smo določili prav tako z odštevanjem binarnih slik po in pred kolapsom mikromehurčka.

## Analiza rezultatov

Shematski prikaz na Slika 5 prikazuje interakcijo med bakterijsko celico in kavitacijskim mehurčkom pri različnih perspektivah s prikazanimi parametri, ki smo jih uporabili pri nadaljnji analizi.

### ZGORNJI POGLED



### STRANSKI POGLED



**Slika 5: Shematski prikaz interakcije mikromehurčka in bakterijske celice iz različnih perspektiv.** Levi sliki predstavljata začetno stanje pred kolapsom mikromehurčka, desni sliki predstavljata mikromehurček z maksimalnim radijem. Pri zgornjem pogledu je določena razdalja med centrom mikromehurčka in centrom celice ( $d_0$ ), ter maksimalni radij mikromehurčka ( $R_{r,max}$ ). Na podlagi teh dveh parametrov smo določili brez-dimenzijsko razdaljo  $\delta$ , ki opisuje razmerje med razdaljo celice in maksimalnim radijem mikromehurčka. Pri stranskem pogledu začetnega stanja mikromehurčka  $d_b$  predstavlja začetno razdaljo med mikromehurčkom in trdno steno z začetnim radijem  $R_0$  pri normalnem okoliškem tlaku in temperaturi.

Pozicijo celic iz analize mikroskopskih slik smo pretvorili v brez-dimenzijsko razdaljo  $\delta$  po enačbi:

$$\delta = \frac{\sqrt{(x_{celica} - x_{center\ mikromehurčka})^2 + (y_{celica} - y_{center\ mikromehurčka})^2}}{R_{r,max}}. \quad \dots(1)$$

kjer  $x_{\text{celica}}$  in  $y_{\text{celica}}$  predstavljata koordinate položaja celice,  $x_{\text{center}}$  mikromehurčka in  $y_{\text{center}}$  mikromehurčka predstavljata koordinate centra mikromehurčka,  $R_{r,\max}$  pa predstavlja maksimalen projiciran horizontalen radij mikromehurčka. Brez-dimenzijska razdalja δ ima razpon med vrednostma 0 in 2, kjer 0 vrednost pomeni da je celica v centru mehurčka, medtem ko vrednost 2 predstavlja lokacijo bakterije na 2x oddaljenosti od projiciranega maksimalnega radija mikromehurčka. Brezdimenzijske razdalje celic iz različnih mikroskopskih slik (začetno stanje, odtrgane ali poškodovane celice) smo potem kategorizirali v gruče s širino  $\Delta\delta = 0,1$  (skupaj 20 gruč). Kategoriziranim podatkom za vsak eksperiment smo potem določili verjetnosti za pričakovane izide odtrganja ali poškodovanja celice. Verjetnost odtrganja ali poškodovanja celice za j-to gručo in i-to eksperimentalno ponovitev je bila določena z enačbami:

$$p_{\text{odtrgana}}^{i,j} = \max \left[ \frac{N_{\text{odtrgana}}^{i,j}}{N_{\text{celica,pred}}^{i,j}}, \frac{N_{\text{celica,pred}}^{i,j} - N_{\text{celica,po}}^{i,j}}{N_{\text{celica,pred}}^{i,j}} \right], \quad \dots(2)$$

$$p_{\text{poškodovana}}^{i,j} = \frac{N_{\text{poškodovana}}^{i,j}}{N_{\text{celica,pred}}^{i,j}}, \quad \dots(3)$$

$$p_{\text{poškodovana,neodtrgana}}^{i,j} = \frac{N_{\text{poškodovana}}^{i,j}}{N_{\text{celica,po}}^{i,j}}. \quad \dots(4)$$

Vrednosti  $N_{\text{celica,pred}}^{i,j}$ ,  $N_{\text{celica,po}}^{i,j}$ ,  $N_{\text{odtrgana}}^{i,j}$  in  $N_{\text{poškodovana}}^{i,j}$  predstavljajo število celic v j-ti gruči i-te eksperimentalne ponovitve v začetnem stanju (pred) ali končnem stanju (po). Verjetnost za poškodovanje celic smo primerjali za začetno stanje ( $p_{\text{poškodovana}}^{i,j}$ ) in tudi na kočno stanje ( $p_{\text{poškodovana,neodtrgana}}^{i,j}$ ), kjer primerjamo verjetnost za poškodovanje ostalih celic, ker za odtrgane celice ne moremo sklepati o živosti.

## Numerične metode

Numerična analiza kavitacijskega mikromehurčka in odziva na bakterijske celice je plod dela sodelavcev v raziskovalni skupini, ki je omogočila natančnejši vpogled v potek kavitacije mikromehurčka in odziva na bakterijske celice. Izvedene so bile numerične simulacije dinamike mehurčka v bližini toge stene, kar nam je omogočilo podrobnejši mehanistični uvid v interakcijo med mikromehurčkom in bakterijskimi celicami. Simulacije vključujejo razrešitev tokovnega polja v bližini mehurčka, dinamike bližnjih suspendiranih kroglic in izračun obtežbe na steno pritrjene bakterijske celice.

## Teoretično ozadje

### Model dinamike mehurčka

Uporabljeni model dinamike tekočin Fluent (Ansys, ZDA) temelji na metodi končnih volumnov skupaj z metodo volumna tekočine za razrešitev stisljivega večfaznega toka. V splošnem je mogoče dinamiko mehurčkov matematično opisati z enačbami ohranitve mase, gibalne količine in energije. V tem primeru sta obravnavani dve fluidni fazi - plinasti mehurček in okoliška tekočina, njuna fazna meja pa je zajeta z reševanjem kontinuitetne enačbe za polje volumskega deleža  $\alpha_l$  tekoče faze. V naslednjem razdelku so količine in lastnosti, značilne za vsako fazo, označene z ustreznim indeksom  $i = g, l$ , ki označujeta plinasto oziroma tekočo fazo.

Enačbo ohranitve mase za kapljevinsko fazo lahko zapišemo kot

$$\frac{\partial \alpha_l \rho_l}{\partial t} + \nabla \cdot (\alpha_l \rho_l \mathbf{U}_l) = 0. \quad \dots(5)$$

Tukaj  $\rho_l$  in  $\mathbf{U}_l$  označujeta gostoto ter hitrostno vektorsko polje tekoče faze. Polje volumskega deleža plinske faze  $\alpha_g$  lahko izračunamo kot  $\alpha_g = 1 - \alpha_l$ . Ko sta znani obe polji volumskega deleža, lahko določimo prostorninsko povprečne lastnosti tekočine  $\phi$  v celotni računski domeni kot  $\phi = \sum_i \alpha_i \phi_i$ . V danem primeru to velja za gostoto  $\rho$ , dinamično viskoznost  $\mu$  in topotno prevodnost  $k$ .

Na podlagi določenih materialnih lastnosti lahko razrešimo enačbo ohranitve gibalne količine (enačba 6) in energije (enačba 7), kar rezultira v znanem skupnem hitrostnem  $\mathbf{U}$  in temperaturnem  $T$  polju.

$$\frac{\partial}{\partial t} (\rho \mathbf{U}) + \nabla \cdot (\rho \mathbf{U} \otimes \mathbf{U}) = -\nabla p + \nabla \cdot \boldsymbol{\tau} + \mathbf{b} \quad \dots(6)$$

$$\frac{\partial}{\partial t} (\rho e) + \nabla \cdot (\mathbf{U}(\rho e + p)) = \nabla \cdot (k \nabla T) \quad \dots(7)$$

Tukaj,  $p$  označuje tlak,  $\mathbf{b}$  masne sile,  $\boldsymbol{\tau}$  tenzor viskoznih napetosti in  $e$  skupno specifično energijo. Tenzor viskoznih napetosti lahko za Newtonske tekočine zapišemo kot

$$\boldsymbol{\tau} = \mu \left[ (\nabla \mathbf{U} + (\nabla \mathbf{U})^T) - \frac{2}{3} (\nabla \cdot \mathbf{U}) \mathbf{I} \right], \quad \dots(8)$$

medtem ko je skupna specifična energija upoštevana kot masno povprečena spremenljivka

$$e = \frac{\sum_i \alpha_i \rho_i e_i}{\sum_i \alpha_i \rho_i}. \quad \dots(9)$$

Skupno specifično energijo posamezne faze  $e_i$  lahko izrazimo kot  $e_i = h_i - \frac{p}{\rho_i} + \frac{|\mathbf{U}|^2}{2}$ , kjer  $h_i$  označuje specifično entalpijo i-te faze, izračunane iz specifične topote dane faze in znanega temperaturnega polja.

Vpliv površinske napetosti obravnavamo na fazni meji med plinasto in kapljevinsko fazo. Skok tlaka na fazni meji kapljevina-plin je modeliran s silo telesa v gibalni enačbi v skladu z modelom kontinuirne površinske sile (Brackbill in sod., 1992) in se lahko izrazi kot

$$\mathbf{b} = \sigma \frac{\rho (\mathbf{v} \cdot \frac{\mathbf{n}}{|\mathbf{n}|}) \nabla \alpha_g}{\frac{1}{2}(\rho_g + \rho_l)}. \quad \dots(10)$$

Tukaj  $\sigma$  označuje površinsko napetost med obema fazama, medtem ko je  $\mathbf{n}$  normala površine mehurčka, definirana kot  $\mathbf{n} = -\nabla \alpha_g$ .

Tekoča faza je modelirana kot stisljiva v skladu s Taitovo enačbo stanja:

$$\left(\frac{\rho}{\rho_{\text{ref}}}\right)^n = 1 + \frac{n(p - p_{\text{ref}})}{K_{\text{ref}}}. \quad \dots(11)$$

Člen  $n$  ustreza eksponentu gostote,  $K_{\text{ref}}$  pa referenčnemu modulu stisljivosti pri referenčnem tlaku  $p_{\text{ref}}$  (tabela 1). Plinska faza je modelirana z zakonom idealnega plina

$$\rho = \frac{p}{R_g^* T'} \quad \dots(12)$$

kjer  $R_g^*$  označuje specifično plinsko konstanto. Z upoštevanjem vsebine mehurčka kot idealnega plina zanemarjamo dejstvo, da kavitacijski mehurčki na splošno vsebujejo mešanico vodne pare in nekondenzirajočih plinov. S tem zanemarimo vsebnost vodne pare v mehurčku in mehanizme prenosa mase med mehurčkom in okoliško kapljevino. Čeprav lahko količina nekondenzirajočih plinov v mehurčku bistveno vpliva na magnitudo odboja mehurčkov in najvišje temperature v mehurčku, to bistveno ne vpliva na dinamiko mehurčkov do prvega kolapsa (Akhatov in sod., 2001). Iz tega razloga vidimo upoštevanje zakona idealnega plina kot pošten približek za trenutno obravnavani pojav.

### Model dinamike kroglice

Rast in kolaps kavitacijskega mikromehurčka lokalno inducirata časovno in prostorsko spremenljivo tokovno polje v okoliški tekočini, kar povzroči gibanje bližnjega krogelnega delca. Gibanje delcev lahko opišemo z gibalnim zakonom:

$$\ddot{x}_p = \frac{F_d}{m_p}. \quad \dots(13)$$

Tukaj  $F_d$  označuje hidrodinamsko silo upora na delec z maso  $m_p$  in pozicijo  $x_p$ . Nadpisane pike označujejo odvode količin po času. Za sferični delec z radijem  $R_p$  lahko silo upora zapišemo kot

$$F_d = \frac{1}{2} \rho_l \pi R_p^2 C_d (\mathbf{u} - \dot{\mathbf{x}}_p) |\mathbf{u} - \dot{\mathbf{x}}_p| \quad \dots(14)$$

kjer  $\rho_l$ ,  $\mathbf{u} = \mathbf{u}(t, x_p(t))$  in  $C_d$  predstavljajo gostoto tekočine, lokalno hitrost toka in koeficient hidrodinamskega upora. Slednjega lahko za krogelne delce zapišemo v obliki Kaskasove enačbe (Yow in sod., 2005):

$$C_d = \frac{24}{Re} + \frac{4}{\sqrt{Re}} + 0,4 \quad \dots(15)$$

in velja za Reynoldsova števila  $Re < 2 \cdot 10^5$ . Reynoldsovo število za kroglico je definirano kot

$$Re = \frac{2R_p \rho_l |\mathbf{u} - \dot{\mathbf{x}}_p|}{\mu_l}. \quad \dots(16)$$

### Model pritrjene celice

Podoben pristop lahko uporabimo v primeru, ko je celica pritrjena na steno. Ob predpostavki sferične oblike celice lahko ocenimo hidrodinamsko silo, ki jo na posamezno bakterijsko celico povzroči bližnji kavitacijski mikromehurček. Za pritrjeno sferično celico s polmerom  $R_c$  lahko silo upora zapišemo kot

$$F_d = \frac{1}{2} \rho_l \pi R_c^2 C_d \mathbf{u} |\mathbf{u}|. \quad \dots(18)$$

Tukaj  $\mathbf{u} = \mathbf{u}(t, x_{c,0})$  je lokalna hitrost toka na lokaciji celice  $x_{c,0}$ . Koeficient upora lahko določimo v skladu z enačbo 15, kjer Reynoldsovo število izračunamo kot

$$Re = \frac{2R_c \rho_l |\mathbf{u}|}{\mu_l}. \quad \dots(19)$$

### **Nastavitev modela**

#### Model dinamike mehurčka

Upoštevani sta dve fazи - plinasti mehurček in okoliška kapljevina tekočina (Slika 5). Rast prvotno stabilnega mikromehurčka (začetni radij  $R_0=1,1 \text{ } \mu\text{m}$ ) dosežemo z

nadtlakom v notranjosti mehurčka (začetni tlak mehurčka  $1,96 \times 10^8$  Pa) v primerjavi s tlakom okolice ( $p_\infty = 101325$  Pa). Temperatura okoljske tekočine je 293,15 K. Mehurček je lociran med  $d_b = 1,5$  µm in 15 µm (korak 1,5 µm) stran od stene, kar v danem primeru rezultira v brez-dimenzijski razdalji mehurček-stena  $\gamma = d_b/R_{r,\max}$  med 0,087 in 1,02 (korak  $\approx 0,1$ ). Plinasto fazo obravnavamo kot zrak, okoliško tekočino pa kot vodo. Upoštevani materialni parametri so zbrani v tabeli 1. Simulacije so izvedene z upoštevanjem osne simetrije. Uporabljeni je ortogonalna numerična mreža z enakomerno resolucijo v bližini mehurčka ( $\Delta x = 44$  nm,  $R_0/\Delta x = 25$ ,  $R_{r,\max}/\Delta x \approx 370$ ). Slednja je bila izbrana na podlagi konvergenčnih študij v prejšnjih raziskavah (Zevnik in Dular, 2020, 2021, 2022). Velikost računskega celic se postopoma povečuje ( $\Delta x_{\max}/\Delta x_{\min} \approx 850$ ) proti robu računske domene, ki je postavljen približno  $50 \times R_{\max}$  stran od centra mehurčka. Skupno število računskega celic znaša približno pol milijona. Računski časovni korak je kontroliran v skladu s Courant–Friedrichs–Lowyjevim pogojem z največjim Courantovim številom 0,2. Robni pogoji na koncu računske domene so upoštevani za tlačni izpust s prevajanjem valov ( $p_\infty = 101325$  Pa,  $T_\infty = 273,15$  K). Na steni je upoštevan pogoj brez zdrsa.

Za vse izračune je bil uporabljen algoritem sklopitev tlaka in hitrosti PISO (Issa, 1986) skupaj z implicitno časovno diskretizacijo prvega reda. Kar zadeva prostorsko diskretizacijo, smo uporabili shemo PRESTO! (Bender, 1981) za interpolacijo tlaka in protitočno shemo drugega reda za interpolacijo gostote, gibalne količine in energije. Fazna meja med mehurčkom in okoliško kapljevinou je zajeta z geometrijsko shemo odsekovno linearne geometrične rekonstrukcije fazne meje (PLIC) (Issa, 1986), ki predpostavlja, da ima fazna meja med dvema tekočinama linearni naklon znotraj računske celice.

Preglednica 1: Upoštevani materialni parametri obeh tekočin.

Lastnost [Enota]	Kapljevina - voda	Plin - zrak
Dinamična viskoznost $\mu$ [Pa s]	$1,003 \times 10^{-3}$	$1,8 \times 10^{-5}$
Toplotna prevodnost $k$ [W/(m K)]	0,6	0,0242
Površinska napetost $\sigma$ [N/m]	-	0,0728
Referenčna gostota $\rho_{\text{ref}}$ [kg/m <sup>3</sup> ]	998,2	-
Referenčni tlak $p_{\text{ref}}$ [Pa]	101325	-
Referenčni modul stisljivosti $K_{\text{ref}}$ [Pa]	$2,2 \times 10^9$	-
EkspONENT gostote $n$ [-]	7,15	-
Specifična plinska konstanta $R_g^*$ [J/(kg K)]	-	287,05

### Model dinamike kroglice

Delce silicijevega dioksida obravnavamo kot kroglice z gostoto 2000 kg/m<sup>3</sup> in polmerom  $R_p = 2$  µm (Silica Microspheres, 2019). Izračunano tokovno polje  $\mathbf{u}(t, \mathbf{x})$  iz

modela dinamike mehurčka na lokaciji kroglice  $x_p$  lahko označimo kot  $\mathbf{u} = \mathbf{u}(t, \mathbf{x}_p(t))$ .

Ker je med eksperimenti upoštevano samo radialno gibanje kroglic, je hitrost radialnega toka  $\bar{u}_r$ , ki poganja gibanje kroglic, upoštevana kot

$$\bar{u}_r(t, r_p) = \frac{1}{2R_p} \int_{z=0}^{z=2R_p} u_r(t, r_p, z) dz, \quad \dots(20)$$

ki služi kot robni pogoj v modelu dinamike kroglice, ki ga razrešimo z numerično integracijo.

### Modeli pritrjene bakterije

Podoben pristop kot pri modelu dinamike kroglice uporabimo tudi pri modelu pritrjene celice. Celice obravnavamo kot kroglice z radijem  $R_c = \left(\frac{1}{8}d_c^3 + \frac{3}{16}d_c^2(l_c - d_c)\right)^{\frac{1}{3}} = 0,45 \pm 0,06 \mu\text{m}$ . Tukaj  $l_c = 1,44 \pm (0,25) \mu\text{m}$  in  $d_c = 0,63 \pm (0,06) \mu\text{m}$  ( $N=30$ ) predstavlja dejansko dolžino in premer bakterijskih celic. Izraz za ekvivalenten celični radij  $R_c$  dobimo preko preračuna ekvivalentnega radija iz dejanskega volumna bakterijske celice ob predpostavki sfero-cilindrične oblike celice.

Hitrost toka  $\bar{\mathbf{u}}$ , ki predstavlja obtežbo na celice, je prevzeta iz modela dinamike mehurčka kot

$$\bar{\mathbf{u}}(t, r_c) = \frac{1}{2R_c} \int_{z=0}^{z=2R_c} \mathbf{u}(t, r_c, z) dz, \quad \dots(21)$$

na podlagi katere lahko skladno z Enačbo (18) določimo pripadajočo silo upora na posamezno bakterijsko celico.

### **Validacija numeričnega modela**

#### Časovni potek radija mikromehurčka

Numerični model dinamike mehurčka je validiran preko eksperimentalnih rezultatov razvoja oblike in velikosti mikromehurčkov. Analiza dinamike mehurčkov je bila izvedena za eksperimentalno pridobljene mehurčke z največjim polmerom nad  $10 \mu\text{m}$ , zaradi omejitev hitre fotografije (časovna ločljivost  $0,7 \mu\text{s}$  in prostorska ločljivost  $0,33 \mu\text{m}/\text{px}$ ). Pomembno je omeniti, da polmer mehurčka  $R_r$  označuje polmer zunanjega obrisa oblike mehurčka iz eksperimentalnih opazovanj (Slika 7a), ki ga lahko razumemo kot navpično projekcijo oblike mehurčka na vodoravno ravnino. Največji polmer

mehurčkov  $R_{r,\max}$  iz eksperimentov se je gibal med 11,0 in 20,5  $\mu\text{m}$  (povprečno 14,5  $\mu\text{m}$ , N=24). Brez-dimensijska razdalja mehurček-stena  $\gamma$  je bila v območju med 0,20 in 0,46 (povprečje 0,30, N=24). Za neposredno primerjavo različnih eksperimentalnih in numeričnih rezultatov so bili polmeri mehurčkov in ustrezní časi pretvorjeni v brez-dimensijsko obliko kot  $R_r^* = \frac{R_r}{R_{r,\max}}$  in  $t^* = \frac{t-t_{\max}}{t_c}$ . Tukaj  $R_{r,\max}$  in  $t_{\max}$  označujeta maksimalni radij mehurčka in pripadajoči čas,  $t_c$  pa čas kolapsa mehurčka.

### Hitrostno polje v bližini mikromehurčka

Inducirano tokovno polje je bilo eksperimentalno okarakterizirano z merjenjem pomikov mikrokroglic silicijevega dioksida med posameznimi dogodki rasti in kolapsa mikromehurčkov. Mikrokroglice so bile z optično pinceto postavljene na različne brez-dimensijske razdalje  $\delta$ , stran od mehurčkov. Isti parameter se uporablja tudi za opis razdalje mehurček-celica (Slika 5). Premiki so bili pridobljeni s sledenjem položaja mikrokroglic.

Na podlagi dobljenih premikov smo ovrednotili največje in časovno povprečne hitrosti kroglic med vsakim dogodkom mikromehurčka. Za validacijo numeričnega modela za napovedovanje razvoja hitrostnega polja v bližini stene smo izmerjene hitrosti krogle primerjali z ustreznimi vrednostmi, kot jih je predvidel numerični model. Primerjava v splošnem nakazuje na to, da numerični model precenjuje magnitudo hitrosti kroglice, vendar je to mogoče pripisati dejству, da so eksperimentalno dobljeni rezultati nagnjeni k podcenjevanju zaradi omejitev s hitro fotografijo (hitra kamera z  $1,44 \times 10^6$  sličic na sekundo rezultira v časovni ločljivosti  $\Delta t = 0,7 \mu\text{s}$ ). Medtem ko numerične simulacije omogočajo veliko boljšo časovno ločljivost z  $\Delta t \ll 0,1 \mu\text{s}$ .

### **Model verjetnosti celičnega dogodka**

Razmerje med vršnimi obtežbami (hidrodinamska sila, strižna napetost na steni) in verjetnostjo pojava posameznega celičnega dogodka (odtrganje, celična smrt) je bilo kvantificirano s prileganjem pridobljenih podatkov na model verjetnosti celičnega dogodka. Slednji je definiran z odsekovno funkcijo s tremi koeficienti. Povezava med izbrano metriko obtežbe in verjetnostjo dogodka celice je določena s potenčno funkcijo, kjer so koeficienti nastavljeni tako, da predstavljajo spodnjo mejno obtežbo, zgornjo mejno obtežbo in pripadajoči eksponent obtežbe. Verjetnost celičnega dogodka pri vršni hidrodinamski sili  $F_{\max}$  je določena v skladu z naslednjo odsekovno funkcijo:

$$P_{\text{event}}(F_{\max}) = \begin{cases} 0, & |F_{\max}| < F_{\text{lth}}, \\ \frac{|F_{\max}|^{\beta_F} - F_{\text{lth}}^{\beta_F}}{F_{\text{uth}}^{\beta_F} - F_{\text{lth}}^{\beta_F}}, & F_{\text{lth}} \leq |F_{\max}| \leq F_{\text{uth}}, \\ 1, & F_{\text{uth}} \leq |F_{\max}|. \end{cases} \quad \dots(22)$$

Tukaj  $F_{lth}$  in  $F_{uth}$  označujeta spodnjo in zgornjo mejno silo. Prvo lahko razumemo kot mejo, da se dogodek za veliko večino celic sploh lahko zgodi ( $P_{event}(F_{max}) \approx 0$ ), medtem ko drugi predstavlja zgornjo mejno silo, pri kateri lahko pričakujemo, da se bo dogodek zgodil za veliko večino celic ( $P_{event}(F_{max}) \approx 1$ ).  $\beta_F$  je tretji modelni koeficient, ki predstavlja eksponent sile. Podoben model je uporabljen tudi za okarakterizacijo verjetnosti celičnega dogodka v povezavi z vršno strižno napetostjo na steni  $\tau_{max}$ :

$$P_{event}(\tau_{max}) = \begin{cases} 0, & |\tau_{max}| < \tau_{lth}, \\ \frac{|\tau_{max}|^{\beta_\tau} - \tau_{lth}^{\beta_\tau}}{\tau_{uth}^{\beta_\tau} - \tau_{lth}^{\beta_\tau}}, & \tau_{lth} \leq |\tau_{max}| \leq \tau_{uth}, \\ 1, & \tau_{uth} \leq |\tau_{max}|. \end{cases} \dots(23)$$

Tudi tukaj  $\tau_{lth}$  in  $\tau_{uth}$  označujeta spodnjo in zgornjo mejo vršnih strižnih napetosti na steni, medtem ko  $\beta_\tau$  predstavlja eksponent strižne napetosti.

Prileganje modela je bilo izvedeno v programskega okolju Matlab z uporabo nelinearne metode najmanjših kvadratov skupaj z algoritmom območja zaupanja. Globalno prileganje je bilo izvedeno za vsak par metrika obtežbe – celični dogodek (skupaj 4 pari).

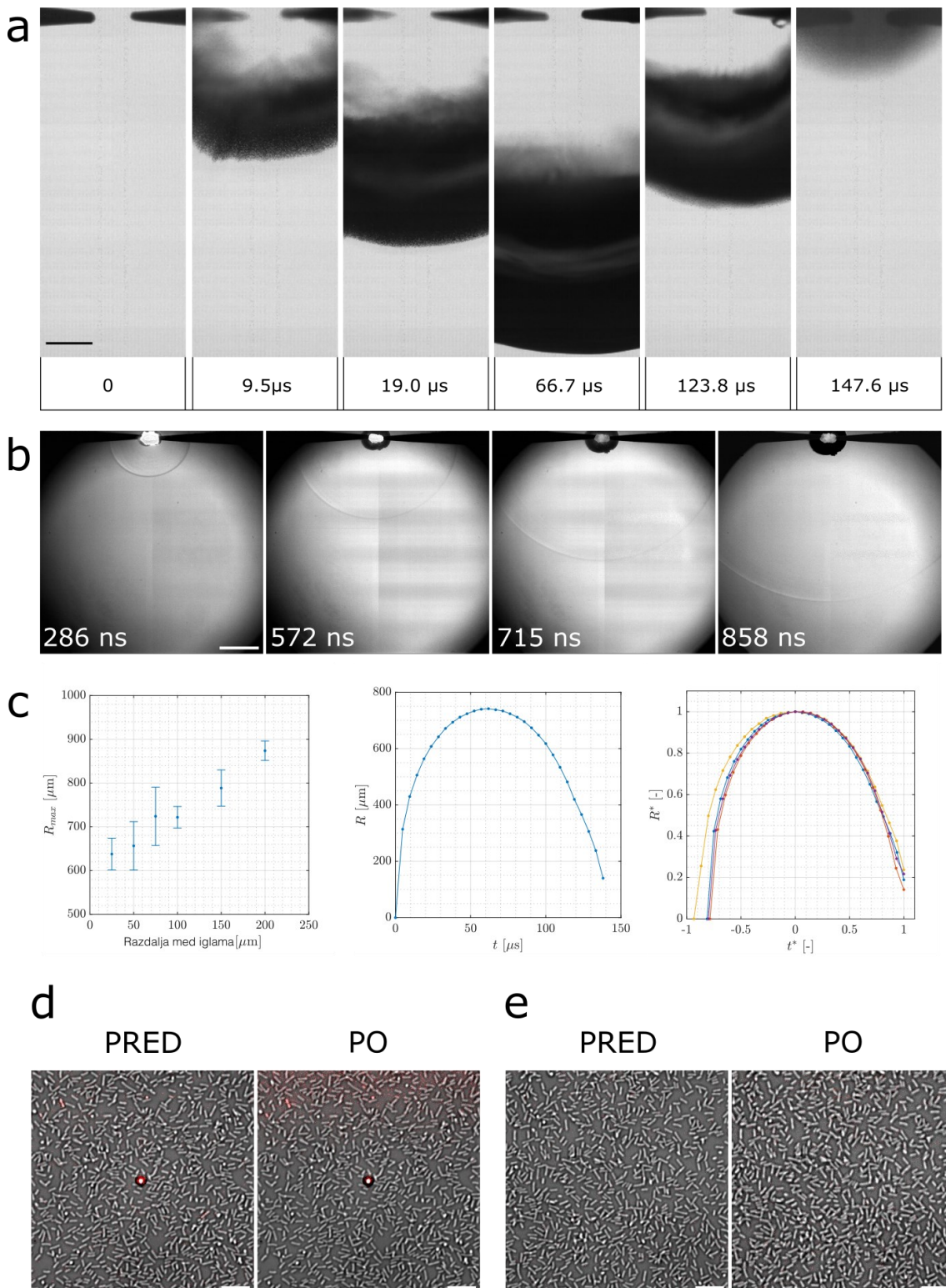
### Statistična analiza

Verjetnost dogodkov bakterijskih celic v odvisnosti od brez-dimenzijske razdalje  $\delta$  smo matematično popisali s krivuljo modela eksponentne enačbe. Parametri prileganja modela z medianama vrednostmi eksperimentalnih podatkov za verjetnost odtrganja celic z enačbo  $P \propto e^{-2\delta}$  je napaka srednjega kvadrata (RMSE) in je znašala 0,039, koeficient determinacije ( $R^2$ ) pa je bil 0,98. Za medianama vrednosti pri verjetnosti za poškodovanje celic pa smo pri enačbi  $P \propto e^{-4\delta}$  določili parametre RMSE=0,044,  $R^2=0,98$ . Za ugotavljanje vpliva tipov curka na odtrganje ali poškodovanje celic smo uporabili Kolmogorov-Smirnov test. p-vrednosti za verjetnosti odtrganja ali poškodovanja celic v odvisnosti od  $\delta$  pri  $\gamma=0.30$  so bile 0,77 in 0,71.

#### 2.2.1.3 Rezultati

Metoda generiranja kavitacijskega mikromehurčka temelji na kombinaciji nastanka zarodnega mehurčka z laserjem in visokonapetostne razelektritve. Pri visokonapetostni razelektritvi pride do nastanka mehurčka v eksperimentalni komori v velikosti med 600 in 900  $\mu\text{m}$ , odvisno od razdalje med pozicionirnima iglama (Slika 6a,c). Ob kolapsu nastanejo tlačni valovi (Slika 6b), ki potujejo skozi eksperimentalno komoro. Čas rasti in kolapsa razelektritvenega mehurčka je bil okrog 130 ms, rast in kolaps mehurčka sta

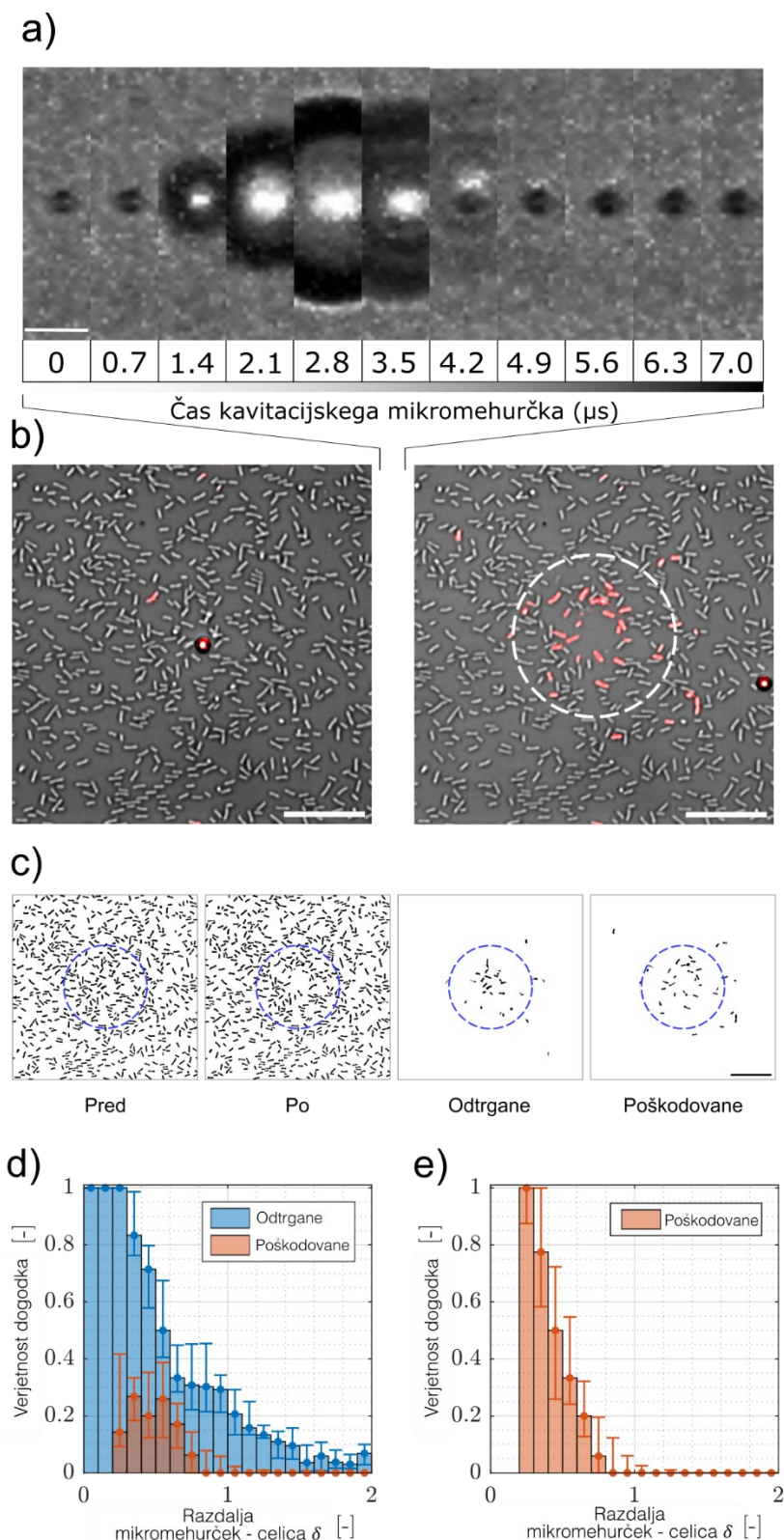
bila simetrična. Razelektritveni mehurček ni imel vpliva na opazovane celice in ni povzročil odtrganja ali poškodovanja celic (Slika 6e).



**Slika 6: Potek visokonapetostne razelektritve v tekočini in vpliv zarodnega mikromehurčka ali tlačnih valov na opazovane bakterijske celice.**

(a) Zaporedje slik rasti in kolapsa mehurčka pri visokonapetostni razelektritvi pri  $75 \mu\text{m}$  medsebojni razdalji med iglama. Merilo:  $100 \mu\text{m}$ . (b) Nastanek tlačnih valov pri nastanku razelektritve pred pojavom kavitacijskega mehurčka. Merilo:  $100 \mu\text{m}$ . (c) Levi graf prikazuje odvisnost maksimalnega radija mehurčka ( $R_{\max}$ ) od medsebojnega razmika med konicama igel. Ročke prikazujejo povprečje štirih ponovitev, napaka je prikazana kot standardna deviacija. Z večanjem razdalje med iglama narašča tudi maksimalen radij mehurčka. Srednji graf prikazuje časovni potek spreminjanja radija mehurčka za eno ponovitev. Desni graf prikazuje spreminjanje brez-dimenzijskega radija –  $R^*$  (radiji normaliziran na maksimalni radij) in brez-dimenzijski čas –  $t^*$  (čas je normaliziran na časovno točko maksimalnega radija mehurčka). Negativne vrednosti predstavljajo čas pred maksimalnim radijem – rast mehurčka, pozitivne vrednosti pa so časovne točke po dosegu maksimalnega radija in je faza kolapsa mehurčka. Graf prikazuje vse štiri posamezne eksperimente. (d) Leva mikroskopska slika prikazuje stanje pred nastankom zarodnega mikromehurčka kjer je v centru vidna magnetna kroglica. Desna slika prikazuje stanje celic po nastanku zarodnega mikromehurčka. Mikroskopske slike so kompozitne slike svetlobne presevne mikroskopije (sivinska slika) in fluorescenčne mikroskopije s PI (rdeči objekti). Primerjava leve in desne slike kaže, da zarodni mehurček ni imel signifikantnega vpliva na okoliške celice – ni prišlo do odtrganja ali poškodb celic. Merilo:  $10 \mu\text{m}$ . (e) Sliki prikazujeta vpliv visokonapetostnega razelektritvenega mehurčka oziroma tlačnih valov na opazovane celice. Položaj celic je bil približno  $4 \text{ mm}$  stran od izvora nastanka razelektritve. Leva slika kaže stanje pred razelektritvijo medtem ko desna slika kaže stanje po razelektritvi. Primerjava slik pred in po dogodku ne kažeta na signifikantne spremembe pri opazovanih celicah. Merilo:  $10 \mu\text{m}$ .

Na oddaljenosti 4-5 mm od vira visokonapetostne razelektritve smo z laserskim pulzom lokalno segreli površino magnetne kroglice, kar je omogočalo rast zarodnega mikromehurčka z mediano radija  $1,1 \mu\text{m}$  ( $N=15$ ). Življenska doba takšnega mehurčka je bila v času med nekaj sto milisekund in nekaj sekundami. Zarodni mehurček ni implodiral. Nastanek zarodnega mikromehurčka ni imel vpliva na odtrganje ali poškodovanje okoliških celic (Slika 6d). Za nastanek nestabilnega kavitacijskega mehurčka (Slika 7a) so bili potrebni tlačni valovi, ki so nastali pri razelektritvi ob nastanku razelektritvenega kavitacijskega mehurčka (Slika 6b). Stabilen zarodni mehurček se je ob prehodu tlačnega vala skrčil, takoj zatem pa eksplozivno razširil (Slika 7a). Mediana maksimalnega radija kavitacijskega mehurčka pri eksperimentih je bila  $15,4 \mu\text{m}$ . Ob kolapsu mehurčka se je ustvaril mikrocurek proti trdni stekelcu, ki je na sliki opazen znotraj mehurčka kot dodaten siv obroč (slika 7a pri  $3,5 \mu\text{s}$  in  $4,2 \mu\text{s}$ ). Za statistično analizo rezultatov smo upoštevali samo eksperimente, kjer je kavitacijski mehurček dosegel ali presegel maksimalni radij  $10 \mu\text{m}$ . Z metodo sicer lahko ponovljivo generiramo kavitacijske mehurčke do treh mikrometrov, vendar zaradi prostorske in časovne resolucijske omejitve (časovna resolucija slik je bila  $0,7 \mu\text{s}$  in prostorska resolucija  $3 \text{ piksle}/\mu\text{m}$ ) smo pri analizi uporabili samo večje mehurčke.



**Slika 7: Kavitacijski mehurček in njegov vpliv na bakterijske celice.**

(a) Tipičen razvoj kavitacijskega mikromehurčka (ptičja perspektiva). Posnetki s hitro kamero prikazujejo zarodni mikromehurček, ki se po prehodu tlačnih najprej skrči in nato eksplozivno raste (1,4-2,8 μs), temu

sledi faza kolapsa mikromehurčka ( $3,5\text{--}4,2 \mu\text{s}$ ). V fazi kolapsa lahko iz spodnje perspektive opazimo nastanek curka proti steklu, ki je viden kot dodatna obročasta struktura znotraj mehurčka. Sekvenca je dolga  $7 \mu\text{s}$ , merilo je  $5 \mu\text{m}$ . (b) Mikroskopske slike pred (levo) in po (desno) kolapsu mikromehurčka. Sliki sta kompozitni sliki presevne svetlobne mikroskopije (sivinska slika) ter fluorescenčne mikroskopije barvila PI (rdeči objekti). Rdeče obarvane celice so se obarvale z barvilm PI, ki kaže na poškodovanje celic. Po kolapsu mikromehurčka opazimo območje v centru mehurčka kjer so bile vse celice odtrgane, potem sledi območje kjer je prišlo do poškodovanja celic (celice so obarvane s PI). Bel črtkan krog na desni sliki prikazuje horizontalno projekcijo maksimalnega radija mehurčka. Merilo je  $20 \mu\text{m}$ . (c) Binarizirane mikroskopske slike pred in po kolapsu mikromehurčka ter binarne slike odtrganih in poškodovanih celic. Moder črtkan krog predstavlja horizontalno projekcijo maksimalnega radija kavitacijskega mehurčka. Merilo je  $20 \mu\text{m}$ . (d) Verjetnost odtrganja (modri stolpci) in poškodovanja (oranžni stolpci) v odvisnosti od brez-dimenzijske razdalje mikromehurček – celica  $\delta$ . (e) Verjetnost poškodovanja za ne-odtrgane celice (oranžni stolpci) v odvisnosti od brez-dimenzijske razdalje mikromehurček – celica  $\delta$ . Rezultati predstavljajo 15 eksperimentalnih ponovitev z maksimalnimi radiji ( $R_{r,\max}$ ) mehurčkov med  $11,1$  in  $24,4 \mu\text{m}$ , mediana  $R_{r,\max}=15,4 \mu\text{m}$ , brez-dimenzijska razdalja mikromehurček – stena ( $\gamma$ ) je bila med  $0,15$  in  $0,58$ , mediana  $\gamma=0,25$ . Skupni število celic je bilo 8646, od tega je bilo 294 primerov odtrganja celic in 257 primerov poškodovanja celic. Stolpci prikazujejo mediana vrednosti, napake so prikazane kot 1. in 3. kvartil verjetnosti za dogodek. Pri obeh grafih (d in e) verjetnost za poškodovanje celic pod  $\delta < 0,2$  niso prikazane ker so bile vse celice v tem območju odtrgane.

Vpliv kavitacijskega mikromehurčka na okoliške pritrjene bakterijske celice *E. coli* je prikazan na Slika 7b. Bakterije so bile enakomerno razporejene po opazovanem vidnem polju s celično gostoto  $0,15\pm0,03 \text{ celic}/\mu\text{m}^2$ . Magnetne kroglice so bile pozicionirane v bližino pritrjenih celic kjer smo izbrani magnetni kroglici z laserskim pulzom ustvarili zarodni mikromehurček. Stabilen mikromehurček je bil izpostavljen tlačnim valovom, ki so nastali ob visokonapetostni razelektritvi. Kavitacijski mikromehurček je agresivno zrastel in implodiral, kar je povzročilo v središču mehurčka popolno odtrganje celic, kateremu je sledilo območje pritrjenih a poškodovanih celic, ki so se obarvale z membransko nepropustnim fluorescentnim barvilm propidijev jodid. Črtkan krog predstavlja horizontalno projekcijo maksimalnega radija mehurčka, ki smo ga pridobili iz zajema slik na hitri kamери. Območje poškodb celic korelira s projiciranim horizontalnim maksimalnim radijem  $R_{r,\max}$ . Po kolapsu mikromehurčka so bili trije možni izidi: celico odtrga, celica ostane pritrjena a poškodovana (obarvajo se s PI) ter mehurček ni imel vpliva na celico – celica je so ostala pritrjena in se ni obarvala s PI. Z računalniško analizo mikroskopskih slik smo lahko identificirali posamezne celice, ki smo jim v binarni obliki določili položaj na mikroskopski sliki.

Združeni rezultati petnajstih eksperimentalnih ponovitev kolapsa mikromehurčka v bližini bakterijskih celic so prikazani na Slika 7d-e. Za primerjavo rezultatov med različnimi ponovitvami smo uporabili brez-dimenzijsko razdaljo med mikromehurčkom in celico  $\delta$ . Ko je vrednosti  $\delta=1$ , to pomeni da je bakterijska celica bila na robu maksimalnega radija mikromehurčka. V primeru vrednosti  $0\leq\delta\leq1$  se je celica nahajala znotraj  $R_{r,\max}$ , v primeru vrednosti  $\delta$  nad 1 pa je to pomenilo, da se je celica nahajala zunaj  $R_{r,\max}$  mehurčka. Rezultati kažejo da je verjetnost za odtrganje celic pri  $\delta\leq0,2$  zelo

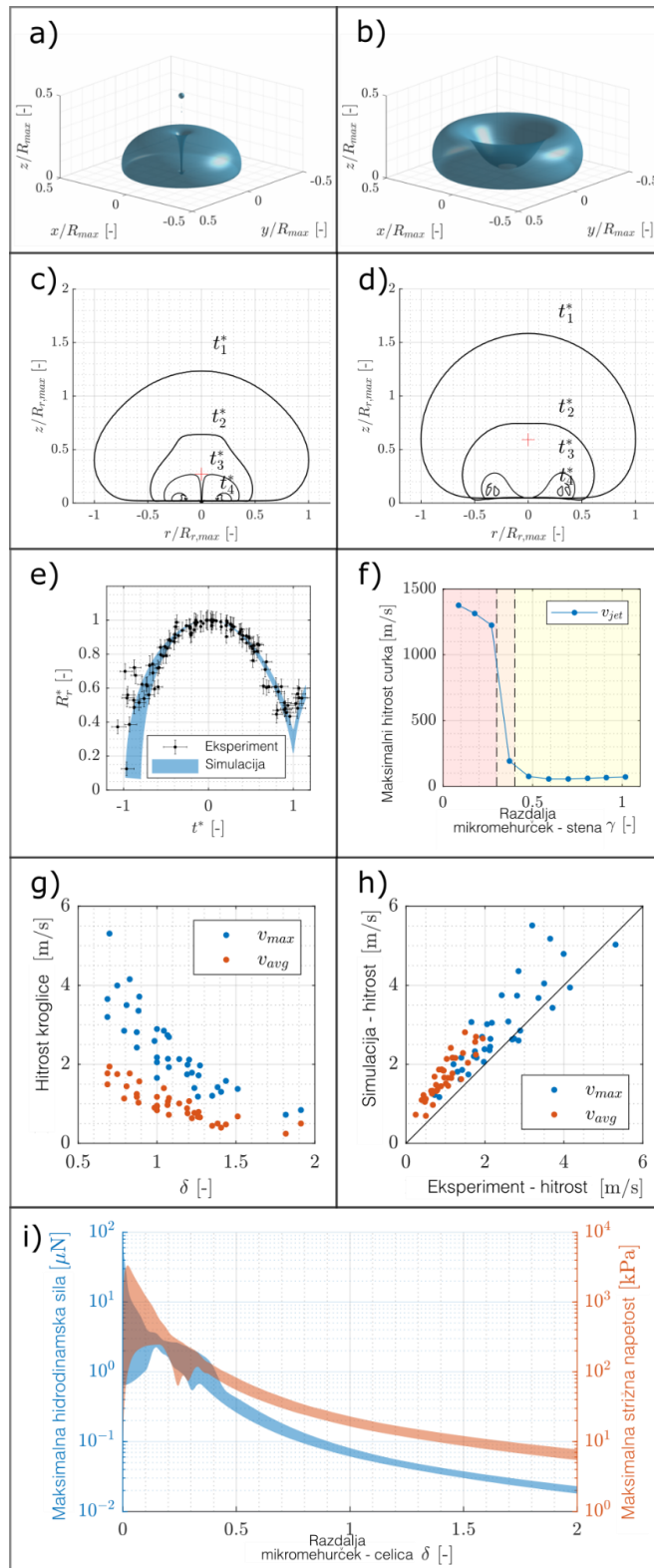
velika, saj je bila večina celic odtrganih, neodvisno od  $R_{r,\max}$ . Pri vrednostih  $\delta > 0,2$  se je verjetnost odtrganja celic zmanjševala eksponentno, verjetnost za odtrganje je bila približno 25 % pri  $\delta = 1$  in približno 10 % pri  $\delta = 1,5$ . Verjetnost za poškodovanje bakterijske celice je prikazano samo za razdalje  $\delta$  nad 0,2 saj so pri nižjih vrednostih bile vse celice odtrgne. Verjetnost poškodovanja pri  $\delta = 0,2$  je bila 100 %, potem pa je sledil hiter eksponentni upad verjetnosti za poškodovanje celice, pri vrednostih  $\delta > 1$  je bila verjetnost že blizu nič. Rezultati kažejo, da se celice lažje odtrgajo od površine kakor pa poškodujejo – minimalna verjetnost za odtrganje celic gre proti vrednosti  $\delta > 2$ , medtem ko je minimalna verjetno za poškodovanje že pi  $\delta > 0,8$ .

Z računskim modelom smo dobili dodaten vpogled na mehanski vpliv kavitacijskega mikromehurčka na bakterijske celice (Slika 8). Rezultati računskih simulacij za kolaps mikromehurčka ob trdni steni je pokazal na dva možna načina nastanka curka, ki sta odvisna od brez-dimenzijskega parametra razdalje  $R_{r,\max}$  in oddaljenosti mikromehurčka od stene. Za mikromehurčke zelo blizu stene  $\gamma \lesssim 0,3$  rezultati nakazujejo na nastanek hitrega in tankega curka proti steni (Slika 8a, c, f). Tak curek lahko doseže maksimalne hitrosti  $1305 \pm 76$  m/s in brez-dimenzijski radij curka  $R_{jet}/R_{r,\max} = 0,021 \pm 0,001$ . Pri mikromehurčkih ki so bolj oddaljeni od površine ( $\gamma \gtrsim 0,4$ ) pa nastane klasičen curek (Slika 8b, d, f), kjer pride do maksimalne hitrosti  $64 \pm 8$  m/s in razmerja  $R_{jet}/R_{r,\max} = 0,30 \pm 0,02$ . Eksperimentalno smo opazili le nastanek klasičnega curka, medtem ko hitrega in tankega curka najverjetneje zaradi tehničnih omejitev hitre kamere nismo zaznali.

Primerjava eksperimentalnega in računskega časovnega poteka spremnjanja radija je prikazano na Slika 8e. Eksperimentalni rezultati brez-dimenzijske projekcije radija  $R_r^*$  se skladajo z rezultati numerične simulacije. Manjše odstopanje je vidno pri začetni fazi rasti mikromehurčka ( $t^* < -0,9$ ). Opažena razlika je lahko zaradi nihanja v okoliškem začetnem tlaku, ki bi lahko bil drugačen kakor smo predpostavili v simulacijah. Ker se maksimalne mehanske sile zgodijo v fazi kolapsa mikromehurčka (Zeng in sod. 2018), smo nastale razlike v začetnih fazah kavitacijskega mehurčka za naš primer zanemarili.

Rezultate za računsko pridobljeno tokovno polje smo potrdili z eksperimentalnimi rezultati določanja tokovnega polja s stekleno kroglico pri rasti in kolapsu posameznega kavitacijskega mikromehurčka. Eksperimentalni rezultati tokovnega polja so prikazani na Slika 8g kjer so prikazane tudi maksimalne in povprečne hitrosti v odvisnosti od  $\delta$ . Z večanjem razdalje od centra mehurčka vidimo neliniaren padec hitrosti toka. Primerjava eksperimentalnih in računskih rezultatov je predstavljena na Slika 8h kjer so eksperimentalne vrednosti nižje od računskih kar je pričakovano zaradi omejitev časovne ločljivosti zajema slik s hitro kamero.

Z validiranim računskim modelom smo izračunali vršne vrednosti strižne napetosti in hidrodinamske sile, ki jih kavitacijski mikromehurček vrši na bakterijsko celico v odvisnosti od  $\delta$ . Slika 8i prikazuje izračunane rezultate za strižno napetost in hidrodinamsko silo v odvisnosti od  $\delta$ , kjer lahko vidimo pri  $\delta < 0,2$  velik raztres rezultatov, ki nakazuje na veliko variabilnost mehanske sile v območju nastanka curka. Veliko variabilnost sil lahko razložimo zaradi pojava dveh tipov curka, ki imata različne hitrosti curkov. Maksimalne mehanske obremenitve v neposrednem središču curka ( $\delta < 0,1$ ) lahko dosežemo vrednosti do desetine  $\mu\text{N}$  in nekaj MPa. Pojavnost maksimalnih mehanskih obremenitev se časovno sklada z nastankom curka in posledično nastankom radialnega toka stran od centra. Omenjene sile pa so zelo kratkožive (nanosekundna časovna skala), saj so v grobem en do dva velikostna razreda krajše kakor sam proces kavitacije mikromehurčka, ki traja nekaj  $\mu\text{s}$ . Vršne mehanske obremenitve znatno upadejo z oddaljevanjem od centra mehurčka, tako da pri razdalji  $\delta = 1$  pričakujemo 20 kPa strižne napetosti in 70 nN hidrodinamske sile. Rezultati se skladajo z eksperimentalnimi rezultati kjer v neposredni bližini centra mehurčka opazimo popolno odtrganje celic, ki nato hitro prične upadati z oddaljevanjem od centra mikromehurčka.

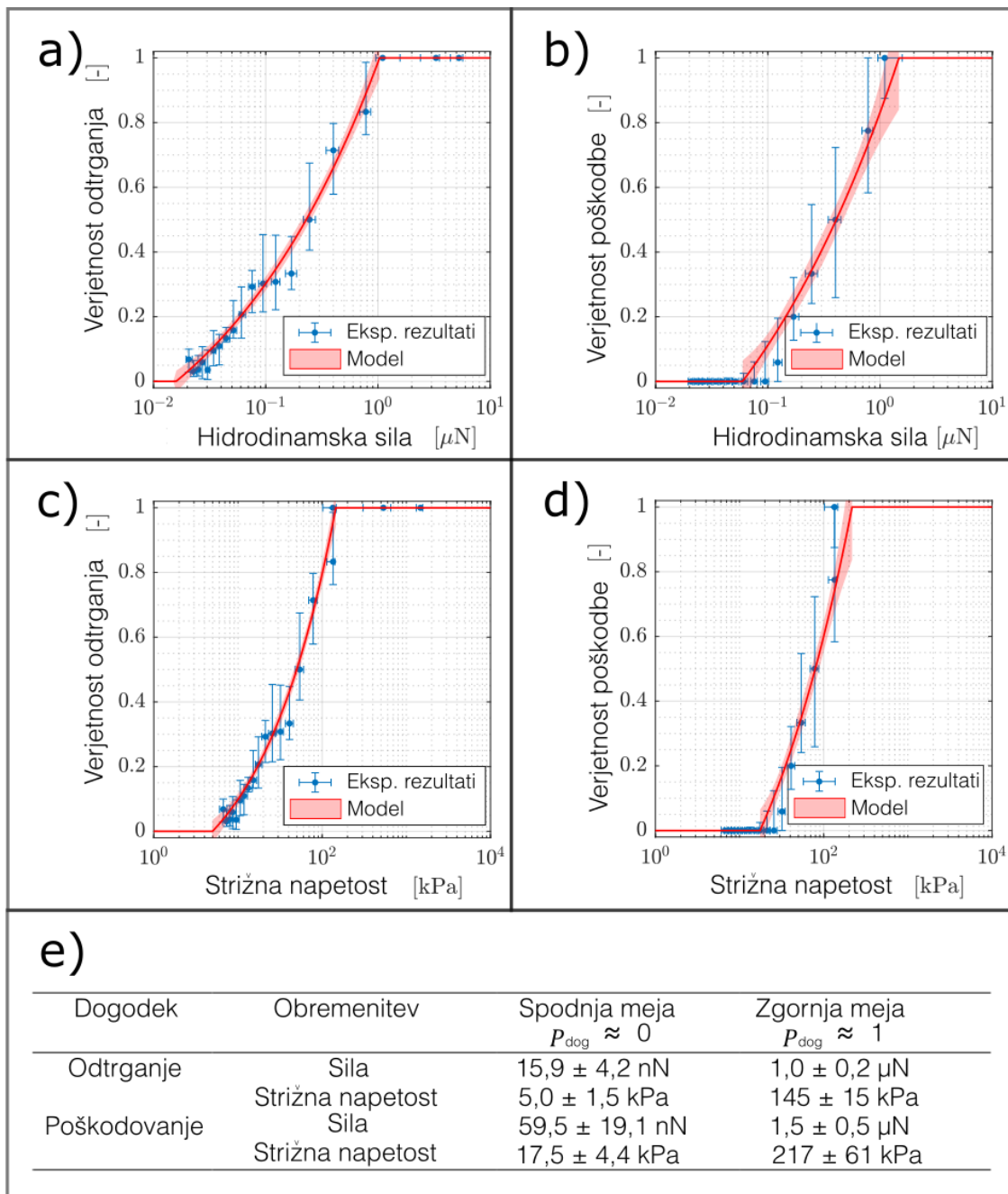


**Slika 8: Računski model kavitacije mikromehurčka in določanje strižne napetosti ter hidrodinamske sile ob kavitaciji mikromehurčka.**

(a,b) Numerični rezultati oblike nastanka dveh tipov curka v času udarca curka v steno ( $z=0$ ). (a) prikazuje obliko hitrega in tankega curka ( $\gamma=0,27$ ), slika (b) prikazuje nastanek klasičnega curka ( $\gamma=0,59$ ). (c)

Časovni potek spremjanja oblike pri kavitaciji mikromehurčka pri  $\gamma=0,27$  kjer nastane hiter in tanek curek. Rdeč križec predstavlja center začetnega stanja mehurčka. Konture oblik mehurčka ustrezano časovnim točkam pri maksimalnem radiju mikromehurčka ( $t_1^*=0$ ), pri polovici maksimalne velikosti ( $t_2^*=0,895$ ), pri nastanku hitrega in tankega curka ob udarcu ob steno ( $t_3^*=0,964$ ) in ob kolapsu preostalega toroidnega mehurčka ( $t_4^*=1,004$ ). (d) Časovni potek spremjanja oblike pri kavitaciji mikromehurčka pri  $\gamma=0,59$  kjer nastane klasičen curek. Rdeč križec predstavlja center začetnega stanja mehurčka. Konture oblik mehurčka ustrezano časovnim točkam pri maksimalnem radiju mikromehurčka ( $t_1^*=0$ ), polovici maksimalne velikosti ( $t_2^*=0,831$ ), ob nastanku hitrega in tankega curka ob udarcu ob steno ( $t_3^*=0,961$ ) in ob kolapsu preostalega toroidnega mehurčka ( $t_4^*=1,008$ ). (e) Časovni potek spremjanja radija mikromehurčka  $R_r$ . Rezultati so predstavljeni v brezdimenzijski obliki, kjer je radij mehurčka  $R_r$  skaliran na maksimalni radij mikromehurčka  $R_{r,max}$ , čas pa je centriran na točko, ko doseže mikromehurček maksimalen radij ob času  $t_{max}$  in skaliran na čas kolapsa mehurčka  $t_c$ . Eksperimentalni rezultati ( $0,20 \leq \gamma \leq 0,46$ , povprečen  $\gamma=0,30$ ,  $N=24$ ) so prikazani s črnimi točkami s predvideno mersko napako ( $\pm 0,67 \mu\text{m}$ ). Rezultati numeričnih simulacij predstavlja moder pas ( $0,18 \leq \gamma \leq 0,48$ , povečanje  $\Delta\gamma \approx 0,1$ ,  $N=4$ ), ki se dobro sklada z eksperimentalnimi rezultati. Preostali numerični rezultati numerične analize pri kolapsu mikromehurčka ob steni:  $R_{r,max}=16,3 \pm 0,5 \mu\text{m}$ ,  $t_{max}=1,58 \pm 0,05 \mu\text{s}$ , in  $t_c=1,73 \pm 0,07 \mu\text{s}$ . (f) Numerični rezultati maksimalne hitrosti curka v odvisnosti od parametra oddaljenosti mikromehurček-stena  $\gamma$ . Obarvana območja predstavljajo nastanek karakteristične oblike curka: rumeno območje predstavlja nastanek klasičnega curka ( $\gamma > 0,4$ ), rdeče predstavlja območje nastanka hitrega in tankega curka ( $\gamma < 0,3$ ). (g) Modre točke predstavljajo eksperimentalne vrednosti hitrosti premikanja kroglice, oranžne točke predstavljajo vrednosti v časovnem povprečju. Število eksperimentalnih ponovitev,  $N=37$ . (h) Primerjava eksperimentalnih in numeričnih rezultatov za maksimalne in povprečne hitrosti. Rezultati kažejo na dobro skladnost rezultatov za maksimalne hitrosti  $v_{max}$  (modre točke, RMSE=0,79,  $R^2=0,73$ ,  $N=37$ ) in za povprečne hitrosti  $v_{avg}$  (oranžne, RMSE=0,75,  $R^2=0,77$ ,  $N=37$ ). (i) Izračunane maksimalne vrednosti hidrodinamske sile (modra) in strižne napetosti (oranžna) na pritrjeno bakterijo v odvisnosti od brez-dimenzijske razdalje med mikromehurčkom in celico  $\delta$ . Rezultati predstavljajo rezultate simulacij za parameter  $\gamma$  med 0,15 in 0,58. Rezultati so predstavljeni na logaritemski  $x$  in  $y$  osi.

Korelациjo med nastalimi vršnimi mehanskimi silami (hidrodinamska sila in strižna napetost) in verjetnostjo za odtrganje ali poškodovanje celic smo dobili s prileganjem potenčnemu modelu (enačba 22 in 23). Parametri modela predstavljajo mejne mehanske obremenitve za verjetnost celičnega odtrganja ali celične poškodbe (Slika 9). Mejne vrednosti za odtrganje bakterije so bile pri 15,9 nN za hidrodinamsko silo in 5 kPa za strižno napetost. Pri poškodovanju celice je bila mejna vrednost hidrodinamske sile 59,5 nN pri strižni napetosti 17,5 kPa. Pri obremenitvah nad 1  $\mu\text{N}$  in 145 kPa lahko pričakujemo, da bo večina celic odtrgnih, medtem ko je visoka verjetnost za poškodovanje celic pri obremenitvah, ki presegajo 1,5  $\mu\text{N}$  in 217 kPa. Te vrednosti lahko pri kolapsu mikromehurčka prevedemo v brez-dimenzijsko razdaljo mikromehurčka in celice  $\delta$  kjer lahko pričakujemo visoko verjetnost odtrganja ali poškodovanja do razdalje  $\delta$  0,41 in 0,38. Oblika curka (hiter in tanek ali klasičen) ni imela signifikantnega vpliva na verjetnost dogodka.



**Slika 9: Mehanske obremenitve bakterijske celice pri kolapsu mikromehurčka**

Verjetnost za odtrganje bakterije (a) in poškodbo bakterije (b) v odvisnosti od hidrodinamske sile. Rdeča črta predstavlja najboljšo napoved modela skupaj s 95 % intervalom zaupanja (rdeče območje okrog črte). Parametri modela za odtrganje  $R^2=0.89$  in RMSE=0.11, ter za poškodovanje:  $R^2=0.66$  in RMSE=0.16. Verjetnost za odtrganja bakterije (c) in poškodbo bakterije (d) v odvisnosti od strižne napetosti. Rdeča črta predstavlja najboljšo napoved modela skupaj s 95 % intervalom zaupanja (rdeče območje okrog črte). Parametri modela za odtrganje  $R^2=0.88$  in RMSE=0.12, ter za poškodovanje:  $R^2=0.66$  in RMSE=0.16. (e) izračunane mejne vrednosti za odtrganje in poškodovanje celice za primer hidrodinamske sile in strižne napetosti. Spodnja meja predstavlja vrednosti, pod katero je zelo majhna verjetnost za dogodek ( $P_{\text{dog}} \sim 0$ ), zgornja meja pa predstavlja vrednosti, okrog katere je zelo velika verjetnost za dogodek ( $P_{\text{dog}} \sim 1$ ).

### 3 RAZPRAVA IN SKLEPI

#### 3.1 RAZPRAVA

Ob kolapsu kavitacijskega mehurčka lahko pride do pojava ekstremnih fizikalno-kemijskih razmer kot so: visoke temperature, nastanek mikrocurkov, tlačnih valov ter nastanek prostih radikalov (Brennen, 1995; Chahine in Hsiao, 2015; Koda in sod., 2003; Suslick in sod., 2011). Omenjene ekstremne razmere bi lahko imele vpliv na obstoj bioloških kontaminantov kot so bakterije ali virusi. Rezultati uporabe kavitacije v literaturi nakazujejo na značilno zmanjšanje živosti bakterijskih celic. Vendar se objavljeni rezultati o učinkovitosti kavitacije znatno razlikujejo, od nekdaj deset odstotkov zmanjšanja števila živih celic pa vse do nekaj logaritmov (Zupanc in sod., 2019). Ker točen mehanizem kavitacije na bakterijske celice ni poznan in ni znano katera komponenta celične stene najbolj pripomore k odpornosti na kavitacijo smo v nalogi proučili vlogo posameznih struktur celične stene pri odpornosti na kavitacijo.

##### 3.1.1 Lipidni dvosloj

Primarno tarčno mesto celičnih poškodb predstavlja citoplazemska membrana, ki je v osnovi fosfolipidni dvosloj. Kot najenostavnnejši modelni sistem za bakterijsko celico smo izbrali fosfolipidne vezikle, ki so sferične strukture, obdane z lipidnim dvoslojem. Obenem smo kot bakterijski model uporabili tudi sferoplaste bakterijske celice *E. coli*, z intaktno citoplazemsko membrano, kjer je bila odstranjena zunanjega membrana in peptidoglikanski sloj. Lipidni vezikli, v mikrometrskem velikostnem rangu, s fluorescentno označeno notranjostjo vezikla so vsebovali 1,2-dioleoil-sn-glicero-3-fosfoholin (DOPC) lipide. Eksperimentalni rezultati z DOPC vezikli kažejo, da so vezikli v puferski raztopini stabilne strukture. Za raztopino, ki je shranjena pri sobni temperaturi in v temi je stabilnost več kot 40 dni. Stabilnost vezikla je odvisna od temperature. Segrevanje raztopine z vezikli do 60 °C ni dalo značilnih sprememb v številu veziklov, medtem, ko je z višanjem temperature prišlo do zmanjšanja števila veziklov. S spremembo temperature se spremeni gibanje molekul v dvosloju, kar vpliva na drugačno pakiranje acilnih verig in polarnih glav, tako z dvigom temperature povzročimo tanjšanje dvosloja in povečanje fluidnosti membrane ter nastanek različnih lipidnih faz (Coderch in sod., 2000; Leonenko in sod., 2004; Simons in Sampaio, 2011). Pri znižanju temperature na -18 °C in -80 °C je bil ravno tako viden upad v številu, obenem pa se je zmanjšal tudi povprečni volumen vezikla. Z nižanjem temperature lahko pride do faznega prehoda med gelsko in tekočo kristalinsko fazo (Balleza, 2012). Znano je, da pri prehodni temperaturi pride do znatnega znižanja upogibne trdnosti, dvosloj se stanjša in permeabilnost za vodo se poveča (Nagle in Wilkinson, 1978; Needham in Evans, 1988). DOPC ima tranzicijsko temperaturo pri -16,5 °C, zato je pri sobni temperaturi v tekoči kristalinski obliki (Ulrich in sod., 1994). Prehod iz dvosloja

iz tekoče v gelsko fazo je v našem primeru povzročilo razpad veziklov. Rezultati kažejo, da so na fazne prehode bolj občutljivi večji vezikli. Obenem ni bilo opazne signifikantne razlike pri -18 °C in -80 °C kar nakazuje, da na stabilnost veziklov predvsem vpliva prehod med različnimi fazami pakiranja lipidov in ne toliko vrednost temperature.

V primeru spremembe ionske jakosti ali osmolarnosti raztopine se stabilnost lipidov zmanjša. Npr. pri spremembi osmolarnosti (dodatek glukoze) se je zmanjšalo število veziklov, kar kaže na ireverzibilne poškodbe oziroma razpad membrane. Pri spremembi ionske jakosti se je poleg zmanjšanja števila veziklov pojavilo tudi puščanje veziklov, kar je bilo vidno kot nižja povprečna intenziteta posameznega vezikla. Podoben učinek kot pri dodatku glukoze je bil opazen tudi pri dodatku etanola v raztopino veziklov. Opažena povečana občutljivost na kemijske spremembe okoliške tekočine kažejo na nestabilnost raztezanja membrane, saj se lipidni dvosloj razpre oziroma raztrga že pri relativnih raztezkih med 2 in 4 % (Boucher in sod., 2007; Doktorova in sod., 2019). Zaradi fluidne organizacije dvosloja lahko pride do začasne poškodbe dvosloja v obliki pore in puščanja snovi iz notranjosti vezikla v okolico, ki se lahko zapre (Leontiadou in sod. 2004) kar smo opazili pri spremembi ionske jakosti.

Dodatek prostih radikalov se je izkazal kot učinkovit način za propad dvosloja. Ob dodatku 1 mM raztopine železovega (II) suflata ( $\text{FeSO}_4$ ) in 1 mM raztopine vodikovega peroksida ( $\text{H}_2\text{O}_2$ ) je prišlo do propada večine veziklov. Do razpada veziklov je prišlo ob presežku kritične koncentracije stresorja. Prosti radikali povzročijo oksidacijo lipidov, kar povzroči reorganizacijo lipidov v dvosloju in nastanek por (Cwiklik in Jungwirth, 2010). Reorganizacija membrane z oksidiranimi lipidi vodi v propad veziklov. Pri dodajanju amfifilnih molekul (surfaktant Triton X-100) v raztopino veziklov smo opazili znatno zmanjšanje števila veziklov. Podobno kot pri prostih radikalih je bilo potrebno doseči oziroma preseči kritično koncentracijo detergenta v raztopini, da je prišlo do popolnega razpada veziklov. Začetni učinek na vezikle smo opazili pri koncentraciji 0,21 mM, medtem ko je bilo viden popoln propad veziklov pri koncentraciji 0,85 mM. Molekule detergenta so v večini primerov inverzno konične oblike in s svojim vstavljanjem v membrane povzročijo stres v lipidnem dvosloju (Atilgan in Sun, 2007). Z višanjem koncentracije molekul v dvosloju inducirajo nastanek por in pri koncentracijah nad kritično micelarno koncentracijo pride do razapljanja dvosloja s strani detergenta (Inque in Kitagawa, 1976).

Za boljše razumevanje mehanizma razpada in odziva dvosloja po dodatku detergenta smo vezikle opazovali direktno pod mikroskopom. Pri direktnem opazovanju razapljanja DOPC veziklov z detergentom Triton X-100 pod mikroskopom smo opazili izrazito dinamično spremenjanje oblik veziklov pred popolnim razapljanjem lipidnega dvosloja. Dodatek detergenta k sferičnim veziklom je povzročil oscilacije in uvihanje membrane, kar je vodilo v nastanek različnih hruškastih in diskastih oblik, sledilo je

izoblikovanje izrastkov in tetrov iz veziklov. Hitre in dinamične spremembe pri dodatku detergenta so vodile v raztplavljanje vezikla. Za natančnejšo razlago opaženih oblik smo spremembe oblik opisali z numeričnimi simulacijami. Molekule detergenta se preferenčno vstavlajo v področja kjer je večja ukrivljenost, kjer ta področja dodatno stabilizirajo, obenem pa lahko povzročijo nastanek nanotub, endoveziklov ali reorganiziranja membrane (Atilgan in Sun, 2007; Drab in sod., 2019; Fošnarič in sod., 2003; Kralj-Iglič in sod., 2000; Kralj-Iglič in sod., 2005). Ker je pri lipidnih dvoslojih »flip-flop« počasen proces (Sudbrack in sod., 2011) je sprememba spontane ukrivljenosti dvosloja zaradi vstavljanja molekul detergenta glavno gonilo za spremembe sferične oblike vezikla. Opazovan fenomen dinamike oblik smo razložili z enostavnim matematičnim modelom Monte Carlo v neravnovesnem stanju. Oblike lipidnega dvosloja smo spremenjali na podlagi dveh parametrov: koncentracije detergenta v dvosloju in prvlaka med molekulami detergenta (združevanje molekul v gruče). Pri nizkih koncentracijah detergenta detergent povzroči nastanek rahlih uvihavanj membrane, ki so se povečala z večanjem koncentracije detergenta v dvosloju. Če se molekule detergenta združeni v skupke inducirajo dodatno ukrivljenost membrane, ki se kaže kot nastanek izrastkov.

Izrazito velike fluktuacije lipidnega dvosloja, ki smo jih opazili po dodatku detergenta, bi lahko bile povzročene tudi s fizikalnimi in mehanskimi stresorji, s katerimi se redno srečujemo pri laboratorijskem delu, ki bi lahko vplivali na stabilnost veziklov in sferoplastov. Pipetiranje z avtomatsko pipeto se vsakodnevno uporablja v raziskovalnih laboratorijih in je lahko tudi vir mehanskega stresa v obliki strižnih sil. Učinek pipetiranja na stabilnost veziklov je bil viden pri 500 ali več ponovitvah pipetiranja, kar je pri rutinskem laboratorijskem delu nerealno visoko. Drugi vir strižnih napetosti je vorteksiranje vzorca kjer 4 minutno vorteksiranje pri rotacijski hitrosti do 3000 obratov na minuto (ang. rpm) ni imelo signifikantnega učinka na vezikle. Rezultati kažejo kot da se je z vorteksiranjem celo povečalo skupno število veziklov. Obenem pa se volumen in intenziteta veziklov nista spremenila, zato predvidevamo, da se je vzorec zgolj dobro premešal in je bil posledično bolj homogen kakor začetni vzorec. V primeru, da smo v vzorec dodali steklene kroglice in nato vorteksirali je bil učinek na lizo veziklov znatno višji. Z dodatkom kroglic v vzorec smo povišali strižne napetosti (Lee in sod., 1998), kar je bilo za vezikle uničujoče. Apliciranje striga z rotacijskim reometrom do strižnih hitrosti (ang. »shear rate«)  $18500\text{ s}^{-1}$  ni dalo signifikantne spremembe v stabilnosti veziklov. De Haas in sod. (1997) so pokazali, da se majhni 1,2-dimiristoil-sn-glicero-3-fosfoholin (DMPC) vezikli obnašajo podobno kot suspenzija trdnih delcev v redčenih raztopinah, kjer je majhna verjetnost, da pride do medsebojnih interakcij med vezikli in v bolj koncentrirani raztopini, kjer interakcija med vezikli ni več zanemarljiva. To nakazuje da strižne sile na makroskopski skali ne bodo imeli znatnega vpliva na mikroskopske delce. Pri eksperimentih so bili vezikli stabilni vse do 1800 bar hidrostatičnega tlaka, ko se je število veziklov zmanjšalo medtem, ko ni bilo

signifikantnega zmanjšanja intenzitete fluorescence veziklov. Molekulam v dvosloju se ob povišanem statičnem tlaku (1000 bar) zmanjša površina in volumen – največji delež sprememb se zgodi v nepolarnem repu. Ob povišanju tlaka se debelina dvosloja bistveno ne spremeni, pričakujemo pa lahko zmanjšanje upogibne konstante (Ding in sod. 2017). Upogibni elastični modul določa fleksibilnost in obliko membrane, vpliva na strukturo in nastanek nelamelarnih lipidnih faz ter vpliva na druge fizikalne in funkcijalne lastnosti membrane (Marsh, 2006). Na upogibnost membran najbolj vpliva sestava dvosloja – na primer negativno nabiti 1,2-dioleoil-sn-glicerol-3-fosfat (DOPG) lipidi se lažje oblikujejo v vezikel kakor nevtralno nabiti lipidi (Nomura in sod., 2001; Nomura in sod., 2004), obenem pa odbojne sile med negativno nabitim glavami lipidov povečajo razmak, kar dodatno stabilizira sferično strukturo vezikla (Kato in sod., 2015).

Iz eksperimentalnega pregleda vpliva mehanskih in fizikalno kemijskih stresorjev izhaja, da so lipidni veziki in sferoplasti zelo občutljive strukture, na katere ima večina uporabljenih stresorjev vpliv, če so le aplicirani dovolj dolgo ali v zadostni količini. Iz tega izhaja, da bi ekstremne razmere, ki se zgodijo ob pojavu kavitacije, lahko imele uničujoč učinek na lipidne vezike. Da bi to dokazali smo uporabili dva tipa kavitacije – akustično in hidrodinamsko. Oba tipa kavitacije sta učinkovito uničila lipidne vezike. Pri hidrodinamski kavitaciji smo uporabili mikro-kavitacijsko napravo z brizgami in krožno zožitvijo premera 0,6 mm, kjer je bila ocenjena povprečna hitrost potovanja vzorca približno 50 m/s. Skozi zožitev smo vzorec potisnili do največ 100-krat, ko je po stotih ciklih propadla večina veziklov. Poleg tega je razvidno, da se je po tretiranju zmanjšal povprečen volumen veziklov. Ker se intenziteta fluorescence ni bistveno spremenila je verjetno med kavitacijo prišlo do nastanka defektov ter puščanja veziklov. To bi lahko imelo pomembne posledice pri uničevanju bakterijskih celic. V primeru, da pride do puščanja citoplazmske membrane bi to lahko pomenilo uničenje celice. Analiza distribucije veziklov po velikosti tekom kavitiranja veziklov nakazuje, da se distribucija veziklov spremeni – večji veziki so bolj dovetni na razpad. Po stotih ciklih ostanejo v suspenziji predvsem veziki z manjšim premerom (okrog enega mikrometra). Pri akustični kavitaciji smo uporabili dve napravi: ultrazvočno banjico in ultrazvočno sondu. Ultrazvočna banjica je imela manjši vpliv na vezike kakor ultrazvočna sonda. Z večanjem izhodne moči pri banjici smo opazili povečan razpad veziklov, vendar se veziklom ni spremenila povprečna fluorescensa, kar nakazuje da pri nežnejšemu tipu akustične kavitacije ne pride tako pogosto do puščanja veziklov. Pri ultrazvočni sondi smo spremenjali jakost soniciranja z nastavljanjem amplitude nihanja. Pri 3  $\mu\text{m}$  amplitudi ultrazvok ni imel znatnega vpliva na vezikle, medtem ko je pri 6  $\mu\text{m}$  amplitudi bil že viden signifikanten upad v številu veziklov. Z nadaljnjam višanjem amplitude je bil opažen eksponenten upad števila veziklov. Nižanje intenzitete fluorescence veziklov kaže na večje puščanje veziklov pri višjih amplitudah, kar je pričakovano, saj akustično valovanje povzroči nastanek oscilacij in začasnih por v dvosloju (Pong in sod., 2006). V primeru, da pore zrastejo preko kritične velikosti pa lahko pride do razpada vezikla

(Marmottant in sod., 2008). Predviden mehanizem razpada veziklov pri soniciranju je zaradi pojava sonoporacije (nastanka por zaradi osciliranja tlaka) ter pojava kavitacije (Miller in sod., 2002; Schroeder in sod., 2009). Distribucija veziklov po velikosti kaže, da z višanjem amplitude ultrazvoka večji vezikli prej razpadajo. To je v skladu z literaturo saj se akustična kavitacija uporablja za pripravo majhnih unilamelarnih veziklov iz velikih multilamelarnih veziklov (Saunders in sod., 1962; Schroeder in sod., 2009).

### **3.1.2 Bakterija *E. coli* in celice z oslabljenimi komponentami celične stene**

Rezultati dinamike lipidnih veziklov so pokazali, da lahko prihaja do znatnih fluktuacij lipidnega dvosloja zaradi delovanja zunanjih dejavnikov. Pri tem lahko lipidni dvosloj razpade, kar bi imelo pogubne posledice za bakterijske celice. Običajno bakterijska celica ni izgrajena samo iz lipidnega dvosloja ampak še iz dodatnih struktur, ki lipidni dvosloj stabilizirajo. Zaradi tega bi lahko bilo delovanje kavitacije na bakterijske celice oslabljeno. Stresorji, ki so se izkazali za zelo učinkovite pri veziklih (kavitacija in vorteksiranje s kroglicami) imajo lahko znaten vpliv na živost bakterijskih celic *E. coli* (Cameron in sod., 2008; Ramanan in sod., 2008; Šarc in sod., 2018; Ho in sod., 2006; Sun in sod., 2018; Zupanc in sod., 2019). Po drugi strani ima detergent Triton X-100 manjši učinek na celice kot pri veziklih saj se vgradi v zunajo membrano, jo oslabi in poveča prepustnost za druge molekule (na primer antibiotike), podobno kot dodatek kelatorja EDTA (Miki in Hardt, 2013), vendar je njegova vgradnja v citoplazemske membrane manjša. Zanimivo, da centrifugiranje celic pri 15000x g povzroči propad 36 % celic *E. coli* (Gilbert in sod., 1990; Pembrey in sod., 1999), kar je primerljivo z učinkom centrifugiranja veziklov.

Razvoj hidrodinamske kavitacijske naprave v laboratorijskem merilu za proučevanje vplivov različnih celičnih struktur na živost bakterijskih celic se je izkazal za zelo težak izziv. V okviru doktorske disertacije nismo uspeli razviti naprave, kjer bi se pojavila kavitacija izključno na testni zožitvi in ne tudi na črpalki ter bi pri tem z uporabo mililitrskih delovnih volumnov dobili zanesljivo delovanje naprave ter vzdržljivost oziroma tesnjenje vseh komponent pri visokih tlakih. Uporabljeni mikro-kavitacijski napravi z zožitvijo, ki smo jo uporabili pri veziklih ni zdržala zadostnega števila pasaž, ki so potrebne pri eksperimentih z bakterijskimi celicami. Pri eksperimentih z bakterijo *E. coli* na potisni postaji s stisnjениm zrakom in Venturijevo zožitvijo (napravo so uporabili Filipić in sod. (2022)) ni prišlo do znatnih sprememb v živosti bakterijske kulture *E. coli* po 1000 pasažah. Pri napravi na rotor-stator črpalki (napravo so uporabili Kolbl Repinc in sod. (2021)) prav tako ni bilo znatnih sprememb v živosti bakterijske kulture *E. coli* po 1000 pasažah. Pri napravi z Venturi zožitvijo in zobato črpalko (napravo so uporabili pri Podbevšek in sod. (2022)) pa smo ugotovili, da že sama črpalka in pretočni ventil vplivata na živost bakterij *E. coli* kar pomeni, da ne moremo zagotovo

ločiti efekt hidrodinamske kavitacije na zožitvi od ostalih stresorjev, ki se pojavljajo na ventilu in črpalki. Poleg tega smo v raziskovalni skupini razvili dodatno mikro-kavitacijsko napravo, kjer preliminarni rezultati kažejo na znaten učinek hidrodinamske kavitacije na bakterije, vendar trenutna vzdržljivost naprave predstavlja eno izmed glavnih šibkih točk, ki onemogoča rutinsko uporabo naprave v raziskovalne namene. Zaradi omenjenih težav smo v nadaljevanju doktorske disertacije vpliv posameznih bakterijskih struktur na živost bakterij pri kavitaciji testirali z uporabo akustične kavitacije z ultrazvočno sondijo.

Pri soniciranju bakterije *E. coli* z ultrazvočno sondijo (20 kHz) in pri 15 µm amplitudi smo opazili eksponenten trend upada živosti celic s konstanto razpada ( $k$ ). Hitro deleče celice (celice v eksponentni fazi rasti) so bile bolj dovetne na propad zaradi soniciranja kakor nedeleče celice v stacionarni fazi rasti. Konstanta razpada celic ( $k$ ) v eksponentni fazi rasti je znašala  $0,16 \pm (0,02)$  ter za celice v stacionarni fazi rasti  $0,03 \pm (0,01)$ . Torej, 90 s soniciranje bakterijske kulture v eksponentni fazi rasti je povzročilo zmanjšanje števila živih celic za 3,4 log, medtem ko je pri celicah v stacionarni fazi rasti prišlo do zmanjšanja števila celic za 1,4 log. Do tega verjetno pride, ker se posameznim plastem celične stene spremeni sestava in struktura. Na primer pri citoplazemski membrani se s spremembom fiziološkega stanja spremeni sestava dvosloja, kar povzroči bolj urejeno stanje molekul v dvosloju, peptidoglikanski sloj ima več navzkrižnih povezav in krajše peptidne verige, LPS sloj se poveča in tudi sinteza EPS gradnikov se poveča (Amsler in sod., 1993; Glauner in sod., 1988; Ivanov in Fomchenkov, 1989; Olsén in sod., 1989; Pisabarro in sod., 1985; Souzu, 1986;).

Da bi preverili vpliv posamezne plasti celične stene na stabilnost celic pri kavitaciji smo spremnigli lastnosti posameznih plasti z dodajanjem kemijskih reagentov ali manipulacije celic na genetskem nivoju. EPS sloj smo modificirali z delecijo genov, ki imajo zapis za tri glavne komponente EPS sloja: kodrasti proteini, PGA in kolanska kislina. Konstanta eksponentnega upada  $k$  se ni signifikantno razlikovala v primerjavi z divjim tipom, tako v eksponentni kot v stacionarni fazi rasti. EPS sloj je najbližja struktura okoliški tekočini oziroma kavitacijskim mehurčkom, zato bi lahko zaradi svoje mehke strukture dušil vpliv kavitacije na celice (Gao in sod., 2014). Torej bi lahko pričakovali povečano občutljivost mutant na soniciranje, vendar v našem primeru deloma oslabljena kapsula ni bila bolj občutljiva na sonikacijo. Kapsularne komponente se obsežneje sintetizirajo pod stresnimi pogojimi (na primer stacionarna faza rasti), vendar pri naših eksperimentih tudi pri mutantah v stacionarni fazi rasti nismo opazili signifikantnih sprememb v stabilnosti bakterijskih kulture v primerjavi s celicami divjega tipa.

Zunanja membrana služi kot dodatna bariera za prehod molekul, obenem pa v kombinaciji s peptidoglikanom služi kot opora celici pri osmotskem tlaku (Delcour,

2008; Rojas in sod., 2018). Konstanta eksponentnega upada  $k$  se tudi v primeru oslabitve zunanje membrane ni signifikantno spremenila v primerjavi z dijjim tipom. Da je dejansko prišlo do reorganizacije zunanje membrane v eksponentno rastočih bakterijskih celicah smo posredno videli preko povečane prepustnosti membransko nepropustnega fluorescentnega barvila propidijevega jodida saj se je pri eksponentnih celicah izpostavljenimi z EDTA povečal delež celic obarvanih s propidijevim jodidom. Pri celicah v stacionarni fazi rasti ni prišlo do signifikantne razlike v prepustnosti barvila v celice. Iz dobljenih rezultatov lahko zaključimo, da zunanja membrana nima večjega vpliva na odpornost celic na kavitaro.

Peptidoglikan je bil dolgo poznan kot edina struktura v celici, ki daje celici mehansko oporo (Auer in Weibel, 2017; Madigan in sod., 2008). V naši raziskavi je oslabljen peptidoglikan znatno senzibiliziral celice za propad pri soniciranju. Za reorganizacijo in oslabitev peptidoglikana smo uporabili dve učinkovini: encim lizocim in antibiotik cefaleksin, ki imata različna načina delovanja na peptidoglikanski sloj. Dodatek lizocima ni signifikantno vplival na konstanto eksponentnega upada. Morfološko se celice tudi niso signifikantno spremene. Kot smo omenili zgoraj, je zunanja membrana fizična pregrada za prehod velikih molekul v celico (npr. lizocima), zato je verjetno, da lizocim ni prišel do peptidoglikana in ga razgradil. V primeru dodatka cefaleksina eksponentnim celicam pa vidimo signifikantno zvišanje konstante razpada ( $k = 0,53 \pm (0,08)$ ). Učinek antibiotika na celicah smo videli kot morfološko spremembo, kjer so bile celice daljše in imele filamentozno rast (dimenzijsi  $5,84 \pm (0,96) \times 0,86 \pm (0,10) \mu\text{m}$ ). Ob dodatku cefaleksina stacionarnim celicam vpliv na propad po soniciranju ni viden, saj deluje antibiotik samo na rastoče celice.

Če povečamo prepustnost zunanje membrane (kombinacija lizocima in EDTA) pa lahko opazimo učinek lizocima, saj se spremeni oblika celic iz paličaste v sferično obliko (sferoplasti). Sferoplasti, pripravljeni iz eksponentnih celic so signifikantno bolj dovezetni za propad pri soniciranju kakor celice divjega tipa v eksponentni fazi rasti. Ravno tako je bila signifikantna razlika pri sferoplastih pripravljenih iz stacionarnih celic ( $k=0,05 \pm (0,01)$ ) v primerjavi celicami divjega tipa v stacionarni fazi rasti. Pri sferoplastih pride do večinske razgradnje peptidoglikanskega sloja in zunanje membrane, tako da ostane intaktna samo notranja membrana (Birdsell in Cota-Robles, 1976; Clifton in sod., 2015; Onitsuka in sod., 1979; Voss, 1964). Zanimivo je, da so bili sferoplasti iz stacionarnih celic bolj stabilni v primerjavi z eksponentnimi sferoplasti, kar nakazuje na bolj rigidno in odporno citoplazemsko membrano stacionarnih celic. V primeru inkubacije celic z antibiotikom cefaleksin, kateri povzroči tvorbo dolgih filamentov, ter EDTA in lizocima nastanejo gigantski sferoplasti, ki imajo premer  $4,5 \pm (1,0) \mu\text{m}$ . Tako pripravljeni sferoplasti so zelo dovezetni za propad med soniciranjem, konstanta  $k$  je znašala  $0,76 \pm (0,32)$ . Podoben učinek soniciranja je bil viden pri liposomih, ki so po velikosti in strukturi zelo podobni uporabljenim veziklom.

To kaže, da samo citoplazemska membrana ni učinkovita pri zaščiti bakterij pred kavitacijo. Potrebne so še druge strukture celične stene.

Dobljeni rezultati nedvoumno kažejo, da ima odločilno vlogo pri stabilnosti celic *E. coli* pri kavitaciji sprememba peptidoglikanskega sloja. Ostali sloji kot ošibljena zunanja membrana ali spremenjen EPS sloj nimata znatnega vpliva. Ker se je pri modifikacijah celične stene spremenila tudi oblika in velikost celic: paličasta, sferična in filamenti bi lahko imela oblika celice tudi vpliv na učinkovitost kavitacije. Primerjava velikosti celic in konstante  $k$  kaže na odvisnost konstante  $k$  od velikosti celic, kar nakazuje, da bi lahko imela tudi velikost celic vpliv na stabilnost celic pri soniciranju. Lahko bi sklepali, da so večje celice bolj občutljive. Podoben trend smo opazili tudi pri veziklih, kjer so najprej razpadli večji vezikli.

Med soniciranjem lahko pride do nastanka prostih reaktivnih radikalov, vendar pričakujemo, da pri soniciranju z nizkimi frekvencami, kot smo ga uporabili v tej disertaciji, ne nastane večja količina prostih radikalov (Jordens in sod., 2016; Mason in sod., 2011; Nasseri in sod., 2017). Za dokaz nastanka radikalov med soniciranjem smo naredili eksperiment z ditiotreitol (DTT), vendar z omenjeno metodo nismo zaznali signifikantne koncentracije prostih radikalov med soniciranjem. Prav tako z lovilcem radikalov – metanolom nismo zaznali signifikantne spremembe v koncentraciji prostih radikalov. Zato sklepamo, da nastanek prostih radikalov ni glavni mehanizem inaktivacije bakterij pri nizko-frekvenčni akustični kavitaciji.

### **3.1.3 Vpliv individualnega kavitacijskega mehurčka na individualno bakterijsko celico**

Opazovanje efekta gruče kavitacijskih mehurčkov na lipidne vezikle, sferoplaste ali bakterije ni enostavno. Problem tako pri hidrodinamski kot pri ultrazvočno inducirani kavitaciji je velika količina energije, ki je s kavitacijo vnesemo v sistem in povzroča intenzivno mešanje lipidnih veziklov oziroma bakterij, kar znatno znižuje ločljivost pri direktnem opazovanju pojava. Za podrobnejše in bolj osnovno razumevanje pojava kavitacije in vpliva kavitacije na bakterijske celice se je potrebno osredotočiti na vpliv posameznega mikrometrskega kavitacijskega mehurčka na individualne bakterijske celice, kar zaradi tehničnih omejitev doslej še ni bilo raziskano. Ker se interakcija med mikromehurčkom in bakterijo dogaja na mikrometrski prostorski in mikrosekundni časovni skali pomeni, da smo na skrajni meji zaznavanja, ki jo omogoča trenutna tehnika. V tej disertaciji smo razvili novo eksperimentalno metodo in opisali kolaps kavitacijskega mikromehurčka z matematičnim modelom, kar predstavlja popolnoma nov pogled na kavitacijo in njen vpliv na bakterijske celice. Poleg tega je ta raziskava ponudila nov vpogled v mehanski odziv bakterijske celice na visokofrekvenčno mehansko obremenitev.

Odziv bakterij na visokofrekvenčne dražljaje so v preteklosti že poskušali raziskovati, vendar so raziskovalci prišli do nasprotajočih ugotovitev. Npr. visokofrekvenčno elektromagnetno polje ni imelo vpliva na rast bakterij *Staphylococcus epidermidis* in *S. aureus*, medtem ko je imelo vpliv na *Pseudomonas aeruginosa* (Salmen in sod., 2018; Wietzikoski Lovato in sod., 2018). Avtorji so inaktivacijo bakterij večinsko pripisali temperaturnemu gradientu in nastanku ROS. Čeprav je pri kavitaciji možen nastanek ROS, je bilo pokazano, da je za generacijo ROS pri gruči mehurčkov potreben daljši čas in veliko kavitacijskih dogodkov (Mason in sod., 2011; Podbevšek in sod., 2022; Yusof in sod., 2016). Zaradi kratkoživosti radikalov in majhne verjetnosti za njihov nastanek je detekcija ROS pri kolapsu enega mehurčka na mikrometrski in nanosekundni prostorski in časovni skali tehnično izredno zahtevna. V nalogi smo nastanek prostih radikalov pri kolapsu mikromehurčka zanemarili.

Ob kolapsu mehurčka lahko v centru mehurčka temperatura naraste vse do nekaj tisoč Kelvinov (Suslick in sod., 1999). Vendar je takšen dvig temperature zelo kratkoživ in je omejen na center mehurčka. Iz preteklih računskih raziskav je znano, da je lahko termičen učinek na bakterijsko celico znaten le v primeru ko je celica v neposrednem kontaktu z mehurčkom (Zevnik in Dular, 2020; Zevnik in Dular, 2021; Zevnik in Dular 2022). Mejna plast s spremenjeno temperaturo okoli mehurčka je zelo majhna, poleg tega je temperaturni dvig pod kritično temperaturo za bakterijske celice, zato lahko temperaturni učinek ob kolapsu posameznega mikromehurčka na bakterijske celice zanemarimo (Mitsuzawa in sod., 2006). Po drugi strani pa bi mehanski stresorji (kompresijske in strižne obremenitve) lahko imeli vpliv na bakterijske celice. Eksperimentalni in računski rezultati kažejo, da je glavni vir mehanskih obremenitev pri kavitaciji nastanek curka proti trdni površini. Ob udarcu curka v steno površine se spremeni smer toka radialno od centra curka, kar povzroči lokalno visoke tlake in strižne sile na pritrjene okoliške bakterijske celice. Pokazali smo, da je maksimalni strig, ki ga občuti bakterija, v rangu MPa in hidrodinamska sila v rangu nekaj deset  $\mu\text{N}$ . Pri tako velikih vršnih obremenitvah lahko pride do poškodb bakterij.

Eksperimentalni rezultati kažejo na tri možne izide ob kolapsu mehurčka na okoliške pritrjene celice – celice se odtrgajo od površine, celice ostanejo pritrjene ampak so poškodovane ali pa kavitacijski mehurček nima efekta na celico. Verjetnost za odtrganje in poškodovanje celic eksponentno pada v odvisnosti od brez-dimenzijske razdalje med mehurčkom in bakterijo. Podoben efekt je bil opažen tudi pri raziskavah z evkarionskimi celicami (Gac in sod., 2007; Hellman in sod., 2008; Jasikova in sod., 2019; O'Connor in sod., 2021; Ohl in sod., 2006; Rau in sod., 2006; Zhou in sod., 2012). Pri kolapsu posameznega mehurčka smo iz eksperimentalnih meritev in matematičnega modela določili, da je za odtrganje celice potrebna hidrodinamska sila v razponu med 15,9 nN in 1  $\mu\text{N}$ . Pri hidrodinamski sili pod 15,9 nN ne pričakujemo odtrganja, medtem ko pri silah nad 1  $\mu\text{N}$  je verjetnost za odtrganje zelo visoka ( $P = 1$ ). Silo odtrganja

bakterijske celice *E. coli* iz steklene površine obdane s PLL so izmerili Potthoff in sod. (2015) s FluidFM metodo, s katero so določili silo odtrganja posamezne bakterijske celice 14 nN. Izmerjena vrednost s FluidFM metodo je primerljiva z našimi rezultati. Mehanske obremenitve, ki so bile potrebne za poškodovanje celice so bile višje, hidrodinamska sila za poškodovanje celic je bila v razredu med 59,6 nN in 1,5  $\mu$ N. Sila za poškodovanje celic se sklada z rezultati raziskovalcev Shiu in sod. (1999), ki so določili silo lize celic *E. coli* pri 3,6  $\mu$ N.

Izračunane najvišje mehanske obremenitve so bile locirane v centru mehurčka zaradi nastanka visokoenergijskega curka, usmerjenega proti steni. Ti rezultati se skladajo z eksperimentalnimi rezultati, ki kažejo na popolno odtrganje celic v samem centru mehurčka. Maksimalna strižna napetost ob steni pri kolapsu mikromehurčka je bila 145 kPa, ki se sklada z raziskavami Zeng in sod. (2018), kjer so poročali o maksimalni strižni napetosti okrog 100 kPa. Računski model je za naš primer pokazal, da ob kolapsu mikromehurčka nastaneta dva tipa curkov: klasičen curek (Dular in sod. 2019) ter zelo tanek in hiter curek (Koch in sod., 2021; Lechner in sod., 2019; Lechner in sod., 2020; Reuter in Ohl, 2021). Klasičen curek je bil viden na eksperimentalnih posnetkih medtem ko nastanek hitrega in tankega curka nismo opazili. Hiter curek je sicer že bil eksperimentalno opažen, vendar pri bistveno večjih (milimetrskih) mehurčkih (Koch in sod., 2021; Lechner in sod., 2020; Reuter in Ohl, 2021a). Iz naših rezultatov izhaja, da tip curka ni imel signifikantnega vpliva na stopnjo odtrganja ali poškodovanja celic *E. coli*.

Rezultati tudi kažejo, da morajo biti bakterije pri kavitaciji v stiku ali v neposredni bližini mehurčka, da ima kavitacija učinek na celice. Kljub temu, da je pri gruči kavitacijskih mehurčkov večina mehurčkov izven mejne razdalje za uničenje bakterij je statistično gledano dovolj neposrednih interakcij mehurček-bakterija, da kavitacija uspešno uničuje bakterije v večjem volumnu in dalj časa trajajoči kavitaciji (npr. pri več pasažah). Seveda se lahko pri gruči kavitacijskih mehurčkov ustvarijo še dodatne mehanske obremenitve, kot so mikro in makro tokovi, ki lahko imajo lahko tudi uničujoč učinek na bakterije (Marmottant in Hilgenfeldt, 2003). Za povečanje učinkovitosti kavitacije je torej potrebno povečati možnosti direktne interakcije med mehurčki in bakterijami – npr. s povečanjem števila pasaž, časa treniranja, ali gostote generiranih mikromehurčkov. Določanje mejnih vrednosti hidrodinamske sile in strižne napetosti pri uničevanju bakterijskih celic *E. coli* predstavlja pomemben korak pri optimizaciji obstoječih in novih metod čiščenja odpadnih voda, ki temeljijo na mehanskem uničenju. Natančnejše razumevanje vpliva posameznega mehurčka na bakterijske celice bo zagotovo omogočilo napredok kavitacijske tehnologije v aplikativne namene čiščenja odpadnih voda.

Prikazani rezultati v okviru doktorske disertacije nakazujejo, da ima hidrodinamska kavitacija uničujoč učinek na fosfolipidne vezikle in bakterijske celice *E. coli*. Kljub pozitivnim rezultatom pa smo opazili, da je uporaba hidrodinamske kavitacije še vedno tehnično zahteven proces, kjer je ponovljivost pojava kavitacije in zanesljivost kavitacijskih naprav še vedno eden izmed glavnih omejujočih problemov ki upočasnujejo napredok tehnologije v aplikativne namene. V okviru naloge smo poskusili natančneje opredeliti proces inaktivacije bakterijskih celic s pomočjo kavitacije. Za aplikativne namene pa bi bilo v prihodnje potrebno preveriti energijsko učinkovitost samega procesa, pri čemer bi lahko umestili učinkovitost čiščenja s kavitacijo med ostale procese čiščenja vode. Direktna primerjava akustične in hidrodinamske kavitacije kaže, da imata metodi različen trend inaktivacije bakterijskih celic. Pri akustični kavitaciji pride na začetku tretiranja do hitrega razpada celic, ki se s časom ustali. Pri hidrodinamski kavitaciji pa je uničenje pri začetnih ciklih tretiranja nižje, nato pa eksponentno narašča z višanjem števila ciklov. Možen vzrok za razliko v fenomenu bi lahko bil različen mehanizem delovanja, ali pa je razlika samo posledica različnega vnosa energije. Poleg tega spremembe v parametrih, kot so amplituda ter frekvenca pri akustični kavitaciji, oziroma spremenjanje geometrije zožitve ter tlačne razlike pri hidrodinamski kavitaciji, lahko različno vplivajo na potek inaktivacije bakterijskih celic. Vplivi teh parametrov pa tudi niso dobro poznani. Čeprav so celice v eksponentni fazi rasti bolj dovezne na propad zaradi kavitacije in je lažje določati razlike med različnimi tretmaji, najdemo v okolju večinoma celice v stacionarni fazi rasti. Zato bi se bilo potrebno v nadalnjih raziskavah še bolj osredotočiti na te celice v izogib precenjevanju učinkovitosti kavitacije pri realnih okoljskih vzorcih. V namene čiščenja odpadnih voda bi bil najboljši izkupiček določenega procesa popolno uničenje celic oziroma sterilizacija. Doseganje popolnega uničenja bakterijskih celic s kavitacijo je najverjetneje malo verjetno saj pri procesu vplivamo samo na določen delež celotnega volumna vzorca, kar pomeni da bi v teoriji potrebovali enormno število ciklov oziroma časa izpostavljenosti kavitaciji. Obenem se z manjšanjem števila celic najverjetneje tudi manjša verjetnost, da bo prišlo do kolapsa mehurčka v neposredni bližini bakterijske celice, kar bi še dodatno podaljšalo čas tretiranja vzorca s kavitacijo. Doprinos k odpornosti na kavitacijo posameznih komponent celične stene smo pokazali pri modelnem predstavniku gram negativne skupine bakterij s tankim slojem peptidoglikana. Gram pozitivne bakterijske celice imajo drugačno sestavo celične stene, kjer je peptidoglikanski sloj veliko debelejši, vendar nimajo zunanje membrane, zato bi bilo potrebno za natančnejše razumevanje odziva celic na kavitacijo preveriti tudi gram pozitivne bakterijske kulture ter druge specializirane oblike bakterijskih celic – na primer spore. Razvoj metode generiranja posameznega mehurčka na mikrometrski skali predstavlja novo metodo, ki omogoča širok spekter uporabe v namene raziskav mehanske karakterizacije bakterijskih celic. Možnost manipuliranja kavitacijskega mehurčka na mikroskopski skali je lahko obetavna metoda za brezkontaktno manipulacijo v mikrofluidnih sistemih, mikrostrukturiranje površin ali delcev. Obenem

bi generiranje mehanskih sil na tako kratki časovni in majhni prostorski skali lahko pripomoglo k zelo natančnim manipulacijam posameznih celic, kjer bi lahko uporabili kavitacijski mehurček kot »nano« skalpel. Z njim bi lahko hitro in natančno ustvarili lokalno poškodbo ali manipulacijo celice za vnos določenih molekul v celico ali selektiven izpust določenih komponent iz celice. Pritrjene bakterije predstavljajo enostaven model začetne faze nastanka biofilma, zato bi lahko omenjena metoda služila tudi za karakterizacijo mehanskih lastnosti biofilma na mikroskopski skali.

### **3.1.4 Pregled doprinosa kandidata in ostalih sodelavcev v okviru doktorske disertacije**

Doktorand Žiga Pandur je naredil vse eksperimente in analizo rezultatov v okviru doktorske naloge, kjer sta mentor (prof. dr. David Stopar) in somentor (prof. dr. Matevž Dular) s svetovanjem, sprotnim spremeljanjem raziskav usmerjala in pomagala doktorandu skozi celoten študij. Dodatno je za celostno razumevanje interakcije med kavitacijskim mehurčkom in bakterijsko celico v disertacijo vključeno delo sodelavca dr. Jure Zevnik, ki je opravil numerične simulacije kolapsa posameznega mehurčka ob togi steni in določil maksimalne sile ob kolapsu mehurčka na bakterijsko celico. Celotno raziskovalno delo skupaj z numeričnimi simulacijami o interakciji med kavitacijskim mehurčkom in bakterijskimi celicami je bilo poslano v pregled za objavo v znanstveni reviji *Science Advances*. Pri spremeljanju dinamike raztapljanja veziklov z detergentom Triton X-100 je dr. Mitja Drab s sodelavci opravil matematičen opis sprememb oblik vezikla zaradi vstavljanja detergenta v fosfolipidni dvosloj, kjer je bilo skupaj z eksperimentalnim opazovanjem pojava objavljeno kot raziskovalen članek v znanstveni reviji *Biophysical Journal*.

## **3.2 SKLEPI**

Na podlagi rezultatov doktorske disertacije podajamo naslednje sklepe.

Lipidni dvosloj (vezikel in sferoplast) je izredno podajna in neraztezna struktura. Zato imata sprememba osmotskega tlaka in ionske jakosti raztopine vpliv na stabilnost lipidnega dvosloja. Pipetiranje in vorteksiranje niso imeli znatnega vpliva na stabilnost veziklov, razen ko smo število ponovitev povečali nerealno visoko. Znaten vpliv na stabilnost lipidnega dvosloja ima vgradnja detergenskih molekul, ki povzroči hitre oscilacije lipidnih veziklov. Za mehanično razlogo oscilacij lipidnih dvoslojev smo uporabili Monte Carlo simulacijo, ki je imitirala neravnotežne pogoje ob začetku raztapljanja lipidnega dvosloja in upoštevala postopno vgradnjo detergента v lipidni dvosloj.

Kavitacija je imela največji učinek na lipidne vezikle in sferoplaste, manj na bakterije v eksponentni fazi in najmanj na bakterije v stacionarni fazi rasti. S selektivnim

spreminjanjem komponent bakterijske celične stene smo ugotovili, da ima največji efekt na odpornost bakterij na kavitacijo peptidoglikanski sloj. Po odstranitvi peptidoglikanskega sloja so bakterije postale zelo občutljive za kavacijo, primerljive občutljivosti lipidnega dvosloja.

Z razvojem nove metode generiranja posameznega kavacijskega mikromehurčka smo preučili vpliv interakcije med izbranim mikromehurčkom in bakterijsko celico. Rezultati kažejo, da ima kavacijski mehurček učinek le če je generiran v neposredni bližini bakterijske celice saj se verjetnost za poškodbo celice znotraj projicirane brez-dimenzijске razdalje bakterija-mikromehurček eksponentno zmanjšuje. Z eksperimentalnimi rezultati smo kalibrirali rezultate matematičnega modela in določili mejne vrednosti hidrodinamske sile in strižne napetosti za poškodovanje bakterijske celice oziroma njeno odtrganje iz površine po interakciji s kavacijskim mikromehurčkom.

### **3.2.1 Potrditev hipotez**

V nalogi sta bili postavljeni dve raziskovalni hipotezi.

**1: Gruča hidrodinamsko generiranih kavacijskih mehurčkov v primerjavi z običajnimi fizikalno-kemijskimi stresorji učinkovito izliza fosfolipidne vezikle, sferoplaste in bakterijske celice.**

Ta hipoteza je bila potrjena. Gruča hidrodinamsko generiranih mehurčkov je zelo učinkovito orodje za uničenje fosfolipidnih veziklov in sferoplastov. Hidrodinamska kavacija je uspešna metoda za uničenje bakterijskih celic, vendar bi bilo potrebno njeni učinkovitost za uspešno komercializacijo povečati.

**2: Z implozijo posameznega kavacijskega mehurčka v bližini bakterijske celice pride do porušenja membranske integritete, kar omogoča lizo bakterijske celice.**

Ta hipoteza je bila v celoti potrjena. Interakcija med kavacijskim mikromehurčkom in bakterijsko celico uniči integriteto bakterijske membrane. Sproščena energija omogoča odtrganje bakterijskih celic in njihovo poškodovanje v obsegu, ki je enak premeru kavacijskega mikromehurčka. Za potrditev hipoteze je bilo potrebno razviti popolnoma nov eksperimentalni pristop, ki omogoča generiranje kavacijskega mikromehurčka v neposredni bližini izbrane bakterijske celice na časovni skali nanosekunde in prostorski skali mikrometra.

## 4 POVZETEK (SUMMARY)

### 4.1 POVZETEK

Kavitacija je pojav parnih mehurčkov v kapljevini, ki hitro in agresivno implodirajo. Sprva je bila kavitacija sprejeta kot nezaželen pojav, saj so se ob kavitaciji turbinskih motorjev pojavile vibracije, povišana glasnost turbinskih motorjev ter erozija materialov (Franc in Michel, 2004). Vendar sproščena energija ob kolapsu mehurčkov lahko uničuje tudi druge materiale, na primer biološke delce kot so bakterijske celice in druge biološke kontaminante. V času ko čista voda postaja luksuzna dobrina, postaja kavitacija ena izmed potencialnih tehnologij za čiščenje in obdelavo vode. Čeprav je bilo narejeno že veliko raziskav na temo uporabe kavitacije za učinkovito razgradnjo bioloških kontaminant v vodi, se trenutno objavljeni rezultati znatno razlikujejo kar nakazuje na slabo razumevanje delovanja kavitacije na biološke vzorce (Zupanc in sod., 2019). Kljub uporabi kavitacije v namene inaktivacije bakterijskih celic in drugih bioloških kontaminant se še vedno smatra sam proces kot fenomen »črne škatlice« kjer ni točno poznan mehanizem delovanja kavitacije na bakterijske celice. Pri hidrodinamski kavitaciji se lokalno pojavljajo ekstremne razmere kot so visoka temperatura, nastanek mikrocurkov z visokimi hitrostmi, tlačnih valov, kisikovih reaktivnih zvrsti (Brennen, 1995; Chahine in Hsiao, 2015; Koda in sod., 2003; Suslick in sod., 2011). Bakterijska celica je visoko-reguliran sistem omejen s celično steno, ki omogoča kemijsko, fizikalno in mehansko stabilnost na okoljske stresorje (Madigan in sod., 2008). Širok spekter ekstremnih razmer ob kolapsu in hiter potek kolapsa mehurčkov še dodatno otežuje določitev točnega mehanizma interakcije kavitacije in bakterijske celice. Poleg tega tudi ni znano katera celična struktura najbolj pripomore k stabilnosti celice pri kavitaciji.

V disertaciji smo s selektivnim pristopom raziskali vpliv kavitacije na lipidne vezikle, bakterijske celice *E. coli* in celice z modificiranimi komponentami posameznih slojev v celični steni. Citoplazemska membrana je eden izmed najbolj osnovnih slojev za obstoj celice saj nadzoruje prehod velikih in nabitih molekul v in iz celice. Gram negativne bakterijske celice imajo poleg citoplazemske membrane še tanek peptidoglikanski sloj, zunanjo membrano in EPS sloj (Madigan in sod., 2008). Kot najbolj enostaven model bakterijske celice smo vzeli DOPC fosfolipidni vezikel, ki je imel v lumnu fluorescentno barvilo (natrijev fluoresceinat), kar nam je omogočilo zajem slik s fluorescentnim konfokalnim mikroskopom. Takšna membranska struktura je osmotsko nestabilna, obenem pa je izredno podajna struktura. Zaradi velikega nabora ekstremnih pogojev, ki nastanejo ob pojavi kavitacije, smo najprej preverili stabilnost veziklov na posamezne fizikalno-kemijske in mehanske stresorje. Fizikalno-kemijski stresorji kot so spremembra ionske jakosti, osmolarnosti so imeli vpliv na stabilnost veziklov. Sprememba temperature je na vezikle imela vpliv le v primeru znižanja temperature pod temperaturo faznega prehoda lipidov (pod -16 °C) ali pri dvigu temperature na 80 °C.

Vstavljanje molekul detergenta v lipidni dvosloj se je izkazal kot zelo učinkovit način uničenja veziklov. Zaradi vstavljanja molekul detergenta v dvosloj je prišlo do znatnih fluktuacij v dvosloju vezikla kar smo opazili kot dinamične spremembe oblike vezikla pred popolnim raztplavljanjem. Nastanek neravnovesnega stanja v dvosloju smo poskusili mehanično razložiti z računskim modelom. Z Monte Carlo računskim modelom smo predpostavili dve spremenljivki, na podlagi katerih smo dobili primerljive rezultate sprememb oblik. Na dinamiko spremicanja oblik pri dodatku detergenta vpliva koncentracija molekul detergenta v dvosloju in tendenca združevanja detergenta v gruče. Predstavljen model nam je omogočil bolj podroben mehaničen vpogled v možne fluktuacije vezikla (lipidnega dvosloja) pred popolno porušitvijo dvosloja.

Mehanski stresorji, ki so prisotni pri rutinskem laboratorijskem delu (pipetiranje in vorteksiranje) niso imeli znatnega vpliva na stabilnost, razen pri zelo visokem številu ponovitev. Centrifugiranje je imelo majhen vpliv na stabilnost veziklov. Povišan hidrostatski tlak ravno tako ni imel učinka. Apliciranje striga z rotacijskim reometrom do hitrosti striženja  $18500\text{ s}^{-1}$  ni vplivalo na stabilnost veziklov. Ko smo dodali v vzorec steklene kroglice in vzorec vorteksirali smo uspešno razbili lipidne vezikle. Rezultati so pokazali, da so vezikli razmeroma stabilni na nizke ionske spremembe, temperaturne spremembe, centrifugiranje in izredno občutljivi na vstavljanje amfifilnih molekul ter visoke strižne sile. Izpostavitev veziklov hidrodinamski kavitaciji se je izkazala kot učinkovita metoda za uničenje veziklov. Vezikle smo izpostavili še akustični kavitaciji s sonotrodo in akustični kavitaciji v ultrazvočni banjici. Akustična kavitacija z ultrazvočno banjico je imela nižji učinek kot kavitacija s sonotrodom.

Bakterija *E. coli* je Gram negativna paličasta bakterija, katere sevi so lahko potencialni patogeni za človeka in se lahko prenašajo preko kontaminiranih vodnih okolij. Bakterijskim celicam smo selektivno oslabili ali odstranili izbrane komponente celične stene: EPS sloj, osibili zunanjou membrano ter spremenili ali odstranili peptidoglikanski sloj. Kot vir kavitacije smo uporabili akustično kavitacijo s sonotrodom, kjer smo pokazali, da je glavna komponenta, ki daje odpornost na kavitacijo peptidoglikanski sloj. Fiziološko stanje bakterijskih celic znatno vpliva na stabilnost celic pri soniciranju – celice v stacionarni fazi rasti so značilno bolj odporne kakor celice v eksponentni fazi rasti. V primeru, ko celici odstranimo zunanjou membrano in peptidoglikanski sloj (sferoplasti), dobimo podoben odziv na soniciranje kot pri liposomih. Kavitacija se je izkazala, kot učinkovit postopek za uničevanje lipidnih veziklov, sferoplastov, bakterijskih celic ali bakterijskih celic s spremenjeno sestavo celične stene. Vezikli in sferoplasti so bili najbolj dovetni za propad pri kavitaciji, medtem ko je pri bakterijskih celicah bilo potrebno dovesti več energije za viden učinek. Za odpornost bakterij na kavitacijo je najbolj pomemben peptidoglikanski sloj, saj se dovetnost za propad zelo poveča, če ga odstranimo. Pri bakterijah z odstranjenim peptidoglikanom postane stabilnost celic na kavitacijo zelo podobna stabilnosti veziklov. Spreminjanje EPS sloja

ali zunanje membrane nima znatnega vpliva na stabilnosti bakterijske celice pri soniciranju.

Vpliv posameznega mikromehurčka na bakterijsko celico še ni bil proučen v literaturi. V nalogi smo razvili metodo za generiranje mikrometrskih kavitacijskih mehurčkov, kar nam je omogočilo neposredno preučevanje interakcije bakterijske celice s kavitacijskim mehurčkom. Z uporabo optične pincete za natančno pozicioniranje zarodnega mehurčka smo lahko hitro in natančno z visokonapetostno razelektritvijo sprožili kavitacijski mikromehurček. Kavitacijski mehurček je imel drastičen vpliv na pritrjene bakterijske celice v neposredni bližini kolapsa mehurčka. Kolaps kavitacijskega mikromehurčka je povzročil odtrganje bakterijskih celic v centru ekspandirajočega mehurčka. Coni odtrganih bakterij je sledila cona s poškodovanimi, a pritrjenimi celicami. Vplivno območje mehurčka za poškodovanje celice je bilo znotraj maksimalnega radija mehurčka, medtem ko je bila verjetnost za odtrganje celic na dvakratni razdalji maksimalnega radija mehurčka. Z računalniško analizo mikroskopskih slik bakterijskih celic smo določili verjetnost za izid interakcije med mehurčkom in bakterijo (odtrgana, poškodovana ali nespremenjena). S pomočjo matematičnega modela smo dobili bolj natančen in dodaten vpogled v dinamiko procesa kavitacije mikromehurčka. Ugotovili smo dva mehanizma nastanka curkov, ki sta odvisna od razdalje mehurčka od trdne stene ( $\gamma$ ). Pri mikromehurčkih, ki so zelo blizu stene ( $\gamma < 0,3$ ) se ustvari hiter in tanek curek, kar je bilo eksperimentalno opaženo pri milimetrskih mehurčkih, v našem primeru generiranja mikromehurčkov pa jih nismo opazili, najverjetneje zaradi resolucijske omejitve uporabljene opreme. Pri mikromehurčkih, ki so oddaljeni od stene  $\gamma > 0,4$  nastane klasičen kavitacijski curek, ki smo ga opazili tudi pri naših eksperimentih. Simulacije so pokazale, da so največje mehanske obremenitve pojavijo ob nastanku curka. Na podlagi modela smo lahko ocenili mejne hidrodinamske sile ter strižne napetosti za odtrganje ali poškodovanje celice, ki sta znašala  $1 \mu\text{N}$  in  $145 \text{ kPa}$  za odtrganje celice ter  $1,5 \mu\text{N}$  in  $217 \text{ kPa}$  za poškodovanje celice. Natančnejše razumevanje vpliva posameznega mehurčka na bakterijske celice bo omogočilo napredok kavitacijske tehnologije v aplikativne namene čiščenja odpadnih voda. Poleg tega novo razvita metoda generiranja kavitacijskih mikromehurčkov in določanje mehanskih lastnosti bakterijske celice omogoča nov vpogled v delovanje bakterijskega sveta.

## 4.2 SUMMARY

A sudden decrease in pressure triggers the formation of vapor and gas bubbles inside a liquid medium (also called cavitation). This leads to many key engineering problems: material loss, noise, and vibration of hydraulic machinery (Franc and Michel, 2004). On the other hand, cavitation is a potentially useful phenomenon: the extreme conditions are increasingly used for a wide variety of applications such as surface cleaning, enhanced chemistry, and wastewater treatment (i.e. bacteria eradication and virus

inactivation). Despite the significant progress, a large gap persists between the understanding of the mechanisms that contribute to the effects of cavitation and its application. Although engineers are already commercializing devices that employ cavitation, we are still not able to answer the fundamental questions such as: how bubbles can clean, disinfect, enhance chemical activity, kill bacteria or what makes bacteria resistant to cavitation phenomena?

In this thesis we approached these fundamental questions by selective modifications of bacterial cell wall structures or by study of simplified cell models such as spherical lipid bilayer structures (vesicles, spheroplasts). Lipid vesicles are widely applied in research, diagnostics, medicine, industry, and as biological model systems. We showed for the first time the effect of hydrodynamic cavitation on vesicle stability and compare it to the effect of well described chemical, physical and mechanical treatments. Fluorescein loaded giant 1,2-dioleoyl-sn-glycero-3-phosphocholine (DOPC) lipid vesicles were treated by hydrodynamic cavitation which is a promising new method for the inactivation of biological samples. Hydrodynamic treatment was compared to various chemical, physical, and mechanical stressors such as ionic strength and osmolarity agents (glucose,  $\text{Na}^+$ ,  $\text{Ca}^{2+}$ , and  $\text{Fe}^{3+}$ ), free radicals, shear stresses (pipetting, vortex mixing, rotational shear stress), high pressure, electroporation, centrifugation, surface active agents (Triton X-100, ethanol), microwave irradiation, heating, freezing-thawing, ultrasound (ultrasonic bath, sonotrode). The fluorescence intensity of the individual fluorescein loaded lipid vesicles was measured with confocal laser microscopy. The distribution of lipid vesicle size, vesicle fluorescence intensity, and the number of fluorescein loaded vesicles was determined before and after the treatment with different stressors. The different environmental stressors were ranked in order of their relative effect on liposome fluorescein release. Of all tested chemical, physical and mechanical treatments for stability of lipid vesicles, the most detrimental effect on vesicles stability had hydrodynamic cavitation, vortex mixing with glass beads and ultrasound. This work provides a benchmark for lipid vesicle robustness to a variety of different physico-chemical and mechanical parameters important in lipid vesicle preparations and applications.

It is known that giant vesicles undergo dynamic morphological changes when exposed to a detergent. The solubilization process may take multiple pathways. In this work, we identify lipid vesicle shape dynamics before the solubilization of 1,2-dioleoyl-sn-glycero-3-phosphocholine giant vesicles with Triton X-100 detergent. The violent lipid vesicle dynamics was observed with laser confocal scanning microscopy and was qualitatively explained via a numerical simulation. A three-dimensional Monte Carlo scheme was constructed that emulated the nonequilibrium conditions at the beginning stages of solubilization, accounting for a gradual addition of Triton X-100 detergent molecules into the lipid bilayers. We suggest that the main driving factor for

morphology change in lipid vesicles is the associative tendency of the TR molecules, which induces spontaneous curvature of the detergent inclusions, an intrinsic consequence of their molecular shape. The majority of the observed lipid vesicle shapes in the experiments were found to correspond very well to the numerically calculated shapes in the phase space of the possible solutions. The results give an insight into the early stages of lipid vesicle solubilization by amphiphilic molecules, which is nonequilibrium in nature and very difficult to study.

The bacterial cell, however, is more complex structure compared to lipid bilayer and more resistant to cavitation. The applications of cavitation in industrial settings are plagued by the lack of the knowledge of the exact mechanism of action of sonication on bacterial cells, variable effectiveness of cavitation on bacteria, and inconsistent data of its efficiency. In this study we have systematically changed material properties of *E. coli* cells to probe the effect of different cell wall layers on bacterial resistance to ultrasonic irradiation (20 kHz, output power 6,73 W, horn type, 3 mm probe tip diameter, 1 ml sample volume). We have determined the rates of sonolysis decay for bacteria with compromised major capsular polymers, disrupted outer membrane, compromised peptidoglycan layer, spheroplasts, giant spheroplasts, and in bacteria with different cell physiology. The non-growing bacteria were 5-fold more resistant to sonolysis than growing bacteria. The most important bacterial cell wall structure that determined the outcome during the sonication was peptidoglycan. If peptidoglycan was remodelled, weakened, or absent the cavitation was very efficient. Cells with removed peptidoglycan had sonolysis resistance equal to lipid vesicles and were extremely sensitive to sonolysis. The results suggest that bacterial physiological state as well as cell wall architecture are major determinants that influence the outcome of bacterial sonolysis.

To evaluate the effect of cavitation on bacterial cell at a fundamental level, one needs to downscale the cavitation process to a single cavitation bubble which is similar in size to a bacterial cell. Here we present a method to deliver a nanoscale spatial and temporal energy quantum to mechanically remove and destroy the individual bacterial cells. The method allows for accurate and fast positioning of the single microbubble on the individual bacterial cell with optical tweezers and triggering of the single violent microscale cavitation event. The interaction between the single cavitation microbubble and the individual bacterial cell was studied with fluorescence microscopy in real time. The results demonstrate that energy delivered during the single cavitation event destroys or detaches bacteria by shear and hydrodynamic stress loads. Mechanical and numerical models were used to estimate the maximal shear stress and hydrodynamic forces for detachment or survival of the individual bacterium.

## 5 VIRI

- Akhatov I., Lindau O., Topolnikov A., Mettin R., Vakhitova N., Lauterborn W. 2001. Collapse and rebound of a laser-induced cavitation bubble. *Physics of Fluids*, 13, 10: 2805-2819.
- Almeida P. F. F., Vaz W. L. C. 1995. Lateral diffusion in membranes. V: *Handbook of biological physics*. Lipowsky R., Sackmann E. (ur.). Amsterdam, Elsevier: 305-357.
- Amir A., Babaeipour F., McIntosh D. B., Nelson D. R., Jun S. 2014. Bending forces plastically deform growing bacterial cell walls. *Proceedings of the National Academy of Sciences*, 111, 16: 5778-5783.
- Amro N. A., Kotra L. P., Wadu-Mesthrige K., Bulychev A., Mobashery S., Liu G. Y. 2000. High-resolution atomic force microscopy studies of the *Escherichia coli* outer membrane: Structural basis for permeability. *Langmuir*, 16, 6: 2789-2796.
- Amsler, C. D., Cho M., Matsumura P.. 1993. Multiple factors underlying the maximum motility of *Escherichia coli* as cultures enter post-exponential growth. *Journal of Bacteriology*, 175: 6238-6244.
- Annegowda H. V., Bhat R., Min-Tze L., Karim A. A., Mansor S. M. 2012. Influence of sonication treatments and extraction solvents on the phenolics and antioxidants in star fruits. *Journal of Food Science and Technology*, 49, 4: 510-514.
- Araújo G. R. d. S., Viana N. B., Gómez F., Pontes B., Frases S. 2019. The mechanical properties of microbial surfaces and biofilms. *The Cell Surface*, 5: 100028, doi: 10.1016/j.tcs.2019.100028: 8 str.
- Atilgan E., Sun S. X. 2007. Shape transitions in lipid membranes and protein mediated vesicle fusion and fission. *Journal of Chemical Physics*, 126: 095102, doi: 10.1063/1.2483862: 10 str.
- Auer G. K., Weibel D. B. 2017. Bacterial cell mechanics. *Biochemistry*, 56, 29: 3710-3724.
- Azuma Y., Kato H., Usami R., Fukushima T. 2007. Bacterial sterilization using cavitating jet. *Journal of Fluid Science and Technology*, 2, 1: 270-281.
- Bangham A. D., Horne R. W. 1964. Negative staining of phospholipids and their structural modification by surface-active agents as observed in the electron microscope. *Journal of Molecular Biology*, 8, 5: 660-668.

- Balasundaram B., Harrison S. T. L. 2006. Study of physical and biological factors involved in the disruption of *E. coli* by hydrodynamic cavitation. *Biotechnology Progress*, 22: 907-913.
- Balleza D. 2012. Mechanical properties of lipid bilayers and regulation of mechanosensitive function. *Channels*, 6: 220-233.
- Bavi N., Nakayama Y., Bavi O., Cox C. D., Qin Q. H., Martinac B. 2014. Biophysical implications of lipid bilayer rheometry for mechanosensitive channels. *Proceedings of National Academy of Sciences*, 111: 13864-13869.
- Bayer M. E., Thurow H. 1977. Polysaccharide capsule of *Escherichia coli*: microscope study of its size, structure, and sites of synthesis. *Journal of Bacteriology*, 130: 911-936.
- Beveridge T. J. 1981. Ultrastructure, chemistry, and function of the bacterial wall. *International Review of Cytology*, 72: 229-317.
- Beveridge T. J., Graham L. L. 1991. Surface layers of bacteria. *Microbiological Reviews*, 55: 684-705.
- Bhuyan M. K., Soleilhac A., Somayaji M., Itina T. E., Antoine R., Stoian R. 2018. High fidelity visualization of multiscale dynamics of laser-induced bubbles in liquids containing gold nanoparticles. *Scientific Reports*, 8: 9665, doi: 10.1038/s41598-018-27663-z: 12 str.
- Birdsell D. C., Cota-Robles E. H. 1976. Production and ultrastructure of lysozyme and ethylenediaminetetraacetate-lysozyme spheroplasts of *Escherichia coli*. *Journal of Bacteriology*, 93, 1: 427-437.
- Blount Z. D. 2015. The natural history of model organisms: The unexhausted potential of *E. coli*. *eLife*, 4: e05826, doi: 10.7554/eLife.05826: 12 str.
- Borkent B. M., Arora M., Ohl C. D., De Jong N., Versluis M., Lohse D., Mørch K. A., Klaseboer E., Khoo B. C. 2008. The acceleration of solid particles subjected to cavitation nucleation. *Journal of Fluid Mechanics*, 610: 157-182.
- Boucher P. A., Joós B., Zuckermann M. J., Fournier L. 2007. Pore formation in a lipid bilayer under a tension ramp: modeling the distribution of rupture tensions. *Biophysical Journal*, 92: 4344-4355.

- Böckmann R. A., Grubmüller H. 2004. Multistep binding of divalent cations to phospholipid bilayers: a molecular dynamics study. *Angewandte Chemie International Edition*, 43: 1021-1024.
- Böckmann R. A., Hac A., Heimburg T., Grubmüller H. 2003. Effect of sodium chloride on a lipid bilayer. *Biophysical Journal*, 85: 1647-1655.
- Brackbill J. U., Kothe D. B., Zemach C. 1992. A continuum method for modeling surface tension. *Journal of Computational Physics*, 100, 2: 335-354.
- Braun V., Rehn K. 1969. Chemical characterization, spatial distribution and function of a lipoprotein (Murein-Lipoprotein) of the *E. coli* cell wall. The specific effect of trypsin on the membrane structure. *European Journal of Biochemistry*, 10: 426-438.
- Braun V., Sieglin U. 1970. The covalent murein-lipoprotin structure of the *Escherichia coli* cell wall. The attachment site of the lipoprotein on the murein. *European Journal of Biochemistry*, 13: 336-346.
- Brennen C.E. 1995. Cavitation and bubble dynamics. Oxford, University Press: 300 str.
- Cameron M., McMaster L. D., Britz T. J. 2008. Electron microscopic analysis of dairy microbes inactivated by ultrasound. *Ultrasonics Sonochemistry*, 15: 960-964.
- Canselier J. P., Delmas H., Wilhelm A. M., Abismail B. 2002. Ultrasound emulsification - An overview. *Journal of Dispersion Science and Technology*, 23: 333-349.
- Cerecedo L. M., Dopazo C., Gomez-Lus R. 2018. Water disinfection by hydrodynamic cavitation in a rotor-stator device. *Ultrasonics Sonochemistry*, 48: 71-78.
- Chahine G. L, Hsiao C. T. 2015. Modelling cavitation erosion using fluid–material interaction simulations. *Interface Focus*, 5: 20150016, doi: 10.1098/rsfs.2015.0016: 12 str.
- Chrysikopoulos C. V., Manariotis I. D., Syrigouna V. I. 2013. Virus inactivation by high frequency ultrasound in combination with visible light. *Colloids and Surfaces B: Biointerfaces*, 107, 1: 174-179.
- Claessens M. M. A. E., Van Oort B. F., Leermakers F. A. M., Hoekstra F. A., Stuart M. A. C. 2004. Charged lipid vesicles: effects of salts on bending rigidity, stability, and size. *Biophysical Journal*, 87: 3882-3893.

- Clifton L. A., Skoda M. W. A., Le Brun A. P., Ciesielski F., Kuzmenko I., Holt S. A., Lakey J. H. 2015. Effect of divalent cation removal on the structure of Gram-negative bacterial outer membrane models. *Langmuir*, 31, 1: 404-412.
- Coderch L., Fonollosa J., De Pera M., Estelrich J., De La Maza A., Parra J. L. 2000. Influence of cholesterol on liposome fluidity by EPR. Relationship with percutaneous absorption. *Journal of Controlled Release*, 68, 1: 85-95.
- Costerton W., Irvin R. T., Cheng K. J. 1981. The bacterial glycocalyx in nature and disease. *Annual Review of Microbiology*, 35, 1: 299-324.
- Cwiklik L., Jungwirth P. 2010. Massive oxidation of phospholipid membranes leads to pore creation and bilayer disintegration. *Chemical Physics Letters*, 486: 99-103.
- Danese P. N., Pratt L. A., Kolter R. 2000. Exopolysaccharide production is required for development of *Escherichia coli* K-12 biofilm architecture. *Journal of Bacteriology*, 182, 12: 3593-3596.
- de Haas K. H., Blom C., van den Ende D., Duits M. H. G., Haveman B., Mellema J. 1997. Rheological behavior of a dispersion of small lipid bilayer vesicles. *Langmuir*, 13, 25: 6658-6668.
- Delcour A. H. 2008. Outer membrane permeability and antibiotic resistance. *Biochimica et Biophysica Acta*, 1794, 5: 808-816.
- Ding W., Palaiokostas M., Shahane G., Wang W., Orsi M. 2017. Effects of high pressure on phospholipid bilayers. *The Journal of Physical Chemistry B*, 121, 41: 9597-9606.
- Doktorova M., LeVine M. V., Khelashvili G., Weinstein H. 2019. A new computational method for membrane compressibility: bilayer mechanical thickness revisited. *Biophysical Journal*, 116: 487-502.
- Drab, M., Stopar D., Kralj-Iglič V., Iglič A. 2019. Inception mechanisms of tunneling nanotubes. *Cells*, 8, 6: 626, doi: 10.3390/cells8060626: 17 str
- Drakopoulou S., Terzakis S., Fountoulakis M. S., Mantzavinos D., Manios T. 2009. Ultrasound-induced inactivation of Gram-negative and Gram-positive bacteria in secondary treated municipal wastewater. *Ultrasonics Sonochemistry*, 16: 629-634.
- Dular M., Požar T., Zevnik J., Petkovšek R. 2019. High speed observation of damage created by a collapse of a single cavitation bubble. *Wear*, 418-419: 13-23.

- Ellison R. T., Giehl T. J. 1991. Killing of Gram-negative bacteria by lactoferrin and lysozyme. *Journal of Clinical Investigation*, 88, 4: 1080-1091.
- Erridge C., Bennett-Guerrero E., Poxton I. R. 2002. Structure and function of lipopolysaccharides. *Microbes and Infection*, 4, 8: 837-851.
- Eskin D. G., Al-Helal K., Tzanakis I. 2015. Application of a plate sonotrode to ultrasonic degassing of aluminum melt: Acoustic measurements and feasibility study. *Journal of Materials Processing Technology*, 222: 148-154.
- Filipić A., Lukežič T., Bačnik K., Ravnikar M., Ješelnik, Košir T., Petkovšek M., Zupanc M., Dular M., Aguirre I. G. 2022. Hydrodynamic cavitation efficiently inactivates potato virus Y in water. *Ultrasonics Sonochemistry*, 82: 105898, doi: 10.1016/j.ultsonch.2021.105898: 9 str.
- Fošnarič, M., Kralj-Iglič V., Bohinc K., Iglič A., May S. 2003. Stabilization of pores in lipid bilayers by anisotropic inclusions. *Journal of Physical Chemistry B*, 107: 12519-12526.
- Franc J. P., Michel J. M. 2004. Fundamentals of cavitation. Dordrecht, Springer Netherlands: 306 str.
- Gac S. L., Zwaan E., van den Berg A., Ohl C. D. 2007. Sonoporation of suspension cells with a single cavitation bubble in a microfluidic confinement. *Lab on a Chip*. 7, 12: 1666-1672.
- Gao S., Lewis G. D., Ashokkumar M., Hemar Y. 2014. Inactivation of microorganisms by low-frequency high-power ultrasound: 1. Effect of growth phase and capsule properties of the bacteria. *Ultrasonics Sonochemistry*, 21, 1: 446-453.
- Gao Y., Ji Y., Li G., An T. 2016. Theoretical investigation on the kinetics and mechanisms of hydroxyl radical-induced transformation of parabens and its consequences for toxicity: influence of alkyl-chain length. *Water Research*, 91: 77-85.
- Gibson K. E. 2014. Viral pathogens in water: occurrence, public health impact, and available control strategies. *Current Opinion in Virology*, 4: 50-57.
- Gilbert P., Pemberton D., Wilkinson D. E. 1990. Synergism within poly-hexamethylene biguanide biocide formulations. *Journal of Applied Bacteriology*, 69: 593-598.

- Glauner B., Höltje J. V., Schwarz U. 1988. The composition of the murein of *Escherichia coli*. Journal of Biological Chemistry, 263: 10088-10095.
- Godlewska R., Wiśniewska K., Pietras Z., Jaguszyn-Krynicka E. K. 2009. Peptidoglycan associated lipoprotein (Pal) of Gram-negative bacteria: function, structure, role in pathogenesis and potential application in immunoprophylaxis. FEMS Microbiology Letters, 298: 1-11.
- Gogate P. R., Pandit A. B. 2005. A review and assessment of hydrodynamic cavitation as a technology for the future. Ultrasonics Sonochemistry, 12, 1-2: 21-27.
- Gogoi A., Mazumder P., Tyagi V. K., Tushara Chaminda G. G., An A. K., Kumar M. 2018. Occurrence and fate of emerging contaminants in water environment: a review. Groundwater for Sustainable Development, 6: 169-180.
- Gregori G., Citterio S., Ghiani A., Labra M., Sgorbati S., Brown S., Denis M. 2001. Resolution of viable and membrane-compromised bacteria in freshwater and marine waters based on analytical flow cytometry and nucleic acid double staining. Applied and Environmental Microbiology, 67: 4662-4670.
- Griffiths B. S., Philippot L. 2013. Insights into the resistance and resilience of the soil microbial community. FEMS Microbiology Reviews, 37, 2: 112-129.
- Gumbart J. C., Beeby M., Jensen G. J., Roux B. 2014. *Escherichia coli* peptidoglycan structure and mechanics as predicted by atomic-scale simulations. PLOS Computational Biology, 10: e1003475, doi: 10.1371/journal.pcbi.1003475: 10 str.
- Heerklotz H., Epand R. M. 2001. The enthalpy of acyl chain packing and the apparent water-accessible apolar surface area of phospholipids. Biophysical Journal, 80: 271-279.
- Hellman A. N., Rau K. R., Yoon H. H., Venugopalan V. 2008. Biophysical response to pulsed laser microbeam-induced cell lysis and molecular delivery. Journal of Biophotonics, 1, 1: 24-35.
- Hiremath P. S., Bannigidad P. 2011. Automated Gram-staining characterisation of bacterial cells using colour and cell wall properties. International Journal of Biomedical Engineering and Technology, 7, 3: 257-265.
- Ho C. W., Chew T. K., Ling T. C., Kamaruddin S., Tan W. S., Tey B. T. 2006. Efficient mechanical cell disruption of *Escherichia coli* by an ultrasonicator and recovery of intracellular hepatitis B core antigen. Process Biochemistry, 41: 1829-1834.

- Horvat M., Pannuri A., Romeo T., Dogsa I., Stopar D. 2019. Viscoelastic response of *Escherichia coli* biofilms to genetically altered expression of extracellular matrix components. *Soft Matter*, 15, 25: 5042-5051.
- Hunter G., Lucas M., Watson I., Parton R. 2008. A radial mode ultrasonic horn for the inactivation of *Escherichia coli* K12. *Ultrasonics Sonochemistry*, 15: 101-109.
- Inque K., Kitagawa T. 1976. Effect of lipid composition on sensitivity of lipid membranes to Triton X-100. *Biochimica et Biophysica Acta Biomembranes*, 426: 1-16.
- Issa R. I. 1986. Solution of the implicitly discretised fluid flow equations by operator-splitting. *Journal of Computational Physics*, 62, 1: 40-65.
- Itoh Y., Wang X., Hinnebusch B. J., Preston III J. F. 2005. Depolymerization of  $\beta$ -1,6-N-acetyl-D-glucosamine disrupts the integrity of diverse bacterial biofilm. *Journal of Bacteriology*, 187: 382-387.
- Itoh Y., Rice J. D., Goller C., Pannuri A., Taylor J., Meisner J., Beveridge T. J., Preston III J. F., Romeo T. 2008. Roles of pgaABCD genes in synthesis, modification, and export of the *Escherichia coli* biofilm adhesin poly- $\beta$ -1,6-N-acetyl-D-glucosamine. *Journal of Bacteriology*, 190: 3670-3680.
- Ivančič T., Jamnik P., Stopar D. 2013. Cold shock CspA and CspB protein production during periodic temperature cycling in *Escherichia coli*. *BMC Research Notes*, 6: 248, doi: 10.1186/1756-0500-6-248: 9 str.
- Ivanov A. I., Fomchenkov V. M.. 1989. Relation between the damaging effect of surface-active compounds on *Escherichia coli* cells and the phase of culture growth. *Mikrobiologija*, 58: 969-975.
- Jasikova D., Rysova M., Kotek M. 2019. Application of laser-induced breakdown cavitation bubbles for cell lysis *in vitro*. *International Journal of Applied Pharmaceutics*, 11, 5: 186-190.
- Jauffred L., Callisen T. H., Oddershede L. B. 2007. Visco-elastic membrane tethers extracted from *Escherichia coli* by optical tweezers. *Biophysical Journal*, 93, 11: 4068-4075.
- Jeucken A., Molenaar M. R., van de Lest C. H. A., Jansen J. W. A., Helms J. B., Brouwers J. F. 2019. A comprehensive functional characterization of *Escherichia coli* lipid genes. *Cell Reports*, 27: 1597-1606.

- Jordens J., Bamps B., Gielen B., Braeken L., Van Gerven T. 2016. The effects of ultrasound on micromixing. *Ultrasonics Sonochemistry*, 32: 68-78.
- Joyce E. M, Wu X., Mason T. J. 2010. Effect of ultrasonic frequency and power on algae suspensions. *Journal of Environmental Science and Health, Part A*, 45: 863-866.
- Kato N., Ishijima A., Inaba T., Nomura F., Takeda S., Takiguchi K. 2015. Effects of lipid composition and solution conditions on the mechanical properties of membrane vesicles. *Membranes*, 5, 1: 22-47.
- Kikuchi K., Sugiura M., Nishizawa-Harada C., Kimura T. 2015. The application of the *Escherichia coli* giant spheroplast for drug screening with automated planar patch clamp system. *Biotechnology Reports*, 7: 17-23.
- Koch A. L., Lane S. L., Miller J. A., Nickens D. G. 1987. Contraction of filaments of *Escherichia coli* after disruption of cell membrane by detergent. *Journal of Bacteriology*, 169: 1979-1984.
- Koch M., Rosselló J. M., Lechner C., Lauterborn W., Eisener J., Mettin R. 2021. Theory-assisted optical ray tracing to extract cavitation-bubble shapes from experiment. *Experiments in Fluids*, 62, 3: 60, doi: 10.1007/s00348-020-03075-6: 19 str.
- Koda S., Kimura T., Kondo T., Mitome H. 2003. A standard method to calibrate sonochemical efficiency of an individual reaction system. *Ultrasonics Sonochemistry*, 10: 149-156.
- Kodama A., Morandi M., Ebihara R., Jimbo T., Toyoda M., Sakuma Y., Imai M., Pu N., Angelova M. I. 2018. Migration of deformable vesicles induced by ionic stimuli. *Langmuir*, 34, 38: 11484-11494.
- Koerner M. M., Palacio L. A., Wright J. W., Schweitzer K. S., Ray B. D., Petracche H. I. 2011. Electrodynamics of lipid membrane interactions in the presence of zwitterionic buffers. *Biophysical Journal*, 101: 362-369.
- Kralj-Iglič V., Iglič A., Hägerstrand H., Peterlin P. 2000. Stable tubular microexovesicles of the erythrocyte membrane induced by dimeric amphiphiles. *Physical Review E, Statistical Physics, Plasmas, Fluids and Related Interdisciplinary Topics*, 61: 4230-4234.

Kralj-Iglič V., Hägerstrand H., Veranic P., Jezernik K., Babnik B., Gauger D. R., Iglič A. 2005. Amphiphile-induced tubular budding of the bilayer membrane. European Biophysics Journal, 34: 1066-1070.

Kumar P., Libchaber A. 2013. Pressure and temperature dependence of growth and morphology of *Escherichia coli*: experiments and stochastic model. Biophysical Jurnal, 105, 3: 783-793.

Lechner C., Lauterborn W., Koch M., Mettin R. 2019. Fast, thin jets from bubbles expanding and collapsing in extreme vicinity to a solid boundary: A numerical study. Physical Review Fluids, 4, 2: 021601, doi: 10.1103/PhysRevFluids.4.021601: 7 str.

Lechner C., Lauterborn W., Koch M., Mettin R. 2020. Jet formation from bubbles near a solid boundary in a compressible liquid: Numerical study of distance dependence. Physical Review Fluids, 5, 9: 093604, doi: 10.1103/physrevfluids.5.093604: 36 str.

Lee S. J., Yoon B. D., Oh H. M. 1998. Rapid method for the determination of lipid from the green alga *Botryococcus braunii*. Biotechnology Techniques, 12: 553-556.

Leonenko Z. V., Finot E., Ma H., Dahms T. E. S., Cramb D. T. 2004. Investigation of temperature-induced phase transitions in DOPC and DPPC phospholipid bilayers using temperature-controlled scanning force microscopy. Biophysical Journal, 86, 6: 3783-3793.

Leontiadou H., Mark A. E., Marrink S. J. 2004. Molecular dynamics simulations of hydrophilic pores in lipid bilayers. Biophysical Journal, 86, 4: 2156-2164.

Li Z. G., Liu A. Q., Klaseboer E., Zhangc J. B., Ohl C. D. 2013. Single cell membrane poration by bubble-induced microjets in a microfluidic chip. Lab on a Chip, 6: 1144-1150.

Lin H. Y., Thomas J. L. 2004. Factors affecting responsivity of unilamellar liposomes to 20 kHz ultrasound. Langmuir, 20: 6100-6106.

Locascio L., Vreeland W., Jahn A., Gaitan M. 2004. Liposomes as model cellular systems, V: Lab-on-Chips for cellomics. Andersson H., van den Berg A. (ur.). Dordrecht, Springer: 59-81.

Lu L., Doak W. J., Schertzer J. W., Chiarot P. R. 2016. Membrane mechanical properties of synthetic asymmetric phospholipid vesicles. Soft Matter, 12: 7521-7528.

- Lucht J. M., Bremer E. 1994. Adaptation of *Escherichia coli* to high osmolarity environments: osmoregulation of the high-affinity glycine betaine transport system proU. FEMS Microbiology Reviews, 14, 1: 3-20.
- Madigan M.T., Martinko J.M., Dunlap P.V., Clark D.P. 2008. Brock biology of microorganisms. 10<sup>th</sup> ed. New Jersey, Pearson Education Inc: 1019 str.
- Maher K., Stevenson D. 1988. Impact frustration of the origin of life. Nature, 331: 612-614.
- Marmottant P., Hilgenfeldt S. 2003. Controlled vesicle deformation and lysis by single oscillating bubbles. Nature, 423: 153-156.
- Marmottant P., Biben T., Hilgenfeldt S. 2008. Deformation and rupture of lipid vesicles in the strong shear flow generated by ultrasound-driven microbubbles. Proceedings of the Royal Society A, Mathematical, Physical and Engineering Sciences, 464: 1781-1800.
- Marsh D. 2006. Elastic curvature constants of lipid monolayers and bilayers. Chemistry and Physics of Lipids, 144: 146-159.
- Mason T. J., Cobley A. J., Graves J. E., Morgan D. 2011. New evidence for the inverse dependence of mechanical and chemical effects on the frequency of ultrasound. Ultrasonics Sonochemistry, 18, 1: 226-230.
- Miki T., Hardt W. D. 2013. Outer membrane permeabilization is an essential step in the killing of Gram-negative bacteria by the lectin RegIII $\beta$ . PLOS One. 8, 7: e69901, doi: 10.1371/journal.pone.0069901: 11 str.
- Miller D. L., Pislaru S. V, Greenleaf J. F. 2002. Sonoporation: Mechanical DNA delivery by ultrasonic cavitation. Somatic Cell and Molecular Genetics, 27: 115-134.
- Mitsuzawa S., Deguchi S., Horikoshi K. 2006. Cell structure degradation in *Escherichia coli* and *Thermococcus sp.* Strain Tc-1-95 associated with thermal death resulting from brief heat treatment. FEMS Microbiology Letters, 260, 1: 100-105.
- Mo S., Coussios C. C., Seymour L., Carlisle R. 2012. Ultrasound-enhanced drug delivery for cancer. Expert Opinion on Drug Delivery, 9, 12: 1525-1538.
- Nagle J. F., Wilkinson D. A. 1978. Lecithin bilayers. Density measurement and molecular interactions. Biophysical Journal, 23: 159-175.

- Nasseri S., Mahvi A. H., Seyedsalehi M., Yaghmaeian K., Nabizadeh R., Alimohammadi M., Safari G. H. 2017. Degradation kinetics of tetracycline in aqueous solutions using peroxydisulfate activated by ultrasound irradiation: Effect of radical scavenger and water matrix. *Journal of Molecular Liquids*, 241: 704-714.
- Needham D., Evans E. 1988. Structure and mechanical properties of giant lipid (DMPC) vesicle bilayers from 20 °C below to 10 °C above the liquid crystal-crystalline phase transition at 24 °C. *Biochemistry*, 27: 8261-8269.
- Nickels J. D., Smith J. C., Cheng X. 2015. Lateral organization , bilayer asymmetry, and inter-leaflet coupling of biological membranes. *Chemistry and Physics of Lipids*, 192: 87-99.
- Nomura F., Inaba T., Ishikawa S., Nagata M., Takahashi S., Hotani H., Takiguchi K. 2004. Microscopic observations reveal that fusogenic peptides induce liposome shrinkage prior to membrane fusion. *Proceedings of the National Academy of Sciences*, 101: 3420-3425.
- Nomura F., Nagata M., Inaba T., Hiramatsu H., Hotani H., Takiguchi K. 2001. Capabilities of liposomes for topological transformation. *Proceedings of the National Academy of Sciences*, 98: 2340-2345.
- Ohl C.-D., Arora M., Ikink R., de Jong N., Versluis M., Delius M., Lohse D. 2006. Sonoporation from Jetting Cavitation Bubbles. *Biophysical Journal*, 91, 11: 4285-4295.
- Ohrdes H., Ille I., Twiefel J., Wallaschek J., Nogueira R., Rosenwinkel K. H. 2018. A control system for ultrasound devices utilized for inactivating *E. coli* in wastewater. *Ultrasonics Sonochemistry*, 40: 158-162.
- Olsén, A., Jonsson A., Normark S. 1989. Fibronectin binding mediated by a novel class of surface organelles on *Escherichia coli*. *Nature*, 338: 652-655.
- Onitsuka M. O., Rikihisa Y., Maruyama H. B. 1979. Biochemical and topographical studies on *Escherichia coli* cell surface. IV. Giant spheroplast formation from a filamentous cell. *Journal of Bacteriology*, 138, 2: 567-574.
- O'Connor J., Akbar F. B., Hutson M. S., Page-McCaw A. 2021. Zones of cellular damage around pulsed-laser wounds. *PloS ONE*, 16, 9: e0253032, doi: 10.1371/journal.pone.0253032: 20 str.

Paliwal S., Mitragotri S. 2006. Ultrasound-induced cavitation: applications in drug and gene delivery. *Expert Opinion on Drug Delivery*, 3, 6: 713-726.

Pandit K. R., Klauda J. B. 2012. Membrane models of *E. coli* containing cyclic moieties in the aliphatic lipid chain. *Biochimica et Biophysica Acta (BBA) - Biomembranes*, 1818, 5: 1205-1210.

Pembrey R. S., Marshall K. C., Schneider R. P. 1999. Cell surface analysis techniques: What do cell preparation protocols do to cell surface properties? *Applied and Environmental Microbiology*, 65, 7: 2877-2894.

Patankar S. V. 1980. Numerical heat transfer and fluid flow. Boca Raton, CRC Press: 214 str.

Patinglag L., Melling L. M., Whitehead K. A., Sawtell D., Iles A., and Shaw K.J. 2021. Non-thermal plasma-based inactivation of bacteria in water using a microfluidic reactor. *Water Research*, 201: 117321, doi: 10.1016/j.watres.2021.117321: 9 str.

Peshkovsky A. S., Peshkovsky S. L., Bystryak S. 2013. Scalable high-power ultrasonic technology for the production of translucent nanoemulsions. *Chemical Engineering and Processing: Process Intensification*, 69: 77-82.

Pisabarro A. G., de Pedro M. A., Vázquez D. 1985. Structural modifications in the peptidoglycan of *Escherichia coli* associated with changes in the state of growth of the culture. *Journal of Bacteriology*, 161: 238-242.

Podbevšek D., Ledoux G., Dular M. 2022. Investigation of hydrodynamic cavitation induced reactive oxygen species production in microchannels via chemiluminescent luminol oxidation reactions. *Water Research*, 220: 118628, doi: 10.1016/j.watres.2022.118628: 11 str.

Podbevšek D., Petkovšek M., Ohl C. D., Dular M. 2021. Kelvin-Helmholtz instability governs the cavitation cloud shedding in Venturi microchannel. *International Journal of Multiphase Flow*, 142: 103700, doi: 10.1016/j.ijmultiphaseflow.2021.103700: 7 str.

Pong M., Umchid S., Guarino A. J., Lewin P. A., Litniewski J., Nowicki A., Wrenn S. P. 2006. *In vitro* ultrasound-mediated leakage from phospholipid vesicles. *Ultrasonics*, 45: 133-145.

Potthoff E., Ossola D., Zambelli T., Vorholt J.A. 2015. Bacterial adhesion force quantification by fluidic force microscopy. *Nanoscale*, 7, 9: 4070-4079.

- Prosperetti A. 2004. Bubbles. *Physics of Fluids*, 16, 6: 1852-1865.
- Pucadyil T. J., Mukherjee S., Chattopadhyay A. 2007. Organization and dynamics of NBD-labeled lipids in membranes analyzed by fluorescence recovery after photobleaching. *Journal of Physical Chemistry B*, 111, 8: 1975–1983.
- Quinto-Su P.A. 2014. A microscopic steam engine implemented in an optical tweezer. *Nature Communications*, 5: 5889, doi: 10.1038/ncomms6889: 7 str.
- Rajasekhar P., Fan L., Nguyen T., Roddick F. A. 2012. A review of the use of sonication to control cyanobacterial blooms. *Water Research*, 46: 4319-4329.
- Ramanan R. N., Ling T. C., Ariff A. B. 2008. The performance of a glass bead shaking technique for the disruption of *Escherichia coli* cells. *Biotechnology and Bioprocess Engineering*, 13: 613-623.
- Rau K. R., Quinto-Su P. A., Hellman A. N., Venugopalan V. 2006. Pulsed laser microbeam-induced cell lysis: time-resolved imaging and analysis of hydrodynamic effects. *Biophysical Journal*, 91, 1: 317-329.
- Reuter F., Ohl C. D. 2021 Nonspherical collapse of single bubbles near boundaries and in confined spaces. V: Cavitation and bubble dynamics. Koukouvinis P., Gavaises M. (ur.). Cambridge, Academic Press: 37-72.
- Reuter F., Ohl C. D. 2021a. Supersonic needle-jet generation with single cavitation bubbles. *Applied Physics Letters*, 118, 13: 134103, doi: 10.1063/5.0045705: 5 str.
- Roberts I. S. 1996. The biochemistry and genetics of capsular polysaccharide production in bacteria. *Annual Review of Microbiology*, 50, 1: 285-315.
- Rogers H. T., Perkins H. R., Ward J. B. 1980. *Microbial cell walls and membranes*. London, Chapman & Hall Ltd: 239-291.
- Rojas E. R., Billings G., Odermatt P. D., Auer G. K., Zhu L., Miguel A., Chang F., Weibel D. B., Theriot J. A., Huang K. C. 2018. The outer membrane is an essential load-bearing element in Gram-negative bacteria. *Nature*, 559, 7715: 617-621.
- Salmen S. H., Alharbi S. A., Faden A. A., Wainwright, M. 2018. Evaluation of effect of high frequency electromagnetic field on growth and antibiotic sensitivity of bacteria. *Saudi Journal of Biological Sciences*, 25, 1: 105-110.

- Saranya N., Devi P., Nithiyanantham S., Jeyalaxmi R. 2014. Cells disruption by ultrasonication. *Bionanoscience*, 4, 4: 335-337.
- Saunders L., Perrin J., Gammack D. 1962. Ultrasonic irradiation of some phospholipid sols. *Journal of Pharmacy and Pharmacology*, 14: 567-572.
- Schlüter-Vorberg L., Prasse C., Ternes T. A., Mückter H., Coors A. 2015. Toxicification by transformation in conventional and advanced wastewater treatment: the antiviral drug acyclovir. *Environmental Science & Technology Letters*, 2: 342-346.
- Schroeder A., Avnir Y., Weisman S., Najajreh Y., Gabizon A., Talmon Y., Kost J., Barenholz Y. 2007. Controlling liposomal drug release with low frequency ultrasound: Mechanism and feasibility. *Langmuir*, 23: 4019-4025.
- Schroeder A., Kost J., Barenholz Y. 2009. Ultrasound, liposomes, and drug delivery: principles for using ultrasound to control the release of drugs from liposomes. *Chemistry and Physics of Lipids*, 162: 1-16.
- Shashi K., Satinder K., Bharat P. 2012. A complete review on: Liposomes. *International Research Journal of Pharmacy*, 3, 7: 10-16.
- Shiu C., Zhang Z., Thomas C. R. 1999. A novel technique for the study of bacterial cell mechanical properties. *Biotechnology Techniques*, 13, 10: 707-713.
- Silhavy T. J., Kahne D., Walker S. 2010. The bacterial cell envelope. *Cold Spring Harbor Perspectives in Biology*, 2, 5: a000414, doi:10.1101/csfperspect.a000414: 16 str.
- Silica Microspheres. 2019. Product Data Sheet 702. Fishers, Bangs Laboratories Inc.: 2 str.
- Simons K., Sampaio J. L. 2011. Membrane organization and lipid rafts. *Cold Spring Harbor Perspectives in Biology*, 3: a004697. doi: 10.1101/csfperspect.a004697.
- Singer S. J., Nicolson G. L. 1972. The fluid mosaic model of the structure of cell membranes. *Science*, 175, 4023: 720-731.
- Sinibaldi G., Occhipinti A., Alves Pereira F., Caprini D., Marino L., Michelotti F., Casciola C. M. 2019. Laser induced cavitation: Plasma generation and breakdown shockwave. *Physics of Fluids*, 31, 10: 103302. doi: 10.1063/1.5119794: 12 str.

- Sleytr U.B., Messner P. 2009. Crystalline bacterial cell surface layers (S-layers) V: Encyclopedia of microbiology. Vol. 1. Schaechter M. (ur.). San Diego, Academic Press/Elsevier Science: 89-98.
- Small E. F., Dan N. R., Wrenn S. P. 2012. Low-frequency ultrasound-induced transport across non-raft-forming ternary lipid bilayers. *Langmuir*, 28: 14364-14372.
- Smith D., Price J., Burby P., Blanco L., Chamberlain J., Chapman M. 2017. The production of curli amyloid fibers is deeply integrated into the biology of *Escherichia coli*. *Biomolecules*, 7, 4: 75, doi: 10.3390/biom7040075: 26 str
- Souzu, H. 1986. Fluorescence polarization studies on *Escherichia coli* membrane stability and its relation to the resistance of the cell to freeze-thawing. I. Membrane stability in cells of differing growth phase. *Biochimica et Biophysica Acta*, 861: 353-360.
- Spiteri D., Chot-Plassot C., Sclear J., Karatzas K. A., Scerri C., Valdramidis V. P. 2017. Ultrasound processing of liquid system(s) and its antimicrobial mechanism of action. *Letters in Applied Microbiology*. 65, 4: 313-318.
- Sudbrack, T. P., Archilha N. L., Itri R., Riske K. A. 2011. Observing the solubilization of lipid bilayers by detergents with optical microscopy of GUVs. *Journal of Physical Chemistry B*, 115: 269-277.
- Sułkowski W. W., Pentak D., Nowak K., Sułkowska A., Goertz M. P., Goyal N., Montano G. A., Bunker B. C. 2005. The influence of temperature, cholesterol content and pH on liposome stability. *Journal of Molecular Structure*, 744-747: 737-747.
- Sun X., Park J. J., Kim H. S., Jin S., Lee S., Om A. S., Yoon j. Y. 2018. Experimental investigation of the thermal and disinfection performances of a novel hydrodynamic cavitation reactor. *Ultrasonics Sonochemistry*, 49: 13-23.
- Sun Y., Sun T. L., Huang H. 2014. Physical properties of *escherichia coli* spheroplast membranes. *Biophysical Journal*, 107, 9: 2082-2090.
- Suslick K. S., McNamara W. B., Didenko Y. 1999. Hot spot conditions during multi-bubble cavitation. V: *Sonochemistry and sonoluminescence*. Crum L. A., Mason T. J., Reisse J. L., Suslick K. S. (ur.). Dordrecht, Springer: 191-204.
- Suslick K. S., Eddingsaas N. C., Flannigan D. J., Hopkins S. D., Xu H. 2011. Extreme conditions during multibubble cavitation: Sonoluminescence as a spectroscopic probe, *Ultrasonics Sonochemistry*. 18: 842-846.

Šarc A., Oder M., Dular M. 2014. Can rapid pressure decrease induced by supercavitation efficiently eradicate *Legionella pneumophila* bacteria?. Desalination and Water Treatment, 57, 5: 2184-2194.

Šarc A., Kosel J., Stopar D., Oder M., Dular. 2018. Removal of bacteria *Legionella pneumophila*, *Escherichia coli*, and *Bacillus subtilis* by (super)cavitation. Ultrasonics Sonochemistry, 42: 228-236

Širok B., Dular M., Stoffel B. 2006. Kavitacija. 1. natis. Ljubljana, i2: 167 str.

Tandiono T., Ow D. S., Driesssen L., Chin C. S., Klaseboer E., Choo A. B., Ohl S. W., Ohl C. D. 2012. Sonolysis of *Escherichia coli* and *Pichia pastoris* in microfluidics. Lab on a Chip. 12, 4: 780-786.

Teran L. A., Rodríguez S. A., Laín S., Jung S. 2018. Interaction of particles with a cavitation bubble near a solid wall. Physics of Fluids, 30, 12: 123304, doi: 10.1063/1.5063472: 12 str.

Thongsomboon W., Serra D. O., Possling A., Hadjineophytou C., Hengge R., Cegelski L. 2018. Phosphoethanolamine cellulose: A naturally produced chemically modified cellulose. Science, 80, 359: 334-338.

Tien H. T., Ottova A. 2003. The lipid bilayer concept: Experimental realization and current applications. V: Membrane science and technology, planar lipid bilayers (BLMs) and their applications. Tien H.T., Ottova-Leitmannova A. (ur.). Amsterdam, Elsevier: 1-73.

Tinevez J. Y., Perry N., Schindelin J., Hoopes G. M., Reynolds G. D., Laplantine E., Bednarek S. Y., Shorte S. L., Eliceiri K. W. 2017. TrackMate: An open and extensible platform for single-particle tracking. Methods, 115: 80-90.

Tuson H. H., Auer G. K., Renner L. D., Hasebe M., Tropini C., Salick M., Crone W. C., Gopinathan A., Huang K. C., Weibel D. B. 2012. Measuring the stiffness of bacterial cells from growth rates in hydrogels of tunable elasticity. Molecular Microbiology, 84, 5: 874-891.

Uehara T., Bernhardt T. G. 2011. More than just lysins: peptidoglycan hydrolases tailor the cell wall. Current Opinion in Microbiology, 14: 698-703.

Ulrich A., Sami M., Watts A. 1994. Hydration of DOPC bilayers by differential scanning calorimetry. Biochimica et Biophysica Acta Biomembranes, 1191: 225–230.

- Vadillo-Rodríguez V., Dutcher J. R. 2011. Viscoelasticity of the bacterial cell envelope. *Soft Matter*, 7: 4101-4110.
- Valap sealant. 2015. Cold Spring Harbor Protocols, doi: 10.1101/pdb.rec082917.
- van den Bogaart G., Hermans N., Krasnikov V., Poolman B. 2007. Protein mobility and diffusive barriers in *Escherichia coli*: consequences of osmotic stress. *Molecular Microbiology*, 64: 858-871.
- Vezenov D., Barrett M. J. 2013. Young's modulus of *B. subtilis* cell wall: measuring and modeling the elasticity of rod-like bacteria. *Biophysical Journal*, 104, 2: 640-641.
- Vollmer W. 2007. Structure and biosynthesis of the murein (peptidoglycan) sacculus. V: The periplasm. Ehrmann M. (ur.). Washington, ASM Press: 198-213.
- Vollmer W., Blanot D., De Pedro M. A. 2008. Peptidoglycan structure and architecture, FEMS Microbiology Reviews, 32, 2: 149-167.
- Voss J. G. 1964. Lysozyme lysis of Gram-negative bacteria without production of spheroplasts. *Journal of General Microbiology*, 35, 2: 313-317.
- Wang X., Preston III J. F., Romeo T. 2004. The pgaABCD locus of *Escherichia coli* promotes the synthesis of a polysaccharide adhesin required for biofilm formation. *Journal of Bacteriology*, 186: 2724-2734.
- Wietzikoski Lovato E. C., Gurgel Velasquez P. A., dos Santos Oliveira C., Baruffi C., Anghinoni T., Machado R. C., dos Reis Lívero F. A., Sato S. W., de Almeida Martins L. 2018. High frequency equipment promotes antibacterial effects dependent on intensity and exposure time. *Clinical, Cosmetic and Investigational Dermatology*, 11: 131-135.
- Wilks J. C., Slonczewski J. L. 2007. pH of the cytoplasm and periplasm of *Escherichia coli*: rapid measurement by green fluorescent protein fluorimetry. *Journal of Bacteriology*, 189, 15: 5601-5607.
- Yao X., Jericho M., Pink D., Beveridge T. 1999. Thickness and elasticity of Gram-negative murein sacci measured by atomic force microscopy. *Journal of Bacteriology*, 181: 6865-6875.
- Young F. R. 1989. Cavitation. New York, McGraw-Hill book company: 418 str.

- Yow H. N., Pitt M. J., Salman A. D. 2005. Drag correlations for particles of regular shape. *Advanced Powder Technology*, 16, 4: 363-372.
- Yusof N. S. M., Babgi B., Alghamdi Y., Aksu M., Madhavan J., Ashokkumar M. 2016. Physical and chemical effects of acoustic cavitation in selected ultrasonic cleaning applications. *Ultrasonics Sonochemistry*, 29: 568-576.
- Zeng Q., Gonzalez-Avila S.R., Dijkink R., Koukouvinis P., Gavaises M., Ohl C.-D. 2018. Wall shear stress from jetting cavitation bubbles. *Journal of Fluid Mechanics*, 846: 341-355.
- Zevnik J., Dular M. 2020. Cavitation bubble interaction with a rigid spherical particle on a microscale. *Ultrasonics Sonochemistry*, 69: 105252, doi: 10.1016/j.ultsonch.2020.105252: 13 str.
- Zevnik J., Dular M. 2021. Liposome destruction by a collapsing cavitation microbubble: A numerical study. *Ultrasonics Sonochemistry*, 78: 105706, doi: 10.1016/j.ultsonch.2021.105706: 15 str.
- Zevnik J., Dular M. 2022. Cavitation bubble interaction with compliant structures on a microscale: A contribution to the understanding of bacterial cell lysis by cavitation treatment. *Ultrasonics Sonochemistry*, 87: 106053, doi: 10.1016/j.ultsonch.2022.106053: 20 str.
- Zhou Y., Yang K., Cui J., Ye J. Y., Deng C. X. 2012. Controlled permeation of cell membrane by single bubble acoustic cavitation. *Journal of Controlled Release*. 157,1: 103-111.
- Zou H., Wang L. 2017. The disinfection effect of a novel continuous-flow water sterilizing system coupling dual-frequency ultrasound with sodium hypochlorite in pilot scale. *Ultrasonics Sonochemistry*, 36: 246-252.
- Zupanc M., Pandur Ž., Stepišnik Perdih T., Stopar D., Petkovšek M., Dular M. 2019. Effects of cavitation on different microorganisms: the current understanding of the mechanisms taking place behind the phenomenon. A review and proposals for further research. *Ultrasonics Sonochemistry*, 57: 147-165.

## ZAHVALA

Najprej bi se rad zahvalil mentorju prof. dr. Stopar David in somentorju prof. dr. Dular Matevž za strokovno pomoč in podporo pri doktorskem študiju. Še posebej bi se zahvalil prof. dr. Dular Matevž, da mi je dal možnost biti del njegove raziskovalne skupine in delati raziskave v okviru ERC projekta »CABUM«.

Zahvalil bi se tudi dr. Zevnik Jure za znanstven doprinos k eksperimentalnemu delu z opravljenimi numeričnimi analizami, g. Godeša Tone za vso tehnično pomoč in izdelavo testnih naprav pri eksperimentih. Zahvalil bi se tudi ostalim sodelavcem za vso pomoč in svetovanje pri delu.

Prav tako bi se zahvalil celotnemu Oddelku za mikrobiologijo na Biotehniški fakulteti, kjer sem lahko izvajal vse mikrobiološke poskuse ter vsem zaposlenim na katedri, ki so mi z nasveti pomagali izboljšati in olajšati izvedbo eksperimentov. Še posebej bi se zahvalil tehnični sodelavki Leskovec Simoni, saj so mi njeni nasveti in pomoč znatno olajšali izvedbo eksperimentov.

Na koncu se iskreno zahvaljujem staršema in bratu, ki so mi vedno stali ob strani tekom študija.

## PRILOGE

**Priloga A:** Objavljen pregledni članek vpliva hidrodinamske kavitacije na mikroorganizme

Vpliv kavitacije na mikroorganizme: trenutno razumevanje mehanizmov kavitacije. Pregled in predlogi za nadaljnje raziskave

Zupanc M., Pandur Ž., Stepišnik Perdih T., Stopar D., Petkovšek M., Dular M. 2019. Effects of cavitation on different microorganisms: the current understanding of the mechanisms taking place behind the phenomenon. A review and proposals for further research. Ultrasonics Sonochemistry, 57: 147-165.

Izvleček:

Nenaden padec tlaka povzroči nastanek parnih in plinskih mehurčkov v kapljevini (imenovano tudi kavitacija). To vodi do številnih (ključnih) inženirskih težav: izgube materiala, hrupa in tresljajev hidravličnih strojev. Po drugi strani pa je kavitacija potencialno uporaben pojav: ekstremni pogoji se vedno pogosteje uporablajo za najrazličnejše aplikacije, kot so površinsko čiščenje, izboljšana kemija in čiščenje odpadne vode (izkoreninjenje bakterij in inaktivacija virusov).

Kljub pomembnemu napredku tehnologije kavitacije pa ostaja velika vrzel med razumevanjem mehanizmov, ki prispevajo k učinkom kavitacije, in njeno uporabo. Čeprav inženirji že komercializirajo naprave, ki uporabljajo kavitacijo, še vedno ne moremo odgovoriti na temeljno vprašanje: Kakšni so natančno mehanizmi, s katerimi lahko mehurčki čistijo, razkužujejo, ubijajo bakterije in povečujejo kemično aktivnost? V članku smo opravili temeljiti pregled nedavnega dela (od leta 2005 naprej) na področju uničevanja mikroorganizmov s pomočjo kavitacije in naj bi služil kot temelj za razvoj tehnologije v prihajajočih letih.



To delo je ponujeno pod Priznanje avtorstva-Nekomercialno-Brez predelav 4.0 Mednarodno licenco



## Effects of cavitation on different microorganisms: The current understanding of the mechanisms taking place behind the phenomenon. A review and proposals for further research



Mojca Zupanc<sup>a</sup>, Žiga Pandur<sup>a,b</sup>, Tadej Stepišnik Perdih<sup>a</sup>, David Stopar<sup>b</sup>, Martin Petkovšek<sup>a</sup>, Matevž Dular<sup>a,\*</sup>

<sup>a</sup> University of Ljubljana, Faculty of Mechanical Engineering, Askerceva 6, 1000 Ljubljana, Slovenia

<sup>b</sup> University of Ljubljana, Biotechnical Faculty, Jamnikarjeva 101, 1000 Ljubljana, Slovenia

### ARTICLE INFO

Keywords:  
Cavitation  
Microorganisms  
Destruction  
Mechanisms  
Review

### ABSTRACT

A sudden decrease in pressure triggers the formation of vapour and gas bubbles inside a liquid medium (also called cavitation). This leads to many (key) engineering problems: material loss, noise, and vibration of hydraulic machinery. On the other hand, cavitation is a potentially useful phenomenon: the extreme conditions are increasingly used for a wide variety of applications such as surface cleaning, enhanced chemistry, and wastewater treatment (bacteria eradication and virus inactivation).

Despite this significant progress, a large gap persists between the understanding of the mechanisms that contribute to the effects of cavitation and its application. Although engineers are already commercializing devices that employ cavitation, we are still not able to answer the fundamental question: What precisely are the mechanisms how bubbles can clean, disinfect, kill bacteria and enhance chemical activity?

The present paper is a thorough review of the recent (from 2005 onward) work done in the fields of cavitation-assisted microorganism's destruction and aims to serve as a foundation to build on in the next years.

### 1. Introduction

The research on the potential of cavitation exploitation is currently an extremely interesting topic. Availability of water is becoming an increasing concern in the globalized world, in both developed and developing countries. Therefore, an efficient and clean disinfection technology, such as optimised employment of cavitation, would be readily welcome to substitute or be combined with the existing ones.

#### 1.1. Problem identification

Due to escalating pollution, the world's clean water supplies are becoming seriously endangered and for a lot of countries, clean water is a luxury that cannot be taken for granted anymore. Therefore, implementing wastewater (WW) recycling and assuring impeccable drinking water sources are becoming more and more important. On one

hand, WW effluents contain pathogenic microorganisms like bacteria (i.e. from genera *Vibrio*, *Enterobacter*, *Escherichia*, *Klebsiella*, *Pseudomonas*) [1] and enteric viruses (i.e. noroviruses and caliciviruses) [2], which can both cause serious infections in organisms that encounter the contaminated water. On the other hand, the main problem for drinking water supply systems is contamination by algae and cyanobacteria. They can cause algal blooms that are not problematic only because they affect the whole water ecosystem but also because of the toxins they release. These toxins are dangerous for many receiving organisms, humans included [3]. To ensure the safe reuse of WW and the use of drinking water, disinfection is an imperative step in the water treatment scheme.

Increasing world's population also leads to augmented food consumption. Due to this more and more attention is given to the production of high-quality food. This means that food preservation, in terms of nutritional, sensory, ensured bioactivity and microbiological

**Abbreviations:** AC, acoustic cavitation; BT, blow through cavitation device; CFU, colony forming units; EOM, extracellular organic matter; HC, hydrodynamic cavitation; HFUS, high frequency ultrasound; LFUS, low frequency ultrasound; LPS, lipopolysaccharides; PC, pump + constriction cavitation device; PFU, plaque forming units; ROS, reactive oxygen species; RS, rotor-stator cavitation device; SEM, scanning electron microscopy; TEM, transmission electron microscopy; CFU, colony forming units; US, ultrasound; VBNC, viable but not culturable; WW, wastewater

\* Corresponding author.

E-mail address: [matevz.dular@fs.uni-lj.si](mailto:matevz.dular@fs.uni-lj.si) (M. Dular).

<https://doi.org/10.1016/j.ultsonch.2019.05.009>

Received 13 February 2019; Received in revised form 26 April 2019; Accepted 8 May 2019

Available online 08 May 2019

1350-4177/ © 2019 The Authors. Published by Elsevier B.V. This is an open access article under the CC BY license (<http://creativecommons.org/licenses/by/4.0/>).

aspect, is of utmost importance [4]. The most important culprits of food spoilage are bacteria, viruses, yeasts and moulds [5].

Another consequence of global population's growth is a more rapid depletion of fossil fuels and fast development of fields like biotechnology, pharmacology and food industry. In order to match the increasing energy demand and to allow these industries to develop further, more effort should be directed into research of novel renewable energy sources and into the search of new and natural sources of compounds. Various types of microorganisms seem to fit both requirements. Algae species from genera like *Nannochloropsis*, *Chlorococcum*, *Scenedesmus*, and *Tetraselmis* are being extensively studied for extraction of lipids to produce biofuels [6]. Similarly, extraction of bioactive compounds like pigments, proteins, antioxidants, lipids, and polysaccharides from yeast (i.e. *Saccharomyces* sp. and *Kluveromyces* sp.) and algae species from genera (i.e. *Dunaliella*, *Chlamydomonas* and *Chlorella*) is also gaining more and more attention [7,8].

Despite completely different final goals, disinfection of water, food preservation and the use of microorganisms for extraction, have one thing in common: Destruction of microorganisms!

### 1.2. Existing methods for microorganism's destruction

Different mechanical and non-mechanical methods for destruction of various types of microorganism have been extensively researched and reported in the literature [8–13]. Commonly used methods for water disinfection include processes, such as chlorination, ozonation, and UV irradiation. These methods are effective to some degree, but they unfortunately also have disadvantages. UV irradiation causes reversible damage to bacteria's DNA [14] and is not very effective when microorganisms are packed into flocs [15]. Chemical disinfection methods like chlorination can result in the formation of by-products [16] and lead to secondary pollution [17,18]. Special attention is also needed when dealing with algae blooms, since using these methods can lead to a release of a toxic compound microcystin [19]. Similarly, thermal pasteurization is still extensively used for food preservation, yet it is not appropriate for all types of food and can result in unwanted effects that impact food's nutritional content and quality [20].

Due to the above-mentioned unwanted side-effects of classical disinfection and destruction methods, the search for alternative, effective, environment-friendly and economical methods with less unwanted effects is increasing. One such promising method is cavitation.

### 1.3. The need for a thorough review

The fields where the introduction of cavitation is considered as a solution are many – pharmacy, chemistry, cleaning, biogas production, waste and drinking water treatment.

In the last decade alone there have been numerous review articles published that deal with cavitation and its ability to destroy microorganisms for purposes of water disinfection [12,18,21–25], food preservation [4,26–28], extraction of bioactive materials [8,10] and its improved efficiency in combination with other methods [29,30].

Most of these review articles focused on acoustic cavitation (AC), which was the first of the cavitation types to be exploited. Also, the focus is usually on either a single microorganism, or a very rudimentary comparison of various cavitation types. Such a limited approach leads to very specific conclusions, which cannot be applied to other cases and are not generally applicable. Unfortunately, they are frequently taken as such, what leads to many dead allies in the progression of this scientific and engineering field.

To maintain the focus, we limited this review to discussion of the mechanical and chemical effects of cavitation on four types of microorganisms (i.e. bacteria, yeast, algae) and viruses in planktonic form. Even though viruses are not living organisms we will name them as microorganisms in this review paper for simplicity. We considered both

AC and hydrodynamic cavitation (HC), as many claim that the latter is more efficient. Additionally, we limited the review to the publications from the last decade.

The main goal of this paper is to review and summarize, which mechanisms are possibly responsible for microorganisms' destruction by cavitation. We considered papers that are explaining the mechanisms behind the effects of cavitation exclusively in distilled/deionized water, tap water, surface water, seawater, artificial sea water, salt solutions, growth medium and different buffer solutions. How AC may promote microorganism's growth (as discussed by Huang et al. [31]) is not in the scope of this review.

One problem, which we noticed during the past years, and which persists in many studies on cavitation exploitation is that the understanding of cavitation is taken very lightly. Hence, in Section 2 we put effort into explaining the main differences of two cavitation types. Another issue is, that conclusions of a certain study are many times disseminated over different types of contaminants – for example, it is argued that a certain type of cavitation reactor, which is efficient for pharmaceutical's removal, will also efficiently destroy bacteria. Unfortunately, this is not necessarily always the case. Section 3 describes characteristics of different microorganisms with the focus on their outer layer where the first effects of cavitation should occur. The core of this manuscript however revolves around the discussion of possible mechanisms by which cavitation acts upon microorganisms, mechanical or chemical. This is thoroughly discussed in Section 4. Finally, in Section 5, we underline problems that hinder accurate comparison of the results reported in the literature. In the end we propose guidelines which should be followed to ensure reproducibility and clearness of the studies and to avoid oversimplification of the problem and uncritical dissemination of the conclusions over various application areas. And this should be done from the perspective of different fields including microbiology, chemistry, physics and engineering. Consequently, such guidelines will hopefully enable faster progression of knowledge and technology, without too many dead ends.

## 2. Cavitation

Cavitation describes a formation of small vapour bubbles (cavities) inside an initially homogeneous liquid medium. It is a rapid physical phenomenon triggered by the sudden decrease in pressure [32]. As the pressure recovers the bubble goes through the violent collapse and possible rebounds. By bubble growth an energy from the surrounding liquid is collected and released by bubble collapses, where extreme conditions can be formed locally. Bubble collapse can cause pressure shocks up to several 100 MPa [33] and if the bubble collapses asymmetrically the so-called microjets with high velocities above 100 m/s can form [34]. In addition the so called hot spots with extreme temperatures in order of several 1000 K [35] can form at the centre of the bubble at its collapse, which can cause the formation of highly reactive radicals [36]. Exact manifestation of cavitation is influenced by liquid properties (temperature, density, viscosity and surface tension) and quality (number of solid particles and amount of dissolved gasses, which can both act as a nuclei).

In general, two types of cavitation are recognized, hydrodynamic and acoustic cavitation. The difference is in the mechanism, which causes the local pressure to drop, while the principles which govern the hydrodynamic bubble and the acoustic bubble are basically the same. Even though there are numerous different expressions for AC frequently used in the literature like ultrasonic cavitation, ultrasonic irradiation, sonication or even, simply, ultrasound (US) they describe the same thing.

### 2.1. Acoustic cavitation

In the case of AC, the necessary low pressures to break down the liquid and generate cavitation are achieved by the propagation of

acoustic waves. This requires high acoustic frequencies – generally 20 kHz and above.

AC has been utilised for over 40 years [37]. Until the present day, almost every chemical research laboratory is equipped with some type of AC generator. In this chapter, we discuss different AC setups and operating conditions under which the experiments on treating micro-organisms are performed. Firstly, we can differentiate the design of AC devices. Ultrasonic waves are usually generated by the piezoelectric transducer, which transforms high-frequency electrical energy into mechanical vibration. The vibrating part can be:

1. A radial probe (also called a sonotrode or horn probe). Sonotrodes are the most common US devices. To operate, the probe of the sonotrode is submerged into the treated liquid. Typical examples of sonotrodes are presented in Al-Juboori et al., Hunter et al. and Liu et al. [38–40]. The probes can be found in various diameters – papers reviewed here use probes with the diameter ranging from 2 mm to 12.7 mm. Majority of the cavitation activity occurs directly below the tip of the radial probe. Since all acoustic energy is transmitted through a small area (the tip of the probe) we can say that sonotrodes generate high-intensity cavitation.
2. On the other hand, piezoelectric transducers can be mounted on the sides of a container. The so-called “ultrasonic baths” (as seen in papers by Monsen et al. and Šarc et al. [41,42]) are also frequently used among researchers. The treated liquid is poured into the bath, where it is exposed to cavitation activity. Cavitation structures occur throughout the volume of the bath, in the anti-nodes of the acoustic waves. This type of cavitation is characterized as low-intensity cavitation because the area through which ultrasound is emitted is large. When using US baths, sometimes the bubbles do not actually collapse (especially if high frequencies are used). Instead, the bubbles oscillate for many acoustic cycles. Extreme conditions associated with the bubble collapse do not occur in this case. Instead, oscillating bubbles produce micro-scale eddies, which induce shear stress on nearby objects. Such cavitation is referred to as “stable cavitation”, whereas cavitation that produces the bubble collapses is also named “transient cavitation”.
3. In addition to sonotrodes and ultrasonic baths other unconventional ultrasonic devices exist. These include hollow radial horns [43], Barrel horn [44], vibrating plates [2,45], or devices producing focused ultrasound [46].

The frequencies at which ultrasonic devices emit the acoustic waves also differ. Most studies are using the piezoelectric transducers with excitation frequency 20 kHz [47,48]. However, researchers use also other frequencies, up to the 3.2 MHz [49], which is the highest used frequency reported in this review paper. In this paper, we refer to frequencies up to 100 kHz as “low frequency US” and to frequencies above 100 kHz as “high frequency US”. By using different transducers in the same device, one can achieve simultaneous excitation with two frequencies [16], where combinations of 17 kHz + 33 kHz and 70 kHz + 100 kHz have been used.

Another important parameter in AC research is its “intensity”. There is, however, no exact definition of cavitation-intensity and therefore different approaches how to describe it exist. Usually, researchers correlate the intensity with the power input to the treated liquid. Therefore, one option is to report the rated electrical power of the specific AC device [44,50,51]. Since not all the electrical energy is converted and emitted as acoustic waves, the second group of researchers tries to evaluate the actual acoustic power. Most commonly acoustic power for sonotrodes and ultrasonic baths is evaluated calorimetrically [22,52]. This method assumes, that all acoustic energy input is eventually dissipated as heat. But even if acoustic power is measured, there are four ways how this is reported in the literature. Acoustic power is either expressed as power (in W), as power over volume (in W/mL or W/L), as power over ultrasound emitting area (W/cm<sup>2</sup>), or even

as total energy emitted per unit of volume (J/mL). When discussing cavitation intensity, it is also important to note how the sample is exposed to the ultrasonic irradiation. Exposure can be either “direct” – the ultrasonic probe is directly submerged into the sample, or in the case of ultrasonic bath the sample is directly poured into the bath [53,54], or “indirect” – where the sample is contained inside a small beaker, vial or some other container. This container with the sample is then placed into a bigger vessel, usually filled with water. Hence, the surrounding water is in direct contact with the surface emitting acoustic waves and thus the sample is indirectly exposed [41,55,56]. Also, in this case the acoustic power is evaluated calorimetrically [55,56]. In the Supplementary material (Table S1), we recalculated all the reviewed data into W/mL.

Furthermore, US devices can be used in continuous mode, as described in Bastarrachea et al. [57] (emit acoustic waves throughout the treatment) or in so-called “duty cycles” – acoustic waves are emitted for specific time. For example, 3 s excitation which is followed by 7 s off time. This cycle is repeated for the time of treatment, as described in Abeledo-Lameiro and Liu et al. [40,58]. Duty-cycles are employed to control the temperature of the samples – in order to eliminate the temperature’s influence on the results. Majority of the papers are treating sample volumes between 100 and 200 mL, where constant temperatures are maintained using water or ice cooling [59]. If the sample volume is large, no cooling is required (for example [43] where 35 L samples are treated). But often the samples are smaller, down to only 1 mL [46] and therefore researchers operate in duty-cycles, which obviously reduces the energy input.

Lastly, we will differentiate two different experimental set-ups employed in AC research. These are “batch” and “flow-through”. Generally, experiments, where AC is harnessed, are in a batch set-up. The treated sample is contained in a beaker or acoustic bath. Because AC zone is rather small, a proper mixing must be provided in order to assure that the whole sample is equally exposed to cavitation activity. While this design is simple, its usability is limited to relatively small samples (as stated, most of the samples are in the range of 100–200 mL). To increase the volume of the sample, some researchers employ the flow-through set-up. Those set-ups have a specially designed smaller cavitation chamber, through which a liquid is fed from a bigger tank. Such arrangements can contain up to 50 L.

The discussed parameters in this chapter together with the respective references are summarised in the Supplementary material and presented in Fig. 1.

## 2.2. Hydrodynamic cavitation

In case of HC, acceleration of the liquid flow causes local pressure drop, which can trigger the cavitation formation – if the pressure drops below saturated pressure at liquid temperature. Depending on the flow conditions, the size of the formed cavitation bubbles varies usually between a few nm to a few mm (in very specific cases even cm [60]). Flow conditions and geometry of the submerged body define the cavitation behaviour and its characteristics. When the bubble forms, most of the energy is captured in the liquid surrounding the bubble, depending on its size and surrounding liquid properties. This energy is released, when the bubble goes through the pressure recuperation. At the same bubble size, the pressure gradient determines the collapse intensity. Depending on the pressure gradient, this energy is released on a different timescale. Different cavitation conditions result in different effects and intensities. The cavitation properties can vary by pressure distribution along the submerged body, flow velocities and liquid properties (temperature, density, viscosity and surface tension) and quality (number of solid particles and amount of dissolved gasses, which can both act as a nuclei) [32].

HC can be in general divided into: 1.) attached cavitation, 2.) cloud shedding cavitation and 3.) supercavitation (Fig. 2). In the case of attached cavitation, the large number of vapor bubbles are close together

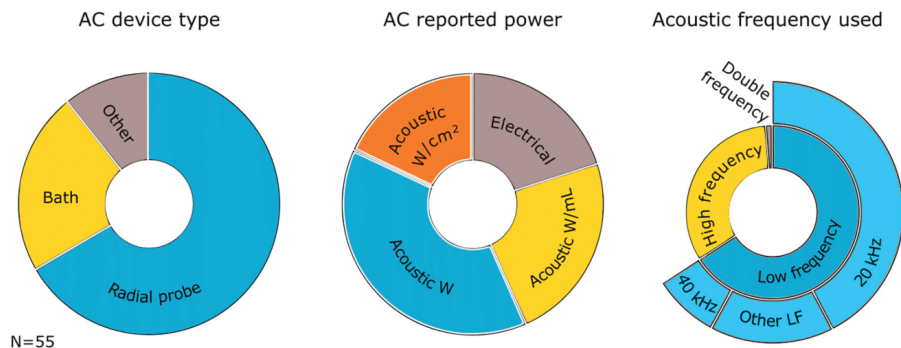


Fig. 1. Papers dealing with AC divided between cavitation device type (left), the reported power (middle) and acoustic frequency the device emits (right); N-number of reviewed papers.

and attached to the leading edge of constriction, forming an attached cloud shape. When flow velocity increases or static pressure additionally drops, the cavitation cloud becomes unstable and starts (partly or completely) to shed from the main cavitation structure (cloud shedding cavitation). If the flow velocity further increases or the pressure drops even lower, the so-called supercavitation forms. It starts when the individual bubbles merge and form a large unified vapor bubble or vapor cloud, which can be stable if the flow conditions do not change once it is formed.

In the reviewed literature three types of cavitation devices were used. They can be divided into: 1.) blow through (BT), 2.) pump + constriction (PC) and 3.) rotor-stator (RS) cavitation devices. Their distribution is graphically presented in Fig. 3, while detailed data is available in Supplementary material (Table S2). Most of the reviewed studies use PC type of devices, where cavitation is most likely already present at the pump impeller, but rare or no remark can be noticed on this issue in the papers. The pump itself is not an issue if it is determined, that it does not cavitate. To exclude the effects of the pump on the results, a BT cavitation device is more suitable. In the case of a BT device, compressed air or a piston is used to push the liquid through the constriction from the first reservoir to the second reservoir. These types of devices are not circular but can be driven as continuously working devices with multiple number of passes with suitable configuration [61,62]. Most configurations with RS devices include pumps for liquid circulation, which can similarly as in the case of PC devices, influence the gathered results. Rare RS designs are capable of operating

without additional circulation pump [63].

One of the advantages of HC is its scalability and its potential to be used on the industrial scale. Nonetheless, one must be aware that scaling effects might be difficult to predict [64]. The reviewed papers were divided by sample volume into three sections: 1.) laboratory, 2.) pilot and 3.) industrial scale cavitation devices (Fig. 3 and Supplementary material Table S2).

### 3. Microorganisms

Microorganisms are microscopic organisms that can exist unicellularly or in a colony of cells. There are prokaryote and eukaryote cell types based on the internal cell structure and other features. Usually prokaryotes are smaller sized than eukaryotes. Prokaryotes have simpler internal cellular organization without enclosed internal membrane structures. Cytoplasm is separated from the surrounding with phospholipid bilayer and extracellular matrix. On the other side, eukaryotes have a more complex structure with additional membrane structures within the cells – called organelles (nucleus, mitochondria, endoplasmatic reticulum, Golgi apparatus, chloroplasts, etc.). Viruses are neither prokaryotes nor eukaryotes since they are not living organisms as they lack many of the attributes of living cells – the most important: they're not a dynamic open system. They also don't have metabolic abilities and replication of their own – they need a host cell [65].

Cell envelope is a sophisticated multi-layered structure and is a

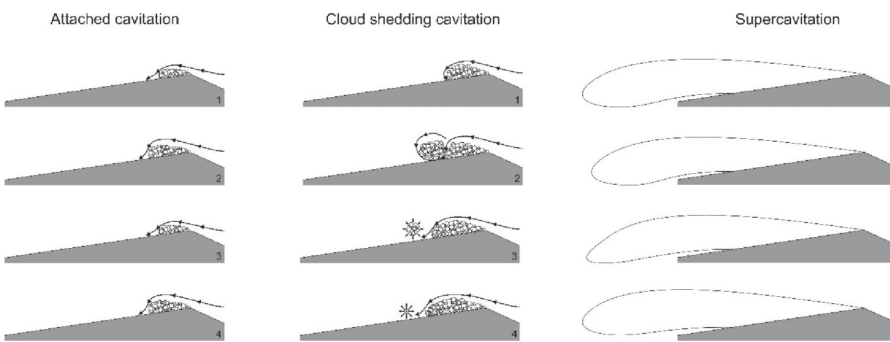


Fig. 2. Types of hydrodynamic cavitation (the flow is from the right to the left).

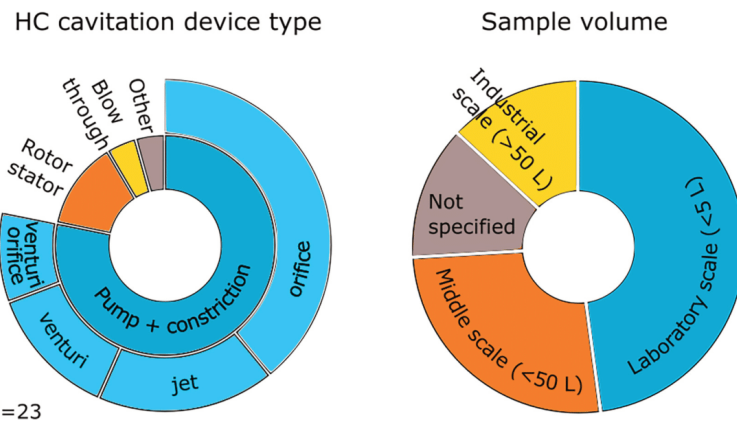


Fig. 3. Papers dealing with HC divided between cavitation device type (left) and sample volume (right); N-number of reviewed papers.

boundary layer between a medium and a cellular cytoplasm [66]. The closest boundary layer to cytoplasm is cytoplasmic membrane. It is a few nm thick and mostly consists of phospholipid bilayer with embedded proteins. Membrane fluidity and heterogeneity are determined with the type of phospholipids, amount of cholesterol and the embedded proteins. Cell membrane can be described as a heterogenic fluid mosaic [67]. Outermost boundary of the cell envelope is an additional layer of matrix called cell wall and gives protection, rigidity and shape to the cell. Cell wall composition varies between microorganisms [65]. Once the membrane is damaged irreversibly, microbial cells will be dead immediately [68]. Therefore, it is important to understand the basics of the cell envelope composition and in this chapter, we describe in detail the outer layer structure of bacteria, yeast and fungi, microalgae, and virus structure (Fig. 4).

Based on their cell wall composition bacteria can be divided into two groups – gram-negative and gram-positive bacteria. Gram-negative bacteria have complex multi-layered structure of the cell wall. They have an outer membrane, which is a second lipid bilayer with polysaccharides – lipopolysaccharides (LPS). LPS molecule consists of lipid A, core oligosaccharide and O-antigen [65]. Between the inner and outer membrane layer is a periplasm with a thin layer (3–8 nm) of peptidoglycan [69]. Peptidoglycan is a polysaccharide composed of covalently linked N-acetylglucosamine and N-acetylmuramic acid. Few amino acids (L-alanine, D-alanine, D-glutamic acid, lysine or diaminopimelic acid) are also present in peptidoglycan, which provide a cross-linking of the long polysaccharide chain. Additional cross-linking occurs by the direct peptide linkage of the amino group of diaminopimelic acid to carboxyl group of the terminal D-alanine. As cell membrane is relatively impermeable to small molecules, integrated transmembrane proteins called porins function as channels for transportation of hydrophilic low molecular weight substances [65].

On the other hand, cell wall of gram-positive bacteria mostly consists of a thick single layer of peptidoglycan and is primarily responsible for the strength of the wall [65]. Peptidoglycan layer is 20–80 nm thick [66]. Besides standard peptidoglycan cross-linking, additional cross-linking occurs mainly by peptide interbridges. Many gram-positive bacteria have teichoic and lipoteichoic acid which are embedded in cell wall and cell membrane. Teichoic acid is partially responsible for the negative charge of the cell. Some bacteria can also form endospores, dormant bacterial structures. Their function is a guarantee of the survival of bacteria in harsh conditions (extreme temperatures, low water activity and nutrient depletion). The outer protective layer of

endospores consists of exosporium (thin protein covering), spore coats (proteins), cortex (loosely cross-linked peptidoglycan), core wall and cytoplasmic membrane [65]. There are a few irregular bacterial cell wall structures and one of them is present in *Mycobacterium*. It stains gram-positive, but its cell wall shares notable features of gram-negative bacteria as it has a pseudo outer membrane. Mycobacterial cell wall core structure encompasses of mycolyl-arabino-galactan-peptidoglycan [70]. Its cell wall is extremely resistant to drugs (small hydrophilic agents) due to low permeability of the cell wall, has a low number of porin molecules and is extremely rich in lipids [71].

Yeast and fungal cell wall share a similar structure. It has two layers: outer layer consists mostly of mannoproteins, while inner layer is microfibrillar and consists mostly of glucans [72]. These compounds are linked with β-1,3 and β-1,6 bonds. β-1,3 glucan chains are coiled spring-like microfibrillar structures that confer elasticity and tensile strength to the cell wall [73]. β-1,6 glucans are amorphous in structure and act as a flexible glue by cross-linking β-1,3 glucan and chitin to the cell wall mannoproteins [74]. The mechanical strength of the wall is mainly due to the inner layer (glucan and chitin) and represents about 50–60% of the cell wall's dry weight [75].

In the case of cyanobacteria, the cell wall is analogous to gram-negative bacteria. An inner murein or peptidoglycan layer supports and strengthens the wall, while the outer lipoprotein layer controls the transport of molecules. The outer gelatinous sheath is providing protection against exposure to high levels of sunlight [76]. Some cyanobacteria form specialized cells for nitrogen assimilation, called heterocyst. Heterocyst are surrounded with thick cell wall containing large amounts of glycolipids, which slows down diffusion of O<sub>2</sub> into heterocyst to maintain anoxic conditions for nitrogen assimilation [65].

In the case of green algae most of their outer wall has a membrane-like trilaminar structure, which exhibits two electron dense sublayers and one sublayer with low electron density between two electron dense layers. These walls have generally highly aliphatic structure. Most of the cell walls contain biopolymers called “algaenan” – an insoluble biopolymer, which is resistant to drastic non-oxidative chemical treatments [77]. Because algae are a large and diverse group, there is also great diversity in chemical compositions of the cell walls [78].

Diatoms on the other hand, have extremely crush-resistant silica cell wall (frustule). Frustules are of different shapes and typically show morphological symmetry [65]. The silica is a polymerised silicic acid and is amorphous with no crystalline structure [79]. The frustule of diatoms can withstand extreme mechanical forces [80].

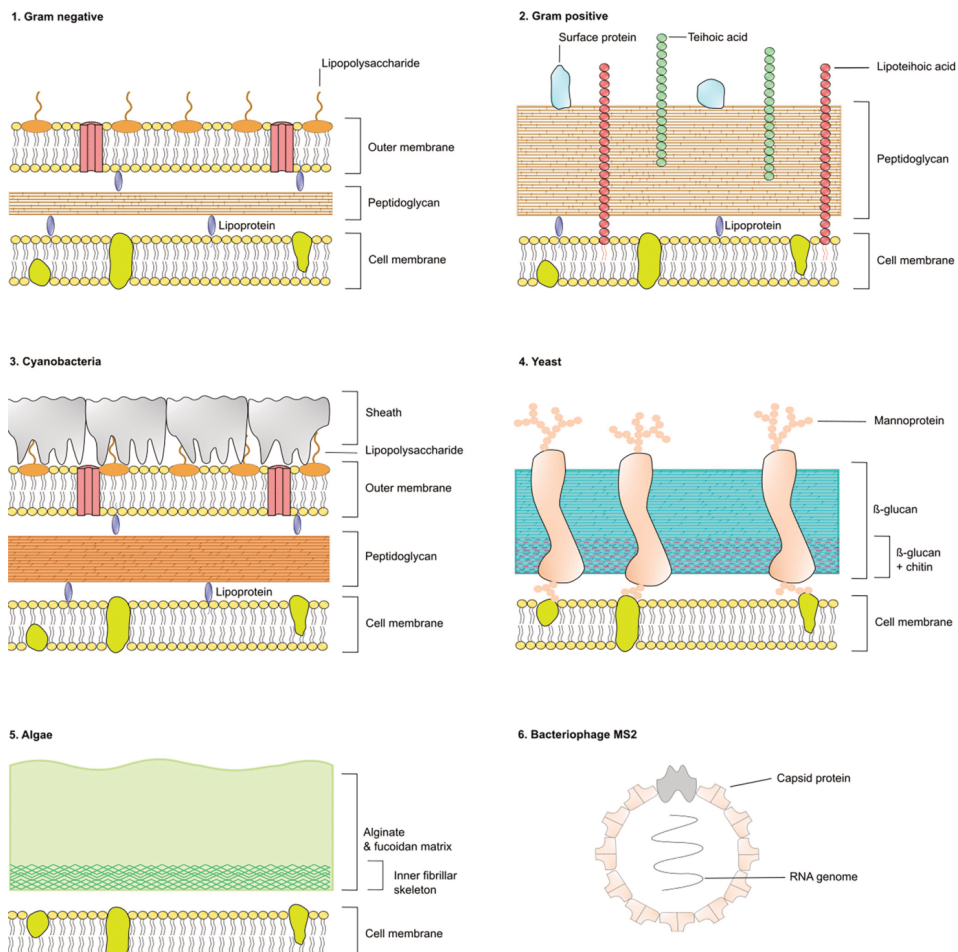


Fig. 4. Cell wall structure of different types of microorganisms and virus structure of bacteriophage MS2. Drawings were adapted from literature [82–85].

Most viruses are smaller than prokaryotic cells, ranging from 20 to 300 nm. Extracellular form poses genome information, surrounded with proteins or other macromolecules, which together form a virus particle. Capsid proteins are monomers or multimers of capsid protein subunits. Viral structure is diverse – usually it is constructed in a highly symmetric way, most common is icosahedral and helical symmetry. Some viruses have additional membrane around capsid – an envelope. Envelope membrane is derived from host cell. Some bacterial viruses possess even more complex structure with icosahedral head and helical tails [65]. High degree of structural diversity of viruses is reflected in a different resistance to physico-chemical treatments. Wide range of pressure resistances is found in-between viruses [81].

#### 4. Cavitation and its possible effects on different microorganisms

Mechanisms responsible for microorganism's inactivation by AC and HC, can be divided into mechanical, thermal and chemical effects [12,20,21,86–88].

##### 4.1. Effects of cavitation

###### 4.1.1. Mechanical and thermal effects

When bubbles in the liquid form and then collapse, extreme conditions can occur that drive the reported mechanical effects such as shock waves, liquid microjets and high shear forces (turbulence and eddies) [59,89–92].

All these mechanical effects are reported to physically damage, weaken or tear the outer layer of different organisms

[12,20,28,91,93,94].

In addition to the above-mentioned effects, in AC another distinctive mechanism – microstreaming, occurs [28,92,95]. By providing high localized shear forces, microstreams can cause serious damage to microorganisms [95] and together with shockwaves generated by bubble collapses facilitate mass transfer processes [92].

Moreover, bubble collapses can cause hotspots – small areas with extremely high temperatures, which can locally damage microorganisms [12,20,92]. Besides this, extreme temperatures can also affect the integrity of the outer layer of microorganisms and make them more susceptible to further damage with reactive species [96].

#### 4.1.2. Chemical effects

Implosion of bubbles and consequently formation of local hot spots is responsible for homolytic cleavage of H<sub>2</sub>O molecules and formation of free radicals ('OH and 'H) [12,91,92]. Being one of the strongest oxidants, 'OH readily oxidize any species they encounter or react between themselves forming H<sub>2</sub>O<sub>2</sub> [54,91,93,97]. Many other species can form ('O<sub>2</sub>H, 'N, 'O, 'O<sub>2</sub>) when different gases air/oxygen are dissolved in water [92,98].

In the case of acoustic cavitation, the number of radicals that reaches the liquid bulk phase depends on the frequencies employed. It has been established that with low ultrasonic frequencies (100 kHz and below) formed bubbles are bigger and their collapses more aggressive. This on one hand releases more energy in terms of shock waves but on the other hand the number of collapses per unit of time is smaller, which hinders diffusion of 'OH into the bulk phase [22,90,92,99,100]. Situation is the opposite for the higher frequencies (above 100 kHz). In this case smaller bubbles are formed, which release less energy. However, the number of collapses is higher, and this facilitates the diffusion of 'OH [54,90,92,99].

Similarly, smaller bubbles and more collapses are favourable for the diffusion of 'OH radicals into the bulk liquid in the case of HC [90]. The efficiency of HC on cell disruption correlates with bubble pressure collapse which depends on cavitation number, presence of dissolved gases, viscosity of the liquid medium, vapour pressure and above all the design of the HC device [10,11,101,102].

#### 4.1.3. Oxidation of microorganism's constituents

Organisms can defend themselves against oxidative stress but when levels of reactive oxygen species (ROS) exceed their antioxidant capabilities oxidative stress ensues [103,104]. OH radicals and H<sub>2</sub>O<sub>2</sub> both act as strong biocides [54,91]. H<sub>2</sub>O<sub>2</sub> has been shown to be effective against bacteria, yeast, microalgae and viruses [105–108] but its effectiveness depends on the concentration applied [105,106,108,109]. H<sub>2</sub>O<sub>2</sub> toxicity is thought to be a consequence of the production of oxidative species like OH radicals intracellularly, but the exact mechanisms of how these reactive species are formed are not yet fully elucidated [108].

Important constituents of microorganisms, that can be affected by oxidation with different reactive species, are polysaccharides, proteins, lipids and DNA [106,107]. As short-lived and electrophilic species, 'OH radicals can attack and oxidise double bonds and sulphydryl groups of these constituents and via chain reactions produce oxidative stress that ends with irreversible consequences for the microorganisms [108–111].

4.1.3.1. Oxidation of proteins. Oxidation of proteins with reactive species can occur in and on the surface of the outer protective layer (protein capsid) as was demonstrated for environmentally important viruses – leviviruses, adenoviruses, caliciviruses and enteroviruses [112,113]. Depending on the oxidant in question protein backbone as well as side chains can be affected with 'OH being the least selective [113]. These oxidation reactions affect virus infectivity and replication by hindering normal functioning of viral constituents [114] or by altering the capsid structure and providing access to interior constituents [96].

Oxidation of proteins can also take place intracellularly when radicals are generated inside the cells from H<sub>2</sub>O<sub>2</sub> [108]. Once formed, 'OH attack electron rich sites like double bonds of the amino acid side chains and backbones [106,110] and can oxidize amino acids such as tyrosine, phenylalanine, tryptophan, histidine, methionine and cysteine. Consequently, the specific function of the corresponding protein is inhibited [108].

4.1.3.2. Oxidation of lipids. When 'OH attack polyunsaturated fatty acids of lipids and cause chain reactions that lead to generation of many other ROS it is referred to as lipid peroxidation [104,109]. This has been reported in numerous studies dealing with effects of free radicals and H<sub>2</sub>O<sub>2</sub> on bacteria and yeast [104,105,108,109,115]. Once the reaction is started, the bacteria cell membrane integrity is affected. Changes in membrane fluidity, permeability and deterioration of membrane's internal organisation in the end lead to free radicals reaching the interior of the cell and causing additional damage to intracellular components [108,115].

4.1.3.3. Oxidation of polysaccharides. One of the distinctive features of gram-negative bacteria is the outer polysaccharide layer [65]. It is reported in the literature that non-radical (H<sub>2</sub>O<sub>2</sub>) and radical ('OH, 'OOR, 'OR and 'ON) ROS can attack polysaccharides. By the scission of the glycoside backbone they cause fragmentation of the biopolymer and cause its fragmentation which changes the functionality of these cell constituents [116]. It was also shown that the susceptibility to radical attack depends on the polysaccharide composition as was demonstrated for sulphated polysaccharides [116].

4.1.3.4. Oxidation of nucleic acids. It was shown that also nucleic acids are susceptible to oxidative stress initiated by ROS. Once inside the cells 'OH can cause a break of the double helix and/or modify nitrogen bases [111,113].

All relevant available literature data, where unambiguous effectiveness results could be deducted, is summarized in tables below and only the maximum recorded effects are given.

#### 4.2. Effects of cavitation on bacteria

In Tables 1–3 results from reviewed articles are presented. One can observe, that researchers employed different cavitation types, treatment times, medium, initial concentration of bacteria, different bacteria species, and therefore the measured inactivation rates differ vastly. More articles were investigating US than HC, therefore more data is available for US.

Effect of bacterial inactivation with US could depend on different operating parameters of the experimental design. High frequency ultrasound (HFUS) resulted in greater inactivation compared to low frequency ultrasound (LFUS) for *Escherichia coli* and *Streptococcus mutans* [56]. In Table 3 positive correlation between higher frequency and greater inactivation for *Staphylococcus epidermidis* can be seen. On the other hand, lower inactivation rate authors observed for HFUS in the case of *Mycobacterium* sp. [54] and *E. coli*, *Klebsiella pneumoniae* [55]. Directly comparing these results might be challenging as researchers used different microorganisms, cavitation operating conditions, treatment times and sample volumes. In addition, increasing power intensity also had a positive effect on inactivation rate as most researchers observed in the case of low frequencies [38,88,117,118], high frequencies [56,99] and with both types of frequencies [54]. Holm et al. [119] observed no effect on *Cobetia marina* and *Enterococcus avium*, but they observed positive effect on *E. coli* and *Vibrio cholerae* at low frequency. They do not offer any suggestions regarding conflicting results between different bacteria.

Different cavitation chamber designs can be utilized to achieve HC. Venturi chamber design seems to be more effective for bacterial inactivation compared to the orifice design [90]. However, multi-hole

**Table 1**  
Review of cavitation effects on gram-negative bacteria reported in the literature.

Species	Characteristics (diameter * length, shape)	Medium	Conc. (CFU/ml)	Proposed mechanism	US freq. (kHz)	Effectiveness (%)			Time (min)	Ref.
						LFUS	HFUS	HC		
<i>Gram-Negative</i>										
<i>Cobetia marina</i>	2.8*1 µm Rod [131]	ASW	2–5 × 10 <sup>6</sup>	M + C	19	90			3.6	[119]
<i>Enterobacter aerogenes</i>	0.7*3.5 µm rod	SS	/	/	20	4.4 <sup>a</sup>			20	[126]
		SS	10 <sup>6</sup>	M	20	5 <sup>a</sup>			40	[88]
		SS	10 <sup>8</sup>	M + C	850		4.4 <sup>a</sup>		20	[99]
<i>Haemophilus influenzae</i>	0.5 µm, round [132]	BS	10 <sup>3</sup>	/	20	99			10	[41]
<i>Klebsiella pneumonia</i>	0.7*1.6 µm rod [133]	BS	10 <sup>5</sup>	M	20	90			15	[55]
		BS	10 <sup>5</sup>	M	580		25		15	[55]
		SS	10 <sup>7</sup>	M	–				5 <sup>a</sup>	[93]
<i>Legionella pneumophila</i>	0.5*2 µm rod [134]	BS	1.5–18 × 10 <sup>3</sup>	M	–				30	[42]
		BS	1.5–18 × 10 <sup>3</sup>	M	33	20			60	[42]
		SS	10 <sup>5</sup>	M	–				3.6 <sup>ac</sup>	[60]
<i>Pseudomonas aeruginosa</i>	0.8*3.1 µm rod [135]	BS	1.0 <sup>c</sup>	M	70	2.7 <sup>b</sup>			3.6	[118]
		BS	1 × 10 <sup>3</sup>	/	20	90			15	[41]
		SS	10 <sup>8</sup>	M	–				3 <sup>a</sup>	[93]
<i>Pseudomonas putida</i>	0.75*3.2 µm rod	DW	/	M	–				100	5p
<i>Pseudomonas syringae</i>	0.9*2.6 µm rod [136]	SS	10 <sup>7</sup>	M	–				6 <sup>a</sup>	[93]
<i>Salmonella enterica</i>	1*3 µm rod [137]	DW	10 <sup>6</sup>	/	24	1 <sup>a</sup>			0.8	[138]
<i>Vibrio cholerae</i>	0.4*3.1 µm rod [139]	ASW	2–5 × 10 <sup>6</sup>	M + C	19	90			0.9	[119]
<i>Surface water coliforms</i>	/	SUW	250	/	20	70.8			15	[38]

LFUS: low frequency ultrasound; HFUS: high frequency ultrasound; HC: hydrodynamic cavitation; ASW: artificial seawater; BS: buffer solution; DW: distilled water; SS: salt solution; SUW: surface water; M: mechanical damage; C: chemical damage; a: log reduction; b: rate of nitrocefin hydrolysis (nmol/mg/s); c: supercavitation; p: number of passes; OD<sub>700</sub> (a.u.); /: data not available.

orifice improves bacterial inactivation compared to a single-hole orifice [90,101]. In multi-hole orifice design, round shaped holes seem to be the most effective, which is attributed to a higher hole number per cross-section [101]. Loraine et al. [93] observed that different nozzle geometry at the same flow rates and total opening area affect the inactivation rate. Slit venturi design proved to be the most energy efficient design for bacterial inactivation, when compared to multi-hole orifice and cylindrical venturi [120]. Increasing discharge pressure has greater positive effect on inactivation in multi-hole orifice, whereas in

venturi it has a negative effect, expressed as lower inactivation rate [90]. Lower cavitation number relates to higher protein release or inactivation rate [93,121]. Increasing nozzle velocity [122], flow rate [101] and cavitation intensity [123] results in an increase of inactivation rates. Loraine et al., Badve et al. and Dalfré Filho et al. [93,120,124] investigated the effect of inlet pressure on inactivation rates. They determined that by elevating the inlet pressure inactivation rates increase but only up to a certain point when a plateau is reached. At further elevation of the pressure the inactivation begins to decrease.

**Table 2**  
Review of cavitation effects on gram-negative bacteria *Escherichia coli* reported in the literature.

Species	Characteristics (diameter * length, shape)	Medium	Conc. (CFU/ml)	Proposed mechanism	US freq. (kHz)	Effectiveness (%)			Time (min)	Ref.
						LFUS	HFUS	HC		
<i>Gram-Negative</i>										
<i>Escherichia coli</i>	0.5*1.5 µm rod	BS	0.5 <sup>e</sup>	M + C	–		70 <sup>b</sup>	1000p	[121]	
		BS	M		20	95		50	[117]	
		GM	1.4 × 10 <sup>11</sup>	M	–		100	3p	[122]	
		SS	10 <sup>3</sup> , 10 <sup>4</sup> , 10 <sup>5</sup>	M	–		80	120	[90]	
		SS	10 <sup>4</sup>	/	20	3.9 <sup>a</sup>		10	[50]	
		ASW	2–5 × 10 <sup>6</sup>	M + C	19	90		1.4	[119]	
		GM	4 × 10 <sup>6</sup>		20	99		3	[39]	
		SS	10 <sup>6</sup>	C	500		1 <sup>a</sup>	10	[56]	
		BS	10 <sup>6</sup>	M	20	4 <sup>b</sup>		4	[53]	
		BS	1 × 10 <sup>3</sup>	/	20	90		15	[41]	
		BS	10 <sup>5</sup>	M	20	91		15	[55]	
		BS	10 <sup>5</sup>	M	580		5	15	[55]	
		BS	/	M	–			93 <sup>b</sup>	1000p	
		DW	10 <sup>6f</sup>	M	–			2.2 <sup>b</sup>	50	
		SS	10 <sup>7</sup>	M	–			5 <sup>a</sup>	60	
		TW	10 <sup>7</sup>	M	–			100	30	
		SS	10 <sup>6</sup> , 10 <sup>8</sup>	/	20	98.1		20	[125]	
		DW	/	C	26	1.7 <sup>a</sup>		3	[1]	
		DW	10 <sup>6</sup>	M + C	–			100	8	
		GM	10 <sup>8</sup>	M	20 + 33	6 <sup>ac</sup>		60	[47]	
		GM	10 <sup>9</sup>	M + C	20	89.1		12	[68]	
		GM	10 <sup>7</sup>	M + C	–			100	14	
		SS	10 <sup>8</sup>	M	–			3.3 <sup>a</sup>	150	
									[60]	

LFUS: low frequency ultrasound; HFUS: high frequency ultrasound; HC: hydrodynamic cavitation; ASW: artificial seawater; BS: buffer solution; DW: distilled water; GM: growth medium; SS: salt solution; TW: tap water; M: mechanical damage; C: chemical damage; a: log reduction; b: release of acid phosphatase; c: dual frequency; p: number of passes; /: data not available.

**Table 3**  
Review of cavitation effects on gram-positive bacteria reported in the literature.

Species	Characteristics (diameter * length, shape)	Medium	Conc. (CFU/ml)	Proposed mechanism	US freq. (kHz)	Effectiveness (%)			Time (min)	Ref.
						LFUS	HFUS	HC		
<i>Gram-Positive</i>										
<i>Bacillus globigii</i> (spores)	0.6 µm [140]	ASW	2–5 × 10 <sup>6</sup>	M + C	19	90			213	[119]
<i>Bacillus halodurans</i>	0.75*2.5 µm rod	DW	/	M	–		100	6p	[122]	
<i>Bacillus subtilis</i>	0.75*2.5 µm rod	GM	1.4 × 10 <sup>11</sup>	M	–		100	4p	[122]	
	SS	10 <sup>7</sup>	M	–		5 <sup>a</sup>	120		[93]	
	SS/GM	/	/	20	4.5 <sup>a</sup>		20		[126]	
	SS	10 <sup>8</sup>	M	850		2.5 <sup>a</sup>	20		[99]	
	SS	10 <sup>5</sup>	M	–		3.8 <sup>a</sup>	120		[60]	
<i>Enterococcus faecalis</i>	0.8*1.1 µm ovoid [141]	BS	103	/	20	75			60	[41]
	DW	10 <sup>6</sup>	M + C	–			100	10	[86]	
<i>Enterococcus avium</i>	1 µm ovoid [142]	ASW	/	M + C	19	90			20.1	[119]
<i>Lactobacillus acidophilus</i>	0.6*3.5 µm rod	SS	10 <sup>4</sup>	/	20	0.6 <sup>b</sup>			10	[50]
<i>Listeria innocua</i>	0.3*1.3 µm rod [143]	GM	10 <sup>8</sup>		20 + 33	4 <sup>ab</sup>			60	[47]
<i>Mycobacterium species Strain (6PY1)</i>	0.4*5 µm rod	GM	10 <sup>6</sup>	M	20	3.2 <sup>a</sup>			35	[57]
<i>Staphylococcus aureus</i>	1 µm coccus [144]	BS	10 <sup>3</sup>	/	20	93			70	[54]
	SS	10 <sup>6</sup> , 10 <sup>8</sup>	/	20	91.7				20	[125]
	GM	10 <sup>9</sup>	M + C	612		43			70	[54]
<i>Staphylococcus epidermidis</i>	0.8*1.0 µm coccus	BS	10 <sup>3</sup>	/	20	81.3			12	[68]
	SS	/	/	20	20				60	[41]
	SS	10 <sup>6</sup>	C	–	0.2 <sup>a</sup>				20	[126]
<i>Staphylococcus pseudintermedius</i>	0.6 µm coccus [145]	SS/GM	/	/	20	0.2 <sup>a</sup>			20	[99]
<i>Streptococcus mutans</i>	0.3 µm coccus [146]	SS	10 <sup>6</sup>	C	500		2 <sup>a</sup>		22	[56]
Seawater bacteria	/	SW	10 <sup>7</sup>	M + C	–		44	15		[120]

LFUS: low frequency ultrasound; HFUS: high frequency ultrasound; HC: hydrodynamic cavitation; ASW: artificial seawater; BS: buffer solution; DW: distilled water; GM: growth medium; SS: salt solution; SW: seawater; M: mechanical damage; C: chemical damage; a: log reduction; b: dual frequency; p: number of passes; /: data not available.

Higher initial cell concentrations led to lower inactivation rates in many of the reviewed articles in AC treatment [39,90,122]. However, Li et al. [125] and Al Bsoul [54] reported no difference between initial concentration on inactivation after 20 min and 70 min treatment, respectively. Loraine et al. [93] observed that with higher initial bacterial concentration, only longer treatment time is needed to achieve comparable inactivation rates at investigated concentration. This hypothesis could answer conflicting results mentioned above. The same correlation of initial concentration and inactivation rates can be seen for different types of HC devices: it has a greater effect for orifices, but only a small effect for venturi geometry [90]. Li et al. [125] speculated about the possibility that with higher cell density ultrasonic waves could act on a higher proportion of bacteria. On the other hand, they suggested also restricted effect of cavitation due to greater aggregation of bacteria.

Moreover, effect of bacterial inactivation could depend on the characteristics of used bacteria. Gao et al. [99] suggested that inactivation of *Bacillus subtilis*, via the breakage of cell wall, with HFUS is a result of rod-shaped cells. They observed lower inactivation rate in the case of LFUS compared to HFUS. Cameron et al. [50] observed unique destruction of rod-shaped *Lactobacillus acidophilus* where most damaged cells had "sheared off" tip of the cells. Gram-positive bacteria seemed to be more resistant to cavitation in comparison to gram-negative. This is assumed to be due to a thicker, more rigid and robust properties of their cell wall [47,50,68,86,93,122,125,126]. Li et al. [125] concluded that primary target for gram-negative bacteria is the outer membrane, while in the case of gram-positive bacteria the target might be cytoplasmic membrane and internal cell structure. Differences between the same gram staining group could be ascribed to the level of cross linking in the outer layer [93]. On the other hand, Gao et al., Koda et al. and Holm et al. [56,88,119,126] did not observe any differences in the destruction of bacteria based on gram staining, shape or size of bacteria. Therefore, Gao et al. [126] proposed thickness of the capsule (cell wall) as one of the physical characteristics which might be responsible for this observation. Capsule is soft and consequently

dampens the shear forces pointed toward the cell membrane. Additionally, they proposed extent of bacterial surface hydrophobicity as a very important parameter for US treatment. Surface of the cavitation bubble is hydrophobic and cavitation bubbles will be attracted to hydrophobic surfaces. Additional protective structures may play a role in bacterial resistance to cavitation treatment as spores of *Bacillus golbigii* are extremely resistant to ultrasound – at least a magnitude higher decimal reduction time was observed [119].

Most of the investigated bacteria were inactivated to more than 70%, but there are also cases where achieved inactivation was not considerable (Tables 1 and 3). For example, Gao et al. [126] observed low inactivation of *Staphylococcus epidermidis* with LFUS (0.2 log after 20 min of treatment). They showed that these bacteria form clusters and observed no effect on structural changes in cells after US treatment. Badve et al. [120] also achieved low inactivation of total bacteria in seawater. In the case of HC, some authors achieved total inactivation of bacteria as a result of treatment. Gram-positive bacteria are probably more resistant to cavitation treatment, as low inactivation can be seen for many species (Table 3). Interestingly, experiments with *Legionella pneumophila* (gram-negative bacteria, Table 1) also show low inactivation in the case of AC or HC, but greater inactivation with supercavitation type of HC [42,60]. They suggest rapid pressure drop as a possible mechanism [60]. Interestingly, for *Staphylococcus aureus* contradictory results are reported (Table 3). Monsen et al. [41] showed only 40% inactivation, whereas Li et al. and Liao et al. [68,125] achieved higher inactivation rates (~81.7%) in shorter treatment time. This dissimilarity of results might be due to different US set-ups – ultrasonic bath and sonotrode, respectively.

A lot of authors observed the effect of cavitation using microscopic techniques (Transmission Electron Microscopy – TEM and Scanning Electron Microscopy – SEM). They concluded that cavitation caused membrane ruptures and damage to the cell wall, morphological changes of cells, empty cell envelopes, occurrence of large vacuoles, cell fragments and shrinkage of cells, etc. [50,53,55,56,68,88,99,121,125,126]. On the other hand, Gao et al. and

Koda et al. [56,99] observed that in the case of *Enterobacter aerogenes* and *Streptococcus mutans* most cells had deformed shape (loss of turgor pressure) but without visually ruptured cell wall after HFUS treatment. Only small number of cells were visually damaged even though inactivation rate was high. Similar observations were also made by Li et al. [125] for *E. coli* with LFUS treatment as a consequence of cell wall composition. It was postulated that HFUS has mechanical and chemical effect on bacteria [99]. Interestingly, Cameron et al. [50] observed small vesicles (< 20 nm) inside and outside of cells as a result of US treatment. They proposed that formation of vesicles was probably a result of emulsification of membrane lipids with cavitation air bubbles. HC seems to selectively damage bacterial cells. Balasundaram and Harrison [121] postulated that this selectivity is due to formation of smaller punctures in the “boundary layer”. They are formed on the outer cell wall of bacteria due to the microjets and result in the leakage of periplasmic enzymes out of the cell. Additionally, they proposed that with different number of passes, different cellular damage can be achieved. At first, outer cell membrane is damaged due to the mechanical effects of cavitation. Then, mechanical and chemical damage occurs in the inner cytoplasmic membrane. Lastly, with longer exposure of the cells to cavitation, more effects can be observed on the outer cell wall. This is probably due to its greater surface area being exposed to the medium. Runyan et al. [118] made similar hypothesis that US can perturb the cell membrane and improve permeability of large hydrophilic molecules as are antibiotics. Šarc et al. [42] proposed that destruction effect in the case of supercavitation is a combination of rapid pressure change and exposure of all the treated volume to the tension forces. Liao et al. and Li et al. [68,125] observed no sublethal subpopulation of damaged cell and therefore concluded that US treatment might be “all or nothing” phenomenon. Cerecedo et al. [86] reached similar observations for HC treatment. Interestingly, Mezule et al. [123] made different observations of *E. coli*, treated with HC. They observed sublethal population, which was metabolically active, but not able to elongate (viable but not culturable cells – VBNC). Liao et al. [68] utilized intriguing insight into the process by monitoring cell membrane potential. They observed a change of membrane potential during treatment with induced peaks after 5 min for *E. coli* and 3 min for *S. aureus*. Cell membrane potential phenomenon might be related to the change of ion channels. Although most authors concluded mechanical and chemical effects are responsible for bacterial destruction, interestingly Spiteri et al. [1] showed involvement of heat shock response genes in US treatment.

In some of the reviewed articles cell destruction was contributed to chemical effect. In the case of HFUS chemical mechanism of destruction might be predominant [56,99]. Additionally, Al Bsoul et al. [54] investigated also formation of H<sub>2</sub>O<sub>2</sub> in distilled water during US treatment. During HFUS and LFUS treatment they detected 148 µM and 15 µM of H<sub>2</sub>O<sub>2</sub>, respectively. Chemical damage was mentioned also for LFUS as Liao et al. [68] suggested that part of cells was damaged intracellularly – ATP level decrease and DNA damage. Their results showed that some cells had intracellular DNA broken and enzymes inactivated without disruption of the cell wall. As a possible mechanism they proposed injection of ROS with cavitation microjets into the cells without damaging cell envelope. Even more compelling are results from Gao et al. [99] where they observed that mechanism of bacterial inactivation with HFUS depends on bacterial species. They concluded that mechanism of inactivation in the case of *B. subtilis* was still predominantly mechanical, while for *S. epidermidis* and *E. aerogenes* it was chemical. Spiteri et al. [1] investigated effects of LFUS on different *E. coli* mutants with different gene deletion affecting specific functional properties. They determined that the strain without oxyR gene was more resistant to treatment. Since oxyR activated genes have direct or indirect antioxidant functions, these results are somewhat interesting. The authors explained this could be due to instability of H<sub>2</sub>O<sub>2</sub> produced during treatment. Besides production of ROS, production of H<sub>2</sub>O<sub>2</sub> is also correlated with decrease of medium's pH. This is the consequence of

nitrous, nitric acid and carbonic acid formation because of dissolved gases [99]. Gashchin and Viten'ko [127] on the other hand offered the following explanation. Bacterial inactivation could be due to chemical instability in the cell wall and membrane, rapid penetration of chemical disinfectants inside the cell, change of pH to alkaline side and formation of OH radicals due to Fenton reaction. Together with the explanations and observations of the chemical effects of cavitation on bacteria inactivation there is also a lot of data available in the literature that investigates the effects of oxidants like H<sub>2</sub>O<sub>2</sub> and 'OH alone on bacteria, mostly on *E. coli*. Labas et al., Flores et al. and Watts et al. [108,111,128] determined toxicity of H<sub>2</sub>O<sub>2</sub> solution on *E. coli*. They proposed that it is not H<sub>2</sub>O<sub>2</sub> by itself that causes oxidation of cell's constituents, but the reactive species derived from it [108,111]. Being a small molecule H<sub>2</sub>O<sub>2</sub> can diffuse through the cell membrane and transform to 'OH via Fenton or Haber-Weiss reaction intracellularly [104,109,129,130]. Whether these reactions take place depends on the presence and amount of superoxide ions and Fe<sup>2+</sup> intracellularly. Flores et al. [111] discussed that the main site of attack of ROS is bacteria outer layer namely the peptidoglycan layer, lipopolysaccharide layer and phospholipid bilayer. They proposed a model describing the mechanism of bacteria's disinfection by H<sub>2</sub>O<sub>2</sub>. First attack of 'OH on the cellular wall is followed by a second attack of 'OH, which results in complete destruction of the cell's outer layer and formation of a lysate from all cell components. On the other hand, Kobayashi et al. and Rahman et al. [109,115] investigated effects of 'OH formed via different treatment processes. Rahman et al. [115] proposed that 'OH formed during sonocatalytic TiO<sub>2</sub> process were responsible for observed lipid peroxidation of *E. coli*'s membrane, while Kobayashi et al. [109] observed toxic effects of different ROS formed from H<sub>2</sub>O<sub>2</sub> under AC on *E. faecalis*.

#### 4.3. Effects of cavitation on yeast and fungi

As can be seen from Table 4 quite a lot of data is available for *Saccharomyces cerevisiae*. Authors either measured the release of intracellular or cell wall constituents but only a small amount of data is available where cell reduction was determined. For *S. cerevisiae* only articles using LFUS were found, whereas for *Aureobasidium pullulans* also HFUS was tested.

A lot of authors concluded that higher US intensities lead to increased release of proteins [40,147–149], polysaccharides [149] and log reductions [88]. Wu et al. [150] additionally observed that also which constituent is released first, depends on intensity. They showed that at lower intensities polysaccharides were released faster than proteins and at higher intensities it was the other way around. Additionally, Gao et al. [99,126] showed that in the case of *A. pullulans* LFUS [126] is more effective than HFUS [99]. Liu et al. and Iida et al. [40,148] for example showed that horn-type sonotrode is more effective than ultrasonic bath. Bystryak et al. [44] additionally showed that higher sonotrode amplitudes provided higher shear forces, which leads to faster and higher release of cell constituents and represents an important parameter in extraction of membrane-bound proteins.

For HC only two articles, both investigating *S. cerevisiae*, were found. Both authors investigated the effect of cavitation number. Balasundaram and Harrison [89] showed that cavitation number affected the release of soluble proteins and extracytoplasmic but not cytoplasmic enzymes. They determined that lower cavitation number is preferable as it results in more intensive cavitation conditions. Albanese et al. [151] on the other hand determined a two-peak model, where yeast cell damage was observed at low cavitation number and then again at very high number. They also concluded that venturi constriction was more effective than orifice plate.

Several authors investigated the effect of cell's initial concentration on cavitation effectiveness. Iida et al. and Zhang et al. [148,149] showed that with increasing the initial cell concentration the amount of protein released decreased, since the number of cavitation bubbles

**Table 4**  
Review of cavitation effects on fungi and yeast reported in the literature.

Species	Characteristics (diameter, shape)	Medium	Conc. (CFU/mL, g cells/mL*, cells/mL <sup>●</sup> , w/v (%)*)	Proposed mechanism	US freq. (kHz)	Effectiveness (%)		Time (min)	Ref.
						LFUS	HFUS		
<i>Aureobasidium pullulans</i> (F)	2–13 µm elongated thin walled	SS	10 <sup>7</sup>	M	20	3 <sup>a</sup>	< 1 <sup>a</sup> < 2 <sup>a</sup>	60	[88]
<i>Saccharomyces cerevisiae</i> (Y)	5–10 µm oval	BS	4.2 × 10 <sup>7</sup> 3.1 × 10 <sup>5</sup>	M + C	850	/	/	60	[99]
			0.5*		–			29 <sup>b</sup>	[89]
								39 <sup>i</sup>	
								27 <sup>j</sup>	
		BS	0.09*	/	/	85 <sup>b</sup>	/	15	[147]
		SS	10 <sup>4</sup>	M	20	3.6 <sup>a</sup>	/	10	[50]
		DW	0.01*	M	20	75 <sup>c</sup>	/	5	[148]
		SS	10 <sup>7</sup> <sup>●</sup>	M	20	42 <sup>d</sup>	/	5	[24]
		DW	/	/	20	0.6 <sup>e</sup>	/	21	[40]
		DW	0.1*	/	20	10 <sup>f</sup> 20 <sup>g</sup>	/	5	[149]
		GM	20*	/	20	18 <sup>e</sup>	/	65	[44]
		DW	0.1*	M	20	92 <sup>b</sup>	/	30	[150]
						84 <sup>h</sup>			

LFUS: low frequency ultrasound; HFUS: high frequency ultrasound ; HC: hydrodynamic cavitation; F: fungi; Y: yeast; BS: buffer solution; DW: distilled water; GM: growth medium; SS: salt solution; M: mechanical damage; C: chemical damage; a: log reduction; b: protein release (%); c: protein release (mg/g); d: tot cell population decline; e: protein release (mg/ml); f: polysaccharide release (dry weight basis: %); g: protein release (dry weight: %); h: polysaccharide release (%); i: extracytoplasmic enzyme release (%); j: cytoplasmic enzyme release (%); p: number of passes; /: data not available.

available for each cell decreased. Similarly, Gao et al. [99,126] showed that the *A. pullulans* inactivation was higher at lower initial concentrations in the case of LFUS and HFUS. They postulated that either viscosity or cell aggregation could be responsible. Higher viscosity lowers the cavitation initiation and higher cell number leads to more cell aggregation and thus bigger resistance to acoustic cavitation. On the other hand, Wu et al. [150] showed that the total amount of released constituents increases with increased concentration but is not correlated to volume. Apar and Özbek [147] found no correlation between effectiveness and cell concentration, while Balasundaram and Harrison [89] showed that an optimal cell concentration exists where the number of interactions between cavities and cells is the highest and leads to the highest release of constituents.

There is no correlation in the literature data proposed between cell shape, size and cavitation effectiveness but for example Iida et al. [148] discussed that the strength of cell wall could play an important role in cell's susceptibility to destruction via forces released during cavitation.

There is not a unique mechanism for cell destruction proposed. Balasundaram and Harrison [89] determined that cavitation only affected the release of cell wall bound and periplasmic (i.e. extracytoplasmic) enzymes. They postulated that the cell wall disruption is in this case the consequence of mechanical effects of cavitation like microjets and shock waves, which caused radial wall motion. Due to these effects, smaller holes in the cell wall developed which led to release of only periplasmic constituents but not bigger intracellular macromolecules. The same cell wall punctures were observed by Cameron et al. [50] who also proposed the same mechanical effects to be the culprit. Similarly, Iida et al. [148] discussed how mechanical effects of cavitation and the strength of microbial cells could be correlated. Since yeast cell are rigid microstreaming is not enough to disrupt them and the rupture will occur only when yeast cells are in proximity of cavitation bubbles. Zhang et al. and Wu et al. [149,150] proposed that the cell wall is initially weakened and broken down followed by the breakage of cell membrane.

Some authors also observed changes in microalgae using SEM and TEM. Balasundaram and Harrison [89] observed only localised cell wall damage and not complete cell disruption. Cameron et al. [50] on the other hand, observed cell fragmentation together with internal damages, uneven cell walls, many cells devoid of content and damages to cell microstructures. Similarly, Wordon et al. [24] observed damages on the outer cell layer, fractioning and extrusion of intracellular constituents. Also, Gao et al. [88] observed both broken and intact cells and Gao et al. [99] observed some cell envelopes that could be the result of

the damage to the yeast cells resulting in the leaking of their inner contents.

As can be seen from Table 4 not many authors investigated the correlation between oxidants formed during cavitation and destruction of yeast cells. Only Balasundaram and Harrison [89] postulated that radicals play an important role. They speculated that after longer treatment times imploding cavities weaken cell walls to a degree where free radicals can break disulphide bonds and result in release of cell wall bound enzyme invertase. There is however data available in the literature that investigates the effect of different oxidant on yeast cells. Steels et al. [105] demonstrated that H<sub>2</sub>O<sub>2</sub> negatively affects survival of *S. cerevisiae* and that outer layer lipid composition plays an important role in cells susceptibility to oxidation. Moradas-Ferreira et al. [103] summarized that H<sub>2</sub>O<sub>2</sub> triggers lipid peroxidation of yeast cell membranes. Brennan et al. [152] observed that H<sub>2</sub>O<sub>2</sub> causes intrachromosomal and interchromosomal recombination leading to mutagenesis, where ·OH is supposed to form in vivo from H<sub>2</sub>O<sub>2</sub> via the metal-catalysed Haber-Weiss reaction. Wang et al. [153] postulated that formation of reactive species like ·OH during plasma treatment are responsible for triggering chain oxidative reactions in cell constituents like cell wall, cell membrane and DNA and eventually inactivation of yeast cells.

#### 4.4. Effects of cavitation on microalgae

Microalgae are a group of photosynthetic microorganisms consisting of cyanobacteria, diatoms and unicellular algae. As can be seen in Tables 5 and 6 microalgae are in general susceptible to inactivation regardless of cavitation type and HFUS appears more efficient than LFUS for many species. There are however some contradictory results in the literature in the case of *Microcystis* sp., *Nannochloropsis* sp. and *Scenedesmus* sp. even though the same medium and mostly the same microorganism's concentration range was used. Using LFUS Joyce et al. and Lürling and Tolman [3,154] detected no significant damage to *Microcystis aeruginosa*, whereas Zhang et al. [155] observed substantial growth inhibition only after 15 days. In the case of *Nannochloropsis* sp. Kurokawa et al. [59] observed very high cell reduction with HFUS while Wang et al. [49] postulated cell structure changes as higher fluorescence of chlorophyll and lipids was emitted when LFUS was used. Besides low immediate damage Kim et al. [156] also determined only slight growth inhibition after 7 days. *Scenedesmus* sp. proved resistant to destruction with AC [154] while Batista et al. [157] achieved very good results with HC. Wang et al. [49] on one hand determined

**Table 5**  
Review of cavitation effects on cyanobacteria and diatoms reported in the literature.

Species	Characteristics (diameter, shape)	Medium	Conc. (cell/mL wt (%)*)	Proposed mechanism	US freq. (kHz)	Effectiveness (%)			Time (min)	Ref.
						LFUS	HFUS	HC		
<i>Anabaena</i> species (CN)	3.3–9.5 µm oval (2006)	GM	/	M	200	92 <sup>a</sup>			60	[165]
<i>Chaetoceros</i> species (D)	2.3–2.5 µm	/	1.1 × 10 <sup>8</sup>	M	2200 20	99 <sup>b</sup> 99 <sup>b</sup>			2 10	[59]
<i>Microcystis</i> species (CN)	4–5 µm oval to spherical [166]	GM GM GM	/ 10 <sup>9</sup> 1.5 × 10 <sup>5</sup>	M + C M M	— 25 20 1320	— 11 <sup>b</sup> 90 <sup>b</sup> Neg	64 <sup>c</sup> 5 102 20	8p 5 102 20	[163] [155] [159]	
		GM	/	M + C	20 580	47 <sup>b</sup>			20	[3]
		GM	2 × 10 <sup>6</sup>	M	20	68 <sup>b</sup>			10	[19]
		GM	6 × 10 <sup>6</sup>	M + C	1146 20	39 <sup>b</sup> 92 <sup>b</sup>			30	[29]
		GM	1.7 × 10 <sup>6</sup>	M + C	—		20 <sup>b</sup>		20	[158]
		GM	3 × 10 <sup>6</sup>	M + C	—		88 <sup>d</sup>		10	[125]
		GM	4.9 × 10 <sup>5</sup>	/	—		99 <sup>b</sup>		18p	[167]
<i>Thalassiosira pseudonana</i> (D)	5 µm	ASW	0.004*	/	20	85 <sup>b</sup>			1.7	[48]

LFUS: low frequency ultrasound; HFUS: high frequency ultrasound; HC: hydrodynamic cavitation; CN: cyanobacteria; D: diatom; ASW: artificial seawater; GM: growth medium; M: mechanical damage; C: chemical damage; a: brightness increase; b: cell reduction; c: cell reduction after 6 days; d: cell reduction after 3 days neg: increased cell concentration; p: number of passes; /: data not available.

higher cell concentration which they ascribed to declumping effect but at the same time proposed cell structure changes due to higher fluorescence of chlorophyll and lipids emitted.

A lot of the authors concluded that the effect of cavitation on microalgae depends on the US frequency [3,49,52,59,158,159] and that higher intensities and longer exposure times correlate to more effective cell destruction [3,19,46,52,154,158–162]. Higher intensities result in more aggressive cavitation which leads to better inactivation but only to a certain point. Excessive intensities can result in formation of too many cavities which interact between themselves resulting in the cushioning effect [162]. Longer exposure times also showed a positive effect on removal of microcystin [19].

Most authors agree that higher inlet pressure [17,157,163] gives the best results in the case of HC. Higher inlet pressure leads to formation of more bubbles and more aggressive bubble collapses which explains the better efficiency [157,163]. There are however contradictory results

about the effect of cavitation number on efficiency. Wu et al. [158] determined higher destruction in the case of increasing cavitation number which they ascribed to higher turbulence. On the other hand, Batista et al. and Xu et al. [157,163] determined better efficiencies with decreasing cavitation number.

Some authors also commented on the correlation between cell concentration and cavitation effectiveness. Xu et al. [163] showed that lower initial concentration yielded better results. Kim et al. [156] observed that in diluted samples the damage to cells is less since interactions between cells and cavitation bubbles are diminished. Halim et al. [161] determined an open-down parabolic relationship between cell destruction and initial concentration. On the other hand, Greenly and Tester [48] showed that concentration does not play an important role but postulated that the volume of the sample may be important for cavitation efficiency. They determined that in the first few seconds the breakage of *Chlamydomonas* sp. cells is the highest.

**Table 6**  
Review of cavitation effects on algae reported in the literature.

Species	Characteristics (diameter, shape)	Medium	Conc. (cell/mL, wt (%)*)	Proposed mechanism	US freq. (kHz)	Effectiveness (%)			Time (min)	Ref.
						LFUS	HFUS	HC		
<i>Chlamydomonas</i> species	3–10 µm spherical thin cell wall	GM	5.5 × 10 <sup>7</sup> –10 <sup>8</sup>	/	1100	85 <sup>a</sup>			7	[46]
		GM	0.007*	/	20	85 <sup>c</sup>			1.7	[48]
		GM	10 <sup>7</sup>	M	20 1146	85 <sup>c</sup> 99 <sup>c</sup>			5.2 2.5	[52]
<i>Chlorella kessleri</i>	2–3 µm ellipsoidal. [169]	GM	1.5 × 10 <sup>6</sup>	/	—				neg	[167]
		GM	2 × 10 <sup>6</sup>	/	20	0 <sup>c</sup>			20	[19]
<i>Chlorococcum</i> species	10–15 µm ellipsoidal thick cell wall [170]	TP	9.5 × 10 <sup>3</sup> 65.5 × 10 <sup>3</sup>	/	40	5 <sup>c</sup>			25	[164]
<i>Dunaliella salina</i>	1.5–3 µm ovoid irregular cell wall	GM	10 <sup>7</sup>	M	1146 20	99 <sup>c</sup> 99 <sup>c</sup>			1.1 5.2	[52]
<i>Isochrysis galbana</i>	5 µm lacking cell wall	TP	0.5*	/	20	85 <sup>c</sup>			0.4	[48]
<i>Nannochloropsis</i> species	1.3–4 µm spherical robust cell wall	TP	0.5*	/	20	55 <sup>c</sup>			2	[48]
		/	1.1 × 10 <sup>10</sup>	M	20 4300	19 <sup>c</sup> 90 <sup>c</sup>			10	[59]
<i>Scenedesmus</i> species	6–8 µm bean shaped [171]	GM	1.9 × 10 <sup>8</sup>	/	—				13 <sup>d</sup>	[156]
		GM	5.2 × 10 <sup>4</sup>	M + C	—				4p 85 <sup>c</sup>	[157]

LFUS: low frequency ultrasound; HFUS: high frequency ultrasound; HC: hydrodynamic cavitation; GM: growth medium; TP: tap water; M: mechanical damage; C: chemical damage; a: chlorophyll release; b: protein release; c: cell reduction; d: dry cell weight reduction; neg: increased cell concentration; p: number of passes; /: data not available.

From the data summarized in Tables 5 and 6 there doesn't seem to be any obvious correlation between the size and shape of the cell and its destruction. However, Wang et al. [49] proposed that cell size, shape or structure could all play an important role in microorganism's destruction when they determined different susceptibility of *Nannochloropsis* sp. and *Scenedesmus* sp. There might however be some correlation between cell wall structure and cavitation efficiency. For example, *Chlamydomonas* sp. and *Dunaliella salina* which have a thin and irregular cell wall, respectively, were both destructed to high degree with all AC frequencies investigated. Greenly and Tester [48] observed that *Nannochloropsis oculata*, which has a robust cell wall, is the most resilient of the species tested. The only microalgae that did not seem to be affected by cavitation were *Chlorella kessleri* and *Chlorococcum* sp. Rajasekhar et al. [19] postulated that this is due to the lack of gas vacuoles, while Halim et al. [164] postulated that the thickness of the cell wall was the culprit. Kim et al. [156] proposed that lower reductions of *Nannochloropsis salinas* were the result of the lack of gas vacuoles and cell structure which is mostly composed of algaelan and cellulose, that give it a more robust structure. Whether cell wall composition is the determining factor in microorganism's susceptibility to destruction with cavitation should be investigated more thoroughly.

Most authors still report that cyanobacteria destruction is in one way or another correlated to the rupture of gas vacuoles which is also in accordance with prior literature. With gas vacuoles ruptured the cyanobacteria lose their ability to float and start sinking to the bottom. Not getting enough light eventually leads to their demise. Gas vacuoles can presumably rupture when the resonance size of cavitation bubble and gas vacuoles are of the same size range [159]. Zhang et al. [159] calculated that at HFUS the sizes are in the same range which could be the reason for their better efficiencies observed in the case of *Microcystis* sp. Jachlewski et al. [43] for example observed that cells without gas vacuoles were also susceptible to HFUS and Jančula et al. [167] achieved the destruction of gas vacuoles without damages to the membranes with HC (no release of toxins). Rajasekhar et al. [19] observed faster effects of LFUS towards *Anabaena* sp. as compared to *Microcystis* sp. under the same treatment conditions, which they ascribed to the former having weaker vacuoles. They also observed no effects on *C. kessleri* which lacked gas vacuoles. Rodriguez-Molares [168] observed immediate destruction of gas vacuoles with LPUS but also their recovery after 24 h. Their recovery however didn't influence the cyanobacteria sedimentation which was still progressing but at a slower pace. To conclude, Lürling and Tolman [154] summarized that the accuracy of calculations of the resonance frequency in the literature is doubtful, which is why more effort should be put into investigation of this.

Kotopoulos et al. [165] postulated a similar mechanism in the case of *Anabaena* sp. where the rupture of heterocyst's membrane is the consequence of US waves coming in resonance with it. Yamamoto et al. [52] proposed the same mechanism in the case of algae *Chlamydomonas concordia* cells, where the radii of the bubble generated by HFUS is supposed to be of the same size range as the algae cell, meaning it causes mechanical resonance of the cells and leads to their destruction. Kurokawa et al. [59] calculated resonance frequencies for *Chaetoceros* sp. and *Nannochloropsis* sp. and determined that they correlate well with the most effective frequency tested.

There are some other mechanisms proposed in the literature. One possibility for microalgae destruction could be the damage of the photosynthetic system (i.e. psycocyanins, chlorophyll) [17,29,43,155,163], which if compromised hinders cyanobacterial growth. Li et al. [17] for example determined a decrease of zeta potential for *Microcystis aeruginosa* after cavitation and proposed that this could lead to cell's instability and enhanced settleability. Jančula et al. [167] on the other hand observed no changes in metabolic activities after HC. Lee et al. [11] investigated *Tetraselmis suecica* and determined that HC causes periplasmic cell disruption with cell bodies intact (i.e. confined to cell wall and membrane) whereas AC causes cytoplasmic disruption with cells split open.

A lot of authors also determined changes in microalgae using SEM and TEM. Rajasekhar et al. and Lürling and Tolman [19,154] observed disrupted filaments which can inhibit the growth of *Anabaena* sp. and *Cylindrospermopsis raciborskii*. Halim et al. [164] observed no changes to *Chlorococcum* sp. under the microscope but they observed complete destruction of *T. suecica*. Xu et al. [163] observed several crucial changes in *M. aeruginosa*. There were changes in the internal layers of the cells, separation of cytoplasm from the cell, condensation and disrupted arrangement of thylakoid membrane in the centre of the cell and destruction of gas vesicles. Jachlewski et al. [43] detected dark membrane-like structures instead of gas vacuoles in natural samples of *M. aeruginosa*. In the laboratory culture that did not contain gas vacuoles they observed severe damage to the outer cell membrane. Li et al. [17] observed smooth cell surface, stripped of extracellular organic matter (EOM), cell rupture after 30 min and cell disintegration after 60 min exposure time. They also observed clear depressions on the cells which pointed to destruction of gas vacuoles. Adam et al. [6] observed changes on the surface of the *N. oculata* cells after LFUS treatment. They also observed disruption of the cell wall which they ascribed to physical effect of cavitation. Batista et al. [157] observed irreversible morphological damages caused to *Scenedesmus* sp. together with cell wall lesions, cavity formation and loss of flotation parts. On the other hand, Bigelow et al. [46] did not use the microscope but only postulated that complete cell fragmentation of *Chlamydomonas* sp. must take place because of the release of proteins and chlorophyll normally located inside the cells.

There are also inconsistencies in the literature whether radicals give any contribution to microalgae cell destruction. Zhang et al. [159] eliminated radicals as a possible mechanism since addition of radical scavenger didn't change their results, whereas Wu et al., Wang et al., Batista et al. and Xu et al. [29,49,157,163] ascribed higher cell reductions to more radicals formed. Joyce et al. [3] tried to give a more thorough explanation and tested the same intensities for HFUS and LFUS. They showed that higher frequencies are more effective and concluded that another important mechanism must be taking place at higher frequencies and proposed formation of a bigger number of radicals. Li et al. [17] observed a correlation between the number of free radicals and microalgae destruction, which starts when 'OH concentration is above 1 μmol/L and for the first time demonstrated that radicals formed during HC could have effect on microalgae cells. There is however data available in the literature that deals with destruction of microalgae with different oxidants alone. H<sub>2</sub>O<sub>2</sub> has been shown to have negative effects on cyanobacteria, algae and diatoms [172–174]. Mikuš et al. [173] detected changes in metabolic system, loss of membrane integrity, cell lysis of *M. aeruginosa* when high enough H<sub>2</sub>O<sub>2</sub> concentration was used. Drabkova et al. [107] additionally determined the negative effects of H<sub>2</sub>O<sub>2</sub> on the photosynthetic system. Gu et al. [175] determined that 'OH formed under photocatalysis were responsible for the first radical-initiated changes in the cyanobacteria outer layer, which eventually led to leakage of cell inclusions like chlorophyll a and proteins. Bai et al. [176] treated algae *Heterosigma akashiwo* and *Skeletonema costatum* with 'OH produced by a novel, very efficient treatment system. When they combined plasma with HC, they observed gaps formed in cell membranes. Since no cellular material leaked from the cells, they speculated that the reason for this is that 'OH passed through these gaps into the cells and caused irreversible damage to DNA.

#### 4.5. Effects of cavitation on viruses

As can be seen in the Table 7 there is not much new data available about effects of cavitation on different types of viruses and only one article is available that studied effectiveness of HC.

MS2 seems very susceptible to inactivation with all types of cavitation [2,51,61] regardless of the initial concentration and medium tested only that in the case of higher concentrations more time for

**Table 7**  
Review of cavitation effects on viruses reported in the literature in the last decade.

Species	Characteristic (diameter)	Medium	Conc. PFU/mL	Proposed mechanism	US freq. (kHz)	Effectiveness (%)			Ref.
						LFUS	HFUS	HC	
MS2 bacteriophage	24–27 nm [113]	BS	10 <sup>6</sup>	/	20	4.62 <sup>a</sup>	30 <sup>b</sup>	[51]	
		BS	10 <sup>4</sup>	/	582	≥3.99 <sup>a</sup>	10 <sup>b</sup>		
		TW	10 <sup>3</sup> –10 <sup>4</sup>	M + C	—	≥99	30	[2]	
Feline calicivirus (FCV-F9)	27–40 nm [113]	BS	10 <sup>6</sup>	/	20	2.67 <sup>a</sup>	30 <sup>b</sup>	[51]	
		BS	10 <sup>4</sup>	/	582	≥4.00 <sup>a</sup>	5 <sup>b</sup>		
Φ X174 bacteriophage	23–27 nm [113]	BS	10 <sup>3</sup> –10 <sup>4</sup>	/	582	90	18	[2]	
Murine norovirus (MNV-1)	28–35 nm [113]	BS	10 <sup>6</sup>	/	20	0.07 <sup>a</sup>	30 <sup>b</sup>	[51]	
		BS	10 <sup>4</sup>	/	—	≥3.79 <sup>a</sup>	30 <sup>b</sup>		

LFUS: low frequency ultrasound; HFUS: high frequency ultrasound; HC: hydrodynamic cavitation; BS: buffer solution; TW: tap water; a: log reduction; b: pulsed mode 30 s on 30 s off; p: number of passes (1L samples); /: data not available.

inactivation was needed [51,61]. The same can be deducted in the case of FCV-F9 and ΦX174 [2,51]. MNV-1 also proved susceptible to inactivation but only in low titres [51] and the authors didn't offer any speculations on the reason why. In the case of MS2, Kosei et al. [61] observed that higher inactivation was achieved when bigger volumes were tested (1 L). This was ascribed to development of more aggressive cavitation in the bigger HC design. Since the cloud radius before collapse is larger in bigger scale device more potent pressure pulse is therefore released, which results in greater effect.

The exact mechanism how cavitation causes virus inactivation is not yet elucidated and there is not yet an explicit mechanism (chemical or mechanical) responsible for the observed effects proposed. Su et al. [51] suggested that the damages inflicted during cavitation on the outer protein capsid itself or recognition sites on the capsid surface could be the reason for virus inactivation. Kosei et al. [61] summarized that 'OH generated during cavitation together with mechanical effects could be held responsible for virus inactivation by affecting viral capsid or genome. There is however a lot of data available in the literature that describes the effects of different oxidants and oxidation treatments (other than cavitation) on different viruses. Cho et al. [112] showed that the inactivation of MS2 phage was the result of OH radicals formed during TiO<sub>2</sub> photocatalysis. The 'OH caused the denaturation of proteins in the protective capsid. Pottage et al. [114] reported that H<sub>2</sub>O<sub>2</sub> vapour very effectively inactivates MS2 and suggested the mechanism behind is the formation of 'OH which can react with thiol groups present in the viral capsid, lipids and genome. Goyal et al. [177] demonstrated the same effectiveness of H<sub>2</sub>O<sub>2</sub> for feline calicivirus. Mayer et al. [113] investigated effects of different water treatment processes on several different viruses, including the ones in Table 7. They showed that the amino acid composition of the capsid plays an important role in virus inactivation with oxidative species. They reported that inactivation by 'OH is correlated with the amount of amino acid tyrosine present in the capsid. To conclude, based on the available literature the composition of the viral outer capsid and the oxidising species in question plays an important role in the pathway of virus inactivation [96,113]. For example, the capsid composition might be responsible for longer inactivation time needed for ΦX1 v74 (hydrophilic capsid) as compared to MS2 (hydrophobic capsid) [2] under the same treatment conditions.

## 5. Discussion and recommendations

### 5.1. Why is it so difficult to compare the data from the literature?

#### 5.1.1. Microbiological aspect

In the reviewed literature authors used organisms at different growth phases for their experiments, but not many investigated its effect on cavitation efficiency. Gao et al. [88] for example observed that

bacteria are of different shape in different growth phases. They proposed that due to this, bacteria could have different biological and physical properties which may both influence the effect of LFUS on bacteria destruction. However, the same authors showed that the rate of destruction of bacteria is comparable regardless of their growth phase in experiments with HFUS [99]. Similarly, Zhang et al. [159] did not find any effect of algae growth phase using LFUS. In contrast, Balasundaram and Harrison [121] noticed higher protein release in rapidly growing *E. coli*. They summarized that slow growing bacteria could strengthen their cell wall which would result in lower destruction rates.

Normally, microorganisms are incubated in growth medium to promote their growth. On the other side, for cavitation, a non-complex water medium is desired as different mediums can affect the cavitation phenomenon [38,50,51]. Therefore, some authors used distilled or deionized water (i.e. purified water) as treatment medium or as a part of culture preparation [40,86,117,122,123,127,149,178]. Purified water has a negative effect on bacteria since it acts as a hypotonic solution, which leads to cell swelling and possible cell burst. Therefore, it could influence the results [117,160]. It is assumed that medium can affect cavitation phenomenon, whereas Loraine et al. [93] postulated that more complex matrix as sewage water does not affect disinfection by HC.

Another problem arises when authors report results on a different scale – logarithmic or decimal. When inactivation results are presented in percentages, 90% sounds like a high number but it only means 1 log in a log scale. With microorganisms, we are dealing with population numbers up to 10<sup>8</sup> or even more. Hypothetically, if initial culture concentration is 10<sup>4</sup> CFU/mL and inactivation rate after treatment is 90%, there are still 10<sup>3</sup> active cells left in suspension. After microorganism's doubling, the cell number is soon going to be even higher than before treatment and therefore the effect of inactivation is nullified.

To determine the effect of treatment, most authors employed the classical plate count method, which is a retrospective method. Additionally, some bacteria in the environment cannot be cultured but are metabolically active cells (VBNC). For example, pathogens in a VBNC state may remain virulent and produce enterotoxins. Therefore, culture-independent techniques are superior to the plate count method for real-time, quantitative assessment of cell viability and functionality. For example, flow cytometry has greater sensitivity compared to classical plate count method [55,125]. When implementing retrospective methods, it is also important to pay attention of keeping samples on ice to reduce cell activity and therefore minimize differences of handling time.

Even though not many authors in the reviewed literature dedicated much thought to these aspects and others not emphasized in this review paper, they could play an important role in cavitation efficiency. Until the effects of growth phase, cell wall integrity and medium on

susceptibility of microorganisms to destruction with cavitation are unequivocally determined, it is difficult to compare the literature data. Similarly, the same can be said for results presentation and detection methods.

#### 5.1.2. Cavitational aspect

Even though cavitation was first observed on ship propellers in 19th century, it is still not fully understood. Due to its complexity and unpredictable nature, the progress in revealing its behaviour and consequences, is slow. Since the mechanisms, that might affect microorganism's destruction are not known, it is extremely difficult to optimise the cavitation treatment. That all details of cavitation phenomenon are still not completely understood can be seen in the reviewed literature. Most of the authors only report that cavitation is present but do not give any specifics on its characteristics. Not only the dispersity of investigated operating conditions, but also their vague description is the reason for poorly reproducible results. The researchers should also clearly state if the sample is in direct or indirect contact with the surface emitting ultrasound.

One of the parameters, generally not adequately described is the intensity of cavitation. As mentioned in Section 2, there is no consensus on the definition of cavitation intensity yet. Despite that, reporting only the electrical power consumption of the cavitating device does not suffice [6,24,41]. Calorimetry is a good method how to estimate the energy, which is actually delivered to the liquid [3]. However, one must be aware that the properties of the generated cavitation will depend also on the surface area, through which the energy is delivered. If the diameter of the US horn tip or the dimensions of the US bath are missing, the experiments are once more impossible to reproduce.

When describing HC operating conditions, the influence of inlet pressure, flow rate or velocities in the constrictions are often considered as critical factors influencing results. Based on previously mentioned parameters cavitation number is often determined and premature conclusions are made i.e. that the highest removal rate is conditioned by this parameter. Since cavitation number itself only vaguely describes the cavitation characteristics [102], most authors misinterpret the results or draw non-relevant conclusions. One must be aware that cavitation behaviour depends on many mutually influencing operating parameters and that changing one of them, will also influence all other parameters. Thus, concluding that one specific parameter influences the results might be misleading. Additionally, by not determining the actual power consumption of cavitating set-ups (i.e. pump together with RS devices) but reporting only the nominal electrical power leads to misconclusions of energy efficiency of the system. Based on the emphasized aspects the conclusions from the reviewed literature are difficult to compare.

#### 5.1.3. Chemical aspect

As discussed in Section 4 different cavitational conditions (i.e. cavitation type, cavitation device and sample treated), can lead to formation of different amounts of reactive species. The pathway of reactive species formation during cavitation is very complex which is implicitly presented in Gagol et al. [98]. Similarly, that different oxidants can provoke various outcomes in microorganisms is discussed in Wigginton et al. [96]. In addition, it should also be taken into consideration that microorganisms can defend themselves against these species but only to a certain degree. Once their defence mechanisms are depleted oxidative stress ensues. It is for example postulated that nutrients present in microorganism's growth medium could influence their defence mechanisms [130]. Additionally, Vázquez et al. [179] reported that "domesticated" laboratory strains compared to environmental strains proved more resistant to oxidative stress. In addition, Gao et al. [99] noticed that radicals formed during cavitation decreased the pH of the solution, which could consequently inactivate investigated microorganisms. Thus, it is evident that a more systematic investigation on the effects of oxidants on different microorganisms must be performed.

It should however be emphasized that even though above-mentioned considerations are taken into account there will always be something else to consider.

Therefore, currently it is hard to compare the available literature since these considerations are not taken into account by most authors. Likewise, it is impossible to conclude whether reactive species induced by cavitation have any effect on microorganism's destruction based on the reviewed literature. A lot of the authors only assumed that radicals could be responsible for microorganism's destruction and cited previous literature but did not corroborated their assumptions in any way (for example by addition of radical scavenger).

#### 5.2. Recommendations and the way forward

- Even though not many authors of the reviewed literature tackle the topic of microorganism's growth phase we recommend that in the future the investigations should be done on microorganisms in stationary phase. In this manner it will be much easier to compare the results and determine if and how growth phase influences effect of cavitation.
- Similarly, to more easily compare the results we recommend that presenting results in logarithmic values is more appropriate.
- Considering the aspect of cavitation, the researchers should report the accurate description of the cavitating geometry. In addition, when possible, images of the cavitation should be provided. These should be, whenever possible, accompanied by measurements of pressure fluctuations which should be reported.
- We observed that many authors use cavitation number as the key parameter, that vaguely describes the cavitation stage. We recommend that together with this they should also give the precise location of pressure measurements, the flow rate, the position of the velocity measurement and the medium temperature (as it was already called upon by Šarc et al. [102]).
- Additionally, the specifics of the medium characteristics, such as pre-treatment (i.e. filtration, deionisation and distillation), the gas and solid particle content, should accompany every report.
- To determine the role of reactive species we recommend that first it should be unequivocally determined whether reactive species are generated during cavitation. Since microorganisms can tolerate oxidative stress to a certain degree, it should be determined which reactive species and in what amount are generated. Only then it would be prudent to determine whether formed species are responsible for destruction of microorganisms.
- The most important oxidants that should always be determined, if authors want to suggest that reactive species are the reason for microorganism's destruction, are  $H_2O_2$  and  $\cdot OH$ . There are numerous different determination methods already described in detail in the literature. Once this is determined also more specific effects of how radicals affect microorganisms should be elucidated by studying which cell constituent is affected (i.e. cell wall and/or intracellular components).

#### 6. Conclusions

As it can be seen from the summarized literature data there are a lot of inconsistencies. It is evident that most of the research is focused on AC and that investigations on the potential of HC for microorganism's destruction have only recently gained more attention. It is also evident that there has not been much progress in terms of developing new ways of cavitation generation especially in the case of HC.

The biggest problem is that most authors only cite previous assumptions regarding cavitation's mechanisms of action and they neither investigate nor offer additional and corroborated new possibilities.

There is however a consensus that a method that would be able to destroy microorganisms in environmental samples or food industry is needed. Cavitation may prove to be such a method and one that could

satisfy all requirements – effectively and relatively quickly destroy microorganisms without any collateral damage such as production of secondary pollutants. But in order to use it most efficiently (to exploit it to its highest potential) the exact mechanisms by which it interacts with microorganisms must be elucidated. This can only be done if scientists from different scientific fields join forces – and this is what ERC project CABUM will focus on in the next 5 years.

#### Acknowledgements

The authors acknowledge the financial support from the Slovenian Research Agency (Core funding No. P2-0401 and Project No. Z2-8188) and the European Research Council (ERC) under the European Union's Framework Program for research and innovation, Horizon 2020 (grant agreement n° 771567 — CABUM).

#### Appendix A. Supplementary data

Supplementary data to this article can be found online at <https://doi.org/10.1016/j.ultrch.2019.05.009>.

#### References

- [1] D. Spiteri, C. Chot-Plassat, J. Seclar, K.A. Karatzas, C. Scerri, V.P. Valdramidis, Ultrasound processing of liquid system(s) and its antimicrobial mechanism of action, *Lett. Appl. Microbiol.* 65 (2017) 313–318, <https://doi.org/10.1111/lam.12776>.
- [2] C.V. Chrysikopoulos, I.D. Manariotis, V.I. Syrigou, Virus inactivation by high frequency ultrasound in combination with visible light, *Colloids Surfaces B Biointerfaces* 107 (2013) 174–179, <https://doi.org/10.1016/j.colsurfb.2013.01.038>.
- [3] E.M. Joyce, X. Wu, T.J. Mason, Effect of ultrasonic frequency and power on algae suspensions, *J. Environ. Sci. Health Part A* 45 (2010) 863–866, <https://doi.org/10.1016/j.ultrch.2014.11.002>.
- [4] A.C. Soria, M. Villamil, Effect of ultrasound on the technological properties and bioactivity of food: a review, *Trends Food Sci. Technol.* 21 (2010) 323–331, <https://doi.org/10.1016/j.tifs.2010.04.003>.
- [5] A. Režek Jambrak, M. Simunek, S. Evačić, K. Markov, G. Smoljanović, J. Frece, Influence of high power ultrasound on selected moulds, yeasts and *Alicyclobacillus acidoterrestris* in apple, cranberry and blueberry juice and nectar, *Ultronics* 83 (2018) 3–17, <https://doi.org/10.1016/j.ultras.2017.02.011>.
- [6] F. Adams, M. Abert-Vian, G. Peltier, F. Chemat, "Solvent-free" ultrasound-assisted extraction of lipids from fresh microalgae cells: a green, clean and scalable process, *Bioresour. Technol.* 114 (2012) 457–465, <https://doi.org/10.1016/j.biortech.2012.02.096>.
- [7] F. Chemat, N. Rombaut, A.G. Sciaire, A. Meullemeestre, A.S. Fabiano-Tixier, M. Abert-Vian, Ultrasound assisted extraction of food and natural products. Mechanisms, techniques, combinations, protocols and applications: a review, *Ultron. Sonochem.* 34 (2017) 540–560, <https://doi.org/10.1016/j.ultrch.2016.06.035>.
- [8] D. Liu, L. Ding, J. Sun, N. Bouissetta, E. Vorobiev, Yeast cell disruption strategies for recovery of intracellular bio-active compounds — a review, *Innov. Food Sci. Emerg. Technol.* 36 (2016) 181–192, <https://doi.org/10.1016/j.ifset.2016.04.017>.
- [9] V.D. Farkade, S.T.L. Harrison, A.B. Pandit, Improved cavitation cell disruption following pH pretreatment for the extraction of β-galactosidase from *Kluveromyces lactis*, *Biochem. Eng. J.* 31 (2006) 25–30, <https://doi.org/10.1016/j.bej.2006.05.015>.
- [10] A.K. Lee, D.M. Lewis, P.J. Ashman, Disruption of microalgal cells for the extraction of lipids for biofuels: processes and specific energy requirements, *Biomass Bioenergy* 46 (2012) 89–101, <https://doi.org/10.1016/j.biombioe.2012.06.034>.
- [11] I. Lee, J.J. Han, Simultaneous treatment (cell disruption and lipid extraction) of wet microalgae using hydrodynamic cavitation for enhancing the lipid yield, *Bioresour. Technol.* 186 (2015) 246–251, <https://doi.org/10.1016/j.biortech.2015.03.045>.
- [12] T. Yusaf, R.A. Al-Juboori, Alternative methods of microorganism disruption for agricultural applications, *Appl. Energy* 114 (2014) 909–923, <https://doi.org/10.1016/j.apenergy.2013.08.085>.
- [13] S.T.L. Harrison, Bacterial cell disruption: a key unit operation in the recovery of intracellular products, *Biotechnol. Adv.* 9 (1991) 217–240.
- [14] S. Drakopoulou, S. Terzakis, M.S. Fountoulakis, D. Mantzarinos, T. Manios, Ultrasound-induced inactivation of gram-negative and gram-positive bacteria in secondary treated municipal wastewater, *Ultron. Sonochem.* 16 (2009) 629–634, <https://doi.org/10.1016/j.ultrch.2008.11.011>.
- [15] H. Ohrdes, I. Ille, J. Twiefel, J. Wallaschek, R. Nogueira, K.-H. Rosenwinkel, A control system for ultrasound devices utilized for inactivating *E. coli* in wastewater, *Ultron. Sonochem.* 40 (2018) 158–162, <https://doi.org/10.1016/j.ultrch.2017.04.017>.
- [16] H. Zou, L. Wang, The disinfection effect of a novel continuous-flow water sterilizing system coupling dual-frequency ultrasound with sodium hypochlorite in pilot scale, *Ultron. Sonochem.* 36 (2017) 246–252, <https://doi.org/10.1016/j.ultrch.2016.11.041>.
- [17] P. Li, Y. Song, S. Yu, Removal of *Microcystis aeruginosa* using hydrodynamic cavitation: performance and mechanisms, *Water Res.* 62 (2014) 241–248, <https://doi.org/10.1016/j.watres.2014.05.052>.
- [18] P. Rajsekhar, L. Fan, T. Nguyen, F.A. Roddick, A review of the use of sonication to control cyanobacterial blooms, *Water Res.* 46 (2012) 4319–4329, <https://doi.org/10.1016/j.watres.2012.05.054>.
- [19] P. Rajsekhar, L. Fan, T. Nguyen, F.A. Roddick, Impact of sonication at 20kHz on *Microcystis aeruginosa*, *Anabaena circinalis* and *Chlorella* sp., *Water Res.* 46 (2012) 1473–1481, <https://doi.org/10.1016/j.watres.2011.11.017>.
- [20] P. Piyantha, E. Mohareb, R.C. McKellar, Inactivation of microbes using ultrasound: a review, *Int. J. Food Microbiol.* 87 (2003) 207–216, [https://doi.org/10.1016/S0168-1605\(03\)00075-8](https://doi.org/10.1016/S0168-1605(03)00075-8).
- [21] P.R. Gogate, Application of cavitation reactors for water disinfection: current status and path forward, *J. Environ. Manage.* 85 (2007) 801–815, <https://doi.org/10.1016/j.jenvman.2007.07.001>.
- [22] X. Wu, E.M. Joyce, T.J. Mason, The effects of ultrasound on cyanobacteria, *Harmful Algae* 10 (2011) 738–743, <https://doi.org/10.1016/j.ultrch.2016.02.020>.
- [23] M.H. Dehghani, Removal of cyanobacterial and algal cells from water by ultrasonic waves — a review, *J. Mol. Liq.* 222 (2016) 1109–1114, <https://doi.org/10.1016/j.molliq.2016.08.010>.
- [24] B.A. Wordon, B. Mortimer, L.D. McMaster, Comparative real-time analysis of *Saccharomyces cerevisiae* cell viability, injury and death induced by ultrasound (20kHz) and heat for the application of hurdle technology, *Food Res. Int.* 47 (2012) 134–139, <https://doi.org/10.1016/j.foodres.2011.04.038>.
- [25] X. He, Y.L. Liu, A. Conklin, J. Westrick, L.K. Weavers, D.D. Dionysiou, J.J. Lenhart, P.J. Mouser, D. Szlag, H.W. Walker, Toxic cyanobacteria and drinking water: Impacts, detection, and treatment, *Harmful Algae* 54 (2016) 174–193, <https://doi.org/10.1016/j.hal.2016.01.001>.
- [26] F. Chemat, Zill-E-Huma, M.K. Khan, Applications of ultrasound in food technology: processing, preservation and extraction, *Ultron. Sonochem.* 18 (2011) 813–835, <https://doi.org/10.1016/j.ultrch.2010.11.023>.
- [27] P.R. Gogate, Hydrodynamic cavitation for food and water processing, *Food Bioprocess Technol.* 4 (2011) 996–1011, <https://doi.org/10.1007/s11947-010-0418-1>.
- [28] J.P.B. de São José, N.J. de Andrade, A.M. Ramos, M.C.D. Vanetti, P.C. Stringheta, J.B.P. Chaves, Decontamination by ultrasound application in fresh fruits and vegetables, *Food Control* 45 (2014) 36–50, <https://doi.org/10.1016/j.foodcont.2014.04.015>.
- [29] X. Wu, E.M. Joyce, T.J. Mason, Evaluation of the mechanisms of the effect of ultrasound on *Microcystis aeruginosa* at different ultrasonic frequencies, *Water Res.* 46 (2012) 2851–2858, <https://doi.org/10.1016/j.watres.2012.02.019>.
- [30] H. Yu, S. Chen, P. Cao, Synergistic bactericidal effects and mechanisms of low intensity ultrasound and antibiotics against bacteria: a review, *Ultron. Sonochem.* 19 (2012) 377–382, <https://doi.org/10.1016/j.ultrch.2011.11.010>.
- [31] G. Huang, S. Chen, C. Dai, L. Sun, W. Sun, Y. Tang, F. Xiong, R. He, H. Ma, Effects of ultrasound on microbial growth and enzyme activity, *Ultron. Sonochem.* 37 (2017) 144–149, <https://doi.org/10.1016/j.ultrch.2016.12.018>.
- [32] J.P. Franc, J.M. Michel, *Fundamentals of Cavitation*, Kluwer Dordrecht, 2004 doi: 10.1007/s13398-014-0173-7\_2.
- [33] C.E. Brennen, *Cavitation and Bubble Dynamics*, Oxford University Press, 1995.
- [34] G.L. Chahine, C.-T. Hsiao, Modelling cavitation erosion using fluid–material interaction simulations, *Interface Focus* 5 (5) (2015) 20150016, <https://doi.org/10.1098/rsfs.2015.0016>.
- [35] K.S. Sudlick, N.C. Eddingsaas, D.J. Flannigan, S.D. Hopkins, H. Xu, Extreme conditions during multibubble cavitation: sonoluminescence as a spectroscopic probe, *Ultron. Sonochem.* 18 (2011) 842–846, <https://doi.org/10.1016/j.ultrch.2010.12.012>.
- [36] S. Koda, T. Kimura, T. Kondo, H. Mitome, A standard method to calibrate sonochemical efficiency of an individual reaction system, *Ultron. Sonochem.* 10 (2003) 149–156, [https://doi.org/10.1016/S1350-4177\(03\)00084-1](https://doi.org/10.1016/S1350-4177(03)00084-1).
- [37] T.J. Mason, Ultron. cleaning: an historical perspective, *Ultron. Sonochem.* 29 (2016) 519–523, <https://doi.org/10.1016/j.ultrch.2015.05.004>.
- [38] R.A. Al-Juboori, V. Aravindhan, T. Yusaf, Impact of pulsed ultrasound on bacteria reduction of natural waters, *Ultron. Sonochem.* 27 (2015) 137–147, <https://doi.org/10.1016/j.ultrch.2015.05.007>.
- [39] G. Hunter, M. Lucas, I. Watson, R. Parton, A radial mode ultrasonic horn for the inactivation of *Escherichia coli* K12, *Ultron. Sonochem.* 15 (2008) 101–109, <https://doi.org/10.1016/j.ultrch.2006.12.017>.
- [40] D. Liu, X.A. Zeng, D.W. Sun, Z. Han, Disruption and protein release by ultra-sonication of yeast cells, *Innov. Food Sci. Emerg. Technol.* 18 (2013) 132–137, <https://doi.org/10.1016/j.ifset.2013.02.006>.
- [41] T. Monsen, E. Lövgren, M. Widerström, L. Wallinder, In vitro effect of ultrasound on bacteria and suggested protocol for sonication and diagnosis of prosthetic infections, *J. Clin. Microbiol.* 47 (2009) 2496–2501, <https://doi.org/10.1128/JCM.02316-08>.
- [42] A. Šarc, M. Oder, M. Dular, Can rapid pressure decrease induced by super-cavitation efficiently eradicate *Legionella pneumophila* bacteria? *Desalin. Water Treat.* 57 (2014) 2184–2194, <https://doi.org/10.1080/19443994.2014.972940>.
- [43] S. Jachiewski, M. Botes, T.E. Cloete, The effect of ultrasound at 256 KHz on *Microcystis aeruginosa*, with and without gas vacuoles, *Water SA* 39 (2013) 171–174, <https://doi.org/10.4314/wsa.v39i1.17>.
- [44] S. Bystryak, R. Santocký, A.S. Peshkovsky, Cell disruption of *S. cerevisiae* by

- scalable high-intensity ultrasound, *Biochem. Eng. J.* 99 (2015) 99–106, <https://doi.org/10.1016/j.bej.2015.03.014>.
- [45] M. Versoza, W. Jung, M.L. Barabád, Y. Lee, K. Choi, D. Park, Inactivation of filter bound aerosolized MS2 bacteriophages using a non-conductive ultrasound transducer, *J. Virol. Methods* 255 (2018) 76–81, <https://doi.org/10.1016/j.jviromet.2018.02.015>.
- [46] T.A. Bigelow, J. Xu, D.J. Steessman, L. Yao, M.H. Spalding, T. Wang, Lysis of *Chlamydomonas reinhardtii* by high-intensity focused ultrasound as a function of exposure time, *Ulrasön. Sonochem.* 21 (2014) 1258–1264, <https://doi.org/10.1016/j.ultsonch.2013.11.014>.
- [47] E.S. Ingugla, B.K. Tiwari, J.P. Kerr, C.M. Burgess, Effects of high intensity ultrasound on the inactivation profiles of *Escherichia coli* K12 and *Listeria innocua* with salt and salt replacers, *Ulrasön. Sonochem.* 48 (2018) 492–498, <https://doi.org/10.1016/j.ultsonch.2018.05.007>.
- [48] J.M. Greenly, J.W. Tester, Ultrasonic cavitation for disruption of microalgae, *Bioresour. Technol.* 184 (2015) 276–279, <https://doi.org/10.1016/j.biortech.2014.11.036>.
- [49] M. Wang, W. Yuan, X. Jiang, Y. Jing, Z. Wang, Disruption of microalgal cells using high-frequency focused ultrasound, *Bioresour. Technol.* 153 (2014) 315–321, <https://doi.org/10.1016/j.biortech.2013.11.054>.
- [50] M. Cameron, L.D. McMaster, T.J. Britz, Electron microscopic analysis of dairy microbes inactivated by ultrasound, *Ulrasön. Sonochem.* 15 (2008) 960–964, <https://doi.org/10.1016/j.ultsonch.2008.02.012>.
- [51] X. Su, S. Zivanovic, D.H. D’Souza, Inactivation of human enteric virus surrogates by high-intensity ultrasound, *Foodborne Pathog. Dis.* 7 (2010) 1055–1061, <https://doi.org/10.1089/fpd.2009.0515>.
- [52] K. Yamamoto, P.M. King, X. Wu, T.J. Mason, E.M. Joyce, Effect of ultrasonic frequency and power on the disruption of algae cells, *Ulrasön. Sonochem.* 24 (2015) 165–171, <https://doi.org/10.1016/j.ultsonch.2014.11.002>.
- [53] H. Lee, B. Zhou, W. Liang, H. Feng, S.E. Martin, Inactivation of *Escherichia coli* cells with sonication, monosonation, thermonication, and manothermonication: Microbial responses and kinetics modeling, *J. Food Eng.* 93 (2009) 354–364, <https://doi.org/10.1016/j.jfoodeng.2009.01.037>.
- [54] A. Al-Bsoul, J.P. Magnin, N. Commeyre-Berne, N. Gondrexon, J. Willison, C. Petrier, Effectiveness of ultrasound for the destruction of *Mycobacterium* sp. strain (6PV1), *Ulrasön. Sonochem.* 17 (2010) 106–110, <https://doi.org/10.1016/j.ultsonch.2009.04.005>.
- [55] E. Joyce, A. Al-Hashimi, T.J. Mason, Assessing the effect of different ultrasonic frequencies on the bacterial viability using flow cytometry, *J. Appl. Microbiol.* 110 (2011) 862–870, <https://doi.org/10.1111/j.1365-2672.2011.04923.x>.
- [56] S. Koda, M. Miyamoto, T. Toma, T. Matsuka, M. Maebayashi, Inactivation of *Escherichia coli* and *Streptococcus mutans* by ultrasound at 500 kHz, *Ulrasön. Sonochem.* 16 (2009) 655–659, <https://doi.org/10.1016/j.ultsonch.2009.02.003>.
- [57] L.J. Bastarrachea, M. Walsh, S.P. Wrenn, R.V. Tikekar, Enhanced antimicrobial effect of ultrasound by the food colorant Erythrosin B, *Food Res. Int.* 2017 (2017) 344–351, <https://doi.org/10.1016/j.foodres.2017.07.012>.
- [58] M.J. Abeledo-Lameiro, E. Ares-Mazás, H. Gómez-Couso, Use of ultrasound irradiation to inactivate *Cryptosporidium parvum* oocysts in effluents from municipal wastewater treatment plants, *Ulrasön. Sonochem.* 48 (2018) 118–126, <https://doi.org/10.1016/j.ultsonch.2018.05.013>.
- [59] M. Kurokawa, P.M. King, X. Wu, E.M. Joyce, T.J. Mason, K. Yamamoto, Effect of sonication frequency on the disruption of algae, *Ulrasön. Sonochem.* 31 (2016) 157–162, <https://doi.org/10.1016/j.ultsonch.2015.12.011>.
- [60] A. Šarc, J. Kosek, D. Stopar, M. Oder, M. Dular, Removal of bacteria *Legionella pneumophila*, *Escherichia coli*, and *Bacillus subtilis* by (super)cavitation, *Ulrasön. Sonochem.* 42 (2018) 228–236, <https://doi.org/10.1016/j.ultsonch.2017.11.004>.
- [61] J. Kosek, I. Gutiérrez-Aguirre, N. Rački, T. Dreo, M. Ravnikar, M. Dular, Efficient inactivation of MS-2 virus in water by hydrodynamic cavitation, *Water Res.* 124 (2017) 465–471, <https://doi.org/10.1016/j.watres.2017.07.077>.
- [62] M. Zupanc, T. Kosjek, M. Petkovsek, M. Dular, B. Kompare, B. Širok, Ž. Blažeka, E. Heath, Removal of pharmaceuticals from wastewater by biological processes, hydrodynamic cavitation and UV treatment, *Ulrasön. Sonochem.* 20 (2013) 1104–1122, <https://doi.org/10.1016/j.ultsonch.2012.12.003>.
- [63] M. Petkovsek, M. Miklak, M. Levstek, M. Stražar, B. Širok, M. Dular, A novel rotation generator of hydrodynamic cavitation for waste-activated sludge disinfection, *Ulrasön. Sonochem.* 26 (2015) 408–414, <https://doi.org/10.1016/j.ultsonch.2015.01.006>.
- [64] M. Dular, I. Khalfa, S. Fuzier, M. Adama Maiga, O. Coutier-Delgosha, Scale effect on unsteady cloud cavitation, *Exp. Fluids* 53 (2012) 1233–1250, <https://doi.org/10.1007/s00348-012-1356-7>.
- [65] M.T. Madigan, K.S. Bender, D.H. Buckley, W.M. Sattley, D.A. Stahl, *Brock Biology of Microorganisms*, 13th ed., Pearson, Boston, 2012.
- [66] V. Vadillo-Rodríguez, J.R. Dutcher, Viscoelasticity of the bacterial cell envelope, *Soft Matter* 7 (2011) 4101–4110, <https://doi.org/10.1039/c0sm01054e>.
- [67] S. Semrau, T. Schmidt, Membrane heterogeneity – from lipid domains to curvature effects, *Soft Matter* 5 (2009) 3174–3186, <https://doi.org/10.1039/b901587i>.
- [68] X. Liao, J. Li, Y. Suo, S. Chen, X. Ye, D. Liu, T. Ding, Multiple action sites of ultrasound on *Escherichia coli* and *Staphylococcus aureus*, *Food Sci. Hum. Wellness* 7 (2018) 102–109, <https://doi.org/10.1016/j.fshw.2018.01.002>.
- [69] V.R.F. Matias, A. Al-Amoudi, J. Dubochet, T.J. Beveridge, Cryo-transmission electron microscopy of frozen-hydrated sections of *Escherichia coli* and *Pseudomonas aeruginosa*, *J. Bacteriol.* 185 (2003) 6112–6118, <https://doi.org/10.1128/JB.185.20.6112-6118.2003>.
- [70] D.E. Minnikin, Chemical principles in the organization of lipid components in the mycobacterial cell envelope, *Res. Microbiol.* 142 (1991) 423–427, [https://doi.org/10.1016/0923-2508\(91\)90114-P](https://doi.org/10.1016/0923-2508(91)90114-P).
- [71] J. Liu, C.E. Barry, G.S. Besra, H. Nikaido, Mycolic acid structure determines the fluidity of the mycobacterial cell wall, *J. Biol. Chem.* 271 (1996) 29545–29551.
- [72] D.E. Levin, Cell wall integrity signaling in *Saccharomyces cerevisiae*, *Microbiol. Mol. Biol. Rev.* 69 (2005) 262–291, <https://doi.org/10.1128/MMBR.69.2.262>.
- [73] R. Kollar, E. Petrakova, G. Ashwell, P.W. Robbins, E. Cabib, Architecture of the yeast cell wall: the linkage between chitin and b(1–3)-glucan, *J. Biol. Chem.* 270 (1995) 1170–1178.
- [74] R. Kollar, B.B. Reinhold, E. Petrakova, H.J.C. Yeh, G. Ashwell, J. Drgonova, J.C. Kapteyn, F.M. Klis, E. Cabib, Architecture of the yeast cell wall: b(1–6)-glucan interconnects mannoprotein, b(1–3)-glucan, and chitin, *J. Biol. Chem.* 272 (1997) 17762–17775.
- [75] F.M. Klis, P. Mol, K. Hellingwerf, S. Brul, Dynamics of cell wall structure in *Saccharomyces cerevisiae*, *FEMS Microbiol. Rev.* 26 (2002) 239–256, [https://doi.org/10.1016/S0168-6458\(02\)00087-6](https://doi.org/10.1016/S0168-6458(02)00087-6).
- [76] P. Sze, *A Biology of the Algae*, WCB/McGraw-Hill, The University of California, 1998.
- [77] B. Allard, J. Templier, Comparison of neutral lipid profile of various trilaminar outer cell wall (TLW)-containing microalgae with emphasis on algaenan occurrence, *Phytochemistry* 54 (2000) 369–380, [https://doi.org/10.1016/S0031-9422\(00\)00135-7](https://doi.org/10.1016/S0031-9422(00)00135-7).
- [78] D.S. Domozochy, M. Ciancia, J.U. Fangen, M.D. Mikkelson, P. Ulvsøv, W.G.T. Willats, The cell walls of green algae: a journey through evolution and diversity, *Front. Plant Sci.* 3 (2012) 1–7, <https://doi.org/10.3389/fpls.2012.00082>.
- [79] E. Pasche, Silicon content of five marine plankton diatom species measured with a rapid filter method, *Limnol. Oceanogr.* 25 (1980) 474–480, <https://doi.org/10.4319/lo.1980.25.3.0474>.
- [80] C.E. Hamm, R. Merkl, O. Springer, P. Jurkoj, C. Maiert, K. Prechtel, V. Smetacek, Architecture and material properties of diatom shells provide effective mechanical protection, *Nature* 421 (2003) 841–843, <https://doi.org/10.1038/nature01416>.
- [81] J.P.P.M. Smelt, Recent advances in the microbiology of high pressure processing, *Trends Food Sci. Technol.* 9 (1998) 152–158, [https://doi.org/10.1016/S0924-2244\(98\)00030-2](https://doi.org/10.1016/S0924-2244(98)00030-2).
- [82] J. Šmarž, D. Šmajš, J. Komrska, V. Krzyžánek, S-layers on cell walls of cyanobacteria, *Micron* 33 (2002) 257–260, [https://doi.org/10.1016/S0968-4328\(01\)0031-2](https://doi.org/10.1016/S0968-4328(01)0031-2).
- [83] T.A. Davis, B. Volesky, A. Mucci, A review of the biochemistry of heavy metal biosorption by brown algae, *Water Res.* 37 (2003) 4311–4330, [https://doi.org/10.1016/S0043-1354\(03\)00293-8](https://doi.org/10.1016/S0043-1354(03)00293-8).
- [84] L. Brown, J.M. Wolf, R. Prados-Rosales, A. Casadevall, Through the wall: Extracellular vesicles in Gram-positive bacteria, mycobacteria and fungi, *Nat. Rev. Microbiol.* 13 (2015) 620–630, <https://doi.org/10.1038/nrmicro3480>.
- [85] M.C. Morais, Breaking the symmetry of a viral capsid, *Proc. Natl. Acad. Sci.* 113 (2016) 11390–11392, <https://doi.org/10.1073/pnas.1613612113>.
- [86] L.M. Cerecedo, C. Dopazo, R. Gomez-Lus, Water disinfection by hydrodynamic cavitation in a rotor-stator device, *Ulrasön. Sonochem.* 48 (2018) 71–78, <https://doi.org/10.1016/j.ultsonch.2018.05.015>.
- [87] X. Sun, J.J. Park, H.S. Kim, S. Jin, S. Lee, A.S. Om, J.Y. Yoon, Experimental investigation of the thermal and disinfection performances of a novel hydrodynamic cavitation reactor, *Ulrasön. Sonochem.* 49 (2018) 13–23, <https://doi.org/10.1016/j.exphermater.2018.02.034>.
- [88] S. Gao, G.D. Lewis, M. Ashokkumar, Y. Hemar, Inactivation of microorganisms by low-frequency high-power ultrasound: 2. A simple model for the inactivation mechanism, *Ulrasön. Sonochem.* 21 (1) (2014) 454–460, <https://doi.org/10.1016/j.ultsonch.2013.06.007>.
- [89] B. Balasundaram, S.T.L. Harrison, Disruption of Brewers’ yeast by hydrodynamic cavitation: process variables and their influence on selective release, *Biotechnol. Bioeng.* 94 (2006) 303–311, <https://doi.org/10.1002/bit>.
- [90] S. Arrojo, Y. Benito, A. Martínez Tarifa, A parametrical study of disinfection with hydrodynamic cavitation, *Ulrasön. Sonochem.* 15 (5) (2008) 903–908, <https://doi.org/10.1016/j.ultsonch.2007.11.001>.
- [91] E.M. Joyce, T.J. Mason, Sonication used as a biocide: a review: Ultrasound as a greener alternative to chemical biocides? *Chim. Oggi.* 26 (2008) 22–26, <https://doi.org/10.1080/14040419.2014.929400>.
- [92] N.S.M. Yusof, B. Babgi, Y. Alghamdi, M. Aksu, J. Madhavan, M. Ashokkumar, Physical and chemical effects of acoustic cavitation in selected ultrasonic cleaning applications, *Ulrasön. Sonochem.* 29 (2016) 568–576, <https://doi.org/10.1016/j.ultsonch.2015.06.013>.
- [93] G. Loraine, G. Chahine, C.T. Hsiao, J.K. Choi, P. Aley, Disinfection of gram-negative and gram-positive bacteria using Dynafets hydrodynamic cavitating jets, *Ulrasön. Sonochem.* 20 (2012) 710–717, <https://doi.org/10.1016/j.ultsonch.2011.10.011>.
- [94] A.K. Lee, D.M. Lewis, P.J. Ashman, Microalgal cell disruption by hydrodynamic cavitation for the production of biofuels, *J. Appl. Phycol.* 27 (2015) 1881–1889, <https://doi.org/10.1007/s10811-014-0483-3>.
- [95] T. Yusaf, Experimental study of microorganism disruption using shear stress, *Biochem. Eng. J.* 79 (2013) 7–14, <https://doi.org/10.1016/j.bej.2013.07.001>.
- [96] K.R. Wiggington, B.M. Pescos, T. Sigstam, F. Bosshard, T. Kohn, Virus inactivation mechanisms: impact of disinfectants on virus function and structural integrity, *Environ. Sci. Technol.* 46 (2012) 12069–12078, <https://doi.org/10.1021/es3029473>.
- [97] M. Klavarotti, D. Mantzavinos, D. Kassinos, Removal of residual pharmaceuticals from aqueous systems by advanced oxidation processes, *Environ. Int.* 35 (2009) 402–417, <https://doi.org/10.1016/j.envint.2008.07.009>.
- [98] M. Gagol, A. Przyjazny, G. Boczkaj, Wastewater treatment by means of advanced

- oxidation processes based on cavitation – a review, *Chem. Eng. J.* 338 (2018) 599–627, <https://doi.org/10.1016/J.CEJ.2018.01.049>.
- [99] S. Gao, Y. Hemar, M. Ashokkumar, S. Patel, G.D. Lewis, Inactivation of bacteria and yeast using high-frequency ultrasound treatment, *Water Res.* 60 (2014) 93–104, <https://doi.org/10.1016/j.watres.2014.04.038>.
- [100] T.J. Mason, A.J. Cobley, J.E. Graves, D. Morgan, New evidence for the inverse dependence of mechanical and chemical effects on the frequency of ultrasound, *Ultrason. Sonochem.* 18 (2011) 226–230, <https://doi.org/10.1016/j.ultrsonch.2010.05.008>.
- [101] B. Balasundaram, S.T.L. Harrison, Optimising orifice geometry for selective release of periplasmic products during cell disruption by hydrodynamic cavitation, *Biochem. Eng. J.* 54 (2011) 207–209, <https://doi.org/10.1016/j.bej.2011.03.002>.
- [102] A. Sarc, T. Stepišnik-Perdih, M. Petkovšek, M. Dulat, The issue of cavitation number value in studies of water treatment by hydrodynamic cavitation, *Ultrason. Sonochem.* 30 (2017) 51–59, <https://doi.org/10.1016/j.ultrsonch.2016.05.020>.
- [103] P. Moradas-Ferreira, V. Costa, P. Piper, W. Mager, The molecular defences against reactive oxygen species in yeast, *Mol. Microbiol.* 19 (1996) 651–658, <https://doi.org/10.1046/j.1365-2958.1996.403940.x>.
- [104] Z.N. Kashmiri, S.A. Mankar, Free radicals and oxidative stress in bacteria, *Int. J. Curr. Microbiol. Appl. Sci.* 3 (2014) 34–40, <https://doi.org/10.1103/PhysRevC.62.014309>.
- [105] E.L. Steele, R.P. Learmonth, K. Watson, Stress tolerance and membrane lipid unsaturation in *Saccharomyces cerevisiae* grown aerobically or anaerobically, *Microbiology* 140 (1994) 569–576, <https://doi.org/10.1099/00221287-140-3-569>.
- [106] G. McDonnell, A.D. Russell, Antiseptics and disinfectants: activity, action, and resistance, *Clin. Microbiol. Rev.* 12 (1999) 147–179.
- [107] M. Drabikova, H.C.P. Matthijss, W. Admiraal, B. Marsalek, Selective effects of H2O2 on cyanobacterial photosynthesis, *Photosynthetica* 45 (2007) 363–369, <https://doi.org/10.3390/catal8100417>.
- [108] M.D. Labas, C.S. Lazar, R.J. Brandi, A.E. Cassano, Reaction kinetics of bacteria disinfection employing hydrogen peroxide, *Biochem. Eng. J.* 38 (2008) 78–87, <https://doi.org/10.1016/j.bej.2007.06.008>.
- [109] Y. Kobayashi, M. Hayashi, F. Yoshino, M. Tamura, A. Yoshida, H. Ibi, M.-C. Lee, K. Ochiai, B. Ogiso, Bactericidal effect of hydroxyl radicals generated from low concentration hydrogen peroxide with ultrasound in endodontic treatment, *J. Clin. Biochem. Nutr.* 54 (2014) 161–165, <https://doi.org/10.3164/jcbn.13>.
- [110] C.L. Hawkins, M.J. Davies, Generation and propagation of radical reactions on proteins, *Biochem. Biophys. Acta – Bioenergy* 1504 (2001) 196–219, [https://doi.org/10.1016/S0005-2728\(00\)00252-8](https://doi.org/10.1016/S0005-2728(00)00252-8).
- [111] M.J. Flores, R.J. Brandi, A.E. Cassano, M.D. Labas, Chemical disinfection with H2O2 – the proposal of a reaction kinetic model, *Chem. Eng. J.* 198–199 (2012) 388–396, <https://doi.org/10.1016/j.cej.2012.05.107>.
- [112] M. Cho, H. Chung, W. Choi, J. Yoon, Different inactivation behaviors of MS-2 phage and *Escherichia coli* in TiO2 photocatalytic disinfection, *Appl. Environ. Microbiol.* 71 (2005) 270–275, <https://doi.org/10.1128/AEM.71.1.270>.
- [113] B.K. Mayer, Y. Yang, D.W. Gerrity, M. Abbassadeegan, The impact of capsid proteins on virus removal and inactivation during water treatment processes, *microbiol. Insights* 8(2) (2015) MBL31441, <https://doi.org/10.4137/MBL31441>.
- [114] T. Pottage, C. Richardson, S. Parks, J.T. Walker, A.M. Bennett, Evaluation of hydrogen peroxide gaseous disinfection systems to decontaminate viruses, *J. Hosp. Infect.* 74 (2010) 55–61, <https://doi.org/10.1016/j.jhin.2009.08.020>.
- [115] M.M. Rahman, K. Nionomiya, C. Ogino, N. Shimizu, Ultrasound-induced membrane lipid peroxidation and cell damage of *Escherichia coli* in the presence of non-woven TiO2 fabrics, *Ultrason. Sonochem.* 17 (2010) 738–743, <https://doi.org/10.1016/j.ultrsonch.2009.12.001>.
- [116] J. Duan, D.L. Kasper, Oxidative depolymerization of polysaccharides by reactive oxygen/nitrogen species, *Glycobiology* 21 (2011) 401–409, <https://doi.org/10.1093/glycob/cwq171>.
- [117] C.W. Ho, T.K. Chew, T.C. Ling, S. Kamaruddin, W.S. Tan, B.T. Tey, Efficient mechanical cell disruption of *Escherichia coli* by an ultrasonicator and recovery of intracellular hepatitis B core antigen, *Process Biochem.* 41 (2006) 1829–1834, <https://doi.org/10.1016/j.procbio.2006.03.043>.
- [118] C.M. Runyan, J.C. Carmen, B.L. Beckstead, J.L. Nelson, R.A. Robison, W.G. Pitt, Low-frequency ultrasound increases outer membrane permeability of *Pseudomonas aeruginosa*, *J. Gen. Appl. Microbiol.* 52 (2006) 295–301, <https://doi.org/10.2323/jgam.52.295>.
- [119] E.R. Holm, D.M. Stamper, R.A. Brizzolara, L. Barnes, N. Deamer, J.A.M. Burkholder, Sonication of bacteria, phytoplankton and zooplankton: application to treatment of ballast water, *Mar. Pollut. Bull.* 56 (2008) 1201–1208, <https://doi.org/10.1016/j.marpolbul.2008.02.007>.
- [120] M.P. Badve, M.N. Bhagat, A.B. Pandit, Microbial disinfection of seawater using hydrodynamic cavitation, *Sep. Purif. Technol.* 151 (2015) 31–38, <https://doi.org/10.1016/j.seppur.2015.07.020>.
- [121] B. Balasundaram, S.T.L. Harrison, Study of physical and biological factors involved in the disruption of *E. coli* by hydrodynamic cavitation, *Biotechnol. Prog.* 22 (2006) 907–913, <https://doi.org/10.1021/bp0502173>.
- [122] Y. Azuma, H. Kato, E. Usami, T. Fukushima, Bacterial sterilization using cavitating jet, *J. Fluid Sci. Technol.* 2 (2007) 270–281, <https://doi.org/10.1299/jfst.2.270>.
- [123] L. Mezule, S. Tsyfinsky, V. Yakushevich, T. Juha, A simple technique for water disinfection with hydrodynamic cavitation: effect on survival of *Escherichia coli*, *Desalination* 248 (2010) 152–159, <https://doi.org/10.1016/j.desal.2008.05.051>.
- [124] J.G. Dalfó Filho, M.P. Assis, A.I.B. Genovesi, Bacterial inactivation in artificially and naturally contaminated water using a cavitating jet apparatus, *J. Hydro-Environ. Res.* 9 (2015) 259–267, <https://doi.org/10.1016/j.jher.2015.03.001>.
- [125] J. Li, J. Ahn, D. Liu, S. Chen, X. Ye, T. Ding, Evaluation of ultrasoundsinduced damage to *Escherichia coli* and *Staphylococcus aureus* by flow cytometry and transmission electron microscopy, *Appl. Environ. Microbiol.* 82 (2016) 1828–1837, <https://doi.org/10.1128/AEM.03080-15>.
- [126] S. Gao, G.D. Lewis, M. Ashokkumar, Y. Hemar, Inactivation of microorganisms by low-frequency high-power ultrasound: 1. Effect of growth phase and capsule properties of the bacteria, *Ultrason. Sonochem.* 21 (1) (2014) 446–453, <https://doi.org/10.1016/j.ultrsonch.2013.06.006>.
- [127] O.R. Gashchin, T.N. Viten'ko, The combined effect of hydrodynamic cavitation, hydrogen peroxide, and silver ions on the *Escherichia coli* microorganisms, *J. Water Chem. Technol.* 33 (2011) 266–271, <https://doi.org/10.3103/S1063455X11040096>.
- [128] R.J. Watts, D. Washington, J. Howsawkeng, F.J. Loge, A.L. Teel, Comparative toxicity of hydrogen peroxide, hydroxyl radicals, and superoxide anion to *Escherichia coli*, *Adv. Environ. Res.* 7 (2003) 961–968, [https://doi.org/10.1016/S1093-0191\(02\)00100-4](https://doi.org/10.1016/S1093-0191(02)00100-4).
- [129] G. Brandi, F. Cattabeni, A. Albano, O. Cantoni, Role of hydroxyl radicals in *Escherichia coli* killing induced by hydrogen peroxide, *Free Radic. Res.* 6 (1989) 47–55, <https://doi.org/10.3109/10715768909073427>.
- [130] K.J. Adolfsen, M.P. Brynildsen, A kinetic platform to determine the fate of hydrogen peroxide in *Escherichia coli*, *PLoS Comput. Biol.* 11 (2015) e1004562, <https://doi.org/10.1371/journal.pcbi.1004562>.
- [131] D.R. Arahal, A.M. Castillo, W. Ludwig, K.H. Schleifer, A. Ventosa, Proposal of *Cobetia marina* gen. nov., comb. nov., within the Family Halomonadaceae, to include the species *Halomonas marina*, *Syst. Appl. Microbiol.* 25 (2002) 207–211, <https://doi.org/10.1078/0723-2020-00113>.
- [132] J.H. Power, B.J. Buster, C.J. Reist, E. Martin, M. Bridges, W.M. Sutherland, R.P. Taylor, B.M. Scheld, Complement-independent binding of microorganisms to primate erythrocytes in vitro by cross-linked monoclonal antibodies via complement receptor 1, *Infect. Immun.* 63 (1995) 1329–1335.
- [133] S. Lu, Y. Han, X. Duan, F. Luo, L. Zhu, S. Li, H. Huang, Cell morphology variations of *Klebsiella pneumoniae* induced by acetate stress using biomimetic vesicle assay, *Appl. Biochem. Biotechnol.* 171 (2013) 731–743, <https://doi.org/10.1007/s12101-013-0368-y>.
- [134] S. Berk, G. Falkiner, E. Garduno, M. Joy, M. Ortiz-Jimenez, R. Garduno, Packaging of live *legionella pneumophila* into pellets expelled by tetrahymena spp. do not require bacterial replication and depends on a Dot/Icm-mediated survival mechanism, *Appl. Environ. Microbiol.* 74 (2008) 2187–2199, <https://doi.org/10.1128/AEM.01214-07>.
- [135] M. Deforet, D. Van Dittmarsch, J.B. Xavier, Cell-size homeostasis and the incremental role in a bacterial pathogen, *Biophys. J.* 109 (2015) 521–528, <https://doi.org/10.1016/j.bpj.2015.07.002>.
- [136] J.-M. Monier, S.E. Lindow, *Pseudomonas syringae* responds to the environment on leaves by size reduction, *Phytopathology* 93 (2003) 1209–1216, <https://doi.org/10.1094/PHYTO.2003.93.10.1209>.
- [137] A. Kawamoto, Y.V. Morimoto, T. Miyata, T. Minamino, K.T. Hughes, T. Kato, K. Namba, Common and distinct structural features of *Salmonella* injectosome and flagellar basal body, *Sci. Rep.* 3 (2013) 1–6, <https://doi.org/10.1038/srep03369>.
- [138] M.C. Cabeza, J.A. Cárcel, J.A. Ordóñez, I. Cambero, L. Dela Hoz, M.L. García, J. Benedito, Relationships among selected variables affecting the resistance of *Salmonella enterica*, serovar *Enteritidis* to thermosonication, *J. Food Eng.* 98 (2010) 71–75, <https://doi.org/10.1016/j.jfoodeng.2009.12.009>.
- [139] T. Chatterjee, B.K. Chatterjee, P. Chakrabarti, Modelling of growth kinetics of *Vibrio cholerae* in presence of gold nanoparticles: effect of size and morphology, *Sci. Rep.* 7 (2017) 1–10, <https://doi.org/10.1038/s41598-017-09357-0>.
- [140] M. Carrera, R.O. Zandomeni, J. Fitzgibbon, J.L. Sagripanti, Difference between the spore sizes of *Bacillus anthracis* and other *Bacillus* species, *J. Appl. Microbiol.* 102 (2007) 303–312, <https://doi.org/10.1111/j.1365-2672.2006.03111.x>.
- [141] A. Kokkinos, C. Passeas, E. Ellopoulos, G. Kalantziopoulos, Cell size of various acidic acid bacteria as determined by scanning electron microscope and image analysis, *Lait* 78 (1998) 491–500, <https://doi.org/10.1051/lait:1998546>.
- [142] J. Yan, Y. Ye, Z. Jian, J. Xie, K. Zhong, S. Wang, H. Hu, Z. Chen, H. Wen, H. Zhang, Enhanced sulfate and metal removal by reduced graphene oxide self-assembled *Enterococcus avium* sulfate-reducing bacteria particles, *Bioresour. Technol.* 266 (2018) 447–453, <https://doi.org/10.1016/j.biortech.2018.07.012>.
- [143] S. Furse, M. Jakubec, F. Ríse, H.E. Williams, C.E.D. Rees, O. Halskau, Evidence that *Listeria innocua* modulates its membrane's stored curvature elastic stress, but not fluidity, through the cell cycle, *Sci. Rep.* 7 (2017) 1–11, <https://doi.org/10.1038/s41598-017-06855-z>.
- [144] J.M. Monteiro, P.B. Fernandes, F. Vaz, A.R. Pereira, A.C. Tavares, M.T. Ferreira, P.M. Pereira, H. Veiga, E. Kurus, M.S. Vannieuwenhze, Y.V. Brun, S.R. Filipe, M.G. Pinho, Cell shape dynamics during the staphylococcal cell cycle, *Nat. Commun.* 6 (2015), <https://doi.org/10.1038/ncomms9055>.
- [145] A. Pomplilio, S. De Nicola, V. Crocetta, S. Guarneri, V. Savini, E. Carretto, G. Di Bonaventura, New insights in *Staphylococcus pseudintermedius* pathogenicity: Antibiotic-resistant biofilm formation by a human wound-associated strain, *BMC Microbiol.* 15 (2015) 1–14, <https://doi.org/10.1186/s12866-015-0449-x>.
- [146] V. Ryan, T.R. Hart, R. Schiller, Size Determination of *Streptococcus-Mutans-10449* by Laser-Light Scattering, *Biophys. J.* 31 (1980) 313–324.
- [147] D. Apar, B. Özbek, Protein releasing kinetics of bakers' yeast cells by ultrasound, *Chem. Biomed. Eng. Q.* 22 (2008) 113–118 <http://hrcak.srce.hr/21403>.
- [148] Y. Iida, T. Tuziuti, K. Yasui, T. Kozuka, A. Towata, Protein release from yeast cells as an evaluation method of physical effects in ultrasonic field, *Ultrason. Sonochem.* 15 (2008) 995–1000, <https://doi.org/10.1016/j.ultrsonch.2008.02.013>.
- [149] L. Zhang, Y. Jin, Y. Xie, X. Wu, T. Wu, Releasing polysaccharide and protein from yeast cells by ultrasound: selectivity and effects of processing parameters,

- Ultrason. Sonochem. 21 (2014) 576–581, <https://doi.org/10.1016/j.ultsonch.2013.10.016>.
- [150] T. Wu, X. Yu, A. Hu, L. Zhang, Y. Jin, M. Abid, Ultrasonic disruption of yeast cells: Underlying mechanism and effects of processing parameters, Innov. Food Sci. Emerg. Technol. 28 (2015) 59–65, <https://doi.org/10.1016/j;ifset.2015.01.005>.
- [151] I. Albanese, R. Ciriminna, F. Meneguzzo, M. Pagliaro, Energy efficient inactivation of *saccharomyces cerevisiae* via controlled hydrodynamic cavitation, Energy Sci. Eng. 3 (2015) 221–238, <https://doi.org/10.1002/ese3.62>.
- [152] R.J. Brennan, B.E.P. Swoboda, R.H. Schiestl, Oxidative mutagens induce intrachromosomal recombination in yeast, Mutat. Res. 308 (1994) 159–167, [https://doi.org/10.1016/0027-5107\(94\)90151-1](https://doi.org/10.1016/0027-5107(94)90151-1).
- [153] Y. Wang, T. Wang, Y. Yuan, Y. Fan, K. Guo, T. Yue, Inactivation of yeast in apple juice using gas-phase surface discharge plasma treatment with a spray reactor, LWT – Food Sci. Technol. 97 (2018) 530–536, <https://doi.org/10.1016/j.lwt.2018.07.049>.
- [154] M. Lürling, Y. Tolman, Beating the blues: is there any music in fighting cyanobacteria with ultrasound? Water Res. 66 (2014) 361–373, <https://doi.org/10.1016/j.watres.2014.08.043>.
- [155] G. Zhang, P. Zhang, H. Liu, B. Wang, Ultrasonic damages on cyanobacterial photosynthesis, Ultrason. Sonochem. 13 (2006) 501–505, <https://doi.org/10.1016/j.ultsonch.2005.11.001>.
- [156] D. Kim, E.K. Kim, H.G. Koh, K. Kim, J.I. Han, Y.K. Chang, Selective removal of rotifers in microalgae cultivation using hydrodynamic cavitation, Algal Res. 28 (2017) 24–29, <https://doi.org/10.1016/j.algal.2017.09.026>.
- [157] M.D. Batista, A.C.B.M. Anhê, J.C. de Souza Inácio, Gonçalves, Use of hydrodynamic cavitation for algae removal: effect on the inactivation of microalgae belonging to genus *scenedesmus*, Water Air Soil Pollut. 228 (2017), <https://doi.org/10.1007/s11270-017-3624-x>.
- [158] Z. Wu, H. Shen, B. Ondruschka, Y. Zhang, W. Wang, D.H. Bremner, Removal of blue-green algae using the hybrid method of hydrodynamic cavitation and ozonation, J. Hazard. Mater. 235–236 (2012) 152–158, <https://doi.org/10.1016/j.jhazmat.2012.07.034>.
- [159] G. Zhang, P. Zhang, B. Wang, H. Liu, Ultrasonic frequency effects on the removal of *Microcystis aeruginosa*, Ultrason. Sonochem. 13 (2006) 446–450, <https://doi.org/10.1016/j.ultsonch.2005.09.012>.
- [160] J.A. Gerde, M. Montalbo-Lomboy, L. Yao, D. Grewell, T. Wang, Evaluation of microalgal cell disruption by ultrasonic treatment, Biore sour. Technol. 125 (2012) 175–181, <https://doi.org/10.1016/j.biortech.2012.08.110>.
- [161] R. Halim, T.W.T. Rupasinghe, D.L. Tull, P.A. Webley, Mechanical cell disruption for lipid extraction from microalgal biomass, Biore sour. Technol. 140 (2013) 53–63, <https://doi.org/10.1016/j.biortech.2013.04.067>.
- [162] U.D. Keris-Sen, U. Sen, G. Soydemir, M.D. Gurrol, An investigation of ultrasound effect on microalgal cell integrity and lipid extraction efficiency, Biore sour. Technol. 152 (2014) 407–413, <https://doi.org/10.1016/j.biortech.2013.11.018>.
- [163] Y. Xu, J. Yang, Y. Wang, F. Liu, J. Jia, The effects of jet cavitation on the growth of *Microcystis aeruginosa*, J. Environ. Sci. Health – Part A 41 (2006) 2345–2358, <https://doi.org/10.1080/10934520600873456>.
- [164] R. Halim, R. Harun, M.K. Danquah, P.A. Webley, Microalgal cell disruption for biofuel development, Appl. Energy. 91 (2012) 116–121, <https://doi.org/10.1039/c2nr30259d>.
- [165] S. Kotpouli, A. Schommartz, M. Postema, Sonic cracking of blue-green algae, Appl. Acoust. 70 (2009) 1306–1312, <https://doi.org/10.1016/j.apacoust.2009.02.001>.
- [166] S. Joung, C. Kim, C. Ahn, K. Jang, Simple method for a cell count of the colonial cyanobacterium, Society 44 (2006) 562–565, <https://doi.org/10.1111/j.1420-9101.2008.01671.x>.
- [167] D. Jančula, P. Mikula, B. Maršálek, P. Rudolf, F. Pochylý, Selective method for cyanobacterial bloom removal: hydraulic jet cavitation experience, Aquac. Int. 22 (2014) 509–521, <https://doi.org/10.1007/s10499-013-9660-7>.
- [168] A. Rodriguez-Molares, S. Dickson, P. Hobson, C. Howard, A. Zander, M. Burch, Quantification of the ultrasound induced sedimentation of *Microcystis aeruginosa*, Ultrason. Sonochem. 21 (2014) 1299–1304, <https://doi.org/10.1016/j.ultsonch.2014.01.027>.
- [169] G. Gartner, B. Uzunov, E. Ingolic, W. Kofler, G. Gacheva, P. Pilarski, L. Zagorchev, M. Odjakova, S. Maya, Microscopic investigations (LM, TEM and SEM) and identification of *Chlorella isolata* R-06/2 from extreme habitat in Bulgaria with a strong biological activity and resistance to environmental stress factors, Biotechnol. Biotechnol. Equip. 29 (2015) 536–540, <https://doi.org/10.1080/13102818.2015.10132838>.
- [170] J.R. Blackwell, E.J. Cox, D.J. Gilmour, The morphology and taxonomy of chlorococcum submarinum (Chlorococcales) isolated from a tidal rockpool, Br. Phycol. J. 26 (1991) 133–139, <https://doi.org/10.1080/00071619100650101>.
- [171] R.S. Gour, A. Chawla, H. Singh, R.S. Chauthan, A. Kant, Characterization and screening of native *Scenedesmus* sp. isolates suitable for biofuel feedstock, PLoS One 11 (2016) 1–16, <https://doi.org/10.1371/journal.pone.0155321>.
- [172] D. Jančula, B. Maršálek, Critical review of actually available chemical compounds for prevention and management of cyanobacteria blooms, Chemosphere 85 (2011) 1415–1422, <https://doi.org/10.1016/j.chemosphere.2011.08.036>.
- [173] P. Mikula, S. Zezulka, D. Jančula, B. Maršálek, Metabolic activity and membrane integrity changes in *Microcystis aeruginosa* – new findings on hydrogen peroxide toxicity in cyanobacteria, Eur. J. Phycol. 47 (2012) 195–206, <https://doi.org/10.1080/09670262.2012.687144>.
- [174] H. Qian, S. Yu, Z. Sun, X. Xie, W. Liu, Z. Fu, Effects of copper sulfate, hydrogen peroxide and N-phenyl-2-naphthalamine on oxidative stress and the expression of genes involved photosynthesis and microcystin disposition in *Microcystis aeruginosa*, Aquat. Toxicol. 99 (2010) 405–412, <https://doi.org/10.1016/j.aquatox.2010.05.018>.
- [175] N. Gu, J. Gao, K. Wang, B. Li, W. Dong, Y. Ma, *Microcystis aeruginosa* inhibition by Zn-Fe-LDHs as photocatalyst under visible light, J. Taiwan Inst. Chem. Eng. 64 (2016) 189–195, <https://doi.org/10.1016/j.jite.2016.04.016>.
- [176] M. Bai, Y. Tian, Y. Yu, Q. Zheng, X. Zhang, W. Zheng, Z. Zhang, Application of a hydroxyl-radical-based disinfection system for ballast water, Chemosphere 208 (2018) 541–549, <https://doi.org/10.1016/j.chemosphere.2018.06.010>.
- [177] S.M. Goyal, Y. Chander, S. Yezli, J.A. Otter, Evaluating the virucidal efficacy of hydrogen peroxide vapour, J. Hosp. Infect. 86 (2014) 255–259, <https://doi.org/10.1016/j.jhin.2014.02.003>.
- [178] M. Olvera, A. Egúia, O. Rodríguez, E. Chong, S.D. Pillai, K. Ilangoan, Inactivation of *Cryptosporidium parvum* oocysts in water using ultrasonic treatment, Biore sour. Technol. 99 (2008) 2046–2049, <https://doi.org/10.1016/j.biortech.2007.02.051>.
- [179] J. Vázquez, K. Grillitsch, G. Daum, A. Mas, G. Beltran, M.J. Torrijas, The role of the membrane lipid composition in the oxidative stress tolerance of different wine yeasts, Food Microbiol. 78 (2018) 143–154, <https://doi.org/10.1016/j.fm.2018.10.001>.

SUPPLEMENTARY DATA

**Table S1:** Reviewed articles grouped by type of device, frequency of sonication, electrical and acoustic power for acoustic cavitation (AC).

Type of the device.	Radial probe (sonotrode)	Ultrasonic bath	Other types
<b>Frequency of sonication</b>			
20 kHz	[1,2,11–20,3,21–30,4,31–35,5–10]	[36,37]	
40 kHz	[29,36,38,39]	[10,40]	[41]
Other low US frequencies used	[29,42–46]	[9,20,35,47,48]	[41]
High US frequencies used	[10,11,29,36,49]	[1,19,32–34,36,50–52]	[31,53–55]
Double frequencies 17 + 33, 70 + 100		[56]	
<b>Electrical power</b>			
40-1000 W	[6,7,21,24,31,44,45]	[25,40]	[18,56]
<b>Acoustic power</b>			
< 0.1 W/mL	[1,10,32,36,43]		[56]
0.1 – 1 W/mL	[1,5,30,35,43,46]		[54]
< 1 W/mL	[8,27]		
<b>Reported in W</b>			
< 15 W	[2,3,11,16,29,33]	[28,37]	
15–100 W	[17,33,34,39,45]	[9,47,48,50]	[55]
< 100 W	[17,20,39,45]		
<b>Reported in W over cm<sup>2</sup></b>			
< 10 W/cm <sup>2</sup>	[22,49]	[19,51]	
10 – 50 W/cm <sup>2</sup>	[19,22,23,42]		
< 50 W/cm <sup>2</sup>	[13–15]		

**Table S2:** Reviewed articles grouped by device type and sample volume for hydrodynamic cavitation (HC).

HC device type		Sample volume			
		Laboratory scale (<5 L)	Middle scale (<50 L)	Industrial scale (>50 L)	Not specified
Pump + constriction	orifice	[57,58]	[59–62]	[63]	[64,65]
	jet	[66]	[67,68]		[69]
	venturi	[48,70,71]			
	venturi, orifice	[72]		[73]	
Rotor-stator		[74,75]		[76]	
Blow-through		[77]			
Other		[78]			

### References

- [1] A. Al Bsoul, J.P. Magnin, N. Commenges-Bernole, N. Gondrexon, J. Willison, C. Petrier, Effectiveness of ultrasound for the destruction of *Mycobacterium* sp. strain (6PY1), *Ultrason. Sonochem.* 17 (2010) 106–110. doi:10.1016/j.ulsonch.2009.04.005.
- [2] S. Gao, G.D. Lewis, M. Ashokkumar, Y. Hemar, Inactivation of microorganisms by low-frequency high-power ultrasound: 2. A simple model for the inactivation mechanism, *Ultrason. Sonochem.* 21 (2014) 454–460. doi:10.1016/j.ulsonch.2013.06.007.
- [3] S. Gao, G.D. Lewis, M. Ashokkumar, Y. Hemar, Inactivation of microorganisms by low-frequency high-power ultrasound: 1. Effect of growth phase and capsule properties of the bacteria, *Ultrason. Sonochem.* 21 (2014) 446–453. doi:10.1016/j.ulsonch.2013.06.006.
- [4] R.A. Al-Juboori, V. Aravinthan, T. Yusaf, Impact of pulsed ultrasound on bacteria reduction of natural waters, *Ultrason. Sonochem.* 27 (2015) 137–147. doi:10.1016/j.ulsonch.2015.05.007.
- [5] L.J. Bastarrachea, M. Walsh, S.P. Wrenn, R. V. Tikekar, Enhanced antimicrobial effect of ultrasound by the food colorant Erythrosin B, *Food Res. Int.* 100 (2017) 344–351. doi:10.1016/j.foodres.2017.07.012.
- [6] M. Cameron, L.D. McMaster, T.J. Britz, Electron microscopic analysis of dairy microbes inactivated by ultrasound, *Ultrason. Sonochem.* 15 (2008) 960–964. doi:10.1016/j.ulsonch.2008.02.012.
- [7] C.W. Ho, T.K. Chew, T.C. Ling, S. Kamaruddin, W.S. Tan, B.T. Tey, Efficient mechanical cell disruption of *Escherichia coli* by an ultrasonicator and recovery of intracellular hepatitis B core antigen, *Process Biochem.* 41 (2006) 1829–1834. doi:10.1016/j.procbio.2006.03.043.
- [8] G. Hunter, M. Lucas, I. Watson, R. Parton, A radial mode ultrasonic horn for the inactivation of *Escherichia coli* K12, *Ultrason. Sonochem.* 15 (2008) 101–109. doi:10.1016/j.ulsonch.2006.12.017.
- [9] E.S. Inguglia, B.K. Tiwari, J.P. Kerry, C.M. Burgess, Effects of high intensity ultrasound on the inactivation profiles of *Escherichia coli* K12 and *Listeria innocua* with salt and salt replacers, *Ultrason. Sonochem.* 48 (2018) 492–498. doi:10.1016/j.ulsonch.2018.05.007.
- [10] E. Joyce, A. Al-Hashimi, T.J. Mason, Assessing the effect of different ultrasonic frequencies on bacterial viability using flow cytometry, *J. Appl. Microbiol.* 110 (2011) 862–870. doi:10.1111/j.1365-2672.2011.04923.x.
- [11] S. Koda, M. Miyamoto, M. Toma, T. Matsuoka, M. Maebayashi, Inactivation of *Escherichia coli* and *Streptococcus* mutans by ultrasound at 500 kHz, *Ultrason. Sonochem.* 16 (2009) 655–659. doi:10.1016/j.ulsonch.2009.02.003.
- [12] H. Lee, B. Zhou, W. Liang, H. Feng, S.E. Martin, Inactivation of *Escherichia coli* cells with sonication, manosonation, thermosonation, and manothermosonation: Microbial responses and kinetics modeling, *J. Food Eng.* 93 (2009) 354–364. doi:10.1016/j.jfoodeng.2009.01.037.
- [13] J. Li, J. Ahn, D. Liu, S. Chen, X. Ye, T. Ding, Evaluation of ultrasoundinduced damage to *Escherichia coli* and *Staphylococcus aureus* by flow cytometry and transmission electron microscopy, *Appl. Environ. Microbiol.* 82 (2016) 1828–1837. doi:10.1128/AEM.03080-15.
- [14] X. Liao, J. Li, Y. Suo, S. Chen, X. Ye, D. Liu, T. Ding, Multiple action sites of ultrasound on *Escherichia coli* and *Staphylococcus aureus*, *Food Sci. Hum. Wellness.* 7 (2018) 102–109. doi:10.1016/j.fshw.2018.01.002.

- [15] M.J. Abeledo-Lameiro, E. Ares-Mazás, H. Goméz-Cousó, Use of ultrasound irradiation to inactivate Cryptosporidium parvum oocysts in effluents from municipal wastewater treatment plants, *Ultrason. Sonochem.* 48 (2018) 118–126. doi:10.1016/j.ulsonch.2018.05.013.
- [16] M. Ashokkumar, T. Vu, F. Grieser, A. Weerawardena, N. Anderson, N. Pilkington, D.R. Dixon, Ultrasonic treatment of Cryptosporidium oocysts, *Water Sci. Technol.* 47 (2003) 173–177.
- [17] D. Apar, B. Özbek, Protein releasing kinetics of bakers' yeast cells by ultrasound, *Chem. Biochem. Eng. Q.* 22 (2008) 113–118. <http://hrcak.srce.hr/21403>.
- [18] S. Bystryak, R. Santockyte, A.S. Peshkovsky, Cell disruption of *S. cerevisiae* by scalable high-intensity ultrasound, *Biochem. Eng. J.* 99 (2015) 99–106. doi:10.1016/j.bej.2015.03.014.
- [19] Y. Iida, T. Tuziuti, K. Yasui, T. Kozuka, A. Towata, Protein release from yeast cells as an evaluation method of physical effects in ultrasonic field, *Ultrason. Sonochem.* 15 (2008) 995–1000. doi:10.1016/j.ulsonch.2008.02.013.
- [20] D. Liu, X.A. Zeng, D.W. Sun, Z. Han, Disruption and protein release by ultrasonication of yeast cells, *Innov. Food Sci. Emerg. Technol.* 18 (2013) 132–137. doi:10.1016/j.ifset.2013.02.006.
- [21] B.A. Wordon, B. Mortimer, L.D. McMaster, Comparative real-time analysis of *Saccharomyces cerevisiae* cell viability, injury and death induced by ultrasound (20kHz) and heat for the application of hurdle technology, *Food Res. Int.* 47 (2012) 134–139. doi:10.1016/j.foodres.2011.04.038.
- [22] T. Wu, X. Yu, A. Hu, L. Zhang, Y. Jin, M. Abid, Ultrasonic disruption of yeast cells: Underlying mechanism and effects of processing parameters, *Innov. Food Sci. Emerg. Technol.* 28 (2015) 59–65. doi:10.1016/j.ifset.2015.01.005.
- [23] L. Zhang, Y. Jin, Y. Xie, X. Wu, T. Wu, Releasing polysaccharide and protein from yeast cells by ultrasound: Selectivity and effects of processing parameters, *Ultrason. Sonochem.* 21 (2014) 576–581. doi:10.1016/j.ulsonch.2013.10.016.
- [24] X. Su, S. Zivanovic, D.H. D'Souza, Inactivation of Human Enteric Virus Surrogates by High-Intensity Ultrasound, *Foodborne Pathog. Dis.* 7 (2010) 1055–1061. doi:10.1089/fpd.2009.0515.
- [25] F. Adam, M. Abert-Vian, G. Peltier, F. Chemat, "Solvent-free" ultrasound-assisted extraction of lipids from fresh microalgae cells: A green, clean and scalable process, *Bioresour. Technol.* 114 (2012) 457–465. doi:10.1016/j.biortech.2012.02.096.
- [26] J.A. Gerde, M. Montalbo-Lomboy, L. Yao, D. Grewell, T. Wang, Evaluation of microalgae cell disruption by ultrasonic treatment, *Bioresour. Technol.* 125 (2012) 175–181. doi:10.1016/j.biortech.2012.08.110.
- [27] J.M. Greenly, J.W. Tester, Ultrasonic cavitation for disruption of microalgae, *Bioresour. Technol.* 184 (2015) 276–279. doi:10.1016/j.biortech.2014.11.036.
- [28] M. Kurokawa, P.M. King, X. Wu, E.M. Joyce, T.J. Mason, K. Yamamoto, Effect of sonication frequency on the disruption of algae, *Ultrason. Sonochem.* 31 (2016) 157–162. doi:10.1016/j.ulsonch.2015.12.011.
- [29] M. Lürling, Y. Tolman, Beating the blues: Is there any music in fighting cyanobacteria with ultrasound?, *Water Res.* 66 (2014) 361–373. doi:10.1016/j.watres.2014.08.043.
- [30] P. Rajasekhar, L. Fan, T. Nguyen, F.A. Roddick, Impact of sonication at 20kHz on *Microcystis aeruginosa*, *Anabaena circinalis* and *Chlorella* sp., *Water Res.* 46 (2012) 1473–1481.

doi:10.1016/j.watres.2011.11.017.

- [31] M. Wang, W. Yuan, X. Jiang, Y. Jing, Z. Wang, Disruption of microalgal cells using high-frequency focused ultrasound, *Bioresour. Technol.* 153 (2014) 315–321. doi:10.1016/j.biortech.2013.11.054.
- [32] X. Wu, E.M. Joyce, T.J. Mason, Evaluation of the mechanisms of the effect of ultrasound on *Microcystis aeruginosa* at different ultrasonic frequencies, *Water Res.* 46 (2012) 2851–2858. doi:10.1016/j.watres.2012.02.019.
- [33] K. Yamamoto, P.M. King, X. Wu, T.J. Mason, E.M. Joyce, Effect of ultrasonic frequency and power on the disruption of algal cells, *Ultrason. Sonochem.* 24 (2015) 165–171. doi:10.1016/j.ulsonch.2014.11.002.
- [34] G. Zhang, P. Zhang, B. Wang, H. Liu, Ultrasonic frequency effects on the removal of *Microcystis aeruginosa*, *Ultrason. Sonochem.* 13 (2006) 446–450. doi:10.1016/j.ulsonch.2005.09.012.
- [35] G. Zhang, P. Zhang, H. Liu, B. Wang, Ultrasonic damages on cyanobacterial photosynthesis, *Ultrason. Sonochem.* 13 (2006) 501–505. doi:10.1016/j.ulsonch.2005.11.001.
- [36] E.M. Joyce, X. Wu, T.J. Mason, Effect of ultrasonic frequency and power on algae suspensions, *J. Environ. Sci. Heal. Part A* 45 (2010) 863–866. doi:10.1016/j.ulsonch.2014.11.002.
- [37] A. Rodriguez-Molares, S. Dickson, P. Hobson, C. Howard, A. Zander, M. Burch, Quantification of the ultrasound induced sedimentation of *Microcystis aeruginosa*, *Ultrason. Sonochem.* 21 (2014) 1299–1304. doi:10.1016/j.ulsonch.2014.01.027.
- [38] R. Halim, T.W.T. Rupasinghe, D.L. Tull, P.A. Webley, Mechanical cell disruption for lipid extraction from microalgal biomass, *Bioresour. Technol.* 140 (2013) 53–63. doi:10.1016/j.biortech.2013.04.067.
- [39] R. Halim, R. Harun, M.K. Danquah, P.A. Webley, Microalgal cell disruption for biofuel development, *Appl. Energy*. 91 (2012) 116–121. doi:10.1039/c2nr30259d.
- [40] T. Monsen, E. Lövgren, M. Widerström, L. Wallinder, In vitro effect of ultrasound on bacteria and suggested protocol for sonication and diagnosis of prosthetic infections, *J. Clin. Microbiol.* 47 (2009) 2496–2501. doi:10.1128/JCM.02316-08.
- [41] M. Versoza, W. Jung, M.L. Barabad, Y. Lee, K. Choi, D. Park, Inactivation of filter bound aerosolized MS2 bacteriophages using a non-conductive ultrasound transducer, *J. Virol. Methods*. 255 (2018) 76–81. doi:10.1016/j.jviromet.2018.02.015.
- [42] E.R. Holm, D.M. Stamper, R.A. Brizzolara, L. Barnes, N. Deamer, J.A.M. Burkholder, Sonication of bacteria, phytoplankton and zooplankton: Application to treatment of ballast water, *Mar. Pollut. Bull.* 56 (2008) 1201–1208. doi:10.1016/j.marpolbul.2008.02.007.
- [43] M.C. Cabeza, J.A. Cárcel, J.A. Ordóñez, I. Cambero, L. De la Hoz, M.L. García, J. Benedito, Relationships among selected variables affecting the resistance of *Salmonella enterica*, serovar Enteritidis to thermosonication, *J. Food Eng.* 98 (2010) 71–75. doi:10.1016/j.jfoodeng.2009.12.009.
- [44] D. Spiteri, C. Chot-Plassot, J. Sclear, K.A. Karatzas, C. Scerri, V.P. Valdramidis, Ultrasound processing of liquid system(s) and its antimicrobial mechanism of action, *Lett. Appl. Microbiol.* 65 (2017) 313–318. doi:10.1111/lam.12776.
- [45] I. Oyane, M. Furuta, C.E. Stavarache, K. Hashiba, S. Mukai, J.M. Nakanishi, I. Kimata, Y. Maeda, Inactivation of *Cryptosporidium parvum* by ultrasonic irradiation., *Environ. Sci. Tech.*

39 (2005) 7294–8. doi:Doi 10.1021/Es0502977.

- [46] U.D. Keris-Sen, U. Sen, G. Soydemir, M.D. Gurol, An investigation of ultrasound effect on microalgal cell integrity and lipid extraction efficiency, *Bioresour. Technol.* 152 (2014) 407–413. doi:10.1016/j.biortech.2013.11.018.
- [47] V.D. Farkade, S.T.L. Harrison, A.B. Pandit, Improved cavitation cell disruption following pH pretreatment for the extraction of  $\beta$ -galactosidase from *Kluveromyces lactis*, *Biochem. Eng. J.* 31 (2006) 25–30. doi:10.1016/j.bej.2006.05.015.
- [48] A. Šarc, M. Oder, M. Dular, Can rapid pressure decrease induced by supercavitation efficiently eradicate *Legionella pneumophila* bacteria?, *Desalin. Water Treat.* 57 (2014) 2184–2194. doi:10.1080/19443994.2014.979240.
- [49] M. Olvera, A. Eguía, O. Rodríguez, E. Chong, S.D. Pillai, K. Ilangovan, Inactivation of *Cryptosporidium parvum* oocysts in water using ultrasonic treatment, *Bioresour. Technol.* 99 (2008) 2046–2049. doi:10.1016/j.biortech.2007.02.051.
- [50] S. Gao, Y. Hemar, M. Ashokkumar, S. Paturel, G.D. Lewis, Inactivation of bacteria and yeast using high-frequency ultrasound treatment, *Water Res.* 60 (2014) 93–104. doi:10.1016/j.watres.2014.04.038.
- [51] C.M. Runyan, J.C. Carmen, B.L. Beckstead, J.L. Nelson, R.A. Robison, W.G. Pitt, Low-frequency ultrasound increases outer membrane permeability of *Pseudomonas aeruginosa*, *J. Gen. Appl. Microbiol.* 52 (2006) 295–301. doi:10.2323/jgam.52.295.
- [52] S. Kotopoulis, A. Schommartz, M. Postema, Sonic cracking of blue-green algae, *Appl. Acoust.* 70 (2009) 1306–1312. doi:10.1016/j.apacoust.2009.02.003.
- [53] S. Jachlewski, M. Botes, T.E. Cloete, The effect of ultrasound at 256 KHz on *Microcystis aeruginosa*, with and without gas vacuoles, *Water SA*. 39 (2013) 171–174. doi:10.4314/wsa.v39i1.17.
- [54] C. V. Chrysikopoulos, I.D. Manariotis, V.I. Syrigouna, Virus inactivation by high frequency ultrasound in combination with visible light, *Colloids Surfaces B Biointerfaces*. 107 (2013) 174–179. doi:10.1016/j.colsurfb.2013.01.038.
- [55] T.A. Bigelow, J. Xu, D.J. Stessman, L. Yao, M.H. Spalding, T. Wang, Lysis of *Chlamydomonas reinhardtii* by high-intensity focused ultrasound as a function of exposure time, *Ultrason. Sonochem.* 21 (2014) 1258–1264. doi:10.1016/j.ultsonch.2013.11.014.
- [56] H. Zou, L. Wang, The disinfection effect of a novel continuous-flow water sterilizing system coupling dual-frequency ultrasound with sodium hypochlorite in pilot scale, *Ultrason. Sonochem.* 36 (2017) 246–252. doi:10.1016/j.ultsonch.2016.11.041.
- [57] I. Lee, J.I. Han, Simultaneous treatment (cell disruption and lipid extraction) of wet microalgae using hydrodynamic cavitation for enhancing the lipid yield, *Bioresour. Technol.* 186 (2015) 246–251. doi:10.1016/j.biortech.2015.03.045.
- [58] Z. Wu, H. Shen, B. Ondruschka, Y. Zhang, W. Wang, D.H. Bremner, Removal of blue-green algae using the hybrid method of hydrodynamic cavitation and ozonation, *J. Hazard. Mater.* 235–236 (2012) 152–158. doi:10.1016/j.jhazmat.2012.07.034.
- [59] B. Balasundaram, S.T.L. Harrison, Study of physical and biological factors involved in the disruption of *E. coli* by Hydrodynamic Cavitation, *Biotechnol. Prog.* 22 (2006) 907–913. doi:10.1021/bp0502173.
- [60] B. Balasundaram, S.T.L. Harrison, Optimising orifice geometry for selective release of

- periplasmic products during cell disruption by hydrodynamic cavitation, *Biochem. Eng. J.* 54 (2011) 207–209. doi:10.1016/j.bej.2011.03.002.
- [61] B. Balasundaram, S.T.L. Harrison, Disruption of Brewers' Yeast by Hydrodynamic Cavitation: Process Variables and Their Influence on Selective Release, *Biotechnol. Bioeng.* 94 (2006) 303–311. doi:10.1002/bit.
  - [62] A.K. Lee, D.M. Lewis, P.J. Ashman, Microalgal cell disruption by hydrodynamic cavitation for the production of biofuels, *J. Appl. Phycol.* 27 (2015) 1881–1889. doi:10.1007/s10811-014-0483-3.
  - [63] L. Albanese, R. Ciriminna, F. Meneguzzo, M. Pagliaro, Energy efficient inactivation of *saccharomyces cerevisiae* via controlled hydrodynamic cavitation, *Energy Sci. Eng.* 3 (2015) 221–238. doi:10.1002/ese3.62.
  - [64] J. Deng, J. Zhou, Experimental Study of the Porous Plate Hydrodynamic Cavitation Device and Removal the Algae in Water, *Adv. Mater. Res.* 800 (2013) 569–572. doi:10.4028/www.scientific.net/AMR.800.569.
  - [65] D. Kim, E.K. Kim, H.G. Koh, K. Kim, J.I. Han, Y.K. Chang, Selective removal of rotifers in microalgae cultivation using hydrodynamic cavitation, *Algal Res.* 28 (2017) 24–29. doi:10.1016/j.algal.2017.09.026.
  - [66] Y. Xu, J. Yang, Y. Wang, F. Liu, J. Jia, The effects of jet cavitation on the growth of *Microcystis aeruginosa*, *J. Environ. Sci. Heal. - Part A Toxic/Hazardous Subst. Environ. Eng.* 41 (2006) 2345–2358. doi:10.1080/10934520600873456.
  - [67] G. Loraine, G. Chahine, C.T. Hsiao, J.K. Choi, P. Aley, Disinfection of gram-negative and gram-positive bacteria using Dynalets hydrodynamic cavitating jets, *Ultrason. - Sonochemistry.* 19 (2012) 710–717. doi:10.1016/j.ultsonch.2011.10.011.
  - [68] J.G. Dalfré Filho, M.P. Assis, A.I.B. Genovez, Bacterial inactivation in artificially and naturally contaminated water using a cavitating jet apparatus, *J. Hydro-Environment Res.* 9 (2015) 259–267. doi:10.1016/j.jher.2015.03.001.
  - [69] Y. Azuma, H. Kato, R. Usami, T. Fukushima, Bacterial Sterilization Using Cavitating Jet, *J. Fluid Sci. Technol.* 2 (2007) 270–281. doi:10.1299/jfst.2.270.
  - [70] D. Jančula, P. Mikula, B. Maršálek, P. Rudolf, F. Pochylý, Selective method for cyanobacterial bloom removal: Hydraulic jet cavitation experience, *Aquac. Int.* 22 (2014) 509–521. doi:10.1007/s10499-013-9660-7.
  - [71] M.D. Batista, A.C.B.M. Anhê, J.C. de Souza Inácio Gonçalves, Use of Hydrodynamic Cavitation for Algae Removal: Effect on the Inactivation of Microalgae Belonging to Genus *Scenedesmus*, *Water. Air. Soil Pollut.* 228 (2017). doi:10.1007/s11270-017-3624-x.
  - [72] M.P. Badve, M.N. Bhagat, A.B. Pandit, Microbial disinfection of seawater using hydrodynamic cavitation, *Sep. Purif. Technol.* 151 (2015) 31–38. doi:10.1016/j.seppur.2015.07.020.
  - [73] S. Arrojo, Y. Benito, A. Martínez Tarifa, A parametrical study of disinfection with hydrodynamic cavitation, *Ultrason. Sonochem.* 15 (2008) 903–908. doi:10.1016/j.ultsonch.2007.11.001.
  - [74] L.M. Cerecedo, C. Dopazo, R. Gomez-Lus, Water disinfection by hydrodynamic cavitation in a rotor-stator device, *Ultrason. Sonochem.* 48 (2018) 71–78. doi:10.1016/j.ultsonch.2018.05.015.
  - [75] L. Mezule, S. Tsypansky, V. Yakushevich, T. Juhna, A simple technique for water disinfection

- with hydrodynamic cavitation: Effect on survival of *Escherichia coli*, Desalination. 248 (2010) 152–159. doi:10.1016/j.desal.2008.05.051.
- [76] X. Sun, J.J. Park, H.S. Kim, S. Jin S. Lee, A.S. Om, J.Y. Yoon, Experimental Investigation of the Thermal and Disinfection Performances of a Novel Hydrodynamic Cavitation Reactor, Ultrason. Sonochem. 49 (2018) 13–23. doi:10.1016/j.ulson.2018.02.034.
- [77] J. Kosek, I. Gutiérrez-Aguirre, N. Rački, T. Drešo, M. Ravnikar, M. Dular, Efficient inactivation of MS-2 virus in water by hydrodynamic cavitation, Water Res. 124 (2017) 465–471. doi:10.1016/j.watres.2017.07.077.
- [78] P. Li, Y. Song, S. Yu, Removal of *Microcystis aeruginosa* using hydrodynamic cavitation: Performance and mechanisms, Water Res. 62 (2014) 241–248. doi:10.1016/j.watres.2014.05.052.

**Priloga B:** Objavljen pregledni članek vpliva mehanskih lastnosti posameznih slojev bakterijske celične stene

Evolucija mehanske stabilnosti od lipidnega dvosloja do kompleksne strukture ovojev bakterijske celične stene

Pandur Ž., Stopar D. 2021. Evolution of mechanical stability from lipid layers to complex bacterial envelope structures. V: Advances in biomembranes and lipid self-assembly. Bongiovanni A., Pocsfalvi G., Manno G., Kralj-Iglič V. (ur.). Cambridge, Academic Press: 207-251.

Izvleček:

Za preživetje v okolju morajo bakterije nenehno ohranjati strukturno celovitost svoje ovojnice. Citoplazemska membrana predstavlja fizično bariero med bakterijsko celico in okoliško tekočino, vendar imajo le redke samo citoplazemske membrano. Večina bakterij je razvila številne dodatne plasti, z namenom premostitve težkih pogojev v okolju. Glavni cilj poglavja je predstavitev različnih struktur bakterijske ovojnice, ki so pomembne za mehansko stabilnost celice. Kronološkega poteka razvoja nastanka struktur bakterijske ovojnice nismo podali, saj so te večinoma neznane, vendar predstavimo mehanski pogled za opazovane sloje celične stene. Predstavljeni so lipidni monosloji in dvosloji, kjer razičemo zakaj takšne strukture so mehansko nestabilne in zakaj so potrebne dodatne površinske plasti. Čeprav je splošno znano, da je peptidoglikan edini strukturni element, ki zagotavlja togost bakterijske ovojnice, nedavne ugotovitve kažejo, da je strižna obremenitev lahko enakomerno porazdeljena med različne plasti. Pri tem ostaja peptidoglikan še vedno bistveni steber v celičnem mehanskem sistemu, vendar le kot del večkompozitne celične pregrade. Predstavili smo tudi vlogo zunanje membrane, S-plasti, kapsule, ovoja in sluzi pri mehanski stabilnosti celice. Čeprav je glavni poudarek po Gramu negativnih in po Gramu pozitivnih bakterijah, je predstavljenih nekaj posebnih primerov prilagoditev bakterijske ovojnice na ekstremna okolja.



## CHAPTER SIX

# Evolution of mechanical stability from lipid layers to complex bacterial envelope structures

Žiga Pandur<sup>a,b</sup> and David Stopar<sup>a,\*</sup>

<sup>a</sup>University of Ljubljana, Biotechnical Faculty, Department of Food Science and Technology, Laboratory of Microbiology, Ljubljana, Slovenia

<sup>b</sup>University of Ljubljana, Faculty of Mechanical Engineering, Ljubljana, Slovenia

\*Corresponding author: E-mail: david.stopar@bf.uni-lj.si

## Contents

1. Introduction	208
2. Lipid monolayers	211
2.1 Lipid monolayer polymorphism	211
2.2 Biological membrane is not a monolayer	212
3. Lipid bilayers	212
3.1 Lipid bilayer mechanical properties	213
3.2 Lipid bilayer bending elastic modulus	214
3.3 Lipid bilayer phase transition	215
3.4 Failure of lipid bilayer stability	215
4. Cytoplasmic membrane layer	216
4.1 Material properties of cytoplasmic membranes	217
4.2 Membrane failure energy	217
5. Peptidoglycan layer	218
5.1 Matching the turgor pressure	219
5.2 Peptidoglycan composition	219
5.3 Peptidoglycan architecture	221
5.4 Biophysical properties of peptidoglycan responsible for stress bearing	222
5.5 Obligate intracellular parasites lack peptidoglycan layer	223
6. Bacterial outer membrane layer	223
6.1 Outer membrane composition	225
6.2 Attachment of the outer membrane to other surface layers	225
6.3 Outer membrane stress bearing	226
6.4 <i>Mycobacterium tuberculosis</i> outer membrane	227
6.5 <i>Deinococcus radiodurans</i> outer membrane	227
7. S-layers	228
7.1 S-layer as a primordial membrane	229
7.2 Antifouling properties of S-layer membranes	230
7.3 S-layer and mineralization	230

8. Capsular layers	231
8.1 Capsule composition	231
8.2 Multifunctional role of capsule	232
9. Extracellular polymeric substances (EPS)	232
10. Sheath layers	233
11. Endospores	233
11.1 Endospore envelope structure	234
11.2 Dissolution of endospore envelope	235
12. How did bacterial envelope evolve?	236
13. Conclusions	237
References	237

## Abstract

To survive in environment, bacteria must constantly maintain structural integrity of their envelope. All bacteria are separated from a surrounding media with a membrane, however only a few have just a membrane envelope layer. Most bacteria have evolved many additional layers to endure harsh conditions in the environment. The focus of this chapter is on different bacterial envelope structures, important for cell mechanical stability. We are not giving a chronological timeline leading to the present-day bacterial envelope structures, as these are largely unknown, but provide mechanistic explanations for the observed molecular assemblies in a given environment. Structural integrity of lipid monolayers and bilayers are reviewed, the reasons are given why they fail mechanically and why additional surface layers are needed. Though peptidoglycan is generally believed to be the sole structural element providing rigidity to the bacterial envelope, some recent findings imply that shear load can be equally distributed and shared between different layers. In this emerging new picture peptidoglycan remains an essential pillar in cell mechanical system but only as a part of a multi-composite cell barrier. The role of the outer membrane, S-layer, capsule, sheath and slime in cell mechanical stability is also discussed. Although the main emphasis is on canonical Gram-negative and Gram-positive bacteria, some fine examples of bacterial envelope adaptations to extreme environments are presented.



## 1. Introduction

Bacteria have no permanent cytoskeletal elements to support their structure and rely on cell envelope to maintain their shape. All bacterial cells are separated from a surrounding media with a membrane envelope but only a few have solely a membrane layer to provide structure, stability, and selectivity. Many additional envelope layers have evolved which help bacteria to maintain their integrity [1]. Cell envelope provides the

intersection between two very different environments; the inner cellular lumen which is a highly regulated homeostatic biochemical system, and an unpredictable outer environment with large fluctuations of chemical and physical parameters [2]. Single cell organisms determine the ultimate physical and chemical boundaries of life on the planet. They can inhabit very low temperature environments down to  $-15^{\circ}\text{C}$  or grow at  $+121^{\circ}\text{C}$ , they can grow at very low or very high pH, low vacuum or pressures up to 1100 bar, they can thrive in hypoosmotic or hyperosmotic medium, at low and high redox potential, high electromagnetic radiation density as well as in radioactive environments [3–11].

Maintaining functional barrier in so diverse environments has resulted in different designs of bacterial envelope, from the most basic resembling a bag of enzymes protected by cytoplasmic membrane in some obligate intracellular bacterial parasites to the most sophisticated multilayer and multi-composite barrier designs found in endospores. Single cell organisms are found in all three domains of life: bacteria, archaea and eukarya. They share similar basic cell plan with cytoplasm enveloped by cell membrane and cell wall. The details, however, differ immensely. In this chapter we will not discuss fungal membrane and semi striated cell wall layers of chitin,  $\beta$ -glucans, manoproteins, and melanins [12]. We will also not discuss structure, composition and chemical bonding in archeal membranes and pseudopeptidoglycan that differs from bacterial peptidoglycan in chemical structure but resembles it in function and physical structure [13]. We will focus on bacterial structures important for cell mechanical stability that have evolved in different bacteria. We will not give a chronological timeline leading to the present-day envelope structures, as these are largely unknown, but provide where possible, mechanistic explanations for the observed bacterial barrier structures.

The literature on bacterial membrane and cell wall structures is very rich and covers in great details chemistry, biochemistry, genetics, and biophysics of different components [14–19]. Bacterial species display different membrane compositions and even the membrane composition of cells belonging to a single species is not constant but depends on the environment and growth condition to which the cells are exposed [20–22]. Bacterial membranes present a large diversity of amphiphilic lipids, including the common phospholipids phosphatidylglycerol (PG), phosphatidylethanolamine (PE) and cardiolipin, the less frequent phospholipids phosphatidylcholine (PC), and phosphatidylinositol (PI) and a variety of other membrane lipids,

such as ornithine lipids, glycolipids, sphingolipids or hopanoids [23]. There are excellent reviews that give an overview about the bacterial membrane lipid structures, different metabolic pathways involved in their formation, and the distribution of membrane lipids and metabolic pathways across taxonomical groups and will not be discussed further [23–26]. Similar for peptidoglycan, there is a high diversity in the composition, sequence of the peptides and cross linkers that varies significantly from species to species and with the growth conditions [27]. We understand well the biogenesis of bacterial S-layers, a proteinaceous surface layer, which is formed by the self-assembly of monomeric proteins into a regularly spaced, two-dimensional array on the surface of bacteria [28]. Comprehensive description of structure, biosynthesis, transport, and assembly of bacterial capsular polysaccharides is known for some bacteria [29]. Although biosynthesis and assembly of structures embedded in cell wall and membrane such as pili, fimbria and flagella are vital for motility and adhesion, they will not be further discussed [30–34].

The main focus of this chapter will be on different surface layers and their contribution to the mechanical stability of bacteria in different environments. There are many known functions of bacterial envelope layers that include but are not limited to enzyme display, transport, motility, adsorption, biofilm formation, interactions with the host, or regulation of the immune system response [35–37]. However, it is often neglected that all surface layers also contribute to the maintenance of cell mechanical integrity. We will begin by reviewing structural integrity of lipid monolayers and bilayers and show how they fail mechanically and why additional surface layers are needed in bacteria. We will next describe the mechanical properties of peptidoglycan which is generally believed to be the sole structure providing rigidity to the bacterial envelope. However, some recent findings imply that shear load can be equally distributed and shared between different layers [38,39]. In this emerging new picture peptidoglycan remains an essential pillar in cell mechanical system but only as a part of a multi-composite cell barrier that needs to be protected as it is highly vulnerable to a variety of chemical attacks. Much like steel reinforced concrete, which provides tensile strength to the construction, but fails on corrosion. We will discuss the role of the outer membrane, S-layer, capsule, sheath and slime in cell mechanical stability. Although the main emphasis will be on canonical Gram-negative and Gram-positive bacteria, we will give some fine examples of surface layer adaptations to extreme environments.



## 2. Lipid monolayers

### 2.1 Lipid monolayer polymorphism

Lipid monolayers, monomolecular films at polar-apolar interface which reduce surface tension, are elemental building blocks of cell membranes and are used extensively as model systems to study adsorption, surface activity, wetting, ordering, lipid phase transitions, and membrane protein-lipid interactions [40–44]. The most obvious geometric feature of lipid monolayers is spontaneous curvature, which is directly related to the lipid molecular geometry [45]. The common bacterial phospholipids such as PE, phosphatic acid, diacylglycerol or cardiolipin, have small polar headgroup to acyl chain ratio which makes them roughly conical in shape and impose a negative monolayer curvature. Monolayer with these lipids bends in such a way that the headgroups come closer together. Less frequently found PC and phosphatidylserine are cylindrical lipids that form a flat monolayer. Conversely, lipids with a large headgroup to acyl chain ratio, such as lysophosphatidylcholine or the large headgroups in PI phosphates confers an inverted conical shape to the lipids, thereby favoring the bending of the membrane into a positive curvature, bending the monolayer away from the headgroups (reviewed in Ref. [46–50]). Polymorphism in lipid monolayers is given in Fig. 1.

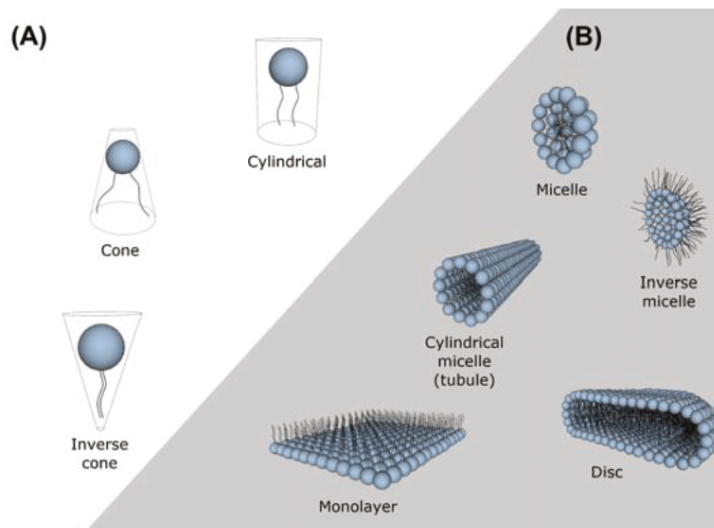


**Fig. 1** Different phospholipid molecular geometries: cylindrical, cone and inverse cone (A); different monolayer aggregates of phospholipid molecules: micelle, inverse micelle, cylindrical micelle (tubule), disc and monolayer (B). Schematic drawings are adapted from Koynova et al. [51] and Patel et al. [52].

## 2.2 Biological membrane is not a monolayer

Lipid monolayers provide a hydrophobic barrier and a good solvent for membrane proteins; however, they do not reflect the structure of biological membrane, which is composed of two monolayers. No known bacteria have their membrane composed of monolayers only. Lipid monolayer bending elasticity is not sufficient to damp the thermal fluctuations. In particular, a loose dynamic monolayer, such as an oil-water interface, has pronounced wrinkles associated with thermal fluctuations and may easily collapse [53]. The surface tension of lipid monolayers decreases with lipid density. At a certain very high surface density, further reduction of the surface tension is not possible, thus the monolayer become unstable at the interface and collapses. Calculations indicate that the energy to deform a monolayer by area compression is significantly greater than that needed to deform it by bending or chain tilting [54]. The collapse of lipid monolayers is dependent on temperature, lipid composition and may be reversible or irreversible [40]. Wrinkling or buckling of monolayer leads to the formation of different 3D lipid aggregates (e.g., bilayer folds, vesicles, tubes, micelles) [55]. The irreversible collapse of lipid monolayer to hexagonal phase or micelles would be detrimental to cell viability.



## 3. Lipid bilayers

Lipid bilayer is the single most important membrane structure found in bacteria (Fig. 2). Since lipid bilayers provide a universal biological membrane matrix, it is expected that many of the mechanical deficiencies of lipid

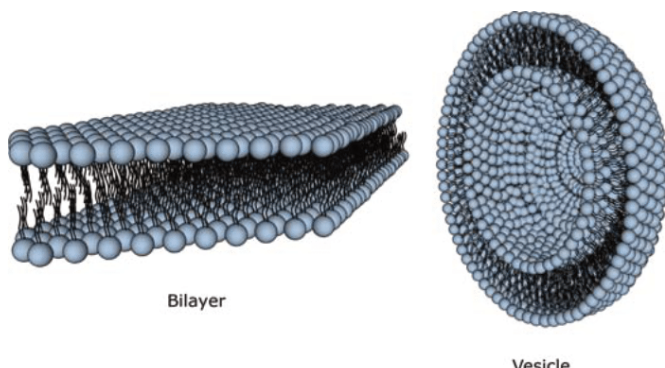


**Fig. 2** Models of phospholipid bilayer and vesicle. Schematic drawings are adapted from Bozzuto et al. [57] and Khan et al. [56].

monolayers are remedied in lipid bilayers. Two factors primarily govern whether a lipid will form a bilayer or not: solubility and shape. For a self-assembled structures such as a bilayers to form, the lipid should have a low solubility in water, which can also be described as a low critical micelle concentration [58,59]. Above the critical micelle concentration molecules will aggregate and form larger structures such as bilayers, micelles or inverted micelles (Fig. 1 and Fig. 2) [60]. Propensity for lipid bilayer depends on shape of the lipid [49,50]. If a particular lipid has too large a deviation from zero intrinsic curvature it will not form a lipid bilayer [61].

### 3.1 Lipid bilayer mechanical properties

The critical mechanical properties of fluid lipid bilayers are bilayer area compressibility/expansion modulus and bilayer bending constant. They determine the bilayer ability to compress, expand, or bend, and its propensity to curve [62]. Lipid bilayer is elastic by nature, giving it the ability to compress and expand and to protect the structural integrity of the cell even in times of mechanical deformation. Compressibility modulus quantifies the response of membrane area to tension, which under physiological conditions may arise from various perturbations, such as changes in osmolarity across the membrane or the addition of lipids or other molecules to one of the membrane's leaflets [63]. Surface flow properties of lipids are directly related to the structural rigidity of membranes [64]. For fluid bilayers the free rearrangement of molecules within the plane means that the structure does not support shear stress, and the shear modulus is by definition zero [65]. Unlike a bulk material, where the resistance to expansion comes from the intermolecular bonds, the resistance to expansion in a bilayer is a result of the extra hydrophobic area exposed to water upon pulling the lipids apart [66]. To a good first approximation the expansion modulus is  $2\gamma$ , where gamma ( $\gamma$ ) is the surface tension of the water-lipid interface. Typically, the expansion modulus is 80–200 mN/m. The values vary strongly with solution conditions [67], but only weakly with tail length and lipid unsaturation [68]. On the other hand, the size of the hydrophilic head group will strongly influence the packing density [69]. A related term to expansion energy is the edge energy, the energy per unit length of a free edge contacting water. This can be thought of as the work needed to create a hole in the bilayer of a unit length. Usually, lipid bilayers begin to rupture at a relative surface expansion of the 2%–4%, which corresponds to an applied tension of 1–25 mN/m [70]. The edge energy is of significant importance in biology as it contributes to the auto-assembly and auto-healing of lipid

bilayer structures [71]. The edge energy enables compartmentalization and resealing after sonoporation or electroporation. Due to the pronounced hydrophobic nature of lipid bilayers spontaneous pore formation is significantly suppressed which enables lipid bilayers to act as a barrier in biological membranes [72]. The mechanical properties of lipid bilayers are further dependent on lipid distribution and composition [68,73–75]. Adding new bilayers (making multilamellar structures) improves mechanical stability of membrane systems in proportion to the degree of lamellarity [76]. However, multilamellar membrane structures are usually not found in bacteria. Most likely due to the transport problems and decreased permeability.

### 3.2 Lipid bilayer bending elastic modulus

Arguably the most important lipid bilayer mechanical property is its bending elastic modulus. Lipid vesicles, for example, are strongly curved. Unlike compressive strain, it is very easy to sustain curvature strains (torques) in a lipid bilayer because of the smallness of its bending elastic modulus, which is typically a few  $k_B T$  up to  $20 k_B T$  [77–79]. Nevertheless, compared to lipid monolayer the elastic bending modulus of the bilayer is doubled [80]. This provides much more stability for the biological membrane. The bending elastic constant of lipid bilayer determines membrane flexibility and a variety of membrane-associated physical and functional properties as reviewed by Marsh [80]. It can control membrane vesicle shape, affect the structure and formation of interlamellar attachments and non-lamellar lipid phases, play an important role in membrane fusion processes, determine the scale of thermally induced elastic bending fluctuations, modulate membrane-membrane interactions, rescales the lateral compressibility that might have functional consequences for membrane insertion of proteins [80]. Together with the spontaneous curvature the bending elastic constants can modulate or control the activity of membrane-associated enzymes and ion channels [81].

Lipid bilayer bending is dependent on its composition. Changes in membrane thickness can affect the bending rigidity of the lipid membrane [82]. Bending rigidity increases with the square of the bilayer thickness. In addition, bending rigidity is dependent on lipid head group charge. For instance, negatively charged dioleoylphosphatidylglycerol (DOPG) liposomes have tendency to become spherical compared to liposomes composed only of neutral lipids [83,84]. The repulsive forces between negative DOPG maximizes their distance and therefore stabilize spherical morphology of lipid bilayer and require larger forces to deform [69]. For example, vesicles

composed of an *Escherichia coli* lipid extract are ~50% less stiff than those containing only DOPG [85]. Similarly, lipids composed of only zwitterionic dimyristoylphosphatidylcholine require approximately half the force to deform compared to DOPG [69]. In *Staphylococcus aureus* and *Caulobacter crescentus* the fraction of DOPG can be as high as 80% and the presence of surface charge stiffens the membrane because the repulsion between the charged lipids effectively resists membrane bending [86]. On the other hand, several peripheral and integral membrane proteins can increase bending and therefore reduce membrane stiffness [87] causing membrane invaginations and evaginations which results in the formation of tubules, vesicles or stacked membrane arrays [88].

### 3.3 Lipid bilayer phase transition

Lipid bilayer mechanical properties are strongly dependent on thermodynamics. The motion of individual lipid molecules at various temperatures is different, which results in different packing of acyl chains and hydrogen bonding between head groups, yielding different lipid phases [89]. Upon heating, lipids undergo a gel-to-liquid crystalline phase transition, which is accompanied by a large entropic change [90]. Changes in the internal energy of lipids with temperature are related to both lipid volume and area changes [91]. For instance, the average volume of a dipalmitoylphosphatidylcholine lipid bilayer changes by about 4% upon melting with the simultaneous lipid area increase of 25% [92,93]. Close to the chain melting transition of lipid bilayers, volume and enthalpy fluctuations increase whereby compressibility display pronounced maxima whereas the sound velocity has its minima [91]. It has been reported that at the transition temperature the bending rigidity significantly drops, bilayer gets thinner and the permeability for water increases [94,95]. In multicomponent lipid bilayers, the presence of saturated and unsaturated lipids with distinct transition temperatures complicates phase behavior. It is interesting to note that bacteria adapt their membrane composition so that they always grow at temperatures above the phase transition of their lipids. For example, if *E. coli* grows at 37 °C it has membrane lipid phase transition at 21 °C, whereas if it grows at 15 °C it has membrane lipid phase transition at 10 °C [96]. It is obvious that bacteria prefer liquid over gel phase membrane.

### 3.4 Failure of lipid bilayer stability

Although relatively stable lipid bilayers can be disrupted by a variety of physico-chemical stressors. The major challenges to lipid vesicle stability

are: mechanical stress [97], oscillating electric field [98,99], static pressure [100], shock waves [101]; hydrolysis [102,103] and chemical assaults by different charged and surface active agents. Vesicles can become transiently porous and leak with no substantial volume change during the process of electroporation [104]. On a longer timescale (e.g. during shear stress) pores may grow to a critical size that leads to lipid bilayer disintegration into several fragments that subsequently reassemble into smaller vesicles. Similar in case of large elongations, the lipid vesicle may deform and fragment to smaller vesicles [97]. The integrity of lipid bilayer may be compromised by lipid hydrolysis. The rate of lipid hydrolysis is dependent on pH [105,106], temperature [105], buffer species [69,107], and ionic strength [108–111]. The ultimate disruption of lipid vesicles is solubilization with surface active molecules (e.g. detergents like Triton X-100). Amphiphilic compounds increase permeability of lipid vesicles by intercalating into the lipid bilayer, which at concentrations higher than critical micellar concentrations, leads to disruption and solubilization of the lipid bilayer [112,113].

Although there are many ways how lipid bilayers can be compromised, from biological point of view, lipid bilayer vulnerability to solubilization by surface-active compounds and failure to sustain osmotic pressure induced expansion are the leading causes of bacterial cell deaths. To curb this, bacteria need to reinforce the lipid bilayer structure or use additional envelope layers.



#### 4. Cytoplasmic membrane layer

Simple homogenous membrane systems such as lipid monolayers or bilayers describe the fundamental physico-chemical properties of biological membranes but fail to describe the complexity of cytoplasmic membrane structures and functions. This is mainly due to a large number of lipid-lipid and lipid-protein interactions found in bacteria. For instance, *E. coli* has more than 100 different head group-acyl chain phospholipid combinations [114]. Such mixtures often exhibit properties intermediate to their components but are also capable of nonlinear phenomena which are not seen in single component systems such as phase separations [115,116]. If some of the lipid components are liquid at a given temperature while others are in the gel phase, the two phases may coexist in spatially separated populations [117]. The phase separation plays a critical role for proteins as they partition into one or the other phase and become locally concentrated or activated.

For example, in *Streptococcus pneumonia* the coexistence of liquid and gel phases minimize bending stress in the ellipsoid geometry defined by the cell wall. Gel phase lipids with high bending rigidity are spontaneously organized at the equator where curvature is minimal, thus marking the future division site, whereas liquid phase membranes are positioned onto the oblong hemispheres [118].

#### 4.1 Material properties of cytoplasmic membranes

Cytoplasmic membrane material properties such as membrane stretching elasticity, its mean curvature, elastic modulus, edge energy, and flexoelectricity are different from simple bilayer model systems [16,79,119]. Biological membranes also have a degree of trans-bilayer asymmetry which increases mechanical stability compared to symmetric bilayers [120]. In sharp contrast to lipid bilayers, cytoplasmic membranes actively maintain, sense, and generate local membrane curvature. This active process is mediated and controlled by specialized proteins that can generate force by polymerization or molecular motors [121]. Maintaining membrane curvature is important because cell has control over processes like membrane scission, septal ring formation, nanotube formation, membrane invaginations, budding, trafficking, fusion, microdomain formation as well as local protein concentration and enzyme activation on membranes [121–130]. For example, four distinct types of membrane topologies can be found in rod-shaped bacteria: the cylindrical shape with zero Gaussian curvature; the curved tip of the septum with negative Gaussian curvature; the concave membrane shape found at the inner surface of the cell poles with positive Gaussian curvature; and the convex membranes found at the outer surface of the cell poles and endospores [131]. Related to membrane curvature is membrane flexoelectricity, a mechanoelectric phenomenon known from liquid crystal physics. In cytoplasmic membrane flexoelectricity manifests itself as the development of polarization upon changes in curvature [132]. Bioflexoelectricity enables membrane structures to function like soft micro and nano machines, sensors and actuators, thus providing important inputs to vital cellular phenomena such as membrane contact, electromotility, and mechanosensitivity [133].

#### 4.2 Membrane failure energy

All the above functions of cytoplasmic membrane are possible only if membrane cohesion force is not exceeded. When cell membrane expands it can reach critical size and ruptures. In hypoosmotic environments water diffuses

into the cell in an attempt to equalize chemical potential inside and outside of the cell resulting in cell volume increase. If critical elastic area compressibility modulus and membrane tensile strength are exceeded the failure energy is reached and cell membrane yields. Membrane failure energy can be increased significantly by cholesterol inclusion [134]. The cholesterol modulates the biological membrane in multiple ways. It changes the fluidity, thickness, compressibility, water penetration and intrinsic curvature of lipid bilayers [135]. The inclusion of cholesterol in lipid bilayers is important factor in increasing lipid bilayer cohesion, but only for lipids where both acyl chains are saturated, or mono or di-unsaturated. Polyunsaturated fatty acids induce greater fluidity because of their higher degree of conformational flexibility [136]. Multiple unsaturation in both lipid chains inhibits the condensing effect of cholesterol in bilayers. The failure energy in sphingomyelin/cholesterol mixture at approximately 40 mol% cholesterol could reach up to 173 mN/m, which is approximately 30-fold larger compared to diarachidonylphosphatidylcholine bilayers [134].

In bacterial membranes, however, cholesterol is absent. Thus, this kind of membrane protection is not an option. Several bacteria have hopanoids as minor membrane components [137]. It has been proposed that hopanoids may have similar function for modulation of molecular order of membranes as sterols in eukaryotic cells [138]. Although inclusion of hopanoids in bacterial membrane may protect bacterial cytoplasmic membrane from excessive expansion, it is not a general mechanism protecting bacteria from hypoosmotic shock. In contrast to eukaryotic cytoplasmic membrane, where membrane is fortified by physical connections to cytoskeleton, bacteria also have only limited temporal connections to the cytoskeleton (i.e. to FtsZ ring during the cell division) [139,140]. Therefore, in order to preserve membrane integrity a completely new design is needed in bacteria to protect cytoplasmic membrane from the adverse environmental effects.



## 5. Peptidoglycan layer

Most of bacteria rely on peptidoglycan in hypoosmotic environments to protect their cytoplasmic membrane [141]. In the bacterial world, one of the most important forces changing cell size and shape is water. Bacterial cytoplasm is a highly salty environment suspended in a less salty surrounding. As bacteria do not have active water transporters, they rely on osmosis for water transport. During water influx cell volume increases, thereby

stretching lipid bilayer until it eventually bursts. Water flux response may occur within milliseconds of osmolarity change [142]. The role of peptidoglycan is to act as a barrier that physically blocks cell to take on too much water. The situation is similar to an inflation of a balloon inside a small box. Once expanding balloon hits the wall it pushes back on the balloon and no more air can be pressurized into the balloon. In contrast to the rigid box, peptidoglycan can reversibly expand providing a fitting fabric for the cell volume under osmotic pressure.

### 5.1 Matching the turgor pressure

In hypoosmotic environments inflow of the water increases the hydrodynamic (turgor) pressure inside the cell which results in cytoplasmic swelling. Force is required to counterbalance turgor pressure. The greater the difference between the osmolyte concentration outside and inside of the cell, the more force is necessary to withstand the pressure. Turgor pressure is defined by the ideal gas law-like,  $P = RT (C_{\text{int}} - C_{\text{ext}})$ , where R is the gas constant, T is the temperature, and  $C_{\text{int/ext}}$  are the internal/external osmolarity, respectively. The turgor pressure in *E. coli* cells can vary in the range from 0.3 to 5 atm. Usually, it is higher in Gram-positive compared to Gram-negative bacteria [38,143]. To protect cell membrane from bursting during hypoosmotic stress bacteria synthesize peptidoglycan with a strength that matches the turgor pressure. For example, in low turgor environment a single layer of peptidoglycan can be enough to control the turgor pressure in *E. coli* [144]. On the other hand, much higher turgor pressure in some Gram-positive bacteria require substantially thicker peptidoglycan (Fig. 3) [27]. The turgor pressure is one of the most important growth parameters for bacteria. For example, during hypoosmotic shock in *B. subtilis* cytoplasmic membrane expands and electrically depolarize. This slows the motion of energy driven bacterial actin homolog MreB, which signals the rate and location of cell-wall synthesis [146]. Consequently, growth arrests, which is a safety measure preventing build-up of osmolytes inside the cell that would cause membrane to burst. If excess membrane is synthesized the growth resumes, which suggests that increased membrane tension is likely responsible for the growth inhibition during hypoosmotic shock [147].

### 5.2 Peptidoglycan composition

The peptidoglycan is composed of glycan strand and peptide stem. The glycan strands are made up of alternating N-acetylglucosamine (GlcNAc) and N-acetylmuramic acid (MurNAc) residues linked by  $\beta$ -1-4 bonds.

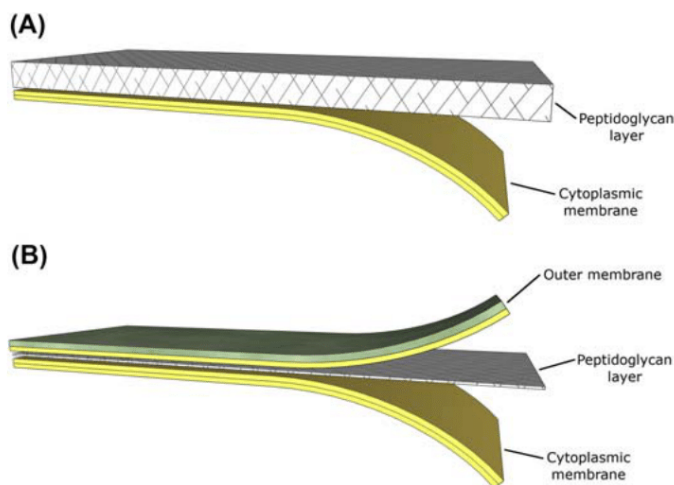


**Fig. 3** Schematic representation of bacterial cell envelope structure in Gram-positive bacteria with a cytoplasmic membrane which for simplicity is depicted to be composed of two identical leaflets and a thick peptidoglycan layer (A), cell envelope in Gram-negative bacteria with cytoplasmic membrane, thin peptidoglycan layer, and asymmetric outer membrane composed of lipopolysaccharide outer leaflet (green) and phospholipid inner leaflet (yellow) (B). The thickness of different layers is presented relative to the cytoplasmic membrane. *Schematic drawings are adapted from Madigan et al. [145].*

The basic disaccharide unit can be repeated several times (e.g. from 2 to 250) [148,149]. The D-lactoyl group of each MurNAc residue is substituted by a penta-peptide stem (usual composition is L-Ala- $\gamma$ -D-Glu-meso-A<sub>2pm</sub>-D-Ala-D-Ala). Cross-linking of the glycan strands generally occurs through neighboring peptide stems between the carboxyl group of D-Ala at position 4 on one peptide stem and the amino group of the diamino acid at position 3 of the other stem, either directly or through a short peptide bridge. Both the glycan and peptide part can be modified. In different bacteria glycan strands can be N-deacetylated, O-acetylated, N-glycosylated [150,151]. Amino acid composition of the peptide stem can vary at all five residues as well as in length and composition of the cross-linker. In addition, peptide stem and cross-linker can be further amidated, hydroxylated, acetylated, or decorated with amino acids or other groups including proteins [27,152]. The fine structure of peptidoglycan is not constant and varies with growth phase and bacterial development [22,153].

Although peptidoglycan is usually considered as a single component material it is best viewed as a composite material. Cytoskeletal filaments such as

MreB are interlinked to peptidoglycan via transmembrane protein MreD, periplasmic protein MreC and penicillin-binding proteins (PBPs) thus interlinking cell cytoskeleton with exoskeleton [154]. MreB is an actin homolog in *E. coli* that forms filaments and is implicated in cell shape maintenance. MreB filaments change peptidoglycan curvature and can exert an inward mechanical force [155,156]. If the intrinsic radius of curvature of MreB is less than the cell radius ( $R$ , ~500 nm) then the cell wall will experience an inward force and will be reshaped. The result is that the steady-state shape of the cell is a cylinder if the MreB filaments are of sufficient stiffness [157]. If MreB is deleted from the cell and the turgor pressure remains cell become spherical. The MreB filament reinforced peptidoglycan layer can be regarded as a fiber-reinforced composite material [156].

### 5.3 Peptidoglycan architecture

Peptidoglycan can form quasi 2D single layer structures in Gram-negative bacteria or thick 3D structures in Gram-positive bacteria. From an architecture point of view the most important peptidoglycan parameter is the degree of cross-linking. The degree of cross-linking varies a lot, from around 20% in *E. coli* to over 90% in *S. aureus* [158]. If we translate this to muropeptide content in *E. coli* most peptidoglycan units appear as monomers or dimers (50% and 40%, respectively), while higher oligomers being a minority [159]. Conversely, in *S. aureus*, the percentage of monomers is low (<10%) and most peptidoglycan units being present as oligomers (lengths up to nonamers were detected by HPLC and up to eicosamers deduced from calculation) [160].

Peptidoglycan architecture can be easily remodeled during growth [159,161]. For example, the transition of *E. coli* from an exponential growth into a resting stationary phase drastically modifies both the composition and architecture of peptidoglycan. The relative abundance of ld-A<sub>2pm</sub>-A<sub>2pm</sub> cross-linked muropeptides increases from approximately 5% to 12% of the total muropeptides [161], the degree of cross-linkage increases from 28% to 38% cross-linked muropeptides, the mean glycan chain length decreases from roughly 33 down to 17 disaccharides per chain, and the lipoprotein-bound muropeptides increases from 9% to 14% [159,161,162]. When peptidoglycan remodels there are two opposing contributions to the Gibbs free energy. During the addition of peptidoglycan basic unit, energy is stored in the activated MurNAc and GlcNAc units which drives the synthesis. This is opposed by the mechanical strain energy change which depends on the shape and size of the cell which increases with cell growth.

When assembly and disassembly reactions exactly balance the peptidoglycan stops growing [156]. The assembly and disassembly process is mediated by transpeptidases and hydrolases and is reversible. The most important enzymes for peptidoglycan architecture remodeling are DD-carboxypeptidase, which belong to the low-molecular weight penicillin-binding proteins (PBP) family. In contrast to the high-molecular weight PBP that synthesize the peptidoglycan, the DD-carboxypeptidase are thought to regulate the degree of cross-linking between glycan chains. By removing the terminal D-alanine from the ends of the peptide side chains, they prevent the transpeptidation reaction. Bacteria often possess several DD-carboxypeptidase and this multiplicity could be important to fine-tune architecture in response to environmental conditions [163–166]. The peptidoglycan synthesis is controlled by cytoskeletal elements from the inside of the cell, whereas peptidoglycan hydrolysis and remodeling are controlled from the enzymes incorporated in the outer membrane. However, recent data indicate that at least in some Gram-negative bacteria, the enlargement of the peptidoglycan layer requires control or activation of peptidoglycan synthases not only from inside the cell but also by synthases associated with the outer membrane, which provides new tools for peptidoglycan remodeling [141].

#### 5.4 Biophysical properties of peptidoglycan responsible for stress bearing

Peptidoglycan is a very efficient biomaterial which provides mechanical strength to bacterial cells. It is light, porous, dynamic, strong and yet in constant flux. The peptidoglycan is viscoelastic solid that allows reversible expansion under pressure and gives cell its shape. Normally peptidoglycan is under dynamic stress in the living cell due to the cell turgor pressure. The pre-stressed state of peptidoglycan can relax if the cytoplasmic membrane is destroyed. For example, in *E. coli* upon membrane dissolution with detergent cell surface area decreased for 45% due to the relaxation of the peptidoglycan [167]. For a spherical cell with radius R and turgor pressure P the tensile stress in the cell wall is isotropic,  $\sigma = PR/h$ , where h is the peptidoglycan thickness. For a cylinder under pressure,  $\sigma_{11}$  and  $\sigma_{22}$  are defined as stresses in the circumferential and axial directions, respectively [156]. Peptidoglycan is more deformable in the direction of the long axis of the cell (elastic modulus  $2.5 \times 10^7 \text{ N m}^{-2}$ ) than in the direction perpendicular to the long axis (elastic modulus,  $4.5 \times 10^7 \text{ N m}^{-2}$ ) [168]. This is consistent with the observation that changes in the volume of osmotically

shocked *E. coli* cells are mainly due to changes in the cell length, whereas cell diameter is virtually constant [169]. It was implied that the anisotropy in elasticity is the consequence of the predominant alignment of the more flexible peptides stems in the direction of the long axis of the cell and of the more rigid glycan strands perpendicular to the direction of the long axis [170]. Peptidoglycan has relatively homogenous pore size distribution: the mean radius of the pores is 2.06 nm for *E. coli* peptidoglycan and 2.12 nm for *B. subtilis* peptidoglycan [171]. From these values it was calculated that globular, uncharged proteins with molecular weights of up 22–24 kDa should be able to diffuse through the relaxed peptidoglycan. If peptidoglycan is stretched, globular proteins of up to 50 kDa or more are able to diffuse through peptidoglycan layer [172].

### 5.5 Obligate intracellular parasites lack peptidoglycan layer

Some obligate intracellular parasitic bacteria, such as *Ehrlichia* and *Anaplasma phagocytophilum*, have only cytoplasmic membrane without peptidoglycan [173]. Obligate intracellular bacteria replicate exclusively within the interior of the living host cells in an osmotically protected niche. Under these conditions peptidoglycan is dispensable. Moreover, the presence of peptidoglycan puts bacteria at risk of detection and destruction by host peptidoglycan recognition factors and downstream effectors [174]. This has resulted in a selective pressure to reduce the levels of peptidoglycan in obligate intracellular parasites. For example, in *Ehrlichia* and *A. phagocytophilum* no genes for peptidoglycan synthesis exist. In some other obligate intracellular parasites genes for peptidoglycan exist but peptidoglycan synthesis has not been detected or peptidoglycan is only transiently present during the bacterial cycle development. Although peptidoglycan is absent in some bacteria (i.e. *Mycoplasmas*, *Planctomyces*, *Chlamydiae*) all the other bacteria have peptidoglycan [27]. It appears that relying solely on cytoplasmic membrane to maintain cell integrity is a very limited strategy in the bacterial world reserved only for the intracellular parasites.



## 6. Bacterial outer membrane layer

Peptidoglycan is a formidable nanomaterial, but it is not immune to destruction and needs protection from adverse environmental factors. Several agents, such as  $\beta$ -lactams (i.e. penicillin, cephalosporin, carbapenems), lipo-peptides (daptomycin), peptide antibiotics (i.e. colistin, polymyxin B) and

ionophores (i.e. monensin, alinomycin) target cell wall [175]. It is interesting to note that Gram-negative bacteria have thinner peptidoglycan layer, yet they are more resistant to antibiotics than Gram-positive bacteria [176]. Some Gram-negative bacteria, such as *Pseudomonas*, are notorious in this regard [177]. There are several strategies how to protect peptidoglycan from destruction (i.e. synthesis of the outer membrane, S-layer, capsule, sheaths, slime) which we will now discuss.

The outer membrane is found mainly in Gram-negative bacteria (Fig. 4). The function of the outer membrane is to serve as a protective barrier that controls the influx and efflux of molecules. It is not immediately obvious why this layer is essential for bacteria. The outer membrane separates the periplasm from the external environment and function as a selective barrier that keeps hydrophobic or amphiphilic compounds that may destroy peptidoglycan from the cell [179,180]. For example, *E. coli* that inhabits the mammalian gut must have cell envelope that is particularly effective at excluding detergents such as bile salts that solubilize the cytoplasmic membrane [181]. This need not be a pressing issue for other Gram-negative bacteria, and their envelopes may differ in species and environment specific ways [14].

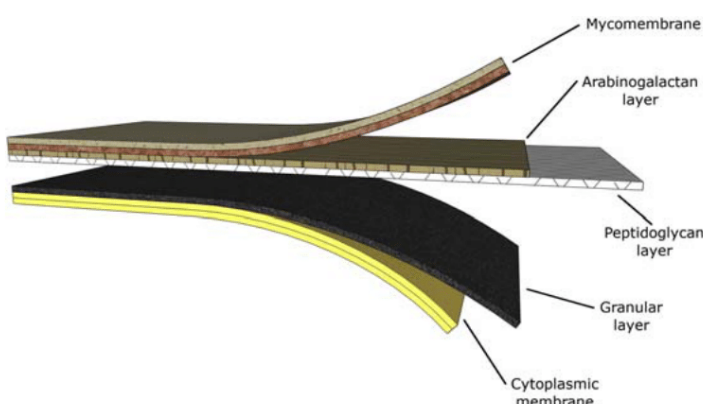


**Fig. 4** Schematic drawing of cell envelope found in members of the order *Corynebacteriales* adapted from Vincent et al. [178]. The inner leaflet of the outer mycomembrane is homogenous and composed of mycolic acid, whereas the outer leaflet is highly heterogeneous and consists of lipids, lipoglycans, and proteins. The thickness of different layers has been estimated to be: cytoplasmatic membrane 6.3 nm; granular layer 3.8 nm, periplasmic space 14.1 nm; peptidoglycan-arabinogalactan layer 6.3 nm; the asymmetric outer membrane 7.5 nm.

## 6.1 Outer membrane composition

The outer membrane is a unique asymmetrical bilayer structure with an inner leaflet composed of phospholipids and an outer leaflet composed mostly of lipopolysaccharides molecules (LPS). The LPS molecule is made of three parts: lipid A, a core oligosaccharide that is usually further subdivided into an inner and outer region; and an O-antigen polysaccharide [182]. Lipid A contains two  $\beta$ -(1–6)-linked glucosamine residues that are phosphorylated and have acylated tails anchoring the LPS molecule into the outer membrane. The inner core is proximal to lipid A and contains a high proportion of negatively charged bacteria-specific sugars, such as 2-keto-3-deoxyoctulosonate and phosphorylated L-glycero-D-manno-heptose. The outer core consists of common sugars, such as hexoses and hexosamines. Negatively charged inner core and lipid A form a dense, divalent cation-stabilized layer [183]. The strong electrostatic bridging interactions of  $\text{Ca}^{2+}$  are essential for the outer membrane structure and function. Without charge screening by divalent cations, the LPS molecule is forced to overcome the thermodynamically unfavorable energy barrier and flips across the hydrophobic bilayer to minimize the repulsive electrostatic forces [184]. Consequently, addition of chelating agents to the outer membrane is a well-established method to permeabilize Gram-negative bacteria and to disrupt its structure in *E. coli* [185,186].

## 6.2 Attachment of the outer membrane to other surface layers

The outer membrane is not a free-floating envelope layer surrounding the bacterial cell, but it is covalently attached to the peptidoglycan. In *E. coli* and other related Gram-negative bacteria, Braun's lipoprotein (LPP) is the only lipoprotein that is responsible for the covalent linkage of the outer membrane to the peptidoglycan [187,188]. LPP is attached to the  $\alpha$ -carboxyl group of meso-A<sub>2</sub>pm residue of peptidoglycan through the  $\epsilon$ -amino functional group of its C-terminal lysine residue while its N-terminal glyceryl-cysteine residue is modified by the addition of three fatty acids that allow incorporation of LPP to the inner leaflet of the outer membrane. LPP contributes to the stress bearing of bacterial cell by covalently linking OM to peptidoglycan layer and by regulating the width of periplasmic space [189]. Another peptidoglycan-associated lipoprotein (Pal) of Gram-negative bacteria is important in attachment of the outer membrane to the peptidoglycan. Pal possesses a region that forms a noncovalent binding pocket for

the m-Dap residue (meso-diaminopimelate) of peptidoglycan [190]. Pal is tethered to the outer membrane via its N-terminal lipid moiety. Pal is transcribed as part of an operon that also encodes two proteins TolB and TolA, with which it interacts [191]. This makes Pal lipoprotein one of the most important mechanical structural elements in the bacterial envelope. It interacts noncovalently with the peptidoglycan layer, outer membrane protein OmpA, LPP, periplasmic protein TolB and the inner membrane protein TolA [192–198]. The Tol-Pal complex, an assembly of lipoproteins, integral membrane proteins and periplasmic proteins interacting with each other and the peptidoglycan, forms a web of covalent and noncovalent contacts between the outer membrane, peptidoglycan layer and the cytoplasmic membrane [199]. During bacterial cell division there are additional interactions in the divisome between the cytoplasmic membrane, peptidoglycan layer and the outer membrane which are guided by FtsK protein [200]. Similarly, FtsN and Tol-pal complex are required for proper invagination of cytoplasmic and outer membranes during constriction in cell division [201]. These examples clearly illustrate the interconnected nature of multi-layer bacterial cell envelope fabric.

### 6.3 Outer membrane stress bearing

The covalently cross-linked peptidoglycan had been thought for decades to be the only envelope layer that matters for bacterial mechanics [202,203]. However, some recent findings indicate that the outer membrane can bear stress loads through large molecular assemblies interlinking the outer and the inner membrane. The outer membrane is actually even more stiff than the cell peptidoglycan and makes a large contribution to cell mechanics [39]. It has been suggested that the stiffness and strength of *E. coli* cells during hyperosmotic shock are largely due to the outer membrane [38,39]. The outer membrane is under negligible or slightly compressive load during steady-state growth. However, steady-state growth is unlikely to be common for bacteria in the environment and bacteria frequently encounter hyperosmotic fluctuations and dynamic mechanical forces, which will engage the load-bearing nature of the outer membrane. Both LPS and proteins contribute to the stiffness of the outer membrane. Compromising the outer membrane, either chemically or genetically, greatly increases deformation of the cell envelope in response to stretching, bending and indentation forces, and induces increased levels of cell lysis upon mechanical perturbation [39]. The outer membrane thus contributes to the bacteria's ability to survive and to tune its mechanical properties based on its environment.

#### 6.4 *Mycobacterium tuberculosis* outer membrane

*Mycobacterium tuberculosis* ability to resist, and persist in the moderately acid environment of the phagosome or phagolysosome has been linked to complex cell envelope with double membrane which acts as a formidable permeability barrier for antibacterial effectors, including protons [204]. The cell envelope of *M. tuberculosis* has an unusual, waxy coating on its surface due to the presence of mycolic acid (Fig. 4). This coating makes cells impervious to Gram-staining, and as a result, *M. tuberculosis* can appear either Gram-negative or Gram-positive. In mycobacteria and corynebacteria, the permeability barrier consists of an outer mycomembrane bilayer composed of mycolic acids and other lipids. Mycolic acids are very-long-chain (C30–C90)  $\alpha$ -alkyl,  $\beta$ -hydroxy fatty acids, which contribute to extremely hydrophobic bacterial surface. The inner leaflet of the outer membrane is homogeneous and mainly composed of mycolic acids. The mycoloyl residues are covalently linked to the cell wall arabinogalactan, which connects peptidoglycan to the outer membrane [178]. The outer monolayer of the outer membrane is heterogenous and composed of various glycolipids, including trehalose monomycolate and trehalose dimycolate which accumulates in a cord-like fashion on the surface of the cells [205]. This provides a thick layer of lipid on the outer part of the cell and protects the tubercle bacillus from noxious chemicals and the host's immune system [206,207]. The composition and amounts of mycolic acids have been shown to affect the virulence, growth rate, colony morphology and permeability of *M. tuberculosis* [208–211]. Mycolic acids in the outer membrane also play a mechanical role [212–214]. The cyclopropane rings in mycolic acids of *M. tuberculosis* contribute to the structural integrity of the cell wall complex and protect cell from oxidative stress [215,216]. Between cytoplasmic membrane and peptidoglycan, there is an extra granular layer which is composed of penicillin-binding proteins, lipoproteins and lipoteichoic acids. The function and precise composition of this layer is still poorly understood [178].

#### 6.5 *Deinococcus radiodurans* outer membrane

The *Deinococcus radiodurans* is well known for its extreme resistance to gamma radiation, UV rays, oxidative stress and desiccation stress [217]. *D. radiodurans* is a Gram-positive bacterium possessing the ability to synthesize carotenoids which bind to the cell envelope and protect against UV and oxidative stress [218]. The structure of the cell envelope of *D. radiodurans* is different from that of the other Gram-positive bacteria (Fig. 5). The complex envelope of

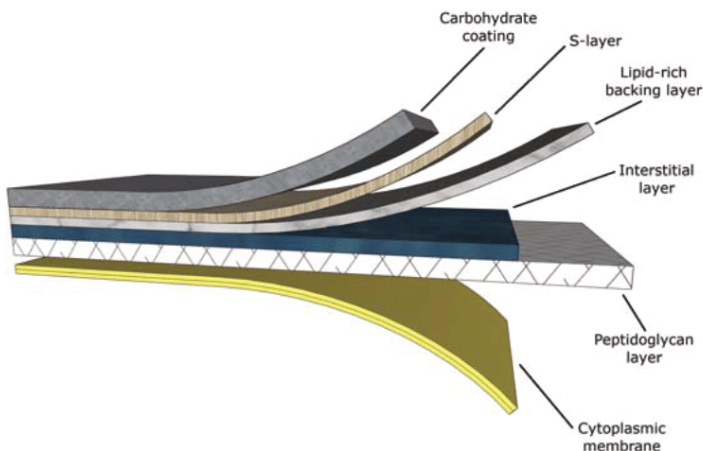


**Fig. 5** *D. radiodurans* envelope structure. The complex structure of cell envelope has been implicated in bacterium extreme resistance to gamma radiation, UV rays, oxidative stress and desiccation stress. Schematic drawing is adapted from Yu et al. [102], Yu et al. [219] and Rothfuss et al. [220].

this organism constitutes a cytoplasmic membrane, a thick peptidoglycan layer, an interstitial layer which is only known to be composed of water soluble proteins, a lipid rich backing layer followed by a hexagonally packed S-surface layer (Hpi) and finally the outermost carbohydrate coat. The composition of the *D. radiodurans* outer membrane is very different from that of Gram-negative bacteria. In contrast to Gram-negative bacteria the outer membrane of *D. radiodurans* has no LPS or usual bacterial phospholipids instead, there are high proportions of glucose-containing phospholipids [221].



## 7. S-layers

The S-layers are frequently observed surface layers in bacteria [222]. It is therefore an exception to the rule that in *E. coli* and *B. subtilis*, the canonical bacterial model systems, the S-layers are absent. Most S-layers are formed by noncovalent, entropy-driven assembly of a single (glyco)protein protomer on the bacterial surface, giving rise to proteinaceous paracrystalline layers (Fig. 6). Generally, a single S-layer is present, constituting 5 to 10% of the total cell protein which is a substantial energy burden for a cell. When the other cell surface components (e.g. capsules, glycocalyx) are absent, S-layer is the outermost cell envelope component. Because many

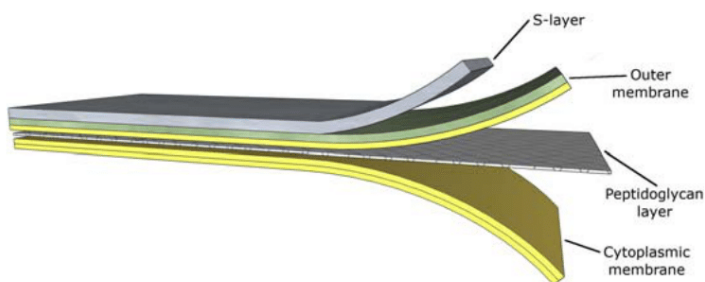


**Fig. 6** S-layer can form as an outermost envelope layer on both Gram-positive and Gram-negative bacteria. Only Gram-negative cell envelope is depicted. The LPS and phospholipid leaflets in the outer membrane are indicated with different colors. The S-layer usually consists of a crystal-like single layer of proteins. The S-layer lattices can have oblique, square, or hexagonal symmetry [223].

bacteria have S-layers it has been speculated that they play important roles in the interaction between the cell and its environment. Various functions have been proposed for S-layers, including shape maintenance and molecular sieving. The S-layer may be a virulence factor, protecting pathogenic bacteria against complement killing, facilitating binding of bacteria to host molecules, or enhancing their ability to associate with macrophages (reviewed in Ref. [224–227]). The S-layer can mechanically reinforce cell envelope by initiating mineral precipitation [228].

### 7.1 S-layer as a primordial membrane

S-layers are the simplest biological (glyco)protein membranes which have developed during the evolution. The S-layer is assembled from identical protein macromolecules. Theoretically, it is not possible to form a closed protein membrane with less redundancy of information. Therefore, it is tempting to speculate that a simple protein membrane capable of dynamic growth could have initiated formation of a barrier membrane envelope in an early stage of biological evolution [229–232]. The S-layers are recognized as versatile patterning elements for the generation of complex supramolecular structures involving other molecules such as lipids, proteins, glycans, and nucleic acids as well as inorganic materials (e.g. nanoparticles). For example, S-layers have been shown to interact specifically with a great variety of amphiphilic molecules (e.g. phosphor- and ether-lipids) generating more complex supramolecular membrane structures with potential for high transmembrane selectivity [233]. When S-layer proteins of *Bacillus stearothermophilus* were recrystallized on positively charged unilamellar

liposomes an inversion of the zeta-potential was observed from +29.1 mV to -27.1 mV. In addition, covalent crosslinked recrystallized S-layer proteins stabilized lipid vesicles. S-layer coated liposomes released only half the amount of liposome enclosed cargo upon exposure to shear forces or ultrasonication or temperature shifts from 25 to 55 °C compared to non-coated liposomes [234] suggesting that S-layer can have a considerable mechanical effect on bacterial cell.

## 7.2 Antifouling properties of S-layer membranes

It was demonstrated that S-layer lattices allow free passage for molecules with a molecular weight of up to 30 kDa and have sharp exclusion limits between molecular weights of 30 and 45 kDa proposing a limiting pore diameter in the range of 3–4.5 nm [235,236]. It appears that molecules capable of penetrating the S-layer have also free passage through the peptidoglycan layer. It is therefore unlikely that S-layers have the potential to function as an effective barrier against lysogenic enzymes and are thus unable to protect peptidoglycan degradation [237]. To allow free passage of molecules S-layers should have antifouling properties [238–240]. It has been suggested that the ultra-low fouling properties of S-layers may be due to their zwitterionic surface properties [241]. In zwitterionic antifouling surfaces ions alternate perfectly in the sub-nanometer scale between positive and negative charges preventing adsorption of naturally occurring molecules, particularly proteins. Alternatively, it has been demonstrated that S-layer could be shedded from the surface to maintain the surface clean [242].

## 7.3 S-layer and mineralization

A unique ecological role was demonstrated for the cyanobacterial S-layer of *Synechococcus* strain GL24. This bacterium was found to induce mineralization of fine-grain gypsum ( $\text{CaSO}_4 \cdot 2\text{H}_2\text{O}$ ) and calcite ( $\text{CaCO}_3$ ) in a fresh water lake [243]. The S-layer has a hexagonal monomer arrangement and provides regularly spaced, chemically identical nucleation sites for mineral growth [228,244,245]. Mineral formation begins within the large holes of the protein array when  $\text{Ca}^{2+}$  binds to negatively charged sites on the S-layer protein and is joined by  $\text{SO}_4^{2-}$ , initiating the formation of a mineral aggregate. Eventually, the S-layer becomes encrusted with mineral and is shed so that cells have a patchy appearance with respect to the location of mineralized portions of their surface. Shedding of S-layer material could be a

common process of bacteria to get rid of mineral depositions on their cell surface thereby maintaining basic vital processes such as growth and division as well as nutrient transport.



## 8. Capsular layers

Capsule polymers are highly flexible hydrocolloids that extend radially from the cell and are rarely cross-linked to one another by covalent bonds (Fig. 7). The most effective linkages between capsule polymers seem to be electrostatic where highly acidic residues can be inter-bridged by divalent metal ions such as  $Mg^{2+}$  or  $Ca^{2+}$ . However, these metals are highly exchangeable and can be displaced by other multivalent species [246]. Capsules are one of the most frequently encountered surface layers [247]. Many species of Gram-positive and Gram-negative organisms are enveloped by a capsule.

### 8.1 Capsule composition

Capsules are comprised of high-molecular-weight capsular polysaccharide chains that are exported across the bacterial cell envelope and retained at the cell surface. The polymers of capsules are branched or unbranched homo- or hetero-polysaccharides but can occasionally be proteinaceous as well [246,248,249]. The chemical composition of capsule displays

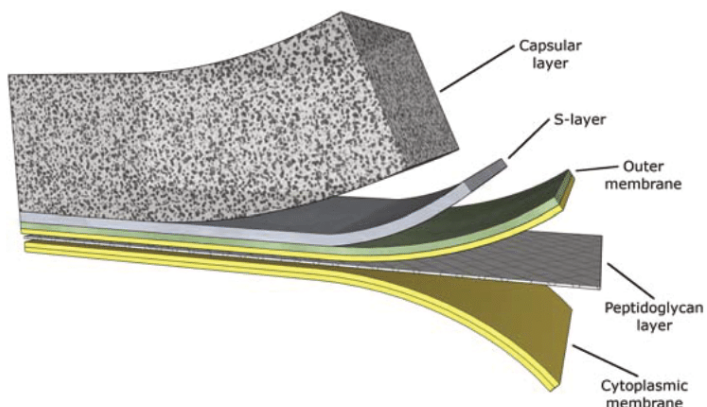


**Fig. 7** Both Gram-positive and Gram-negative bacteria may have capsular layer. Only Gram-negative envelope structure is depicted with a relatively thick gel like capsular layer. The capsular layer can have various thickness and can extend up to several  $\mu m$  into the extracellular space [145].

remarkable diversity even within a single species. For instance, *E. coli* has over 80 different capsular (K antigen) serotypes [250,251]. *E. coli* capsules have been subdivided into four groups based on structural, biochemical, and genetic criteria (reviewed in Whitfield [252]). Capsule polysaccharides in groups 1 and 4 have shorter carbohydrate chains, which are covalently linked to the lipid A core of the outer membrane producing K<sub>LPS</sub> molecules [253,254]. Longer chain polysaccharides form capsules independently of covalent attachment to LPS. For example, K30<sub>CPS</sub> is anchored noncovalently to the bacterial surface by an outer membrane lectin, Wzi [255]. Capsular polysaccharides in groups 2 and 3 are thought to be linked to the surface via a diacylglycerolphosphate moiety [256].

## 8.2 Multifunctional role of capsule

In Gram-negative bacteria capsule is linked covalently and noncovalently to the outer membrane, which in turn is connected to the peptidoglycan and the cytoplasmic membrane. The viscoelastic nature of capsule strengthens the envelope [257]. Extending great distances from the cell surface (often up to several micrometers), capsules are used as cementing substances, to bind bacteria together into microcolony formats, to bind the cells to substrata, or to form flocs, eventually developing large biofilms which cover surfaces [258,259]. Capsular polysaccharides offer physical barrier to antibiotics or bind to cationic antibiotics, thus lowering peptidoglycan degradation. Capsule prevents bacterial cell desiccation due to hydrated nature of polysaccharides keeping all envelope layers moist and lubricated, capsule facilitate bacteria to adhere onto host cell surface, help the bacteria to escape from host immune response by inhibiting complement cascade, prevent antibody opsonization, and preclude the recognition by macrophage [260]. Capsular proteins represent a major virulence factor together with toxins, adhesins [261], LPS, and exopolysaccharides [262].



## 9. Extracellular polymeric substances (EPS)

Like capsules, bacterial extracellular polymeric substances or slimes include a wide range of extracellular homo and heteropolymers [248,263]. They are abundant in nature and are weakly adsorbed to the cell or float freely in the aqueous milieu. They are frequently the most abundant components of biofilms. Sometimes bacteria overproduce their capsular materials but for some reason, fail to anchor them securely to their surfaces.

Such polymers are sloughed off into the surroundings and float freely until they become associated with other solid surfaces or bacteria. Electron microscopy of natural biofilms or suspended flocs frequently reveals envelope and other cellular debris from lysed bacteria intermixed with intact cells throughout a polymeric matrix; this matrix was initially part of a capsule but is now more appropriately classified as extracellular slime or EPS since it is no longer entirely associated with the cell [249].



## 10. Sheath layers

Sheaths are less frequently encountered envelope structures than capsules or EPS in the bacterial world [247]. Sheaths are tubes enclosing linear chains of cells composed of an amorphous polymeric network. Sheaths are found in *Thiothrix spp.*, *Thioploca spp.* or some cyanobacteria [264,265]. In *Thioploca* sheaths, for example, cells can even glide within the sheath [264]. The sheaths are an integral peripheral structure of these genera and have far-reaching design purposes over and above those of more usual bacteria [266]. Sheaths precipitate iron (*Sphaerotilus*) or manganese (*Leptothrix*) oxides [267]. For *Leptothrix discophora*, the manganese-oxidizing capability is determined by proteins within the sheath [268,269]. *Leptothrix* spp. sheaths comprises a metal-impregnated organic matrix that may be synthesized and excreted as globules from the surface of the bacterial cell envelope. Transfer to the immature sheath skeleton by globule, threads or pili like secretions contributes to the thickening of the sheath layer in which aqueous-phase inorganic elements began to deposit, resulting in high electron density fibrous structure [270]. Sheaths play important roles in ecosystems by accumulating biologically important elements and induce the crystallization of unexpected mineral phases [271]. This bacteria may also possess capsule which is structurally differentiated from the sheath, the outer membrane, as well as S-layer (Fig. 8) [272,273].



## 11. Endospores

In terrestrial (soil) environments where many bacteria found potentially lethal extreme conditions which includes cycles of heat and cold, freezing and thawing, physical abrasion, extreme desiccation, exposure to corrosive chemicals, attack by other organisms and their extracellular degradative enzymes, or prolonged exposure to solar radiation there are many

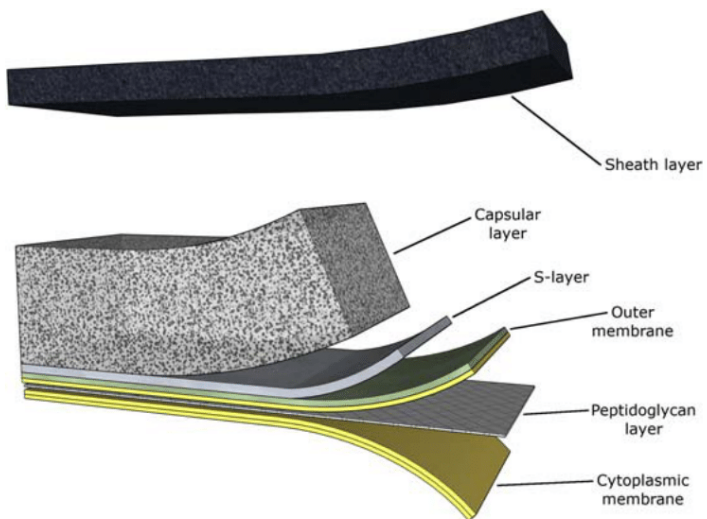


**Fig. 8** Sheath layer is a dislocated structural layer of some bacteria that encloses chains of bacterial cells. Sheath layers are usually metal-impregnated organic matrices. Schematic drawing of Gram-negative envelope structure with additional sheath layer was adapted from Madigan et al. [145].

spore forming bacteria [274]. Endospores are the toughest living biological structure known that can survive extreme conditions for years. A sporulating bacterium cannot predict beforehand how long or in what environment it will spend its dormant state. Therefore, the sporulating cell must prepare for the worst each time it undergoes differentiation. There are several reasons why endospores can survive harsh environments as reviewed by Nicholson et al. [274]. These factors include the genetic makeup of the sporulating species, the precise sporulation conditions, the spore coats, the relative impermeability of the spore core, the low water content of the hydrated spore's core, the high level of minerals in the spore core, the saturation of spore DNA with  $\alpha/\beta$ -type small acid-soluble proteins (SASP), and repair of damage to macromolecules during spore germination and outgrowth.

### 11.1 Endospore envelope structure

The distinct morphological feature of endospore is its layered envelope structure. It is reminiscent of, but much more sophisticated version of the vegetative bacterial envelope structure. The core of the endospore is surrounded, by the inner spore membrane, germ cell wall, cortex, outer spore

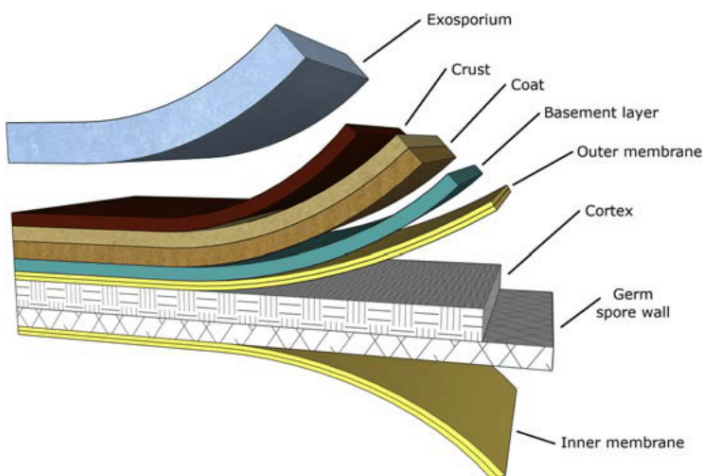


**Fig. 9** Bacterial endospore is the most complex biological cell envelope structure known. The multiple layer structure of the spore envelope protects genome, which is housed in partially dehydrated core. Both germ cell wall and cortex layer are composed of peptidoglycan but with different architecture. The outer membrane is derived from mother forespore phospholipid membrane. The coat has four distinct sublayers: basement layer, inner coat, outer coat, and crust. The outermost protective layer exosporium may not be present in all endospores. Schematic drawing is adapted from literature by McKenney et al. [275], Stewart et al. [277] and Cogliati et al. [276].

membrane, coat, and exosporium (Fig. 9). There are four layers in spore coat observed in thin-section electron microscopy of the *B. subtilis*: a basement layer, a lamellar inner coat, a more coarsely layered outer coat and a recently identified layer named the crust [275]. The coat has an important role in limiting access of hydrolyzing enzymes to the peptidoglycan-containing cortex. In some species, such as *B. anthracis*, a different type of outermost layer exists, called the exosporium [278]. The exosporium is a distinct glycoprotein layer that surrounds the spore and is separated by a gap called the interspace. In *Bacillus cereus* and its close relatives *B. anthracis* and *Bacillus thuringiensis*, the exosporium consists of a crystalline two-dimensional basal layer adorned with hair-like projections [279].

## 11.2 Dissolution of endospore envelope

Although an endospore is mainly a dormant structure fit for the long-term bacterial survival, spores must be able to germinate rapidly when nutrients become available. Spores continually monitor their surroundings using an

array of germination receptors embedded in the inner spore membrane. Germinants of *B. subtilis* include sugars, amino acids, peptidoglycan fragments and ions [280,281]. As germinants will reach their receptors traversing the spore coat and cortex, the coat must ultimately be both protective and permeable. The endospore coat can therefore be conceptualized as a molecular sieve that excludes large molecules, such as lysozyme, while allowing the passage of small-molecule germinants [282,283]. Most of the layered structures of the endospore are rapidly lost upon germination: the coat is shed, and the cortex is degraded by cell wall hydrolases. The germ cell wall is retained to serve as a primer for vegetative cell wall assembly. The inner spore membrane becomes the plasma membrane, whereas the fate of the outer spore membrane is less clear. It may be lost during spore germination, but there is at least one organism (*Acetonema longum*) in which it persists after germination, thus generating a double membrane vegetative cell akin to Gram-negative bacteria [284].



## 12. How did bacterial envelope evolve?

The bacterial envelope is an extremely complex and diverse layered structure of vital importance for bacteria. Although it is very important to know how the envelope evolved, we do not have at present a definite answer. Helpful suggestions are coming from whole-genome sequencing, molecular biology, biochemistry, biophysics and bioinformatics studies [285–287]. For example, we have vague ideas how the outer membrane might have evolved. During endospore formation Gram-positive bacteria have temporally two membranes. Contrary to other endospore formers *A. longum* keeps the outer membrane even after germination [284]. Hence, it is possible that Gram-negative bacteria evolved from an ancestral endospore-forming Gram-positive bacteria [286]. During the process, the thickness of the peptidoglycan was reduced, and teichoic acids were lost, presumably before the acquisition of the LPS molecules. Currently however, there are too many unknowns in this scenario. One thing is to keep the second membrane, the other is to make it functional (i.e. connect it to the peptidoglycan, target protein to the other membrane, change physiology to allow for lower turgor pressures, transport nutrient across two membranes, and many other modifications we find in modern Gram-negative bacteria). Nevertheless, with the new research tools at our disposal we may be in a position to provide some meaningful answers to these questions.



### 13. Conclusions

Bacterial cell envelope is a multicomponent multilayer composite material of exquisite complexity. Bacteria take advantage of physical interactions between envelope molecular components to achieve mechanical stability and selectivity unmatched in biology. These interactions are typically complex and cannot be easily and quantitatively deciphered. Progress is being made in developing a quantitative understanding of the interactions important for cell envelope biogenesis and integrity. We have a general idea how mechanical forces influence molecular chemistry of the envelope and how mechanical stress shape and reshape the cell. We are beginning to appreciate that cell mechanics is not revolving solely around peptidoglycan layer but is an integrated response of all cell envelope layers. The cell envelope structure is interconnected on many different levels. Envelope molecular constituents foremost participate in building a particular layer structure (i.e. lipid bilayer, peptidoglycan, outer membrane, capsule, sheath) where they have distinct molecular interactions within the layer. However, there are also numerous covalent and non-covalent interactions between adjacent layers (i.e. LPP connecting the outer membrane to peptidoglycan) or trans-layer connections between distant layers (i.e. Pal interconnecting the cytoplasmic membrane to the outer membrane via peptidoglycan) that we are beginning to unravel. Multiple interlayer connections reinforce envelope structure. Being light, strong, flexible, porous, and selective cell envelope will continue to inspire engineers to make exciting new material composite structures. However, many molecular details of bacterial cell envelope endurance are still missing and await further theoretical explanation.

### References

- [1] H.T. Tien, A. Ottova, The lipid bilayer concept: experimental realization and current applications, *Memb. Sci. Technol.* (2003) 1–73.
- [2] J.J. Thwaites, N.H. Mendelson, Mechanical behaviour of bacterial cell walls, *Adv. Micro. Physiol.* (1991) 173–222.
- [3] E.M. Rivkina, E.I. Friedmann, C.P. McKay, D.A. Gilichinsky, Metabolic activity of permafrost bacteria below the freezing point, *Appl. Environ. Microbiol.* 66 (2000) 3230–3233.
- [4] K. Takai, K. Nakamura, T. Toki, U. Tsunogai, M. Miyazaki, J. Miyazaki, H. Hirayama, S. Nakagawa, T. Nunoura, K. Horikoshi, Cell proliferation at 122 °C and isotopically heavy CH<sub>4</sub> production by a hyperthermophilic methanogen under high-pressure cultivation, *Proc. Natl. Acad. Sci. U.S.A.* 105 (2008) 10949–10954.
- [5] C. Schleper, G. Pühler, B. Kuhlmann, W. Zillig, Life at extremely low pH, *Nature* 375 (1995) 741–742.

- [6] H. Liu, Y. Zhou, R. Liu, K.-Y. Zhang, R. Lai, *Bacillus solisalsi* sp. nov., a halotolerant, alkaliphilic bacterium isolated from soil around a salt lake, *Int. J. Syst. Evol. Microbiol.* 59 (2009) 1460–1464.
- [7] G. Horneck, Survival of microorganisms in space: a review, *Adv. Space Res.* 1 (1981) 39–48.
- [8] R.D. Sleator, C. Hill, Bacterial osmoadaptation: the role of osmolytes in bacterial stress and virulence, *FEMS Microbiol. Rev.* 26 (2002) 49–71.
- [9] M.G. Liebensteiner, N. Tsesmetzis, A.J.M. Stams, B.P. Lomans, Microbial redox processes in deep subsurface environments and the potential application of (per)chlorate in oil reservoirs, *Front. Microbiol.* 5 (2014).
- [10] G. Beretta, A.F. Mastorgio, L. Pedrali, S. Saponaro, E. Sezenna, The effects of electric, magnetic and electromagnetic fields on microorganisms in the perspective of bioremediation, *Rev. Environ. Sci. Bio/Technology.* 18 (2019) 29–75.
- [11] A. Krisko, M. Radman, Biology of extreme radiation resistance: the way of *Deinococcus radiodurans*, *Cold Spring Harb. Perspect. Biol.* 5 (2013) a012765–a012765.
- [12] N.A.R. Gow, J.-P. Latge, C.A. Munro, The fungal cell wall: structure, biosynthesis, and function, *Microbiol. Spectr.* 5 (2017).
- [13] S.-V. Albers, B.H. Meyer, The archaeal cell envelope, *Nat. Rev. Microbiol.* 9 (2011) 414–426.
- [14] T.J. Silhavy, D. Kahne, S. Walker, The bacterial cell envelope, *Cold Spring Harb. Perspect. Biol.* 2 (2010) a000414–a000414.
- [15] D.-J. Scheffers, M.G. Pinho, Bacterial cell wall synthesis: new insights from localization studies, *Microbiol. Mol. Biol. Rev.* 69 (2005) 585–607.
- [16] G.K. Auer, D.B. Weibel, Bacterial cell mechanics, *Biochemistry* 56 (2017) 3710–3724.
- [17] J.A.H. Romaniuk, L. Cegelski, Bacterial cell wall composition and the influence of antibiotics by cell-wall and whole-cell NMR, *Philos. Trans. R. Soc. B Biol. Sci.* 370 (2015) 20150024.
- [18] A.J.F. Egan, R.M. Cleverley, K. Peters, R.J. Lewis, W. Vollmer, Regulation of bacterial cell wall growth, *FEBS J.* 284 (2017) 851–867.
- [19] C. Paradis-Bleau, G. Kritikos, K. Orlova, A. Typas, T.G. Bernhardt, A genome-wide screen for bacterial envelope biogenesis mutants identifies a novel factor involved in cell wall precursor metabolism, *PLoS Genet.* 10 (2014) e1004056.
- [20] M.F. Brown, Lipid polymorphism and membrane properties, in: R. Epand (Ed.), *Lipid Polymorph. Membr. Prop.*, Academic press, San Diego, CA, 1997, pp. 285–356.
- [21] W. Dowhan, Molecular basis for membrane phospholipid diversity: why are there so many lipids? *Annu. Rev. Biochem.* 66 (1997) 199–232.
- [22] G.W. Huisman, D.A. Siegele, M.M. Zambrano, R. Kolter, Morphological and physiological changes during stationary phase, in: F.C. Neidhardt (Ed.), *Escherichia Coli Salmonella Typhimurium Cell. Mol. Biol.*, American Society for Microbiology, Washington DC, 1996, pp. 1672–1682.
- [23] C. Sohlenkamp, O. Geiger, Bacterial membrane lipids: diversity in structures and pathways, *FEMS Microbiol. Rev.* 40 (2016) 133–159.
- [24] C. Ratledge, S.G. Wilkinson, *Microbial Lipids LK*, Academic press, London, 1988 [etc.] SE – .. dl.; 25 cm. <https://wur.on.worldcat.org/oclc/898843218>.
- [25] H. Goldfine, Bacterial membranes and lipid packing theory, *J. Lipid Res.* 25 (1984) 1501–1507.
- [26] J.E. Cronan, Bacterial membrane lipids: where do we stand? *Annu. Rev. Microbiol.* 57 (2003) 203–224.
- [27] W. Vollmer, Structural variation in the glycan strands of bacterial peptidoglycan, *FEMS Microbiol. Rev.* 32 (2008) 287–306.

- [28] R.P. Fagan, N.F. Fairweather, Biogenesis and functions of bacterial S-layers, *Nat. Rev. Microbiol.* 12 (2014) 211–222.
- [29] L.M. Willis, C. Whitfield, Structure, biosynthesis, and function of bacterial capsular polysaccharides synthesized by ABC transporter-dependent pathways, *Carbohydr. Res.* 378 (2013) 35–44.
- [30] M. Lukaszczuk, B. Pradhan, H. Remaut, The biosynthesis and structures of bacterial pili, *Subcell Biochem.* (2019) 369–413.
- [31] O. Mol, B. Oudega, Molecular and structural aspects of fimbriae biosynthesis and assembly in *Escherichia coli*, *FEMS Microbiol. Rev.* 19 (1996) 25–52.
- [32] R. Liu, H. Ochman, Stepwise formation of the bacterial flagellar system, *Proc. Natl. Acad. Sci. U.S.A.* 104 (2007) 7116–7121.
- [33] K. Dimmitt, S. Bradford, M. Simon, Synthesis of bacterial flagella. I. Requirement for protein and ribonucleic acid synthesis during flagellar regeneration in *Bacillus subtilis*, *J. Bacteriol.* 95 (1968) 801–810.
- [34] O.A. Soutourina, P.N. Bertin, Regulation cascade of flagellar expression in Gram-negative bacteria, *FEMS Microbiol. Rev.* 27 (2003) 505–523.
- [35] A. Cockayne, Bacterial cell walls, in: *Encycl. Immunol.*, Elsevier, 1998, pp. 320–323.
- [36] M.-P. Chapot-Chartier, S. Kulakauskas, Cell wall structure and function in lactic acid bacteria, *Microb. Cell Factories* 13 (2014) S9.
- [37] X. Liu, H.M. Grabherr, R. Willmann, D. Kolb, F. Brunner, U. Bertsche, D. Kühner, M. Franz-Wachtel, B. Amin, G. Felix, M. Onghena, T. Nürmberger, A.A. Gust, Host-induced bacterial cell wall decomposition mediates pattern-triggered immunity in *Arabidopsis*, *Elife* 3 (2014).
- [38] H. Hwang, N. Paracini, J.M. Parks, J.H. Lakey, J.C. Gumbart, Distribution of mechanical stress in the *Escherichia coli* cell envelope, *Biochim. Biophys. Acta Biomembr.* 1860 (2018) 2566–2575.
- [39] E.R. Rojas, G. Billings, P.D. Odermatt, G.K. Auer, L. Zhu, A. Miguel, F. Chang, D.B. Weibel, J.A. Theriot, K.C. Huang, The outer membrane is an essential load-bearing element in Gram-negative bacteria, *Nature* 559 (2018) 617–621.
- [40] S. Baoukina, S.J. Marrink, D.P. Tieleman, Structure and dynamics of lipid monolayers: theory and applications, in: *Biomembr. Front.*, Humana Press, Totowa, NJ, 2009, pp. 75–99.
- [41] D. Risović, A. Penezić, V. Čadež, S. Šegota, B. Gašparović, Surface free energy tuning of supported mixed lipid layers, *RSC Adv.* 6 (2016) 52475–52484.
- [42] S.A. Akimov, V.A.J. Frolov, P.I. Kuzmin, J. Zimmerberg, Y.A. Chizmadzhev, F.S. Cohen, Domain formation in membranes caused by lipid wetting of protein, *Phys. Rev. E* 77 (2008) 051901.
- [43] B.L. Stottrup, S.L. Keller, Phase behavior of lipid monolayers containing DPPC and cholesterol analogs, *Biophys. J.* 90 (2006) 3176–3183.
- [44] M. Elderdfi, A.F. Sikorski, Langmuir-monolayer methodologies for characterizing protein-lipid interactions, *Chem. Phys. Lipids* 212 (2018) 61–72.
- [45] D. Koller, K. Lohner, The role of spontaneous lipid curvature in the interaction of interfacially active peptides with membranes, *Biochim. Biophys. Acta Biomembr.* 1838 (2014) 2250–2259.
- [46] L.V. Chernomordik, M.M. Kozlov, Protein-lipid interplay in fusion and fission of biological membranes, *Annu. Rev. Biochem.* 72 (2003) 175–207.
- [47] G. Di Paolo, P. De Camilli, Phosphoinositides in cell regulation and membrane dynamics, *Nature* 443 (2006) 651–657.
- [48] J. Zimmerberg, M.M. Kozlov, How proteins produce cellular membrane curvature, *Nat. Rev. Mol. Cell Biol.* 7 (2006) 9–19.

- [49] T.J. McIntosh, S.A. Simon, Roles of bilayer material properties in function and distribution of membrane proteins, *Annu. Rev. Biophys. Biomol. Struct.* 35 (2006) 177–198.
- [50] O.S. Andersen, R.E. Koepp, Bilayer thickness and membrane protein function: an energetic perspective, *Annu. Rev. Biophys. Biomol. Struct.* 36 (2007) 107–130.
- [51] R. Koynova, B. Tenchov, Transitions between lamellar and nonlamellar phases in membrane lipids and their physiological roles, *OA Biochem.* 1 (2013).
- [52] V. Patel, R. Lalani, D. Bardoliwala, S. Ghosh, A. Misra, Lipid-based oral formulation strategies for lipophilic drugs, *AAPS PharmSciTech* 19 (2018) 3609–3630.
- [53] A.R. Thiam, B. Anttony, J. Wang, J. Delacotte, F. Wilfing, T.C. Walther, R. Beck, J.E. Rothman, F. Pincet, COPI buds 60-nm lipid droplets from reconstituted water-phospholipid-triacylglyceride interfaces, suggesting a tension clamp function, *Proc. Natl. Acad. Sci. U.S.A.* 110 (2013) 13244–13249.
- [54] P.I. Kuzmin, S.A. Akimov, Y.A. Chizmadzhev, J. Zimmerberg, F.S. Cohen, Line tension and interaction energies of membrane rafts calculated from lipid splay and tilt, *Biophys. J.* 88 (2005) 1120–1133.
- [55] S. Baoukina, L. Monticelli, H.J. Risselada, S.J. Marrink, D.P. Tieleman, The molecular mechanism of lipid monolayer collapse, *Proc. Natl. Acad. Sci. U.S.A.* 105 (2008) 10803–10808.
- [56] M. Khan, N. Dosoky, J. Williams, Engineering lipid bilayer membranes for protein studies, *Int. J. Mol. Sci.* 14 (2013) 21561–21597.
- [57] G. Bozzuto, A. Molinari, Liposomes as nanomedical devices, *Int. J. Nanomed.* 10 (2015) 975–999.
- [58] J.N. Israelachvili, Interactions of biological membranes and structures, in: *Intermol. Surf. Forces*, Elsevier, 2011, pp. 577–616.
- [59] H. Heerklotz, R.M. Epand, The enthalpy of acyl chain packing and the apparent water-accessible apolar surface area of phospholipids, *Biophys. J.* 80 (2001) 271–279.
- [60] D. Lombardo, M.A. Kiselev, S. Magazù, P. Calandra, Amphiphiles self-assembly: basic concepts and future perspectives of supramolecular approaches, *Adv. Condens. Matter Phys.* 2015 (2015) 1–22.
- [61] N. Fuller, R.P. Rand, The influence of lysolipids on the spontaneous curvature and bending elasticity of phospholipid membranes, *Biophys. J.* 81 (2001) 243–254.
- [62] R.M. Venable, F.L.H. Brown, R.W. Pastor, Mechanical properties of lipid bilayers from molecular dynamics simulation, *Chem. Phys. Lipids* 192 (2015) 60–74.
- [63] M. Doktorova, M.V. LeVine, G. Khelashvili, H. Weinstein, A new computational method for membrane compressibility: bilayer mechanical thickness revisited, *Biophys. J.* 116 (2019) 487–502.
- [64] G. Espinosa, I. Lopez-Montero, F. Monroy, D. Langevin, Shear rheology of lipid monolayers and insights on membrane fluidity, *Proc. Natl. Acad. Sci. U.S.A.* 108 (2011) 6008–6013.
- [65] A.V. Granato, The shear modulus of liquids, *J. Phys. IV* 06 (1996) C8-C1–C8-C9.
- [66] D. Boal, Mechanics of the Cell, second ed., *Mech. Cell*, 2012, pp. 1–608.
- [67] C.A. Rutkowski, L.M. Williams, T.H. Haines, H.Z. Cummins, The elasticity of synthetic phospholipid vesicles obtained by photon correlation spectroscopy, *Biochemistry* 30 (1991) 5688–5696.
- [68] W. Rawicz, K.C. Olbrich, T. McIntosh, D. Needham, E. Evans, Effect of chain length and unsaturation on elasticity of lipid bilayers, *Biophys. J.* 79 (2000) 328–339.
- [69] N. Kato, A. Ishijima, T. Inaba, F. Nomura, S. Takeda, K. Takiguchi, Effects of lipid composition and solution conditions on the mechanical properties of membrane vesicles, *Membranes (Basel)* (2015) 22–47.

- [70] P.-A. Boucher, B. Joós, M.J. Zuckermann, L. Fournier, pore formation in a lipid bilayer under a tension ramp: modeling the distribution of rupture tensions, *Biophys. J.* 92 (2007) 4344–4355.
- [71] M. Asgari, A. Biria, Free energy of the edge of an open lipid bilayer based on the interactions of its constituent molecules, *Int. J. Non Lin. Mech.* 76 (2015) 135–143.
- [72] T. Portet, R. Dimova, A new method for measuring edge tensions and stability of lipid bilayers: effect of membrane composition, *Biophys. J.* 99 (2010) 3264–3273.
- [73] S. Ali, J.M. Smaby, M.M. Momsen, H.L. Brockman, R.E. Brown, Acyl chain-length asymmetry alters the interfacial elastic interactions of phosphatidylcholines, *Biophys. J.* 74 (1998) 338–348.
- [74] B. Brüning, R. Stehle, P. Falus, B. Farago, Influence of charge density on bilayer bending rigidity in lipid vesicles: a combined dynamic light scattering and neutron spin-echo study, *Eur. Phys. J. E.* 36 (2013) 77.
- [75] P. Girard, J. Prost, P. Bassereau, Passive or active fluctuations in membranes containing proteins, *Phys. Rev. Lett.* 94 (2005) 088102.
- [76] D. Vorselen, F.C. MacKintosh, W.H. Roos, G.J.L. Wuite, Competition between bending and internal pressure governs the mechanics of fluid nanovesicles, *ACS Nano* 11 (2017) 2628–2636.
- [77] H. Bermúdez, D.A. Hammer, D.E. Discher, Effect of bilayer thickness on membrane bending rigidity, *Langmuir* 20 (2004) 540–543.
- [78] R. Phillips, T. Ursell, P. Wiggins, P. Sens, Emerging roles for lipids in shaping membrane-protein function, *Nature* 459 (2009) 379–385.
- [79] A.G. Petrov, Flexoelectricity of model and living membranes, *Biochim. Biophys. Acta Biomembr.* 1561 (2002) 1–25.
- [80] D. Marsh, Elastic curvature constants of lipid monolayers and bilayers, *Chem. Phys. Lipids* 144 (2006) 146–159.
- [81] J.C. Bozelli, W. Jennings, S. Black, Y.H. Hou, D. Lameire, P. Chatha, T. Kimura, B. Berno, A. Khondker, M.C. Rheinstädter, R.M. Epand, Membrane curvature allosterically regulates the phosphatidylinositol cycle, controlling its rate and acyl-chain composition of its lipid intermediates, *J. Biol. Chem.* 293 (2018) 17780–17791.
- [82] S. Purushothaman, P. Cicuta, O. Ces, N.J. Brooks, Influence of high pressure on the bending rigidity of model membranes, *J. Phys. Chem. B* 119 (2015) 9805–9810.
- [83] F. Nomura, M. Nagata, T. Inaba, H. Hiramatsu, H. Hotani, K. Takiguchi, Capabilities of liposomes for topological transformation, *Proc. Natl. Acad. Sci. U.S.A.* 98 (2001) 2340–2345.
- [84] F. Nomura, T. Inaba, S. Ishikawa, M. Nagata, S. Takahashi, H. Hotani, K. Takiguchi, Microscopic observations reveal that fusogenic peptides induce liposome shrinkage prior to membrane fusion, *Proc. Natl. Acad. Sci. U.S.A.* 101 (2004) 3420–3425.
- [85] G.F. White, K.I. Racher, A. Lipski, F.R. Hallett, J.M. Wood, Physical properties of liposomes and proteoliposomes prepared from *Escherichia coli* polar lipids, *Biochim. Biophys. Acta Biomembr.* 1468 (2000) 175–186.
- [86] H.A. Faizi, S.L. Frey, J. Steinkühler, R. Dimova, P.M. Vlahovska, Bending rigidity of charged lipid bilayer membranes, *Soft Matter* 15 (2019) 6006–6013.
- [87] P.W. Fowler, J. Hélie, A. Duncan, M. Chavent, H. Koldsoe, M.S.P. Sansom, Membrane stiffness is modified by integral membrane proteins, *Soft Matter* 12 (2016) 7792–7803.
- [88] N. Jamin, M. Garrigos, C. Jaxel, A. Frelet-Barrand, S. Orlowski, Ectopic neo-formed intracellular membranes in *Escherichia coli*: a response to membrane protein-induced stress involving membrane curvature and domains, *Biomolecules* 8 (2018) 88.
- [89] K. Simons, J.L. Sampaio, Membrane organization and lipid rafts, *Cold Spring Harb. Perspect. Biol.* 3 (2011) a004697–a004697.

- [90] D. Balleza, Mechanical properties of lipid bilayers and regulation of mechanosensitive function, *Channels* 6 (2012) 220–233.
- [91] T. Heimburg, Mechanical aspects of membrane thermodynamics. Estimation of the mechanical properties of lipid membranes close to the chain melting transition from calorimetry, *Biochim. Biophys. Acta Biomembr.* 1415 (1998) 147–162.
- [92] J.F. Nagle, D.A. Wilkinson, Lecithin bilayers. Density measurement and molecular interactions, *Biophys. J.* 23 (1978) 159–175.
- [93] D. Needham, E. Evans, Structure and mechanical properties of giant lipid (DMPC) vesicle bilayers from 20.degree.C below to 10.degree.C above the liquid crystal-crystalline phase transition at 24.degree., *Clin. Biochem.* 27 (1988) 8261–8269.
- [94] R. Dimova, B. Pouliquen, C. Dietrich, Pretransitional effects in dimyristoylphosphatidylcholine vesicle membranes: optical dynamometry study, *Biophys. J.* 79 (2000) 340–356.
- [95] B. Gumić-Audenis, F. Sanz, M.I. Giannotti, Impact of galactosylceramides on the nanomechanical properties of lipid bilayer models: an AFM-force spectroscopy study, *Soft Matter* 11 (2015) 5447–5454.
- [96] T. Heimburg, Phase Transitions in Biological Membranes, 2019, pp. 39–61.
- [97] P. Marmottant, T. Biben, S. Hilgenfeldt, Deformation and rupture of lipid vesicles in the strong shear flow generated by ultrasound-driven microbubbles, *Proc. R. Soc. A Math. Phys. Eng. Sci.* 464 (2008) 1781–1800.
- [98] K.A. Riske, R. Dimova, Electro-deformation and poration of giant vesicles viewed with high temporal resolution, *Biophys. J.* 88 (2005) 1143–1155.
- [99] T. Portet, F. Camps I Febrer, J.M. Escoffre, C. Favard, M.P. Rols, D.S. Dean, Visualization of membrane loss during the shrinkage of giant vesicles under electropulsation, *Biophys. J.* 96 (2009) 4109–4121.
- [100] W. Ding, M. Palaiokostas, G. Shahane, W. Wang, M. Orsi, Effects of high pressure on phospholipid bilayers, *J. Phys. Chem. B* 121 (2017) 9597–9606.
- [101] Y.R. Sliozberg, Structural Changes in Lipid Vesicles Generated by the Shock Blast Waves: Coarse-Grained Molecular Dynamics Simulation, 2013.
- [102] H. Wu, L. Yu, Y. Tong, A. Ge, S. Yau, M. Osawa, S. Ye, Enzyme-catalyzed hydrolysis of the supported phospholipid bilayers studied by atomic force microscopy, *Biochim. Biophys. Acta Biomembr.* 1828 (2013) 642–651.
- [103] S.R. Tabaei, M. Rabe, H. Zetterberg, V.P. Zhdanov, F. Höök, Single lipid vesicle assay for characterizing single-enzyme kinetics of phospholipid hydrolysis in a complex biological fluid, *J. Am. Chem. Soc.* 135 (2013) 14151–14158.
- [104] R.L. Knorr, M. Staykova, R.S. Gracià, R. Dimova, Wrinkling and electroporation of giant vesicles in the gel phase, *Soft Matter* 6 (2010) 1990–1996.
- [105] W.W. Sułkowski, D. Pentak, K. Nowak, A. Sulkowska, M.P. Goertz, N. Goyal, G.A. Montano, B.C. Bunker, The influence of temperature, cholesterol content and pH on liposome stability, *J. Mol. Struct.* 744–747 (2005) 737–747.
- [106] M.P. Goertz, N. Goyal, G.A. Montano, B.C. Bunker, Lipid bilayer reorganization under extreme pH conditions, *Langmuir* (2011) 5481–5491.
- [107] M.M. Koerner, L.A. Palacio, J.W. Wright, K.S. Schweitzer, B.D. Ray, H.I. Petrache, Electrodynamics of lipid membrane interactions in the presence of zwitterionic buffers, *Biophys. J.* 101 (2011) 362–369.
- [108] M.M.A.E. Claessens, B.F. Van Oort, F.A.M. Leermakers, F.A. Hoekstra, M.A.C. Stuart, Charged lipid vesicles: effects of salts on bending rigidity, stability, and size, *Biophys. J.* 87 (2004) 3882–3893.
- [109] A. Kodama, M. Morandi, R. Ebihara, T. Jimbo, M. Toyoda, Y. Sakuma, M. Imai, N. Pu, M.I. Angelova, Migration of deformable vesicles induced by ionic stimuli, *Langmuir* (2018).

- [110] R.A. Böckmann, A. Hac, T. Heimburg, H. Grubmüller, Effect of sodium chloride on a lipid bilayer, *Biophys. J.* 85 (2003) 1647–1655.
- [111] R.A. Böckmann, H. Grubmüller, Multistep binding of divalent cations to phospholipid bilayers: a molecular dynamics study, *Angew. Chem. Int. Ed.* 43 (2004) 1021–1024.
- [112] K. Inque, T. Kitagawa, Effect of lipid composition on sensitivity of lipid membranes to triton X-100, *Biochim. Biophys. Acta Biomembr.* 426 (1976) 1–16.
- [113] B.R. Casadei, C.C. Domingues, E. De Paula, K.A. Riske, Direct visualization of the action of triton X-100 on giant vesicles of erythrocyte membrane lipids, *Biophys. J.* 106 (2014) 2417–2425.
- [114] A. Jeucken, M.R. Molenaar, C.H.A. van de Lest, J.W.A. Jansen, J.B. Helms, J.F. Brouwers, A comprehensive functional characterization of *Escherichia coli* lipid genes, *Cell Rep.* 27 (2019) 1597–1606.e2.
- [115] J.-W. Park, D.J. Ahn, Temperature effect on nanometer-scale physical properties of mixed phospholipid monolayers, *Colloids Surf. B Biointerfaces* 62 (2008) 157–161.
- [116] H.M. Seeger, G. Marino, A. Alessandrini, P. Facci, Effect of physical parameters on the main phase transition of supported lipid bilayers, *Biophys. J.* 97 (2009) 1067–1076.
- [117] M. Edidin, The state of lipid rafts: from model membranes to cells, *Annu. Rev. Biophys. Biomol. Struct.* 32 (2003) 257–283.
- [118] P. Calvez, J. Jouhet, V. Vié, C. Durmorth, A. Zapun, Lipid phases and cell geometry during the cell cycle of *Streptococcus pneumoniae*, *Front. Microbiol.* 10 (2019).
- [119] Y. Sun, T.-L. Sun, H.W. Huang, Physical properties of *Escherichia coli* spheroplast membranes, *Biophys. J.* 107 (2014) 2082–2090.
- [120] L. Lu, W.J. Doak, J.W. Schertzer, P.R. Chiarot, Membrane mechanical properties of synthetic asymmetric phospholipid vesicles, *Soft Matter* 12 (2016) 7521–7528.
- [121] H.T. McMahon, E. Boucrot, Membrane curvature at a glance, *J. Cell Sci.* 128 (2015) 1065–1070.
- [122] M. Pinot, S. Vanni, E. Ambroggio, D. Guet, B. Goud, J.-B. Manneville, Feedback Between Membrane Tension, Lipid Shape and Curvature in the Formation of Packing Defects, 2018.
- [123] H.T. McMahon, J.L. Gallop, Membrane curvature and mechanisms of dynamic cell membrane remodelling, *Nature* 438 (2005) 590–596.
- [124] Y. Shibata, J. Hu, M.M. Kozlov, T.A. Rapoport, Mechanisms shaping the membranes of cellular organelles, *Annu. Rev. Cell Dev. Biol.* 25 (2009) 329–354.
- [125] A. Martyna, B. Bahsoun, M.D. Badham, S. Srinivasan, M.J. Howard, J.S. Rossman, Membrane remodeling by the M2 amphipathic helix drives influenza virus membrane scission, *Sci. Rep.* 7 (2017) 44695.
- [126] H.P. Erickson, M. Osawa, FtsZ constriction force — curved protofilaments bending membranes, *Subcell Biochem* (2017) 139–160.
- [127] T.N.V. Saaki, H. Strahl, L.W. Hamoen, Membrane curvature and the tol-pal complex determine polar localization of the chemoreceptor tar in *Escherichia coli*, *J. Bacteriol.* 200 (2018).
- [128] H. Alimohamadi, B. Ovryn, P. Rangamani, Modeling membrane nanotube morphology: the role of heterogeneity in composition and material properties, *Sci. Rep.* 10 (2020) 2527.
- [129] W. Römer, L. Berland, V. Chambon, K. Gaus, B. Windschieg, D. Tenza, M.R.E. Aly, V. Fraisier, J.-C. Florent, D. Perrais, C. Lamaze, G. Raposo, C. Steinem, P. Sens, P. Bassereau, L. Johannes, Shiga toxin induces tubular membrane invaginations for its uptake into cells, *Nature* 450 (2007) 670–675.
- [130] I.K. Jarsch, F. Daste, J.L. Gallop, Membrane curvature in cell biology: an integration of molecular mechanisms, *J. Cell Biol.* 214 (2016) 375–387.

- [131] H. Strahl, J. Errington, Bacterial membranes: structure, domains, and function, *Annu. Rev. Microbiol.* 71 (2017) 519–538.
- [132] Q. Deng, L. Liu, P. Sharma, Flexoelectricity in soft materials and biological membranes, *J. Mech. Phys. Solid.* 62 (2014) 209–227.
- [133] V. Vitkova, A.G. Petrov, Lipid Bilayers and Membranes, 2013, pp. 89–138.
- [134] D. Needham, R.S. Nunn, Elastic deformation and failure of lipid bilayer membranes containing cholesterol, *Biophys. J.* 58 (1990) 997–1009.
- [135] S.-T. Yang, A.J.B. Kreutzberger, J. Lee, V. Kiessling, L.K. Tamm, The role of cholesterol in membrane fusion, *Chem. Phys. Lipids* 199 (2016) 136–143.
- [136] S.E. Feller, K. Gawrisch, A.D. MacKerell, Polyunsaturated fatty acids in lipid bilayers: intrinsic and environmental contributions to their unique physical properties, *J. Am. Chem. Soc.* 124 (2002) 318–326.
- [137] G. Ourisson, M. Rohmer, K. Poralla, Prokaryotic hopanoids and other polyterpenoid sterol surrogates, *Annu. Rev. Microbiol.* 41 (1987) 301–333.
- [138] J.P. Sáenz, D. Grosser, A.S. Bradley, T.J. Lagny, O. Lavrynenko, M. Broda, K. Simons, Hopanoids as functional analogues of cholesterol in bacterial membranes, *Proc. Natl. Acad. Sci. U.S.A.* 112 (2015) 11971–11976.
- [139] Y.-L. Shih, L. Rothfield, The bacterial cytoskeleton, *Microbiol. Mol. Biol. Rev.* 70 (2006) 729–754.
- [140] C. Di Ciano-Oliveira, A.C.P. Thirone, K. Szaszi, A. Kapus, Osmotic stress and the cytoskeleton: the R(h)ole of Rho GTPases, *Acta Physiol.* 187 (2006) 257–272.
- [141] A. Typas, M. Banzhaf, C.A. Gross, W. Vollmer, From the regulation of peptidoglycan synthesis to bacterial growth and morphology, *Nat. Rev. Microbiol.* 10 (2012) 123–136.
- [142] M. Jansen, A. Blume, A comparative study of diffusive and osmotic water permeation across bilayers composed of phospholipids with different head groups and fatty acyl chains, *Biophys. J.* 68 (1995) 997–1008.
- [143] J.T. Mika, P.E. Schavemaker, V. Krasnikov, B. Poolman, Impact of osmotic stress on protein diffusion in *Lactococcus lactis*, *Mol. Microbiol.* 94 (2014) 857–870.
- [144] J.C. Gumbart, M. Beeby, G.J. Jensen, B. Roux, *Escherichia coli* peptidoglycan structure and mechanics as predicted by atomic-scale simulations, *PLoS Comput. Biol.* 10 (2014) e1003475.
- [145] M.T. Madigan, J.M. Martinko, P.V. Dunlap, D.P. Clark, *Brock Biology of Microorganisms*, twelfth ed., Pearson Education, San Francisco, 2009.
- [146] E.R. Rojas, K.C. Huang, J.A. Theriot, Homeostatic cell growth is accomplished mechanically through membrane tension inhibition of cell-wall synthesis, *Cell Syst.* 5 (2017) 578–590.e6.
- [147] E.R. Rojas, K.C. Huang, Regulation of microbial growth by turgor pressure, *Curr. Opin. Microbiol.* 42 (2018) 62–70.
- [148] R.C. Hughes, Autolysis of *Bacillus cereus* cell walls and isolation of structural components, *Biochem. J.* 121 (1971) 791–802.
- [149] I.G. Boneca, Z.-H. Huang, D.A. Gage, A. Tomasz, Characterization of *Staphylococcus aureus* cell wall glycan strands, evidence for a new  $\beta$ -N-acetylglucosaminidase activity, *J. Biol. Chem.* 275 (2000) 9910–9918.
- [150] D. Sychantha, A.S. Brott, C.S. Jones, A.J. Clarke, Mechanistic pathways for peptidoglycan O-acetylation and de-O-acetylation, *Front. Microbiol.* 9 (2018).
- [151] M.-H. Laaberki, J. Pfeffer, A.J. Clarke, J. Dworkin, O-acetylation of peptidoglycan is required for proper cell separation and S-layer anchoring in *Bacillus anthracis*, *J. Biol. Chem.* 286 (2011) 5278–5288.
- [152] A.K. Yadav, A. Espaillat, F. Cava, Bacterial strategies to preserve cell wall integrity against environmental threats, *Front. Microbiol.* 9 (2018).

- [153] M.A. de Pedro, F. Cava, Structural constraints and dynamics of bacterial cell wall architecture, *Front. Microbiol.* 6 (2015).
- [154] T. Kruse, J. Bork-Jensen, K. Gerdes, The morphogenetic MreBCD proteins of *Escherichia coli* form an essential membrane-bound complex, *Mol. Microbiol.* 55 (2005) 78–89.
- [155] F. van den Ent, C.M. Johnson, L. Persons, P. de Boer, J. Löwe, Bacterial actin MreB assembles in complex with cell shape protein RodZ, *EMBO J.* 29 (2010) 1081–1090.
- [156] S.X. Sun, H. Jiang, Physics of bacterial morphogenesis, *Microbiol. Mol. Biol. Rev.* 75 (2011) 543–565.
- [157] H. Jiang, F. Si, W. Margolin, S.X. Sun, Mechanical control of bacterial cell shape, *Biophys. J.* 101 (2011) 327–335.
- [158] F. Chattaway, Microbial cell walls and membranes, *Biochem. Educ.* 10 (1982) 33.
- [159] B. Glauner, J. V Höltje, U. Schwarz, The composition of the murein of *Escherichia coli*, *J. Biol. Chem.* 263 (1988) 10088–10095.
- [160] M.A. Snowden, H.R. Perkins, Peptidoglycan cross-linking in *Staphylococcus aureus*. An apparent random polymerisation process, *Eur. J. Biochem.* 191 (1990) 373–377.
- [161] A.G. Pisabarro, M.A. de Pedro, D. Vázquez, Structural modifications in the peptidoglycan of *Escherichia coli* associated with changes in the state of growth of the culture, *J. Bacteriol.* 161 (1985) 238–242.
- [162] B. Blasco, A.G. Pisabarro, M.A. de Pedro, Peptidoglycan biosynthesis in stationary-phase cells of *Escherichia coli*, *J. Bacteriol.* 170 (1988) 5224–5228.
- [163] D. Gully, D. Gargani, K. Bonaldi, C. Grangeteau, C. Chaintreuil, J. Fardoux, P. Nguyen, R. Marchetti, N. Nouwen, A. Molinaro, P. Mergaert, E. Giraud, A peptidoglycan-remodeling enzyme is critical for bacteroid differentiation in bradyrhizobium spp. during legume symbiosis, *Mol. Plant Microbe Interact.* 29 (2016) 447–457.
- [164] A.S. Ghosh, C. Chowdhury, D.E. Nelson, Physiological functions of D-alanine carboxypeptidases in *Escherichia coli*, *Trends Microbiol.* 16 (2008) 309–317.
- [165] D.E. Nelson, K.D. Young, Contributions of PBP 5 and DD-carboxypeptidase penicillin binding proteins to maintenance of cell shape in *Escherichia coli*, *J. Bacteriol.* 183 (2001) 3055–3064.
- [166] K.D. Young, Bacterial shape, *Mol. Microbiol.* 49 (2004) 571–580.
- [167] A.L. Koch, S.L. Lane, J.A. Miller, D.G. Nickens, Contraction of filaments of *Escherichia coli* after disruption of cell membrane by detergent, *J. Bacteriol.* 169 (1987) 1979–1984.
- [168] X. Yao, M. Jericho, D. Pink, T. Beveridge, Thickness and elasticity of gram-negative murein sacculi measured by atomic force microscopy, *J. Bacteriol.* 181 (1999) 6865–6875.
- [169] G. Van Den Bogaart, N. Hermans, V. Krasnikov, B. Poolman, Protein mobility and diffusive barriers in *Escherichia coli*: consequences of osmotic stress, *Mol. Microbiol.* 64 (2007) 858–871.
- [170] W. Vollmer, P. Born, Bacterial cell envelope peptidoglycan, in: *Microb. Glycobiol.*, Elsevier, 2010, pp. 15–28.
- [171] R.C. Hughes, P.F. Thurman, E. Stokes, Estimates of the porosity of *Bacillus licheniformis* and *Bacillus subtilis* cell walls, *Z. für Immunitätsforsch. Exp. Klin. Immunol.* 149 (1975) 126–135.
- [172] W. Vollmer, J.-V. Holtje, The architecture of the murein (peptidoglycan) in gram-negative bacteria: vertical scaffold or horizontal layer(s)? *J. Bacteriol.* 186 (2004) 5978–5987.
- [173] M. Lin, Y. Rikihisa, *Ehrlichia chaffeensis* and *Anaplasma phagocytophilum* lack genes for lipid A biosynthesis and incorporate cholesterol for their survival, *Infect. Immun.* 71 (2003) 5324–5331.

- [174] C. Otten, M. Brilli, W. Vollmer, P.H. Viollier, J. Salje, Peptidoglycan in obligate intracellular bacteria, *Mol. Microbiol.* 107 (2018) 142–163.
- [175] K. Bush, Antimicrobial agents targeting bacterial cell walls and cell membranes, *Rev. Sci. Tech. l’OIE*. 31 (2012) 43–56.
- [176] H. Nikaido, Bacterial resistance to antibiotics as a function of outer membrane permeability, *J. Antimicrob. Chemother.* 22 (1988) 17–22.
- [177] Z. Pang, R. Raudonis, B.R. Glick, T.-J. Lin, Z. Cheng, Antibiotic resistance in *Pseudomonas aeruginosa*: mechanisms and alternative therapeutic strategies, *Biotechnol. Adv.* 37 (2019) 177–192.
- [178] A.T. Vincent, S. Nyongesa, I. Morneau, M.B. Reed, E.I. Tocheva, F.J. Veyrier, The mycobacterial cell envelope: a relict from the past or the result of recent evolution? *Front. Microbiol.* 9 (2018).
- [179] K.L. May, M. Grabowicz, The bacterial outer membrane is an evolving antibiotic barrier, *Proc. Natl. Acad. Sci. U.S.A.* 115 (2018) 8852–8854.
- [180] H. Nikaido, Molecular basis of bacterial outer membrane permeability revisited, *Microbiol. Mol. Biol. Rev.* 67 (2003) 593–656.
- [181] D.G. Thanassi, L.W. Cheng, H. Nikaido, Active efflux of bile salts by *Escherichia coli*, *J. Bacteriol.* 179 (1997) 2512–2518.
- [182] B. Bertani, N. Ruiz, Function and biogenesis of lipopolysaccharides, *EcoSal Plus* 8 (2018).
- [183] A.V. Hughes, D.S. Patel, G. Widmalm, J.B. Klauda, L.A. Clifton, W. Im, Physical properties of bacterial outer membrane models: neutron reflectometry & molecular simulation, *Biophys. J.* 116 (2019) 1095–1104.
- [184] L.A. Clifton, M.W.A. Skoda, A.P. Le Brun, F. Ciesielski, I. Kuzmenko, S.A. Holt, J.H. Lakey, Effect of divalent cation removal on the structure of gram-negative bacterial outer membrane models, *Langmuir* 31 (2015) 404–412.
- [185] H.-L. Alakomi, A. Paananen, M.-L. Stuiko, I.M. Helander, M. Saarela, Weakening effect of cell permeabilizers on gram-negative bacteria causing biodeterioration, *Appl. Environ. Microbiol.* 72 (2006) 4695–4703.
- [186] L. Leive, Release of lipopolysaccharide by EDTA treatment of *E. coli*, *Biochem. Biophys. Res. Commun.* 21 (1965) 290–296.
- [187] V. Braun, K. Rehn, Chemical characterization, spatial distribution and function of a lipoprotein (Murein-Lipoprotein) of the *E. coli* cell wall. The specific effect of trypsin on the membrane structure, *Eur. J. Biochem.* 10 (1969) 426–438.
- [188] V. Braun, U. Sieglin, The covalent murein-lipoprotein structure of the *Escherichia coli* cell wall. The attachment site of the lipoprotein on the murein, *Eur. J. Biochem.* 13 (1970) 336–346.
- [189] M. Mathelié-Guinlet, A.T. Asmar, J.-F. Collet, Y.F. Dufrêne, Lipoprotein Lpp regulates the mechanical properties of the *E. coli* cell envelope, *Nat. Commun.* 11 (2020).
- [190] R. Godlewska, K. Więsławska, Z. Pietras, E.K. Jagusztyn-Krynicka, Peptidoglycan-associated lipoprotein (Pal) of Gram-negative bacteria: function, structure, role in pathogenesis and potential application in immunoprophylaxis, *FEMS Microbiol. Lett.* 298 (2009) 1–11.
- [191] A. Kovacs-Simon, R.W. Titball, S.L. Michell, Lipoproteins of bacterial pathogens, *Infect. Immun.* 79 (2011) 548–561.
- [192] M. Leduc, K. Ishidate, N. Shakibai, L. Rothfield, Interactions of *Escherichia coli* membrane lipoproteins with the murein sacculus, *J. Bacteriol.* 174 (1992) 7982–7988.
- [193] E. Bouveret, R. Derouiche, A. Rigal, R. Lloubes, C. Lazdunski, H. Benedetti, Peptidoglycan-associated lipoprotein-TolB interaction. A possible key to explaining the formation of contact sites between the inner and outer membranes of *Escherichia coli*, *J. Biol. Chem.* 270 (1995) 11071–11077.

- [194] T. Clavel, P. Germon, A. Vianney, R. Portalier, J.C. Lazzaroni, TolB protein of *Escherichia coli* K-12 interacts with the outer membrane peptidoglycan-associated proteins Pal, Lpp and OmpA, Mol. Microbiol. 29 (1998) 359–367.
- [195] E. Cascales, A. Bernadac, M. Gavioli, J.-C. Lazzaroni, R. Lloubes, Pal lipoprotein of *Escherichia coli* plays a major role in outer membrane integrity, J. Bacteriol. 184 (2002) 754–759.
- [196] E. Bouveret, H. Bénédetti, A. Rigal, E. Loret, C. Lazdunski, In vitro characterization of peptidoglycan-associated lipoprotein (PAL)-peptidoglycan and PAL-TolB interactions, J. Bacteriol. 181 (1999) 6306–6311.
- [197] E. Cascales, M. Gavioli, J.N. Sturgis, R. Lloubes, Proton motive force drives the interaction of the inner membrane TolA and outer membrane Pal proteins in *Escherichia coli*, Mol. Microbiol. 38 (2000) 904–915.
- [198] C. Deprez, R. Lloubès, M. Gavioli, D. Marion, F. Guerlesquin, L. Blanchard, Solution structure of the *E. coli* TolA C-terminal domain reveals conformational changes upon binding to the phage g3p N-terminal domain, J. Mol. Biol. 346 (2005) 1047–1057.
- [199] Y.-C. Yeh, L.R. Comolli, K.H. Downing, L. Shapiro, H.H. McAdams, The Caulobacter tol-pal complex is essential for outer membrane integrity and the positioning of a polar localization factor, J. Bacteriol. 192 (2010) 4847–4858.
- [200] A.M. Berezuk, S. Glavota, E.J. Roach, M.C. Goodyear, J.R. Krieger, C.M. Khursigara, Outer membrane lipoprotein RlpA is a novel periplasmic interaction partner of the cell division protein FtsK in *Escherichia coli*, Sci. Rep. 8 (2018) 1–14.
- [201] M.A. Gerding, Y. Ogata, N.D. Pecora, H. Niki, P.A.J. de Boer, The trans-envelope Tol-Pal complex is part of the cell division machinery and required for proper outer-membrane invagination during cell constriction in *E. coli*, Mol. Microbiol. 63 (2007) 1008–1025.
- [202] A.L. Koch, Orientation of the peptidoglycan chains in the sacculus of *Escherichia coli*, Res. Microbiol. 149 (1998) 689–701.
- [203] J. V Höltje, Growth of the stress-bearing and shape-maintaining murein sacculus of *Escherichia coli*, Microbiol. Mol. Biol. Rev. 62 (1998) 181–203.
- [204] O.H. Vandal, C.F. Nathan, S. Ehrt, Acid resistance in *Mycobacterium tuberculosis*, J. Bacteriol. 191 (2009) 4714–4721.
- [205] K. Takayama, C. Wang, G.S. Besra, Pathway to synthesis and processing of mycolic acids in *Mycobacterium tuberculosis*, Clin. Microbiol. Rev. 18 (2005) 81–101.
- [206] P.J. Brennan, H. Nikaido, The envelope of mycobacteria, Annu. Rev. Biochem. 64 (1995) 29–63.
- [207] M. Daffé, P. Draper, The envelope layers of mycobacteria with reference to their pathogenicity, Adv. Microb. Physiol. (1997) 131–203.
- [208] E. Dubnau, J. Chan, C. Raynaud, V.P. Mohan, M.-A. Lanéelle, K. Yu, A. Quémard, I. Smith, M. Daffé, Oxygenated mycolic acids are necessary for virulence of *Mycobacterium tuberculosis* in mice, Mol. Microbiol. 36 (2002) 630–637.
- [209] M.S. Glickman, J.S. Cox, W.R. Jacobs, A novel mycolic acid cyclopropane synthetase is required for cording, persistence, and virulence of *Mycobacterium tuberculosis*, Mol. Cell. 5 (2000) 717–727.
- [210] J. Liu, C.E. Barry, G.S. Besra, H. Nikaido, Mycolic acid structure determines the fluidity of the mycobacterial cell wall, J. Biol. Chem. 271 (1996) 29545–29551.
- [211] Y. Yuan, Y. Zhu, D.D. Crane, C.E. Barry III, The effect of oxygenated mycolic acid composition on cell wall function and macrophage growth in *Mycobacterium tuberculosis*, Mol. Microbiol. 29 (1998) 1449–1458.
- [212] C. Asselineau, J. Asselineau, Trehalose-containing glycolipids, Prog. Chem. Fats Other Lipids 16 (1978) 59–99.

- [213] C.E. Barry, R.E. Lee, K. Mdluli, A.E. Sampson, B.G. Schroeder, R.A. Slayden, Y. Yuan, Mycolic acids: structure, biosynthesis and physiological functions, *Prog. Lipid Res.* 37 (1998) 143–179.
- [214] A. Zureck, G. P. Kubica, L. G. Wayne (editors), the mycobacteria — a sourcebook, Part A and Part B (microbiology series volume 15). 1553 S., 225 abb., 122 tab. New York-basel 1984. Marcel dekker. \$ 295.00. ISBN: 0-8247-7009-9 (Part A), 0-8247-1917-4 (Part B), *J. Basic Microbiol.* 25 (1985) 662–662.
- [215] K.M. George, Y. Yuan, D.R. Sherman, C.E. Barry, The biosynthesis of cyclopropanated mycolic acids in *Mycobacterium tuberculosis*, *J. Biol. Chem.* 270 (1995) 27292–27298.
- [216] Y. Yuan, R.E. Lee, G.S. Besra, J.T. Belisle, C.E. Barry, Identification of a gene involved in the biosynthesis of cyclopropanated mycolic acids in *Mycobacterium tuberculosis*, *Proc. Natl. Acad. Sci. U.S.A.* 92 (1995) 6630–6634.
- [217] J.R. Battista, Against all odds:the survival strategies of *Deinococcus radiodurans*, *Annu. Rev. Microbiol.* 51 (1997) 203–224.
- [218] D. Slade, M. Radman, Oxidative stress resistance in *Deinococcus radiodurans*, *Microbiol. Mol. Biol. Rev.* 75 (2011) 133–191.
- [219] J. Yu, T. Li, S. Dai, Y. Weng, J. Li, Q. Li, H. Xu, Y. Hua, B. Tian, A tamB homolog is involved in maintenance of cell envelope integrity and stress resistance of *Deinococcus radiodurans*, *Sci. Rep.* 7 (2017) 45929.
- [220] H. Rothfuss, J.C. Lara, A.K. Schmid, M.E. Lidstrom, Involvement of the S-layer proteins Hpi and SlpA in the maintenance of cell envelope integrity in *Deinococcus radiodurans* R1, *Microbiology* 152 (2006) 2779–2787.
- [221] B.G. Thompson, R. Anderson, R.G.E. Murray, Unusual polar lipids of *Micrococcus radiodurans* strain Sark, *Can. J. Microbiol.* 26 (1980) 1408–1411.
- [222] U.B. Sleytr, P. Messner, D. Pum, M. Sára, Occurrence, location, ultrastructure and morphogenesis of S-layers, in: *Cryst. Bact. Cell Surf. Proteins*, Elsevier, 1996, pp. 5–33.
- [223] U.B. Sleytr, B. Schuster, E.-M. Egelseer, D. Pum, S-layers: principles and applications, *FEMS Microbiol. Rev.* 38 (2014) 823–864.
- [224] M. Sara, E.M. Egelseer, Functional aspects of S-layers, in: U.W. Sleytr, P. Messner, D. Pum, M. Sara (Eds.), *Cryst. Bact. Cell Surf. Proteins*, Academic press, Austin, Tex, 1996, pp. 103–131.
- [225] U.B. Sleytr, P. Messner, Crystalline surface layers on bacteria, *Annu. Rev. Microbiol.* 37 (1983) 311–339.
- [226] P. Messner, K. Steiner, K. Zarschler, C. Schäffer, S-layer nanoglycobiology of bacteria, *Carbohydr. Res.* 343 (2008) 1934–1951.
- [227] P. Messner, E.M. Egelseer, U.B. Sleytr, C. Schäffer, Bacterial surface layer glycoproteins and “non-classical” secondary cell wall polymers, in: *Microb. Glycobiol.*, Elsevier, 2010, pp. 109–128.
- [228] J. Šmarda, D. Šmajš, J. Komrska, V. Krzyžánek, S-layers on cell walls of cyanobacteria, *Micron* 33 (2002) 257–277.
- [229] U.B. Sleytr, R. Plohberger, The dynamic process of assembly of two-dimensional arrays of macromolecules on bacteria cell walls, *Electron Microscopy Mol. Dim.* (1980) 36–47.
- [230] D. Pum, P. Messner, U.B. Sleytr, Role of the S layer in morphogenesis and cell division of the archaeabacterium *Methanocorpusculum sinense*, *J. Bacteriol.* 173 (1991) 6865–6873.
- [231] U. Sleytr, Bacterial S-layers, *Trends Microbiol.* 7 (1999) 253–260.
- [232] U.B. Sleytr, M. Sára, D. Pum, B. Schuster, P. Messner, C. Schäffer, Self-assembling protein systems: microbial S-layers, in: S.R. Fahnestock, A. Steinbüchel (Eds.),

- Biopolym, Wiley-VCH Verlag GmbH & Co. KGaA, Weinheim, Germany, 2005. Online.
- [233] U.B. Sleytr, P. D, E. E.M, I. N, S. N, S-layer proteins, in: Knoll. Wolfgang (Ed.), Handb. Biofunctional Surfaces, Pan Stanford Publishing, 2013, pp. 507–568.
  - [234] C. Mader, S. Küpcü, M. Sára, U. Sleytr, Stabilizing effect of an S-layer on liposomes towards thermal or mechanical stress, *Biochim. Biophys. Acta Biomembr.* 1418 (1999) 106–116.
  - [235] P. Messner, C. Schäffer, E.-M. Egelseer, U.B. Sleytr, Occurrence, structure, chemistry, genetics, morphogenesis, and functions of S-layers, in: Prokaryotic Cell Wall Compd, Springer Berlin Heidelberg, Berlin, Heidelberg, 2010, pp. 53–109.
  - [236] T. Pavkov-Keller, S. Howorka, W. Keller, The structure of bacterial S-layer proteins, *Prog. Mol. Biol. Transl. Sci.* (2011) 73–130.
  - [237] M. Sára, U.B. Sleytr, Molecular sieving through S layers of *Bacillus stearothermophilus* strains, *J. Bacteriol.* 169 (1987) 4092–4098.
  - [238] M. Sára, U.B. Sleytr, Charge distribution on the S layer of *Bacillus stearothermophilus* NRS 1536/3c and importance of charged groups for morphogenesis and function, *J. Bacteriol.* 169 (1987) 2804–2809.
  - [239] K. Gruber, U.B. Sleytr, Influence of an S-layer on surface properties of *Bacillus stearothermophilus*, *Arch. Microbiol.* 156 (1991) 181–185.
  - [240] S. Weigert, M. Sára, Surface modification of an ultrafiltration membrane with crystalline structure and studies on interactions with selected protein molecules, *J. Membr. Sci.* 106 (1995) 147–159.
  - [241] Y.-L. Ji, Q.-F. An, Q. Zhao, W.-D. Sun, K.-R. Lee, H.-L. Chen, C.-J. Gao, Novel composite nanofiltration membranes containing zwitterions with high permeate flux and improved anti-fouling performance, *J. Membr. Sci.* 390–391 (2012) 243–253.
  - [242] A. Chandramohan, E. Duprat, L. Remusat, S. Zirah, C. Lombard, A. Kish, Novel mechanism for surface layer shedding and regenerating in bacteria exposed to metal-contaminated conditions, *Front. Microbiol.* 9 (2019).
  - [243] J.B. Thompson, F.G. Ferris, Cyanobacterial precipitation of gypsum, calcite, and magnesite from natural alkaline lake water, *Geology* 18 (1990) 995.
  - [244] S. Schultze-Lam, G. Harauz, T.J. Beveridge, Participation of a cyanobacterial S layer in fine-grain mineral formation, *J. Bacteriol.* 174 (1992) 7971–7981.
  - [245] S. Schultze-Lam, T.J. Beveridge, Physicochemical characteristics of the mineral-forming S-layer from the cyanobacterium *Synechococcus* strain GL24, *Can. J. Microbiol.* 40 (1994) 216–223.
  - [246] R.J.C. McLean, T.J. Beveridge, Metal-binding capacity of bacterial surfaces and their ability to form mineralized aggregates, in: H.L. Ehrlich, C.L. Brierley (Eds.), *Microb. Miner. Recover.*, McGraw-Hill Publishing Co., New York, 1990, pp. 185–222.
  - [247] T.J. Beveridge, L.L. Graham, Surface layers of bacteria, *Microbiol. Rev.* 55 (1991) 684–705.
  - [248] T.J. Beveridge, Ultrastructure, chemistry, and function of the bacterial wall, *Int. Rev. Cytol.* (1981) 229–317.
  - [249] C. Whitfield, Bacterial extracellular polysaccharides, *Can. J. Microbiol.* 34 (1988) 415–420.
  - [250] K. Jann, B. Jann, Polysaccharide antigens of *Escherichia coli*, *Clin. Infect. Dis.* 9 (1987) S517–S526.
  - [251] I. Orskov, F. Orskov, B. Jann, K. Jann, Serology, chemistry, and genetics of O and K antigens of *Escherichia coli*, *Bacteriol. Rev.* 41 (1977) 667–710.
  - [252] C. Whitfield, Biosynthesis and assembly of capsular polysaccharides in *Escherichia coli*, *Annu. Rev. Biochem.* 75 (2006) 39–68.
  - [253] P.A. Amor, C. Whitfield, Molecular and functional analysis of genes required for expression of group IB K antigens in *Escherichia coli*: characterization of the his- region

- containing gene clusters for multiple cell-surface polysaccharides, *Mol. Microbiol.* 26 (1997) 145–161.
- [254] P.R. MacLachlan, W.J. Keenleyside, C. Dodgson, C. Whitfield, Formation of the K30 (group I) capsule in *Escherichia coli* O9:K30 does not require attachment to lipo-polysaccharide lipid A-core, *J. Bacteriol.* 175 (1993) 7515–7522.
- [255] S. Sachdeva, N. Kolimi, S.A. Nair, T. Rathinavelan, Key diffusion mechanisms involved in regulating bidirectional water permeation across *E. coli* outer membrane lectin, *Sci. Rep.* 6 (2016) 28157.
- [256] E.C. Gotschlich, B.A. Fraser, O. Nishimura, J.B. Robbins, T.Y. Liu, Lipid on capsular polysaccharides of gram-negative bacteria, *J. Biol. Chem.* 256 (1981) 8915–8921.
- [257] G.R. de S. Araújo, N.B. Viana, F. Gómez, B. Pontes, S. Frases, The mechanical properties of microbial surfaces and biofilms, *Cell Surf.* 5 (2019) 100028.
- [258] J.W. Costerton, R.T. Irvin, K.J. Cheng, The bacterial glycocalyx in nature and disease, *Annu. Rev. Microbiol.* 35 (1981) 299–324.
- [259] M.E. Bayer, H. Thurow, Polysaccharide capsule of *Escherichia coli*: microscope study of its size, structure, and sites of synthesis, *J. Bacteriol.* 130 (1977) 911–936.
- [260] I.S. Roberts, The biochemistry and genetics of capsular polysaccharide production IN bacteria, *Annu. Rev. Microbiol.* 50 (1996) 285–315.
- [261] D.A. Rasko, V. Sperandio, Anti-virulence strategies to combat bacteria-mediated disease, *Nat. Rev. Drug Discov.* 9 (2010) 117–128.
- [262] H.-J. Wu, A.H.-J. Wang, M.P. Jennings, Discovery of virulence factors of pathogenic bacteria, *Curr. Opin. Chem. Biol.* 12 (2008) 93–101.
- [263] T.J. Beveridge, The structure of bacteria, in: J.S. Poincexter, E.R. Leadbetter (Eds.), *Bact. Nat.*, Plenum Publishing Corp., New York, 1989, pp. 1–65.
- [264] J.M. Larkin, W.R. Strohl, Beggiatoa, Thiotricha, and Thioploca, *Annu. Rev. Microbiol.* 37 (1983) 341–367.
- [265] R.Y. Stanier, G.C. Bazaine, Phototrophic prokaryotes: the cyanobacteria, *Annu. Rev. Microbiol.* 31 (1977) 225–274.
- [266] T.J. Beveridge, The bacterial surface: general considerations towards design and function, *Can. J. Microbiol.* 34 (1988) 363–372.
- [267] W.C. Ghiorse, Biology of iron-and manganese-depositing bacteria, *Annu. Rev. Microbiol.* 38 (1984) 515–550.
- [268] L.F. Adams, W.C. Ghiorse, Characterization of extracellular Mn<sup>2+</sup>-oxidizing activity and isolation of an Mn<sup>2+</sup>-oxidizing protein from Leptothrix discophora SS-1, *J. Bacteriol.* 169 (1987) 1279–1285.
- [269] F.C. Boogerd, J.P. de Vrind, Manganese oxidation by Leptothrix discophora, *J. Bacteriol.* 169 (1987) 489–494.
- [270] M. Furutani, Assemblage of bacterial saccharic microfibrils in sheath skeleton formed by cultured leptothrix sp. strain OUMS1, *J. Mar. Sci. Res. Dev.* 3 (2013).
- [271] C.S. Chan, Microbial polysaccharides template Assembly of nanocrystal fibers, *Science* 303 (2004) 1656–1658 (80–).
- [272] T.J. Beveridge, R.J. Doyle, *Metal Ions and Bacteria*, Wiley, 1989.
- [273] L.L. Graham, R. Harris, W. Villiger, T.J. Beveridge, Freeze-substitution of gram-negative eubacteria: general cell morphology and envelope profiles, *J. Bacteriol.* 173 (1991) 1623–1633.
- [274] W.L. Nicholson, N. Munakata, G. Horneck, H.J. Melosh, P. Setlow, Resistance of *Bacillus* endospores to extreme terrestrial and extraterrestrial environments, *Microbiol. Mol. Biol. Rev.* 64 (2000) 548–572.
- [275] P.T. McKenney, A. Driks, P. Eichenberger, The *Bacillus subtilis* endospore: assembly and functions of the multilayered coat, *Nat. Rev. Microbiol.* 11 (2013) 33–44.
- [276] S. Cogliati, J. Gabriel Costa, Bacterial spores and its relatives as agents of mass destruction, *J. Bioterrorism Biodefense* 07 (2016).

- [277] G.C. Stewart, The exosporium layer of bacterial spores: a connection to the environment and the infected host, *Microbiol. Mol. Biol. Rev.* 79 (2015) 437–457.
- [278] C. Steichen, P. Chen, J.F. Kearney, C.L. Turnbough, Identification of the immunodominant protein and other proteins of the *Bacillus anthracis* exosporium, *J. Bacteriol.* 185 (2003) 1903–1910.
- [279] L. Kailas, C. Terry, N. Abbott, R. Taylor, N. Mullin, S.B. Tzokov, S.J. Todd, B.A. Wallace, J.K. Hobbs, A. Moir, P.A. Bullough, Surface architecture of endospores of the *Bacillus cereus*/*anthracis*/*thuringiensis* family at the subnanometer scale, *Proc. Natl. Acad. Sci. U.S.A.* 108 (2011) 16014–16019.
- [280] D. Paredes-Sabja, P. Setlow, M.R. Sarker, Germination of spores of *Bacillales* and *Clostridiales* species: mechanisms and proteins involved, *Trends Microbiol.* 19 (2011) 85–94.
- [281] I.M. Shah, M.-H. Laaberki, D.L. Popham, J. Dworkin, A eukaryotic-like ser/thr kinase signals bacteria to exit dormancy in response to peptidoglycan fragments, *Cell* 135 (2008) 486–496.
- [282] A.I. Aronson, P. Fitz-James, Structure and morphogenesis of the bacterial spore coat, *Bacteriol. Rev.* 40 (1976) 360–402.
- [283] A. Driks, *Bacillus subtilis* spore coat, *Microbiol. Mol. Biol. Rev.* 63 (1999) 1–20.
- [284] E.I. Tocheva, E.G. Matson, D.M. Morris, F. Moussavi, J.R. Leadbetter, G.J. Jensen, Peptidoglycan remodeling and conversion of an inner membrane into an outer membrane during sporulation, *Cell* 146 (2011) 799–812.
- [285] M. Hegreness, R. Kishony, Analysis of genetic systems using experimental evolution and whole-genome sequencing, *Genome Biol.* 8 (2007) 201.
- [286] W. Vollmer, Bacterial outer membrane evolution via sporulation? *Nat. Chem. Biol.* 8 (2012) 14–18.
- [287] D. Zerbib, Bacterial cell envelopes: composition, architecture, and origin, in: D. Miklavčič (Ed.), *Handb. Electroporation*, Springer International Publishing, Cham, 2017, pp. 417–436.

**Priloga C:** Dovoljenje založnika Elsevier za vključitev objavljenega raziskovalnega dela v doktorsko disertacijo z naslovom: A Monte Carlo study of giant vesicle morphologies in nonequilibrium environments (Biophysical Journal).

A Monte Carlo study of giant vesicle morphologies in nonequilibrium environments

Author: Mitja Drab, Žiga Pandur, Samo Penič, Aleš Iglič, Veronika Kralj-Iglič, David Stopar

Publication: Biophysical Journal

Publisher: Elsevier

Date: 19 October 2021

© 2021 Biophysical Society.

Journal Author Rights

Please note that, as the author of this Elsevier article, you retain the right to include it in a thesis or dissertation, provided it is not published commercially. Permission is not required, but please ensure that you reference the journal as the original source. For more information on this and on your other retained rights, please visit: <https://www.elsevier.com/about/our-business/policies/copyright#Author-rights>

BACK CLOSE WINDOW

**Priloga D:** Dovoljenje založnika Elsevier za vključitev objavljenega raziskovalnega dela v doktorsko disertacijo z naslovom: Evolution of mechanical stability from lipid layers to complex bacterial envelope structures (Academic Press).

Dear Žiga Pandur,

Thank you for contacting us.

As an Elsevier author, you retain the right to include the chapter embedded in your thesis (provided that this is not to be published commercially) whether in full or in part, subject to proper acknowledgment; see <https://www.elsevier.com/about/policies/copyright> for more information.

As this is a retained right, no written permission from Elsevier is necessary.

Please let me know if you have any queries.

Thank you.

Kind regards,

Thomas Rexson Yesudoss

Copyrights Coordinator

ELSEVIER | HCM - Health Content Management

Visit [Elsevier Permissions](#)

**From:** Administrator

**Date:** Wednesday, December 07, 2022 10:11 AM GMT

Dear Customer

Thank you for contacting Elsevier's Permissions Helpdesk.

This is an automated acknowledgement to confirm we have received your query. Ticket number 221207-017508 has been opened on your behalf and we aim to respond within two business days.

Regards,

Permissions Helpdesk

**From:** Žiga Pandur

**Date:** Wednesday, December 07, 2022 10:11 AM GMT

Dear Mr./Ms.,

I'm asking about permission for a book chapter: Chapter Six Evolution of mechanical stability from lipid layers to complex bacterial envelope structures (Book: Advances in Biomembranes and Lipid Self-Assembly, <https://doi.org/10.1016/bs.abl.2020.09.005>), where as an author I would include chapter the in doctoral thesis?

Thank you and best regards,  
Žiga Pandur